NTNU

Norwegian University of
Science and Technology

Voltage Source Converter Technology for Offshore Grids

Interconnection of Offshore Installations in a Multiterminal HVDC Grid using VSC

Pål Kristian Myhrer Vormedal

Master of Science in Energy and Environment

Submission date: June 2010

Supervisor: Olav B Fosso, ELKRAFT

Co-supervisor: Magnus Gustafsson, Statnett SF

Norwegian University of Science and Technology
Department of Electric Power Engineering

Problem Description

Supply of offshore installations from the onshore grid has been an important topic for several years. The motivation has been both economical and environmental. Local electricity supply of offshore installations based on gas turbines is expensive due to low efficiency, as well as that these installations are contributing significantly to the emission of green house gases from Norway. Few implementations have been made due to the complexity and the expenses of such installations. The focus on offshore wind farms and the developments of the converter technology have again made this as a candidate solution. The Voltage Source Converter (VSC) technology has several advantages over the conventional HVDC, though still there are limitations.

The MSc work should build on the project work: Voltage source converter technology for offshore grids - Interconnection of offshore installations in a multiterminal HVDC grid using VSC from the autumn 2009.

This work will be concentrated on the further development of the conceptual model of an offshore grid and the implementation of the model in the PSS/E software.
The model should be applied in a dynamic analysis of the multiterminal HVDC system.

The studies conducted should be focused on principles of operation for the multiterminal VSC HVDC grid, and possible interaction with the AC grids.

Trondheim, June 2010
Prof. Olav Bjarte Fosso
Supervisor

Assignment given: 22. January 2010
Supervisor: Olav B Fosso, ELKRAFT

Preface

Writing this master thesis has been a valuable and rewarding experience in my education. It has been motivating to get the possibility to thoroughly study a topic that I find very interesting.

I would like to thank my supervisor, Professor Olav Bjarte Fosso, and the scientific community at the Department of Electrical Power Engineering and Sintef Energy, for their guidance and advice. I am very grateful for the collaboration with Statnett SF. I have received a lot of support and guidance from my co-supervisor Magnus Gustafsson and other people at Statnett working with similar projects.

I appreciate the information given to me by various manufacturers, platform operators and consultant agencies, especially Per-Erik Björklund at ABB, who has contributed considerable.

Finally, I want to express my appreciation to my fellow students for a good working environment with rewarding discussions and many laughs, and to Marte Tangvald for all her support and encouragement.

Pål Kristian Myhrer Vormedal

Trondheim, June 2010

Abstract

This master thesis has investigated the possible application of voltage source converters (VSC) for the interconnection of offshore installations, i.e. wind farms and petroleum platforms, in a multiterminal DC (MTDC) grid. The master thesis is written at the Norwegian University of Science and Technology, Department of Electric Power Engineering and is a continuation of the project written during the autumn of 2009. The work has been carried out in cooperation with Statnett SF, the Norwegian TSO, as a contribution to an ongoing research and development program on offshore electrification.

The motivation behind this thesis is the possibilities the VSC technology bring about for the realization of renewable wind energy far from shore and supplying petroleum installations from the main onshore grid, thus reducing emissions.

A theoretical study has been conducted, describing the VSC technology from basic operation to topics related to the implementation of a high power rated offshore MTDC grid. A suggested model of a small power system was established in the simulation program PSS®E. The model consisted of a four converter MTDC connecting three separate AC systems. One of the AC systems was a simplified representation of a main onshore grid, and the other two were small offshore AC grids made up of a wind farm and a petroleum platform. The MTDC was modeled using ABB's HVDC Light Open model v 1.1.9-2, developed for use in PSS®E.

A series of dynamic simulations have been performed using the model to demonstrate and analyze the principles of operation for a MTDC and the interaction between the AC systems and the MTDC. The dynamic simulations demonstrate the basic operation of a MTDC with a master-slave control scheme for the active power control, as implemented in the HVDC Light model. The simulation results confirm the functionality of a MTDC as described in the theoretical analysis of the technology.

The analysis based on both the literature and simulations conclude that VSC technology is a realistic solution for an offshore grid with the objective of supporting passive network installations far from shore. Simulation results conclude that an advanced control system for the active power control operation (Poption) of all the converters in a MTDC may greatly improve the performance of the system following a disturbance. Both theoretically and through simulations it has been demonstrated that the VSC MTDC provides stability improvements to the connected AC grid, by actively controlling the injected active and reactive power to the grid. The possibility to use the MTDC as an alternative path for transferring large amounts of power has been investigated, and this was found to be beneficial for the system. The difficulties related to fault protection in a MTDC have been highlighted, and a theoretical analysis concluded that the protection scheme using IGBT circuit breakers is the preferred solution with present available technology.

Table of Contents

List of tables

List of figures

The figures of chapter 12, displaying the simulation results from the cases, are not listed here, but are found in the analysis of each respective case, as indicated in the list of contents. In addition, the figures in the appendices are also not listed here.

Abbreviations

AC	Alternating current
AVR	Automatic voltage regulator
BBC	Bang-bang control
CLOD	Composite load model (petroleum platforms)
DC	Direct current
DFIG	Doubly fed induction generator
DLL	Dynamically loaded library
FACTS	Flexible AC transmission systems
GTO	Gate turn off transistor
HVDC	High voltage direct current
IGBT	Insulated gate bipolar transistor
IGBT-CB	Insulated gate bipolar transistor current breaker (valve)
LCC	Line Commutated current source Converters
MMC	Modular multilevel converter
MTDC	Multiterminal DC system with VSC
MVA	Mega volt ampere
NTNU	Norwegian university of science and technology
PassNetOp	Passive net operation (converter setting)
PCC	Point of common coupling
Pctrl	Active power control (converter setting)
PlossAdjust	Active power loss adjusting
POI	Point of interconnection
Poption	Active power control option (converter model parameter)
PSS®E	Power system simulator for engineering
pu	Per unit
PWM	Pulse width modulation
R&D	Research and development
SIL	Surge impedance loading
SLD	Single line diagram
SM	Submodule
STATCOM	STAtic synchronous COMpensator
SVC	Static VAR compensator
TCR	Thyristor-controlled reactor
TSC	Thyristor-switched capacitor
TSO	Transmission system operator
UdcCtrl	DC voltage control (converter setting)
VSC	Voltage cource converter
WRIG	Wound rotor induction generator
XLPE	Cross linked polyethylene

1 Introduction

1.1 Problem background

Offshore wind power has proven to be a renewable energy source with a high potential. The North Sea has a vast amount of wind energy, with the largest energy per area densities located at such distances from shore to imply that HVDC is the preferred solution for subsea transmission.

The Norwegian petroleum platforms in the North Sea use electricity from local gas fired turbines. These gas turbines have much less efficiency than onshore generation of electricity, and also release large amounts of green house gases. Therefore, supplying the platforms with power from onshore transmitted by HVDC will result in benefits both from economic and environmental protection perspectives.

In the European liberalized electricity market, the interconnections between countries are very important to facilitate cross-border trade of electricity and to improve the reliability of the grid.

This is the background for a high interest in the use of voltage source converter (VSC) technology in a multiterminal HVDC grid as a potential solution for the integration of the wind farms and petroleum installations into the onshore grid. Such a grid could later be extended to incorporate interconnections between countries for power transmission. The reason for using DC instead of AC is that for the distances involved (more than 100 km) there would be a very large reactive production in the AC cable that would lead to unacceptable high losses and voltage problems. The Norwegian TSO, Statnett SF, is currently carrying out several research and development studies regarding offshore grids, and has, as an external company, suggested the topic of this master thesis. The master thesis is a continuation of the literature specialization project from the autumn of 2009 on the same topic.

1.2 Purpose of the master thesis

The motivation for this master thesis has the following two main objectives:

- The first objective is to further develop a conceptual model of a multiterminal VSC HVDC offshore grid and implement the model in the PSS®E software.
- The second objective is to apply the simulation model in a dynamic analysis of the multiterminal HVDC system. The studies conducted should be focused on principles

of operation for the multiterminal VSC HVDC grid, and possible interaction with the AC grids.

1.3 Overview of previous work

Voltage source converters for transmission purposes can be considered as a new, yet proven technology, with several commercial projects over the last decade. Numerous experiments and simulations have been performed and documentation on the subject, in the form of papers, articles and thesis, is plentiful. For offshore purposes there has been a strong focus on the possibility of using VDC HVDC for the interconnection of large wind farms to the onshore grid, and there is an extensive amount of literature on this subject. Supplying platforms with power in a point to point connection from the main grid have also been covered in several articles and analyses, for instance documentation of the Troll A project. However there are not many offshore projects in commission to this date, and hence not a strong practical experience. Also the research material on multiterminal configurations, especially protection and power control, is somewhat limited. A reason for the inadequate information regarding protection could be that the DC breaker technology is not yet developed for the highest ratings, and the manufacturers are therefore restrictive with regards to this information.

1.4 Layout of report

The contents of this master thesis may be divided into three parts. The first part is mainly a theoretical study, chapters 2 to 6, helpful for understanding the rest of the master thesis. Most of this theoretical study was conducted during the literature specialization project in the autumn of 2009. The second part, chapters 7 to 10, describes the implementation of the suggested power system in a simulation model for use in PSS®E. The third part, chapters 11 to 13, of the master thesis presents the simulations that were performed and includes an analysis of the subsequent simulation results.

Chapter 2 is a thorough description the VSC technology, from the basic operation of the converter to the possibilities of creating an offshore HVDC grid using VSC.

Chapter 4, on AC power systems and stability definitions, is to be considered as a short summary of important aspects necessary for the power system analyses. As the chapter primarily is repetition, a reader with experience in power system analysis would not have to read the chapter in order to understand the rest of the master thesis.

2 Voltage source converter technology

2.1 Semiconductors

Semiconductor devices, that are used for power electronic applications such as HVDC, are classified into *uncontrolled, half-controlled and fully-controlled* semiconductors depending upon the controllability of their ON and OFF states. Power diodes belong to the uncontrolled semiconductor devices category where as thyristors are in the half-controlled group since their switching-on is controlled. Fully-controlled semiconductors allow controlling both switching-on and switching-off. Hence the term *"switch"* in power electronics often refers to the fully controlled semiconductor devices [11].

Although power transistors are the most common types of switches, there are also special types of fully controlled thyristors that belong to the same group, for instance the Gate-Turn-Off thyristor, GTO. In VSC HVDC the most commonly used fully controlled semiconductor is the Insulated Gate Bipolar Transistor, IGBT, which combines some of the advantages of other available switches [12].

HVDC transmission using self-commutated VSC-based systems with insulated-gate bipolar transistor (IGBT) valve and Pulse Width Modulation (PWM) was introduced in the late 1990s. Since then the progression to higher voltage and power ratings for these converters has roughly paralleled that for thyristor valve converters in the 1970s. Figure 2.1.1 illustrates solid-state converter development for the two different types of converter technologies using thyristor valves and IGBT valves [13].

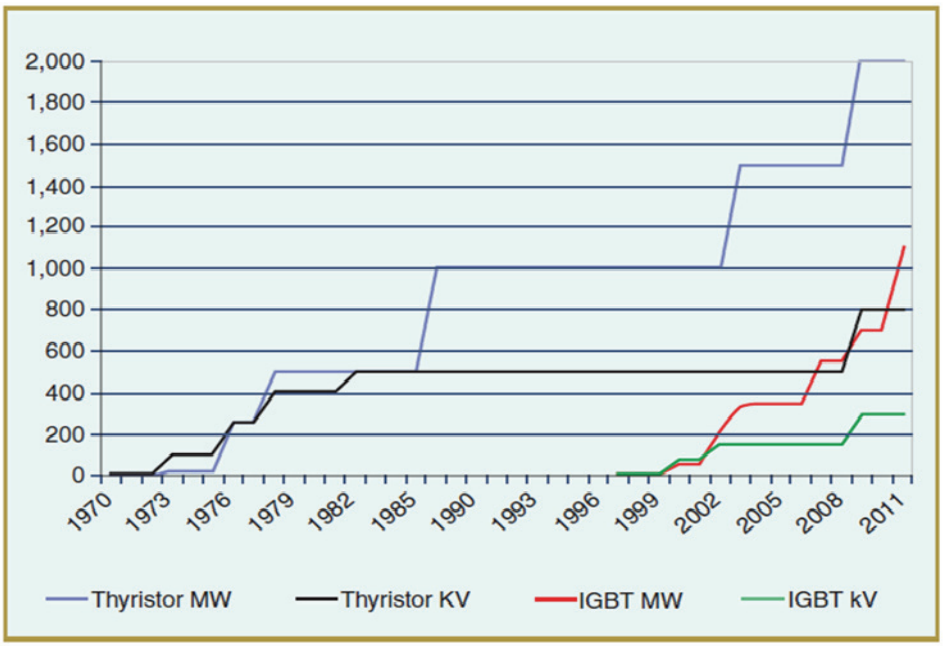

Figure 2.1.1: Development in semiconductors [13]

As can be seen from figure 2.1.1, technological developments in the IGBTs the last ten years have led to a dramatic increase in power- and voltage- handling capabilities of the voltage source converters. The first VSC project at Hellsjön in 1997 used ±10 kV, 3 MVA, and now ABB offers its converter type M9 with ±320 kV and a base power of around 1200 MVA [7]. To further exemplify the development of IGBTs, the book *Power electronics-Converters, Applications, and Design* [12] from 2003 say that IGBTs are available in module ratings as large as 1700 V and that voltage ratings of up to 2 – 3 kV were projected. Today producers supply commercially available IGBT modules with ratings of up to 6500 V [14], and for instance Mitsubishi have made projections that they will soon have modules of 9000 V [15].

2.2 Basic VSC technology

2.2.1 Fundamental converters

This chapter describes the basic operating principles of the VSC by tracking its topology back to the simplest switch mode DC-DC converters, namely step-down (Buck) converter and step-up (Boost) converters. Switch mode refers to the high frequency switching of the electronic valves (IGBTs) involved in the energy conversion process. Step-up and step-down DC-DC converters are shown in figure 2.2.1. A rigorous discussion of these DC-DC converters can be found in [12]. The following is mainly based on the work presented in [11].

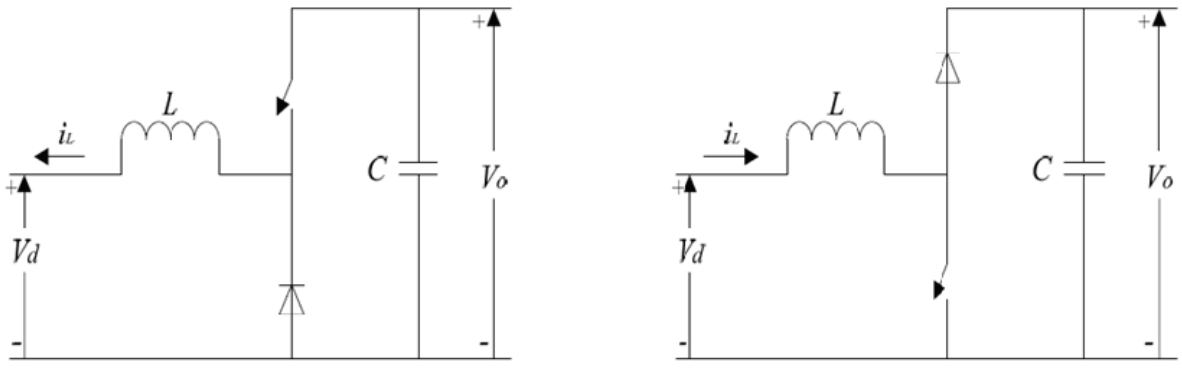

Step-down converter Step-up converter

Figure 2.2.1: Basic DC-DC converters [11]

Note that in figure 2.2.1 the step-down and step-up converters convey power in opposite directions. In order to conduct current, the switches in the converters must be forward biased in addition to providing the pulse width modulated signals to the switch gates. When the switches are forward biased, the voltage relations will be given by:

$$V_d = D_1 V_o \tag{2.1}$$

for the step-down converter and:

$$V_d = (1 - D_2) V_o \tag{2.2}$$

for the step-up converter respectively.

D_1 and D_2 are duty ratios of the switches for the step-down and step-up converters respectively. The duty ratio of a switch is defined as the ratio of its ON-state time during one cycle to one period of the switching frequency.

$$D = \frac{T_{on}}{T_s} \tag{2.3}$$

And

$$T_s = \frac{1}{f_s} \tag{2.4}$$

Here *fs* is the switching frequency. This relation is shown in the following diagram.

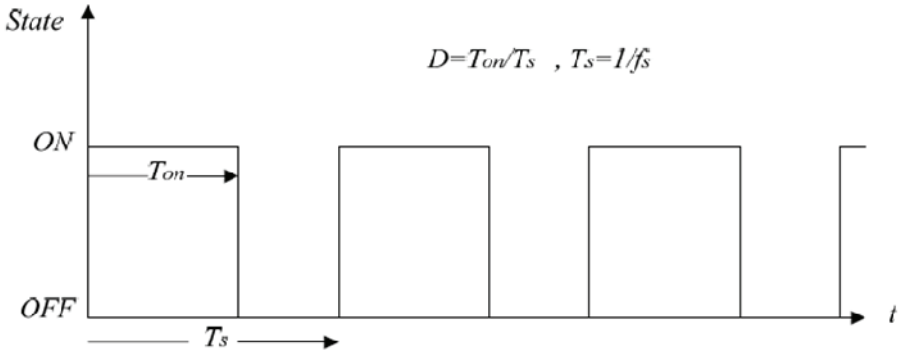

Figure 2.2.2: Duty cycle of a switch [11]

The biasing of the switches depends on the difference of the Thevenin's equivalent voltages of the external networks connected on the left and right sides of the converter. If the gates are reverse biased while supplied with the switching pulses, there will be no current flow and the input-output voltage relations given by equations (2.3.) and (2.4) will no more hold true. Since the step-down and step-up converters transfer power only to the left and to the right sides respectively, it would be possible to combine the two to make a bidirectional DC to DC converter as shown in figure 2.2.3.

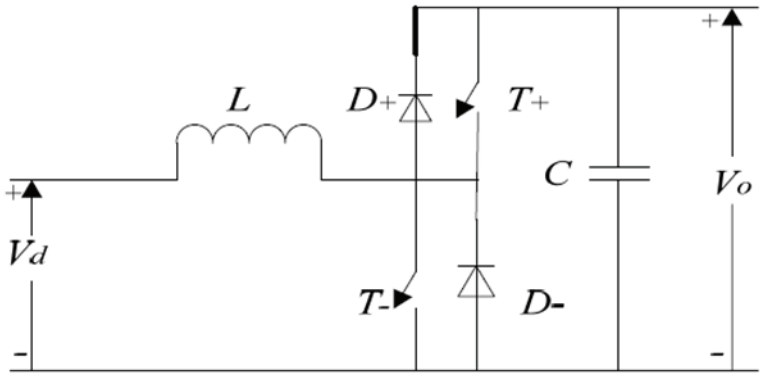

Figure 2.2.3: Bidirectional DC-DC converter [11]

Equations (2.3) and (2.4) must be equal for continuous bidirectional power conversion.

$$V_d = D_1 V_o = (1 - D_2) V_o \rightarrow D_2 = 1 - D_1 \tag{2.5}$$

Equation (2.5) indicates that *T*+ and *T*- are complementary; meaning when *T*+ is in ON-state *T*- will be in OFF-state and vice versa.

After rearranging the switches and splitting the DC capacitor into two, we get the following topology shown in figure 2.2.4.

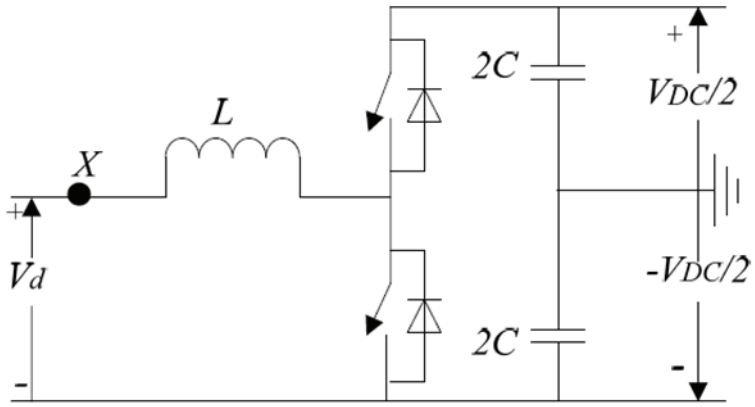

Figure 2.2.4: Rearrangement of the bidirectional DC-DC converter [11]

We define the phase voltage as the voltage of point *X* with reference to the earth.

$$\begin{aligned} V_{ph} &= V_d + \frac{-V_{DC}}{2} \\ &= D_1 V_{DC} + \frac{-V_{DC}}{2}, \qquad 0 \le D_1 \le 1 \\ &= (2D_1 - 1)\frac{V_{DC}}{2} \end{aligned} \tag{2.6}$$

Assigning $K = 2D_1 - 1$,

$$V_{ph} = \frac{KV_{DC}}{2}, \qquad -1 \le K \le 1 \tag{2.7}$$

By varying the constant *K*, it is possible to interface different levels of DC voltages of the same or opposite polarities for bidirectional power flow.

If we now replace the constant *K* with a sinusoidal function of variable amplitude, we can get a sinusoidal phase voltage (V_{ph}). This is done by using Pulse Width Modulation (PWM), which is explained in the following section.

2.2.2 Pulse Width Modulation (PWM)

The output AC- voltage in a switch-mode inverter is obtained by switching the transistors in a certain way. Figure 2.2.5 shows a half bridge single-phase switch-mode converter. The voltage V_d is assumed to be a constant DC- voltage, v_{AN} is the output AC voltage and i_o is the AC- current.

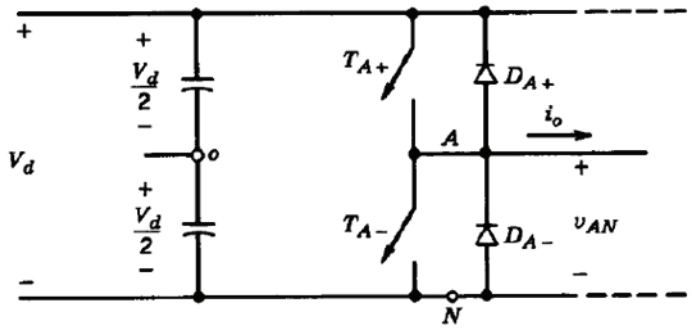

Figure 2.2.5: One-leg switch mode inverter [12]

In order to control the switching, a signal needs to be given to the transistors. This is achieved by using a pulse width modulated switching scheme. A control signal $v_{control}$ is compared with a triangular signal v_{tri} in order to decide which of the transistors T_A+ and T_A- that should be conducting. This is shown in equation (2.8) and (2.9), and in figure 2.2.6.

$$v_{control} > v_{tri} \quad \Rightarrow \quad T_{A+} \text{ is on} \quad \Rightarrow \quad v_{Ao} = \frac{1}{2}V_d \tag{2.8}$$

$$v_{control} < v_{tri} \quad \Rightarrow \quad T_{A-} \text{ is on} \quad \Rightarrow \quad v_{Ao} = -\frac{1}{2}V_d \tag{2.9}$$

The control signal $v_{control}$ is a sinusoidal signal with the frequency *f* equal to the desired output voltage frequency of the converter. The triangular signal has constant amplitude V_{tri} and

frequency f_s. As can be seen from the lower part of figure 2.2.6, the voltage v_{Ao} is not a sinusoidal wave, and the fundamental component $(v_{Ao})_1$ has to be filtered out. Since the voltage is of a very high frequency, the filters can be small. However, it is inevitable that harmonics of a higher order is produced [12][16].

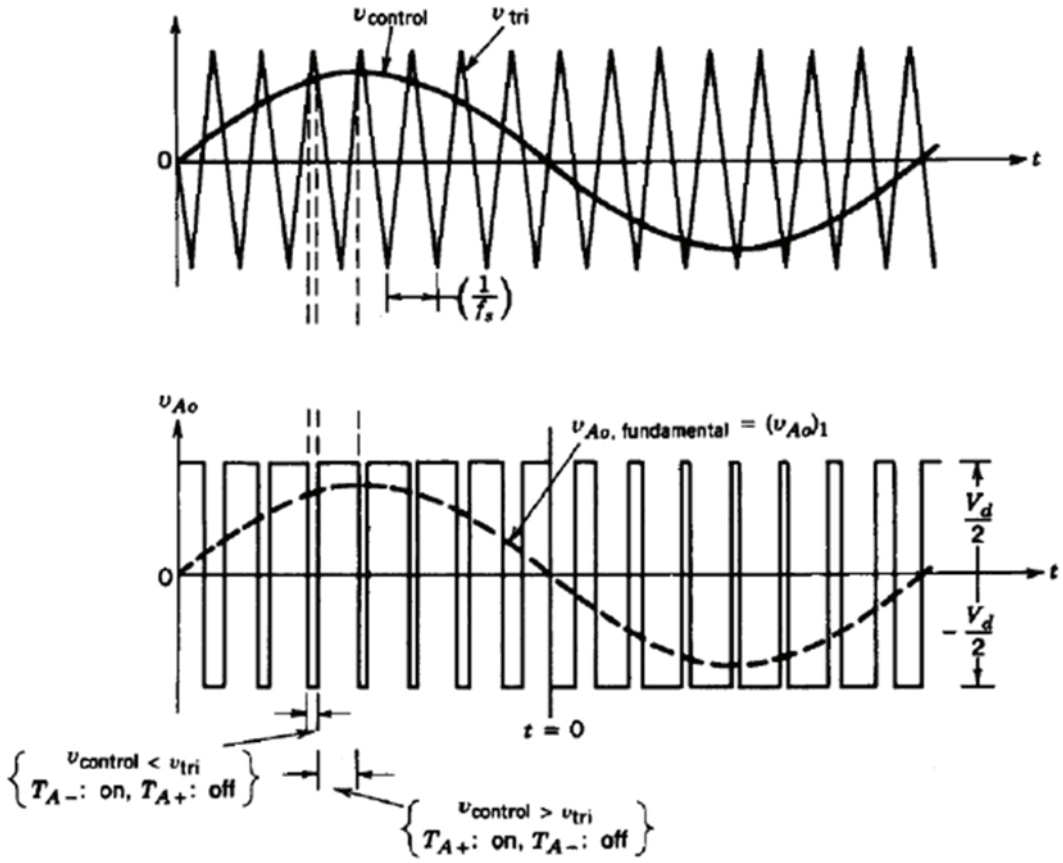

Figure 2.2.6: Pulse-width modulation of a single-phase converter [12]

As long as the amplitude of $v_{control}$ is smaller than the amplitude of v_{tri}, the amplitude of the fundamental component of the output voltage $(v_{Ao})_1$ is proportional with the amplitude of the control signal $v_{control}$. This is called linear modulation. The factor m_a in equation (2.10) is called modulation ratio.

$$(v_{Ao})_{1,peak} = \frac{v_{control,peak}}{v_{tri,peak}} \frac{V_d}{2} = m_a \frac{V_d}{2} \tag{2.10}$$

The phase voltages will in time domain be

$$V_{ph} = \frac{V_{DC} m_a \sin(\omega t)}{2} \tag{2.11}$$

And in phasor domain be

$$\hat{V}_{ph} = \frac{m_a V_{DC}}{2\sqrt{2}} \angle 0^o \tag{2.12}$$

The bidirectional converter together with the sinusoidal PWM consist the half bridge single phase switch mode converter. Three of the half bridge single phase converters connected in parallel and with sinusoidal modulation signals of 120^o apart from each other constitute the three phase switch mode converter, also known as Voltage Source Converter (VSC). The phrase "Voltage Source" refers to the fact that the polarity of DC voltage in VSC is fixed for both rectifier and inverter mode of operations. For thyristor based converters, it is the polarity of current which is fixed for both modes of operations. The three phase bidirectional converter (VSC) is shown in figure [16][11]. There exists other more complex methods for pulse width modulation, for example Space Vector PWM, but descriptions of this will not be emphasized in this project.

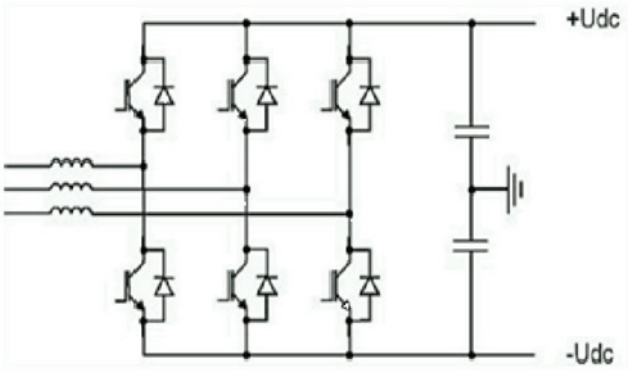

Figure 2.2.7: Voltage source converter [17]

2.3 Comparison of HVDC technologies:

Two basic converter technologies are used in modern HVDC transmission systems. These are conventional line-commutated current source converters (LCC) and self-commutated voltage source converters (VSC) [13].

Line-commutated converters require a relatively strong synchronous voltage source in order to commutate. Commutation is the transfer of current from one phase to another in a synchronized firing sequence of the thyristor valves. Each valve is comprised of a suitable number of series-connected thyristors to achieve the desired DC voltage rating. The three-phase symmetrical short circuit capacity available from the network at the converter connection point should be at least twice the converter rating for converter operation [18][19].

Line-commutated current source converters can only operate with the AC current lagging the voltage, so the conversion process demands reactive power. Reactive power is supplied from the AC filters, which look capacitive at the fundamental frequency, shunt banks, or series capacitors that are an integral part of the converter station. Any surplus or deficit in reactive power from these local sources must be accommodated by the AC system [13].

This difference in reactive power needs to be kept within a given band to keep the AC voltage within the desired tolerance. The weaker the system or the further away from generation, the tighter the reactive power exchange must be to stay within the desired voltage tolerance. Proper control of the converter and its associated reactive power compensation allows the AC system voltage to be held within a fairly tight and acceptable range. Unlike a generator or static VAr compensator (SVC), a conventional HVDC converter cannot provide much dynamic voltage support to the AC network. [18]

The LCC produces considerable AC side current harmonics that require filter banks. The large space footprint of such equipment will make it challenging for installation on an offshore platform [19].

The disadvantages of LCC-based HVDC can to a great extent be overcome by the VSC. HVDC conversion technology using voltage source converters can not only control active and reactive power independently but also provide dynamic voltage regulation to the AC system, as will be described in chapter 3. The VSC generates a voltage on the AC-side and is able to operate in weak networks. Since it operates at a much higher frequency than the LCC, it produces considerably less harmonics. A negative aspect is that due to this higher frequency switching losses increase [18][19].

Table 2.1: Comparison of LCC and VSC [20]

Attributes	**Classical LCC HVDC**	**VSC HVDC**
Converter technology	Thyristor valve, grid commutation	Transistor valve (IGBT), self commutation
Max converter rating at present	6400 MW, ±800 kV (overhead line)	1200 MW, ±320 kV (cable)
Active power flow control	Continuous ±0.1 Pr to ±Pr (Changing power direction normally takes some time due to the change of polarity)	Continuous 0 to ±Pr
Reactive power demand	Reactive power demand = 50 % of active power transfer	No reactive power demand
Independent control of active and reactive power	No	Yes
Typical system losses (These values are decreasing)	2.5 % - 4.5 %	4 % – 6 %
Scheduled maintenance	Typically < 1 %	Typically < 0.5 %
Multi- terminal configuration	Complex	Possible, limitations are explained later in the project
Relative size	4	1

To summarize, the conventional or classic HVDC (LCC) is efficient at transferring large amounts of bulk power due to the high thyristor ratings. It is however dependent on strong AC grids at both converter- stations and is vulnerable to commutation failure. VSC HVDC has lower transfer ratings and higher losses in the converters, but has the capacity to connect passive grids and provide dynamic compensation.

The figures below illustrate the structure of both LCC and VSC, how the semiconductors are stacked in modules which then constitute the phase legs of the converters.

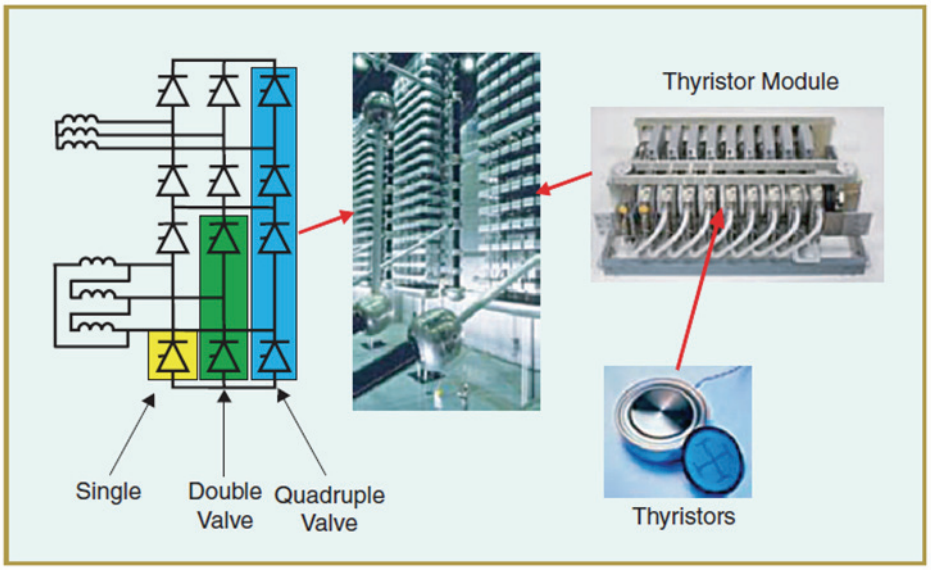

Figure 2.3.1: Structure of LCC [13]

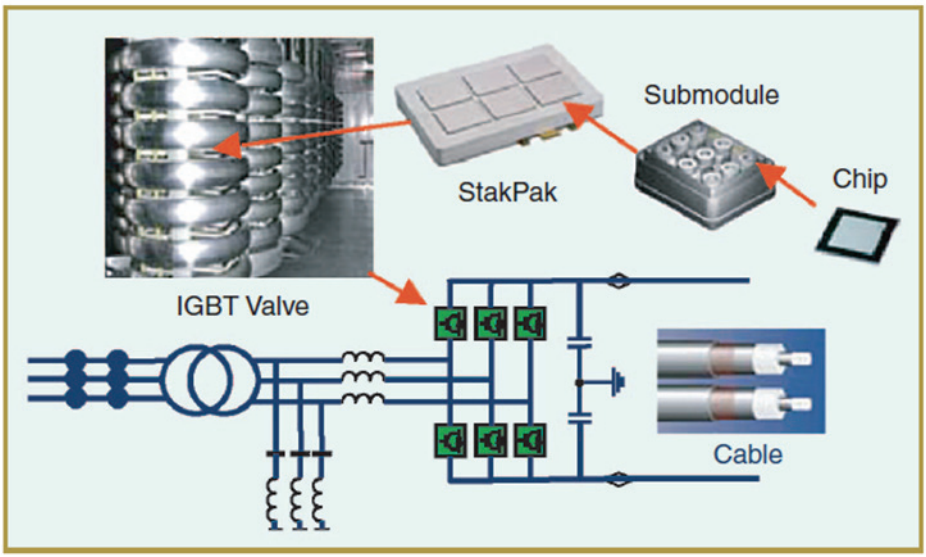

Figure 2.3.2: Structure of VSC [13]

2.4 Multilevel VSC – topology

From the introduction of commercially VSC projects until now, ABB have been the market leading supplier of the technology for VSC transmission. Their product, known as HVDC Light, has ensured that the basic HVDC VSC is now well established technology through a number of installations world-wide. This VSC technology has been based on a two-level design. Siemens is in the process of building their first commercial HVDC VSC installation in San Francisco with a rating of 400 MW, ±200 kV with an 80 km sea cable across the bay interlinking the AC grid. This VSC technology is based on multilevel design, and is called HVDC PLUS. Areva is still developing their HVDC VSC technology and has experience with STATCOM but has so far not published information on any commercial installation of HVDC VSC [21].

To make high voltages in HVDC transmission applications controllable by semiconductors with a blocking ability of a few kilovolts, multiple semiconductors are connected in series, the amount depending on the DC voltage. To ensure uniform voltage distribution not only statically but also dynamically, all devices connected in series in one converter leg have to switch simultaneously with the accuracy in the microsecond range. As a result, high and steep voltage steps are applied at the AC converter terminals which require extensive filtering measures. From the figure below it can be seen that a two-level converter, where the voltage is created with PWM, have a voltage characteristic that is far away from the desired sinusoidal shape. The high voltage steps needs extensive filtering and also exerts high stresses on the converter components.

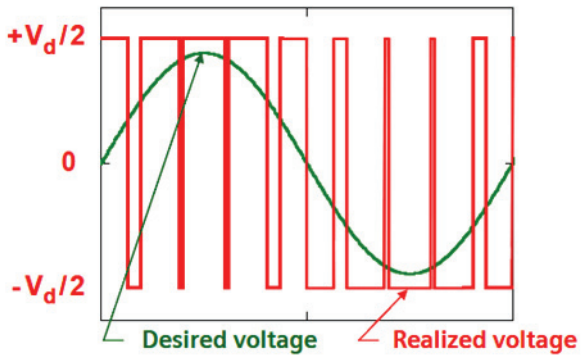

Figure 2.4.1: Two-level converter voltage [22]

Both the size of voltage steps and related voltage gradients can be reduced or minimized if the AC voltage generated by the converter can be selected in smaller increments than at the two-level design. The finer the gradation, the smaller is the proportion of harmonics and the lower is the emitted high-frequency radiation. Converters with this capability are called *multilevel converters*. Furthermore, the switching frequency of individual semiconductors can be reduced. Since each switching event creates losses in the semiconductors, converter losses can be effectively reduced.

There are different possible topologies for multilevel converters. Figure 2.4.2 shows two possible solutions, conventional multilevel converter and a more advanced modular multilevel converter (MMC). Each converter consists of six converter legs and figure 2.4.2 depicts the principle design of two of these legs (one phase) [22].

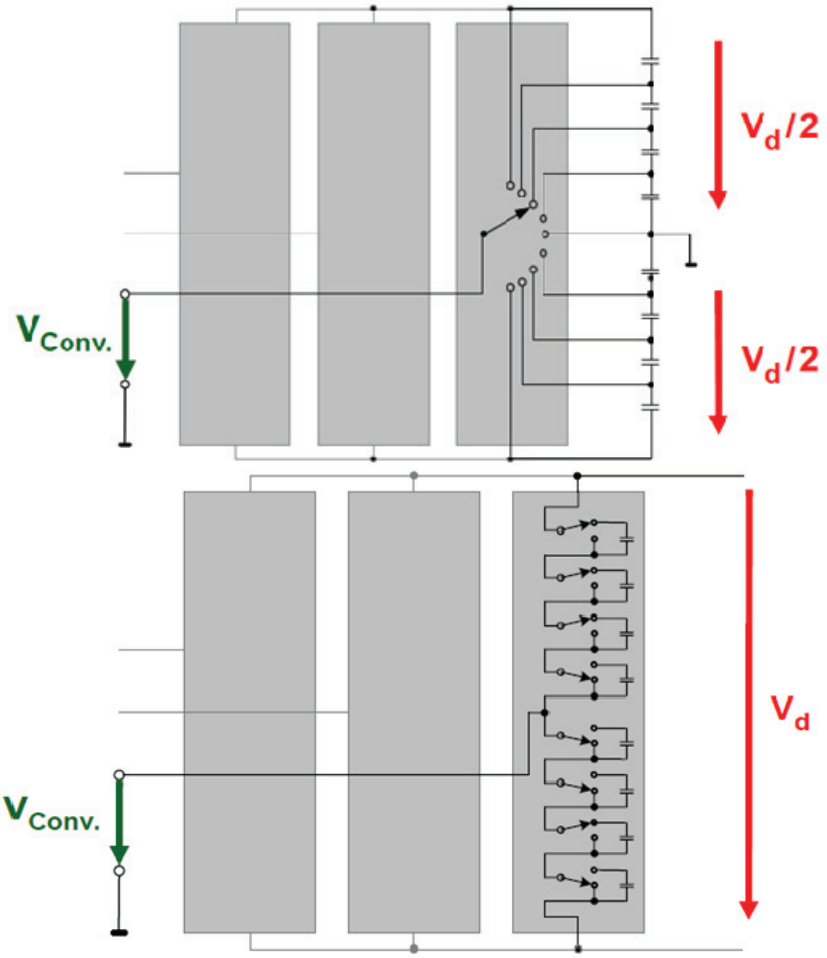

Figure 2.4.2: Multilevel VSC concepts [22]

Siemens HVDC PLUS is a voltage source converter with MMC, and this design can be used as a basis for further understanding multilevel converters, figure 2.4.3.

In this design each of the six converter legs consist of a number of submodules (SM) connected in series with each other and with one converter reactor. Each of the submodules contains an IGBT half bridge as switching element and a DC storage capacitor.

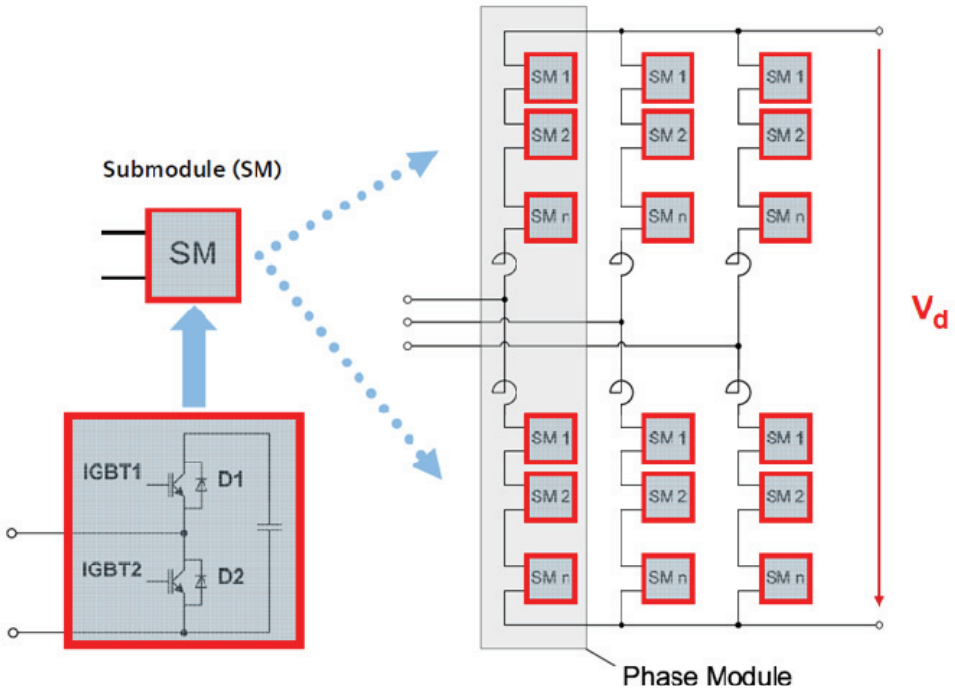

Figure 2.4.3: Modular multilevel converter [22]

It is thereby possible to separately and selectively control each of the individual submodules in a converter leg. In principle this means that the two converter legs of each phase module represent a controllable voltage source. The total voltage of the two converter legs in one phase unit equals the DC voltage, and by adjusting the ratio of the converter leg voltages in one phase module, the desired sinusoidal voltage at the AC terminal can be achieved [22].

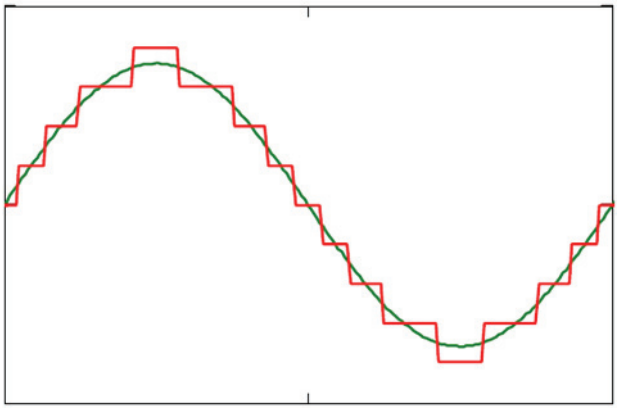

Figure 2.4.4: AC voltage with multilevel converter [22]

From figure 2.4.4 it can be seen that there is very small need for AC voltage filtering to achieve a clean voltage with multilevel converter, in comparison to the two-level converter with PWM in figure 2.4.2. Multilevel converters will have a much lower stress on the phase reactors, filters and capacitors in the converter compared to two-level. A more detailed study of the multilevel design can be investigated in [22].

2.5 Main Components of VSC:

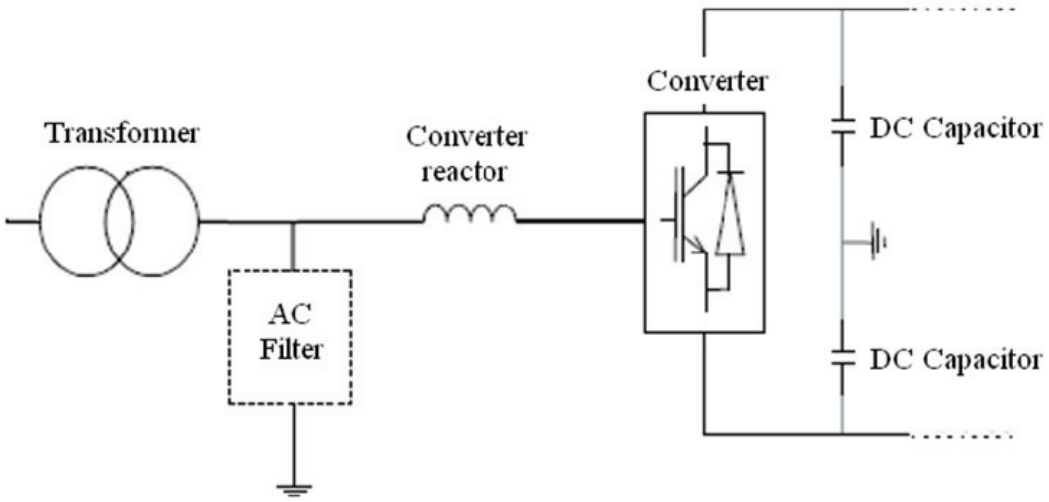

Figure 2.5.1: Main components of a VSC [11]

Transformer
Usually, the converters are connected to the AC system via transformers. The transformer has the main purpose of transforming the AC voltage in to a level suitable to the converter.

Converter reactor
The converter reactor is one of the key components in a voltage source converter to permit continuous and independent control of active and reactive power. There is one converter reactor per phase.

The main purposes of the converter reactor are:

- to provide low-pass filtering of the PWM pattern to give the desired fundamental frequency voltage. The converter generates harmonics related to the switching frequency. The harmonic currents are blocked by the converter reactor, and the harmonic content on the AC bus voltage is reduced by the AC filter.
- to provide active and reactive power control. The fundamental frequency voltage across the reactor defines the power flow (both active and reactive) between the AC and DC sides.
- to limit the short-circuit currents

DC capacitors
The primary objective of the valve DC side capacitor is to provide a low-inductance path for the turned-off current and also to serve as an energy store that supports the DC voltage. The capacitor also reduces the harmonics ripple on the direct voltage. Disturbances in the system (e.g. AC faults) will cause DC voltage variations. The ability to limit these voltage variations depends on the size of the DC side capacitor. A multilevel concept is, as explained in the previous section, completely different with respect to the capacitor. There the total capacitor is the sum of all the smaller capacitors of the submodules.

AC filter

In addition to the series inductance of the reactor, AC filters can be used to eliminate the voltage harmonics entering into the AC system. A typical AC filter is a shunt connected high pass filter containing two or three earthed or unearthed filter branches tuned in the order of the PWM frequency. The rating of the filters depend on the performance requirements and magnitude of the harmonics, but a typical filter for a two-level converter is somewhere between 10 to 30 % of the rated power. As explained preciously, multilevel converters produce les harmonics and therefore require smaller filters.

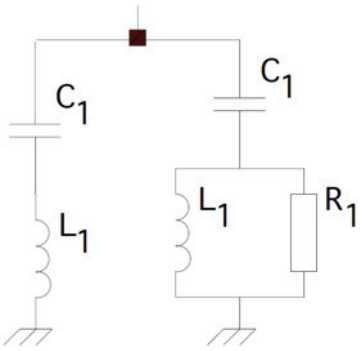

Figure 2.5.2: Example of AC filter [7]

2.6 DC cables

This description of the physical construction for HVDC cables is made with a reference to ABB's HVDC Light submarine cables especially designed for VSC application. The essential elements like insulation and protection screen of the cable systems are very similar, independently of the manufacturer.

The polymeric insulation system of HVDC Light deep sea submarine cables consists of the conductor screen, insulation material and insulation screen. The insulation material is cross linked polyehylen (XLPE). Submarine cables have a lead alloy sheath with a polyethylene sheath (inner jacket) extruded over the lead sheet. The polyethylene sheath provides mechanical and corrosion protection for the lead sheath. The tensile armor consists of galvanized round steel wires close to each other twisted round the cable and flooded with bitumen in order to obtain effective corrosion protection. It is needed when the cable is laid in the sea, and also offers mechanical protection against impacts and abrasion if the cable is not buried to safe depth in the seabed. The outer cover of the submarine cables consists of two layers of polypropylene yarn, the inner one impregnated with bitumen. The submarine cables can be installed on all types of seabed, and can be buried or be protected by covers [7].

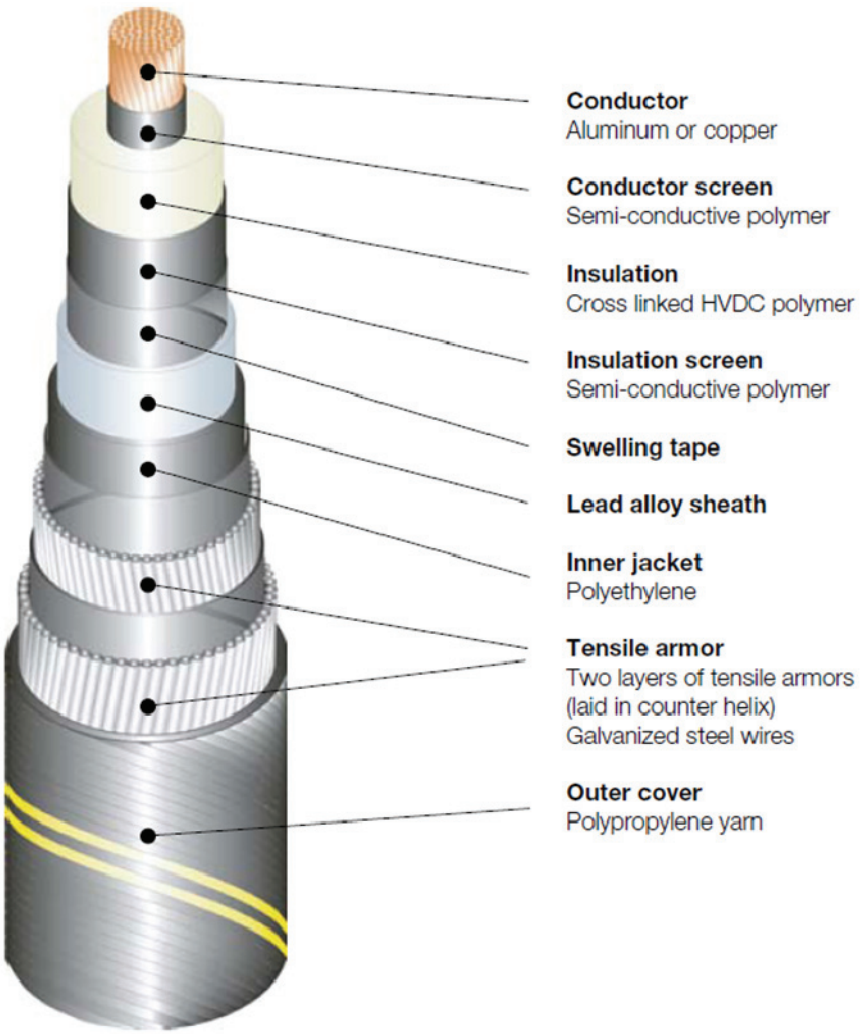

Figure 2.6.1: DC cable [7]

2.7 Power flow

A VSC HVDC system has the advantage compared to a traditional LCC HVDC system that the VSC converter can provide separate control of active and reactive power. This is done by controlling the amplitude and phase angle of the produced AC voltage, which is obtained by changing the control signal $v_{control}$ as described in chapter 2.2.2.

Consider a system topology as shown in figure 2.7.1.

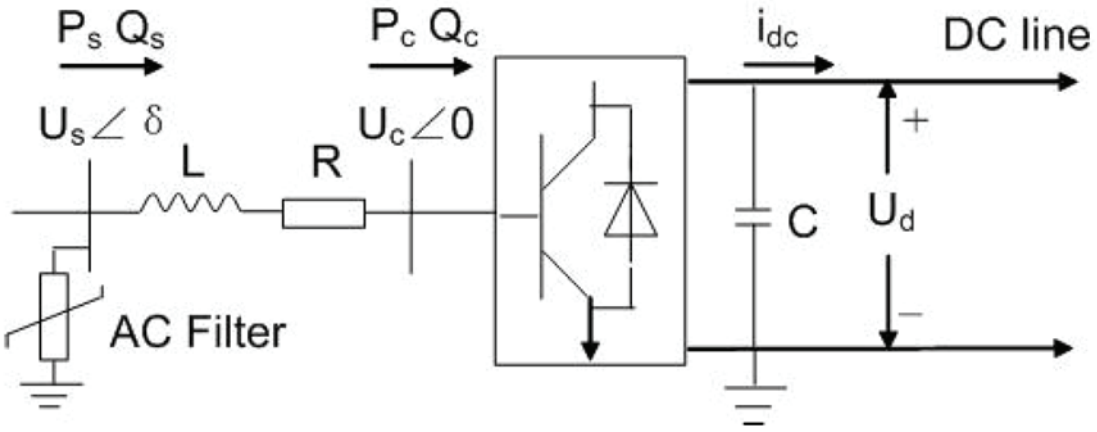

Figure 2.7.1: Power flow in VSC [23]

Assume the power flowing from the AC system into the converter, corresponding to rectifier mode of operation for the converter. The voltage V_c lags V_s with the angle δ. By neglecting the resistance R, the power transferred to the converter from the AC system can be derived as in equation (2.13) [23].

$$\mathbf{S_C} = P_C + jQ_C = \mathbf{V_C} \bullet \mathbf{I}^* = \mathbf{V_C}\left[\frac{\mathbf{V_S} - \mathbf{V_C}}{j\omega L}\right]^* = V_C\left[\frac{V_S\cos(\delta) + jV_S\sin(\delta) - V_C}{j\omega L}\right]^* \tag{2.13}$$

With the resistance neglected, the active power from the AC system equals the received active power at converter. The expression for the active power is found from equation (2.13) in equation (2.14) by dividing the imaginary part of the numerator by $j\omega L$, and multiply it with V_C.

$$|P_S| = |P_C| = V_C\left[\frac{V_S\sin(\delta)}{\omega L}\right] = \frac{V_C V_S}{\omega L}\sin(\delta) \tag{2.14}$$

The reactive power Q_C consumed by the converter is found from equation (2.13) in equation (2.15), by dividing the real part of the numerator by $j\omega L$, and multiply it with V_C.

$$Q_C = V_C\left[\frac{V_S\cos(\delta) - V_C}{\omega L}\right] = \frac{V_C V_S\cos(\delta) - V_C^2}{\omega L} \tag{2.15}$$

Correspondingly to the power into the converter, the expression for the power delivered by the AC system is given in equation (2.16).

$$\mathbf{S_S} = P_S + jQ_S = \mathbf{V_S} \bullet \mathbf{I}^* = \mathbf{V_S}\left[\frac{\mathbf{V_S} - \mathbf{V_C}}{j\omega L}\right]^* = V_S\left[\frac{V_S - V_C\cos(\delta) - jV_C\sin(\delta)}{j\omega L}\right]^* \tag{2.16}$$

The reactive power drawn from the AC system is expressed in equation (2.17).

$$Q_S = \frac{V_S^2 - V_S V_C \cos(\delta)}{\omega L} \tag{2.17}$$

In traditional HVDC systems with LCC converters, the direction of the active power flow is changed by changing the firing pulse to the thyristors so that the DC voltage changes polarity, while the direction of the DC current remains the same [12]. To change the direction of the active power flow in VSC converters the direction of the DC current is changed, while the DC voltage polarity is the same, see figure 2.7.2 below. In this case, the rectifier becomes an inverter, and vice-versa. Considering the system in figure 2.7.1 and equation (2.14), the power flow direction would change if the voltage V_c was made to lead V_s.

In a traditional HVDC system, the converts consume reactive power independently of active power flow direction. In VSC HVDC systems, the reactive power can be controlled at each converter according to (2.15).

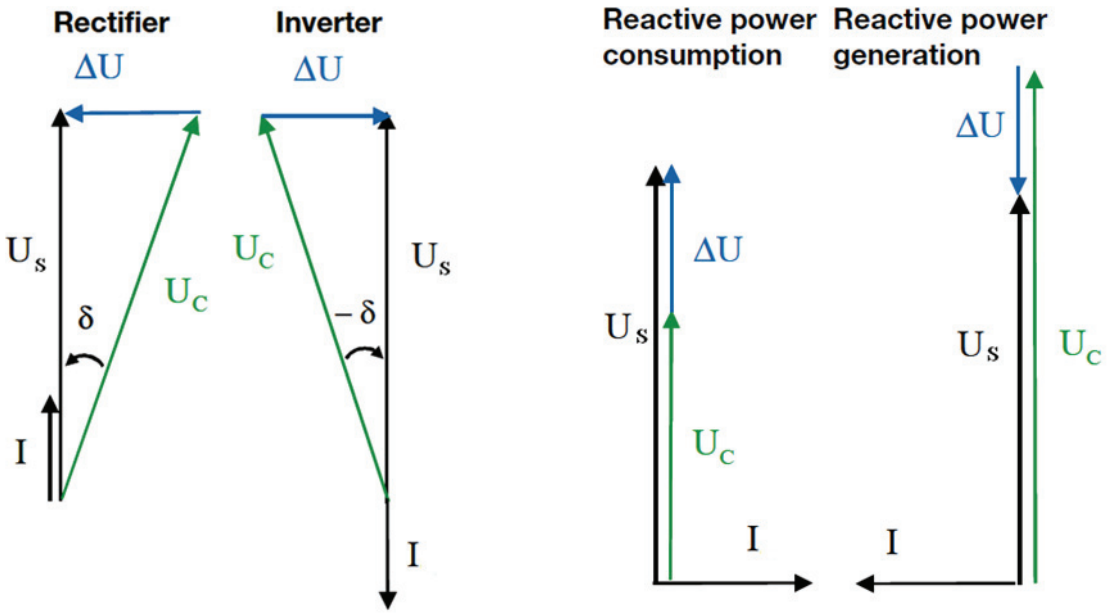

Figure 2.7.2: VSC mode of operations [7, modified]

To summarize:

Changing the phase angle controls the active power flow between the converter and the filter bus and consequently between the converter and the AC network.

- If the U_C is in phase-lag, the active power flows from AC to DC side (rectifier)
- If the U_C is in phase-lead, the active power flows from DC to AC side (inverter)

Changing the amplitude difference between the filter voltage U_S and the converter voltage U_C controls the reactive power flow between the converter and the filter bus and consequently between the converter and the AC network.

- If $U_S > U_C$, there is reactive power consumption.
- If $U_C > U_S$, there is reactive power generation.

The fact that a VSC system can control both active and reactive effect independently at each converter station makes the VSC very suitable for projects were the gridsituation is challenging, such as connection of offshore systems. Because the VSC system provide quick control of reactive compensation for voltage support, the need for additional compensating equipment such as SVC, is reduced [24].

2.8 Control during normal operation of VSC

As can be seen from the equations in the previous section, the VSC converter has two controllable variables in order to control the active and reactive power at its terminals. By applying a phase shift δ to the sinusoidal control signal $v_{control}$, the output voltage will get the same phase shift. By increasing the modulation ratio m_a, the amplitude on the output AC-voltage will increase, according to equation (2.12) [16].

These two controllable variables (δ and m_a) mean that VSC has two degrees of freedom. In comparison, thyristor based converter has only one degree of freedom, i.e. the firing angle (α). Degree of freedom refers to the number of independently alterable parameters and is an indication of the maximum number of independently controllable output quantities. This higher flexibility together with its fixed voltage polarity for both rectifier and inverter modes of operation make VSC-HVDC the core component in developing multiterminal DC systems (MTDC), which will be discussed in chapter 2.10 [11].

In VSC the active power can be continuously controlled from full power export to full power import. Normally each station controls its reactive power flow independently of the other station. However, the flow of active power to the DC network must be balanced, which means that the active power leaving the DC network must be equal to the active power coming into the DC network, minus the losses in the VSC HVDC system. A difference in power would imply that the DC voltage in the system would rapidly increase or decrease, as the DC capacitor increases its voltage with increased charge [7]. Each converter can either be set to regulate the AC voltage by adjusting the reactive power at the connection busbar, or set to operate at constant reactive power. In addition to the above mentioned parameters, the DC-voltage has to be controlled by one of the converters. The other converter controls the active power, based on an active power set point.

Assume the rectifier has constant DC voltage control and the inverter has constant active power control. If the inverter increases the voltage angle δ due to a change on the active

power set point, the active power from the inverter to the AC system will increase according to equation (2.14). With no change in the power transfer at the rectifier, the capacitance on the DC side will discharge and the DC voltage will decrease. The rectifier has to increase the voltage angle to transfer more power to the DC link in order to charge the capacitances and increase the DC voltage. The general equation (2.18) explains the mechanism, where $v_{\text{capacitance}}$ is the voltage over the DC side capacitance, C is the total DC capacitance and i is the current flowing through the capacitance due to imbalance of active power between the two converters.

$$v_{\text{capacitance}} = \frac{1}{C}\int_0^t i\,dt \tag{2.18}$$

In a traditional HVDC system, a communication link between the two converter stations is needed in order to control the power flow. The voltage is measured in one end, and the DC voltage is controlled in the other end so that the voltage difference divided by the DC line or cable resistance equals the set point of the DC current [25]. A VSC HVDC system does not require any communication between the two converters. The converters communicate through the measured DC voltage at each end.

2.9 P-Q diagram

Figure 2.9.1 depicts the P-Q diagram for HVDC Light back-to-back, i.e. with no distance between the two stations. The first and second quadrants represent the rectifier, and the third and fourth the inverter. A positive value of Q indicates the delivery of reactive power to the AC network [5]. If the connection transfers 90 % active effect referred to the rating, the converters at each end of the connection can contribute with approximately ± 50% reactive effect. Even if there is no transfer of active power, the converters can still act as a STATCOM in their connected AC grid [16].

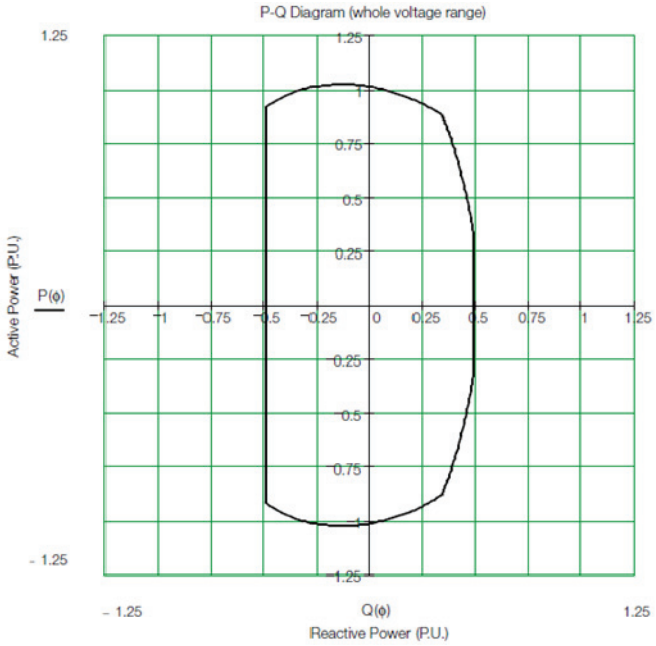

Figure 2.9.1: P-Q diagram for HVDC Light [7]

The following explanation of the P-Q diagram refers to figure 2.9.2 below, and is based on documents provided by ABB (The manufacturer of HVDC Light).

There are mainly three factors that limit the capability seen from a power system stability perspective:

1. The first one is the maximum current through the IGBTs. This will give rise to a maximum MVA circle in the power plane where maximum current and actual AC voltage is multiplied. If the AC voltage decreases so will also the MVA capability.
2. The second limit is the maximum DC voltage level. The reactive power is mainly dependent on the voltage difference between the AC voltage the VSC can generate from the DC voltage and the grid AC voltage. If the grid AC voltage is high the difference between the maximum DC voltage and the AC voltage will be low. The reactive power capability is then moderate but increases with decreasing AC voltage. This makes sense from a stability point of view.
3. The third limit is the maximum DC current through the cable.

The different limits are shown in figure 2.9.2. For a decreasing AC voltage level the maximum DC voltage level will vanish and the maximum current level (MVA limit) will decide the capability. For high AC voltages the DC voltage limit is quite restrictive but it will most likely not be desirable to inject reactive power into the AC system in the case of already high AC system voltages. The absorbing reactive capacity given by the MVA circle is hence much more important for a high AC voltage.

There is also a steady state minimum DC-voltage level limit for HVDC Light. This may prohibit continuous operation at absorbing large amount of reactive power, and is the reason for the limit of -0.5 pu reactive power in figure 2.9.1.

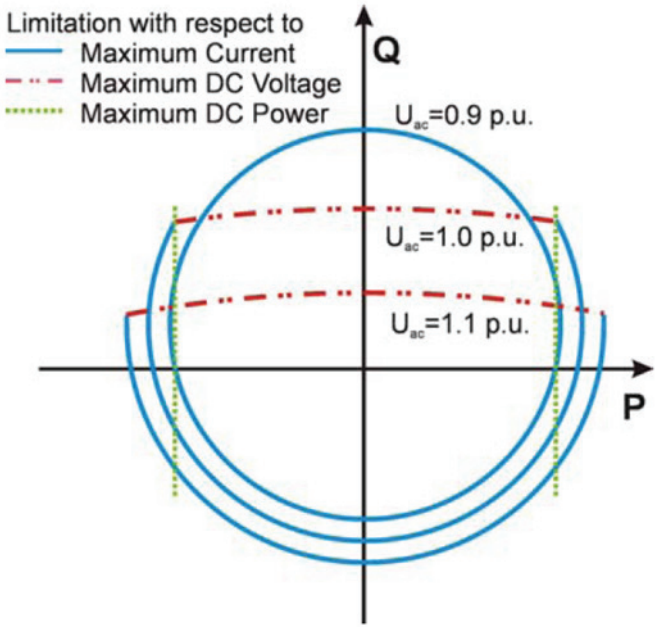

Figure 2.9.2: Restrictions on a HVDC light P-Q diagram [26]

The capability curve for a VSC can be compared to the capability curve for a generator. Maximum DC voltage level corresponds to maximum field current in the rotor winding and IGBT current corresponds to armature current.

A VSC transmission system can virtually instantly take any working point within the capability chart [27][26].

2.10 Black start

Restoring power after a wide-area power outage, or blackout, can be difficult and time-consuming, as power plants need to be restarted under the condition of no power supply from the AC grid, as this is a dead grid. This means a so-called black start needs to be performed. To provide a black start in an onshore grid based on thermal production, power stations are typically equipped with small diesel generators which can be used to start larger generators (of several megawatts capacity), which in turn can be used to start the main power station generators. It is costly to provide such a large standby capacity at a power station.

An offshore AC grid, powered with HVDC from land, may have to be restored after a total shut down caused to a failure in the HVDC transmission or the offshore AC system. Therefore, it is a necessity that the converters can initiate a black start of a dead and passive

grid. It is thoroughly explained in previous chapters how a VSC can convert the DC voltage of the DC side storage capacitor into an AC voltage by switching on and off the converter bridges according to the pre-determined switching pattern. Using pulse width modulation, the VSC will create an AC side voltage which contains a fundamental component equal to the AC reference voltage in magnitude, phase and frequency. During an offshore black start one of the VSC HVDC converter stations is connected to the main AC grid (an active grid in contrast to a dead grid) and the DC capacitors can be charged through this converter. The DC link voltage can be hold to a reference value by putting the onshore converter in DC voltage control mode. During normal power transmission operation, the AC reference voltage is determined by active power (or DC voltage) and reactive power (or AC voltage) control, and the observed AC network voltage as well. During the black start, the AC voltage reference is created according to the pre-determined magnitude, phase angle and frequency. Voltage source converters can provide effective voltage and frequency stabilization during the restoring process when the network experiences dramatic changes from zero short-circuit power to normal short-circuit power. This will make the restoration less complicated and more reliable

During transition from black start control to normal power flow control no transient should be noticed, as the on-line measured active and reactive power will be used as initial active and reactive power settings in the power control mode. It is not necessary that the loads and generations must be balanced during this transition as the VSC HVDC can adjust the power in a wide range from absorption to generation up to rated power of the HVDC. [28]

A detailed description of a full scale testing of black start using VSC HVDC can be further investigated in [28].

2.11 Multiterminal VSC HVDC (“Super grid”)

One of the main challenges for the technology development of multiterminal HVDC is that there have been no real demanders for it, and therefore no market for the technology. For onshore applications it has proven too costly and the AC grid has been sufficient. However in recent years there has been a stronger focus on the possibilities for electrification of petroleum installations in combination with the connection of offshore electricity production in Europe. With a large scale electrification of both loads and production offshore there is a potential for an offshore multiterminal HVDC with interconnectors in the North Sea [29].

Until now HVDC has been used for point to point transmission with two terminals and in a few cases three terminals. It has been considered very complicated to build a meshed HVDC network. HVDC using VSC technology makes it more realistic to consider real HVDC grids, with more than two interconnections. In fact, in industrial drive systems the parallel operation of multiple VSCs is common practice [19].

In LCC the DC current can only flow in one direction. This means that changing the power direction involves changing the polarity of the transmission. This is not a problem with two terminals, but becomes more problematic with multiterminal schemes. VSC, on the other hand, can allow current in both directions and there is no need to change the polarity when the direction of power is changed. This makes building a HVDC grid with VSC easier than with LCC because power can be reversed at an intermediate tap independently of the main power flow direction without switching to reverse voltage polarity [13]. Another advantage with VSC is that disturbances in the AC grid do not cause commutation failure that severely affects the DC transmission. VSC HVDC grid will be more immune to disturbances in the AC grid [30].

Despite the advantages of VSC, a DC network faces several challenges:

- Standardization
- Control of power
- Protections and DC breakers
- Earthing

2.11.1 Standardization

As long as HVDC was mainly point to point transmission the need of standardization has not been urgent. With HVDC grids the situation changes as in this case the grid will inevitably have to be built in stages and the different parts will have no contact with each other in the beginning. If voltage, protection principles and power flow control are not in some way standardized it might not be possible to connect the different parts into an overall grid at a later stage. This makes it important to have a discussion on standards at an early time [30].

2.11.2 Protection

This section, covering protection, is made rather comprehensive, as the subject is very important. Today, the main arguments against a realization of high power DC grids are issues related to switching and protection [31].

2.11.2.1 Available technology

Faults on the DC bus or in the DC cables (or lines) are probably the most severe challenge facing a DC grid with VSC. AC grids are fed by large generators and transformers which both offer a high inductance, and the resulting high impedance limits the short circuit currents in case of faults. Similarly, LCC HVDC has a very large reactor at the converter which limits short circuit currents. Voltage source converters however, are, by themselves, defenseless against DC faults. Their anti-parallel diodes conduct as rectifier bridges to feed the fault, and their IGBTs are helplessly by-passed, unable to extinguish the fault current. The AC side will

feed current into the DC side fault only limited by the reactance in the AC grid, the converter transformer and the converter phase reactor. Because the short circuit currents in DC grids are limited by much smaller impedances than the AC grids the theoretical short circuit currents could reach extreme values.

Today, in present two terminal schemes, these faults are taken care of by opening the breakers on the AC side in both converters. This solution is less attractive when more than two terminals are involved because the whole DC side will lose its voltage for several hundred milliseconds. DC breaker protections have to be designed to make sure that only the faulted part of the grid is disconnected. In order to clear a DC fault, the fault must be starved of the fault current for a period long enough for the plasma to be extinguished and there is no possibility of re-striking when the voltage reappears. The protections would also have to make sure that if zone one protections does not operate properly a zone two protections should operate and take out a somewhat bigger part of the grid. The major part of the grid should still be able to continue operation. Such a solution, that can maintain the DC voltage on most of the grid, will be a necessity for larger DC grids. The only way to achieve this is to use some sort of DC breakers. [30][31][32]

The kind of DC breakers that would serve the power- and voltage- ratings required in a DC cable grid does not exist today. The requirements differ from ordinary AC breakers on at least two important parameters. First they will have to break DC current, and then they will have to be much faster than AC breakers. High power circuit breakers designed for AC systems are mechanical devices, using either vacuum or SF6 to extinguish the occurring arc. The natural zero crossing in AC grids is essential for the operation and determines the short circuit turn-off capability of mechanical circuit breakers. In DC application no natural zero crossing exists, leading to the fact that present circuit breaker technology is not able to break large DC currents. The high speed will be necessary because, as explained, the impedance in a DC grid is quite low. The fault currents will rise very rapidly towards very high values unless interrupted within a few milliseconds.

Even though a “conventional” DC breaker is not available for the necessary transmission ratings there is however a possible solution with the required qualities. By series connection of IGBTs a “valve” is created that can be applied to break the current. This will be very similar to a converter leg in a VSC, but the valve will be directed in the opposite direction compared to the converter, thus producing the ability to block currents from the AC grid into the DC grid. Such a valve is very big, voluminous and expensive compared to AC breakers from conventional power systems. Despite the drawbacks with the valve, this solution is the only realistic available method to break short circuit currents in a high rated DC grid. Hence the DC circuit breakers in the examples for grid protection presented later in the chapter will be referred to as IGBT circuit breakers (IGBT-CB). As the current continuously would pass through the IGBTs this solution involves high losses [30][25][31].

This IGBT-CB design is relatively simple but it does not have bidirectional blocking capability. When the DC current through the VSC is in the direction of the dashed arrow, the IGBTs in the CB are blocking and thereby cutting off the flow of current to the DC network.

When the DC current has the direction of the solid arrow, it cannot be blocked by the IGBT-CB as there is a path through the anti-parallel diodes. For this reason, when a line is to be completely isolated, the blocking of the IGBT-CB must be accompanied by the blocking of the IGBTs in the VSC [31].

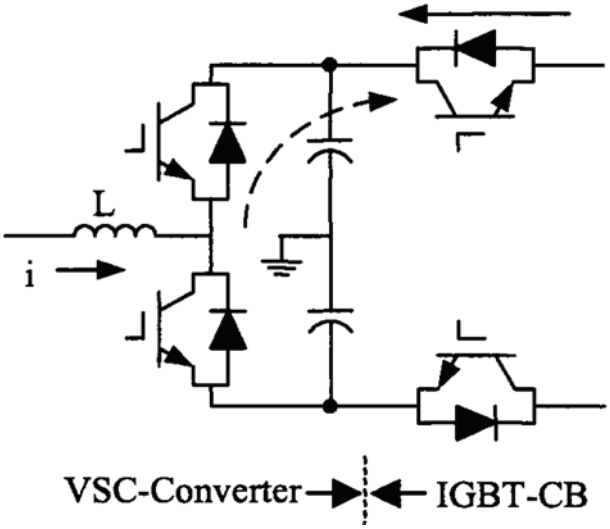

Figure 2.11.1: Placement of IGBT-CB [31]

Another alternative to the IGBT-CB is some sort of resonance circuit to superimpose an oscillatory discharge on the direct current. The oscillatory discharge has to give the result that the current should cross zero after a short period of time, at which point a conventional circuit breaker could be applied. The resonance breaker would avoid the high losses in the IGBT breaker, and would also be smaller and less expensive. However this technology has not yet been developed to serve as a DC circuit breaker in case of faults in the necessary ratings of a DC grid. Nevertheless, this seems to be a theoretically feasible solution, but require more technical development and testing. The resonance breaker is actually used by ABB in HVDC Classic (LCC) including the multiterminal application in North America. For classic HVDC this breaker is used for the metallic return switching from bipolar to monopolar operation. For this a conventional SF6 breaker with resonance circuit is used up to a couple of thousand Amperes, but it is not used to break fault current [21]. Reference [33] proposes a resonance solution, illustrated in figure 2.11.2, where the current through the main switch is brought to zero by providing an alternate path for the DC load current with the help of an auxiliary switch and resonant components. The circuit consists of the main switch T_1, the auxiliary switch T_2, resonant components L_r and C_r along with diodes D1, D2, and D3. The main switch T_1 is in the main current path connecting the source V_s to the load. The load is considered to be an RL load. Under normal operating conditions, the switch T_1 is ON carrying the load current I_m , and the auxiliary switch T_2 remains OFF [33].

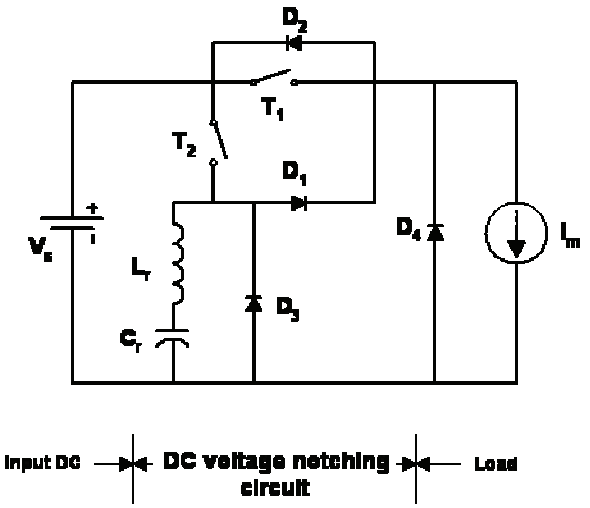

Figure 2.11.2: Resonance circuit breaker [33]

To summarize there are today basically three alternative methods for DC fault clearing that are feasible. All three have been used by ABB in HVDC VSC installations [21].

- AC breaker with DC switches
- DC Resonance Breaker
- IGBT DC circuit breaker

In addition to these there is a constant technology development in this area, leading to new inventions as described in [34] and [35].

The first one is a circuit-opening device for interrupting heavy currents by means of an explosive charge, described as:

"A circuit-opening device comprising an explosive circuit-breaker which consists of a hollow conductor housing an explosive cartridge, an explosive charge and a detonator and also an operating current relay in the form of, say, a low-voltage spark gap, a trigatron or thyratron, the place where the electric circuit is opened being in the form of two parallel branches, one of which includes only an explosive circuit-breaker and serves continuously to carry the operating current while the other branch includes an explosive circuit-breaker and a series-connected operating current relay, which normally does not pass the operating current."[34]

This solution will necessarily have to be replaced after being used.

The latter on is an invention that essentially consists in direct current being passed through a gas discharge device, and the density of the gas filling the current channel of the gas discharge device is at the same time reduced to a critical value at which the direct current is broken [21][35].

2.11.2.2 Possible protection schemes

Protection using AC breakers

This procedure illustrates protection in a DC grid after a fault is detected, using the AC breakers connected to the converter stations.

1) Transistors are blocked
2) All AC breakers are opened
3) Current and voltage in the DC system decrease to 0
4) Localization of fault
5) Isolation of fault with DC- switch
6) Short deblocking of converters to balance voltage
7) Closing of AC breakers
8) DC- capacitors are energized via diodes
9) Deblocking of capacitors

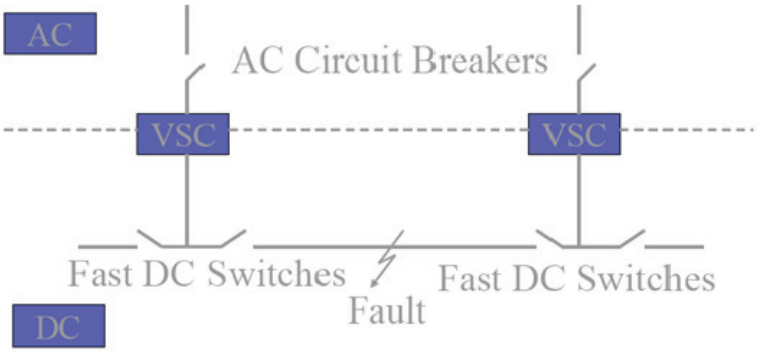

Figure 2.11.3: Protection using AC breakers [21]

By opening all AC breakers (step 2) all offshore AC grids powered by the DC grid will shut down. A somewhat more detailed method, referred to as *"Hand-shaking method"*, is described in [36]. This employs an advanced fault detecting technique.

Protection using IGBT-CB (DC breakers)

The following protection scheme, using IGBT-CBs, demonstrates how the use of AC breakers can be avoided in case of fault in the DC grid. This method is entirely based on [31].

In order to extinguish the fault current, it is necessary to block all the VSCs and IGBT-CBs thus causing a brief disruption of service. The faulted transmission line section has to be identified quickly (based on feature extraction of the voltage and current waveforms as explained later). If the fault has been verified as permanent rather than temporary, the fast DC

switches (SW) on either end of identified faulted DC line are opened. The IGBT-CBs and the Converter Stations unblock and the remaining VSC-HVDC system resumes service.

Fast DC Switches, in this example, are relatively cheap mechanical switches that are placed at both ends of each DC line. They which can isolate a DC line after the fault current has been extinguished, but they are not capable of breaking any fault current. They can be compared to an arc divider of an AC grid, see figure below.

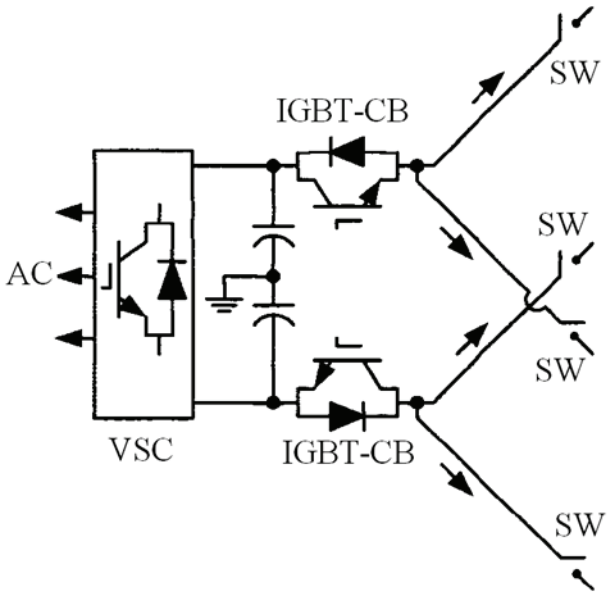

Figure 2.11.4: Protection using DC breakers [31, modified]

Immediate Effect of DC fault on converter stations

A DC fault draws large currents from the VSCs on both ends of the faulted line because of the large potential differences between the DC voltages of the VSCs and the short circuit voltage at the fault (which is close to zero). The size of the large currents depends on the line resistances and inductances (proportional to distance) between the fault and the VSCs. The large currents quickly discharge the DC capacitors of the nearest two VSCs so that their DC voltages drop abruptly. These two concomitant factors: the decrease in the DC voltages of the neighbouring converters and the increase in their DC currents, form the basis of reliable detection.

Blocking of IGBT-CBs and converter stations

When the VSC detect a fault in one of their interconnected lines or cables, both the converters and the IGBT-CBs block so that the fault current ceases to be fed from the AC grid through the severed converter stations. The fault current is then drawn from the capacitors of the affected converter stations. As the closest converters to the fault start blocking, they in turn set up the conditions for the next converters, which are electrically further away from the fault, to block. At the end of the sequential severing of all VSCs, the DC network is isolated from any source that can feed the fault. Given sufficient time for the arc to de-ionize, the fault is self-clearing. Otherwise, the fault is possibly a permanent fault.

Verification of Permanent/Temporary Fault

After all the IGBT-CBs and all the VSCs have blocked and sufficient time has been given for the fault to extinguish naturally, a test is performed to verify if the fault is temporary or permanent. This consists of momentarily unblocking the IGBT-CBs on either side of the identified faulted line. Because the DC capacitors of all the blocked VSCs are continually being charged by the anti-parallel diodes, the capacitor charges are momentarily transferred to the DC network to raise the network voltage. Thus, the voltage sensors at the network node of each VSC will record sustained DC voltages in the case when the fault has been cleared. However, if the fault is permanent, the DC voltages will return to zero, which is the voltage of the permanent fault.

Fault Isolation and Restoration

When the fault is temporary, all VSCs can unblock, and the MTDC system resumes operation. When the fault is permanent, the control stations on either end of the permanently faulted line open the fast DC switches, thereby isolating the fault. In the first step towards restoration, the IGBT-CBs and VSCs on either side of the faulted line are unblocked so that the DC network becomes charged. When the other stations detect the network voltage, their IGBT-CBs and VSCs unblock and the MTDC system resumes operation without the isolated line.

DC switchyard

With the appropriate DC breakers needed in a DC grid there are different possibilities for how they could be applied to the grid in detail. The figure below shows an HVDC switchyard that would look very much the same as an AC switchyard. This configuration would make it possible to maintain the function of the switchyard with a fault on any part of the yard and maintain operation of all healthy cables and converters at a fault at any converter or cable [30].

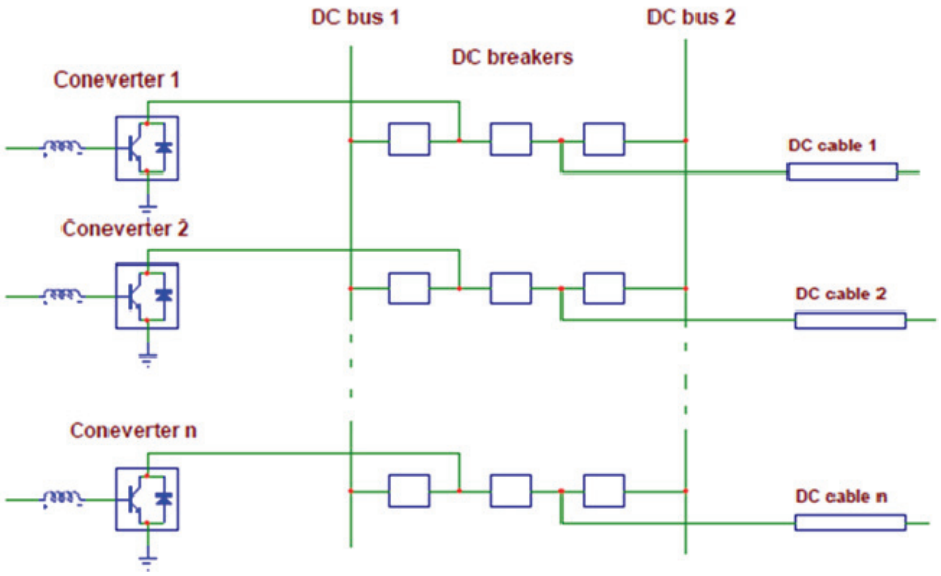

Figure 2.11.5: Possible DC switchyard [30]

2.11.2.3 Fault detection

With a fast DC breaker for each branch it is possible to achieve rapid and selective fault clearing in a DC grid in a similar manner as in an AC grid. This will however require a fast and selective fault detection scheme that will identify in which branch the fault is located. The total fault clearing time will be the sum of fault detection time and breaker operation time [21].

An appropriate ground rule placed on the detection and identification schemes is that only the local information at each VSC is to be used [31]. This ground rule concerning local information means that the faulted line should be identified at each connected VSC. The detection of the DC fault is based on the measurements of the voltages across the DC capacitors and the currents passing through the IGBT-CB. When the pre-set thresholds of the DC voltages and the incremental DC currents are crossed simultaneously for a preset time, the VSC and DC breakers assume that there is a fault.

Precautions should be taken to ensure that AC faults cannot be mistaken by the DC fault detection. It has been found that the strategy of blocking the IGBTs of the VSC when AC faults occur isolates the effects of AC faults on the DC system. The DC capacitors of the VSC also filter out the effects of AC fault disturbances thus smoothing the currents flowing through the IGBT-CBs. As a result, the currents through the IGBT-CBs have low changes in current over time (dI/dt). In contrast, DC faults are associated with rapid changes in current since there is a large voltage difference between the DC capacitor voltage and the voltage at the fault location. Thus, a very rapid change in current through the DC breakers is essential to confirm a DC fault. This ensures that an AC fault cannot be mistaken by the DC fault detection.

Reference [31] explains how to properly determine on what line the DC fault is with measurements of the following:

- Large initial current change- the initial change of a branch current of the faulted line is the largest, whereas the initial change of the branch current in each un-faulted line is small.
- Rise-time of the first wavefront- this relates to the fact that the faulted branch currents have the longest rise time. The initial long rise time is related to the growth of fault currents which are drawn from the DC capacitors closest to the fault.
- Oscillation Pattern- the subsequent oscillations in the current patterns bear the resonance frequency of the L-C-R circuits of the transmission line models.

To measure the distance to the fault will be difficult, and may have to rely on very rapid processors with the ability to analyze these transients [25].

2.11.3 Power flow control

In a two terminal VSC transmission the power flow is fully controlled. In a DC grid it might not be possible to control currents in all lines in the same way. This is due to the fact that it is only possible to control the current if the grid has as many branches as nodes, and a grid is likely to have much more branches than nodes. One of the advantages with a grid is that fewer converter stations are needed. The drawback is the loss of controllability of the current in the branches of the grid. Power flow calculations need to be done to make sure that no branch is overloaded [30]. This should normally be possible, but it might lead to low utilization of some branches.

A MTDC is expected to consist of several VSC HVDC terminals connected to each other by a DC network. The MTDC should work with a fixed DC voltage level or within a small window of upper and lower limits. Each of the terminals should be able to adopt different control strategies depending upon the terminals specific needs. The voltage source converters should monitor and control DC side parameters as well as AC side parameters [11].

There are different methods for the control of load sharing in a VSC MTDC system. One way to do so is by slave-master configuration where there is one master-terminal dedicated for the DC bus voltage regulation and others are set for constant power control mode. In this control scheme the functionality of the whole MTDC link always depends on the presence of the master-terminal in the grid, leading to breakdown of the whole system during failure of the master-terminal.

An alternative solution to avoid this problem is the use of DC voltage regulation by voltage margin control method with modified droop characteristics at several terminals, as thoroughly described in [37]. This is comparable to the concept of power - frequency droop control in AC systems, and can be extended to DC systems. According to the voltage margin method, each converter will regulate the DC voltage as long as the power flow through the converter is within the upper and lower limits and the reference DC voltages of the terminals are offset from one another by a certain voltage margin. Converters are to be equipped with a direct voltage droop characteristic that regulates the amount of power that is fed into or absorbed from the AC system [37].

The DC droop control is achieved by using P controller in the DC voltage controller of the converter terminal. The higher the value for the P controller, the less droop would be attained for the terminal and this forces the terminal to respond more to changes in DC voltage variations of the DC mesh system.

The energy stored in the DC capacitances, and directly controlling the DC voltage, serves conveniently as a measure for unbalances in the system. This is analogous to the energy storage of the inertia of synchronous generator used for droop control in AC systems [29].

To avoid an abrupt disconnection of the converter at a critical voltage level, DC-bus under voltage load shading (UVLS) can be used beginning from some level higher than the critical DC voltage level. This is DC-grid analogous of under frequency load shading scheme in AC grid [37].

Power flow control in MTDC is an issue that requires more research before the implementation and construction of an offshore grid is possible. However, a master thesis on the subject, [11], concludes that: *"Voltage margin method merged with DC voltage droop control results in the most robust and reliable operation of MTDC systems without the need for fast communication system between terminals."* [11]

2.11.4 Earthing

For the specific aspect addressed in this section it is not noted any major difference between the LCC and VSC concept.

VSC systems can be developed in a monopole with earth or metallic return or a bipole arrangement, as depicted in figure 2.11.6.

A bipole arrangement with a fully insulated return conductor offers the following advantages:

- Two poles of opposite polarity but with the same voltage amplitude simplify the design of the converter transformer and opens for possible configurations without converter transformers.
- Higher transmission voltage between the + and - pole reduce the DC current and thereby the thermal rating and the losses.
- In case of a fault on one of the poles the remaining pole will still be able to transfer 50 % of the rated power.

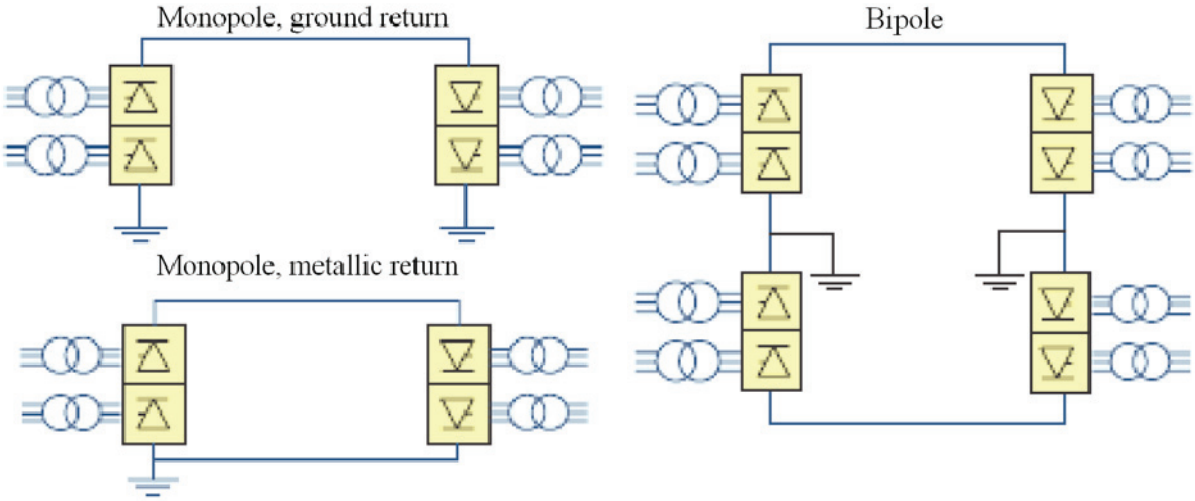

Figure 2.11.6: Monopole and bipole arrangements [38]

Based on the above aspects together with the capability of a higher transmission capacity, the bipolar configuration seems advantageous. The following evaluation of an HVDC grid earthing strategy is based on information from reference [39], and is carried out with bipole configuration as a starting point. A bipolar grid may, during its development, contain sections of monopolar configuration.

The two fundamental earthing strategies are high impedance earth, to isolate the system, and low impedance earth, directly earthed systems.

During earth faults in high impedance earthed HVDC grids, the fault currents are effectively limited. On the other hand the equipment in the grid will be subjected to large over-voltages, up to twice the normal operating voltage, see figure 2.11.7. This fact, together with difficulties to implement an effective and selective protection system for earth faults are strong arguments against high impedance earthed HVDC grids.

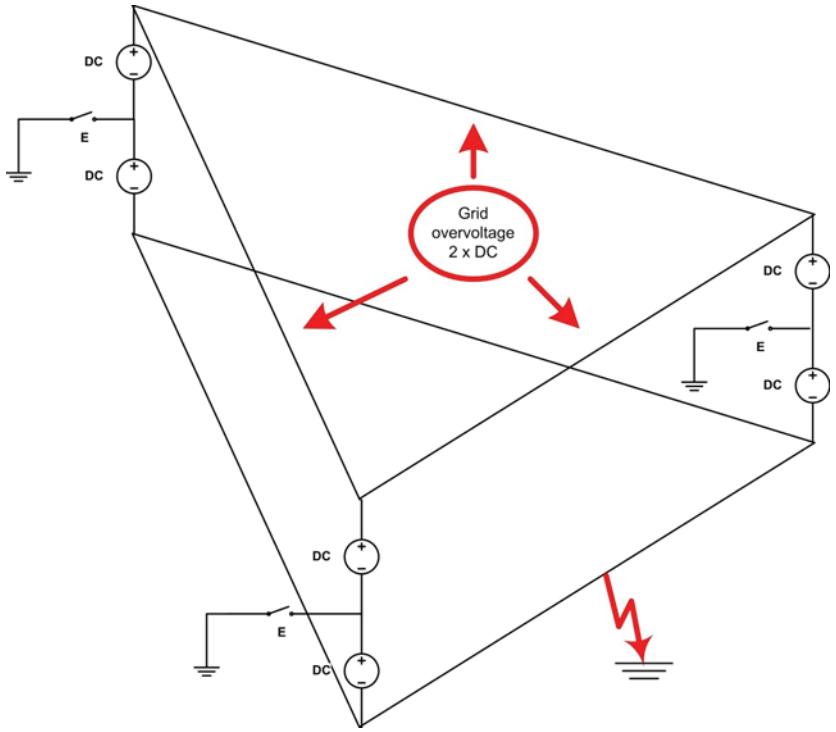

Figure 2.11.7: High impedance earthing [39]

During earth faults in low impedance or directly earthed, bipolar HVDC grids, the over-voltages are limited meanwhile the earth fault currents may reach extreme values, see figure 2.11.8 below. With effective and fast HVDC breakers available, this grid configuration looks attractive.

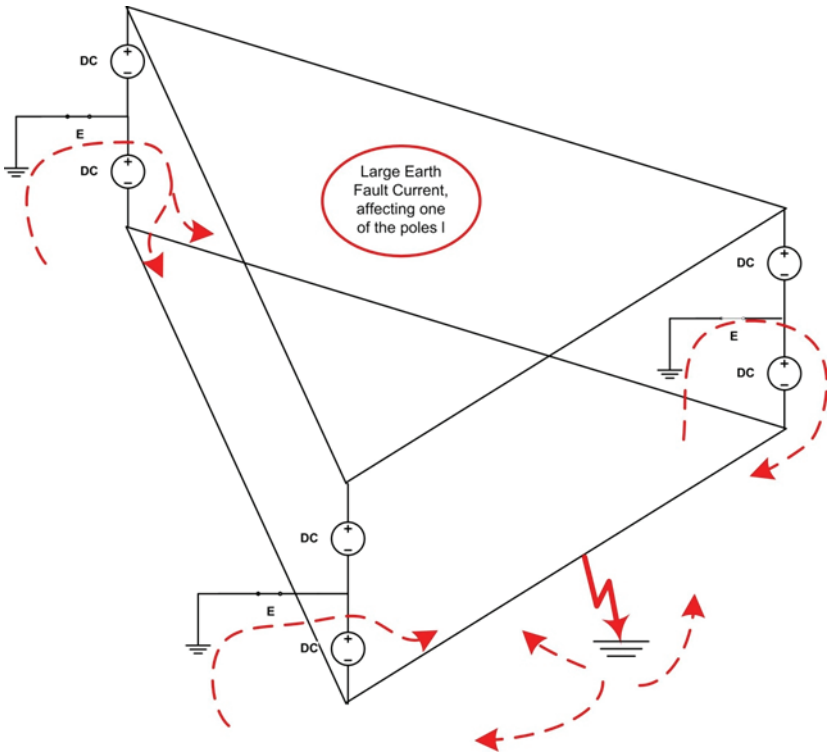

Figure 2.11.8: Low impedance earthing [39]

The information provided by [39] concludes that, in view to what has been presented above and the cost implication of increased voltage stresses on semiconductor valves, the directly earthed DC grid does seem to be the preferred choice of the two alternatives considered.

2.12 Advantages with VSC

This chapter is meant as a short summary of the major advantages with VSC, presented in this report, that make this converter technology suitable for electrification of offshore installations.

Independent control of active and reactive power

Voltage source converter (VSC) transmission system technology has the advantage of being able almost instantly to change its working point within its capability. The converter operates with high frequency pulse width modulation (PWM) and thus has the capability to rapidly control both active and reactive power, independently of each other, to keep the voltage and frequency stable. This can be used to support the grid with the best mixture of active and reactive power during stressed conditions [7][13].

The capability to supply weak and passive networks

Whereas conventional HVDC LCC require a relatively strong synchronous voltage source in order to commutate, the VSC, which uses IGBTs in order to control the direction of the current, does not run the risk of commutation failure [13]. The voltage source converter is not

dependant on a high short circuit capability in its interconnected system. This is a property necessary for the connection of weak offshore grid.

Lower space requirements
The LCC produces considerable AC side current harmonics that require filter banks. The large space footprint of such equipment will make it challenging for installation on an offshore platform [19]. Since VSC operates at a much higher frequency than the LCC, it produces considerably less harmonics, and therefore requires smaller filters. With multilevel VSC the need for filtering is almost zero.

Black start capabilities
Black start capability is a feature that is essential for a passive offshore system powered from land by HVDC.

Possibilities for multiterminal DC
Despite technological challenges in the protection schemes, VSC will have the possibility to be applied in a multiterminal DC grid. The voltage sharing could be governed by a DC droop control and the direct voltage would serve as a measure for unbalances in the system.

Improved dynamic performance and stability
A voltage source converter is in many ways identical to a STATCOM, and can therefore support the dynamic performance of the connected AC grid, as described in the chapter on system stability later in the report. Fast control of active and reactive power of VSC HVDC systems can improve power grid dynamic performance during disturbances. For example, if a severe disturbance threatens system transient stability, fast power run-back and even instant power reversal control functions can be used to help maintain synchronized power grid operation. VSC HVDC systems can also provide effective damping to mitigate electromechanical oscillations by active and reactive power modulation [20].

2.13 Constraints with VSC

Corresponding to the last chapter, this chapter aims to highlight some of the challenges related to offshore interconnection using VSC.

Absolute dynamic current rating
The main drawback of the VSC is its limited current capability. Even for very short durations, over-currents cause thermal stresses that degrade or cause permanent damage to the switching elements. In the case of a grid-side fault the system voltage is temporarily reduced. Since the current is limited, the power that can be fed to the AC system is reduced as well and the onshore VSC cannot regulate the direct voltage. A very fast reduction of the offshore power system generation, in case of wind farm, or demand is required to keep the scheme in operation [19].

Protection and fault handling
The handling of DC faults is challenging in terms of isolating the fault. In a system without DC breakers a fault results in that the entire DC system has to be disconnected on the AC side. The DC breaker technology is not yet a mature enough technology, as thoroughly described in chapter 2.10.2 [40].

High losses
Due to the higher frequency switching losses are higher in VSC compared to LCC. There is a continuous technological development in this field and the losses are being reduced. The figure below shows the development for reduction of losses in HVDC light (ABB). Technological development in the recent years has lead to losses in VSC approaches the losses in LCC.

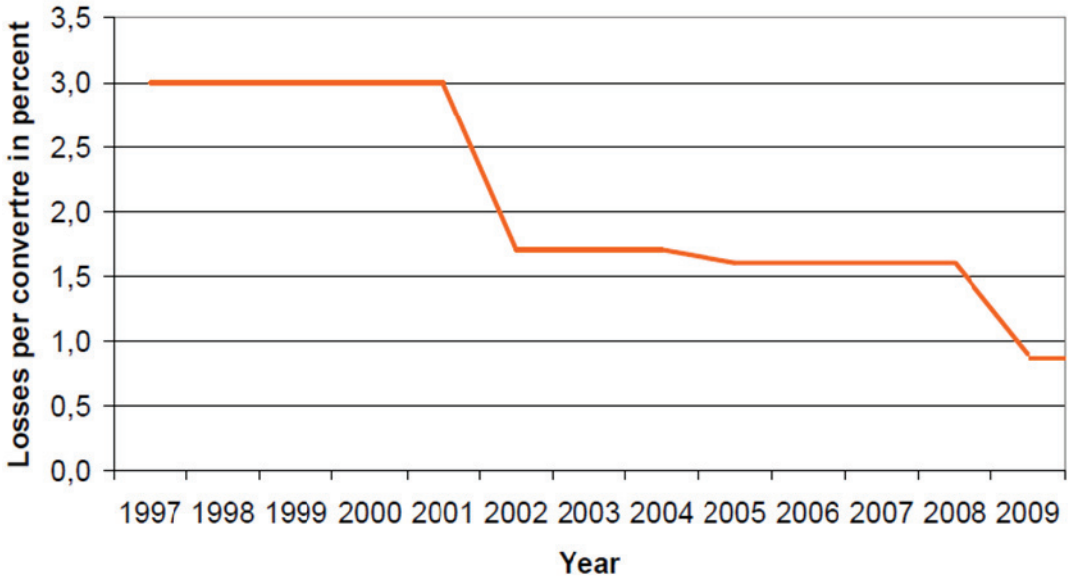

Figure 2.13.1: Reduction of converter losses [41]

2.14 Relevant projects using VSC

The following examples of application are included to demonstrate that many of the possibilities associated with the VSC technology are not just theoretical, but actually proven in commercial projects.

Stability improvement of weak grids (Cross Sound Cable):
The Cross Sound Cable is a 330 MW, ±150 kV submarine VSC project supplying controllable power transmission to Long Island (US). It became an important power supply route to Long Island when restoring the network during the big blackout in the northeastern United States in 2003. During the thunderstorms that occurred before the networks were completely restored,

several +100 to –70 MVAr swings were noticed over 20 seconds, and still the AC voltage was kept constant [7].

Interconnection of offshore platform (Troll A and Valhall in 2010):
With the Troll A project VSC transmission converters were, for the first time, being installed offshore on a platform. Troll has two parallel systems operating at ±60 kV, each capable of providing 44 MW, which provide redundancy for each other. The transmission system directly feeds a high voltage variable speed synchronous machine designed for compressor drive with variable frequency and variable voltage. Valhall has a one cable system operating at ±150 kV and 78 MW with earth return in the screen. The distance is 292 km [7][21].

Black start (Estlink):
The Estlink is a 350 MW, ± 150 kV VSC transmission project with submarine and land cables, that connects Estonia to Finland and the Nordpool marked. The black start capability is implemented at the Estonian side, which means the converter is automatically switched to black start operation if the AC grid is lost. This makes a fast restoration possible after a blackout in the Estonian network. The link has been in operation since the end of 2006 [7].

3 Suggested system for modeling

In the autumn of 2009 a literature study on voltage source technology was carried out and resulted in a project report for the Norwegian University of Science and Technology (NTNU), Department of Electrical Power Engineering. The project report concludes that a system model should be created and used to investigate the dynamic performance of a multiterminal VSC HVDC. Figure 3.1.1 illustrates the suggested power system for modeling.

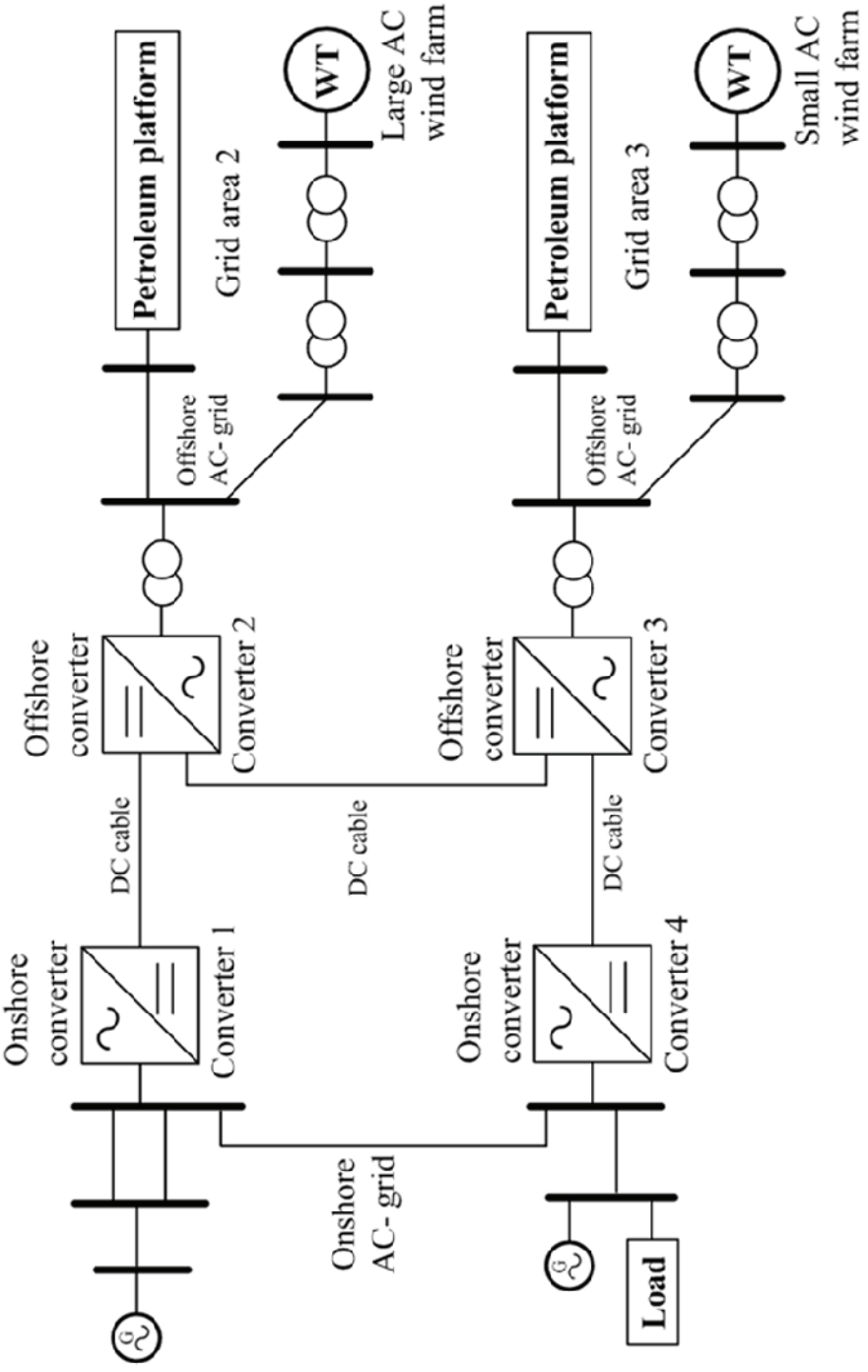

Figure 3.1.1: Power system for dynamic analysis

The power system consists of a small onshore AC grid and a four-converter multiterminal HVDC system with two offshore VSC nodes. Each offshore voltage source converter supplies an offshore AC system composed of wind power generation and load on the petroleum platforms. These offshore AC systems are referred to as area 2 and area 3 as they are connected by converter 2 and 3 respectively.

The simplicity of the onshore grid makes it possible to more thoroughly examine causes and effects in the dynamic simulations. The motive for simulating on a modeled grid instead of an existing physical one is the possibility to extract generic qualities and characteristics of the VSC and the interaction between VSC transmission and the AC grids.

This master thesis is written in cooperation with Statnett SF, the Norwegian TSO, as a contribution to an ongoing research and development (R&D) program on offshore electrification. The HVDC transmission capacities and converter ratings are therefore chosen to be in the same range as other projects investigated in this R&D program. This will hopefully provide some comparative benefits between the simulation models in the different projects.

The R&D program suggests the following capacities for the HVDC grid:

- Total HVDC transmission capacity of around 1000 MW, i.e. the onshore converters should have a rating no less than 1000 MW
- The offshore converters connecting the platforms and wind farms should be in the range of about 400 MW.

The distances between converters in the HVDC grid should be above the lengths where AC cable transmission can compete with HVDC cable transmission, and this is normally in the range of up to 100 km. Above this distance the reactive losses that occur due to the capacity of the AC cables are so high that they prevent the use of AC cables as a realistic alternative for large power transfer. A report on loss evaluation of HVAC and HVDC transmission solutions for large offshore wind farms [8] from 2005 concludes that a HVAC solution leads to the lowest losses for distances of up to 55–70 km from the shore. The choice of distances between converters in this generic simulation model is set to be 200 km. There are four converters which are connected with three cable sections, i.e. the total HVDC transmission distance is 600 km.

The HVDC grid may be viewed as one large two-terminal transmission system between the onshore converters, and two smaller converters that are either feeding power into or absorbing power from this system, see figure 3.1.2.

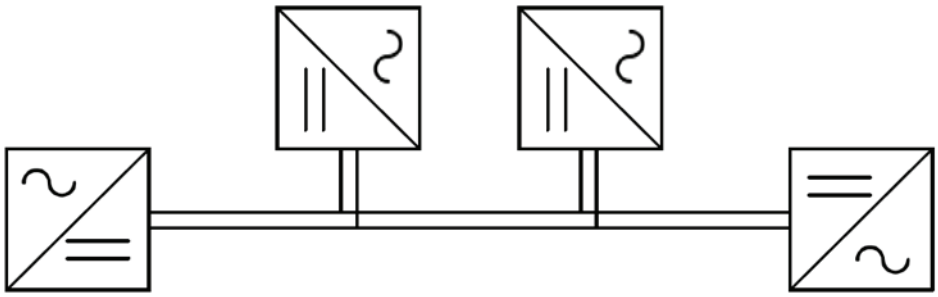

Figure 3.1.2: Simplified illustration of the HVDC system

The power consumption on the petroleum platforms is dimensioned to 120 MW for each platform. This is assumed to be a realistic size seen in comparison to the installed power of existing Norwegian platforms. For instance the Valhall platform will be supplied 78 MW from shore using VSC HVDC which will be operational in 2010, and the total installed power on the Ekofisk field is approximately 170 MW. The petroleum platform models are to be connected to the offshore AC grid at 132 kV.

The two wind farms are not set to the same installed capacity. This is because it enables the dynamic investigation of offshore areas with either a large or a smaller wind farm in the same simulation model. The capacities chosen are 250 MW for the wind farm connected to offshore area 2 (large wind farm) and 100 MW for the wind farm connected to offshore area 3 (small wind farm).

The cable distance between the converter station of offshore converter 2 and the large wind farm is set to 30 km. The cable distance between the small wind farm and offshore converter 3 is set to 5 km. The cable distance between the offshore converter station and the petroleum platform is 3 km for both offshore areas.

The power system has been modeled and analyzed using the power system simulation program PSS®E. The voltage source converters have been represented with ABB's HVDC Light model developed for use in PSS®E.

An argument could be made that the rating of the MTDC is over dimensioned for the many cases analyzed in this master thesis that only investigates the offshore electrification and not large power transfer. The reason for the large power rating in these cases is that the modeled MTDC should represent a real system build for both large power transfer between onshore connection points and electrification of offshore installations. Different simulation cases are then created to more clearly illustrate operational aspects connected to each of the two areas of application. This makes the general functionality of the MTDC easier to analyze. In addition, a situation where there is no need for large power transfer, but the offshore installations are connected is entirely realistic.

4 AC power systems and stability definitions

The following chapter is a brief derivation and summary of the relations and equations that influence power transfer capability and stability in an AC grid. The motivation for including this in the project is that it will more clearly describe the function of compensation in networks and also important relations in power system stability. The content of this chapter is based on the power system stability books by Kundur and Machowski [42][43], and these books are referred to for a more detailed description of the topics.

4.1 Power line description and modeling

A transmission power line can be analyzed on a per phase basis in terms of the distributed parameters:

$$z = R + j\omega L = \text{series impedance per unit length/phase} \quad (4.1)$$

$$y = G + j\omega C = \text{shunt admittance per unit length/phase} \quad (4.2)$$

where R is the series resistance, L is the series inductance, G is the shunt conductance and C is the shunt capacitance. The shunt conductance G is due to leakage currents along insulator strings and corona. In power lines, its effect is small and usually neglected.

The simplified equivalent electric circuit of a power line may be reduced to the following figure:

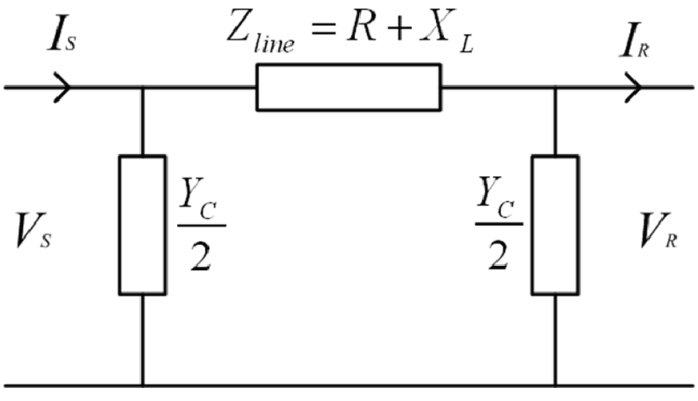

Figure 4.1.1: π-equivalent of a power line

Where Z_{line} [Ω] is the total series impedance for the line length and Y_C [S] is the total shunt admittance for the line length. A simplification is made that half of the lines distributed shunt admittance is placed at each end of the line. To represent the equivalent circuit using only ohmic components the admittances in each end of the cable are replaced by $-j2X_C$ as:

$$j\frac{Y_C}{2} = j\omega\frac{C}{2} = \frac{1}{-j2X_C} \tag{4.3}$$

The π- equivalent (named for its similarity with the Greek letter) is a good approximation for short and medium-length lines (length up to about 200 km) [46]. For very short lines the admittance may often be neglected.

Table 4.1 below displays typical parameter values for overhead lines for 400 kV, 50 Hz. These values are used in the onshore grid model. Detailed calculations of the branch parameters used in PSS®E may be found in Appendix A.

Table 4.1: Parameter values for overhead lines [43]

V_n, f_n	R [Ω/km]	$X_L = \omega L$ [Ω/km]	$B = \omega C$ [μS/km]
400 kV, 50 Hz	0.018	0.265	5.360

In PSS®E, the basic transmission line model is a π-equivalent connected between network buses. The required parameter data to model the π-equivalent is comprised of [1]:

- One series impedance (R + jX).
- Two admittance branches ($jB_{ch}/2$) representing the line's capacitive admittance (line charging).
- Two admittance branches (G + jB) for shunt equipment units (e.g. reactors) that are connected to and switched with the line. The system modeled in this thesis does not have any such shunt equipment.

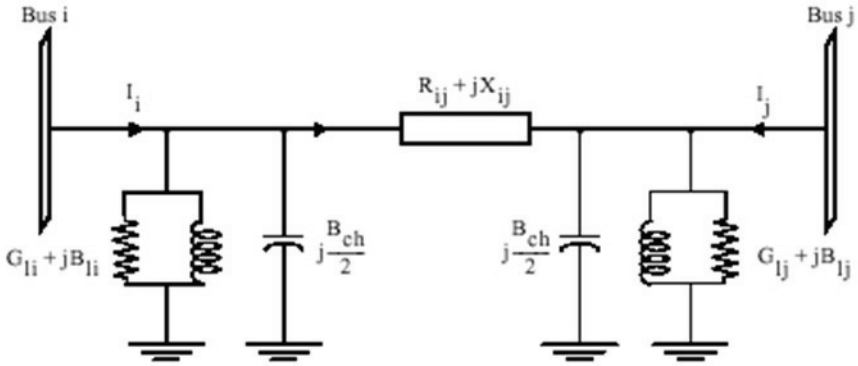

Figure 4.1.2: Branch model in PSS®E [1]

4.2 AC cables

AC cables may be described electrically with the same elements as transmission lines. However the series impedance and shunt admittance of power cables have different values from transmission lines due to the construction of the cables. The shunt susceptance in cables is much higher than in transmission lines because the conductors are closer to each other, and

the conductors are surrounded by metallic screens. Hence the capacitive charging of the cable is substantial for long cable distances, i.e. the cable produce large amounts of reactive power.

The cable parameter data for a subsea cable with the capacity to transport 250 MW for 30 km and 100 MW for 5 km was needed in the model to connect the wind farms to the offshore converter stations. With the help of Thomas Skånøy of Siemens, the cable data of table 4.2 were chosen for the model. It is emphasized that these are only reasonable example values for the cables and does not describe any definite products of Siemens or others. The voltage levels indicated are those necessary for the quantity of power transmission.

Table 4.2: Parameter values for subsea cables [44]

P [MW]	Distance [km]	U [kV]	R [Ω/km]	X [Ω/km]	C [µF/km]	B [µS/km]
250	30	245	0.060	0.128	0.170	53.380
100	5	132	0.110	0.150	0.140	43.960

A comparison between the AC lines and AC cables show that the susceptance of the cables is much higher than of the lines. The petroleum platforms are supplied with a 3 km cable with the same parameter values as the cable connecting the small wind farm.

Cross linked polyethylene (XLPE) is one of the most commonly used elastomer as solid insulation in high power apparatus. Elastomers are polymeric materials that exhibit elastic properties similar to rubber. The electric properties of polyethylene (PE) as insulation are outstandingly good. It has high breakdown strength and does not contain polar groups, and therefore has a low relative permittivity and dissipation factor. Disadvantages are that polyethylene ages on exposure to light and oxygen, and they are sensitive to partial discharges, which mean that the insulation should be free of voids internally and at the surfaces. Cross linking renders the PE infusible and suitable for service temperatures up to 125 °C, thus permitting cables to carry high current densities. [45]

High voltage subsea AC cables need to have a lead sheath to avoid problems with with water treeing in the cross linked polyetylen insulation material. The field strength is high and diffusion of water into the insulation is not accepted. [46]

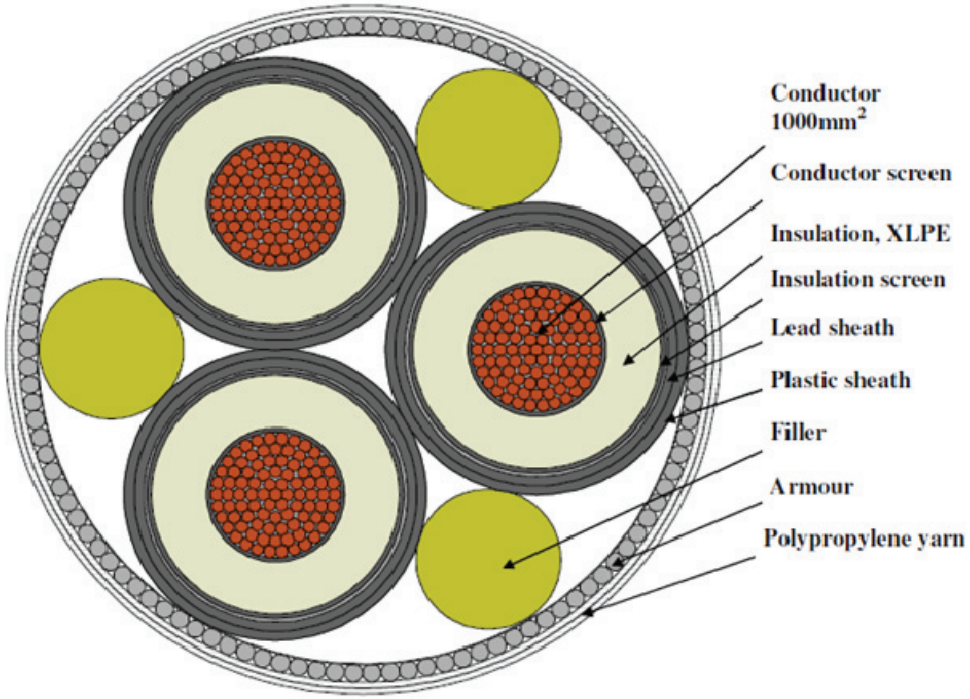

Figure 4.2.1: Cross section of a HVAC XPLE subsea cable, illustration [47]

4.3 Surge Impedance Loading (SIL)

Whit reference to equations (4.1) and (4.2) and neglecting the shunt conductance G, transmission lines and cables can be described by their characteristic impedance Z_C according to equation:

$$Z_C = \sqrt{\frac{z}{y}} = \sqrt{\frac{R + j\omega L}{j\omega C}} = \sqrt{\frac{L}{C}}\left(1 - j\frac{R}{2\omega L}\right) \tag{4.4}$$

If the losses are neglected, the characteristic impedance is commonly referred to as the surge impedance. It has the dimension of a pure resistance and is equal to [42]:

$$Z_C = \sqrt{\frac{L}{C}} \tag{4.5}$$

The power delivered by a transmission line when it is terminated by its surge impedance is known as the natural load or surge impedance load (SIL). The *SIL* can be expressed according to equation (4.6).

$$\text{SIL} = \frac{V_0^2}{Z_C} \tag{4.6}$$

V_0 is the rated voltage of the line or cable and Z_C is the characteristic impedance of the line or cable (losses neglected). If a line is loaded at a level below SIL, the line will produce reactive power. The effect from the shunt capacitance is bigger than the effect from the series inductance. On the other side, if a line is loaded at a level above SIL, the line will consume reactive power due to the increased current in the line. The effect from the shunt capacitance is dependent of the voltage, and hence approximately constant.

The *SIL* of a cable is much higher than for a transmission line for the same voltage. This is due to the high capacitance, as can be seen by comparing table 4.1 and Table 4.2. A typical power cable will not be able to transfer power equal to *SIL*, because of the thermal limit. In the case with an offshore wind farm connected to the grid with AC cables, the reactive power produced by the cable will be highest when the cable is connected, but the active power transfer from the wind farm is small. The higher the active power, the more reactive power is consumed in the series inductance. However, at full power AC cables will still produce large amounts of reactive power.

4.4 Strength of AC systems and short circuit ratio

The normal parameter for measuring the strength at a busbar in an AC network is short circuit power (*SC MVA)*. The definition of short circuit power is given in equation (4.7)

$$\text{SC MVA} = I_{fault} \cdot V_{AC} = \frac{V_{AC}^2}{Z_{Th}} \tag{4.7}$$

I_{fault} is the fault current for a three phase fault with zero impedance at the busbar, V_{AC} is the nominal line voltage [kV] at the bus and Z_{Th} is Thevenin impedance [Ω] seen from the bus experiencing the fault.

Even though the short-circuit impedance is equal to zero, the fault current will be limited by the Thevenin impedance. The Thevenin impedance for the given busbar corresponds to the diagonal element in the node impedance matrix for the system. The diagonal elements Z_{ii} of the node impedance matrix is the total impedance between bus *i* and ground in a system. Physically, this means that the fault current has to return through impedances from ground other places in the power system, see figure 4.4.1.

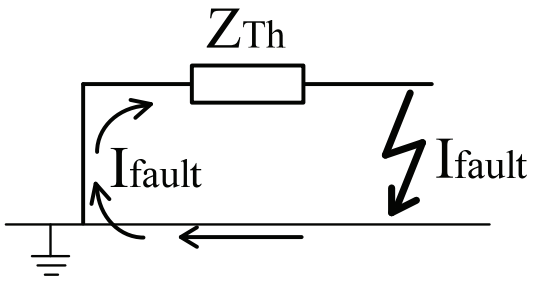

Figure 4.4.1: Illustration of short circuit current

In fault studies, a generator is represented as Norton equivalent, with a current source in parallel to the generator impedance connected to earth, se figure 4.4.2. The current source has infinite internal impedance.

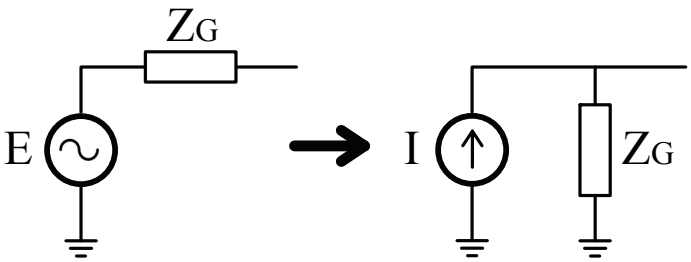

Figure 4.4.2: Thevenin and Norton equivalent

The closer a generator is located to a busbar, the more will it contribute to reducing the Thevenin impedance seen from the busbar because it creates a shorter electrical distance to ground. More lines connected to the busbar will also contribute to reducing the Thevenin impedance, as from the busbar the lines are seen to be in a parallel path to ground. Hence, this will also increase the short circuit power.

An important parameter when investigating AC systems with HVDC links is the short circuit ratio (SCR). SCR is the relation between the converter power rating of the HVDC link and the short circuit power at the converter bus, and describes the AC system strength in HVDC applications.

$$SCR = \frac{SC\_MVA}{P_{HVDC}} = \frac{V_{AC}^2}{Z_{Th} \cdot P_{HVDC}} \tag{4.8}$$

When connecting a traditional HVDC link using thyristor converters, a rule of thumb is that the SCR should be larger than 3. The same requirement does not apply for VSC HVDC as the voltage source converters do not need a strong grid in the commutation process. However, the HVDC Light model used in the simulation model, as will be described in chapter 8, is developed and verified for SCR > 3 at the strongest AC system. The model has also been tested in sample cases for lower SCR, and it is estimated that the model is possible to use down to SCR=1.4, in most cases with good enough results. It is recommended to let the

converter connected to the strongest AC system to be in DC voltage control mode [2]. In the developed simulation model, the short circuit ratio at the converter in DC voltage control is calculated to SCR = 3.632, which means that the HVDC Light model is verified for the simulation applications performed in this thesis. The calculations of SCR is found in appendix A.

4.5 Electrical relations in the system

The following chapter is a brief derivation and summary of the relations equations influence power transfer capability in an AC grid. The motivation for including this in the project is that it will more clearly describe the function of compensation in networks and also important relations in power system stability. The content of this chapter is based on the power system stability books by Kundur and Machowski [15][30], and these books are referred to for a more detailed description of the topics.

Equation (4.1) and (4.2) describes the electrical properties of a power line in terms of distributed parameters, and equation (4.4) defines the characteristic impedance of a line.

An additional required definition is:

$$\gamma = \sqrt{zy} = \alpha + j\beta = \text{propagation constant} \tag{4.9}$$

In typical power lines $R << \omega L$. This means that losses in the characteristic impedance of equation (4.4) may be neglected for simplified analytical expressions in high voltage lines.

$$Z_C = \sqrt{L/C} \tag{4.10}$$

$$\gamma = j\beta = j\omega\sqrt{LC} \tag{4.11}$$

Hence Z_C is a real number (i.e. a pure resistance) and $\gamma = j\beta$, where β is called the phase constant. The β is a distributed parameter [rad/km], and if l is the length between two buses in a system then:

$$\theta = \beta l = \textit{electrical length or line angle} \tag{4.12}$$

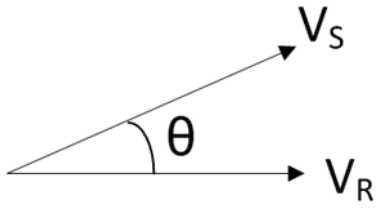

Figure 4.5.1: Electrical length

The power transferred between a sending and a receiving bus is given by the following equation, when the only approximation is that line losses are neglected:

$$P_R = \frac{V_S V_R}{Z_C \sin\theta} \sin\delta \tag{4.13}$$

In this equation δ is the voltage angle between the sending and receiving bus.

For a short line *sin* θ can be replaced by θ in radians. Hence:

$$Z_C \sin\theta = Z_C\theta = \sqrt{L/C}\,\omega\sqrt{LC}l = \omega Ll = X_L \tag{4.14}$$

where X_L is the series inductive reactance. The expression for power transferred therefore reduces to the more familiar form:

$$P_R = \frac{V_S V_R}{X_L} \sin\delta \tag{4.15}$$

Equation (4.15) shows that real power P depends on the product of phase voltages and the sine of the angle δ between their phasors. In power networks, node voltages must be within a small percentage of their nominal values. Hence such small variations cannot influence the value of real power. The conclusion is that, when X_L is constant, large changes of real power, from negative to positive values, correspond to changes in the sine of the angle δ.

However, from equation (4.13) it is worth noting that line performance is determined by the characteristic impedance Z_C and the electrical length θ. The objective of compensation is to modify these parameters to create the desired voltage and power characteristics. When the compensation device injects or absorbs reactive current, the system impedance appears to change and hence the voltage and power characteristics also change. Shunt capacitive compensation in effect decreases Z_C and increases β, whereas shunt inductive compensation increases Z_C and decreases β.

Holding X_L constant, the characteristic $P(\delta)$ becomes sinusoidal, and is referred to as the power–angle characteristic, while the angle δ is referred to as the power angle or the load angle. Because of stability considerations, the system can operate only in that part of the characteristic which is shown by a solid line in figure 4.5.2. The characteristic will have higher amplitudes for smaller values of X_L.

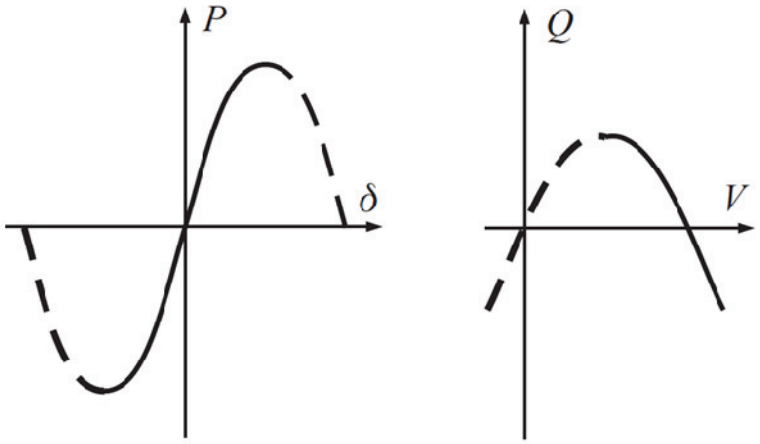

Figure 4.5.2: Stability regions [43]

The per-phase reactive power leaving the element is expressed as:

$$Q = \frac{V_S V_R}{X_L}\cos\delta - \frac{V_R^{\,2}}{X_L} \tag{4.16}$$

The term *cos δ* is determined by the value of real power because the relationship between the sine and cosine is $\cos\delta = \sqrt{1 - \sin^2\delta}$. Using this relation and equation (4.15) gives:

$$Q = \sqrt{\left(\frac{V_S V_R}{X_L}\right)^2 - P_R^2} - \frac{V_R^2}{X_L} \tag{4.17}$$

The characteristic *Q(V)* corresponds to an inverted parabola depicted in figure 4.5.2. Because of stability considerations, the system can operate only in that part of the characteristic which is shown by a solid line. The smaller the reactance X_L, the steeper the parabola, and even small changes in *V* cause large changes in reactive power. The inverse relationship also takes place: a change in reactive power causes a change in voltage.

The above analysis points out that *Q - V* and *P - δ* form two pairs of strongly connected variables. Therefore it is important to remember that voltage control strongly influences reactive power flows and vice versa. Similarly, when talking about real power *P* one should remember that it is connected with angle δ. That angle is also strongly connected with system frequency f, and hence the pair P - f is also strongly connected and important for understanding power system operation and stability [42][43].

4.6 Stability definitions

The knowledge of basic stability relations is important in understanding the dynamic behavior of power systems. In this chapter these basic concepts for power system stability are defined and explained. More detailed descriptions can be further investigated in [42][43][48].

"Power system stability is the ability of an electric power system, for a given initial operating condition, to regain a state of operating equilibrium after being subjected to a physical disturbance, with most system variables bounded so that practically the entire system remains intact."

This definition applies to an interconnected power system as a whole. Often, however, the stability of a particular generator or group of generators the stability of particular loads is also of interest [48].

The previous chapter showed that three quantities are important for power system operation: (i) angles of nodal voltages δ, also called power or load angles; (ii) frequency f; and (iii) nodal voltage magnitudes V. These quantities are especially important from the point of view of defining and classifying power system stability. Hence power system stability can be divided into: (i) rotor (or power) angle stability; (ii) frequency stability; and (iii) voltage stability, as illustrated in figure 4.6.1 below. As power systems are nonlinear, their stability depends on both the initial conditions and the size of a disturbance. Consequently, angle and voltage stability can be divided into small- and large-disturbance stability [43].

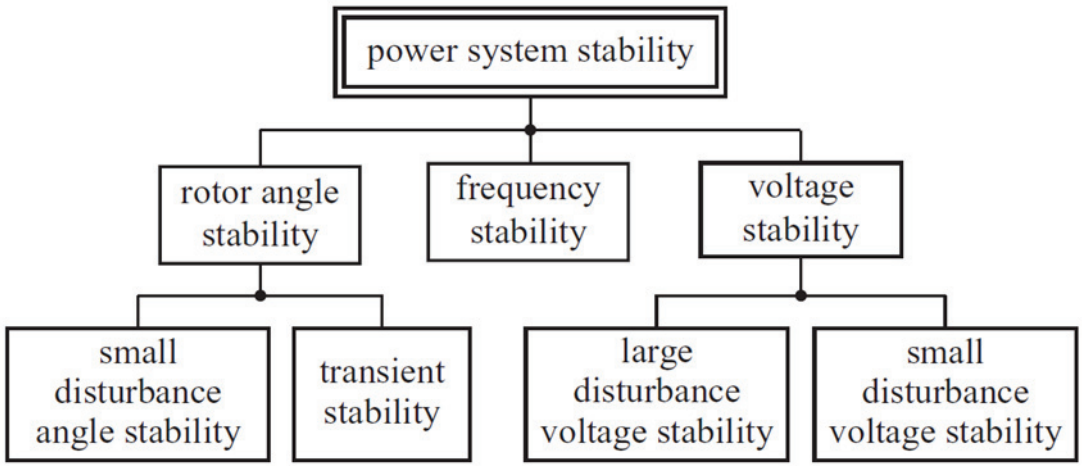

Figure 4.6.1: Power system stability [43]

Rotor angle stability refers to the ability of synchronous machines of an interconnected power system to remain in synchronism after being subjected to a disturbance. It depends on the ability to restore and maintain equilibrium between electromagnetic torque and mechanical torque of each synchronous machine in the system. A fundamental factor in this problem is the manner in which the power outputs of synchronous machines vary as their rotor angles change. If one generator temporarily runs faster than the system, the angular position of its

rotor relative to the system will advance, and the generator will assume more of the total load, depending on the power – angle relationship. The increased electrical power output will then exceed the constant mechanical power on the generator, thereby reducing the speed difference and angular separation. The power – angle relationship is highly nonlinear, and beyond a certain limit, an increase in angular separation is accompanied by a decrease in power transfer leading to a further increase in the angular separation. Instability results if the system cannot absorb the kinetic energy corresponding to these rotor speed differences.

Voltage stability is the ability of a power system to maintain steady acceptable voltages at all buses in the system under normal operating conditions and after being subjected to a disturbance. A system enters a state of voltage instability when a disturbance, increase in load demand or change in system condition causes a progressive and uncontrollable drop in voltage. A criterion for voltage stability is that, at a given operating condition for every bus in the system, the bus voltage magnitude increases as the reactive power injection at the same bus is increased. The main factor causing voltage instability is the inability of the power system to meet the demand for reactive power. The driving force for this is the loads, which tend to quickly restore the power consumed in response to a disturbance. Restored loads increase the stress on the high voltage network by increasing the reactive power consumption and causing further voltage reduction.

The distinction between rotor angle stability and voltage stability is actually not based on a weak coupling between variations in $P - \delta$ and $Q - V$. In fact, the coupling is strong for stressed conditions and both rotor angle stability and voltage stability are affected by pre – disturbance active power as well as reactive power flows. Instead, the distinction is based on the specific set of opposing forces that experience sustained imbalance and the principal system variable in which the consequent instability is apparent.

Frequency stability refers to the ability of a power system to maintain steady frequency following a severe system upset resulting in a significant imbalance between generation and load. It depends on the ability to restore and maintain equilibrium between system generation and load, with minimum unintentional loss of load. Instability that may result, occurs in the form of sustained frequency swings leading to tripping of generating units and loads.

The definitions of power system stability described above are simplified classifications for understanding and developing corrective measures. In any given situation, any one form of instability may not occur in its pure form. This is particularly true in highly stressed systems and for cascading events; as systems fail, one form of instability may ultimately lead to another form.

4.7 Compensating

4.7.1 SVC

Static VAR compensators (SVCs) based on conventional thyristors have been used in power systems since the 1970s. The role of the SVC is to adjust the amount of reactive power compensation to the system, and in that way control voltage at the bus to which they are connected. A flexible and continuous reactive power compensation scheme that operates in both the capacitive and inductive regions can be constructed using shunt elements of thyristor-switched capacitors (TSC) and thyristor-controlled reactors (TCR). Using these elements it is possible to design a variety of SVC systems [43].

Figure 4.7.1 illustrates the characteristic of an SVC consisting of a controllable reactor and a fixed capacitor. The composite characteristic is derived by adding the individual characteristics of the components.

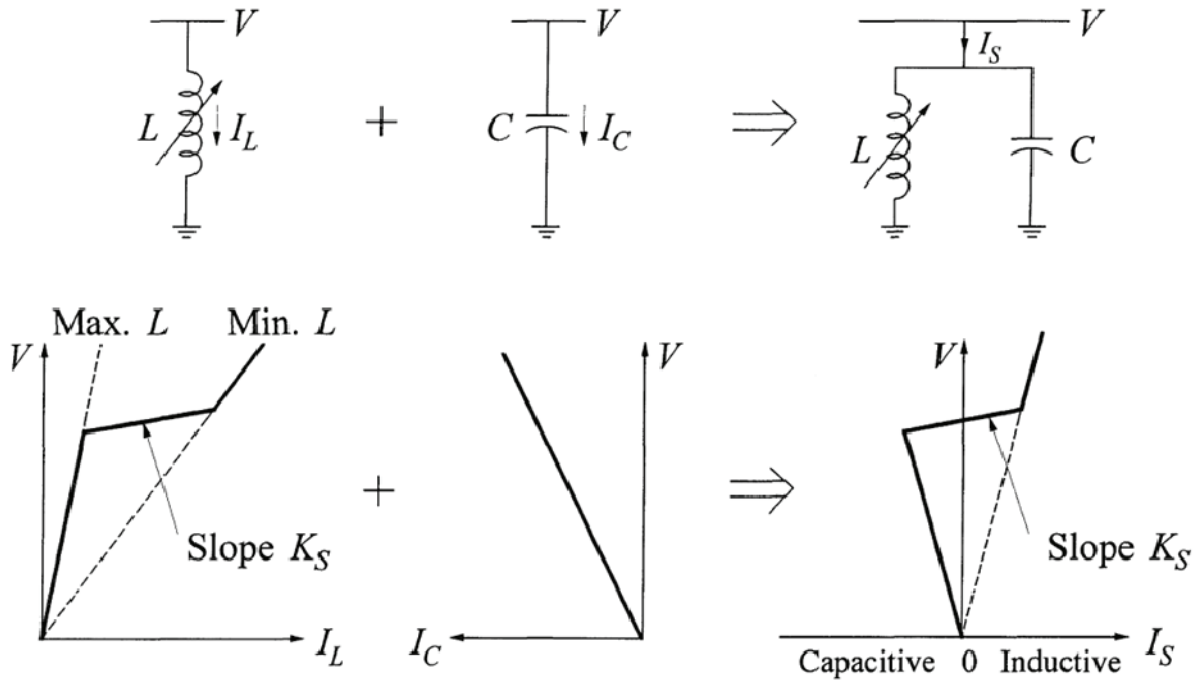

Figure 4.7.1: Composite characteristic of SVC [42]

The voltage at the point of intersection with the vertical axis is equal to the desired voltage. This is the steady state working area and around this voltage the composite characteristic is very flat. If the system voltage were to decrease, the SVC would produce a reactive current, and the new bus voltage would be at the intersection between the SVC characteristic and the system reactive load characteristic. Without the SVC, the new voltage would be at the

intersection between the new system reactive load characteristic and the V – axis. This voltage would be much lower than the voltage achieved with the VSC [42].

The disadvantages with SVC arise if the voltage suddenly drops below the working area. In figure 4.7.2, this part of the characteristic is denoted by II that corresponds to a parabola $Q = B_{max} \cdot V^2$. This is the maximum value of the capacitive susceptance when all the capacitors are switched on and the reactors switched off [43]. This means that as the reactive power production is proportional to voltage squared, the SVC contributes the least when it is most needed. For instance if the voltage drops to 0.8 pu, the SVC would not be able to supply more than 0.64 pu reactive power.

The part of the characteristic denoted by III corresponds to a parabola $Q = B_{min} \cdot V^2$, that is the minimum value of the susceptance when all the reactors are switched on and all the capacitors switched off.

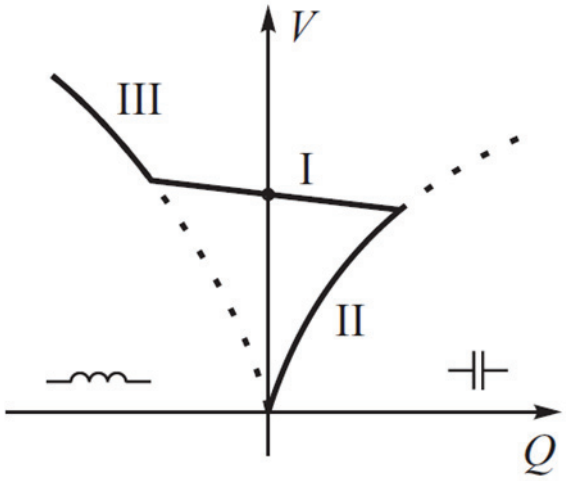

Figure 4.7.2: Q – V relations of SVC [43]

4.7.2 STATCOM

The *static compensator* (STATCOM) provides shunt compensation in a similar way as the SVCs but utilizes the voltage source converter (VSC). Consequently it incorporates a very high content of power electronics but its conventional components are reduced to only a transformer and a capacitor. The operating principle of the STATCOM is illustrated in figure 4.7.3. On the DC side of the voltage source converter, there is only a capacitor. The voltage source converter is equipped with a pulse width modulation (PWM) controller operating with two control parameters *m* and ψ.

A change in *m* enables the converter to change the magnitude of the AC voltage and therefore it influences a change of alternating current flowing through the transformer reactance *X*:

$$I_{AC} = \frac{(V_i - V_{AC})}{jX} \tag{4.18}$$

If $V_{AC} > V_i$ then I_{AC} leads V_i and reactive power is delivered to the busbar. The compensator acts like a capacitor. Conversely if $V_{AC} < V_i$ then I_{AC} lags V_i and reactive power is drawn from the bus. The compensator acts like a reactor. For a transformer reactance of 0.1 pu, a ±10% change in V_{AC} produces a ±1 pu change in the inserted reactive power. Changing ψ, responsible for the phase of AC voltage, makes it possible to control the active power fed to the capacitor, which is necessary to keep a constant value of the DC voltage. To compensate reactive power in a power system, the STATCOM must be equipped with an automatic voltage regulator (AVR). Its function is to enforce appropriate reactive power changes by affecting the regulation parameters m and ψ of the converter controller.

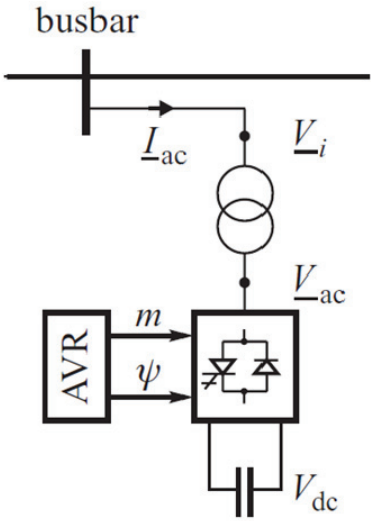

Figure 4.7.3: STATCOM [43]

Figure 4.7.4 depicts the V – I and V – Q characteristics of the STATCOM. The V – I characteristic shows that the STATCOM holds the current constant when the voltage falls below the working area, as opposed to the SVC where the current decrease linearly. The consequence is that the STATCOM offers better reactive compensation during voltage dips because the reactive power varies linearly with voltage, compared to the SVC where reactive power decrease with the voltage squared.

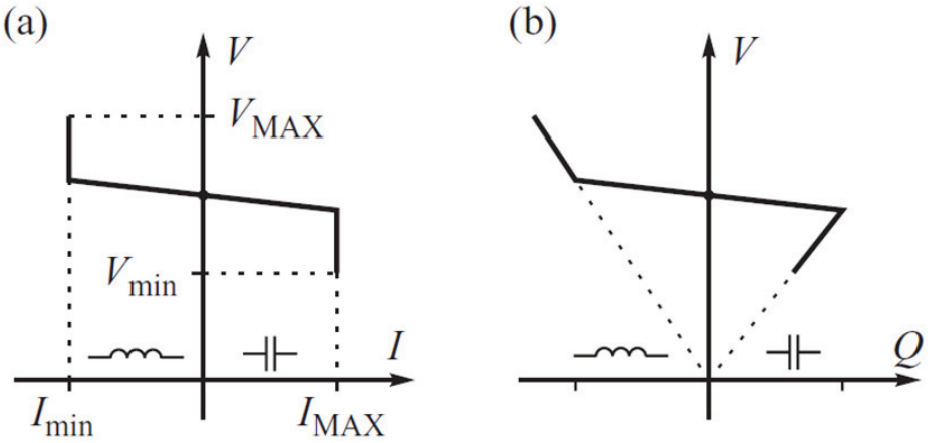

Figure 4.7.4: STATCOM characteristics, a) V – I, b) V – Q [43]

4.8 Dynamic stability improvement by FACTS devices

This chapter describes the dynamic stability improvements achieved by exploiting the features of FACTS devices, especially STATCOM, following a large disturbance. The motivation for including this chapter is to illustrate the benefits of having a VSC in the system, as the converters of the VSC transmission essentially are STATCOMs. The STATCOM improves the stability limit of the power system, first by raising the power-angle curve as much as possible to maximize the decelerating area, and then fully utilizing it in counterbalancing the accelerating area. Basic knowledge of the equal-area criterion is required to understand this topic. A brief repetition will be provided, and more detailed descriptions can be investigated in reference [30]. The following is mainly a summary of the work of M.H. Haque [40][41].

Transmission lines in a modern interconnected power system are heavily loaded to meet the growing demand of power transmission. One of the consequences of such a stressed system is the threat of losing stability following a disturbance. Improvement of first swing stability limit is recognized as one of the important issues in power system operation. A power system can be considered as first swing stable if the angles of all machines in center of angle reference frame increases until a peak is reached where the angle starts returning to the stable equilibrium point.

The first swing stability limit of a single machine infinite bus system can be determined through the equal-area criterion. During the faulted period, the electrical power output of the machine decreases drastically while the mechanical power input remains more or less constant. The machine therefore acquires excess energy which accelerates the machine. The excess energy during the faulted period can be represented by an area called accelerating area. To maintain stability, the machine must return the excess energy once the fault is cleared. The excess energy returning capability of the machine in post fault period is represented by another area called decelerating area. The electrical power output of the machine during deceleration is higher than the mechanical input power, thus decreasing the rotor speed. The

equal-area method is illustrated with a three phase fault in figure 4.8.1 below. In this figure area 1-2-3-4 is the acceleration area and area 4-5-6-7 is the decelerating area. To remain stable the decelerating area must equal the accelerating area before the rotor angle reaches the angle corresponding to point 8. Beyond point 8 the electrical power $P_E(\delta')$ is less than the mechanical power P_m and the rotor experiences a net acceleration torque which further increases its angle. The rotor makes an asynchronous rotation and loses synchronism with the system.

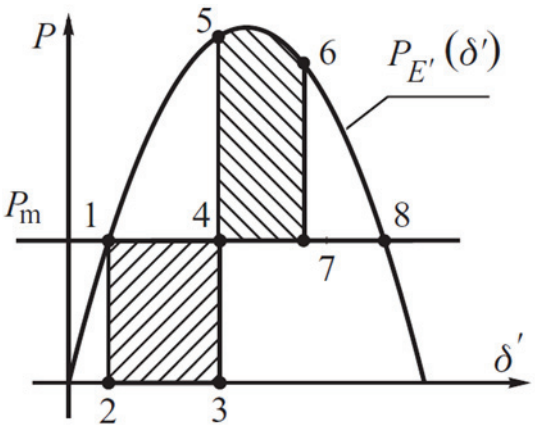

Figure 4.8.1: Equal-area method [43 - modified]

To summarize, the stability of the system can be improved by enlarging the decelerating area and this requires raising the power-angle curve of the system. Furthermore it is observed that the fault clearing time, pre-fault mechanical power input and the electrical output as function of rotor angle are major factors in determining the size of the areas, and hence if the machine will regain stability after the fault [43][49].

Flexible AC transmission systems (FACTS) devices are found to be very effective in improving both stability and damping of a power system by dynamically controlling the power-angle curve of the system.

Continuous and discontinuous controls are very commonly used for FACTS devices to improve the dynamic performance of power systems. For small disturbances, the continuous control is found to be very effective for damping improvement even though it may not utilize the full capability of the device. However, for large disturbances, a full control or bang-bang control (BBC) is needed to improve stability of the system. The bang-bang control operates a FACTS device at its full rating, but the mode of operation is changed (from inductive to capacitive or vice versa) at some discrete points.

The first swing stability limit of a simple system in the presence of a STATCOM is maximized first by enlarging the decelerating area as much as possible and then fully utilizing it in counterbalancing the accelerating area. Enlarging the decelerating area requires raising the power-angle curve in early part of the post-fault period.

The following example is taken from [49]. The model, as depicted in figure 4.8.2, is a single machine connected to an infinite bus and a STATCOM connected to the transmission line at an intermediate bus m. The dynamics of the machine, in the classical model, can be represented by the following differential equations.

$$\frac{d\delta}{dt} = \omega \tag{4.19}$$

$$\frac{d\omega}{dt} = \frac{1}{M}(P_m - P_e - D\omega) \tag{4.20}$$

Here δ, ω, *M, D, P_m* and *P_e* are the angle, speed, moment of inertia, damping coefficient, input mechanical power and output electrical power, respectively, of the machine.

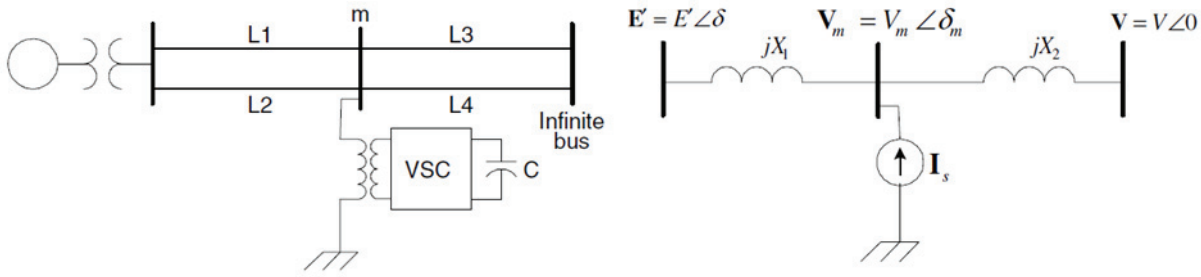

Figure 4.8.2: Network model with STATCOM [49]

With reference to equation (4.15), the electrical power from the machine is given by:

$$P_{e0} = \frac{E'V}{X_1 + X_2}\sin\delta = P_{\max}\sin\delta \tag{4.21}$$

Here P_{e0} is the power without STATCOM. A STATCOM is capable of injecting controllable reactive power into the system, and this is represented by a shunt reactive current source I_s. The electrical power output in the presence of a STATCOM (P_{e1}) can be written as:

$$P_{e1} = P_{\max}\sin\delta + f_1(\delta)I_s = (P_{e0} + \Delta P_{e1}) \tag{4.22}$$

$$f_1(\delta) = \frac{E'X_2}{X_1 + X_2}\sin(\delta - \delta_m) \tag{4.23}$$

Consequently, from the equations the STATCOM increases or decreases the electrical power curve, depending on if the current is inductive or capacitive. For a given system reactance X ($= X_1 + X_2$), ΔP_{e1} depends on reactance X_2 and hence the location of the STATCOM.

Figure 4.8.3 shows the power-angle curves of the machine when the STATCOM operates at its full capacitive rating ($I_s = I_s^{\max}$) as well as at full inductive rating ($I_s = I_s^{\max}$). For

comparison, the power-angle curve of the machine without the STATCOM ($I_s = 0$) is also shown in the figure.

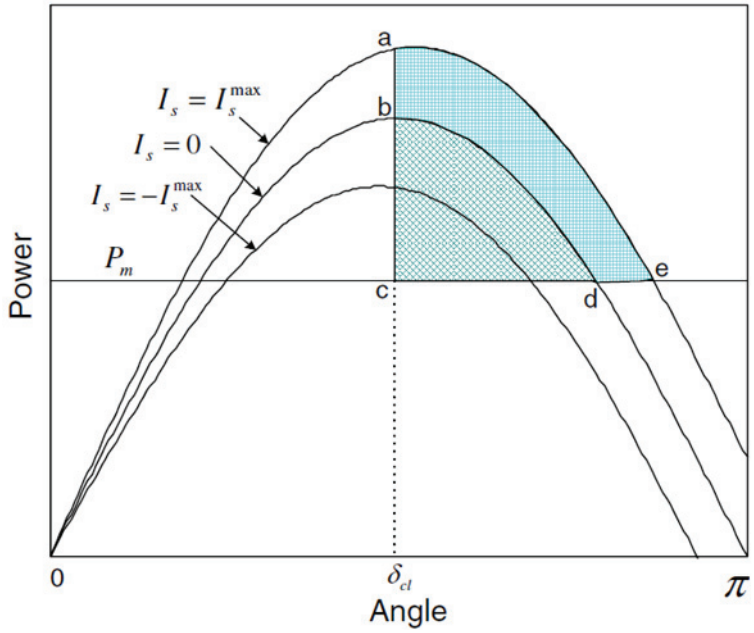

Figure 4.8.3: Compensation with STATCOM [49]

For a fault clearing angle of δ_{cl}, area b-c-d represents the decelerating area without the STATCOM. However, when the STATCOM is added, the decelerating area is increased by the area a-b-d-e. This increase in the deceleration area, provided by the compensation of the STATCOM, greatly improves the first swing stability of the machine.

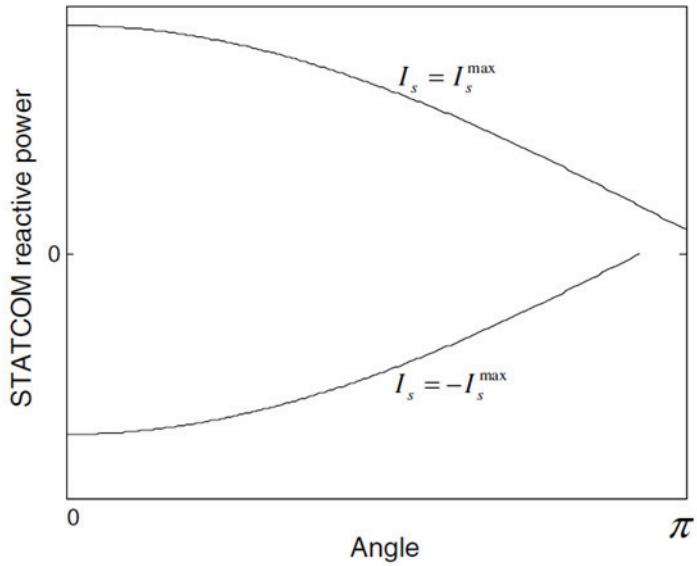

Figure 4.8.4: Reactive power capability of STATCOM [49]

A typical variation of reactive power supplied by the STATCOM (when it operates at full inductive and capacitive ratings) is shown in figure 4.8.4. In practice, the STATCOM can operate anywhere in between the two curves shown in the figure.

5 Petroleum requirements

5.1 Voltage quality:

From a platform operator's point of view, the dimensioning concern when electrifying a platform will normally be the compressors, which are in the range of a few tens of MW and powered through a frequency converter. They compress gas to a higher pressure at the outflow than at the inflow. For the highest levels of power, a load commutated inverter (LCI) will be used. The LCI has a thyristor inverter and a thyristor rectifier which in turn feeds a synchronous machine that drives the compressor. When the frequency converter experiences a dip in the supply voltage to around 70 – 80 percent of nominal voltage, the thyristors will start blocking, the motor starts to retard and no power or torque will be supplied to the compressor. If the absence of torque has a too long duration, the gas will come in return through the compressor in a so-called surge. This may damage the compressor, and is unacceptable. In Norway this has been known to happen at both Kårstø and Kollsnes. If the compressors have to be stopped, this will bring about flaring of gas or stop in the production [5].

In addition to the frequency converters powering compressors, there are also a large amount of rotating motors on the platform necessary for normal operation. These motors would also stop following a long duration dip in the supply voltage.

In the technical requirements for Statoil, the largest Norwegian petroleum company, it is specified that a frequency converter should handle a loss of power for 200 ms, and electronic protection in switch boards should tolerate 500 ms loss of power [5]. If a fault occurs in the VSC transmission system, and the protection scheme using AC breakers is applied, the offshore AC grid would have to be disconnected by the use of AC breakers before the converters shut-down and the fault is removed. Provided that the DC fault is quickly identified and cleared, this would take a minimum of a few seconds [53]. As explained, this will result in production shut down at the platform. Instead, if the platform was supplied from more than one cable connected in a multiterminal solution, the faulted cable could be disconnected without eliminating power supply to the platform. However, the disconnection of the cable would require DC breakers, and this technology is not yet available for high voltages, as explained in chapter 2.11 [5].

A more detailed overview of the requirements for the Norwegian petroleum installations can be further investigated in the NORSOK standards. They are developed by the Norwegian petroleum industry to ensure adequate safety, value adding and cost effectiveness for existing and future petroleum industry developments. The NORSOK standards are prepared to complement available international standards and fill the broad needs of the Norwegian petroleum industry. They also refer to international standards that include provisions to the NORSOK standard [52].

5.2 Security of supply:

Petroleum platforms with local power generation normally have a requirement that one of the main generators should be able to shut down without affecting production. Typical configurations are 2 × 100 % or 3 × 50 % of total power demand. With these configurations, planned maintenance can be performed with full production. It is assumed that if one of these platforms were to be supplied by one VSC HVDC cable from the onshore grid, the reliability and regulation of power supply would be approximately the same as with local power generation [54][5].

A different scenario occurs in a petroleum field where many platforms have local power production. The probability that all the power generation should trip at the same time would be negligible. If the platforms were connected to each other by AC cables, the remaining platforms could supply emergency power if one of the platforms experienced a fault. Should such a field of platforms be supplied by only one DC cable from shore, there would no longer be selectivity in case of a fault on the transmission cable. Selectivity is a fundamental requirement in protection philosophy and implies that only the faulted section of the grid should be disconnected. In this scenario all the fault-free platforms would lose their power supply, and the reliability would decrease [5]. Selectivity is a major concern with the electrification of the offshore installations, and implies a multiterminal solution to ensure security of supply.

5.3 Availability and maintenance time

Due to the high economic losses associated with shut-down of petroleum platforms, it is necessary that the power supply have an eminent availability. This means that the VSC transmission design must allow maintenance activities (forced and scheduled) to be performed with minimum curtailment of the system operation. The majority of equipment in a VSC station is normal high-voltage and low-voltage equipment (breakers, disconnectors, transformers, capacitors, reactors, low-voltage power distribution and motor control systems, etc) that require normal service. The IGBT valves require a minimum of maintenance.

The maintenance work would be reduced with the use of exchange modules or components instead of repair, in the case of a failure. In addition, there should be incorporated extensive redundancies for essential systems such as cooling systems, duplicated control systems and station service power, to allow for most of the maintenance work to be done with no interruption of operation. The redundancy in protection, control and service systems is very important as empirically these systems influence the reliability to the same extent as the electric power components in the transmission systems. As indicated previously, the cables should also have redundancy, as a failure on the cable itself is the most critical scenario, and the repairs could take months. I.e. for optimization of reliability, the petroleum fields should

be supplied from more than one cable ashore, and these cables could be connected offshore in a multiterminal DC system [5][7][50].

Compared with local generation on the platforms, power transfer from shore has less need for maintenance, so planned maintenance can be performed when the production on the platform is closed for regular maintenance. In Statoil, this happens every other year or more infrequent [5].

5.4 Observed reliability and availability

The actual availability of power supply on petroleum platforms will necessarily vary between different platforms. However, Statoil has provided some statistics that gives a reasonable estimate of the situation for the locally powered Norwegian offshore platforms. The availability of power supply is 98 % of the total time. Approximately half of the unavailability is considered forced, in other words unforeseen failures which lead to a stop in the production while maintenance and repairs are performed. The remaining half of unavailability is scheduled unavailability (planned maintenance), which, as previously described, will not affect the production on the facility as long as the installed power generation is 2 × 100 % or 3 × 50 % of total power demand [5].

Table 5.1: Availability of locally powered platforms [5]

Availability	98 %
Scheduled unavailability	1 %
Forced unavailability	1 %

The VSC HVDC manufacturer ABB claims an availability of above 98 % for their commercial projects. The availability may be increased if more strategic spare parts are kept on stock for fast repair in case of an unplanned outage of the HVDC transmission due to faults. For normal VSC substations, when excluding the DC cable, the values in table 5.2 are statistical averages that correspond well with ABB delivered HVDC Light projects. The reliability measure is the forced outage rate in outages/year. The unavailability measure is made up by the forced and unforced (scheduled) unavailability, i.e. the times (in % of one year) when the transmission is out of service. (Availability % = 100 % - unavailability %).

Table 5.2: Availability of VSC (HVDC Light - ABB) [50]

Forced outage rate	1 -2 outages/year
Forced unavailability	0.3 – 0.5 %
Unforced (scheduled) unavailability	< 0.4 %
Availability	> 99.0 %

The performance of existing HVDC links in operation world-wide is reported bi-annually by Cigré B4. However, for a true offshore environment there is at the time of writing only experience with one VSC HVDC link that has supplied power to the Troll A gas platform since 2005 [55]. Electrification of the Norwegian Valhall platform is being executed, and the VSC transmission will be operational in 2010.

It is clear from a comparison of the values for locally powered platforms and VSC transmission systems that the availability of power supply is in the same range should the platform be powered from shore using VSC HVDC. When only looking at the converter substations, the availability of power is actually higher with VSC transmission compared with local generation (0.3 – 0.5 % against 1 % forced unavailability).

6 Choice of wind generator system

In the autumn of 2009, a preliminary theoretical study on wind power technology was performed in preparation for this master thesis. The study contained a thorough presentation of the possible wind generator systems available for offshore wind farms. This chapter is a summary of the study's conclusion on offshore wind generator configuration and the main arguments for this decision.

In proportion to rotation speed, wind turbine concepts may be classified into fixed speed, limited variable speed and variable speed. Variable speed wind turbines are classified into wind generator systems with partial-scale and full-scale power converters, based on the rating of the power converter related to the generator capacity.

According to the study of different wind generator systems, the developing trends of wind generator systems may be summarized as a movement towards a variable speed concept. Variable speed operation is very attractive for a number of reasons, including reduced mechanical stress and increased power capture by keeping the tip speed ratio constant [56][17].

Figure 6.1.1 illustrates the generator system of a variable speed wind turbine with partial-scale converter. This configuration is known as the doubly fed induction generator system (DFIG) or Scherbius machine [56].

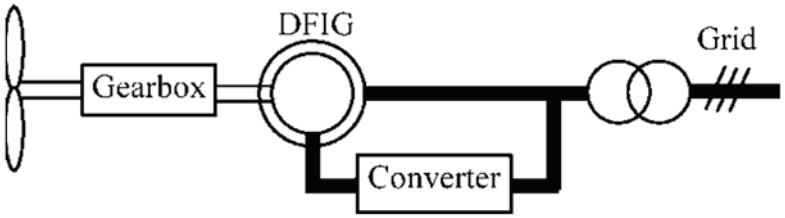

Figure 6.1.1: Double fed induction generator (DFIG) [13]

The generator is a wound rotor induction generator (WRIG) with the stator connected directly to the grid, and the rotor connected through a power electronic converter. Typically, the variable speed range is ± 30% around the synchronous speed of the grid. The rating of the power electronics converter is only 25–30% of the generator capacity, which makes this concept attractive and popular from an economic point of view [57]. While the rotor speed varies, the DFIG can supply power at constant voltage and constant frequency [58]. The converter is a partial-scale back-to back converter, which is a four-quadrant converter. This means that the DFIG can produce or absorb an amount of reactive power.

Compared with fixed speed generators, DFIG offers more advantages such as speed control, reduced flicker, and four-quadrant active and reactive power capabilities. Compared with a full-scale converter, the full scale power converter can perform smooth grid connection over

the entire speed range. However, because the total amount of generated power has to pass through the power converter, the full scale power converter has higher losses. A full-scale converter is also more expensive due to higher costs associated with power electronic components [57][17].

In onshore applications, the variable speed systems have an additional advantage. In case of a temporary fault, the turbine speed can be reduced and rotational energy extracted from the rotor to support the system stability and frequency. This ability to support the grid by extracting the kinetic energy of the rotor requires an additional regulator in the DFIG converter, as the rotor frequency and the grid frequency are decoupled [59]. In a small offshore AC grid, connected through a VSC transmission system, these problems are handled by the control capabilities for frequency and power of the VSC [60]. In other words, the stability advantages of wind turbines with variable speed are no longer as important for the offshore systems investigated in this project, as long as the interconnecting converter is operational. In the event that the converter is not operational this may however prove beneficial during short duration island operation of the offshore grid.

On background of the reasons given in this chapter, a decision was made to model the offshore wind farms in the simulation model as DFIG wind turbines.

7 Wind modeling in PSS®E

As described previously in chapter 6, the decision has been made to model the offshore wind power plants in the simulation model as Doubly Fed Induction Generator (DFIG) systems.

PSS®E v32 provides four different generic wind models for dynamic modeling, including DFIG. These are:

- Type 1. Direct connected Conventional Induction Generator
- Type 2. Wound rotor Induction Generator with Variable Rotor Resistance
- **Type 3. Doubly-Fed Induction Generator**
- Type 4. Full Size Converter Unit

Because the DFIG wind model is listed as type 3, all the dynamic models included in the DFIG representation have the prefix WT3 (Wind Type 3). The total dynamic representation of the DFIG system comprises the following models:

- WT3G: generator/converter model
- WT3E: electrical (converter control) model
- WT3T: mechanical control (wind turbine) model
- WT3P: pitch control model.

There are two different generator/converter models available in PSS®E v32, namely WT3G1 and WT3G2.

The WT3G2 model is a new generator model and is recommended for new dynamic setups because it includes improvements in the original WT3G1. However, as will be explained later in this chapter, the WT3G1 model was chosen for the simulation model in this master's thesis.

The electrical control model WT3E1 can be used with WT3G1 as well as with the improved WT3G2 models. The turbine and pitch control models are also compatible with both generator models.

7.1 Choice of generator system

The PSS®E user manual provides example sets of the dynamic data input with reference to GE 1.5 MW Wind Turbine for both WT3G1 and WT3G2. Originally, the intention was to use the G2 model in the simulations, and this model was implemented in a series of example models to study and validate the dynamic performance of the model during different case studies. The recommended value for the parameter VLTFLG is 2 in the electrical model WT3E1when used in connection with WT3G2, and this was applied for the test simulations.

The output from these simulations showed that the dynamic wind model with WT3G2 was in many cases not able to restore the bus voltage and active power generation following a nearby fault that was quickly cleared.

The following example illustrates the phenomena.

A wind park with 100 aggregated wind turbines is connected to bus number 1. Bus number 1is connected through a transformer to bus number 2 at a higher voltage level. Bus number 2 is connected to the main grid of a large system from an example case named savnw, provided in the PSS®E v32 package.

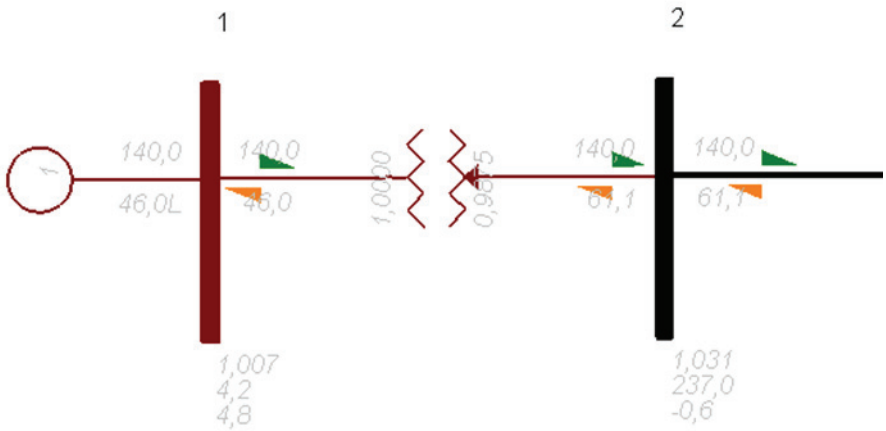

Figure 7.1.1: SLD of test simulations for wind farm

The following dynamic simulation was performed on the system using both WT3G1 and WT3G2 models. When using WT3G1 the recommended value for VLTFLG is 1.

Dynamic simulation event

Time [sec]	Event
0.00	Normal operation
0.20	Bus fault on bus 2
0.30	Bus fault cleared

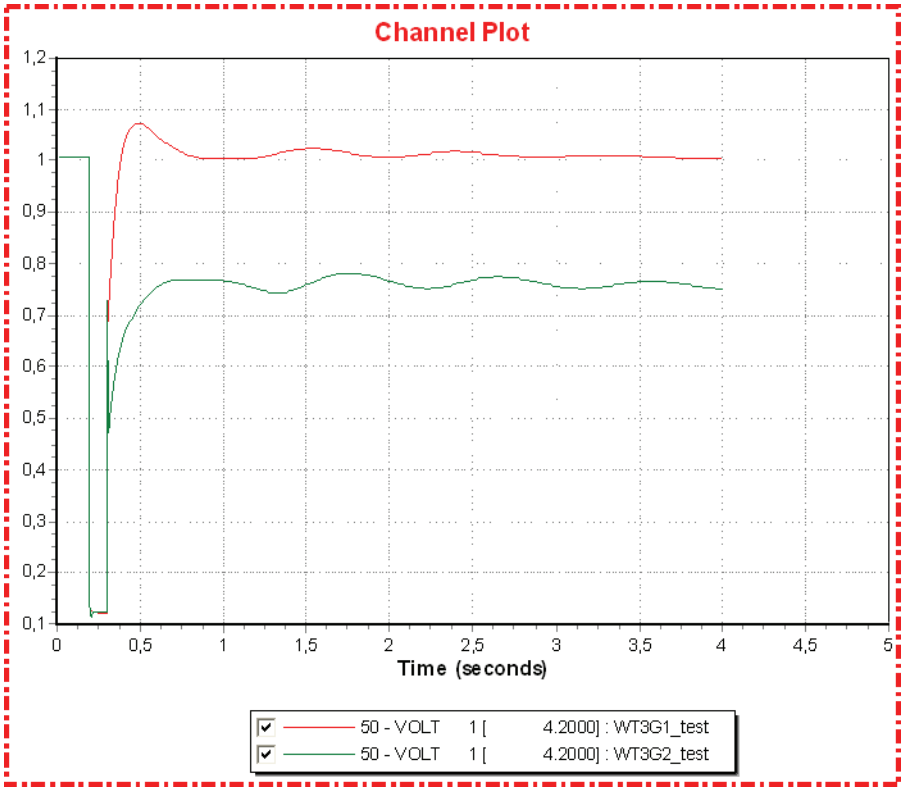

Figure 7.1.2: Voltage comparison of wind generator models [pu]

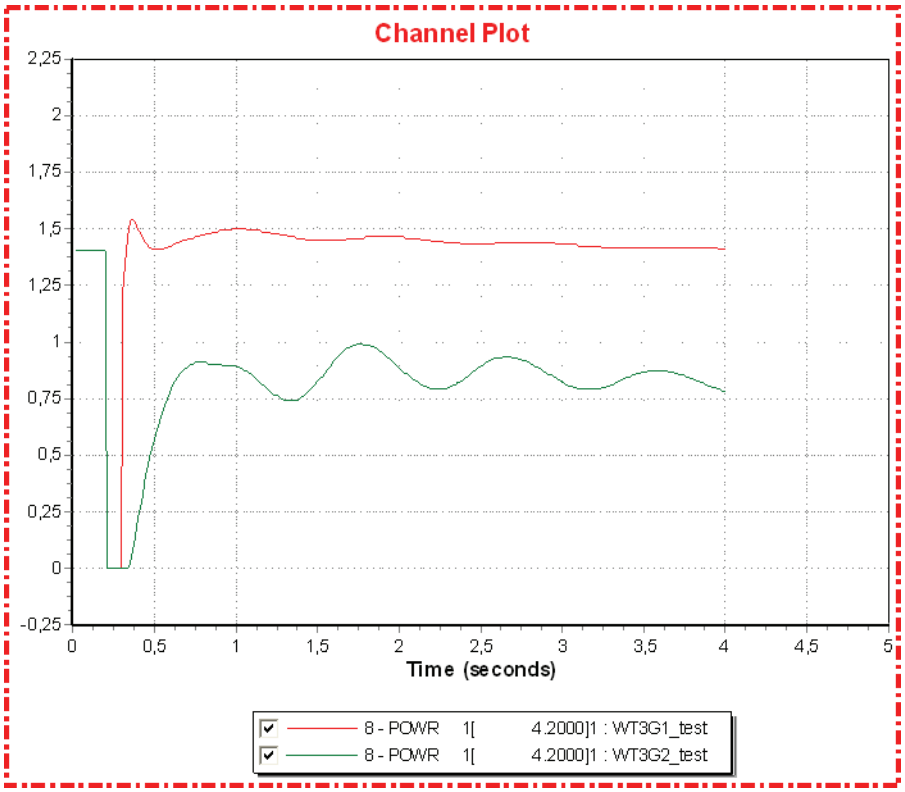

Figure 7.1.3: Active power comparison of wind generator models [pu]

From these simulation results it is clear that the parameter values provided and recommended in PSS®E v32 for WT3G2 does not give a realistic dynamic behavior following a short duration fault nearby. Several simulations were performed experimenting with different voltage levels, system cases and dynamic parameters, but the reason for the generator models performance was not discovered. It was, however, possible to achieve a reasonable dynamic performance with WT3G2 by setting VLTFLG = 0 in WT3E1, and thereby bypassing the terminal voltage control, as explained later in the section on block diagrams. This alternative was not selected for the simulations performed in this master thesis because the older generator model, WT3G1, demonstrated a realistic dynamic behavior with the recommended terminal voltage control. A decision was therefore made that the WT3G1 model was to be used as this model displayed a proper dynamic behavior in connection with a complete control system.

7.2 Aggregation of wind turbines

The provided dynamic wind model is referred to the 1.5 MW GE DFIG wind turbine. In most simulation studies, including this thesis, the object is to examine the total effect of a wind farm, i.e. multiple wind turbines. This can be performed with the same dynamic model by specifying in the generator model the number of original wind turbine units that will be lumped into one equivalent machine in the power flow case. For N lumped machines, the *Mbase* of the original machine must be multiplied by N in the power flow case.

Simulations were performed using the same base case (example case savnw, PSS®E v32) as described previously in the comparison between WT3G1 and WT3G2. A wind farm, represented by one generator in the power flow, is connected to bus number 1. Bus number 1is connected through a transformer to bus number 2 at a higher voltage level, in which again is connected to the main grid of the larger system from the example case, see figure 7.1.1.

The simulations used three different sizes of wind farms (1,10 and 100 wind turbines) to determine if the dynamic behavior of the aggregated wind turbines were a realistic way to model multiple wind turbines.

The dynamic simulation case was as follows:

Time [sec]	**Event**
0.00	Normal operation
0.20	Bus fault on bus 2
0.30	Bus fault cleared

Figure 7.2.1 depicts the dynamic voltage at bus number 1 following the short duration bus fault at bus 2 for all the three wind farm sizes. The voltage behavior is almost identical in all the cases, and this is a strong indication that the aggregation of multiple wind turbines into one equivalent unit is a very good approximation with respect to voltage.

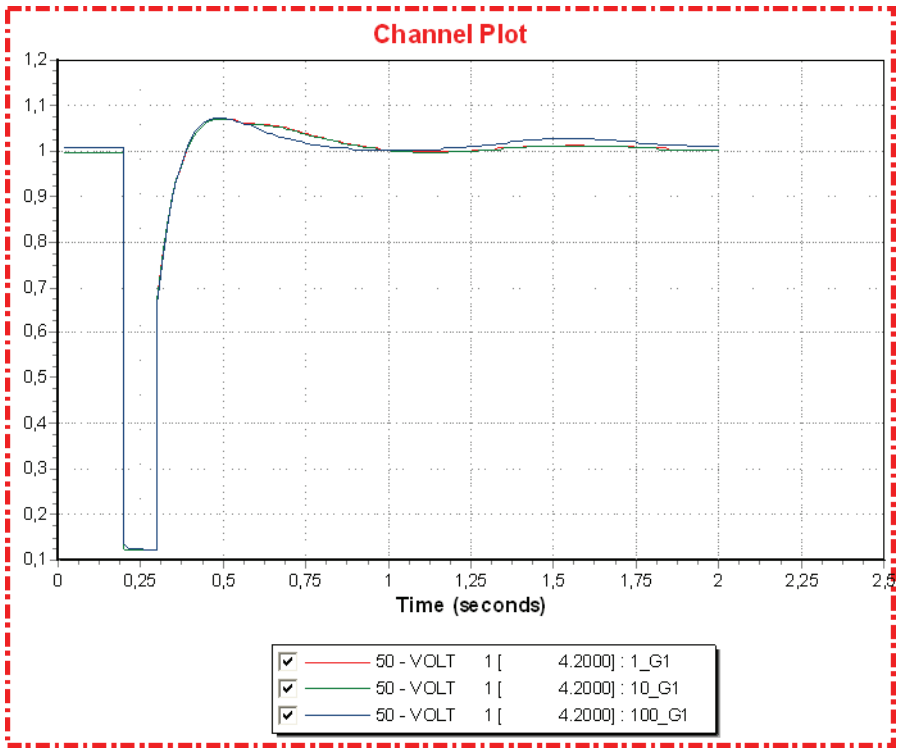

Figure 7.2.1: Voltage comparison of aggregated wind farms [pu]

Also, when it comes to generated active power, the behavior of the aggregated wind turbines are almost identical to the single wind turbine (keep in mind that system power reference is S_{ref} = 100 MVA).

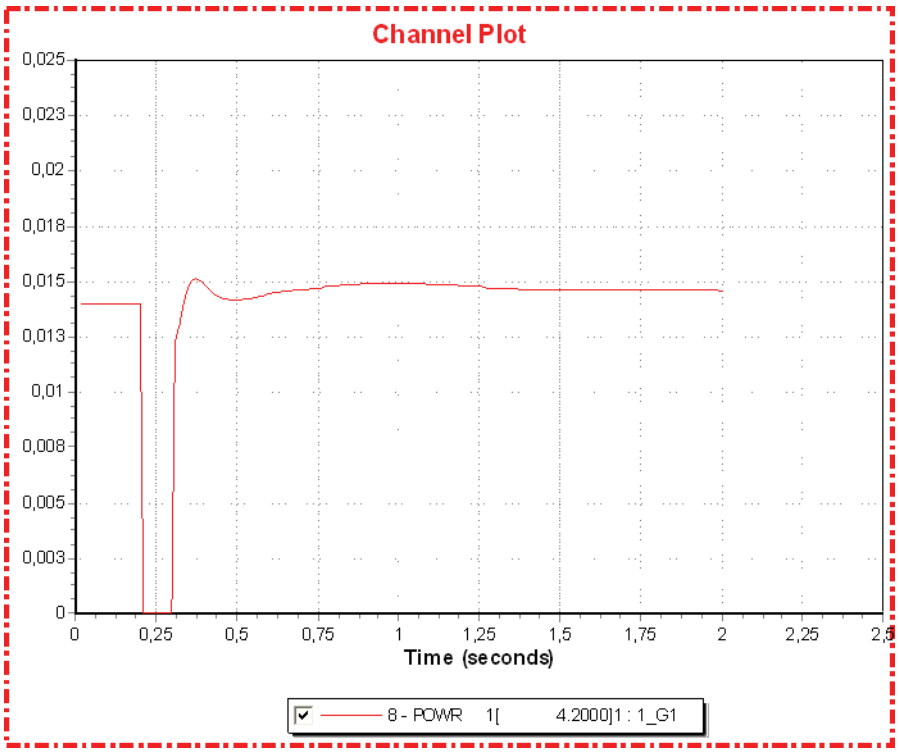

Figure 7.2.2: Power generation of a single wind turbine [pu]

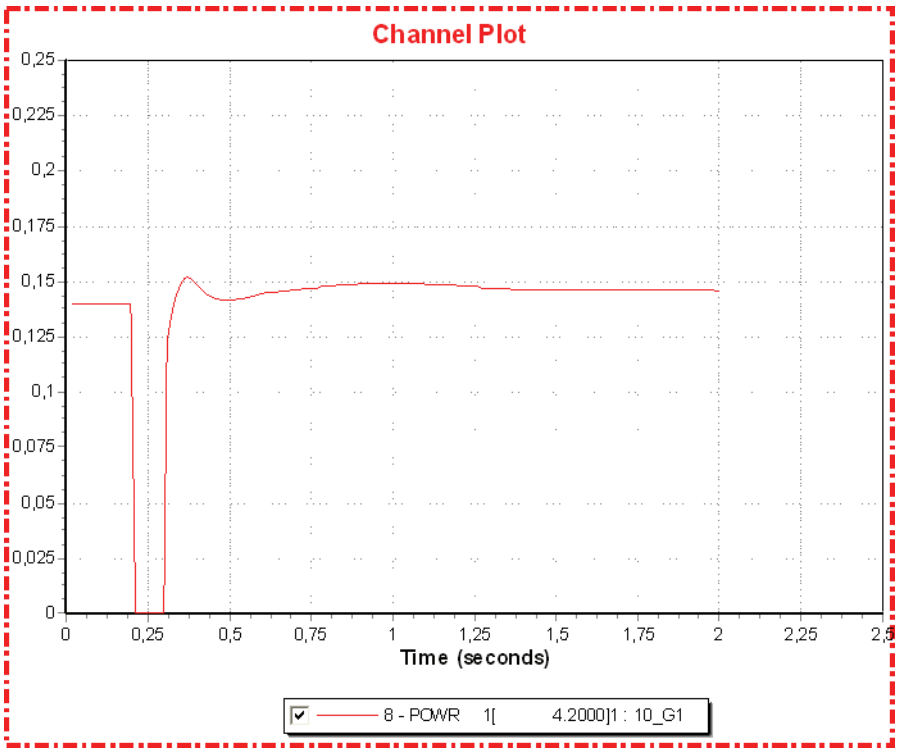

Figure 7.2.3: Power generation of a 10 turbine wind farm [pu]

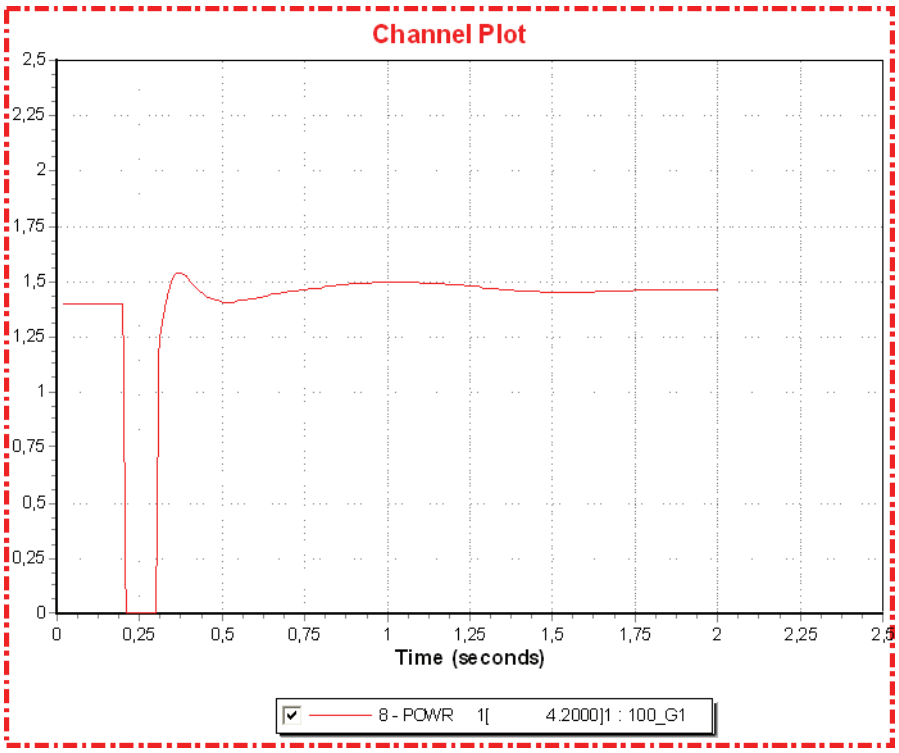

Figure 7.2.4: Power generation of a 100 turbine wind farm [pu]

The conclusion from these simulations is that the aggregated wind farms exhibit almost identical performance compared to a single wind turbine. Using one equivalent generator to represent a large wind farm with this modeling method is therefore considered an acceptable

and reasonable simplification. The wind farms in the simulation model investigated in this master thesis will be modeled in this manner.

7.3 Power flow modeling

This section highlights some of the important aspects to consider when modeling the wind farm in the power flow case.

As explained, the entire wind farm is modeled as one generator in the power flow. The correct *Mbase* value for this generator will be the *Mbase* value of the single wind turbine model multiplied with the number of wind turbines in the wind farm. The *Mbase* for one of the 1.5 MW wind turbines is 1.7 MVA.

The generator's *Xsource* should have the same value as the equivalent reactance, *Xeq*, of the dynamic generator model. *Xsource* is a per unit (pu) value based on the given *Mbase*, and consequently shall not be multiplied with the number of wind turbines. The value for *Xeq* was 0.8 in the data set for the dynamic wind models, and this value was therefore used as the value for *Xsource*.

The question could be asked whether or not the value for *Xsource* is referred to the rotating mass of the turbine or of the complete DFIG system. This is because most of the reactive generation in a DFIG originates from the converter. The consequence of this is that the value for *Xsource* would be too small if it was only referred to the rotating mass and not the entire system. However, an assumption is made that because the parameter data for the GE wind turbine is provided in the PSS®E user manual the values are intended for the direct use in simulations, and the value for *Xsource* probably covers both the rotating mass and converter.

In the simulations the wind farms were set to operate within a power factor of 0.95. The model data allows the dynamic response of the turbine to operate at a higher reactive power generation, the limit is a power factor of 0.9.

Reference [61] states that the GE 1.5 MW DFIG wind turbine has a terminal voltage of 690 V. The voltage level for the collector bus in a wind farm normally lies between 20 and 35 kV. In this thesis 22 kV was selected. The next voltage level is determined by the necessary voltage needed to transfer the generated power in subsea cables to the PCC of the converter station. In wind farm terminology this bus is sometimes referred to as the point of interconnection (POI), as this is where the wind farm is connected to the main grid. For the largest wind farm this voltage level is 245 kV and for the smaller wind farm the cable is operated at 132 kV. Figure 7.3.1 shows the single line diagram from PSS®E illustrating the different power levels associated with the largest wind farm (offshore area 2).

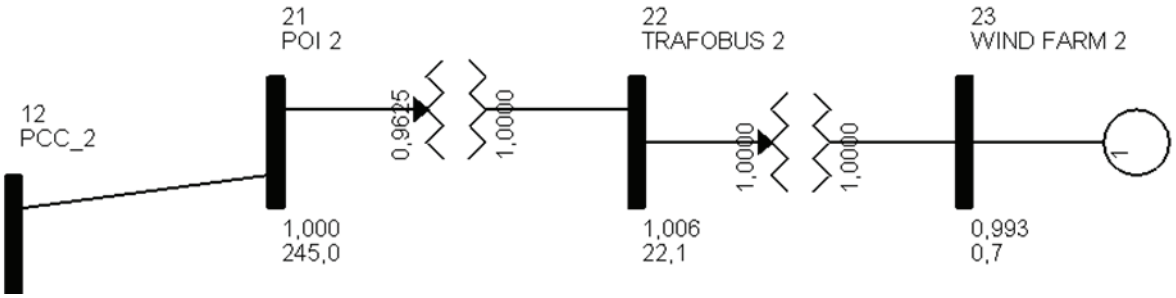

Figure 7.3.1: Offshore voltage levels (offshore area 2)

Both in the dynamic file and in the power flow file a parameter must be set indicating which bus should have its voltage regulated by the wind farm. In this respect, there are two possible distinctive alternatives.

1. The wind farm regulates its own bus voltage, i.e. the voltage that the generator is connected to. The transformers regulate the voltage of the following buses.
2. The wind farm regulates the voltage at the POI, i.e. the high voltage bus connected to the rest of the grid. In this case, the transformer between the POI and the collector bus regulates the voltage at the collector bus which connects all the individual wind turbines of the wind farm through the step up transformer.

A detailed comparison between these two alternatives is an interesting case that could be further investigated. This would involve theory on transformer settings and their voltage control. Such a comprehensive analysis is not included in the scope of this work. In the simulations involved in this thesis the second alternative was chosen after advice from [6], i.e. the wind farm regulates the POI.

7.4 Dynamic wind model

The modeling of the offshore wind farms have been implemented with dynamic parameters provided in the PSS®E manual for a GE 1.5 MW wind turbine. In addition to the data set, the PSS®E manual includes block diagrams for the models and data sheets with a name that describes the meaning of each parameter. However, there is no further information of important conditions for normal behavior of the model in dynamic simulations.

This chapter aims to remedy this situation with a rather comprehensive analysis of the block diagrams to better understand the dynamic behavior of the wind model. The analysis has been made with the help of Professor Kjetil Uhlen [59].

Figure 7.4.1 illustrates the interaction between the four dynamic models that make up the dynamic representation of the DFIG wind model.

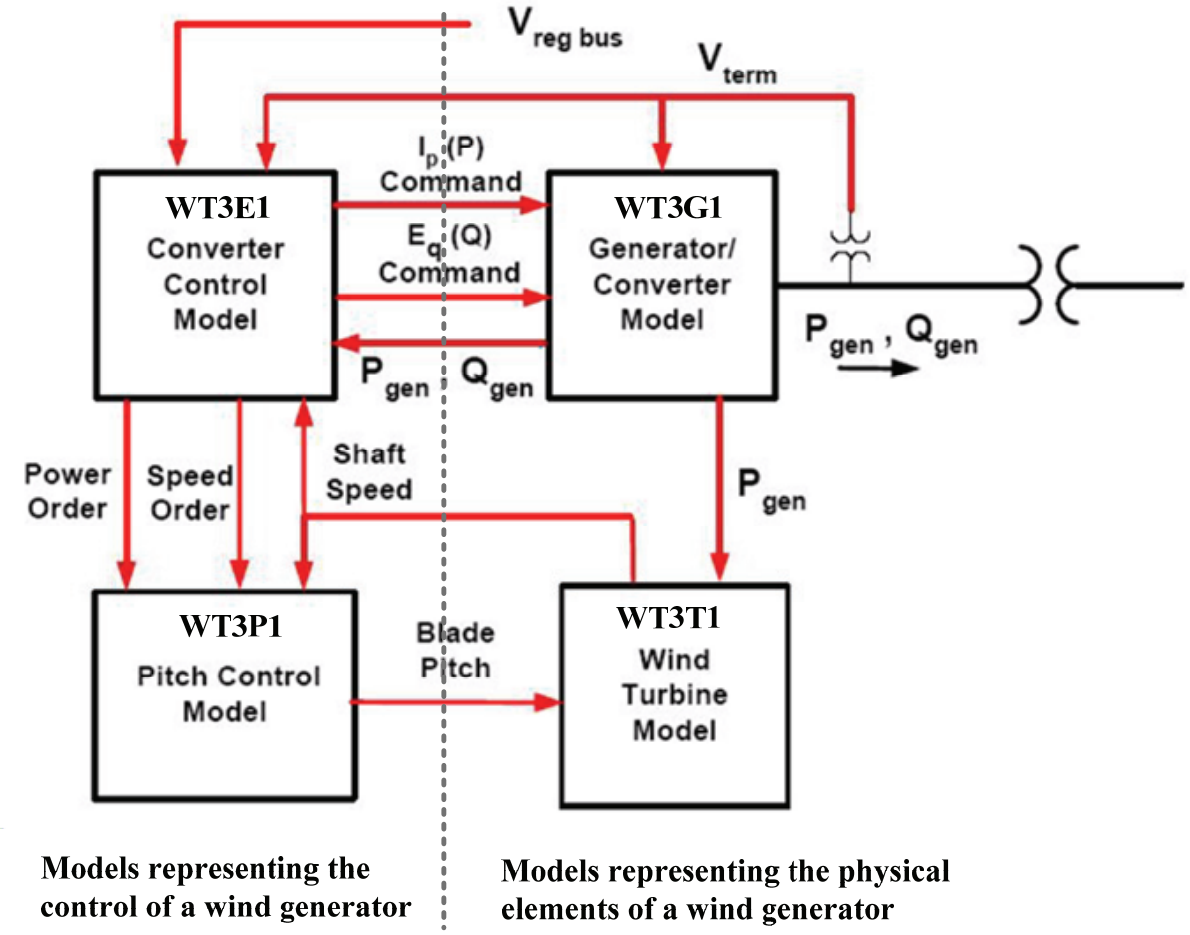

Figure 7.4.1: Interaction of the dynamic wind models [1]

Figure 7.4.1 has been divided to show which models represent the physical elements of a wind turbine and which models represent the control of the wind turbine generator.

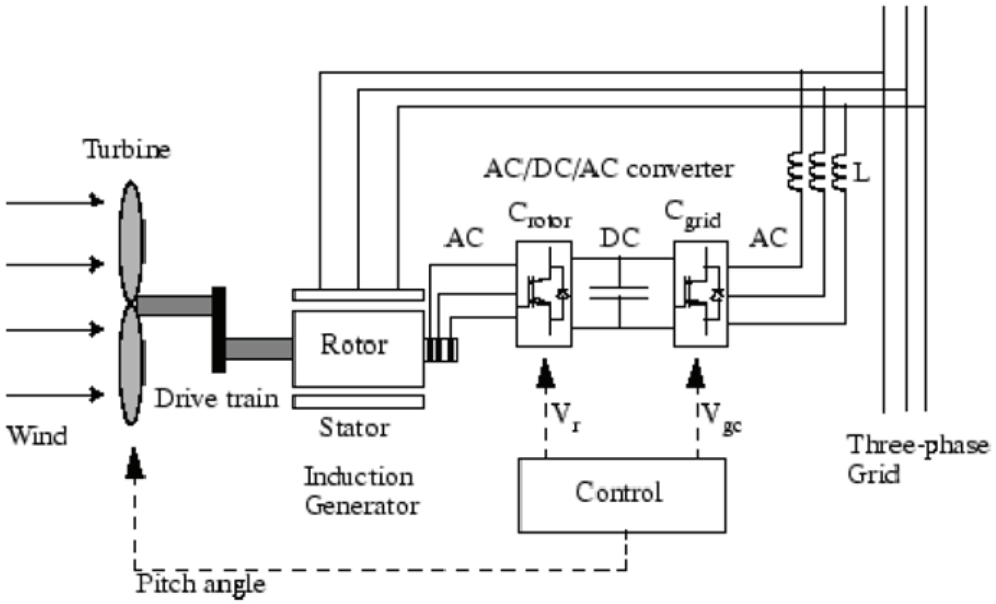

Figure 7.4.2: DFIG wind turbine system [60]

As can be seen in figure 7.4.2 below, illustrating a DFIG, the control system of a physical wind turbine regulates both the pitch angle of the turbine and the converter that governs the rotor voltage, and thereby controls the power output.

7.4.1 WT3E1:

The most comprehensive model with respect to parameters is the electrical (converter control) model. It receives information about the active and reactive electrical power output from the generator model, the shaft speed from the turbine model and the voltage levels at both the terminal and the bus selected for voltage control. The electrical model is made up of two control systems that regulate the active and the reactive power command to the generator/converter model (WT3G1).

The active power control receives information on the electric power output from the generator and compares this to a set of parameters in the model that links shaft speed and active power output. The turbine speed associated with the present active power level is then compared to input of the actual shaft speed of the turbine. The torque regulator then creates an active power command (I_{Pcmnd}) that is sent to the generator model and controls the mechanical torque. A speed order, giving an optimal speed reference with respect to power, and a power order, is sent to the pitch control model.

The reactive power control is slightly more complex as there are different options the user has to decide depending on the choice of generator model and the application of the wind model. The parameters that have to be decided are the integer constants (ICONS) for VARFLG and VLTFLG, se figure 7.4.3.

The possible choices for VARFLG are:

0 - Constant Q control
1 - Wind Plant reactive power control
-1 - Constant power factor control

The possible choices for VLTFLG are:

0 - Bypass terminal voltage control
1 - E_{qcmd} limits are calculated as $V_{Term} + XIQ_{min}$ and $V_{Term} + XIQ_{max}$, i.e., limits are functions of terminal voltage
2 - E_{qcmd} limits are equal to XIQ_{min} and XIQ_{max}

By setting VARFLG = 0 (constant Q control) the Q_{cmd} is given by the reactive power from the power flow. If the VARFLG is set to 1, the terminal voltage at the voltage regulated bus is compared against the reference voltage to create the voltage error. This error is used to compute the Q_{cmd}. Constant power factor control, VARFLG = -1, means that the Q_{cmd} is determined using a power factor angle reference input.

After the Q_{cmd} is created, it is compared against the value of the generators reactive power (Q_{elec}) and the error goes through an integrator that creates a voltage reference. This voltage

reference is compared to the terminal voltage of the generator and the computation of the resultant reactive power control, or more precisely voltage command E_{qcmd}, is dependent on the ICON chosen for VLTFLG. If the VLTFLG is set to 0, the integral of the error between Q_{cmd} and Q_{elec} is used directly to compute the voltage command E_{qcmd}. If the VLTFLG is set to 1, the voltage error between the reference voltage and the terminal voltage (V_{Term}) is multiplied by a gain and integrated to compute the voltage command E_{qcmd}, with E_{qcmd} limits calculated as $V_{Term} + XIQ_{min}$ and $V_{Term} + XIQ_{max}$, i.e., limits are functions of terminal voltage. By setting VLTFLG to 2 the same integration of the voltage error will take place, but the E_{qcmd} limits are equal to the constants XIQ_{min} and XIQ_{max}. VLTFLG = 2 is the recommended parameter setting for WT3G2.

In the simulations performed in this master's thesis the generator model WT3G1 was chosen and the recommended values for the parameters are VLTFLG = 1 and VARFLG = 1. These ICONS have been used for all the dynamic simulations in this project.

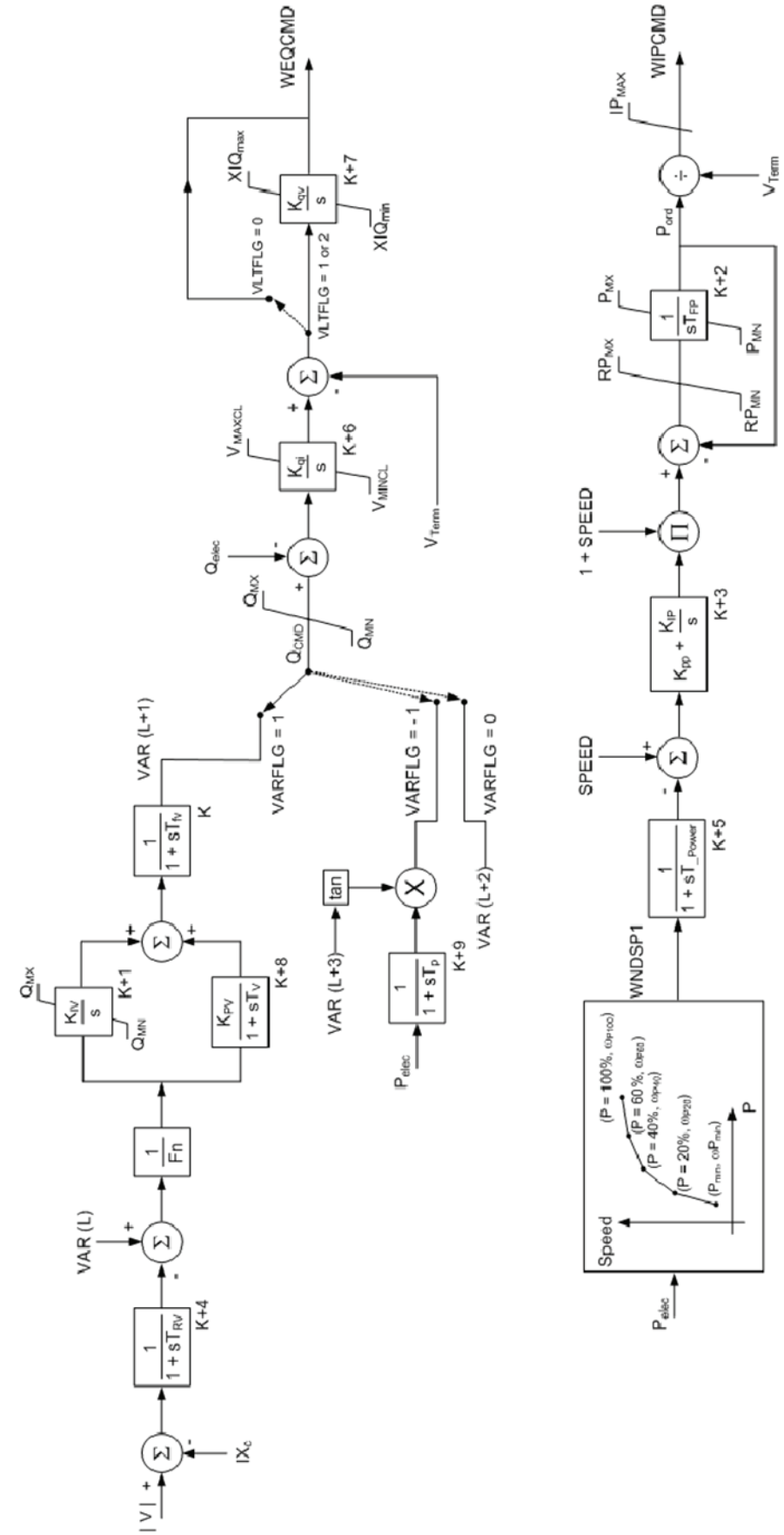

Figure 7.4.3: WT3E1, electrical (converter control) wind model [1]

7.4.2 WT3G1

The generator/converter model receives the active power command (I_{Pcmnd}) and the reactive power command (E_{qcmd}) from the WT3E1 along with feedback of the terminal voltage. The reactive power command is actually a voltage command signal that is divided by the X_{eq}, an equivalent reactance of the generators effective reactance, to create a flux current command. The output of the generator model is a controlled current source that computes the required injected current into the network in response to the flux and active current commands. In PSS®E, along with most simulation programs, all sources in the system are modeled as a current injection.

The electromagnetic (flux) generator dynamics are neglected in this dynamic modeling of the generator. The motivation for doing this is that in a controlled DFIG this dynamic behavior is much faster than for instance in a synchronous machine, and will therefore not be as significant.

The generator/converter model includes a phase-locked loop (PLL) to synchronize the generator rotor currents with the stator. The function of the PLL is to establish a reference frame for the WT3G1 voltages and currents shown in the phase diagram in figure 7.4.5. The output of the PLL is the angle δ which defines the displacement between the network reference real axis and the machines' internal reference X axis. In steady-state Vx = V_{term}. In the case of a system disturbance, the rate of change is limited by the PLL logic.

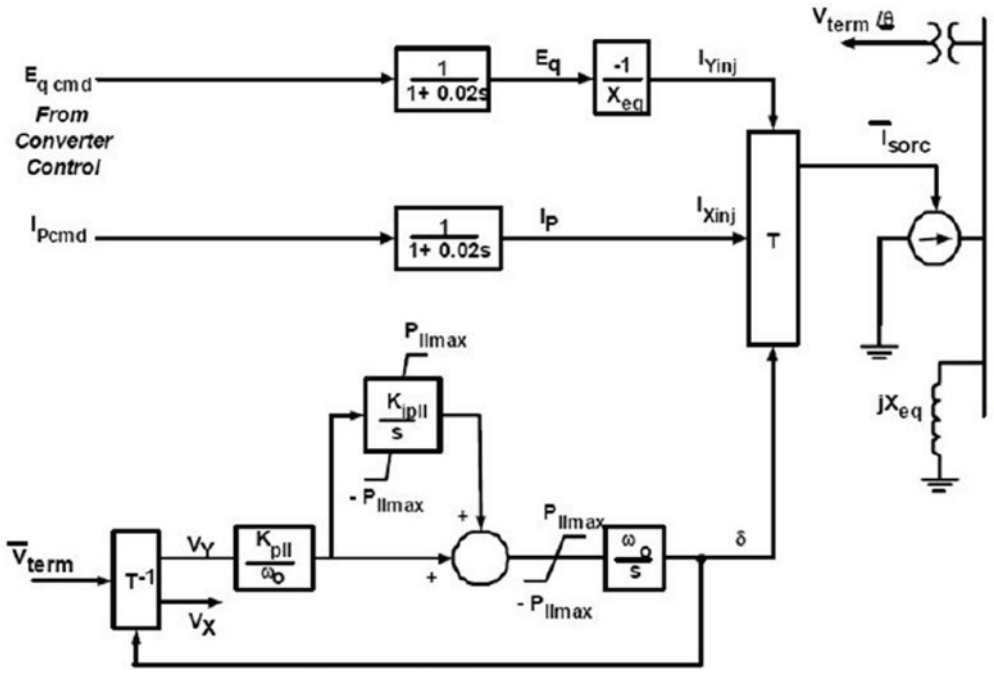

Figure 7.4.4: WT3G1, generator/converter wind model [1]

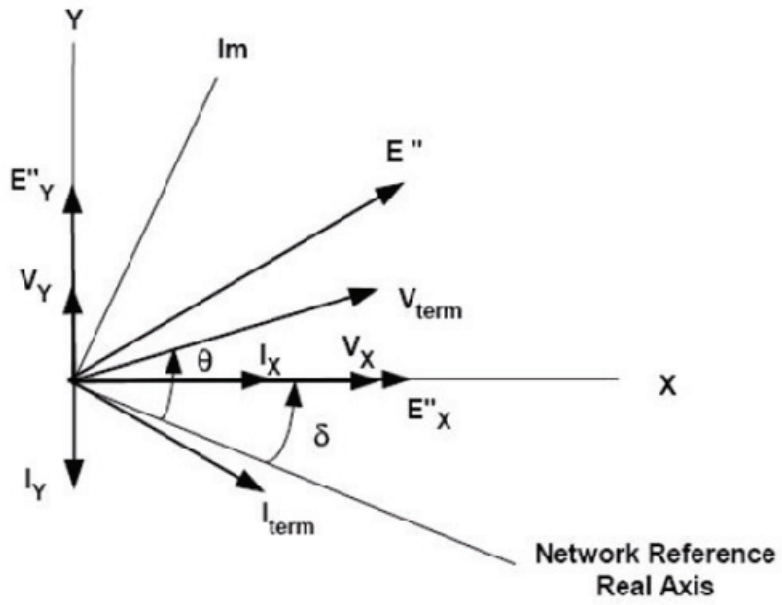

Figure 7.4.5: WT3G1 phasor diagram [1]

7.4.3 WT3P1

The pitch model, figure 7.4.6, receives input on speed order (WNDSP1) and power order (WPCMND) from the electrical model and input on the shaft speed (SPEED) from the wind turbine model. These orders are the desired values or set points of the regulator.

The pitch control regulates the mechanical (turbine) model and the function of the pitch control model is to extract as much mechanical power from the available wind as possible in the turbine model, without exceeding the rating of the equipment.

In the pitch compensation the power order is compared to a power reference (P_{MX}) input decided by the user. P_{MX} describes the maximum allowable power generation of the wind model. If the power order is larger than P_{MX} the pitch compensation control circuit will produce a pitch command to pitch the blades out of the wind, and thereby reduce the power.

The speed order and actual shaft speed are compared to create a speed error (ω_{err}) which is integrated in the control circuit called pitch control. This control circuit also produces a pitch command which will either increase or decrease the actual shaft speed in the WT3T1 model to match the speed order from the electrical model. The two pitch commands are then added together in a resulting total pitch command (θ_{cmnd}) that is integrated with respect to the blade response time constant. The models final output is the blade pitch (WPITCH), which is an input to the wind turbine model.

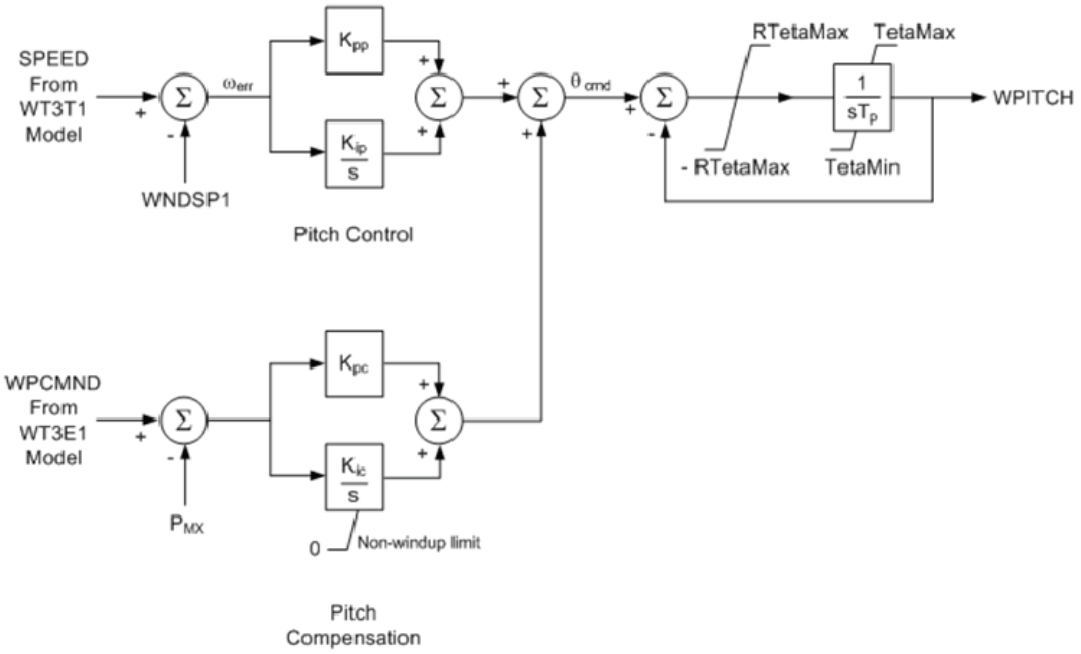

Figure 7.4.6: WT3P1, pitch wind model [1]

7.4.4 WT3T1

The wind turbine model is the combination of a mechanical model and a very simple aero dynamical model. Using the electromechanical swing equations of a rotating machine and the speed set point from the pitch control, the model computes the turbine speed that in turn determines the blade pitch and the generated power.

The mechanical model can simulate on either one-mass system or two-mass system. In a one-mass mechanical system, the shaft is represented by one stiff shaft, and the inertia of the turbine and the generator can be represented by one total inertia constant. In a two-mass mechanical system, the total shaft is represented by two shafts, which can be twisted independently of one another within a certain limit. If the two-mass system is to be used, the parameter H_{tfrac} must be given a value between zero and one which defines the turbines inertia fraction. To simulate on the one-mass mechanical system H_{tfrac} is set to zero.

The complete block diagram for the turbine control is given in figure 7.4.7.

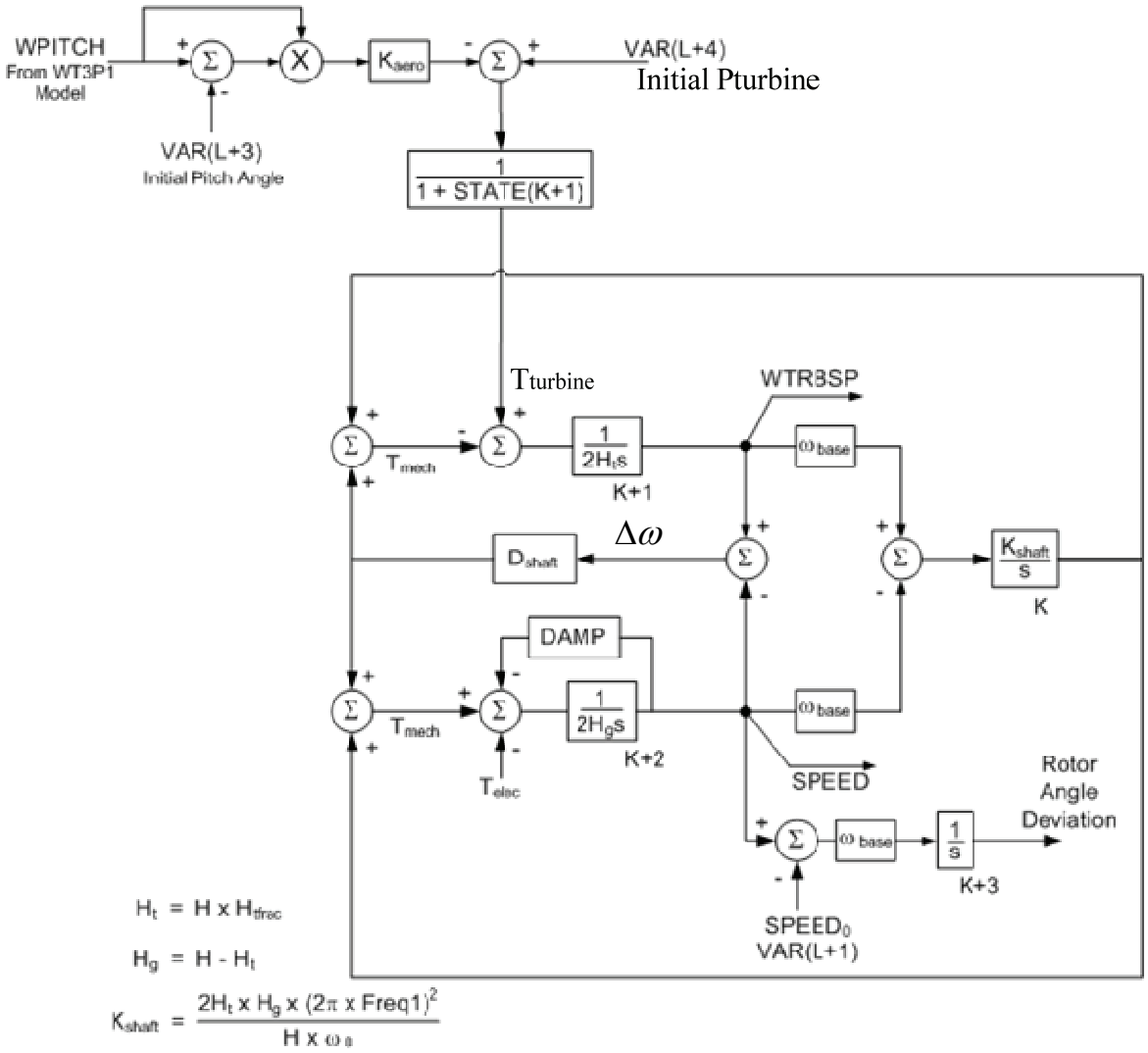

Figure 7.4.7: WT3T1, turbine (mechanical) wind model [1, modified]

The block diagram of the turbine model is described by the following equations, giving the relationship between change in rotor speed and torque.

$$\dot{\omega}_t = \frac{1}{2H_t}(T_{turb} - T_{mech}) \tag{7.1}$$

$$\dot{\omega}_g = \frac{1}{2H_g}(T_{mech} - T_{elec}) \tag{7.2}$$

$$T_{mech} = K_{shaft}(\Delta\theta) + D_{shaft}\Delta\omega \tag{7.3}$$

In the parameter data files for GE 1.5 MW wind turbine the parameter for H_{tfrac} is set to zero, i.e. the one-mass mechanical system is used in all the simulations. This results in a much simpler block diagram as the internal turbine shaft speed deviation disappears. The turbine inertia integrator (K+1) falls away and reduces the turbine control to the simplified block diagram of figure 7.4.8.

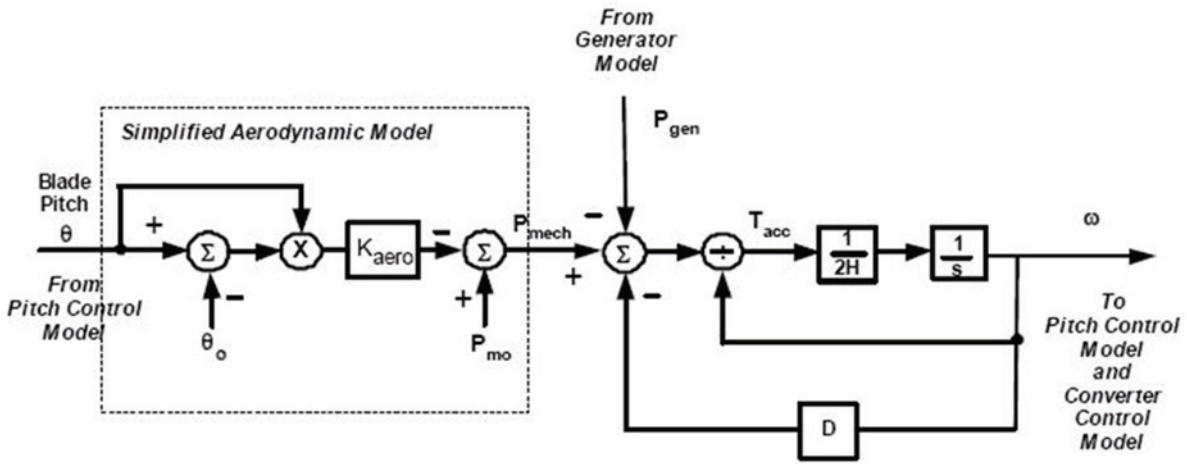

Figure 7.4.8: WT3T1, one-mass turbine (mechanical) wind model [17]

The new equation describing the rotor angle deviation reduces to:

$$\dot{\omega} = \frac{1}{2H_{tot}}(T_{turb} - T_{elec}) \tag{7.4}$$

As this is relatively non complex model, the damping (D/DAMP) shown in the diagrams is comprised of the mechanical damping of the turbine shaft and any electrical damping in the generator.

Appendix C contains the parameter data for the dynamic implementation of the wind turbines.

8 HVDC Light Open model Version 1.1.9-2

The contents of this chapter is mainly based on information from the HVDC Light model documentation i.e. reference [2][3] and the document *"It's time to connect"* [7]. In addition, many of the modeling decisions were taken based on advice from Per-Erik Björklund [9] of ABB and results from test simulations.

8.1 Choice of simulation model for VSC

There are two simulation model alternatives when using PSS®E to investigate VSC systems, namely PTI's model library VSC model and ABB's HVDC Light VSC model created for use in PSS®E. The PTI model was originally created in cooperation with ABB about ten years ago. It was implemented with information corresponding to ABB's model at that time with regards to both power flow and dynamic behavior. However, the ABB dynamic simulation model at that time is now considered to have had extensive fundamental flaws. ABB have, on occasions, made test-runs with the PTI model, but not found the dynamic response to be satisfactory compared to the behavior of their product HVDC Light [9]. ABB is today, as previously described in the report, the leading supplier of VSC projects in the market, and is considered to have an extensive experience with VSC technology. An important problem with the use of PTI's model for this master thesis is that it is restricted to two-terminal operation, while the situation to be analyzed includes a multiterminal system. The choice of simulation model was therefore to use ABB's PSS®E HVDC Light Open model (Version 1.1.9-2).

8.2 Power and voltage ratings

HVDC Light is a module based technology with power ratings from 101 MW to 1216 MW. To increase the power of the converters, modules are placed in series and parallel in order to increase the current and voltage. The current and voltage rating of the different modules are shown in table 8.1 below.

Table 8.1: Modules for HVDC Light [7]

HVDC Light® modules		Currents		
		580A (2 sub)	1140A (4 sub)	1740A (6 sub)
Voltages	± 80 kV	M1	M2	M3
	± 150 kV	M4	M5	M6
	± 320 kV	M7	M8	M9

The intentional use of the system modeled in this master thesis is to investigate the possibilities for large power transfer in a multiterminal HVDC system with interconnected offshore AC systems. The choice of HVDC light converter modules in the model have to consider the necessary power levels of the offshore AC grids, the required power transfer capacity and also a standardization of the voltage levels, as previously described. Considering these requirements, the HVDC light modules chosen for the converters are M7 offshore and M9 onshore, with a base power of respectively 405 MVA and 1216 MVA. Both modules operate on the same DC voltage level of ±320 kV, which necessarily must be the equal in order to combine them in a multiterminal DC grid.

Table 8.2: Module ratings of M7 and M9 [7]

Converter modules	M7	M9
Max DC voltage (pole to ground) [kV]	320	320
Base power [MVA]	405	1216
DC current [A]	627	1881

8.3 Power flow representation:

8.3.1 Converter representation

The following section describes how the HVDC light model, developed by ABB, is correctly represented in PSS®E power flow simulation using standard generator elements from PSS®E.

Figure 8.3.1 below illustrates a simplified single line diagram for a HVDC Light converter station.

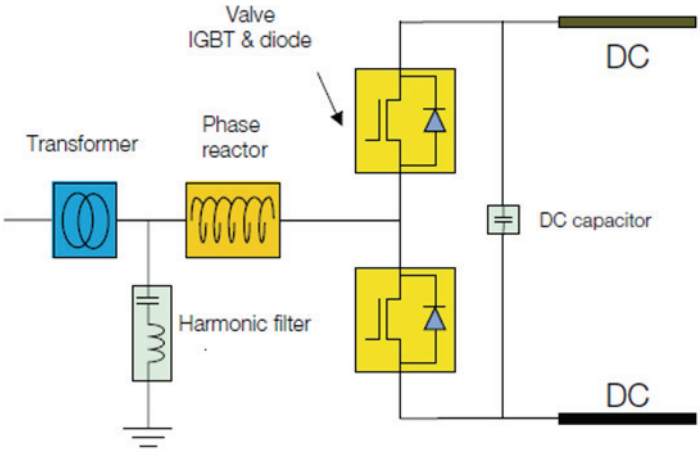

Figure 8.3.1: SLD for a HVDC Light converter station [7]

In PSS®E the converter station is modeled by creating two buses as seen in figure 8.3.2, a filter bus and a PCC bus (Point of Common Coupling).

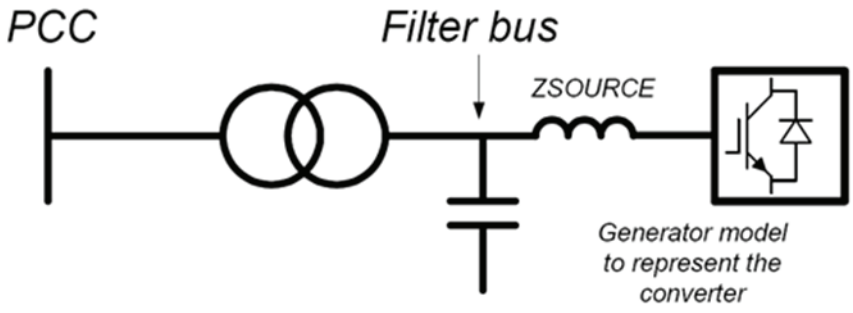

Figure 8.3.2: PSS®E representation of a converter station [2]

The voltage source converter is modeled as a synchronous generator connected to the filter bus. The *Mbase* value for the generator should be specified in accordance with the MVA rating of the HVDC Light converter, which means 405 MVA and 1216 MVA for the M7 and M9 converters respectively. The generator impedance *Z Source* is used in PSS®E for specifying the converters commuting reactance L as seen in figure 8.3.2. The reactive component, *X Source*, should be set equal to the per unit impedance of the AC series reactors, and the resistive part, *R Source*, is set equal to zero.

The harmonic filter in figure 8.3.1 is represented by the reactive power generation of the fixed shunt AC filter capacitors connected to the same filter bus as the generator. Additionally, a two-winding converter transformer has to be added connecting the filter bus to the Point of Common Coupling (PCC). The transformer tap changer position is on the PCC side of the transformer, and regulates the voltage on the filter bus. The voltage level on the filter bus is 416 kV for both M7 and M9, and the voltage on the PCC bus is decided by the user. The complete modeling of one converter station in a PSS®E single line diagram is seen in figure 8.3.3 below.

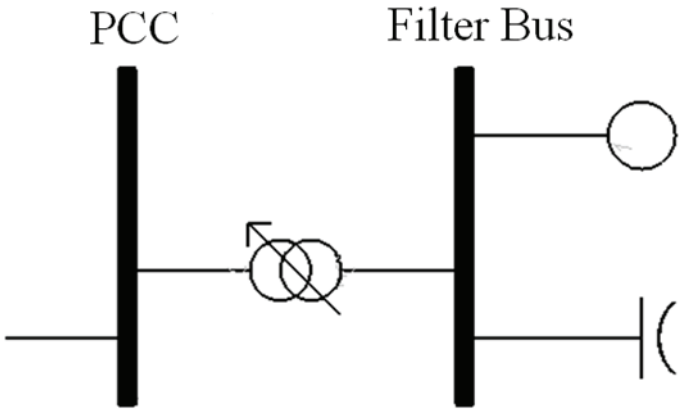

Figure 8.3.3: SLD of converter model in PSS®E

The DC cables between converters are not modeled in the power flow. For power flow simulations the user must specify the active power flow of each converter in the DC system. In a multiterminal system this may seem rather complex, but the following rules apply [2]:

- The power references follow the PSS®E references for the generic generator model, meaning that if there is a negative power generation, the converter receive power from the AC system and injects power in the DC system (rectifier operation). If the power generation is positive, the converter receives power from the DC system and injects it in the AC system (inverter operation).
- The absolute total value of all the negative power generation must be larger than the total positive power generation. This is because the injected power in the DC system (negative sign) must be larger than the output due to losses.
- The user must select the power levels in such a way that a realistic level of losses is attained. This should include transmission losses in the DC cable and converter losses.
- The user must select a combination of active and reactive power that is within the P-Q diagram in figure 8.3.4. The figure describes the P-Q capability of a HVDC Light converter station as one single unit, and the defined P-Q operating area is therefore referred to the PCC bus. This includes the effect of the converter, series reactor, shunt filter and power transformer. The user must therefore decide the Qmin and Qmax limits of the generator on the filter bus so that the converter stations operating area on the PCC bus lies within the P-Q diagram, while keeping in mind the constant reactive power generation from the shunt filter and the reactive consumption of the transformer and *Z Source*. It should be noted that the given P-Q diagram is a guaranteed steady state possible operation area. Dynamically the limits may be increased somewhat for short time periods [9].

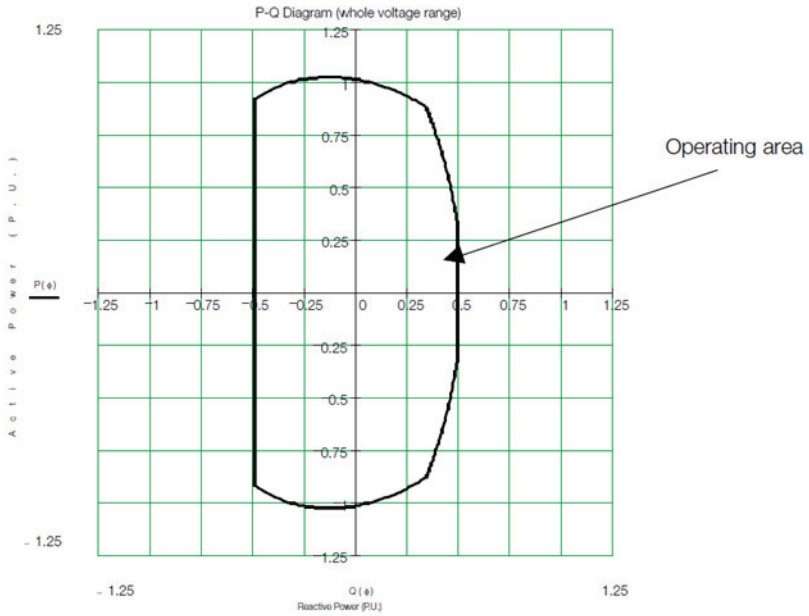

Figure 8.3.4: P-Q capability of HVDC Light [2]

8.3.2 Losses

As mentioned, the DC cables are not modeled in the power flow. The power combination of the converters has to be defined by the user so that the power balance in the DC system is maintained. The power going into the rectifiers must equal the power going out from the inverters and the power loss in the system, as described by equation (8.1).

$$P_{Loss} = -P_{total\_rectifier} - P_{total\_inverter} \tag{8.1}$$

The power loss in the system consists of the converter loss and the cable loss.

The converter losses are estimated to 0.0165 pu of nominal losses when the converters operate at nominal load. This can be seen by comparing the sending power with the receiving power when the system has a back-to-back configuration, i.e. no cable losses.

Table 8.3: Converter losses in HVDC Light [7]

Converter	DC voltage	DC current	DC Cable	Sending power	Receiving power (MW)					
types	kV	A	Cu in mm²	MW	Back-to-back	50 km	100 km	200 km	400 km	800 km
M7	320	627	300	408.1	396.4	391.4	388.8	382.9	370.6	
M8	320	1233	1200	802.2	775.7	772.8	770.1	764.2	752.5	729.0
M9	320	1881	2800	1224.4	1184.1	1180.8	1178.1	1172.2	1160.5	1137.0

$$P_{converter\_loss} = \frac{P_{sending} - P_{receiving}}{2 \cdot P_{sending}} = \frac{1224.4 - 1184.1}{2 \cdot 1224.4} = 0.016457 \cong 1.65\% \tag{8.2}$$

The converter losses are dynamically calculated as a constant part representing the no load losses, and a load dependant loss which is estimated to be linear with the load. It is assumed that the same estimation applies in the power flow. The no load losses are estimated to 0.3 pu of the nominal losses. The load losses are estimated to 0.7 pu of the nominal losses and decrease linearly with the transferred power.

The cable losses are calculated as:

$$P_{cable\_loss} = 2 \cdot R_{cable} \cdot I_{DC}^2 \tag{8.3}$$

Rcable is the cable resistance in one cable. The DC current of a two-terminal system is found by dividing the sending power on the DC side, $P_{sending\_DC}$, by the DC voltage multiplied by 2. The converter loss for one converter is subtracted from the power going into the rectifier in order to find the sending DC power. The DC voltage has to be multiplied by 2 because the given DC voltage level is pole to ground. In a multiterminal DC system finding every DC current is a little more complex, but the principle is the same.

$$I_{DC} = \frac{P_{sending\_DC}}{2 \cdot V_{DC}} \tag{8.4}$$

In reference [7], an overview of resistance at 20 ºC for different submarine cables is presented. In this thesis, data for the largest cable is used, with a copper conductor area of 2400 mm^2. This cable was chosen due to the transfer requirements of the system. If the M9 converters transfer the rated power and in addition the large wind farm offshore supplies the platform at the other offshore converter, the total power transfer at the middle cable section would equal more than 1320 MW. The cable chosen has a power rating of 1389 MW when the cables are laid close to each other on the sea bed, which is reasonable to assume from an economic point of view. The resistance for this cable is 0.0073 Ω/km at 15 ºC. According to [10][46] the resistance, within a typical temperature range for cable conductors, increase linearly described by:

$$R_\theta = R_{\theta 0}(1 + \alpha(\theta - \theta_0) \tag{8.5}$$

Where

θ	is the temperature
θ_0	is the reference temperature
α	is the temperature coefficient, 0.0038 [1/K] for copper
$R_{\theta 0}$	is the reference resistance
R_θ	is the actual resistance at the temperature θ

For the chosen cable and with an assumption that the working temperature of the cable is approximately 60 ºC the resistance in the cable is:

$$R_{60°C} = 0.0073 \cdot (1 + 0.0038 \cdot (60 - 15)) = 0.00855\ \Omega/\text{km} \tag{8.6}$$

As each of the cable lengths are modeled to be 200 km the resistance for each cable section is:

$$R_{cable} = 0.00855 \cdot 200 = 1.710\ \Omega \tag{8.7}$$

The system losses have to be calculated based on the different power flow situations of each scenario.

It is difficult to theoretically calculate the exact system losses that match the dynamic representation of the system. In these cases the HVDC Light model supplies a helpful function called PlossAdjust (active power loss adjusting). PlossAdjust is a parameter (value) that is created at initialization. It is defined as the difference between the initial dynamic losses and the power flow losses. The parameter is used to fine tune the power flow losses to get a perfect match between power flow and dynamic initialization. PlossAdjust is kept constant during the dynamic simulation. If the power flow losses do not match the dynamic losses at the initialization, and the difference is large, a warning message is written in the PSS®E output window.

The message looks like:

```
ch
"Relatively high PlossAdjust (xx MW) at dynamic initialization,
increase/decrease converter power from dc system in load flow"
```

The *"power from dc system"* is the power from DC to AC system, i.e. the same as the power given to the generators used as converter representation in power flow. Small changes in the power generation at the converters corresponding to the recommended PlossAdjust can then be made in the power flow case.

8.3.3 Simulation system specific power flow modeling

The HVDC Light Open Model from ABB includes example files for all the converter modules containing the default power flow values. Almost all these values are to be used unaltered as they are calculated by ABB and connected to the performance of the HVDC Light converters. This section will only describe the additional alterations that must be made specifically for this HVDC system.

In the power flow simulations, all the offshore AC grids require a swing machine to balance out the power flow in the isolated systems. The generator model of the offshore converter will be designated as swing machine (bus IDE = 3). This is the correct modeling decision as in real systems the VSC converter handles the power unbalances of these kinds of small interconnected grids. If the wind power generation offshore exceeds the offshore load, the converter will assume rectifier operation and deliver the excess power to the DC grid. Reversely if the offshore load is larger than the generation the converter will supply power from the DC grid to the offshore AC system (inverter operation).

The voltage level at the converters' PCC bus may be decided by the user. In this system the voltage level at the PCC is 400 kV for the onshore converters 1 and 4, 245 kV for converter 2 and 132 kV for converter 3.

The power generation and reactive power limits must be decided by the user specifically for each scenario in accordance with the P-Q diagram, as previously explained. The actual power values are listed in the description of the different scenarios.

The default values provided in the HVDC Light model are applied for all the other parameters related to the converters. This includes the generator, filter bus, fixed shunt, power transformer and PCC.

8.4 Dynamic modeling

8.4.1 User model CABBOM

The dynamic behavior of the multiterminal HVDC Light transmission is modeled by the user model CABBOM interacting with the representation in the power flow model as shown in figure 8.4.1.

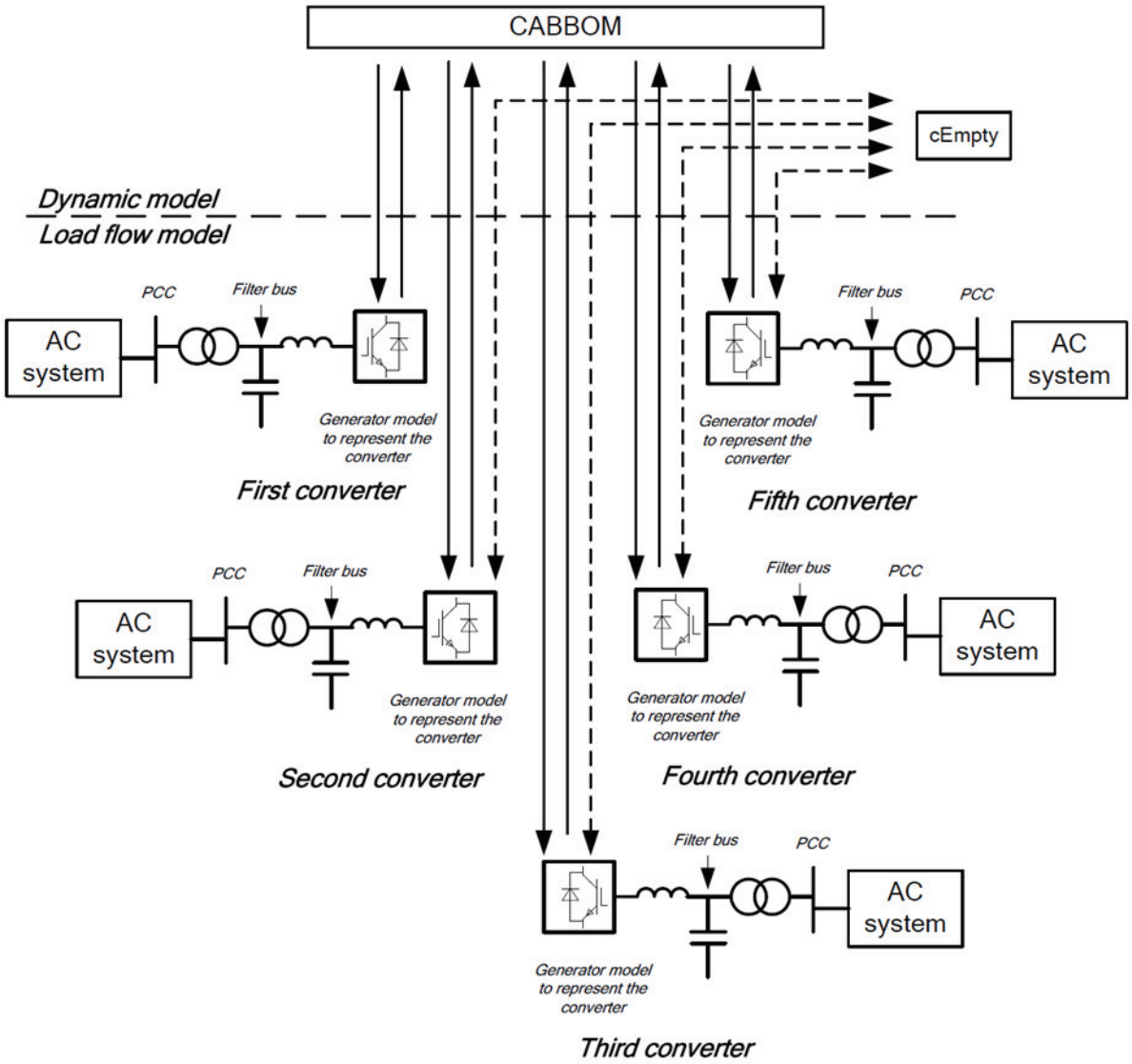

Figure 8.4.1: Power flow and dynamic interaction [3]

The user model CABBOM is applied as the "primary" dynamic model for the generator used as the first converter in PSS®E. Still CABBOM controls all the converters in the transmission.

An additional "dummy" user model cEmpty is applied as the "primary" dynamic model for each generator used as the second to fifth converters. Without this "dummy" user model,

PSS®E will disconnect the related converters in the dynamic simulation. This "dummy" model does nothing, the code is empty.

The possible theoretical number of converters in a multiterminal HVDC Light scheme is in principle not limited. However, for practical reasons, as the PSS®E VAR-vector is limited to 500 elements for a user model, the limit in this model is five terminals.

Normally, when using external user models in PSS®E, the creation of dynamically loaded library (DLL) is required in order to perform the dynamic simulations. This is not necessary in this case as the HVDC Light model includes a pre - compiled model specific user DLL. Therefore, provided that no other user models are applied, there is no need to create any additionally DLLs.

8.4.2 DC system

As mentioned in the chapter on power flow representation, the DC side is represented as a dynamic model only, i.e. no electrical representation in the power flow. Both the converters and the cables of the system have capacitances with corresponding time constants T according to equation (8.8)

$$T = 2 \bullet \frac{\frac{1}{2} \bullet C \bullet U_{DC,nom}^2}{P_{nom}} = \frac{C \bullet U_{DC,nom}^2}{P_{nom}} \tag{8.8}$$

Where:

- C is the capacitance pole to ground, i.e. converter capacitance or the cable capacitance in one cable [F]
- $U_{DC,nom}$ is the nominal DC voltage pole to ground [kV]
- P_{nom} is the nominal power of the system [MW]

T is the charging time of the capacitance [sec], and the DC model is based on simple integrator blocks according to equation (8.9)

$$\text{Integrator block} = \frac{1}{Ts} \tag{8.9}$$

The DC system is represented by a three node model between each converter as shown in figure 8.4.2. The nodes are numbered as 1, 2, 3, etc. Node 1, 3, 5, 7 and 9 represent the converter bus and node 2, 4, 6, 8 represents the "fictive" midpoint of the each cable branch. Each node is provided with a capacitance, for node 1, 3, 5, 7 and 9 this is typically the converter DC capacitance, and node 2, 4, 6 and 8 the cable branch capacitance. The

connections between the nodes are made by R-L circuits, where R and L correspond to the cable.

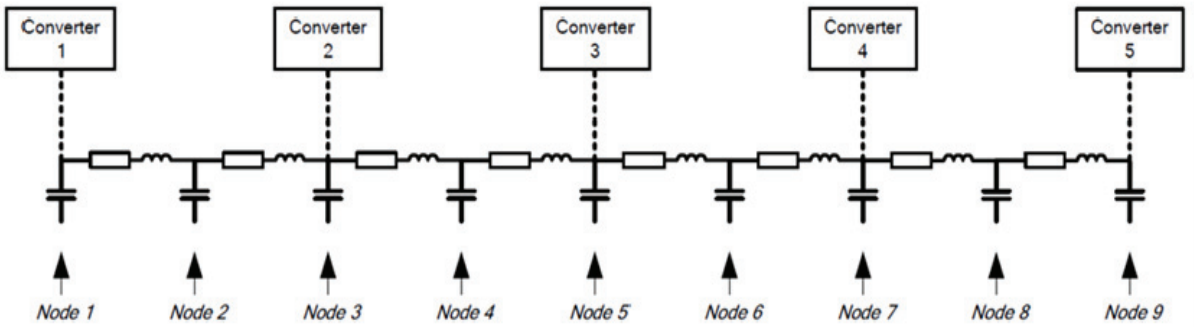

Figure 8.4.2: Dynamic DC system representation [3]

According to equation (8.8), the time constant is proportional to the capacitance of the cable, which is proportional to the length of the cable. Hence, there is a linearly dependency between the length of the cable and the cable's time constant. The time constant for the converters remains unchanged for increased cable length.

The DC voltage at the converter set to regulate the DC voltage is calculated as the integration of the net injected current via the integrator. The net current is the difference in active power injection by the converters, minus losses, divided by the DC voltage. For the other converters, the DC voltage is calculated by subtracting or adding the voltage drop due to the resistivity in the system.

8.4.3 Converter control model

The HVDC Light converter control recognizes the following actions:

- AC voltage control or reactive power control
- Active power control or DC voltage control
- Current output limitation
- Internal converter voltage limitations

It should be noted that only one converter in the DC system can be in DC voltage control. The DC voltage controlling converter acts as a slack bus in the DC system and is balancing the active power to maintain a proper DC voltage. It should also be noted that each converter can be independently set in AC voltage control or reactive power control.

The principles of the control system are shown in figure 8.4.3.

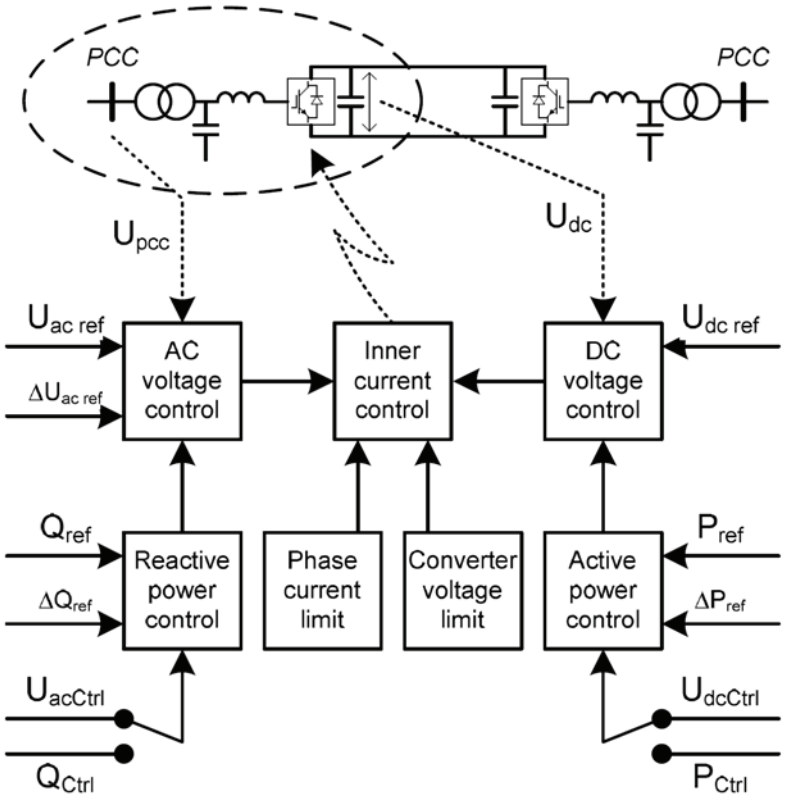

Figure 8.4.3: Converter control model [2]

8.4.4 Passive net operation

The offshore converters in the simulation model are set in passive net operation. This is a control mode to be used in the following applications:

- Black start, to restore an AC system after a black out.
- Offshore wind farm applications, passively receive all power generated at the wind farm.

The control principles for a HVDC Light converter in an offshore wind farm AC system are different from a converter connected in a large transmission system. The converter must control frequency and voltage in the offshore grid. This means the HVDC converter station functions as a swing bus in the offshore system and exchanges power with the offshore grid in order to regulate any unbalances in the isolated system. The passive mode of an HVDC Light converter is implemented with the functions for voltage and frequency control. This means that the passive net operation control mode is suitable for offshore wind farm application.

8.4.5 Chopper

During onshore faults, the possibility for power transmission from the DC system to the main grid onshore is limited. This transmission limitation has nothing to do with converter capability or control. The explanation is that the onshore AC voltage is very low, compare to equation (8.10) describing power transmission:

$$S = \sqrt{3} \cdot U \cdot I^{*} \tag{8.10}$$

In the case of an onshore AC fault combined with net power transmission from the offshore grid to the DC system, the active power from the DFIG generators must be reduced quickly to avoid charging of the DC cable, or burn the excess of power with a DC chopper. A DC chopper is a resistor in the DC system with high energy capability. The DC chopper evacuates the surplus of energy during network faults, when a power transmission is not possible [51].

The latter is found to be an attractive solution, and the possibility to include a chopper at the converter is implemented in the HVDC Light model.

If the onshore fault have a considerably longer time than specified for the chopper design, or is more frequent than expected, the chopper may be overstressed. The chopper capability is defined as the time in seconds, in which the chopper can maintain the DC system nominal power. The model is provided with a chopper supervision which is assumed to be used in combination with an offshore wind farm, and it is only possible to activate at a converter in DC voltage control mode and with a chopper activated (typically an onshore converter).

8.4.6 Time step recommendations

The dynamic behavior HVDC Light model is verified by comparison with identical test cases in PSCAD/EMTDC. The model performance showed:

- Virtually identical results as PSCAD/EMTDC for PSS®E time steps in the range 0.5-10 ms for typical transmissions between regular AC systems.
- A time step dependency in results, for a converter in the mode Passive Net operation.

The recommendations for PSS®E simulation time steps are as follows:

- For general system studies, 10 ms time step is acceptable. Using 5 ms or less, in most cases do not give any added value
- For cases including Passive net operation, a time step of 1 ms is recommended. Especially in cases with AC system recovery during “Black start” or with offshore wind farm applications.

In combination with the choice of the time step, there is a user parameter controlling the gain reduction (UacQGainRed) that may be useful. The parameter is to be used at weak systems, and specific for weak AC systems in combination with large time step (10 ms). At weak AC systems and a large time step there is a risk for numerical oscillations, using the gain reduction remove these oscillations.

8.4.7 Fault simulation and converter trip

Chapter 2.11 thoroughly describes aspects associated with faults in the DC grid and different protection schemes for multiterminal HVDC grids. Following a fault on a DC cable, the faulted cable should be disconnected using some sort of fast DC circuit breakers. The technology for high power DC circuit breakers is not developed yet and the HVDC Light model does not support simulation of a fault in the DC cables. However, an approximation can be made to simulate such a protection scheme. With reference to figure (3.1.1), a fault on the DC cable between converter 4 onshore and converter 3 offshore can be simulated by tripping converter 4 while keeping converter 3 in operation. The premise for this simplification is the existence of very fast DC circuit breakers of the correct power rating. This simplification involves that the DC system will contain the same capacitance after the fault even though the capacitance from the faulted cable realistically should be excluded. The effect of this is negligible according to Per – Erik Björklund of ABB HVDC power systems [9].

A converter has to be tripped in a correct way and this is done with the PSS®E command “Disconnect Bus”. For a proper Trip, both the filter bus and the power transformer (between filter bus and PCC bus) shall be out of service, both those activities are performed in one operation with the “Disconnect Bus” command on the filter bus.

The proper converter trip explained above will automatically change the integer constant parameter, named Debl, that denotes the converter’s operation from deblocked (normal operation, Debl = 1) to blocked (operation interrupted, Debl = 0).

After a converter trip, the converter can be set back in operation again. To do this both the filter bus must be changed from bus IDE = 4 (disconnected) to bus IDE = 2 (generator bus) and the power transformer must be changed back to “in service”. After that (immediately or after a certain simulated time) the converter control parameter Debl must be set to 1 again (Deblocked, normal operation. These operations must be performed “manually” by the user in the network case and the dynamic model.

8.4.8 Simulation system specific dynamic modeling

This section gives an overview of the actual inputs in the dynamic model for the system investigated in this thesis. The system is not a straight forward system to model as it combines both a multiterminal operation with different converter modules. Due to the relative complexity of the system and the lack of previous work done in modeling such a system with the HVDC Light model, several assumptions have had to been made. These assumptions were made in cooperation with Per-Erik Björklund, the reference person for the HVDC Light Open Model User Guide. The actual data sheet for the dynamic model is for restricted use. The parameters and values that are of specific interest for this system model are therefore explained in this chapter, instead of showing the complete system model data sheet.

Converter 1 is chosen to be the DC voltage regulating converter due to its proximity to the swing machine of the onshore grid, and thereby the converter connected to the strongest AC grid. The filter bus of converter 1 is chosen as the filterbus number for the HVDC Light converter model, i.e. the first converter which uses CABBOM as the primary dynamic model for the generator.

The number of converters in the system is inserted, in this case a total of 4 converters.

The reactive power control is set to AC voltage control for all the converters.

For the active power control option (Poption) the two offshore converters are set to passive net operation, PassNetOp. Converter 1 controls the DC voltage (UdcCtrl) and converter 4 is in active power control (Pctrl). For most simulations performed both converter 1 and 4 have choppers (ChopCtrl) activated at their converter stations. When this is not the case the alterations in ChopCtrl will be described clearly.

There is a control parameter called iCtrlParamAlt associated with the active power control option that should be altered from its default value in the case of offshore wind farm applications. This is done for converter 2 and 3.

For the nominal direct voltage, pole to ground, the HVDC Light standard value of 320 kV was used. This is the operating voltage of both the M7 and M9 modules that were used in the system model.

The choice for nominal power, in MW, for the DC system is not clearly given as in a two terminal system with equal sized converters. M7 converters operate at a nominal power of 405 MW and M9 operate at 1216 MW. As the M9 converters are the dimensioning components of the system the choice was made to set the DC system nominal power to 1216 MW. The value of the system's nominal power is important because it serves as the basis for other parameter values and results.

The cable and converter time constants are referred to the nominal power. The default value for the HVDC Light converter time constant is 0.004 seconds, regardless of converter module. This value was kept for the M9 modules, but the new time constants for the M7 modules are calculated as:

$$T_{M7\_converter} = 0.0040 \cdot \frac{405\ [\mathrm{MW}]}{1216\ [\mathrm{MW}]} = 0.00133 \text{ seconds} \tag{8.11}$$

Test simulations were performed with this time constant for the offshore converters and the following warning message was created:

```
************  ABB HVDC Light® ****************

Simulation time:                              0.2000002
User model: CABBOM, Dc System
Version: 1.1.9-2
Filterbus node number in PSS/E, Conv  1:          101
Filterbus node number in PSS/E, Conv  2:          102
Warning and Error messages

Total registered errors:                            2
Number of written error messages:                   2

1) Converter capacitance is to small, Modified to a minimum value,
DC-node No=           3
2) Converter capacitance is to small, Modified to a minimum value,
DC-node No=           5

*******  ABB HVDC Light®, End of messages CABBOM, Dc System *******
```

The smallest time constant that did not result in the message was empirically found to be 0.0016 seconds, and this was applied in the model. The impact this slightly higher value has on the simulations is assumed to be negligible.

Default time constants for the a 100 km long M9 cable was multiplied by 2 to find the correct time constant for the 200 km cables used in the system. As previously explained, the time constants for cables are approximately proportional with the length of the cable.

Another result of setting the nominal power equal to the rating for M9 is that the DC system's current reference will be:

$$I_{DC\_ref} = \frac{P_{DC\_nom}}{2 \cdot U_{DC\_nom}} = \frac{1216\ [\mathrm{MW}]}{2 \cdot 320\ [\mathrm{kV}]} = 1.90 \text{ kA} \tag{8.12}$$

While the current reference for the M7 converters offshore are:

$$I_{M7\_ref} = \frac{P_{M7\_nom}}{2 \cdot U_{M7\_nom}} = \frac{405\ [\mathrm{MW}]}{2 \cdot 320\ [\mathrm{kV}]} = 0.633 \text{ kA} \tag{8.13}$$

The consequence of this is that when plotting simulation results for the offshore M7 converters, the current will reach a value of 0.33 pu at full effect.

As explained in the section on power flow modeling, the value for the ohmic resistance in the DC cable is calculated to 1.71 Ω for each DC cable.

The value for the cable inductance is calculated from a default value to a value corresponding to the correct cable lengths, assuming a linear dependency between cable length and inductance.

8.5 Limitations of the HVDC Light Open Model

In the user guide for multiterminal HVDC Light Open Model the following is mentioned as a limitation of the model:

"In the HVDC Light Open model, the dc voltage control is not fully represented. The consequence of that is that for some cases, when the converter in dc-voltage control operates as rectifier, sometimes after a disturbance, the dc system is not capable to recover. The situation is characterized by a dc voltage at approximately 0.9 pu and all converters are in constant modulation index limitation.

The recommendation when using the HVDC Light Open model is to avoid the combination:

- *Rectifier operation*
- *DC-voltage control*

It should be pointed out, that this is not a limitation of the HVDC Light technology, rather a limitation of the Open model."

This would naturally cause a restriction on the simulations that could be performed with the system model. In the case of low wind power generation, the onshore converter in UdcCtrl would also be in rectifier mode, supplying the offshore petroleum platforms.

ABB was contacted and inquired on how often this limitation occurred. The response was that they had noticed that the multiterminal Open Model could in some cases have a poorer performance if the UdcCtrl was assigned to a converter in rectifier operation. This happened mainly after an AC fault in or near the converter. The limitation is only discovered in the multiterminal Open Model, it is not found in the "Detailed model" or the Open Model 2 terminal.

Several test simulations was performed with converter 1 operating in UdcCtrl and as a rectifier while being subjected to a nearby AC fault, and the model behavior described in the user guide never occurred. As the limitation does not seem to be present in the created system model, and the detection of the limitation is easily detected by a constant DC voltage of

around 0.9, the decision was made to continue the simulations with the multiterminal HVDC Light Open Model.

Other limitations with the model that restrict the possible simulations are:

- The model does not have the possibility to simulate a DC fault, and the subsequent protection schemes of the MTDC.
- The model has only implemented a master – slave active power control scheme, not the *"Voltage margin method merged with DC voltage droop"*, as described in chapter 2.11.

8.6 Errors discovered in the model

During the work done with the HVDC Light model, a few irregularities was discovered with the model. ABB have been notified and the following will be more thoroughly investigated and corrected in the next version of the model.

- The model documentation [2] explains that a valid converter trip involves both disconnecting the filter bus and putting the power transformer out of service. It states that if only the filter bus is disconnected, then the transformer will remain in service and PSS®E will handle this similar to a solid fault on the filter bus. However, simulations performed showed that the transformer is put out of service following a disconnection of the filter bus.

- When plotting the electric power generation of a converter that is subjected to a trip (disconnect bus), the plotted value of $P_{electric}$ will remain constant and equal to the pre fault value even after the converter trip. This is just a problem in the plotting, and not an error in the simulation model. This has been investigated, and the transferred power and converter current falls to zero as they should do.

- The following warning message occurred during dynamic initialization. It states that the reference current limit (0.3286204) is initialized above system current limits (1.077440), when it is clearly not. This did not prevent dynamic simulations, and was ignored on the advice from reference [9].

```
************  ABB HVDC Light® ****************

 Simulation time:                          -2.0000001E-03
 User model: CABBOM
 Version: 1.1.9-2
 Converter number:               1
 Filterbus node number in PSS/E:                    101
 Warning and Error messages

 Total registered errors:                             1
 Number of written error messages:                    1

   1) IREF_LIM initialized above current limit:  0.3286204,   1.077440

 *******  ABB HVDC Light®, End of messages CABBOM, Converter *******
```

9 Petroleum platform modeling

9.1 CLOD model

The petroleum platforms are represented in the power flow simulations as a normal load, specifying the active (MW) and reactive load (MVAr). In the dynamic models the platforms are represented using the PSS®E model CLOD. The CLOD type models replace all constant power, current, and admittance load with a composite load consisting of induction motors, lighting and other types of equipment such as would be fed from many typical substations. It is intended for use in situations where it is desirable to represent loads at the dynamic level, as distinct from the algebraic characteristic level used in power flow, but where detailed dynamics data is not available. The models allow the user to specify a minimum amount of data stating the general character of the composite load. It uses this data internally to establish the relative sizes of motors modeled in dynamic detail and to establish typical values for the detailed parameter lists required in the detailed modeling.

The make-up of the composite load is specified by CON(J) through CON(J+4) of CLOD. These CONs specify the percentage of the total load (as shown in the power flow case) that is due to large motors, small motors, magnetizing current, discharge lighting, constant MVA devices, and voltage sensitive load. The percentages may be specified arbitrarily on the basis of the user's knowledge of the nature of the particular plant, feeder, or substation.

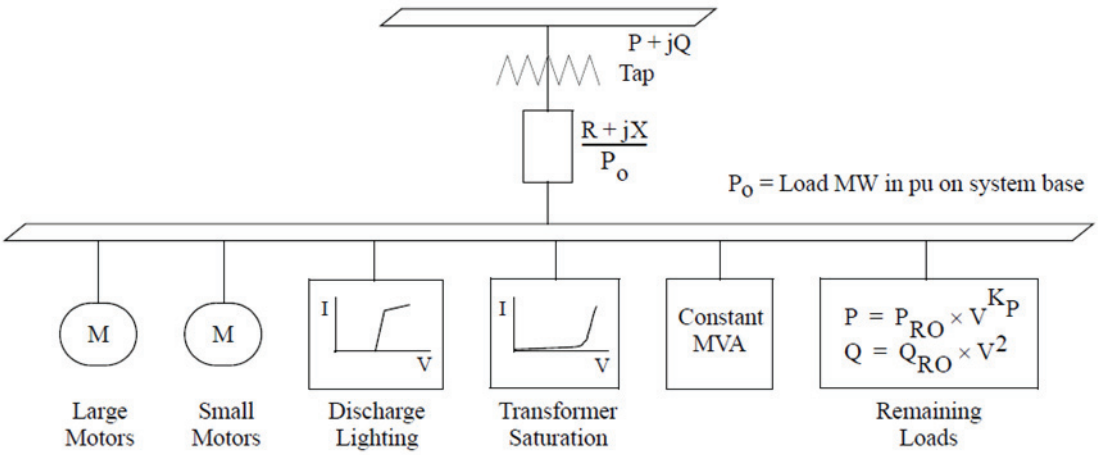

Figure 9.1.1: Illustration of the CLOD model [1]

The parameters (CONS) needed to model the electrical load on the petroleum platforms are based on a simplified model of the Norwegian platform Gjøa. The single line diagram (SLD) and additional information are supplied by Statoil [5], but several assumptions and simplifications have been made. The large motors have been defined as rotating motors not connected through a converter and larger than 0.5 MW. The value for small motors and

discharge lightning have some uncertainty, but their combined size relative to the total load is known, and an assumption has been made on their internal load allocation. The PSS®E user manual informs that the value of CON(J+2) stating the percentage of load current due to magnetizing should not exceed about 10 %. For the platform model this value is assumed to be 1 %, which includes both the main platform transformer and smaller distribution transformers [4].

The largest components of the platform load are the compressors powered through converters. Due to the converters this load will not directly experience voltage changes in the AC grid on the opposite side of the converter. The impact of voltage changes depends on how the converter controls the load voltage in relation to the changes in the grid voltage. Seen form the AC grid, the combination of compressor and converter will have an approximately constant active effect demand when experiencing moderate voltage variations. A simplification has therefore been made that this part of the platform load is modeled to behave as a constant MVA load in the CLOD model. All real loads remaining on the bus after applying the specified percentages varies as the voltage is raised to the K_P power. In this modeling there is, however, no remaining load, and the value of K_P is put to zero. By entering R and X values in per unit (pu) of the load MW base, a user may add some distribution transformer impedance or distribution line impedance. These values are set to zero, but values for the cable supplying the platform with power have been included in the model as explained in the chapter on subsea cable parameters.

Table 9.1: Platform model parameters [5]

CONs	Value	Description
J	24.02	% large motor
J+1	2.05	% small motor
J+2	1.00	% transformer exciting current
J+3	1.85	% discharge lighting
J+4	72.08	% constant power
J+5	0.00	K_P of remaining
J+6	0.00	Branch R (pu on load MW base)
J+7	0.00	Branch X (pu on load MW base)

I, 'CLODxx', LID, CON(J) to CON(J+7) /

Busnr 'CLODBL' 1 24.02 2.05 1.85 1 72.08 0 0 0

(LID is an explicit load identifier)

Figure 9.1.2: CLOD input in dynamic file

9.2 Problems with the model

In the implementation and test runs of the CLOD model an unexpected dynamic behavior was discovered.

The CLOD model with the given petroleum platform parameters is supposed to consists of around 26 percent rotating machines, se table 9.1. The model therefore possesses a large amount of inertia which means that the platform load should be able to ride through a short duration fault in island operation. The voltage on the connected bus would naturally fall during the fault, but the load should still be connected to the system. This is also the models behavior in most cases, but there is one event where this does not happen.

After a disconnection and following reconnection of neighbouring buses, it appears that the CLOD model disappears from the system. The model data sheets indicate that the model is still in service in the system, but the effect of the model is no longer present. The power consumption from the load represented by the CLOD model falls to zero.

As described in the chapter on the HVDC Light model, the correct way to trip a converter in the VSC model is to use the PSS®E command disconnect bus on the filter bus; this is buses 5 and 6 in the figure 9.2.1.

One intended area of application for the simulation system created is the investigation of offshore island operation during a short duration trip of the converter. This could then be a problem as the converter is tripped with the disconnect bus command, and the CLOD model does not exhibit a realistic dynamic response following a disconnection of neighbouring buses. To illustrate the problem, the following graphs depict the response of the CLOD model to different disturbances, with reference to the example system in figure 7.2.1.

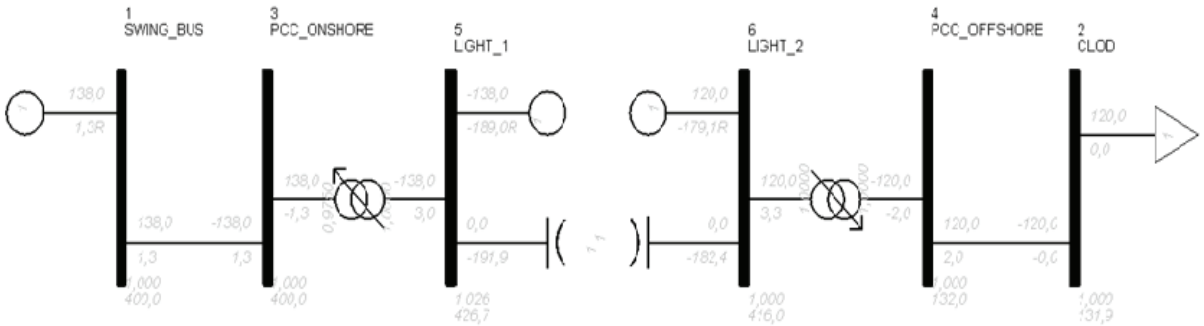

Figure 9.2.1: SLD of CLOD test simulation

Simulation 1:

Time	Event
0.00	Normal operation
0.20	Bus fault on bus 2 (where CLOD is connected)
0.30	Bus fault cleared

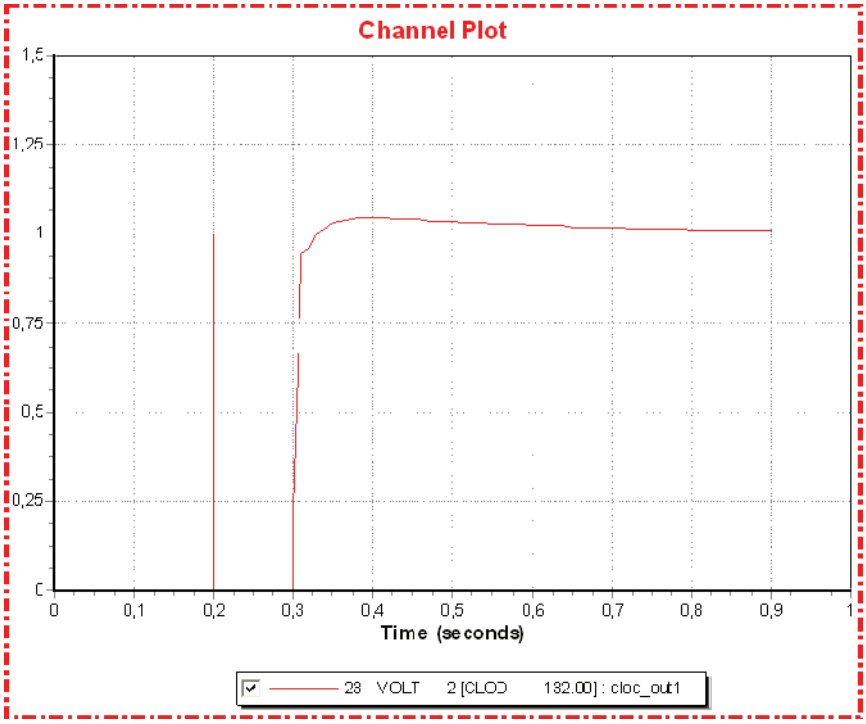

Figure 9.2.2: Simulation 1, CLOD voltage [pu]

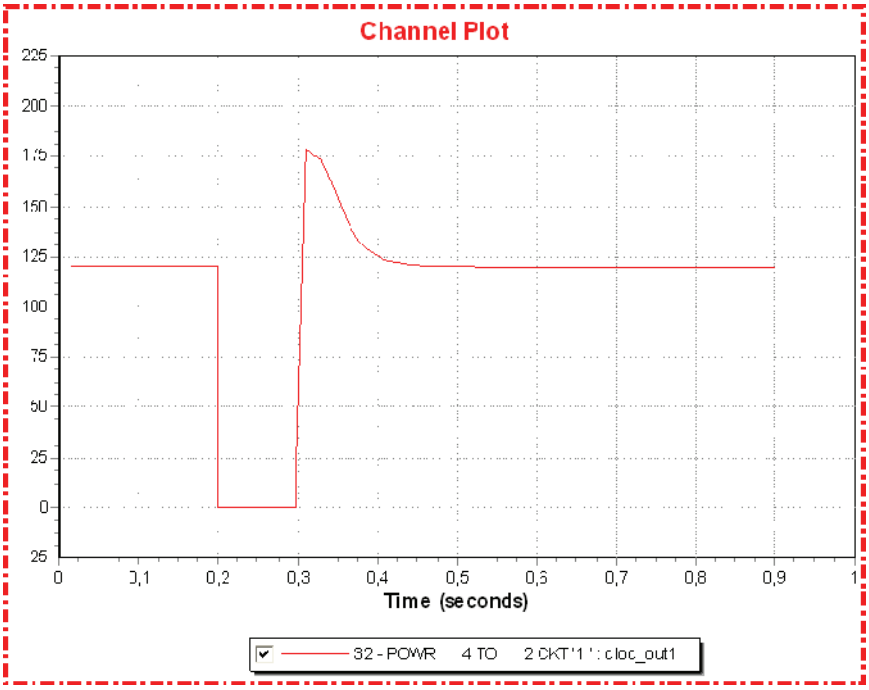

Figure 9.2.3: Simulation 1, CLOD power consumption [MW]

Simulation 2:

Time	Event
0.00	Normal operation
0.20	Bus fault on bus 6 (filter bus)
0.30	Bus fault cleared

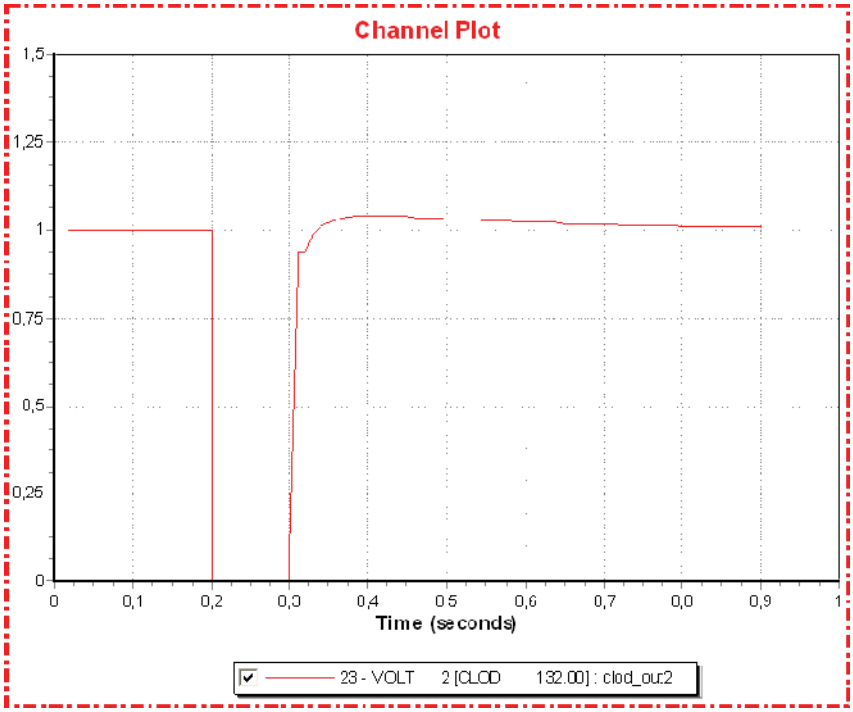

Figure 9.2.4: Simulation 2, CLOD voltage [pu]

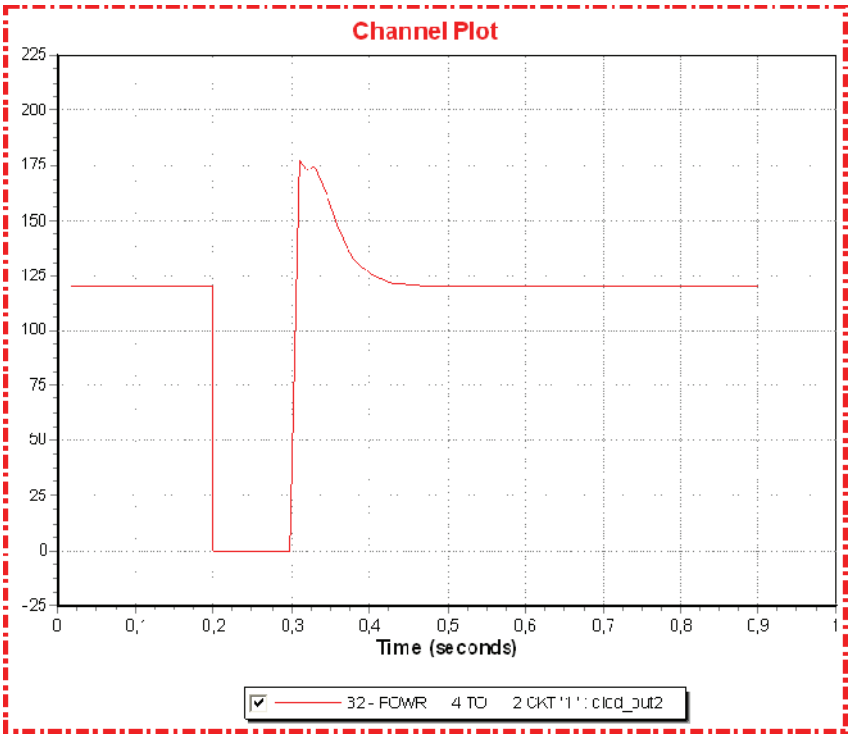

Figure 9.2.5: Simulation 2, CLOD power consumption [MW]

Simulation 3:

Time	Event
0.00	Normal operation
0.20	Disconnect bus 2 (where CLOD is connected)
0.30	Bus 2 reconnected and branches back in service

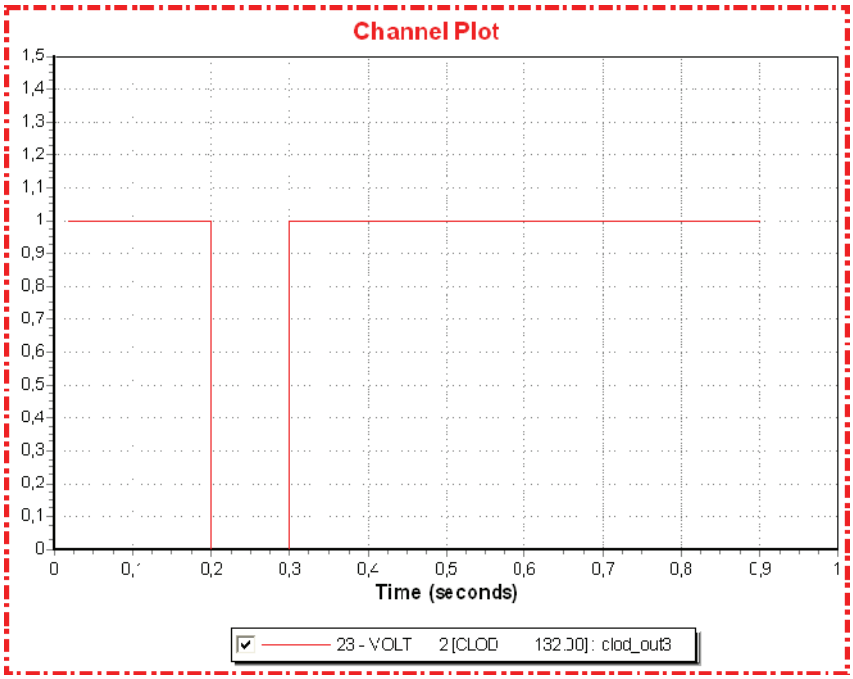

Figure 9.2.6: Simulation 3, CLOD voltage [pu]

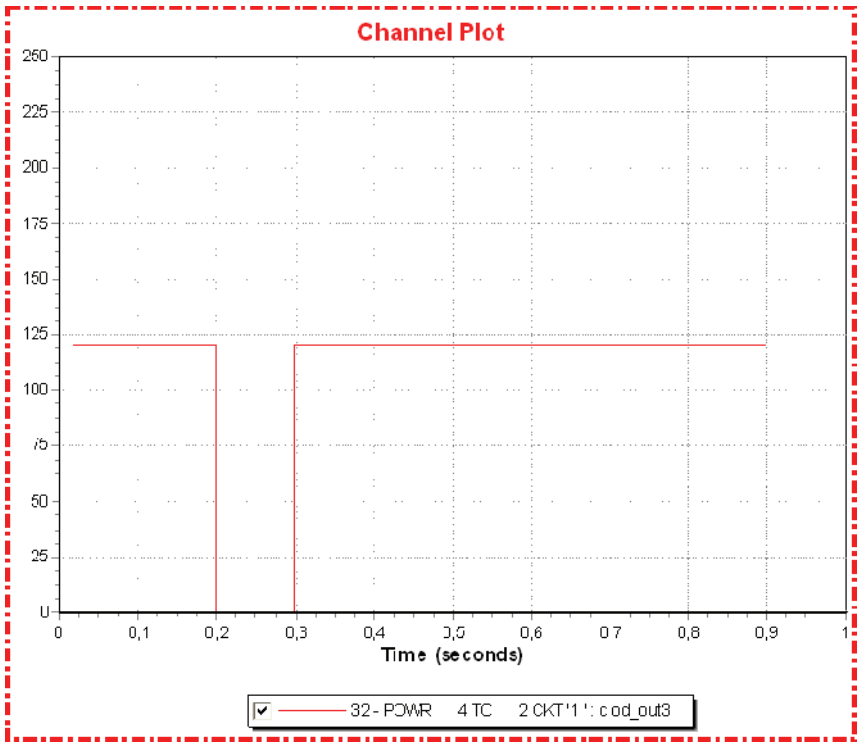

Figure 9.2.7: Simulation 3, CLOD power consumption[pu]

Simulation 4:

Time	Event
0.00	Normal operation
0.20	Disconnect bus 6 (trip converter)
0.30	Converter, buses, transformer and branch offshore back in operation

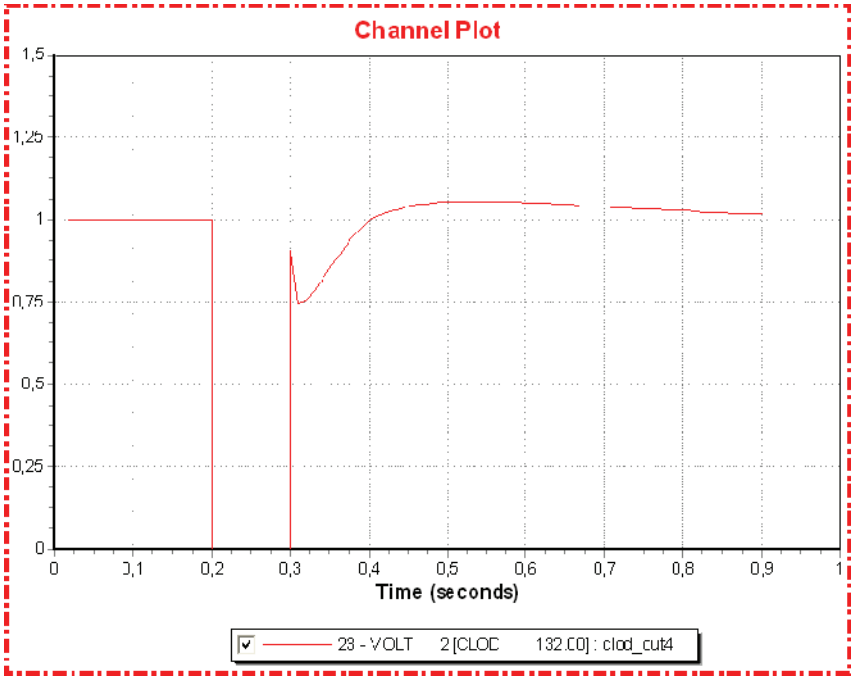

Figure 9.2.8: Simulation 4, CLOD voltage [pu]

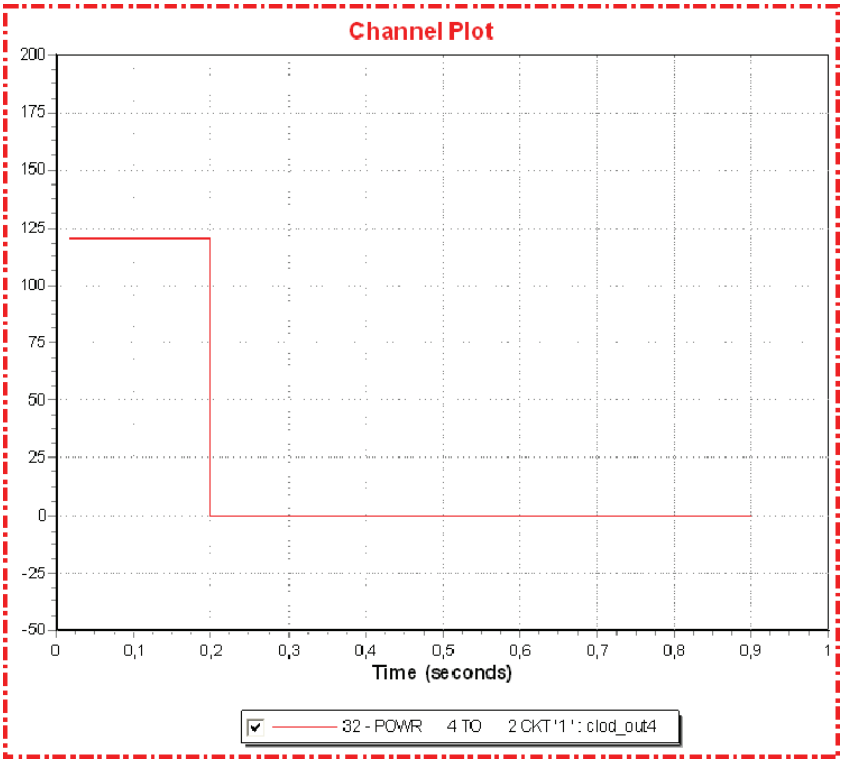

Figure 9.2.9: Simulation 4, CLOD power consumption [MW]

The figures illustrating the voltage on the CLOD bus and power to the CLOD load in the event of a bus fault, on either the CLOD bus or a bus close by, show that the CLOD model exhibits a realistic and reasonable dynamic behavior in these cases.

In the case where the CLOD bus is disconnected and subsequently reconnected, the power consumed and voltage does not display a reasonable dynamic performance following the disturbance. The voltage and power simply rises to the pre fault values without an oscillatory transient settling. However, the power consumption in the load is still present in the system, i.e. the load is still in service. From the last figure it is clear that the load is no longer active in the system as there is no power consumption at the CLOD bus following the reconnection of the system. This behavior results in a difficulty analyzing dynamic island operation following a short duration trip of the offshore converter.

The PTI support at Siemens in Trondheim was contacted about the problem of why this load model that contains a large portion of rotating machines is not able to remain in service during such a nearby disconnection, but an explanation was not discovered.

The solution to this problem was the implementation of more rotating machines in the offshore grid in the form of the wind machines. The inertia of the wind machines enables the offshore grid to remain operational following a trip of the interconnecting converter as the wind farm can regulate active and reactive power to support the grid. Even in the case of low pre fault power generation at the wind farms the CLOD model remains in service while the converter is disconnected. The dynamic behavior offshore, in the case of a small wind farm with very low wind power generation, does not display an acceptable performance with respect to power balance and voltage level. This is more thoroughly described in the chapter on dynamic simulations. However, the important objective at of keeping the CLOD model in operational in the simulation model is solved. It is considered that this solution to the CLOD problem does not compromise the value of the simulation model, as the wind farms offshore was intended to be modeled anyway.

The following figures illustrate the dynamic behavior of the CLOD model when the wind farm is implemented offshore. As seen in figure 9.4.12, the CLOD model remains operational after a disconnection of the nearby converter bus.

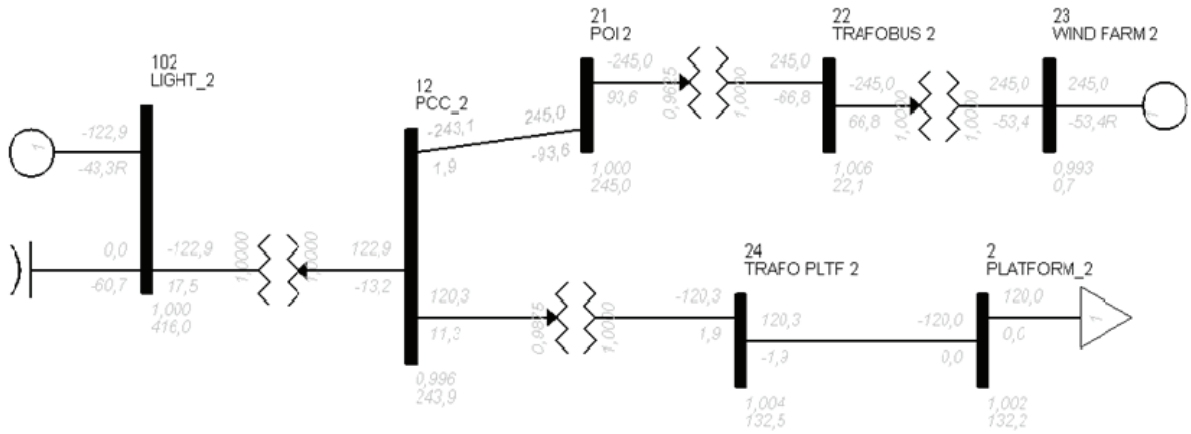

Figure 9.2.10: Offshore area consisting of both wind farm and petroleum platform

Simulation 5:

Time	Event
0.00	Normal operation
0.20	Disconnect bus 102 (trip converter)
0.30	Converter, buses, transformer and branch offshore back in operation

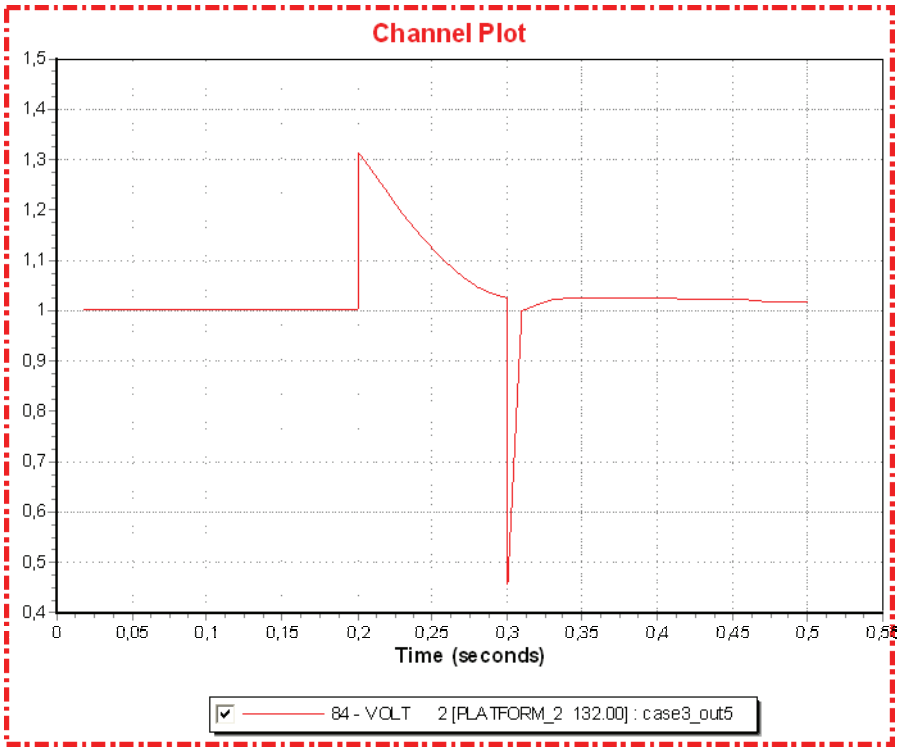

Figure 7.2.11: Simulation 5, CLOD voltage [pu]

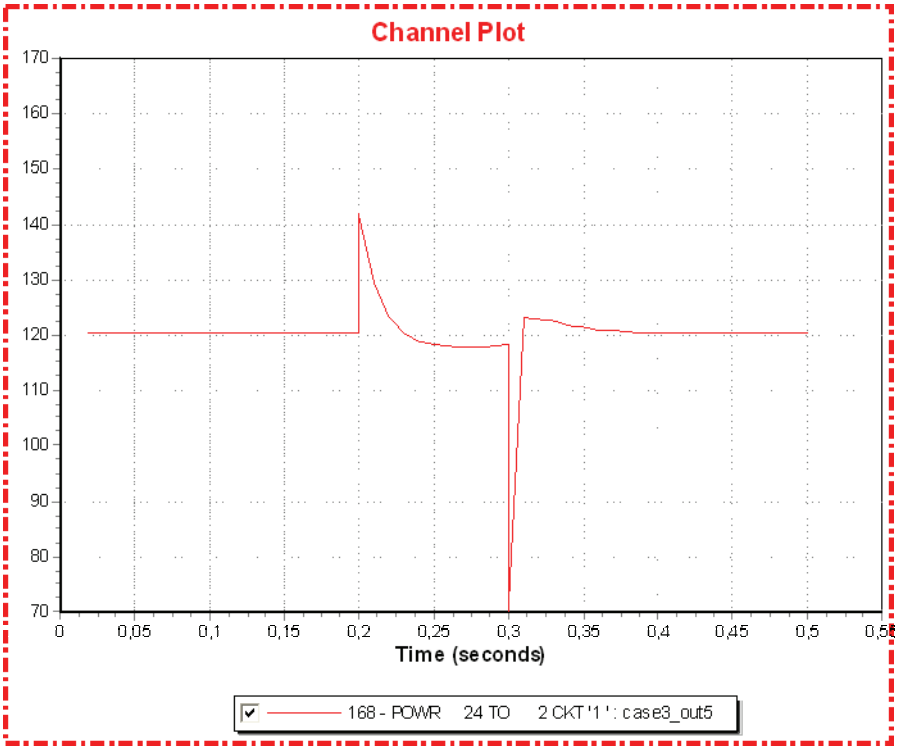

Figure 9.2.12: Simulation 5, CLOD power consumption [MW]

An alternative solution could have been to model the petroleum platforms in more detail using specific models for the representation of rotating machines and compressor converters. The necessary platform parameter data was not available so this alternative was not chosen, but could be a possible suggestion for further work on the simulation model.

10 Simulation model

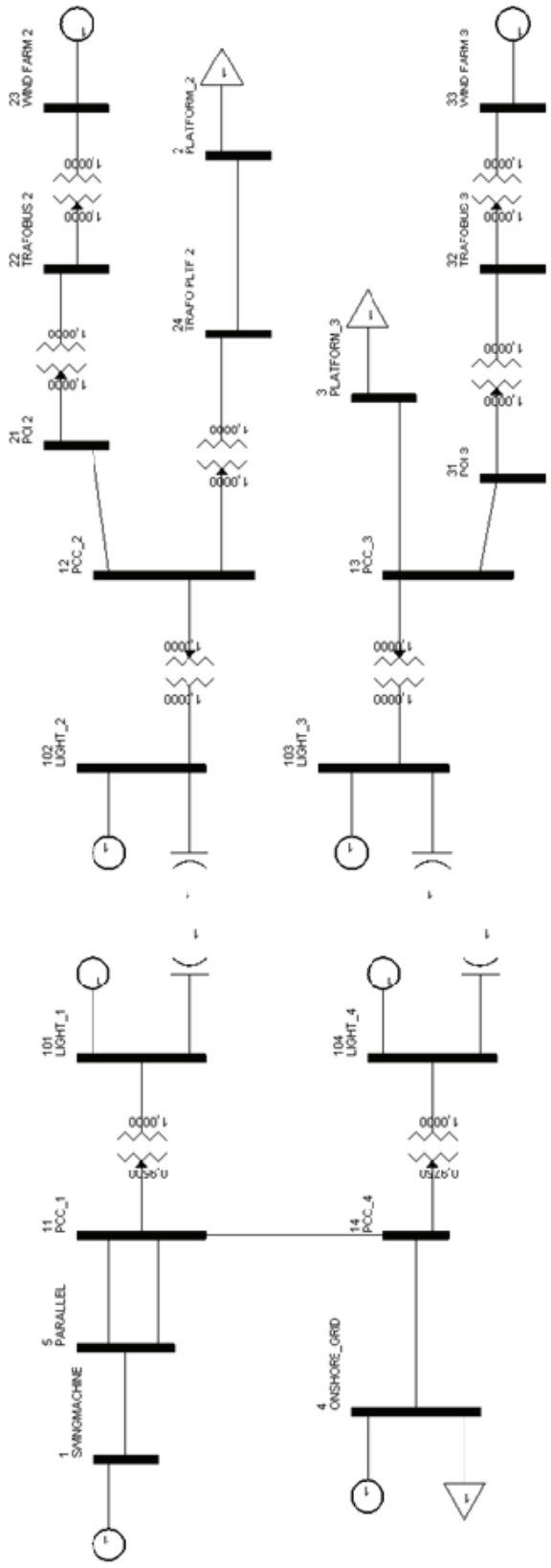

Figure 10.1.1: SLD of the developed simulation model

Figure 10.1.1 depicts the single line diagram (SLD) of the simulation model developed for analysis in PSS®E. The model is created according to the suggested power system described in chapter 3, see figure 3.1.1.

The voltage source converters 1 to 4 in the system are given the names Light_1 to Light_4 in the simulation model, as they are modeled using the HVDC Light dynamic model.

Larger figures of the separate AC grids of the model can be found in appendix D.

11 Description of intended simulations

11.1 Power flow scenarios

The objective for the simulation model developed in this master thesis is to investigate general principles of operation for a MTDC grid. In order to fully examine the functionality of the modeled MTDC, the simulation model must be subjected to a variety of disturbances under different power flow situations. As a result, three different power flow scenarios have been created using almost the exact same dynamic system model. These power flow scenarios are the basis for all the dynamic simulations performed in this thesis. The different power flow scenarios will be described in this chapter.

As described in chapter 3, the installed active effect at the offshore wind farms is 250 MW for the large wind farm at offshore grid area 2 and 100 MW for the small wind farm at offshore grid area 3. The active load at each petroleum platform is 120 MW. Bus number 4, intended to represent a portion of the onshore grid, has both a load and a generator connected. The generator is in the power flow set to generate 200 MW and the load consumes 900 MW. The reason for the relative large load on bus 4 is to create an onshore grid that is in the same magnitude as the rating of the onshore converters. The generator on bus number 1 is the swing machine of the onshore system, and represents the remaining portion of the underlying onshore grid.

With this as a basis for the systems AC components the following power flow scenarios are defined and created:

Large wind generation:

The wind farms generate 98 % of the installed effect, i.e. the large wind farm generates 245 MW and the small wind farm generates 98 MW.

Small wind generation:

The wind farms generate 15 % of the installed effect, i.e. the large wind farm generates 37.5 MW and the small wind farm generates 15 MW.

Large power transfer:

The wind farms produce 98 % of the installed effect. The generator on bus number 4 is removed, but the 900 MW load on bus 4 remains.

The motivation for the large and small wind generation scenarios is to examine the dynamic behavior of the HVDC grid both when the power flow is in the direction from onshore to offshore grids and reversely offshore to onshore. There is a net surplus of power offshore in the large wind generation scenario, and a net deficit in the small wind generation scenario.

The large power transfer scenario is used to investigate a situation with large onshore power transfer, and the possible advantages that the VSC HVDC grid provides in the case of an onshore disturbance. The generator on bus 4 is removed to prevent it from increasing its power output to meet the load demand on the same bus during the disturbance in the onshore grid. Thus, maintaining the need for a large onshore power transfer from the generator at bus 1 to the load at bus 4.

The active power at converter 4, operating in Pctrl, is set to zero for all the power flow scenarios. This is primarily done to more clearly investigate the change in the converter operation following the disturbance. However, in both the large power transfer and large wind generation power flow scenarios, the active power at converter 4 should be set to zero if the objective was to minimize the active losses. This is because the excess power from offshore area 4 has a shorter transmission distance to converter 1 compared to converter 4.

Table 11.1: Power flow scenarios

Power flow scenario	**Wind farm 2**	**Wind farm 3**	**Petroleum platforms**	**Onshore load, bus 4**	**Generator bus 4**
Large wind generation	+245 MW	+98 MW	-120 MW	-900 MW	+200 MW
Small wind generation	+37.5 MW	+15 MW	-120 MW	-900 MW	+200 MW
Large power transfer	+245 MW	+98 MW	-120 MW	-900 MW	disconnected

The power flow scenarios were solved before the dynamic simulations could be performed. The power flow solutions are not included in this report as the results are of no analytical importance when it comes to analyzing the MTDC. The power flow model is created using standard PSS®E system components, and the correct power flow in the MTDC was calculated as described in chapter 8.3, and using PlossAdjust. Before performing the dynamic simulations, the generators have to be converted to Norton equivalents, and the loads have to be converted according to their voltage dependency. The loads can be converted as constant current, constant admittance or constant power loads. Table 11.2 shows the load composition that was used in the conversion. The values are based on recommendations from Statnett SF for normal loads.

Table 11.2: Load composition in a normal load [16]

Load representation	**P [%]**	**Q [%]**
Constant power	40	30
Constant current	40	20
Constant admittance	20	50

11.2 Overview of the dynamic cases

This master thesis aims to analyze and describe the principles of operation for the multiterminal HVDC grid (MTDC) and interaction between the MTDC and the AC grids. To do this, a number of different event cases have been defined to help investigate the dynamic behavior of the system following a disturbance or a dynamical alteration of the model. The motivation for each of the cases is to highlight a certain response in the system model, as explained in the presentation of the cases.

Table 11.3: Overview of dynamic simulation cases

Case	Event	Investigate the … (motivation)	Power flow scenarios
Case 1	Disconnection of converters and alterations of DC voltage control	-response and behavior of UdcCtrl converter (DC slack bus). -HVDC Light model's response following the disconnection.	-Large wind gen. -Small wind gen.
Case 2	Disturbance in the onshore AC grid	-effect on the offshore AC grids. -behavior of the HVDC system, including converters.	-Large wind gen. -Small wind gen.
Case 3	Disturbance in the offshore AC grids	-effect on the onshore AC grid. -behavior of the HVDC system, including converters.	-Large wind gen. -Small wind gen.
Case 4	Disconnection (trip) of the offshore converter stations	-dynamic island operation of the offshore AC grids seen in relation to the protection schemes for a MTDC grid.	-Large wind gen. -Small wind gen.
Case 5	Disruption of a large offshore wind power generation	-performance in the affected offshore AC grid. -response of the HVDC system.	-Large wind gen.
Case 6	Disconnection of both onshore converter stations at the same time	-effect on the DC voltage with either a net power surplus or a net power deficit in the offshore areas. -behavior of the choppers.	-Large wind gen. -Small wind gen.
Case 7	Fault in the long onshore line (bus 11 - 14) during large onshore power transfer	-use of the VSC MTDC system for security of supply and stability support in the onshore grid.	-Large power transfer
Case 8	Onshore AC disturbances with various scenarios for large onshore power transfer	-stability improvements brought on by the presence of the VSC HVDC during various large power transfer scenarios.	-Large power transfer -Large power transfer scenario modified

The disturbances subjected to the system in each case are individually chosen for each separate case, depending on the behavior desired to be highlighted and investigated. In all the

cases investigated, there is performed more than one dynamic simulation; either the system is subjected to various disturbances, or to different power flow scenarios. The argument for this is that it enables a comparative analysis of the results.

12 Dynamic simulations

This chapter is a description of the various dynamic simulations performed with the simulation model, and an analysis of the results. The explanations and analysis of the system behavior is based on the simulation results combined with information from the HVDC Light documentation [2][3] and discussions with Per-Erik Björklund of ABB [9]. For simplicity the multiterminal VSC HVDC system in the model is referred to as the MTDC. This includes both the cables and converter stations.

The events in the simulation description often include the terms bus fault and line fault. For the simulations performed in this master thesis the following definitions apply:

- A bus fault is a three-phase short circuit which is applied to the busbar with impedance equal to zero, so that the voltage at the connection point is zero during the fault.
- A line fault is a three-phase short circuit applied at the given line with impedance equal to zero, and the fault occurs close to the first mentioned busbar.

The time in the event description of each simulation is given in seconds.

The system values selected for plotting in this report vary between the cases depending on the attention for the analysis. However, in almost all the cases the converters' active and reactive power generation and the DC voltage are plotted as these values are very important for understanding the response and performance of the MTDC, which is the main motivation for the simulations performed in this work.

The power flow scenario applied in each simulation is put in parenthesis just above the event description.

The system power reference is 100 MVA.

12.1 Case 1

During the dynamic simulations of case 1 it is important to remember that the starting values for the converters active power control option (Poption) is

Converter 1 - UdcCtrl = DC voltage control
Converter 2 - PassNetOp = Passive net operation
Converter 3 - PassNetOp = Passive net operation
Converter 4 - Pctrl = Active power control

The reader should also keep in mind an error discovered in the plotting of dynamic results for the converters, as described in chapter 8.6. After a converter is tripped, the plotted power generation of the converter does not fall to zero, but remains constant and equal to the pre fault value. This is just a problem in the plotting and not an error in the simulation model, the transferred converter power and converter current falls to zero as they should do. This behavior is illustrated in the first simulation by a comparison of the figures plotting converter power and converter current.

Simulation 1 (Large wind generation)

Time	Event
0.00	Normal operation
0.20	Disconnect (trip) converter 2

Simulation 1 describes the operation of the converter set in DC voltage control (UdcCtrl). Prior to the disturbance, offshore area 2 has a net power surplus of 122.9 MW that is delivered to the HVDC system and transferred to converter 1 and 3. Offshore area 3 has a net power deficit of 22.6 MW that is supplied by the HVDC system through converter 3. As converter 2 is disconnected, the pre fault power balance of the HVDC system is disturbed because the power into the MTDC from converter 2 disappears and the power extracted from the MTDC at converter 3 remains the same. As a result of this new power situation, the stored energy in the capacitances of the MTDC, i.e. the converter and cable capacitances, is discharged through converter 3. The discharge of the capacitances leads to a decrease in the DC voltage for the MTDC, as described in chapter 2.8 and 2.10.2. The voltage decrease of the entire MTDC is detected by the DC voltage controlling converter, in this case converter 1, which changes its operating point in the P-Q diagram to increase the power delivered to the MTDC. The objective of converter 1 is to create a new power balance in the MTDC and recharge the system capacitances, thereby restoring the DC voltage to the desired value. The onshore AC system connected to converter 1 suddenly experiences a change in the power exchange with converter 1. Going from delivering power to the onshore grid pre fault, converter 1 absorbs power from the onshore grid after the disturbance, and this change in power flow occurs very rapidly. This leads to the general rule of thumb for VSC HVDC systems that the converter selected for DC voltage control should be the converter connected to the strongest, and thereby most flexible AC grid.

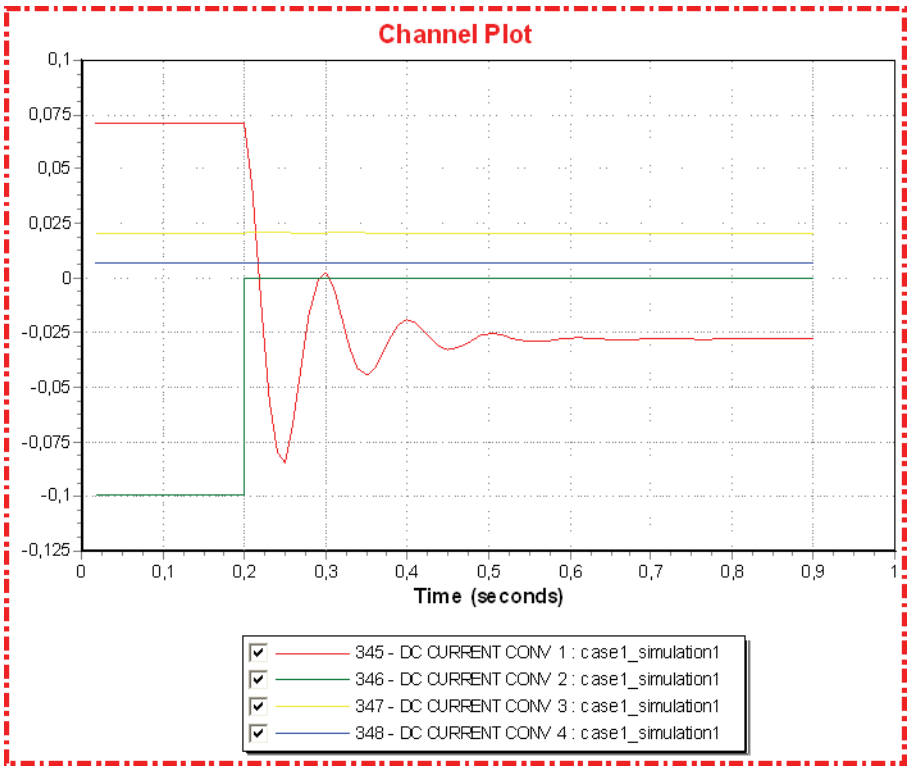

Figure 12.1.1: Converter DC current [pu]

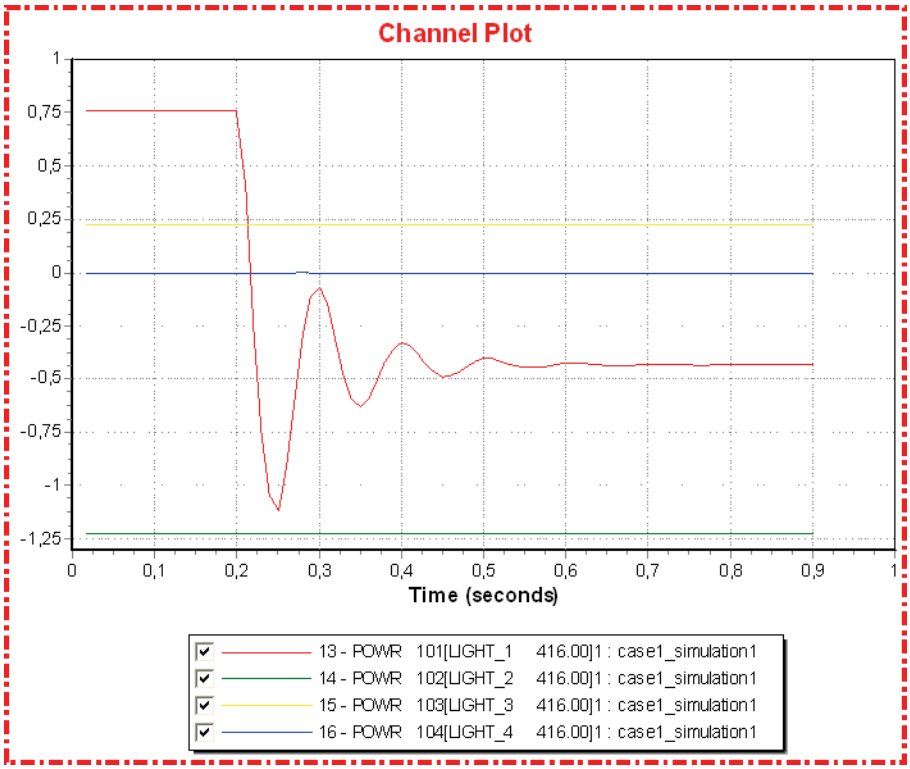

Figure 12.1.2: Converter active power [pu]

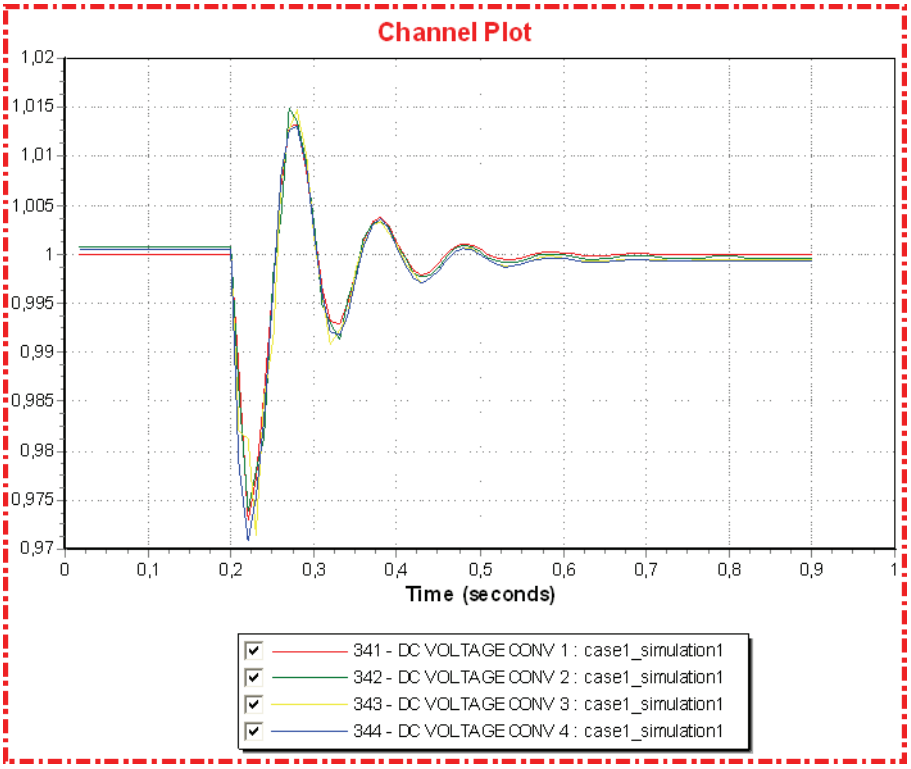

Figure 12.1.3: Converter DC voltage [pu]

Simulation 2 (Large wind generation)

Time	Event
0.00	Normal operation
0.20	Disconnect (trip) converter 1 (UdcCtrl converter)

In this simulation, converter 1 operating in UdcCtrl is disconnected. The immediate new situation following the disturbance is that no power results in a stop of power delivery onshore from the MTDC while there is a net power injection to the MTDC offshore of approximately 100 MW. The result is that more energy is stored in the MTDC, the system capacitances are charged above their desired set point and the DC voltage increases. About 0.6 seconds following the disturbance the DC voltage reaches 1.1 pu. At this point converter 4, set to operate in Pctrl, changes its P-Q operating point and starts delivering power to the onshore grid, thus creating a power balance that maintains the DC voltage at 1.1 pu. The action of converter 4 is not a general principle of operation for converters in Pctrl, but an "emergency UdcCtrl" build into the ABB HVDC Light model that enables converters in Pctrl to change their active power generation, thus limiting the maximum value of the DC voltage.

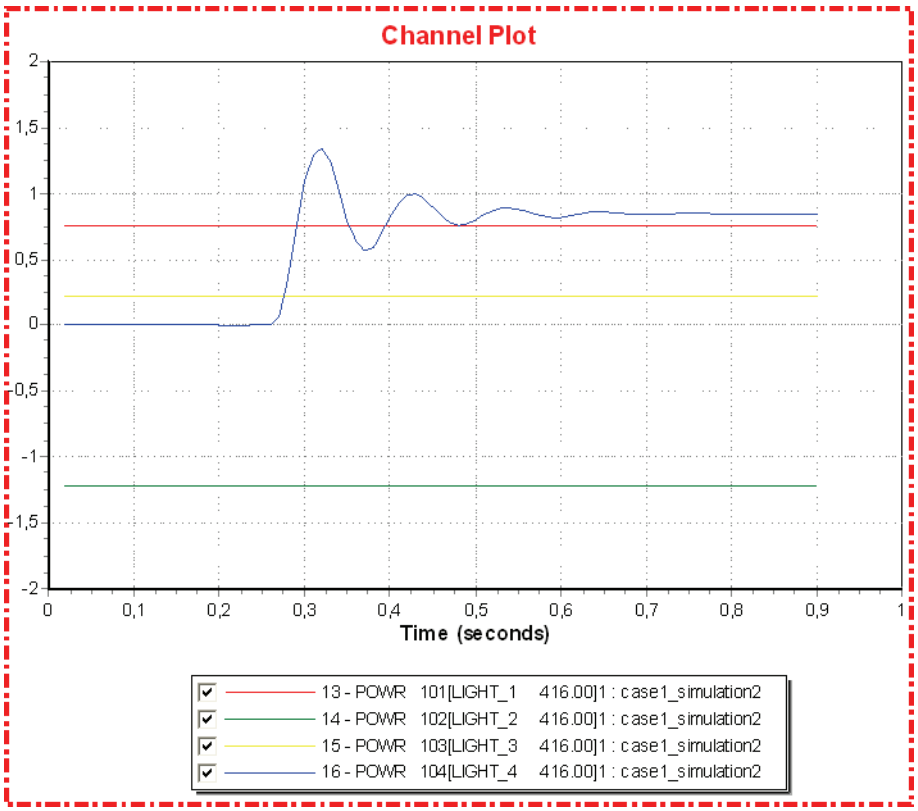

Figure 12.1.4: Converter active power [pu]

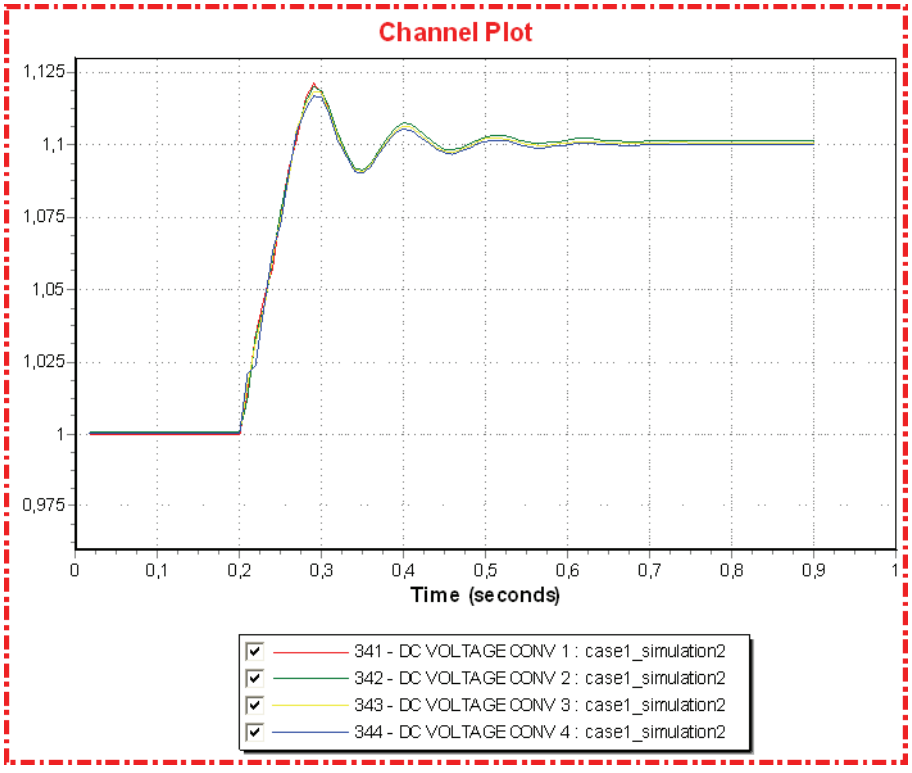

Figure 12.1.5: Converter DC voltage [pu]

Simulation 3 (Small wind generation)

Time	Event
0.00	Normal operation
0.20	Disconnect (trip) converter 1 (UdcCtrl converter)

The disturbance in simulation 3 is the same as in simulation 2, disconnection of the UdcCtrl converter 1, but the power flow scenario is different. In the small wind farm scenario there is a net deficit of around 188 MW offshore that is supplied by converter 1 through the DC system. As converter 1 is disconnected, the stored energy in the DC capacitances is discharged through converter 2 and 3, thus reducing the DC voltage. About 0.3 second following the disturbance the DC voltage reaches 0.9 pu, at which point the "emergency UdcCtrl" of the model is activated and converter 4 starts delivering power to the MTDC from the onshore AC grid. Converter 4 creates a new power balance in the MTDC that prevents the capacitances from being fully discharged, and the voltage from falling below 0.9 pu.

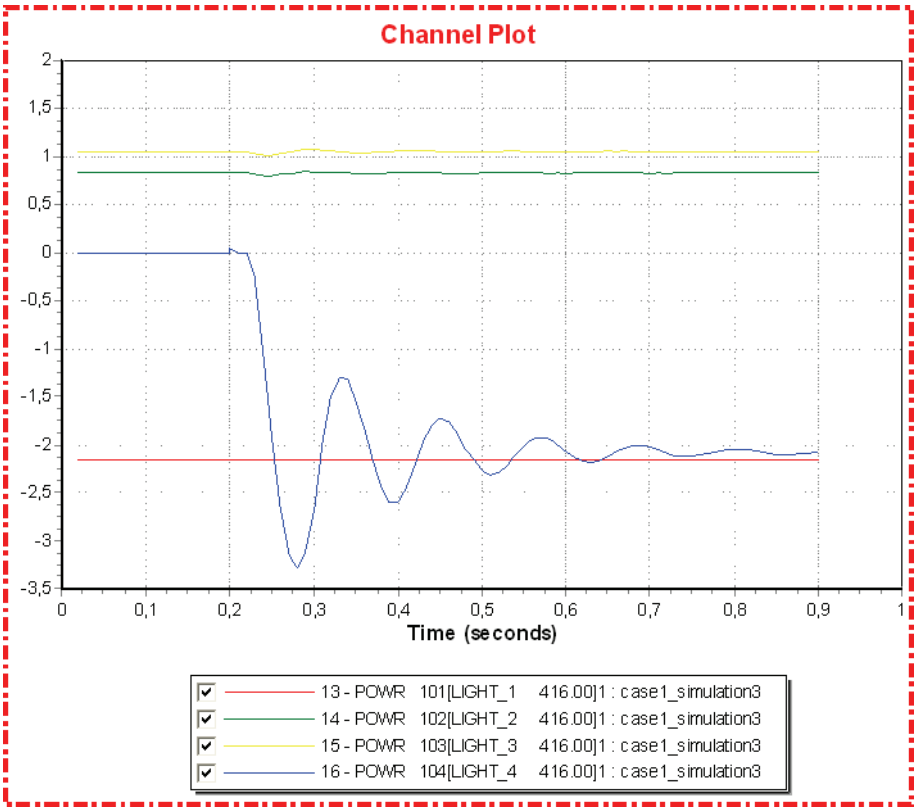

Figure 12.1.6: Converter active power [pu]

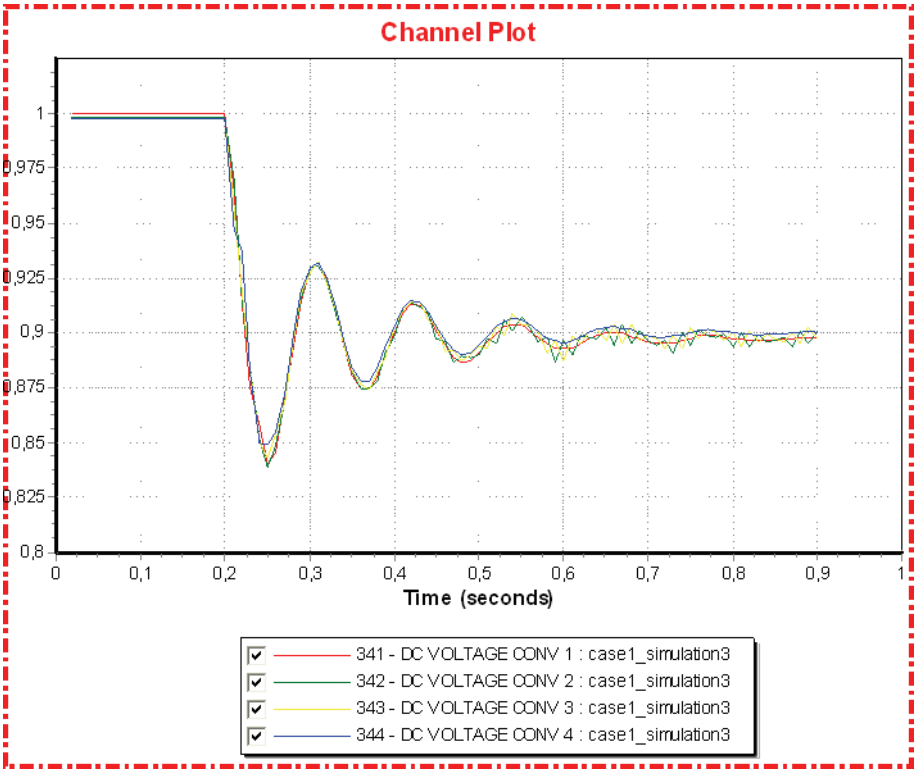

Figure 12.1.7: Converter DC voltage [pu]

Simulation 4 (Large wind generation)

Time	Event
0.00	Normal operation
0.20	Disconnect (trip) converter 1 and change Poption for converter 4 to UdcCtrl

This simulation is performed to investigate a possible alternative control strategy for DC voltage rather than the one implemented in the HVDC Light model and described chapter 2.11.3 as master - slave configuration, where one converter is permanently set as the master-terminal controlling DC voltage. The problem with the master-slave configuration is that the MTDC system always depends on the presence of the master-terminal in the grid, leading to breakdown of the whole system during failure of the master-terminal. The idea investigated in this simulation is that the MTDC could operate with a control strategy where all the converters are ranked according to their ability to serve as the DC voltage controlling converter. In the case of a failure of the DC voltage controlling converter, the role of UdcCtrl is simply transferred to the highest ranked converter still operating in the MTDC.

With reference to this specific simulation model, the converter with the highest ability to assume UdcCtrl following a failure at converter 1, is converter 4, which is connected to the same relatively strong onshore AC grid. Converters 2 and 3 are not suitable as they are connected to small offshore AC grids with limited possibilities for flexible power generation.

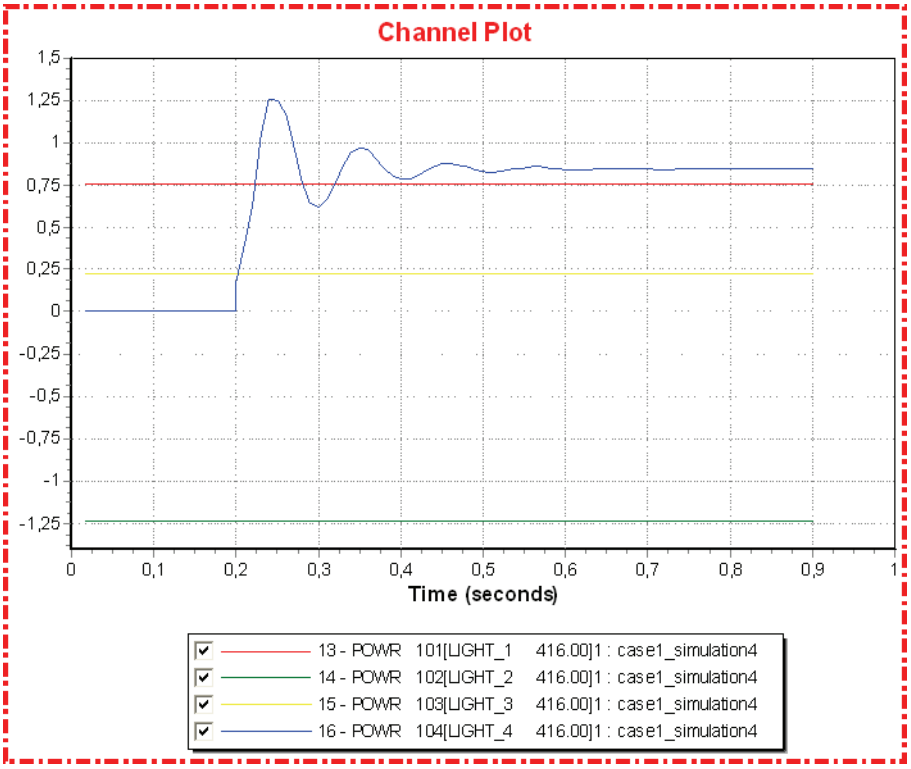

Figure 12.1.8: Converter active power [pu]

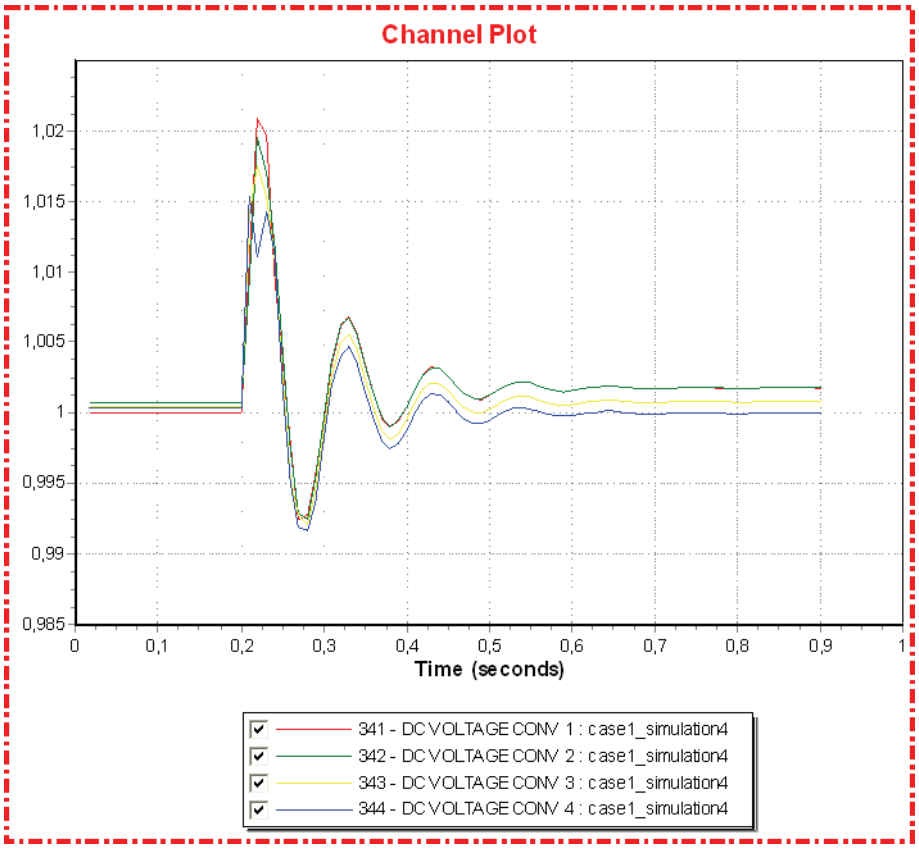

Figure 12.1.9: Converter DC voltage [pu]

In simulation 4, at the same time converter 1 is tripped, the active power control option (Poption) of converter 4 is changed from Pctrl to UdcCtrl. Simulation 4 is comparable to that of simulation 2, where Poption for converter 4 remains in Pctrl following the trip of converter 1.

The dynamic response shows that converter 4 changes its working point in the P-Q diagram immediately after the disturbance, aiming to maintain the power balance in the MTDC. In simulation 2 the power flow in converter 4 remained constant until the DC voltage reached the value of 1.1 pu, thereby initiating the emergency UdcCtrl. As a result of the immediate response of converter 4 in simulation 4, the DC voltage only experiences a few small oscillations before settling at the desired value of 1.0 pu. The oscillations are due to transient power imbalances as converter 4 attempts to establish the correct power injection to the MTDC.

The conclusion drawn from the comparison of the two simulations is that an advanced control system for the active power control operation (Poption) of all the converters in a MTDC may greatly improve the performance of the system following a disturbance. If the disturbance prohibits the Poption designated for a converter, the control system should be able to alter the Poption of the converters to the most suitable combination for the new system situation.

12.2 Case 2

The motivation for the simulations performed in case 2 and case 3 is to illustrate the decoupling effect of using a VSC HVDC grid to connect separate AC systems. In case 2 the effects offshore following an onshore disturbance are investigated.

Simulation 1 (Large wind generation)

Time	Event
0.00	Normal operation
0.20	Line fault on line 5 – 11 (id1)
0.30	Disconnect (Trip) faulted line

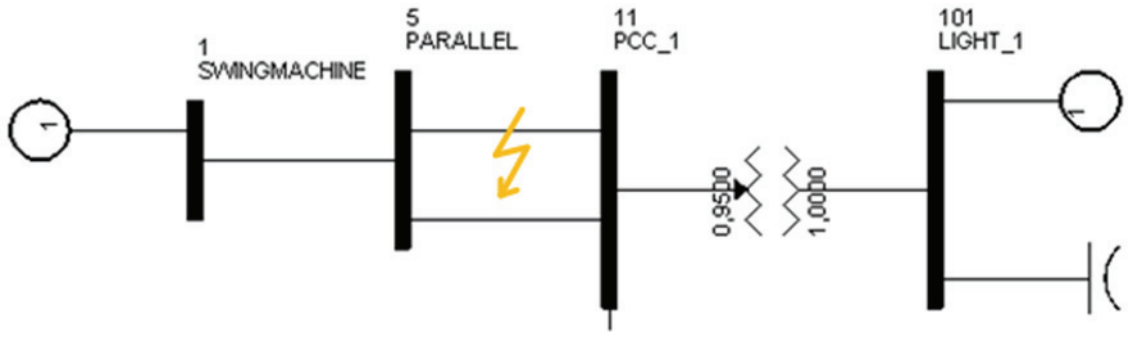

Figure 12.2.1: Dynamic simulation disturbance

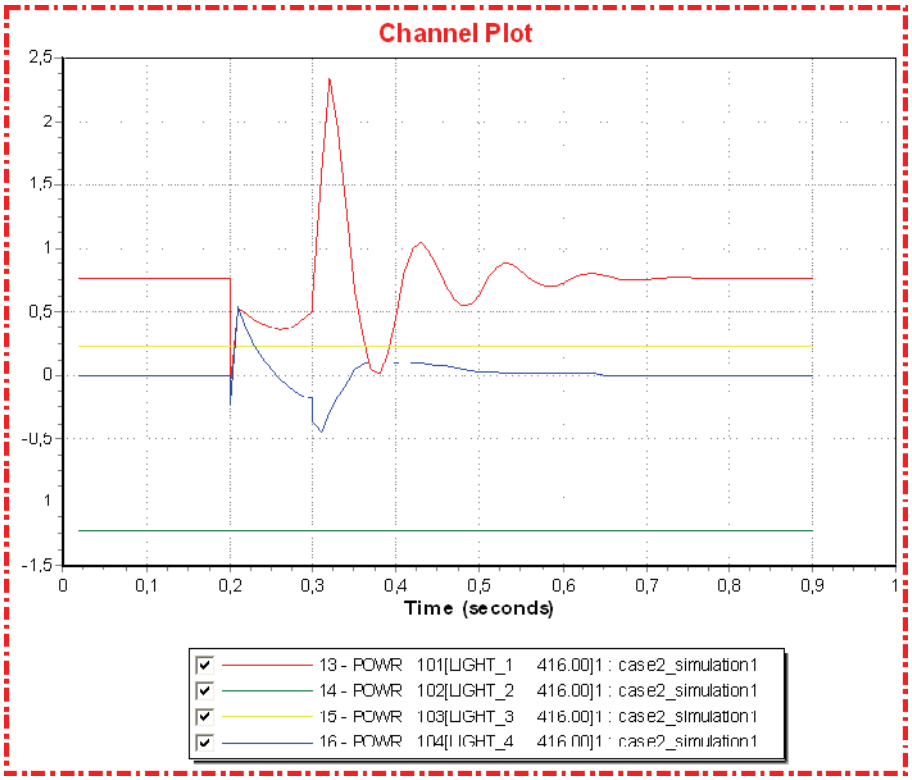

Figure 12.2.2: Converter active power [pu]

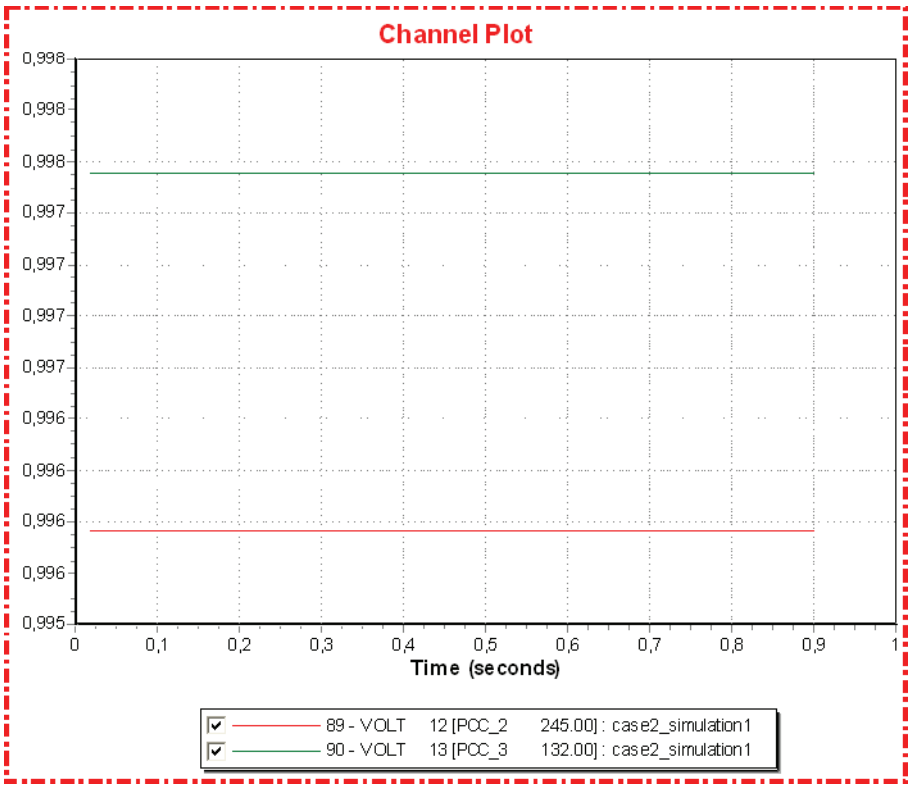

Figure 12.2.3: Offshore AC voltages [pu]

The simulation results show that the offshore AC grids are unaffected by the onshore disturbance. The entire MTDC remains operational and the offshore converters do not change their working points, but continue to exchange exactly the same amount of active and reactive power with the offshore AC grids. The MTDC is the only connection between the onshore AC grid, experiencing the disturbance, and the offshore AC grids. As the offshore converters do not change their behavior at all, the offshore AC grids do not experience any consequences from the disturbance onshore. The offshore systems are completely unaffected, the voltages and wind power generation remains constant during the entire simulation.

A comment should be made about the actions of converter 4 in simulation 1. This converter is set in Pctrl with an active power production of 0.0 MW. Despite this control setting the converter immediately changes power generation following the disturbance. An explanation for this behavior has not been discovered. The DC voltage is nowhere near the limits of 0.9 and 1.1 pu that would initiate the "emergency UdcCtrl", thus allowing converter 4 to change power generation. A similar situation occurs in case 7, simulation 1, as explained later in the description of case 7. The explanation in case 7 is that the phase locked loop of the converters control system is unable to handle the swift changes in the phase angle of the onshore AC grid. This leads to a faulted converter control. The grid and event situation of case 7 is not identical to this simulation 1 of case 2, but it is possible that the explanation for the response of converter 4 is the same.

Simulation 2 (Large wind generation)

Time	Event
0.00	Normal operation
0.20	Bus fault at bus 14
0.30	Clear bus fault

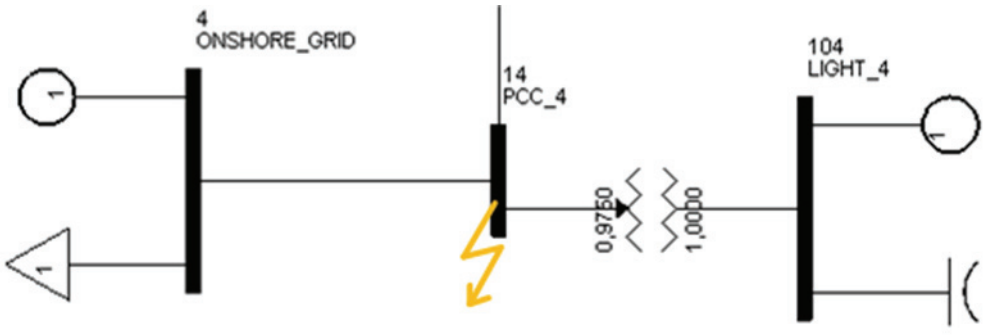

Figure 12.2.3: Dynamic simulation disturbance

In simulation 2 a temporary bus fault is applied at an onshore bus close to converter 4. The offshore converters demonstrate the same behavior as described in simulation 1, their active and reactive power exchange with the offshore AC grids remain the same following the onshore disturbance. The offshore AC grids are therefore unaffected by the onshore fault.

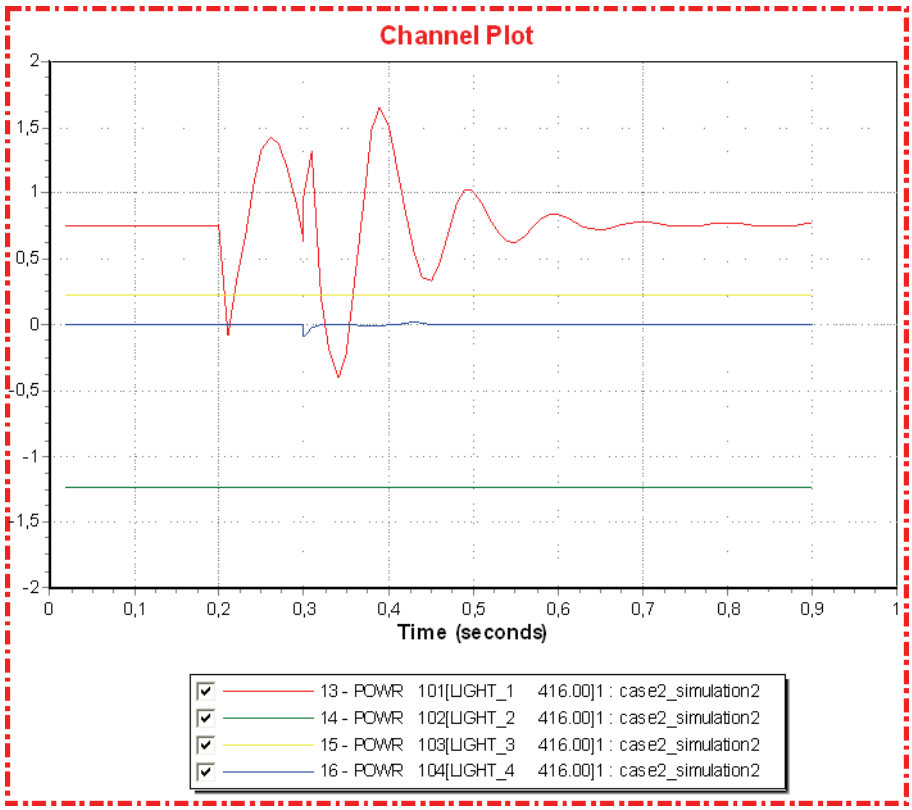

Figure 12.2.5: Converter active power [pu]

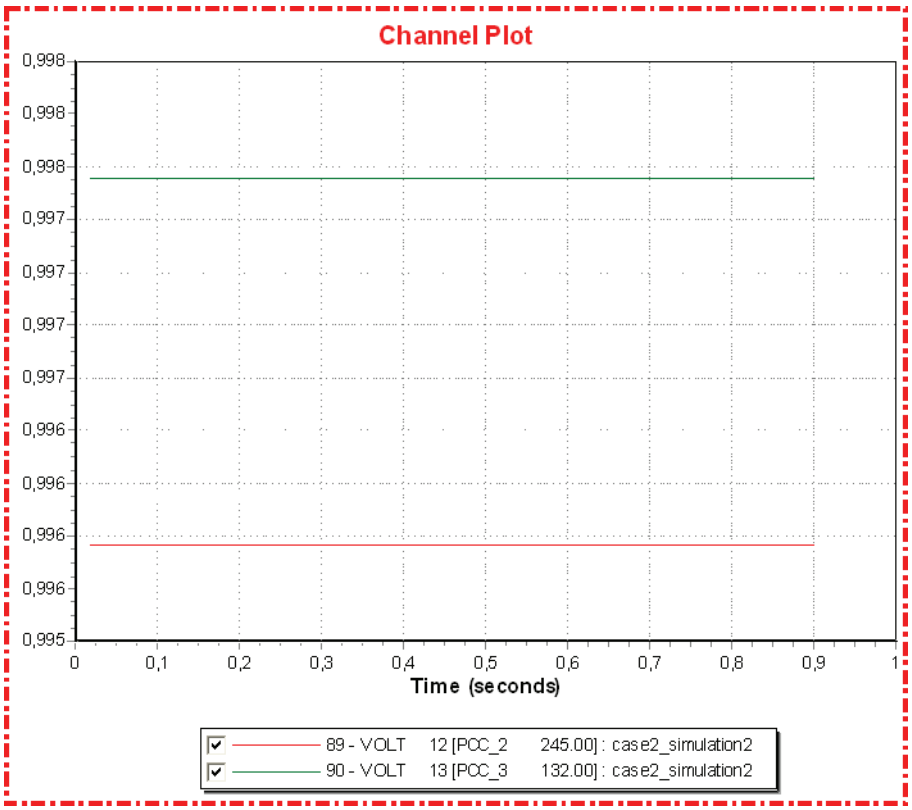

Figure 12.2.6: Offshore AC voltages [pu]

Simulation 3 (Small wind generation)

Time	Event
0.00	Normal operation
0.20	Line fault on line 5 – 11 (id1)
0.30	Disconnect (Trip) faulted line

The sequence of events subjected to the system in simulation 3 is the same as in simulation 1, see figure 12.2.1. However, the small wind generation power flow scenario is applied, instead of the large wind generation scenario used in simulation 1.

A comparison of simulation 1 and 3 illustrates the difference of having a net surplus or a net deficit of power offshore in the case of an onshore disturbance. The onshore disturbance occurs in the proximity of converter 1 in UdcCtrl, and limits the ability for converter 1 to inject power into the MTDC in order to properly control the DC voltage.

Prior to the disturbance, converter 1 supplied the necessary power to the offshore AC grids through the MTDC. During the duration of the line fault, the power delivered to the MTDC from converter 1 is very limited. As the offshore converters aim to deliver the same amount of power to the offshore AC grids, simultaneously as the power into the MTDC is limited, the result is a negative power balance in the MTDC. This leads to a discharge of energy from the DC capacitors and a subsequent fall in DC voltage. The offshore converters struggle to maintain the power delivered to the offshore AC grids as the DC voltage drops. Although the converter currents increase, the converters are unable to deliver the constant required pre fault amount of power to the offshore grids. The offshore AC grids experience a fall in the active power supplied from their converters and their AC voltage falls as seen in figure 12.2.11.

The DC voltage falls below 0.9 pu after approximately 0.3 seconds after the disturbance. At this time converter 4 assumes emergency UdcCtrl, thereby injecting power into the MTDC and increasing the DC voltage. When the faulted line is disconnected, converter 1 is again able to deliver the necessary power to the MTDC and resumes control of the DC voltage which stabilizes at 1.0 pu after a few oscillations. The offshore converters may then return to their desired power exchange and the offshore AC grids returns to their pre fault behavior.

It should be noted that the converter 4 display the same unexplained performance as described in simulation 1, a small change in active power prior to “emergency UdcCtrl” operation.

The reactive power generation a converter 1 exceeds the steady state limit for a short transient spike immediately after the faulted line is disconnected. Dynamically the converters may exceed the reactive power limit depicted in figure 2.9.1 by around 10 percent for a very short time. However, the reason for the performance depicted in figure 12.2.9 is most likely that during a time step the control system of CABBOM (HVDC Light model) and PSS®E solves the simulation equations separately. This may result in improper values, especially in connection to fault or disconnection of fault [9].

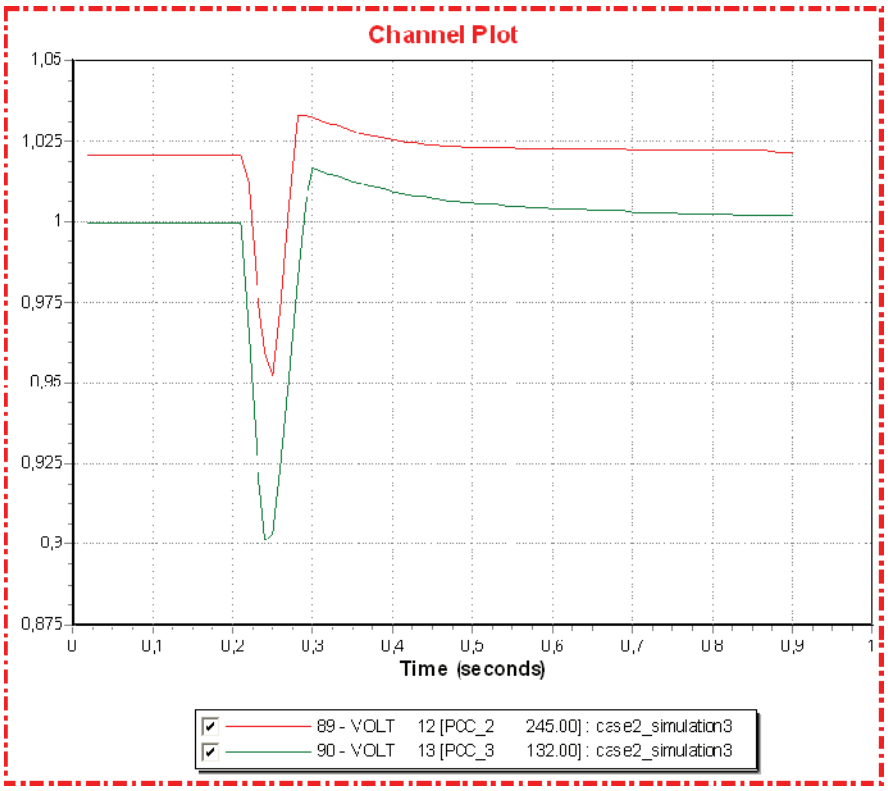

Figure 12.2.7: Offshore AC voltages [pu]

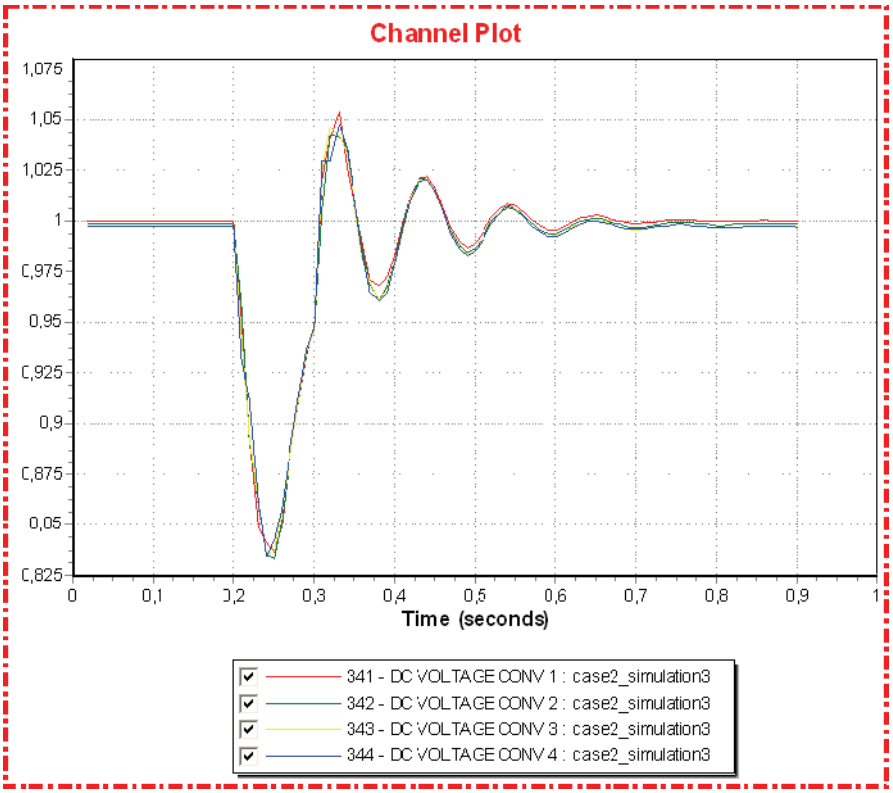

Figure 12.2.8: Converter DC voltage [pu]

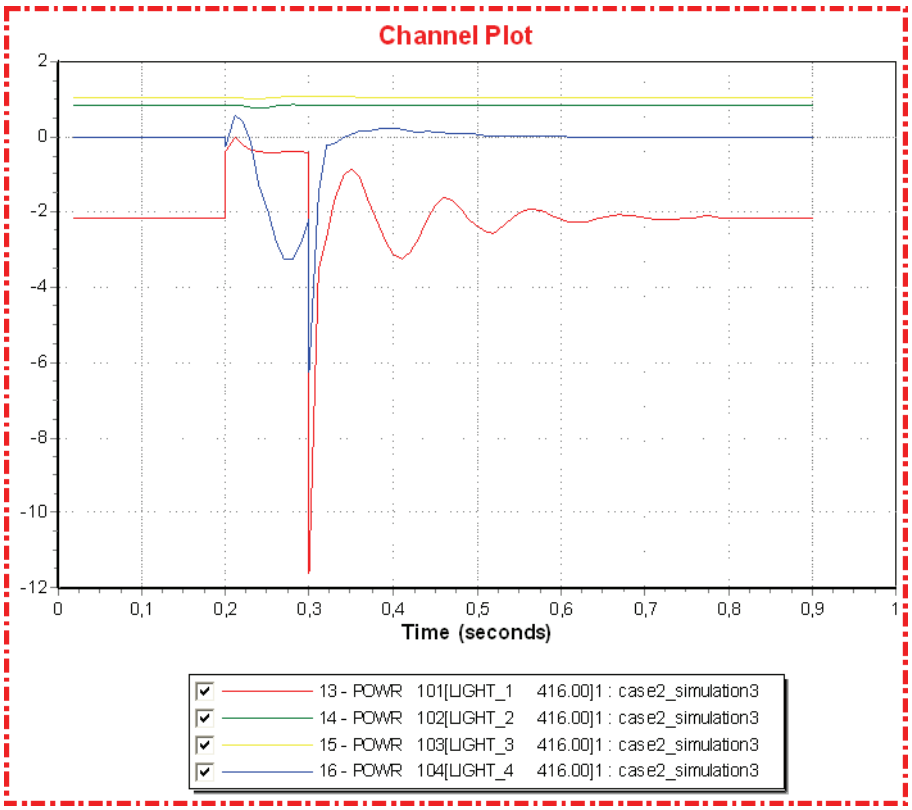

Figure 12.2.9: Converter active power [pu]

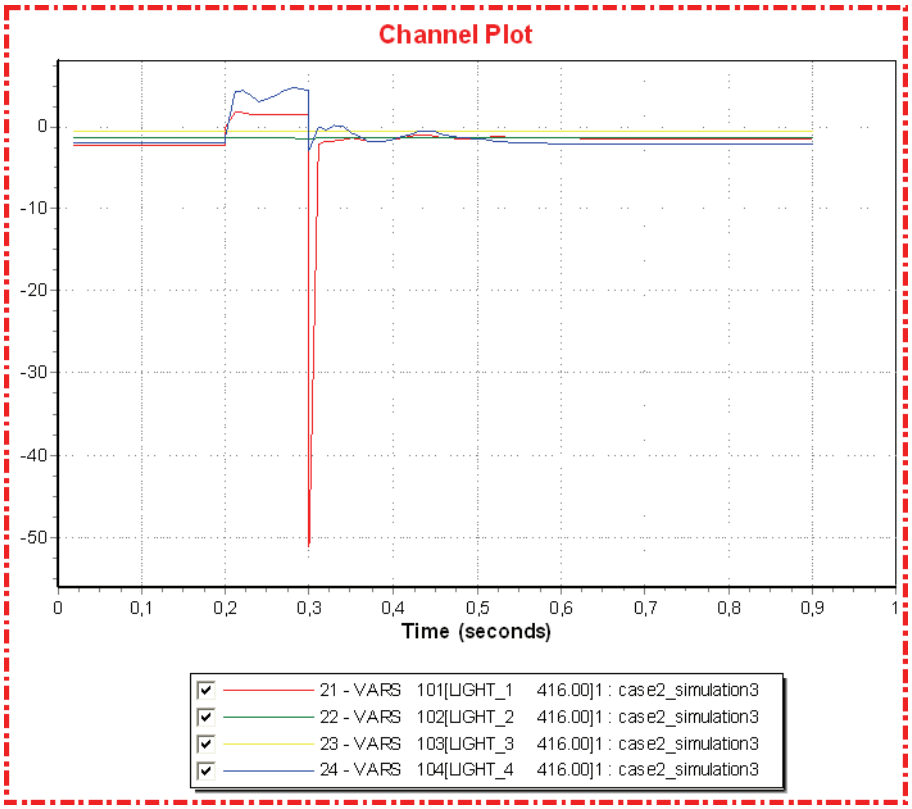

Figure 12.2.10: Converter reactive power [pu]

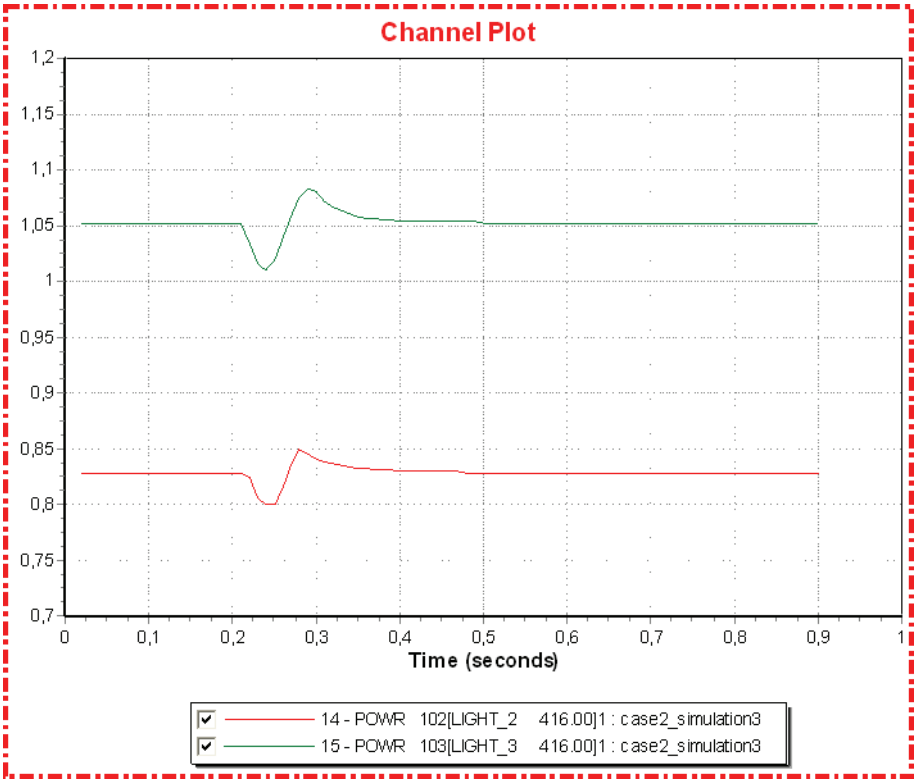

Figure 12.2.11: Offshore AC voltages [pu]

Simulation 4 (Small wind generation)

Time	Event
0.00	Normal operation
0.20	Bus fault at bus 14
0.30	Clear bus fault

The sequence of events subjected to the system in simulation 4 is the same as in simulation 2, see figure 12.2.3, but the small wind generation power flow scenario is applied.

Contrary to the response investigated in simulation 3, the offshore AC grids are not affected by the onshore disturbance of simulation 4. The reason is that this onshore disturbance does not obstruct the onshore power flow to converter 1 and into the MTDC, provided that the onshore grid can dynamically supply the necessary power. Converter 1 is therefore able to carry out a proper control of the DC voltage by maintaining the power balance of the MTDC. In simulation 3 the offshore converters had a reduction in the delivered power to the AC grids due to the fall of the DC voltage. As the DC voltage in simulation 4 remains at the desired value of 1.0 pu, the offshore converters will not change their behavior. The result is that the offshore AC grids are not affected by the onshore fault in simulation 4.

The minor oscillations of the DC voltage are caused transient power imbalances in the MTDC due to the power oscillations of converter 1 following the onshore disturbance.

Another reason for the successful performance of the MTDC following the disturbance, in addition to the location of the bus fault relative to converter 1, is the relative modest power deficit offshore. Converter 1 is only able to deliver as much power as the onshore AC grid is able to transfer to the converter. If the power injection required to maintain DC power balance were of a much larger scale, the onshore AC grid might not be able to transfer such quantities of power while being subjected to a bus fault.

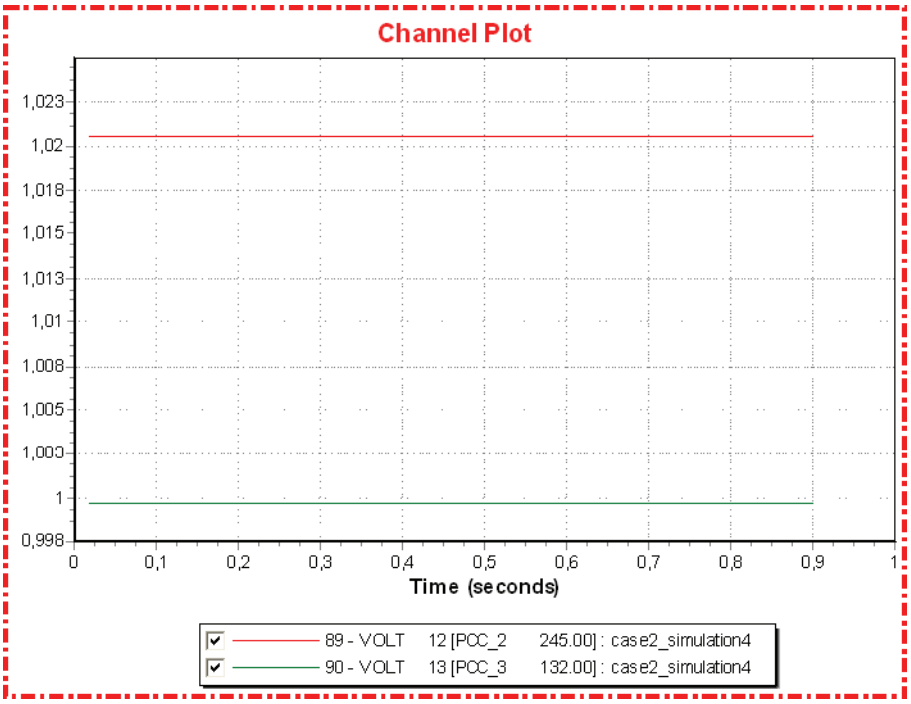

Figure 12.2.12: Offshore AC voltages [pu]

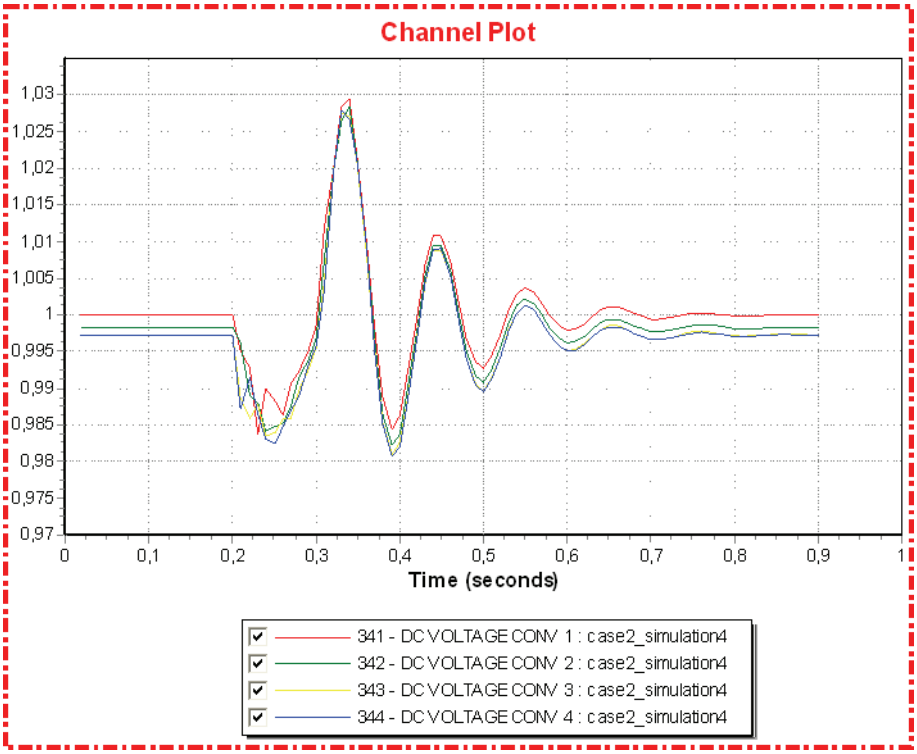

Figure 12.2.13: Converter DC voltage [pu]

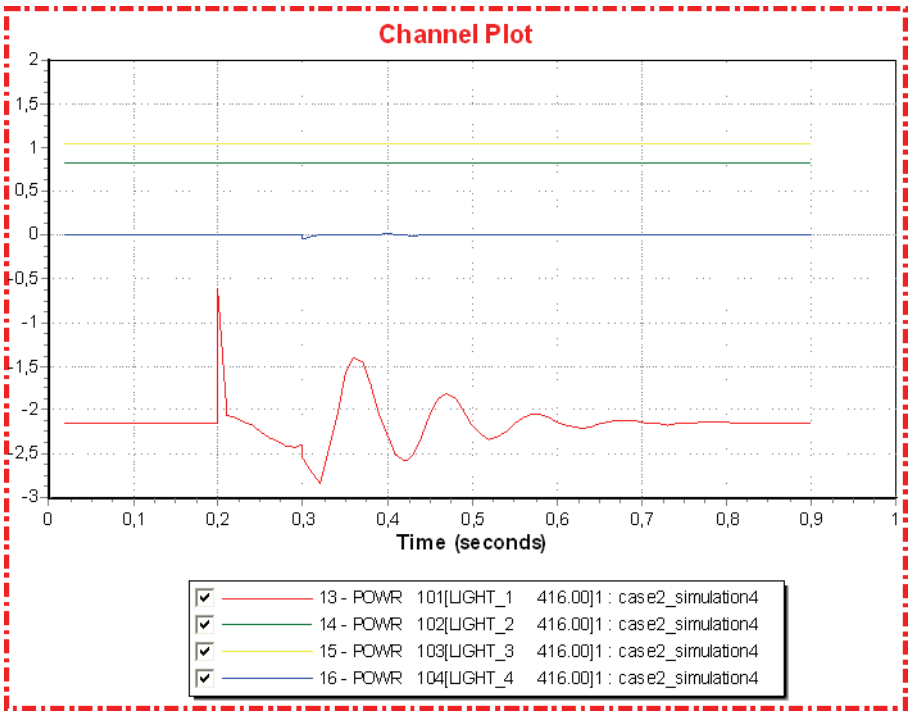

Figure 12.2.14: Converter active power [pu]

12.3 Case 3

The motivation for case 3 is to demonstrate the decoupling effect of using a VSC MTDC to connect separate AC grids, just like in case 2. Contrary to case 2, the disturbance now occurs in an offshore AC system, and the following behavior of the onshore AC grid is investigated. Only the large wind generation power flow scenario is applied for the simulations performed in case 3 and all the disturbances are performed in relation to the large wind farm of offshore area 2. An offshore AC fault that removes the large power generation of wind farm 2 will have the largest disturbing effect on the system, compared to other offshore AC faults.

Simulation 1 (Large wind generation)

Time	Event
0.00	Normal operation
0.20	Bus fault at bus 12 (PCC 2)
0.30	Clear bus fault

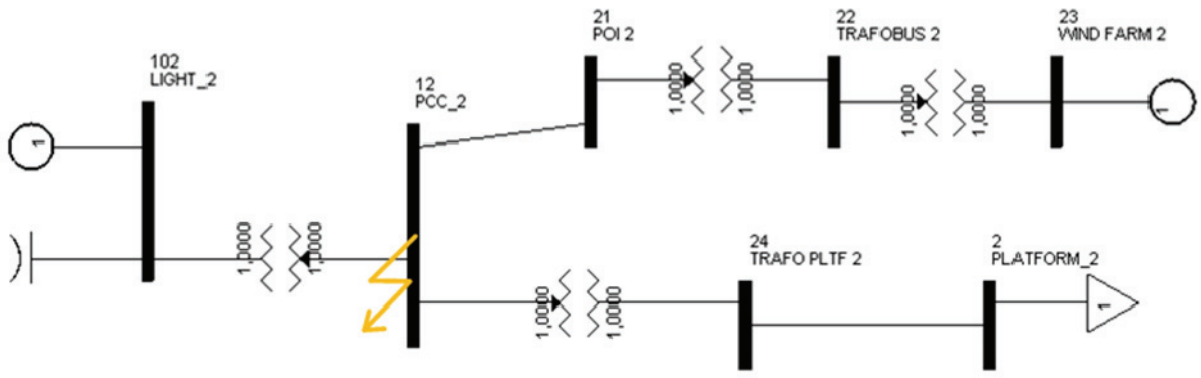

Figure 12.3.1: Dynamic simulation disturbance

Simulation 1 investigates the event of a bus fault on the PCC in offshore area 2. As the voltage falls to zero, no active power can be exchanged between the offshore area 2 and converter 2.

The results from simulation 1, show that the voltage in the onshore system is practically unaffected by the temporary bus fault offshore. The impact on the onshore grid due the offshore fault is an increase in the onshore power generation to allow converter 1 to maintain the power balance in the MTDC following the loss of power from converter 2. Provided that the onshore AC grid is flexible enough with respect to power generation, the offshore fault will not bring about any severe consequences for the stability onshore.

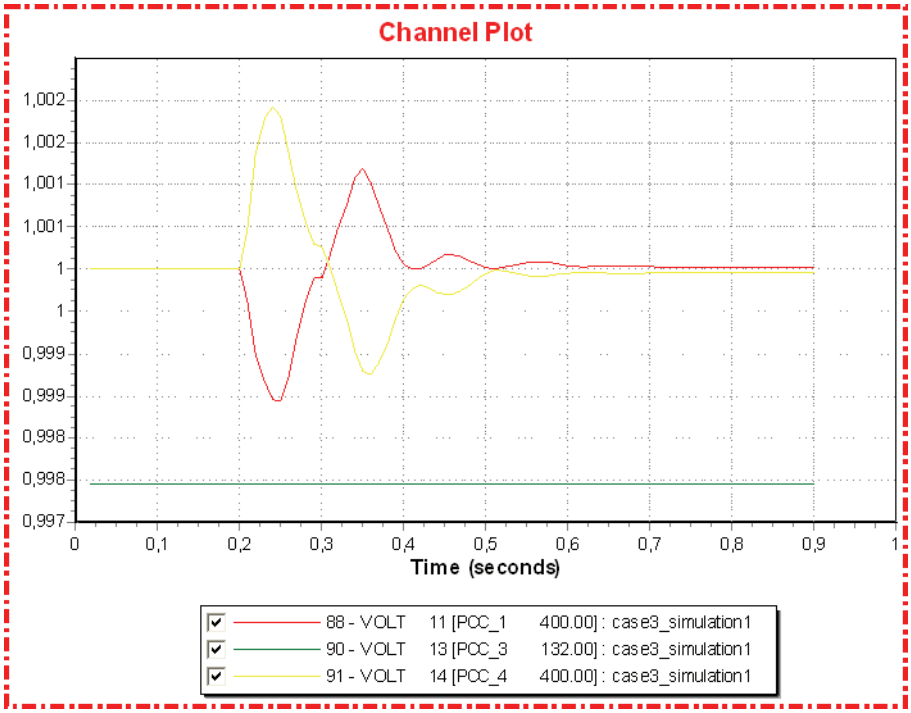

Figure 12.3.2: AC voltages [pu]

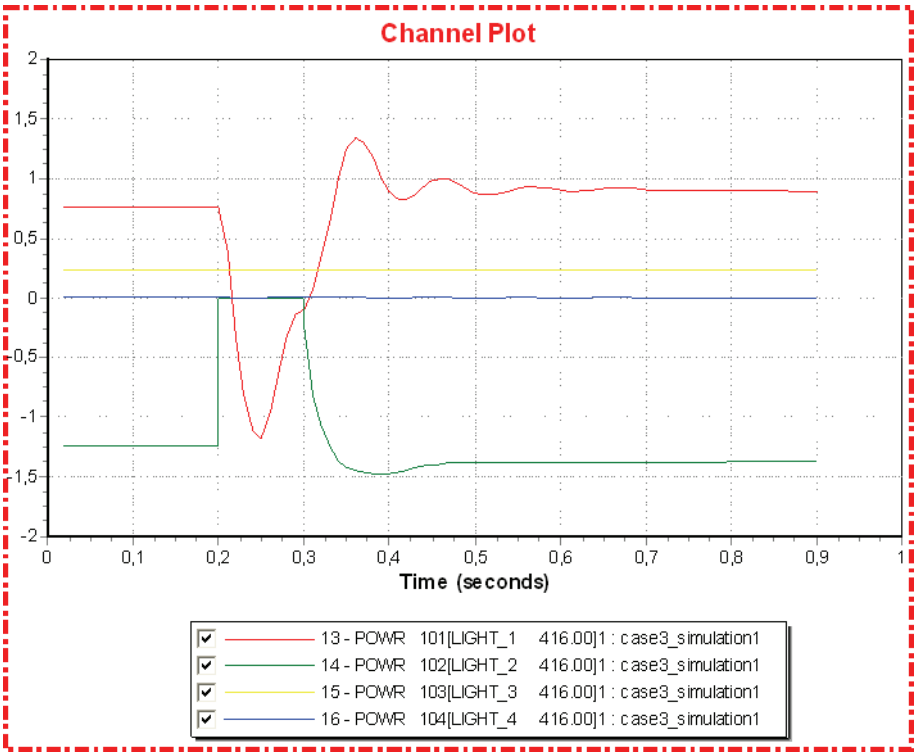

Figure 12.3.3: Converter active power [pu]

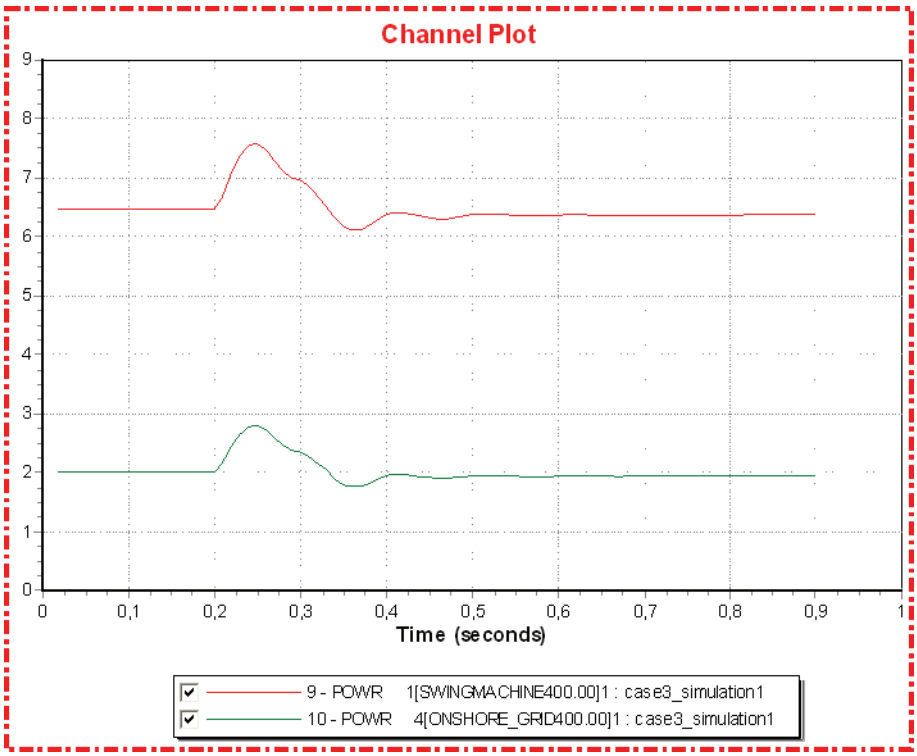

Figure 12.3.4: Onshore generators active power [pu]

Simulation 2 (Large wind generation)

Time	Event
0.00	Normal operation
0.20	Disconnect generator at bus 23 (wind farm 2)

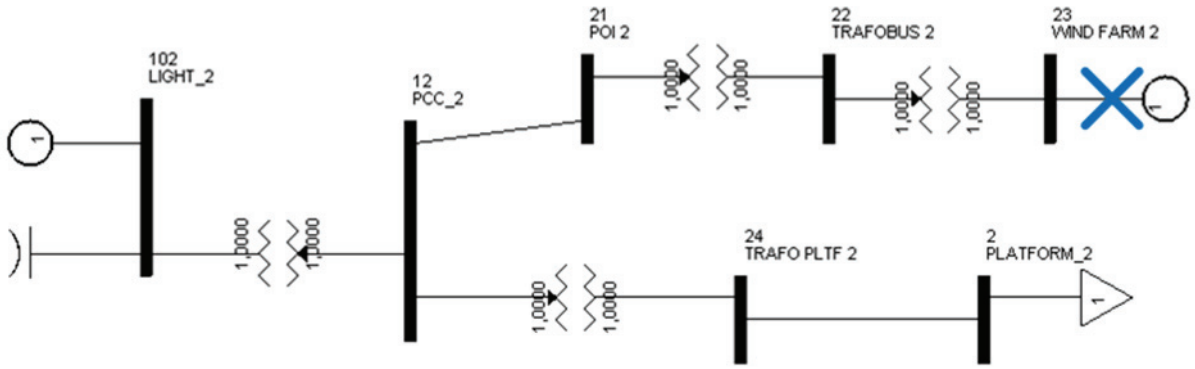

Figure 12.3.5: Dynamic simulation disturbance

Simulation 2 investigates a disconnection of the large wind farm at offshore area 2.

The consequences onshore following the offshore disturbance are quite similar to those of simulation 1. The power generation onshore increases to compensate for the disappearance of

wind farm 2. Compared to simulation 1, the onshore generation must increase more as petroleum platform 2 continues to be supplied from converter 2 in this simulation. The small oscillations in the onshore voltage are due to the transients in the active and reactive power flow following the disturbance. The offshore disturbance does not have an effect on the stability of the onshore system.

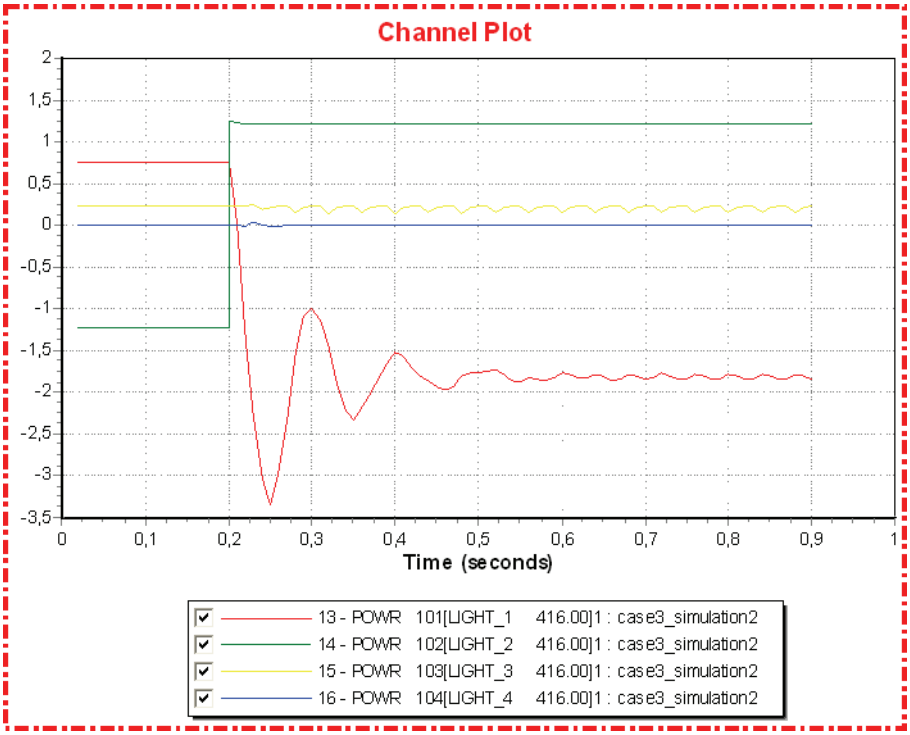

Figure 12.3.6: Converter active power [pu]

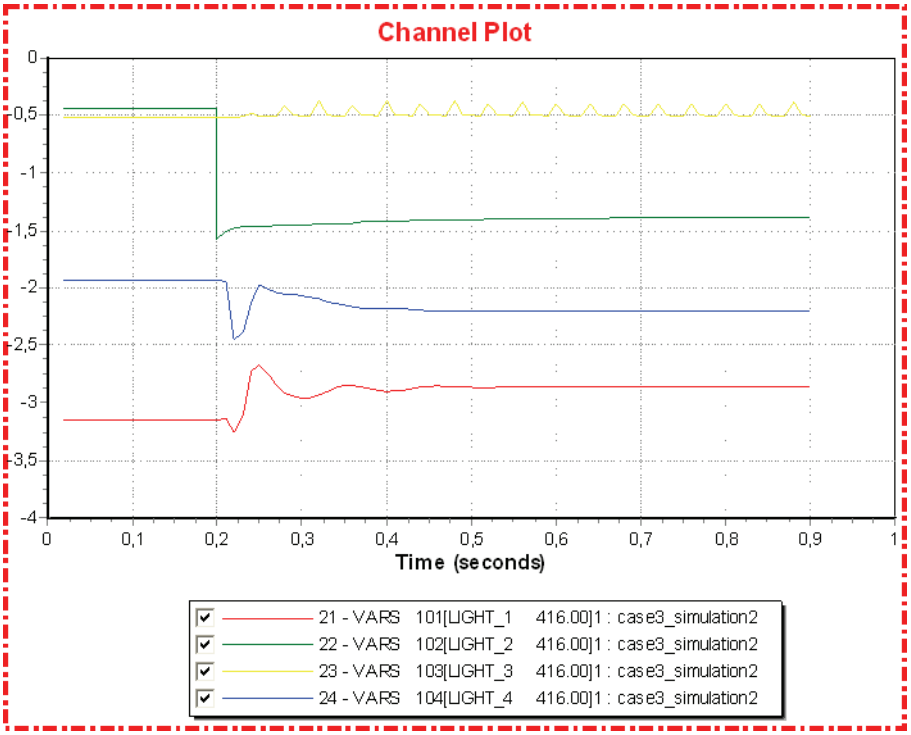

Figure 12.3.7: Converter reactive power [pu]

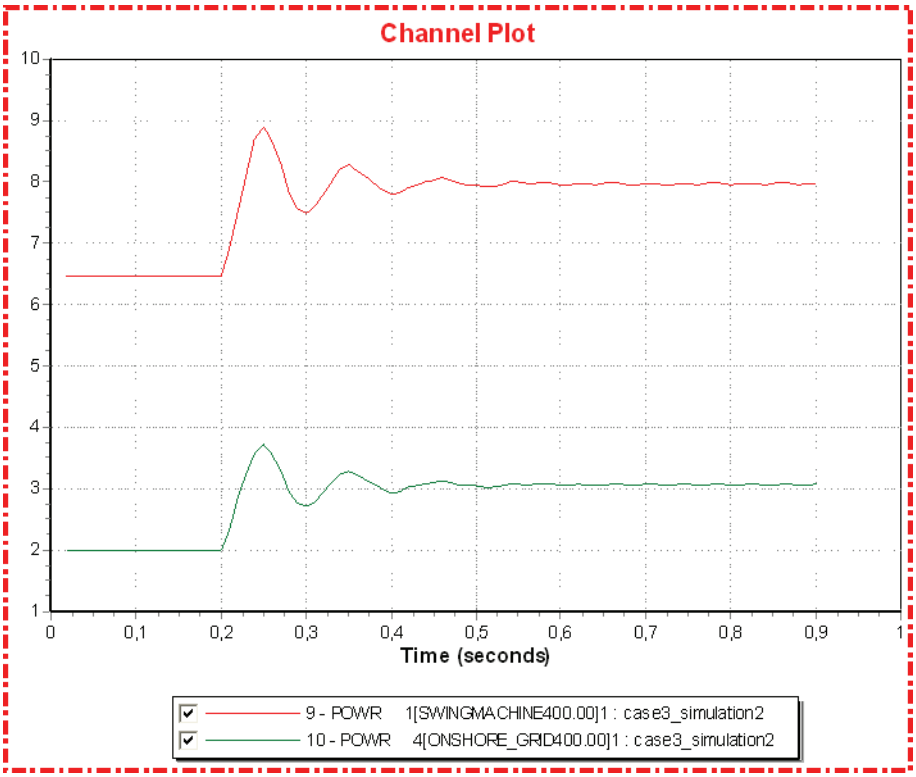

Figure 12.3.8: Onshore generators active power [pu]

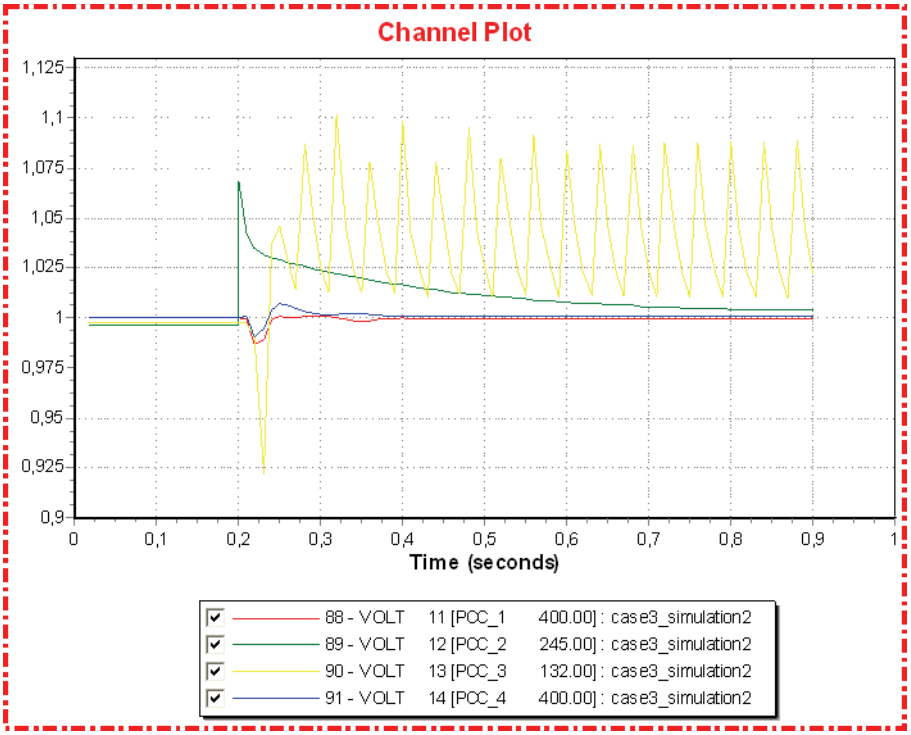

Figure 12.3.9: AC voltages [pu]

12.4 Case 4

The simulations in case 4 aim to investigate the temporary dynamic island operation of the offshore AC grids seen in relation to the protection schemes for a MTDC grid. The two protection schemes applied in the simulations are described in chapter 2.11.2.2, as protection using IGBT current breakers (IGBT-CB) and protection using AC breakers.

The two protection schemes involve different durations for the offshore island operation. The idea behind the simulations is to analyze and compare the two protection schemes with respect to offshore grid performance. Both the large wind generation and the small wind generation power flow scenarios are applied.

Exact values for the time duration of the necessary island operation associated with each protection scheme has been difficult to acquire. For protection using AC breakers reference [30] indicates a down time of "several hundred milliseconds" while [53] assumes that "Provided that the DC fault is quickly identified and cleared this would take a minimum of a few seconds". Protection using IGBT-CB is entirely based on reference [31] which states that "it is necessary to block all the VSCs and IGBT-CBs thus causing a brief disruption of service".

Without any concrete values the following has been defined for the simulations:

- Protection using IGBT-CB leads to offshore island operation for 0.05 seconds.
- Protection using AC breakers leads to offshore island operation for 2.00 seconds.

Protection using IGBT-CB is analyzed with simulation 1 and 3, and protection using AC breakers is analyzed with simulation 2 and 4.

Unfortunately, for most of the simulations performed in this case, the offshore area 3 demonstrated an unrealistic behavior. Among other irregularities, the wind farm consumed power whereas the petroleum platform supplied power, as will be demonstrated in simulation 1. The explanation for this behavior in offshore area 3 was not discovered. The wind farm and petroleum platform in offshore area 3 are modeled with exactly the same parameters as those in offshore area 2, apart from the fact that wind farm 3 have fever wind turbines lumped together. As a result of these unresolved problems with the model, only offshore area 2 will be used for the analysis in case 4.

Simulation 1 (Large wind generation)

Time	Event
0.00	Normal operation
0.20	Disconnect (trip) converter 2 and 3
0.25	Reconnect converter 2 and 3 and the associated power transformers

Simulation 1 analyses the short duration island operation associated with protection using IGBT-CB in the large wind generation power flow scenario. The simulation is also used to demonstrate the unrealistic performance of offshore area 3, as an explanation for why only offshore area 2 is analyzed in this simulation case.

The figure below depicts the active power generation of the wind farms. Both offshore areas have a petroleum platform load of 120 MW (CLOD model). As seen in the figure, wind farm 2 reduces its power generation to match the load and losses in the isolated system, thus creating a power balance. Wind farm 3 on the other hand does not try to generate as much power as possible to balance the load in the isolated system. Instead, the wind farm starts to consume more than 100 MW of active power that is somehow delivered from the petroleum platform. The speed of the wind turbines increase and the voltages in offshore area 3 are unsatisfactory. The dynamic response of the wind farm and the CLOD model in offshore area 3 is unrealistic, indicating that there is either a problem with the models or an error has been made in the modeling. As no such error has been discovered, the offshore area 3 has been excluded from the simulations of case 4.

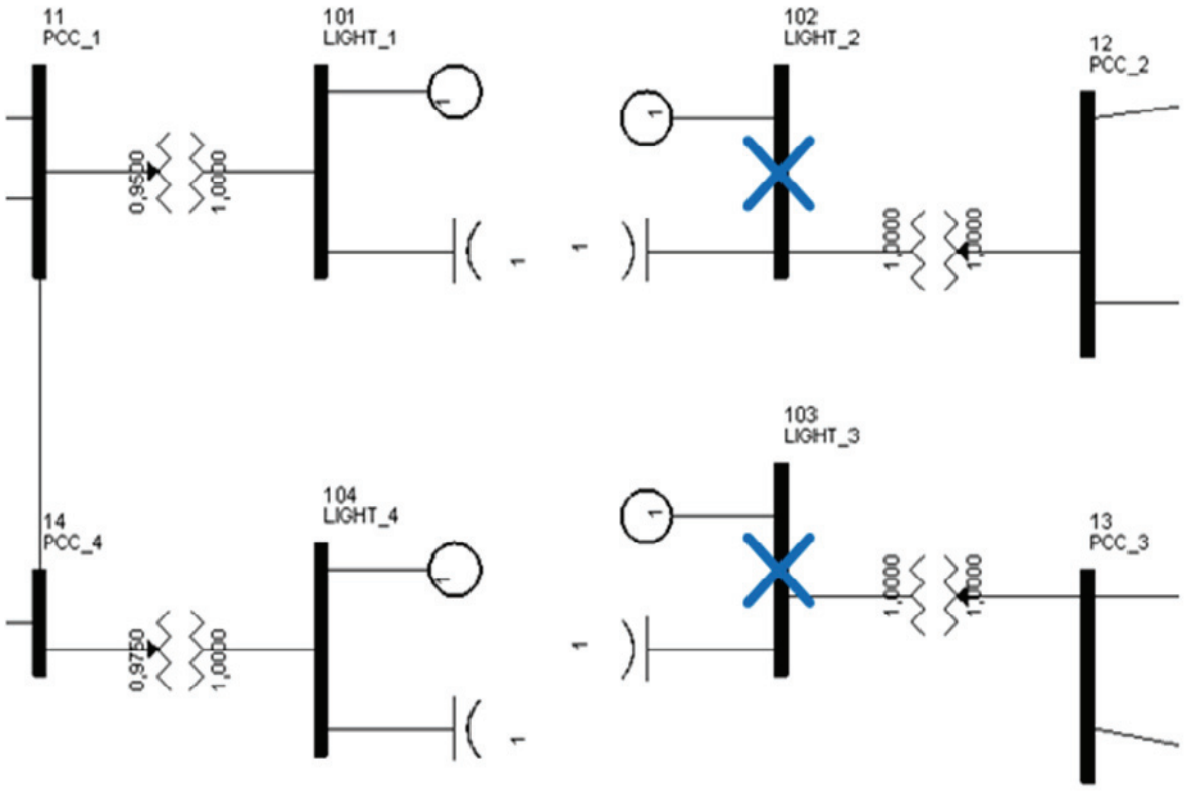

Figure 12.4.1: Dynamic simulation disturbance

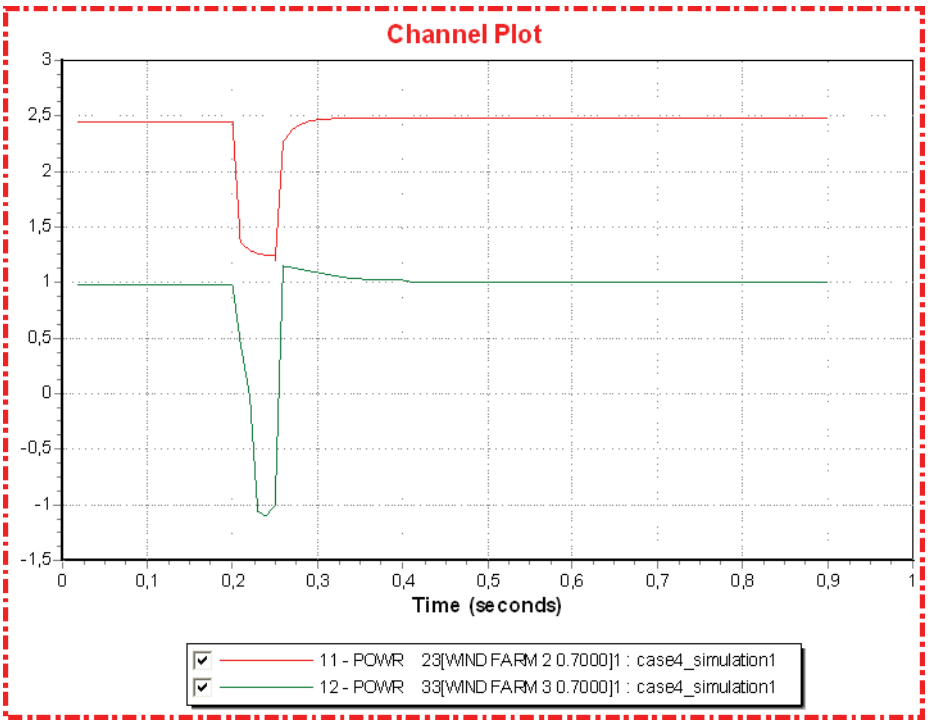

Figure 12.4.2: Wind power generation [pu]

The following figures plot the speed of the wind farm, power delivered to the petroleum platform and voltages in offshore area 3.

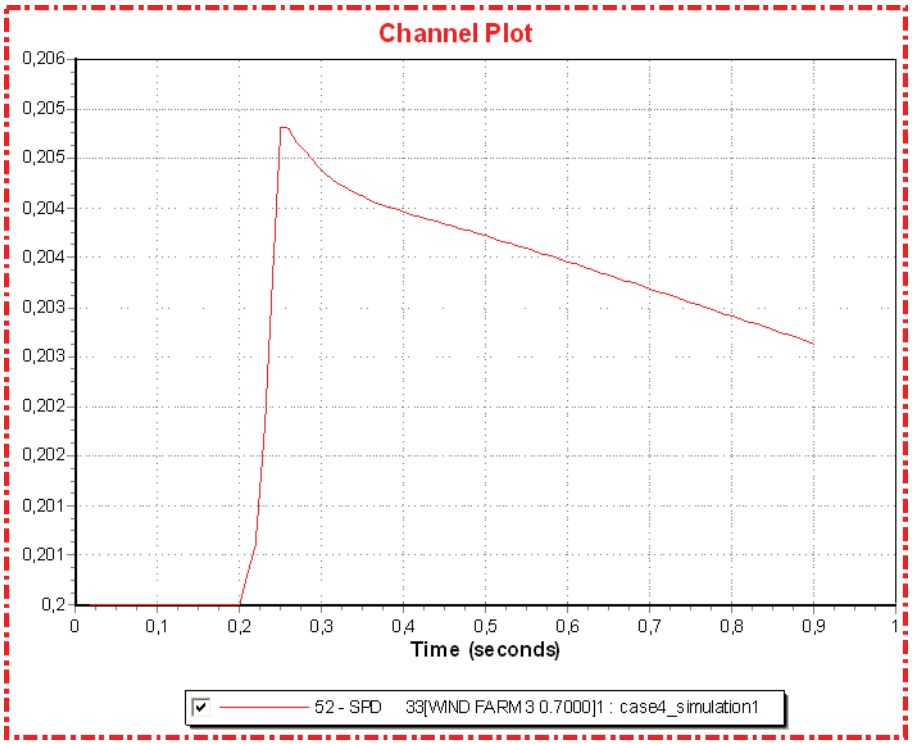

Figure 12.4.2: Turbine speed, wind farm 3 [pu]

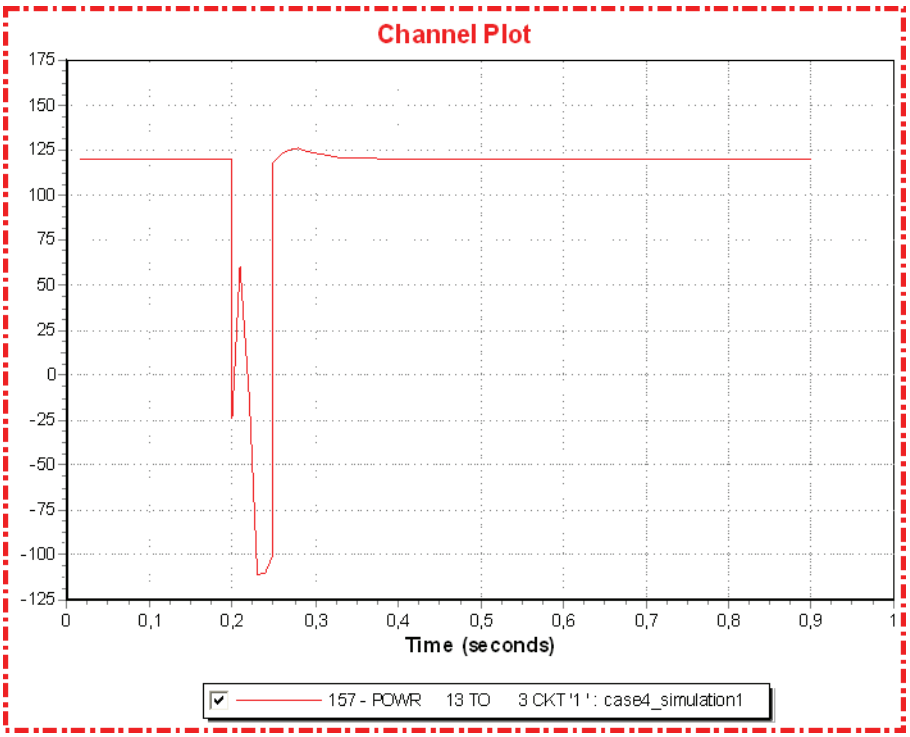

Figure 12.4.4: Active power to platform 3 [MW]

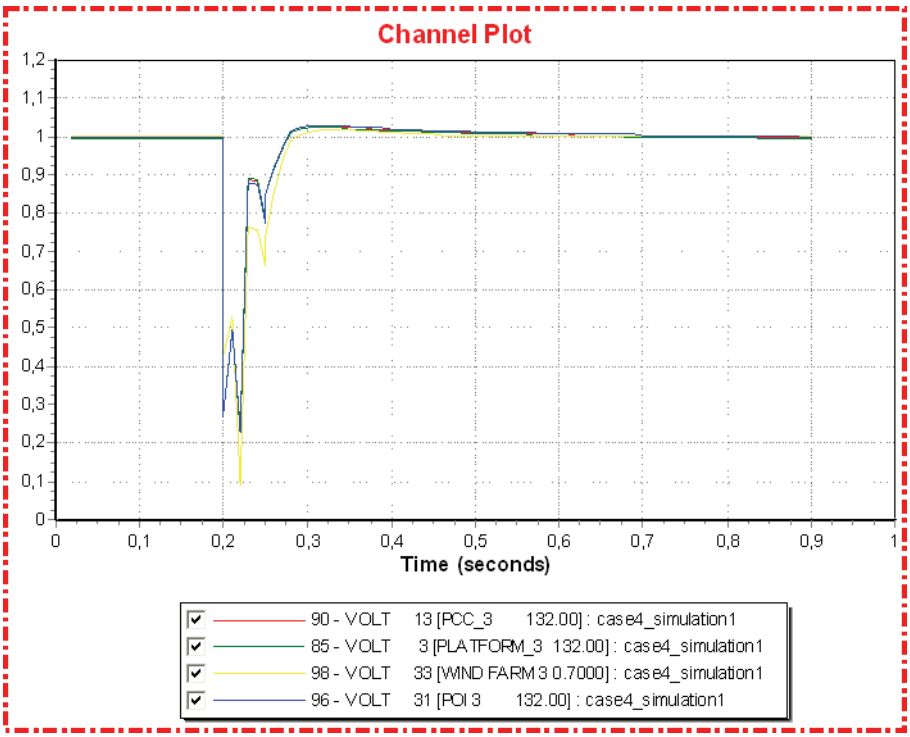

Figure 12.4.5: AC voltage, offshore area 3 [pu]

The next figures illustrate the response in offshore area 2, which is interpreted as a realistic behavior.

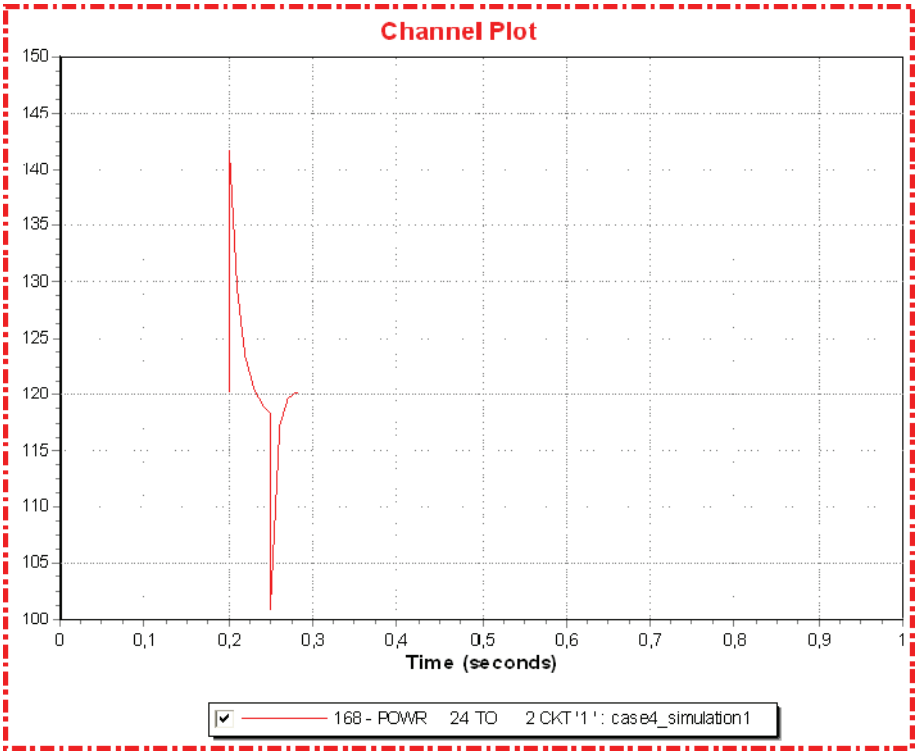

Figure 12.4.6: Active power to platform 2 [MW]

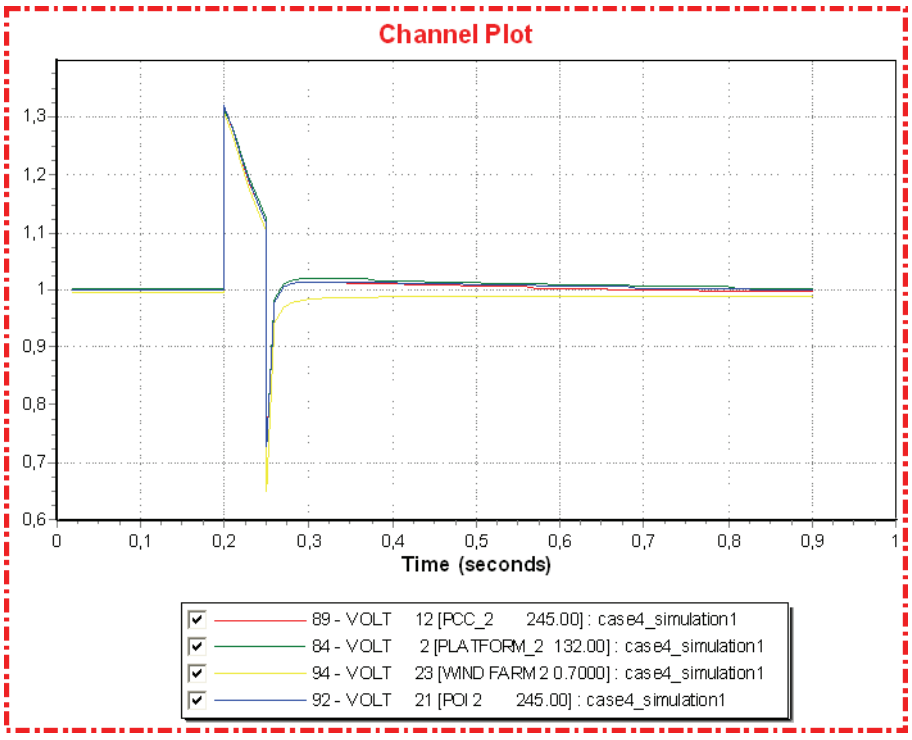

Figure 12.4.7: AC voltage, offshore area 2 [pu]

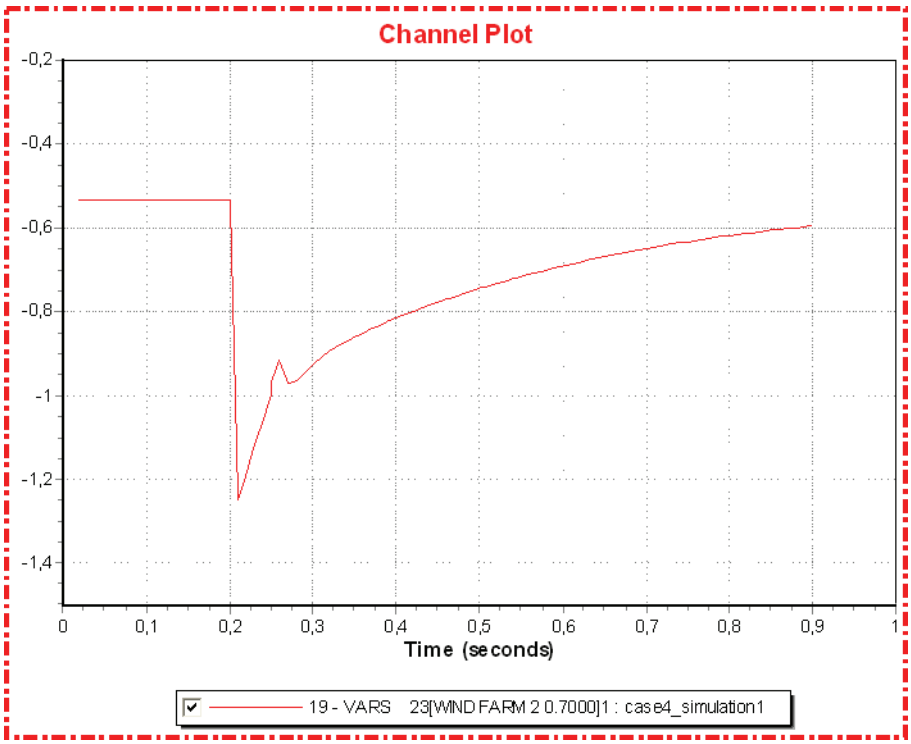

Figure 12.4.8: Reactive power generation, wind farm 2 [pu]

Offshore area 2 exhibits an acceptable realistic behavior during the island operation and following reconnection of the converter. The power delivered to the petroleum platform experiences both a surge followed by a sag, both in the shape of a spike. However, the transients only lasts for a so short duration that the power supply is acceptable for the petroleum platform, se chapter 5.1. The voltage in offshore area 2 is above the desired value, reaching 1.31 pu directly after the disconnection of the converter. The reason for the high voltages is related to the high reactive power generation of the large cable connecting wind farm 2 to PCC 2. At the time of the disturbance, the wind farm changes from generating reactive power to consuming reactive power, trying to reduce the voltages in offshore area 2. The wind farm is set to regulate the POI 2, bus number 21. The wind farm immediately consumes the maximum dynamic limit with respect to reactive power, but then decease this reactive consumption. Because wind farm 2 reduces its power output to create an offshore power balance, the excess energy produced during the island operation is stored as kinetic energy in the wind turbines. The speed of the wind turbines and the offshore frequency therefore increases as the converter is disconnected, and returns, however, to pre fault values shortly after the converter is reconnected.

Simulation 2 (Large wind generation)

Time	Event
0.00	Normal operation
0.20	Disconnect (trip) converter 2 and 3
2.20	Reconnect converter 2 and 3 and the associated power transformers

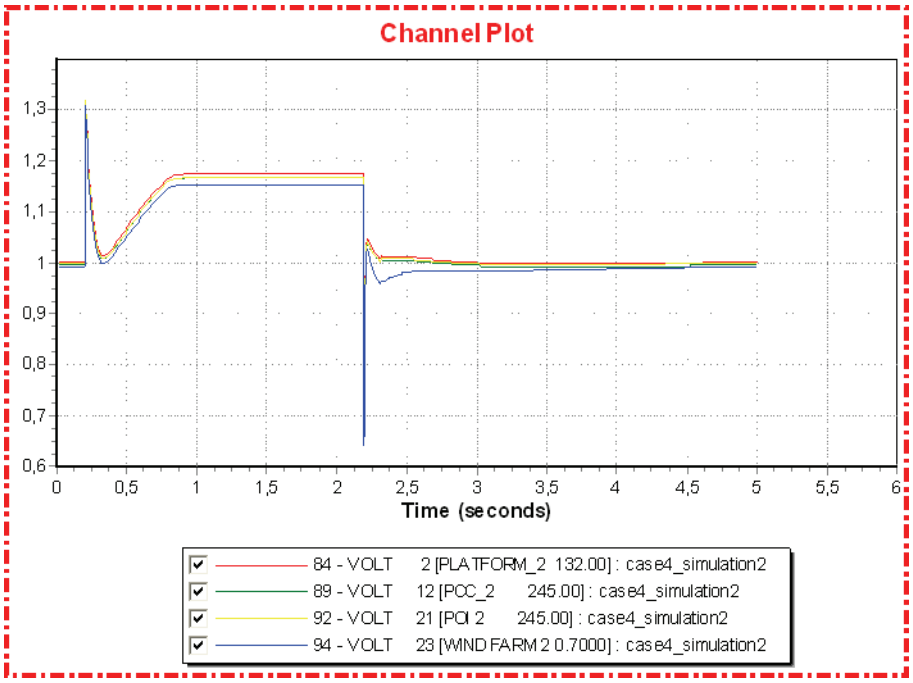

Figure 12.4.9: AC voltage, offshore area 2 [pu]

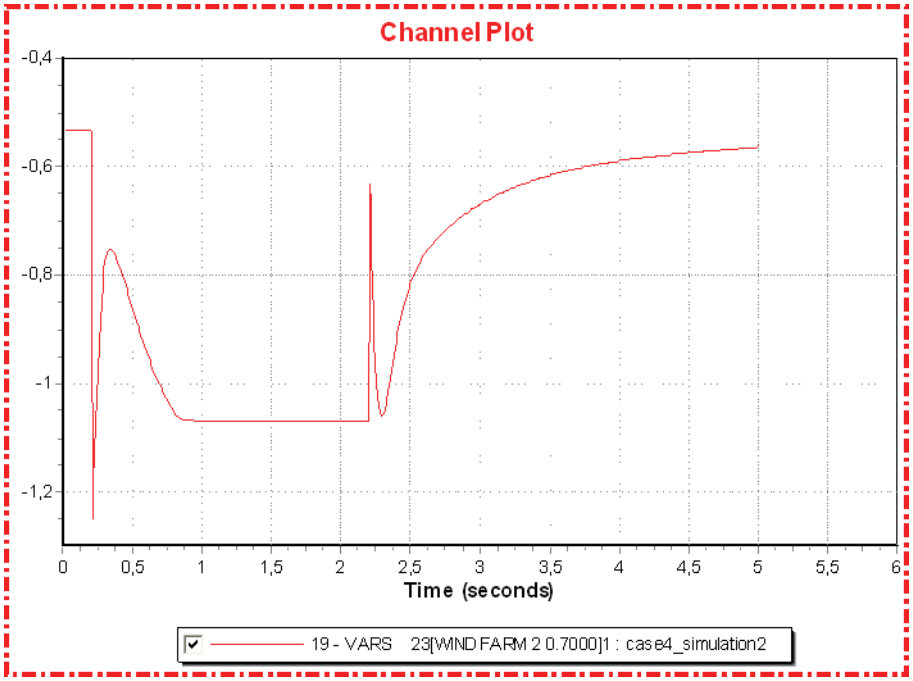

Figure 12.4.10: Reactive power generation, wind farm 2 [pu]

Simulation 2 investigates the longer duration island operation connected to the protection scheme using AC breakers. The results show similar performance in the offshore area 2 as in simulation 1. Wind farm 2 reduces the power generation to match the load, the speed in the wind farm increase, along with the frequency in the offshore system. The voltage is high

during island operation due to the high reactive production in the large AC cable. When the converter is connected this reactive power is delivered to the MTDC. In island operation, however, this is not possible. The wind farm consumes as much reactive power as possible given the dynamic model parameters. In conclusion, the voltage and frequency in offshore area 2 are above the desired value, but the power delivered to the petroleum platform is acceptable.

Simulation 3 (Small wind generation)

Time	Event
0.00	Normal operation
0.20	Disconnect (trip) converter 2 and 3
0.25	Reconnect converter 2 and 3 and the associated power transformers

Simulation 3 investigates the short duration converter disconnection associated with protection using IGBT-CB, and employs the small wind generation power flow scenario. Prior to the disturbance wind farm 2 generates 37.5 MW and the platform load consumes 120 MW. Hence, there is a net power deficit in offshore area 2 at the time of disturbance. Wind farm 2 rapidly increases its power output immediately after the converter is disconnected, and the power output peaks at 125 MW. The extra power generation of the wind farm exhausts the rotating energy of the turbines, leading to a reduction in the wind turbine speed and the offshore frequency. As in the previous simulations the voltages offshore increase due to high reactive generation in the AC cable. The behavior following reconnection of the converter is unproblematic.

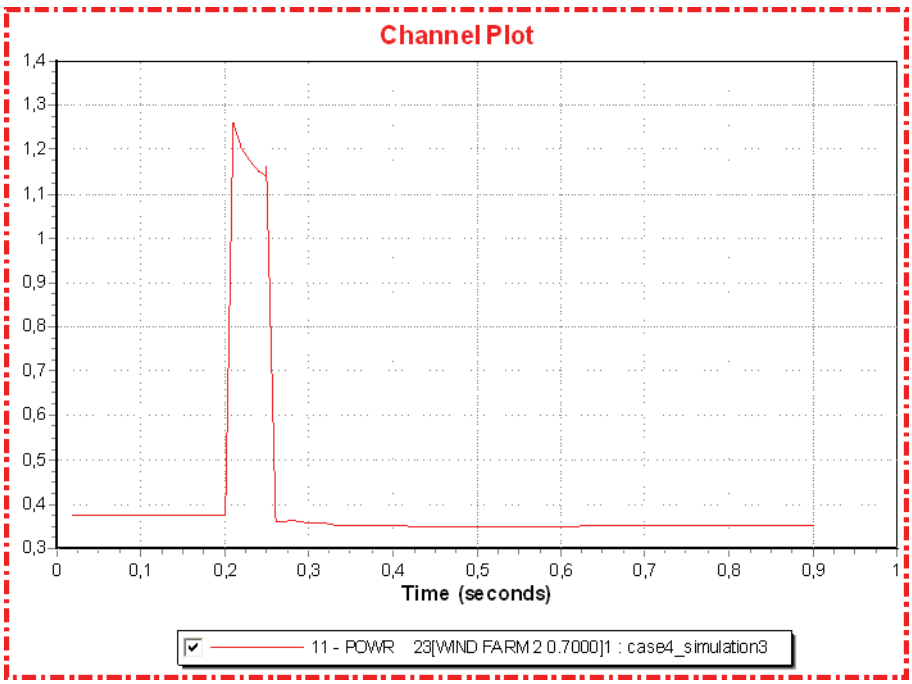

Figure 12.4.11: Active power generation, wind farm 2 [pu]

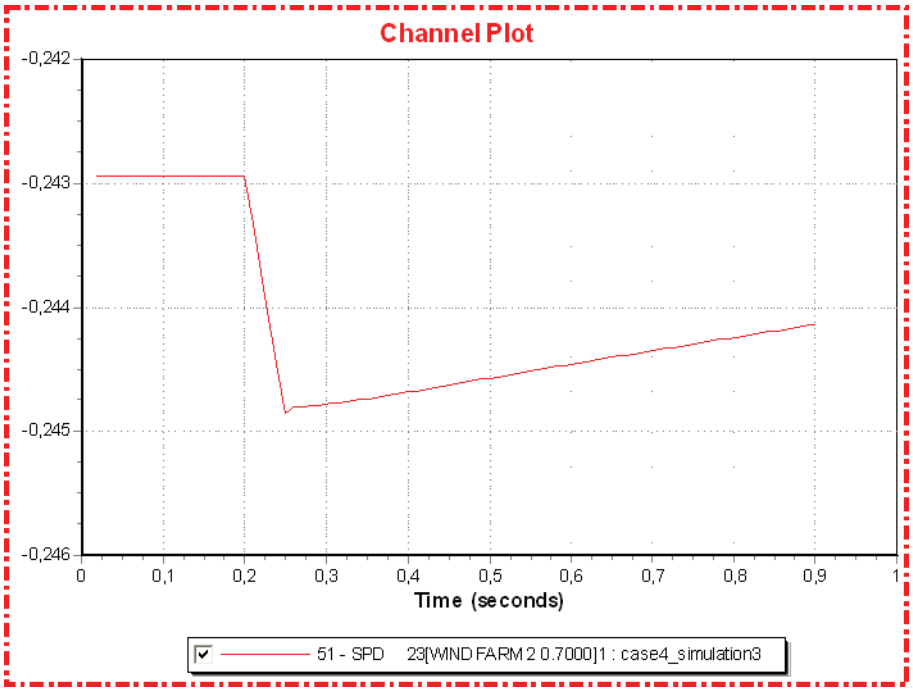

Figure 12.4.12: Turbine speed, wind farm 2 [pu]

Simulation 4 (Small wind generation)

Time	Event
0.00	Normal operation
0.20	Disconnect (trip) converter 2 and 3
2.20	Reconnect converter 2 and 3 and the associated power transformers

Simulation 4 combines the small wind generation power flow scenario and protection using AC breakers, leading to an island operation of 2 seconds. Like in simulation 3, the wind farm increases its power output by drawing power from the rotating energy of the turbines. The consequence is a falling speed in the wind turbines and a lower offshore frequency during island operation. After an initial peak of around 1.27 pu, the voltage stabilize at a lower value than in the other simulations in case 4. This is a result of stable high reactive power consumption in the wind turbines and a pre fault low power generation. The voltage of around 1.07 pu is nevertheless higher than the desired value. Following the reconnection of the converter, wind farm 2 generates less power compared to the pre fault situation. This is to increase the turbine speed to the desired level.

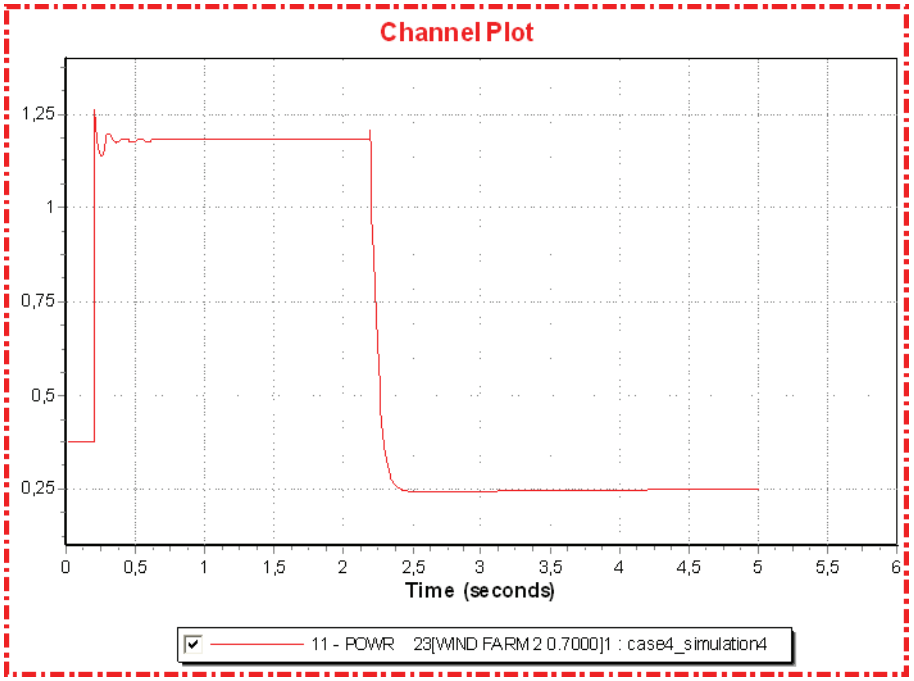

Figure 12.4.13: Active power generation, wind farm 2 [pu]

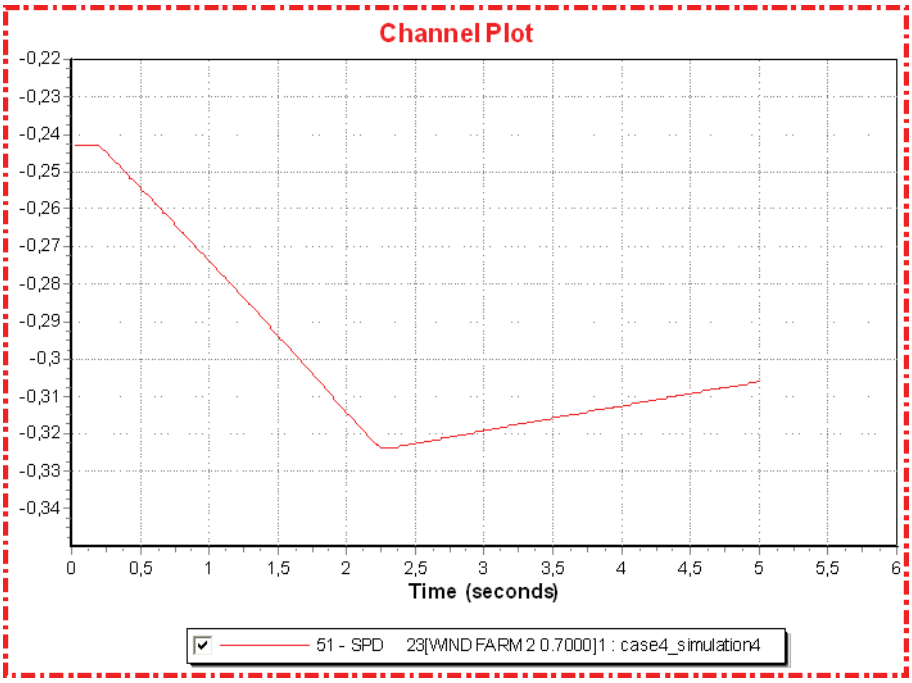

Figure 12.4.14: Turbine speed, wind farm 2 [pu]

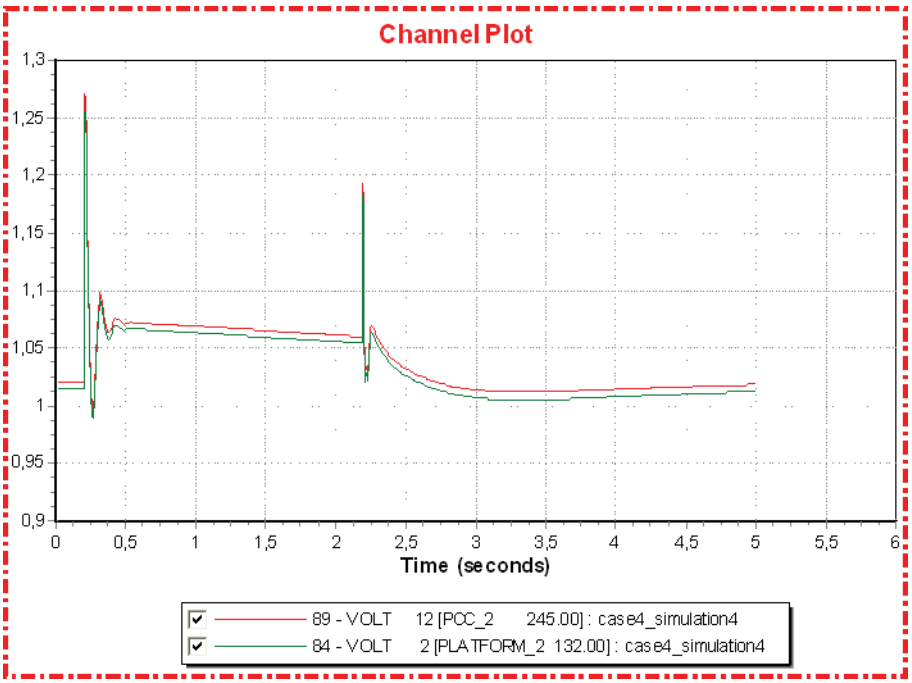

Figure 12.4.15: AC voltage, offshore area 2 [pu]

12.4.1 Comments to case 4 and SVC Light

The motivation for the simulations performed in case 4 was to investigate the dynamic island operation of the offshore AC grids seen in relation to the protection schemes for a MTDC. However, the extent of the simulations was limited due to problems with the simulation model. Thus, some of the intended simulations could not be performed. The limiting modeling problems with respect to the intended simulations and analysis of case 4 are:

- The CLOD model representing the petroleum platforms displayed an unrealistic behavior following a trip of a nearby, power supplying bus, as explained in chapter 9.2.
- Offshore area 3 did not behave in a realistic manner during island operation.

The problem with the CLOD model is the most important limitation for the analysis of case 4. The model could not operate correctly in an island system without being connected to rotating machines. The consequence is that a comparative analysis of the protection schemes' effect on offshore island operation is impossible with the CLOD model, when the petroleum platform is the only component in the offshore system. Unfortunately, connected offshore AC systems that only consist of petroleum installations will probably be very dominant for a realistic implementation of VSC HVDC for interconnection of offshore installations. In addition, for a situation where the offshore AC system consists of both a wind farm and petroleum installations it is impossible to expect the wind farm to be operative constantly. During very high wind speeds the wind turbines may be turned off to prevent mechanical damage, and shut down during maintenance must also be expected.

The problem with offshore area 3 prevents an investigation of island operation where the wind farm has a smaller rating than in offshore area 2.

These problems cause inadequate simulation results, and the subsequent analysis is not able to create general conclusions for the protection schemes based on the simulations.

SVC Light

The dynamic behavior in offshore area 2 demonstrates that the power system performance is acceptable for all the simulations performed, both for 0.05 and 2 seconds duration of the island operation. As explained, this acceptable performance is largely due to the stabilizing effect of the offshore wind farm. The wind farm can quickly change active and reactive power to regulate the system.

An offshore AC system without any wind generation would need an alternative solution to control the system performance during island operation. Such a solution could be a dynamic energy storage, for instance ABB's product *SVC Light with Energy Storage* [62].

SVC Light is ABB's STATCOM concept, utilizing voltage source converters, and combining this with a battery storage makes up the SVC Light with Energy Storage. Having both capacitors and batteries, it can control both reactive power (Q), as an ordinary SVC Light, and active power (P) by means of the batteries.

Using modern electronics, SVC Light with Energy Storage can feed the grid with exactly the right amount of reactive and active power needed at each instant, independently of one another. The Energy Storage can release energy into a load during peak periods and charge surplus energy when demand is low. The SVC Light with Energy Storage serves as a dynamic power source. It supports the grid continuously with reactive power, and in the event of loss of generation, the Energy Storage pushes active power into the grid until the grid is reconfigured

At present, the rated power and capacity are typically in the 20 MW range for tens of minutes, but the technology permits up to 50 MW for periods of 60 minutes and more. ABB has targeted industrial, distribution and transmission level energy storage applications. The focus is particularly on applications that require the combined use of continuous reactive power control and short-time active power.

As the Energy Storage can level out intermittent production and support demand response, its functionality is valuable in the realization of renewable energy sources.

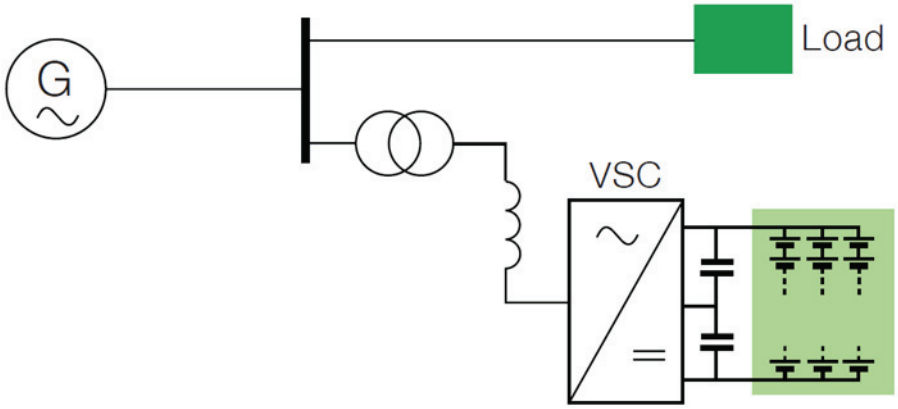

Figure 12.4.16: SVC Light with Energy Storage [62]

12.5 Case 5

The simulations of case 5 are used to investigate the response in an offshore AC grid following the sudden disruption of a large offshore wind power generation. The actions taken by the connected converter to stabilize the offshore AC grid are analyzed. The events of simulation 1 are identical to those of simulation 2 in case 3, see figure 12.3.5, but the attention in this simulation is concentrated on the offshore performance.

Simulation 1 (Large wind generation)

Time	Event
0.00	Normal operation
0.20	Disconnect generator at bus 23 (wind farm 2)

Simulation 2 investigates a disconnection of the large wind farm at offshore area 2. The cable connecting the wind farm to the rest of the offshore AC grid remains in operation. This is to examine the effect of the cables reactive power generation, as it is electrified, but carries no load current, se chapter 4.3 describing SIL.

Immediately after the disturbance, the voltage in offshore area 2 experiences a moderate increase to approximately 1.07 pu before being reduced towards 1.00 pu. The reason for the voltage increase is the high reactive power produced in the subsea cable.

Converter 2, operating in PassNetOp, immediately changes P-Q working point, going from rectifier to inverter mode of operation. The converter also absorbs much of the reactive power in order to control the offshore AC voltage.

It appears that due to the operation of the converter, connecting the offshore AC grid to the MTDC, there are no severe consequences for the offshore AC grid following the disconnection of the associated wind farm.

It is observed that the events of simulation 2 results in a power oscillation between converter 1 and converter 3 in the MTDC. As a result the DC voltage is not able to stabilize at a steady state value after the disturbance, but have a saw tooth shaped oscillation around 1.00 pu. The active and reactive power performance of converter 3 also creates unfavorable system behavior in offshore area 3, for instance a voltage that oscillates around 1.05 pu and an uneven power generation of wind farm 3.

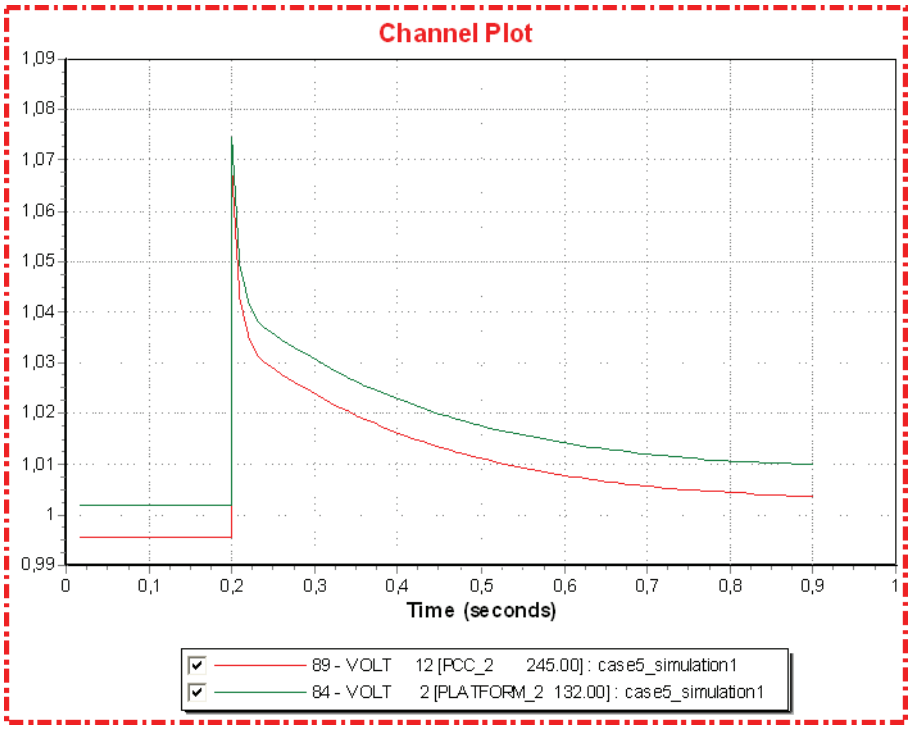

Figure 12.5.1: AC voltage, offshore area 2 [pu]

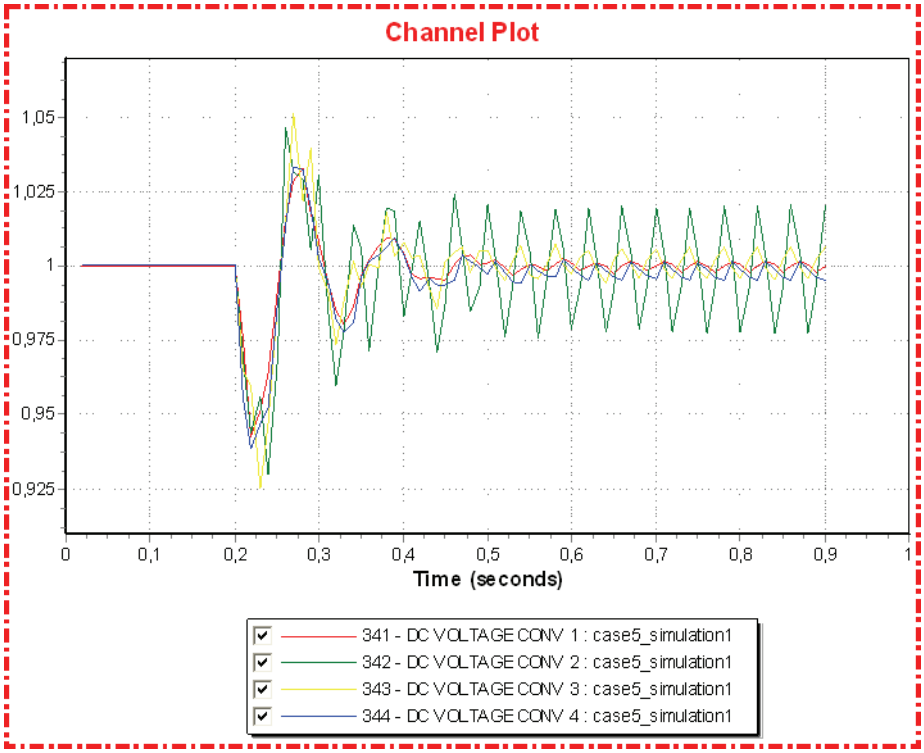

Figure 12.5.2: Converter DC voltage [pu]

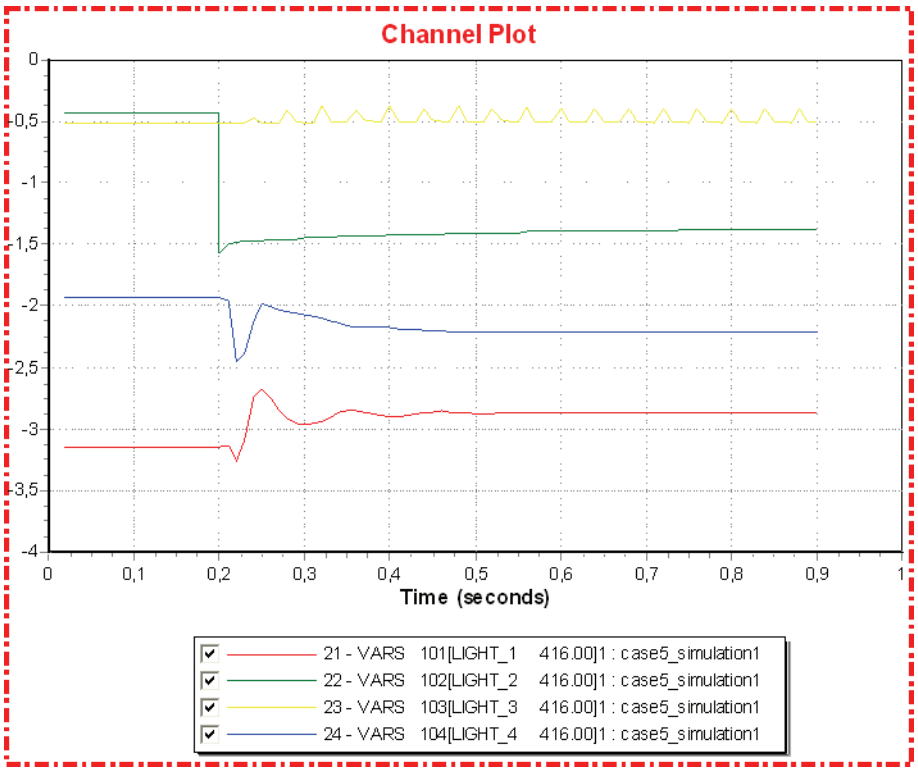

Figure 12.5.3: Converter reactive power [pu]

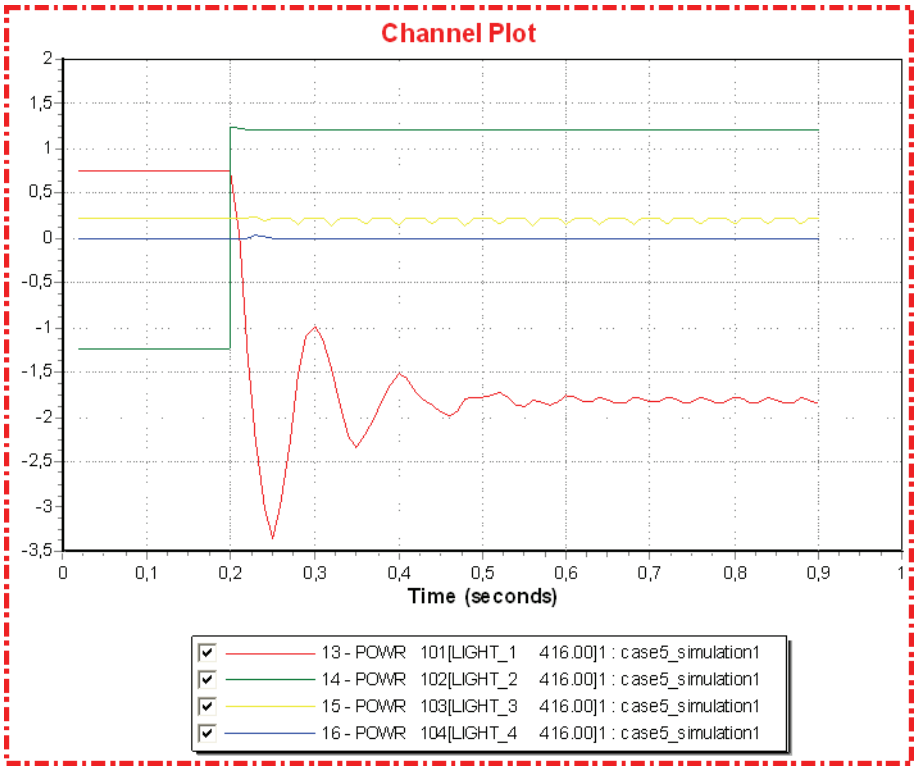

Figure 12.5.4: Converter active power [pu]

Simulation 2 (Large wind generation)

Time	Event
0.00	Normal operation
0.20	Line fault on cable 21 – 12
0.30	Disconnect (trip) faulted line

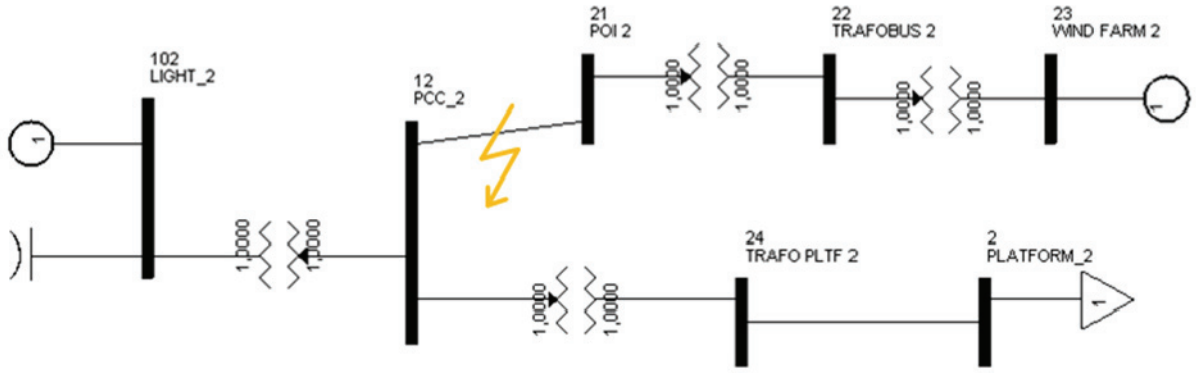

Figure 12.5.6: Dynamic simulation disturbance

Simulation 2 investigates the dynamic response in offshore area 2 following a line fault (more precisely cable fault) in the cable connecting wind farm 2 with the rest of offshore area 2, and a subsequent trip of the faulted cable.

The results show that the offshore AC voltage quickly recovers to the pre fault value, after the faulted cable is disconnected, due to the response of the converter. The power delivered to the petroleum platform initially experiences an overshoot before stabilizing at the pre fault value.

The overshoot is related to the swing equations of rotating machines described in equations (4.18) and (4.19). No power could be transferred to the petroleum platform during the duration of the line fault. As a consequence, the rotating machines, modeled implicitly in the CLOD model, will exhaust their rotating energy to provide the same amount of work at the platform. There is a negative power balance of the machines; the mechanical power out of the machine is larger than the electrical power into the machine. This leads to a reduction of the machine speed. Following the trip of the faulted line, the converter is again able to transfer power to the offshore AC grid, supplying power to the petroleum platform. To restore the pre fault situation in the machines, the power transferred to the petroleum platform following the disconnection will assume a higher value for a limited time duration. This is the explanation for the power overshoot. It is not possible to plot the speed of the platform machines as the petroleum platforms are modeled using the CLOD model.

Despite the response of the converter, a short-circuit fault in the offshore AC grid will prevent power from being delivered to the petroleum platform. Seen in relation to the requirements of a maximum 200 ms loss of power to the petroleum platforms described in chapter 5.1, such a fault must therefore be quickly cleared.

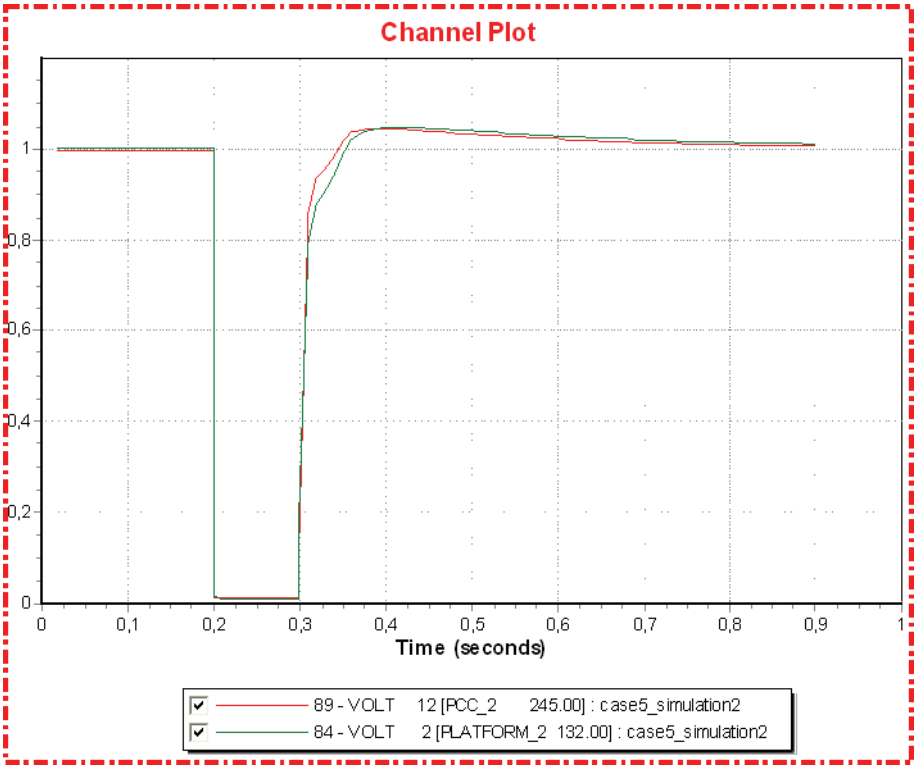

Figure 12.5.7: AC voltage, offshore area 2 [pu]

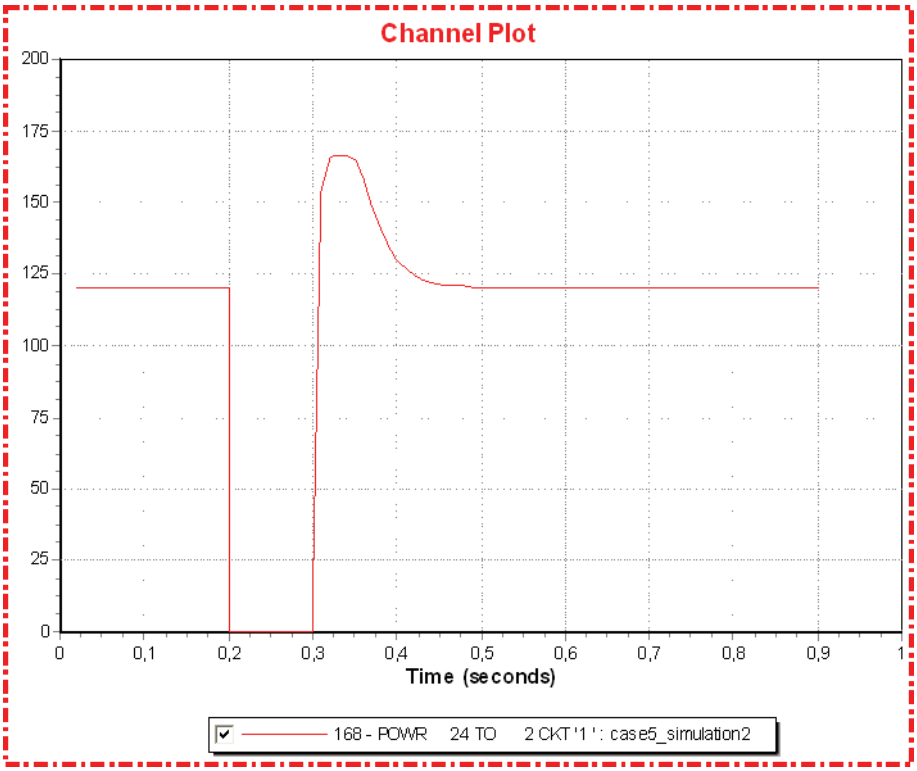

Figure 12.5.8: Active power to platform 2 [MW]

12.6 Case 6

The motivation for the simulations performed in case 6 is to examine the behavior of the MTDC following a disconnection of both the onshore converters. The remaining DC system in operation will then consist of the three DC cables, the onshore choppers associated with the onshore converters and the offshore converters in PassNetOp. In addition, the capacitances of the onshore converters remain in the system after the converters are disconnected. After the disconnection of the onshore converters, operating in UdcCtrl and Pctrl, there are no converters in the MTDC able to operate as the dynamic slack bus maintaining MTDC power balance and controlling the DC voltage. The offshore converters cannot assume this task because they are connected to weak AC systems with very limited flexibility in the power generation.

The small wind generation scenario is applied to demonstrate a situation with a net power deficit offshore, leading to a discharge of the DC capacitances. Oppositely, the large wind generation scenario demonstrates a situation with a net power surplus offshore, thus charging the DC capacitances.

Simulation 1 (Small wind generation)

Time	Event
0.00	Normal operation
0.20	Disconnect (trip) converter 1 and 4

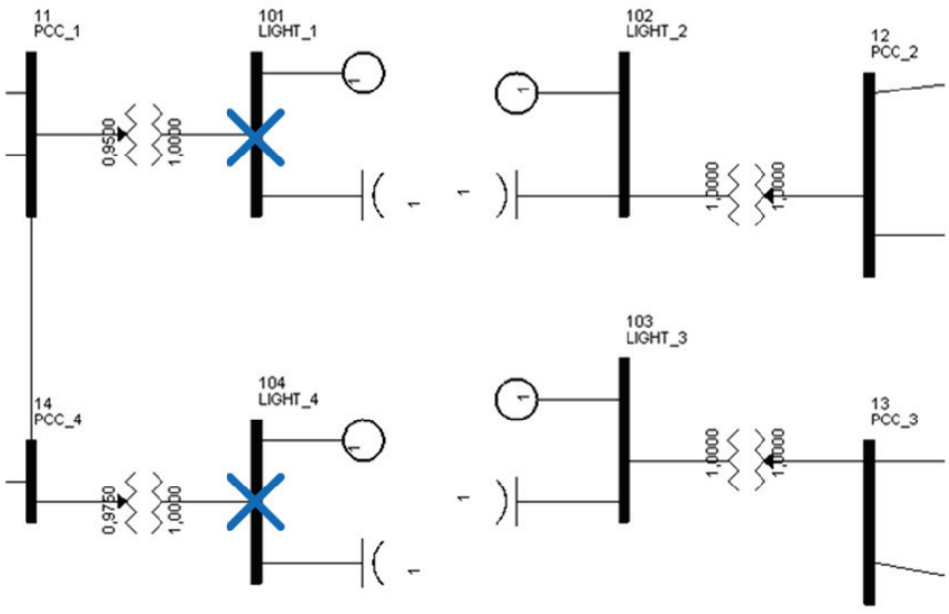

Figure 12.6.1: Dynamic simulation disturbance

Prior to the disconnection of the onshore converters, the offshore converters are operating in inverter mode supplying power to the offshore AC grids. The situation after the disturbance is that no power is injected into the MTDC while the offshore converters continue to deliver power from the MTDC to the offshore AC grids. The offshore converters remain in this operation after the disconnection because they are set in PassNetOp, aiming to support the offshore AC grids. The negative power balance will discharge the DC capacitances and the DC voltage drops. The offshore converters increase their converter current trying to deliver the constant amount of power, but as the energy of the MTDC is discharged, the converter power falls. The offshore converters fail to regulate the offshore grid performance and the voltage of the offshore grids also drop.

The DC voltage continues to drop linearly for 0.114 seconds after the disturbance until it reaches 0.5 pu. At this point the system collapses, and the simulation results showing the DC voltage is no longer applicable, but illustrates the collapse of the MTDC.

With the simplification of a linear fall in the power from the offshore converters to the offshore AC grids, an estimate has been made of the delivered energy from the MTDC before the collapse. This was then compared to the stored energy in the MTDC at the time of disconnection of the onshore converters. Approximately 69.2 percent of the stored energy in the MTDC was extracted before the collapse. For calculations see appendix E.

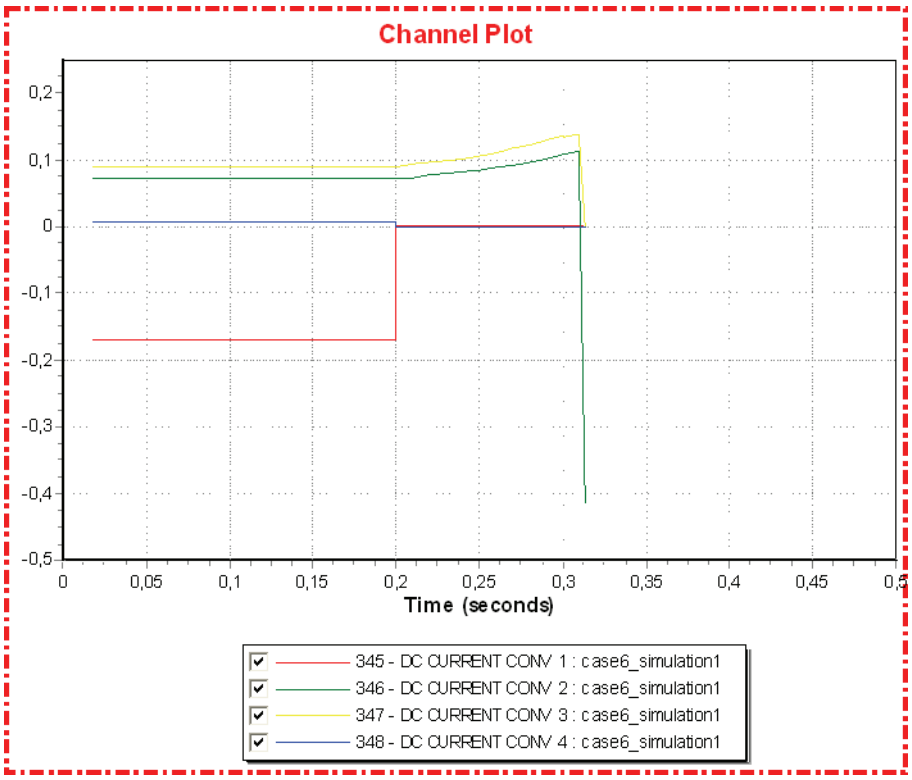

Figure 12.6.2: Converter DC current [pu]

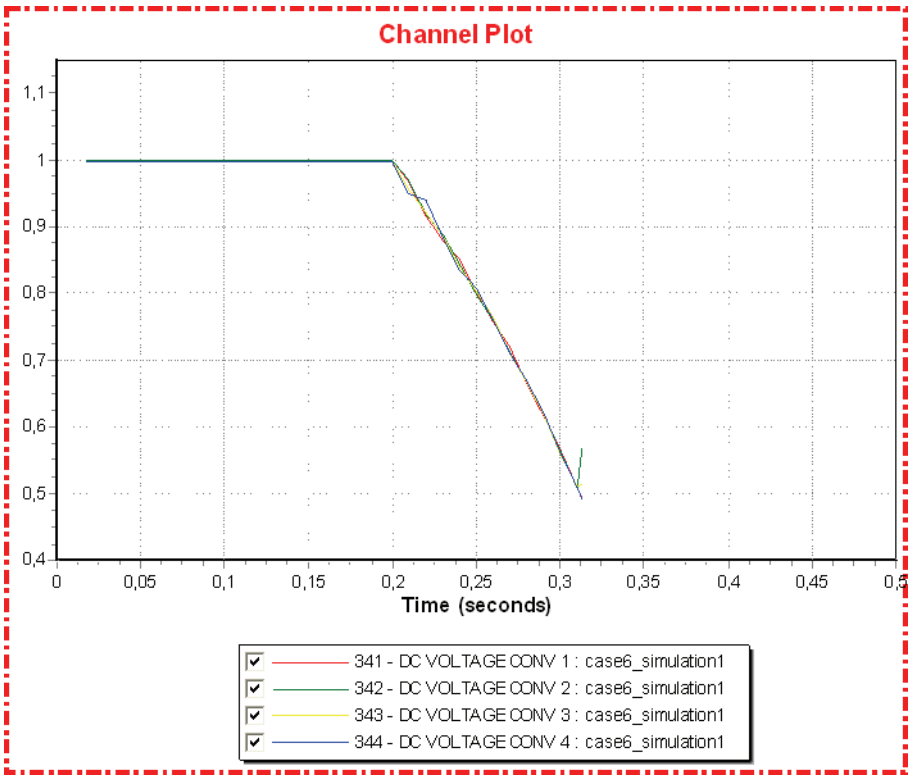

Figure 12.6.3: Converter DC voltage [pu]

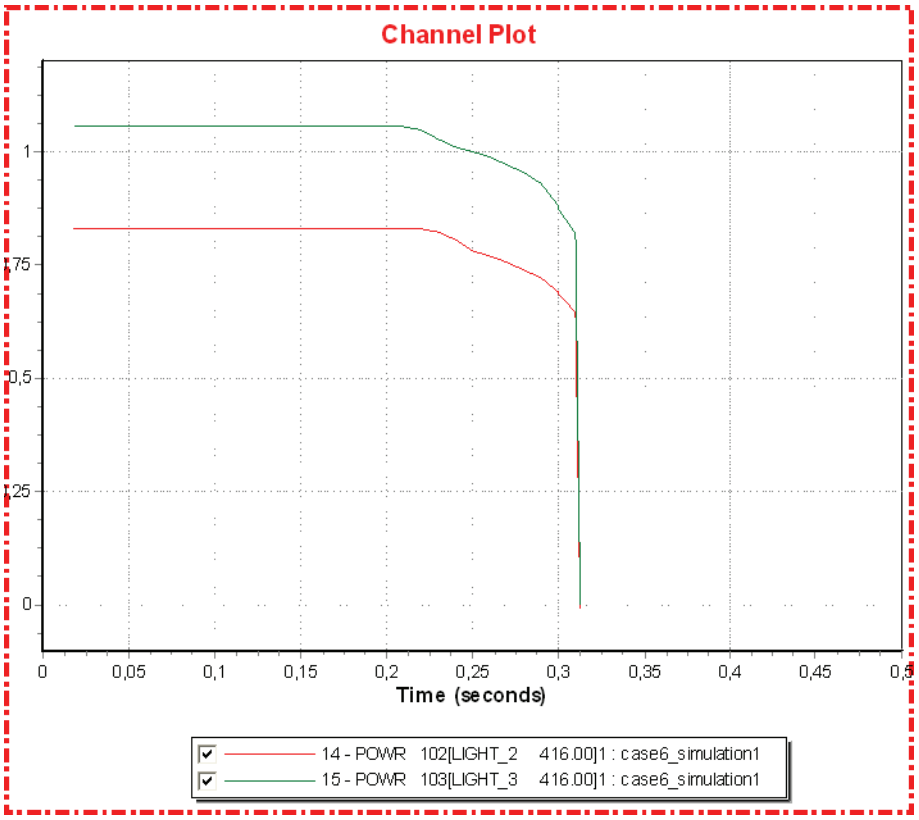

Figure 12.6.4: Offshore converters active power [pu]

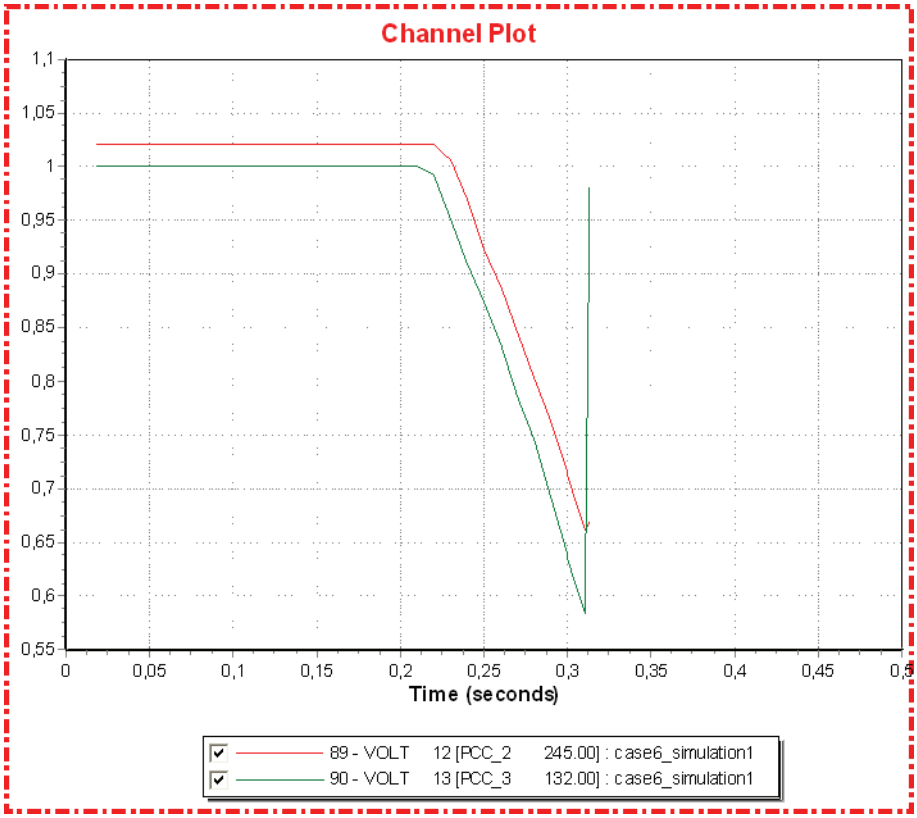

Figure 12.6.5: Offshore AC voltages [pu]

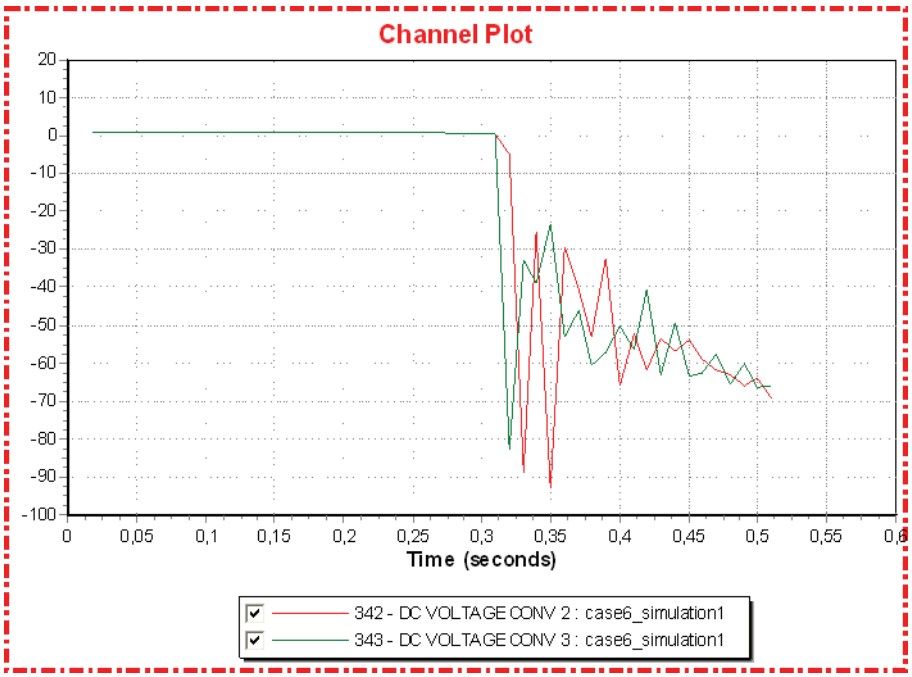

Figure 12.6.6: Converter DC voltage [pu]

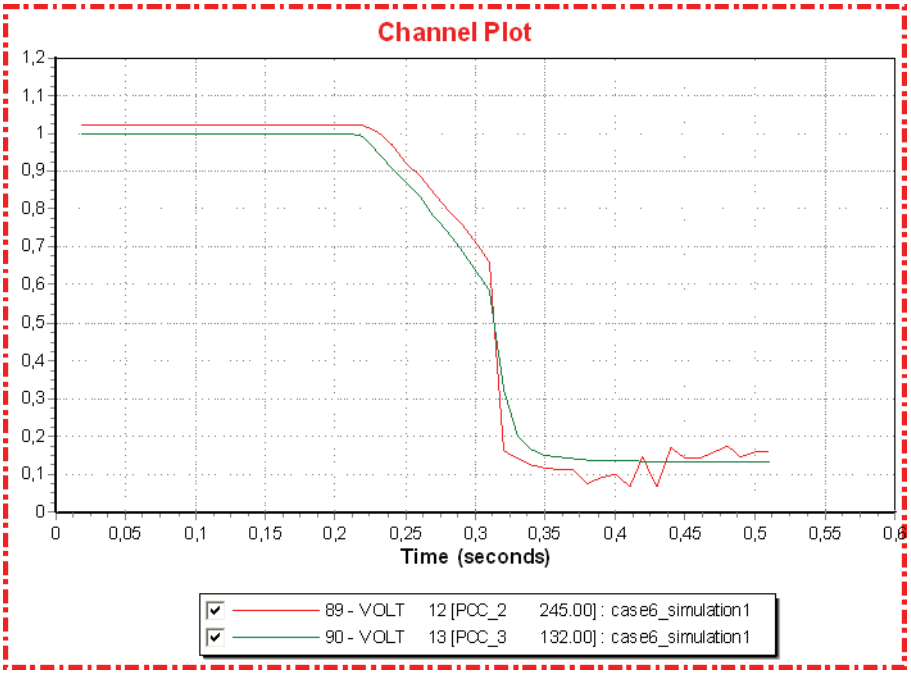

Figure 12.6.7: Offshore AC voltages [pu]

Simulation 2 (Large wind generation)

Time	Event
0.00	Normal operation
0.20	Disconnect (trip) converter 1 and 4

Simulation 2 demonstrates the function of onshore choppers, as described in chapter 8.4. The disconnection of the onshore converters results in a MTDC with no converters capable of controlling the DC voltage. As the offshore converters operate in PassNetOp they passively receive the net power surplus from the offshore AC grids leading to a charging of the DC capacitors, and the DC voltage rises.

When the DC voltage rise above a pre defined level, in this case 1.25 pu, the choppers, located close to the disconnected onshore converters, come into operation. The choppers dissipate excess energy in the MTDC in large power pulses, se figure 12.6.9. This action discharges the DC capacitances, and the DC voltage falls almost immediately to around 0.94 pu. The sequence of events is then repeated until a converter with the ability to control the DC voltage is reconnected or the chopper reaches its energy capacity, at which point it will be disconnected and the MTDC will be overcharged and collapse.

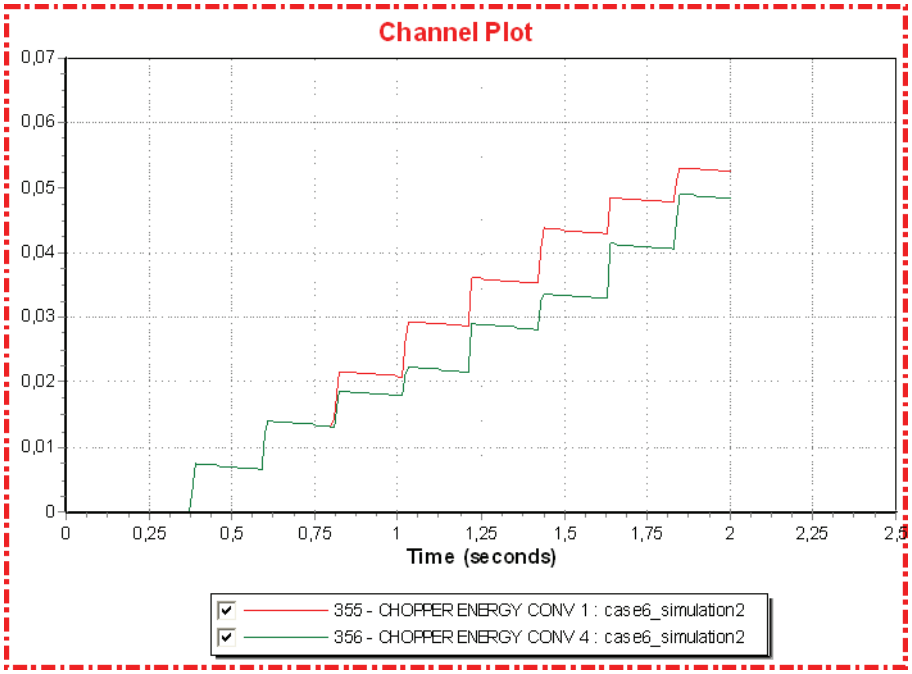

Figure 12.6.8: Dissipated chopper energy [pu]

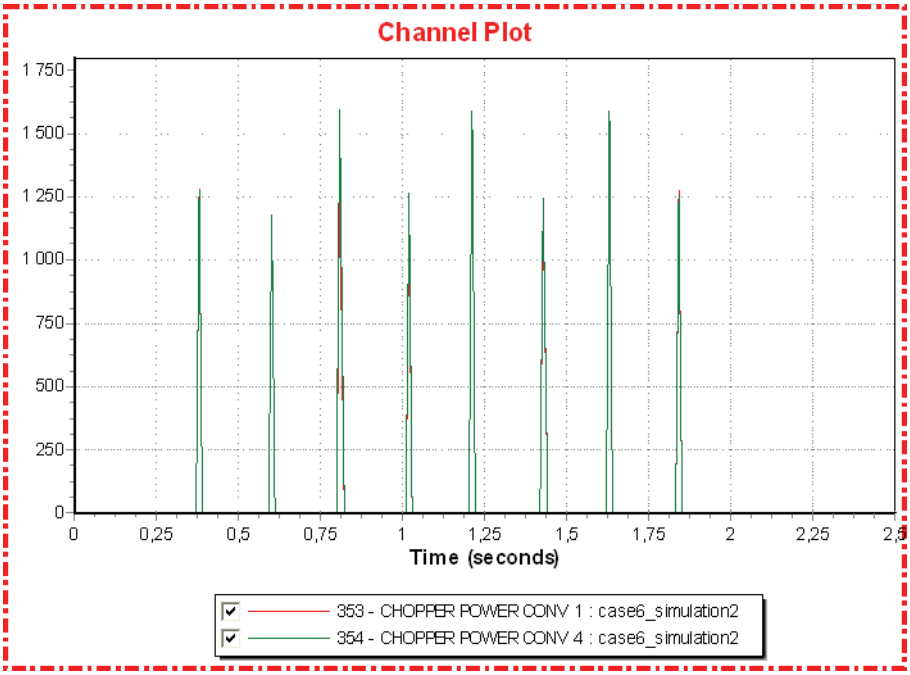

Figure 12.6.9: Dissipated chopper power [pu]

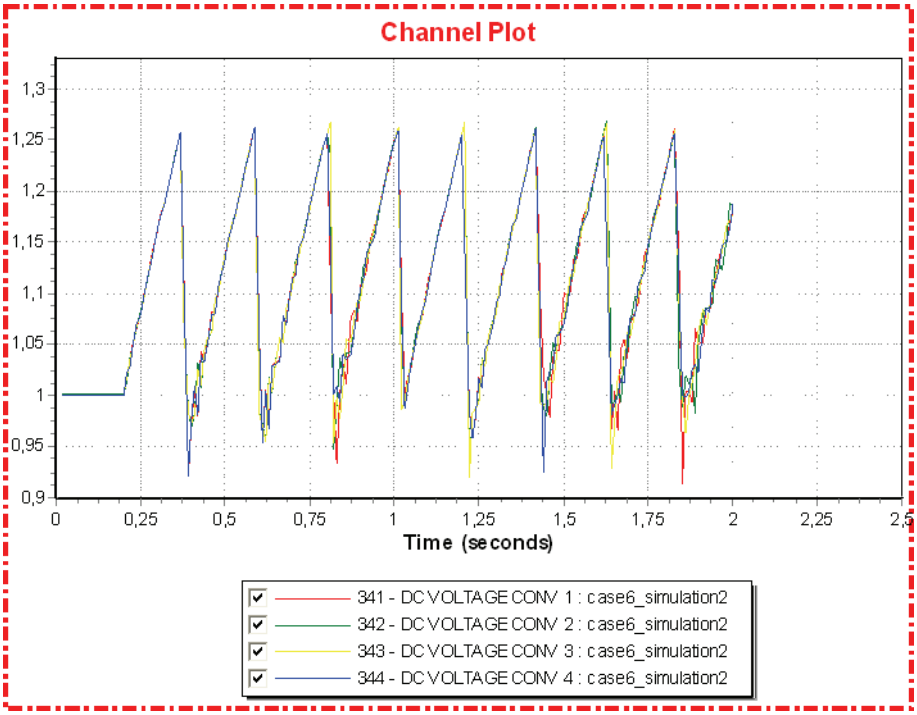

Figure 12.6.10: Converter DC voltage [pu]

Simulation 3 (Large wind generation)

Time	Event
-0.00	Remove the choppers connected to the onshore converters
0.00	Normal operation
0.20	Disconnect (trip) converter 1 and 4

Simulation 3 demonstrates the situation described previously when both the onshore converters are disconnected and there are no choppers in operation. The consequences for the MTDC are opposite to those in simulation 1 where the small wind generation scenario was applied.

The DC voltage rises linearly following the disconnection of the onshore converters, due to the constant power injected by the offshore converters. When the DC voltage reaches 1.75 pu, about 0.6 seconds after the disturbance, the dynamic results of the simulation model start to behave in an unrealistic manner indicating a complete collapse of the MTDC. Offshore converter 2 changes operation mode from rectifier to inverter, and delivers almost 1700 MW to offshore area 2. Considering that the rating of converter 2 is 405 MW in steady state and that offshore area 2 has a net power surplus of around 123 MW, there is absolutely no reason for converter 2 to deliver 1700 to the offshore AC grid. As a result, the voltage at offshore area 2 rises to 7.5 pu, and the wind farm consumes large amounts of power. All these results indicate that the system collapses as the DC voltage reaches 1.75 pu.

The following warning message from the HVDC Light model is printed at the time of collapse. This message indicates that the DC voltage is too high and that the converters should

be disconnected to protect the equipment. The disconnection must be handled manually by the user.

```
************  ABB HVDC Light® ****************

 Simulation time:                          0.7929934
 User model: CABBOM
 Version: 1.1.9-2
 Converter number:               1
 Filterbus node number in PSS/E:                  101
 Warning and Error messages

 Total registered errors:                           1
 Number of written error messages:                  1

   1) TripOrder activated du to high Udc. SoftTrip implemented as Ipcc
      calculated to zero.

 *******  ABB HVDC Light®, End of messages CABBOM, Converter *******


 ************  ABB HVDC Light® ****************

 Simulation time:                          0.7929934
 User model: CABBOM
 Version: 1.1.9-2
 Converter number:               2
 Filterbus node number in PSS/E:                  102
 Warning and Error messages

 Total registered errors:                           1
 Number of written error messages:                  1

   1) TripOrder activated du to high Udc. SoftTrip implemented as Ipcc
      calculated to zero.

 *******  ABB HVDC Light®, End of messages CABBOM, Converter *******


 ************  ABB HVDC Light® ****************

 Simulation time:                          0.7929934
 User model: CABBOM
 Version: 1.1.9-2
 Converter number:               3
 Filterbus node number in PSS/E:                  103
 Warning and Error messages

 Total registered errors:                           1
 Number of written error messages:                  1

   1) TripOrder activated du to high Udc. SoftTrip implemented as Ipcc
      calculated to zero.

 *******  ABB HVDC Light®, End of messages CABBOM, Converter *******


 ************  ABB HVDC Light® ****************

 Simulation time:                          0.7929934
 User model: CABBOM
 Version: 1.1.9-2
 Converter number:               4
 Filterbus node number in PSS/E:                  104
 Warning and Error messages

 Total registered errors:                           1
 Number of written error messages:                  1

   1) TripOrder activated du to high Udc. SoftTrip implemented as Ipcc
      calculated to zero.

 *******  ABB HVDC Light®, End of messages CABBOM, Converter ******
```

At the same time as the message is printed, the converter current in all the converters are set to zero. The MTDC system shuts down.

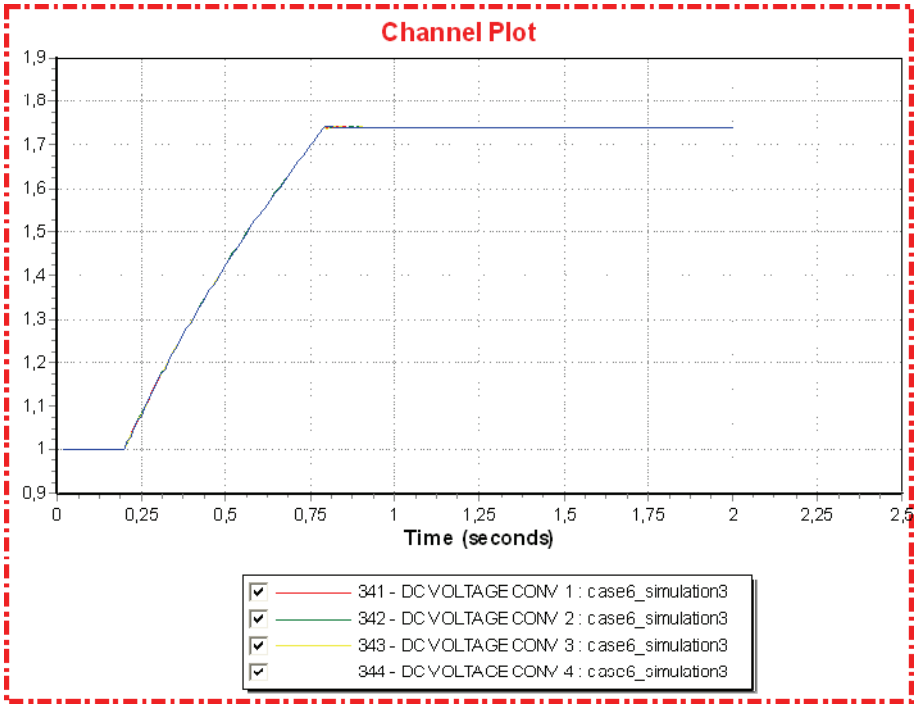

Figure 12.6.11: Converter DC voltage [pu]

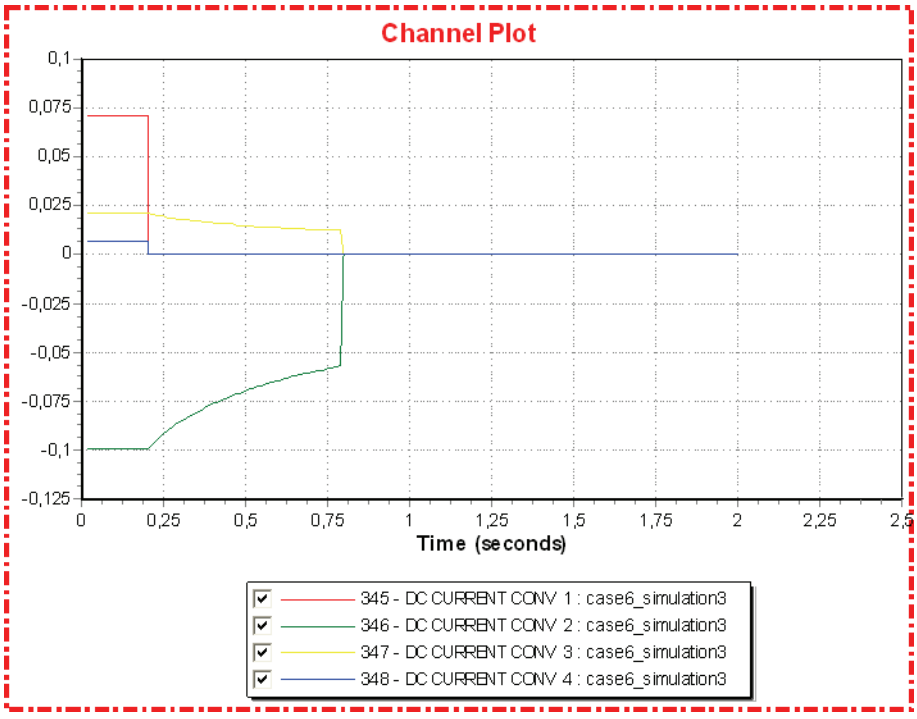

Figure 12.6.12: Converter DC current [pu]

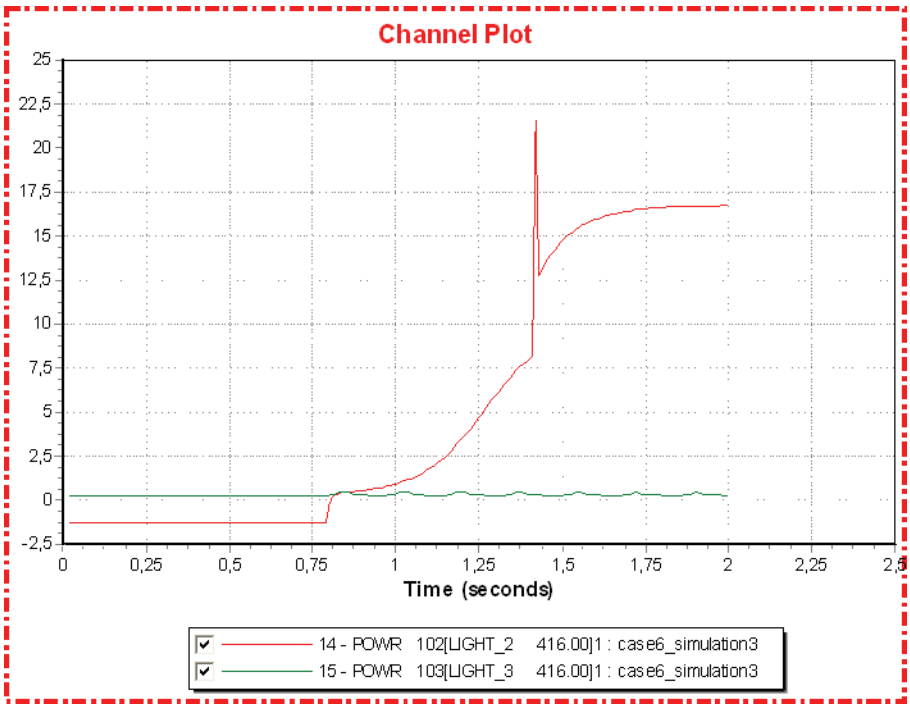

Figure 12.6.13: Offshore converters active power [pu]

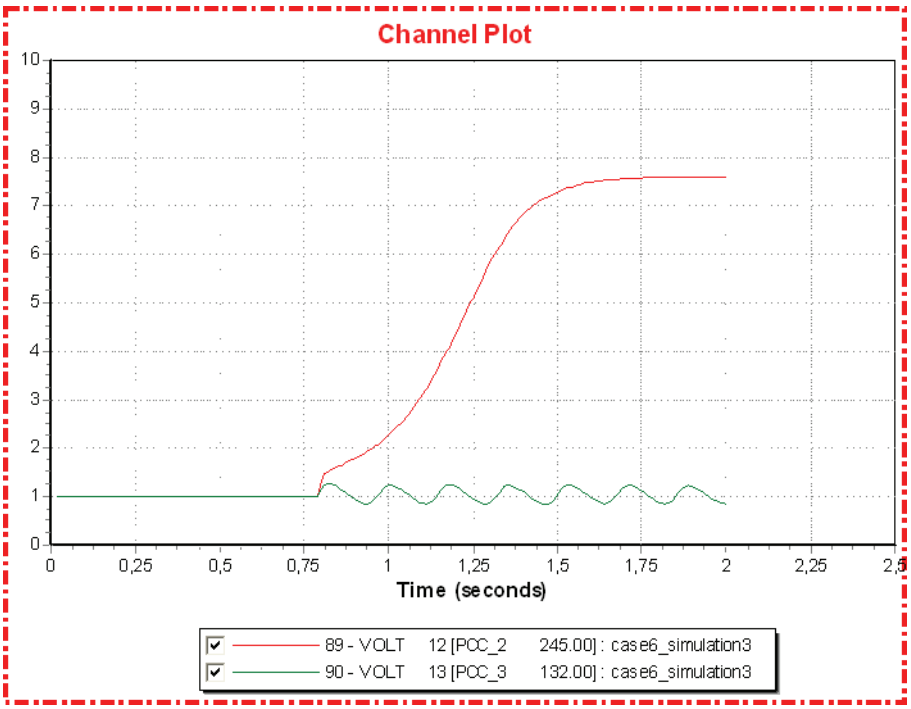

Figure 12.6.14: Offshore AC voltages [pu]

12.7 Case 7

Case 7 investigates the use of the MTDC as an alternative path for transferring large amounts of power in the case of an onshore disturbance that prohibits large power transmission within the onshore grid. An onshore AC grid with two converter connections to a MTDC, like the system modeled in this thesis, would consequentely have the ability to use the MTDC for improving the security of supply. The importance of a well developed control system for regulating the active power control option (Poption) of the converters is also demonstarted. Simulation 1 is intended as a reference case demonstrating the system response when no alterations in Poption are made. The large power transfer power flow scenario is used for both the simulations in case 7.

The onshore system may be viewed as two parts following the disconnection of the line between bus 11 and 14. These parts are referred to as the upper part, consisting of bus 1, 5, 11 and 101, and the lower part, consisting of bus 4, 14 and 104, of the onshore grid.

Simulation 1 (Large power transfer)

Time	Event
0.00	Normal operation
0.20	Line fault on line 14 – 11
0.30	Disconnect (trip) faulted line

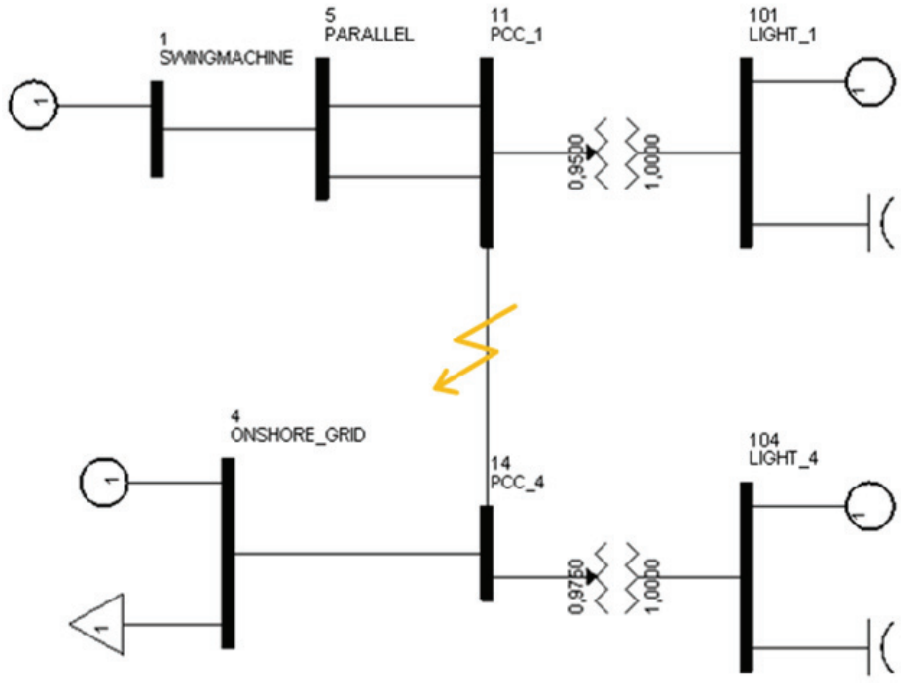

Figure 12.7.1: Dynamic simulation disturbance

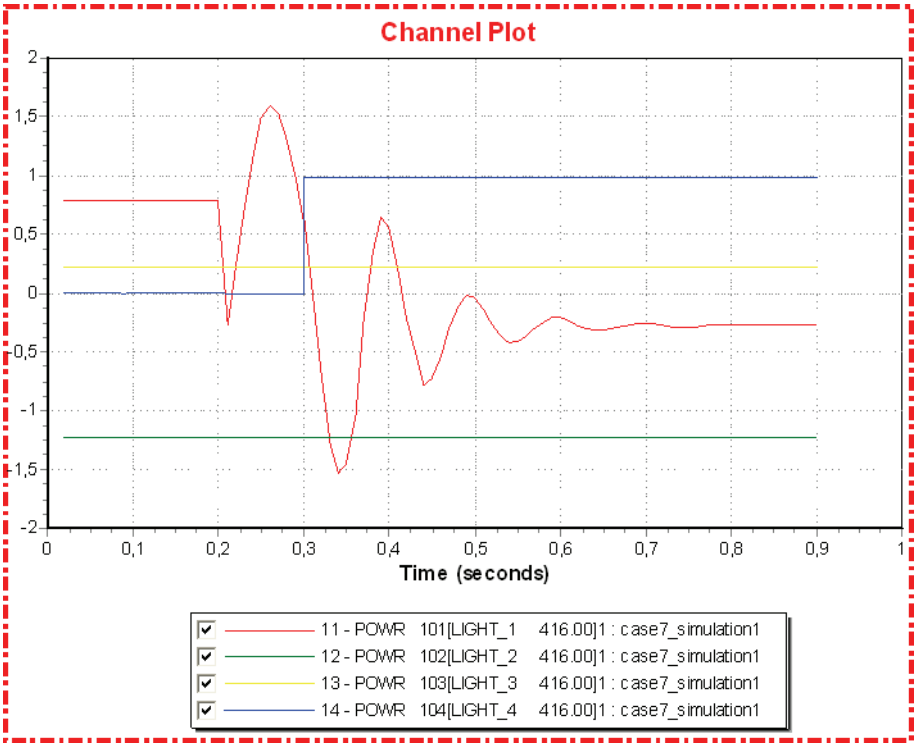

Figure 12.7.2: Converter active power [pu]

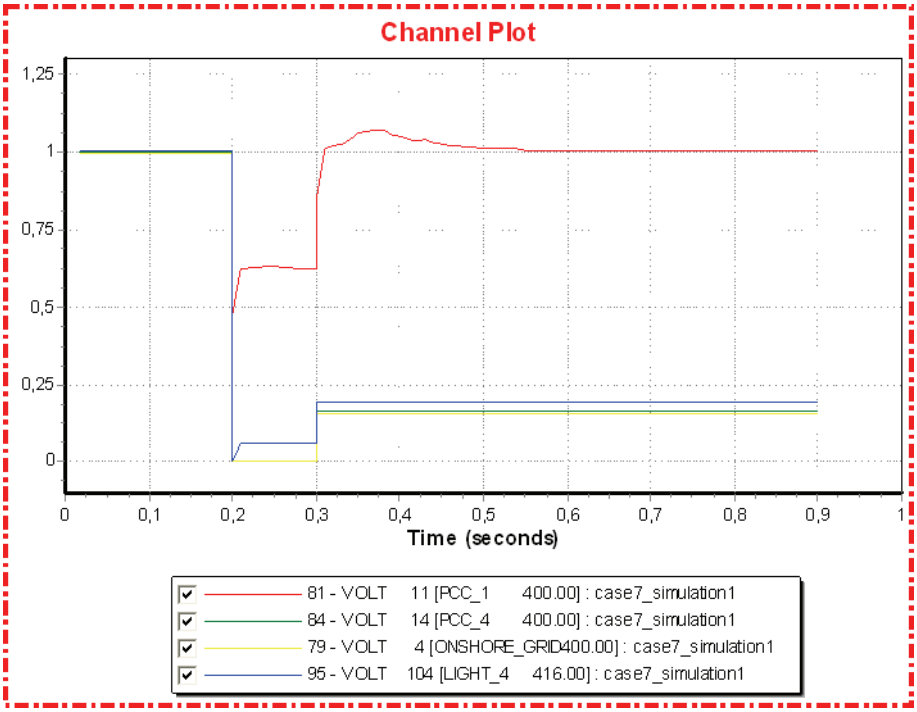

Figure: 12.7.3: Onshore AC voltages [pu]

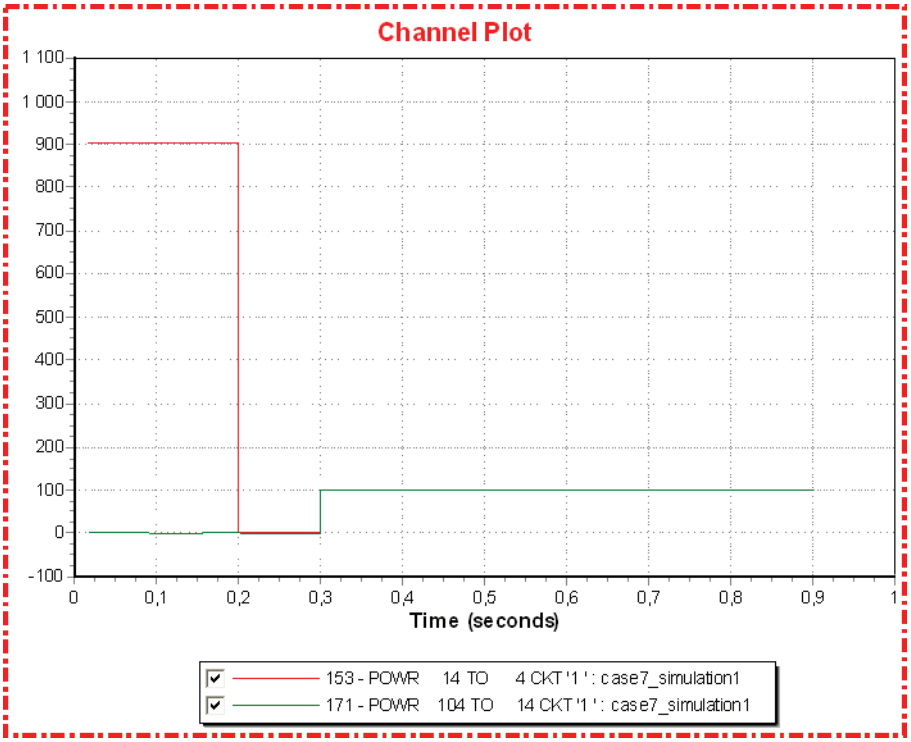

Figure 12.7.4: Onshore power flow [MW]

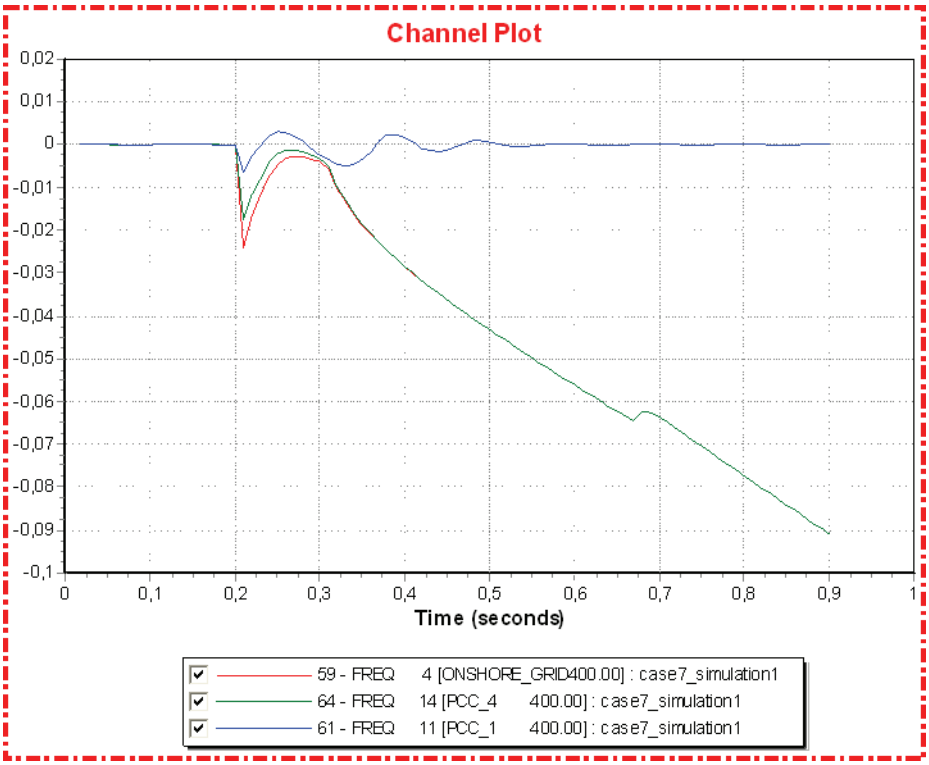

Figure 12.7.5: Onshore frequency [pu]

The results from simulation 1 demonstrate how the MTDC system is unable to maintain an acceptable system performance in the lower part of the onshore system when the Poption of converter is not altered to match the new situation. Following the disconnection of the faulted

line, the lower part of the onshore grid is isolated from the upper part of the onshore grid, including the generator at bus 1 supplying most of the power to the load at bus 4.

Converter 4 remains in Pctrl after the disturbance and therefore tries to keep its active power output at the same level as prior to the disturbance, which was 0.0 MW. However, from the plot illustrating the converter power, it is clear that converter 4 changes its active power output to 100 MW (1 pu) immediately after the faulted line is disconnected leading to isolation of the lower part of the grid. The explanation for this behavior is related to the two different principal philosophies for converter control, Pctrl and PassNetOp, in addition to the mandatory UdcCtrl.

In Pctrl a converter follows the phase angle of the connected AC system, and indirectly the frequency, using a PLL. The control system operates in the dq–reference frame and calculates a current order that is injected or absorbed from the AC system using a current regulator. The entire control principle is based on the assumption that the AC system phase angle (and frequency) is decided by the AC system, not the converter. In the situation investigated in simulation 1, there is no generator in the lower part of the onshore AC grid following the disconnection of the fault, and the PLL attempts to synchronize up against something that does not exist. The PLL tries to follow the AC system phase angle, but the only component in the isolated system that controls a phase angle is the converters PLL. The fundamental condition for the control philosophy for Pctrl is false, and the system does not function as intended. The collapse in lower part of the grid results in a very rapid change in phase angle that the PLL control system is unable to follow. The error in the angles then leads to the active power from converter 4 to bus 4 and 14.

When a converter operates in PassNetOp the assumption is that the converter is the strongest component in the connected AC system, and therefore controls the phase angle, i.e. the PLL has a constant position. The AC system therefore follows the converter.

The collapse in the lower part is clear from the figures illustrating voltage and frequency, despite the active power error in converter 4.

Simulation 2 (Large power transfer)

Time	Event
0.00	Normal operation
0.20	Line fault on line 14 – 11
0.30	Disconnect (trip) faulted line and change Poption for converter 4 to PassNetOp

The disturbance subjected to the onshore AC grid is exactly the same as in simulation 1, but the Poption of converter 4 is manually altered from Pctrl to PassNetOp as the faulted line is disconnected.

The dynamic response of simulation 2 offers very interesting results, both in the MTDC and in the onshore AC grid.

Converter 4 immediately changes P-Q working point and extracts large amounts of power from the MTDC to supply the lower onshore grid, following the disconnection and change in Poption. The result is that the DC voltage experience a large and rapid fall to around 0.65 pu, before converter 1 is able to restore the power balance in the MTDC. The DC voltage then experiences a few transient oscillations before stabilizing at 1.0 pu.

The power consumption in the load at bus 4 does not immediately reach the pre fault level of 900 MW, but experience one oscillatory swing around 700 MW before increasing to 900 MW. The explanation for this behavior is most likely connected to the parameters given for conversion of system loads prior to the dynamic simulation, see table 11.2. The load is 40 percent dependent on voltage and 20 percent dependent on voltage squared. As the voltage also experience the same oscillatory swing before reaching the pre fault value of 1.0 pu, the power demand at the load is limited by the voltage level.

In addition to the active power delivered, converter 4 also adjusts the reactive power supply to the lower onshore grid to regulate the AC voltage. The frequency in the lower part of the grid stabilizes at a slightly lower level than prior to the disturbance.

By changing Poption for converter 4 from Pctrl to PassNetOp as the lower onshore grid is isolated from the power generation at bus 1, converter 4 starts acting as the dynamic slack bus, controlling the lower onshore grid. The result is that voltage, frequency and power balance is maintained at the desired level. This emphasizes the importance of a flexible and well developed control system for the Poption of the converters in a MTDC, as explained in previous cases.

Realistically it is possible that the control system will not be fast enough to change the Poption of converter 4, leading to a Black Out of the lower onshore part. Converter 4 could then be used to initiate a Black Start.

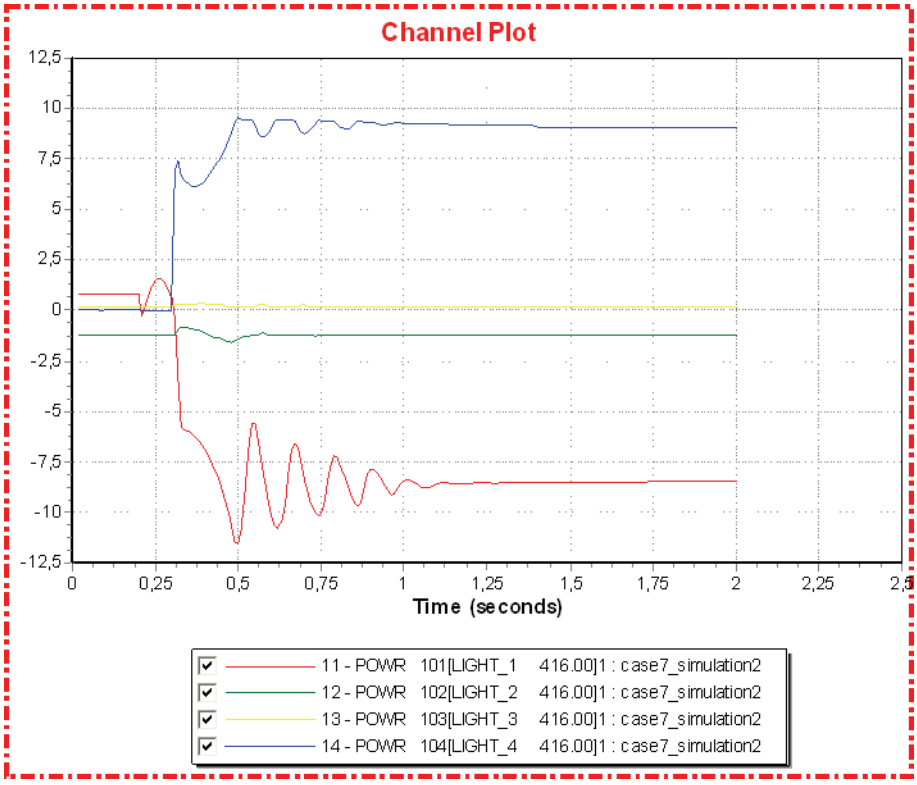

Figure 12.7.6: Converter active power [pu]

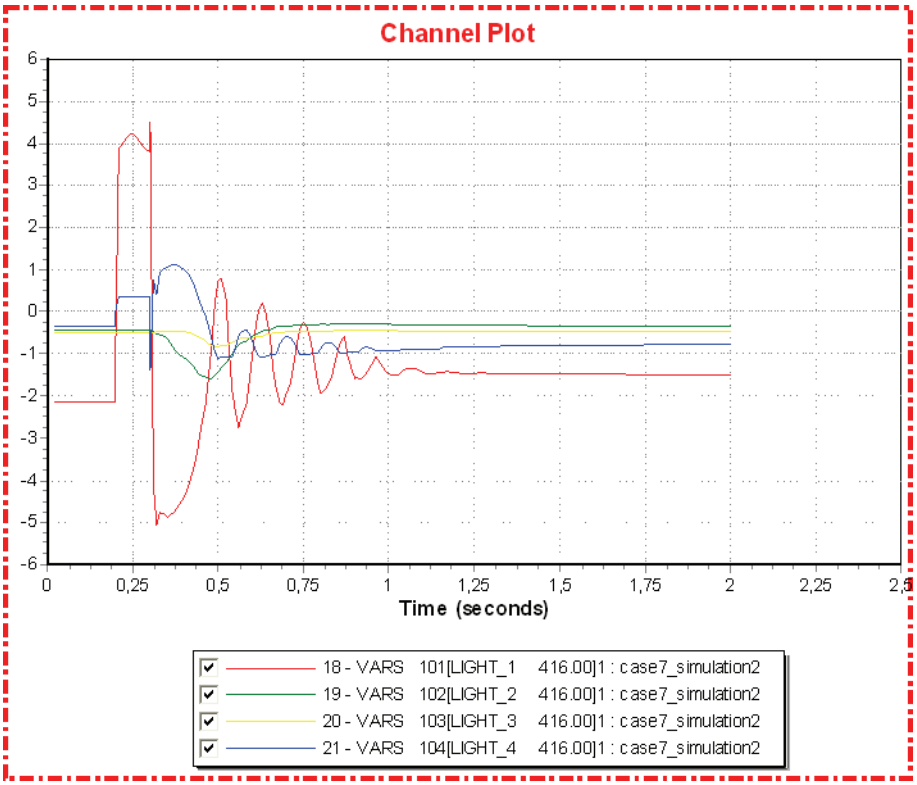

Figure 12.7.7: Converter reactive power [pu]

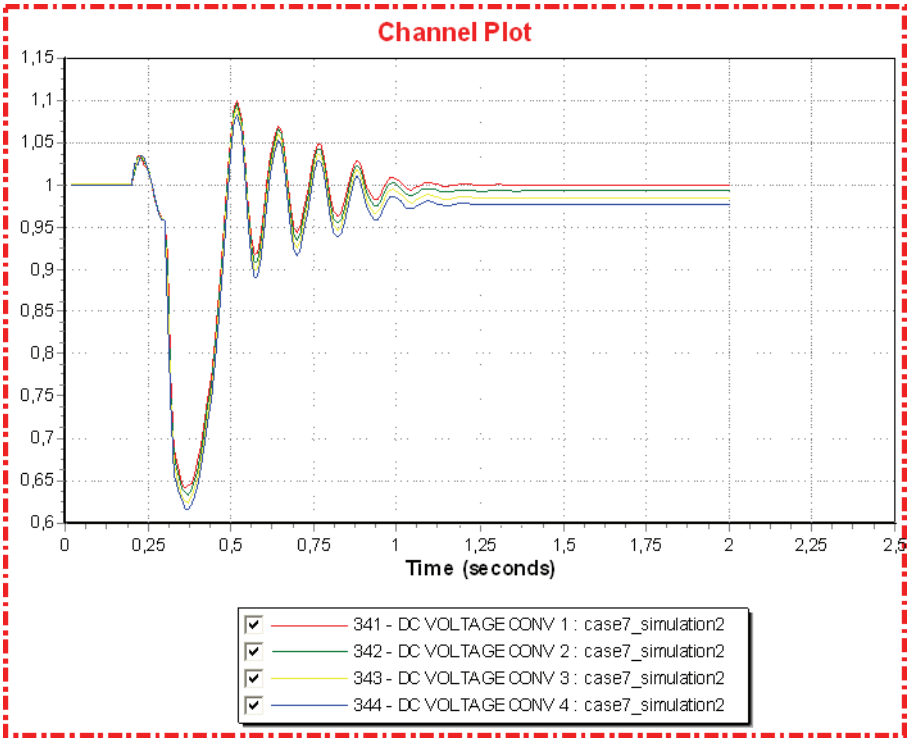

Figure 12.7.8: Converter DC voltage [pu]

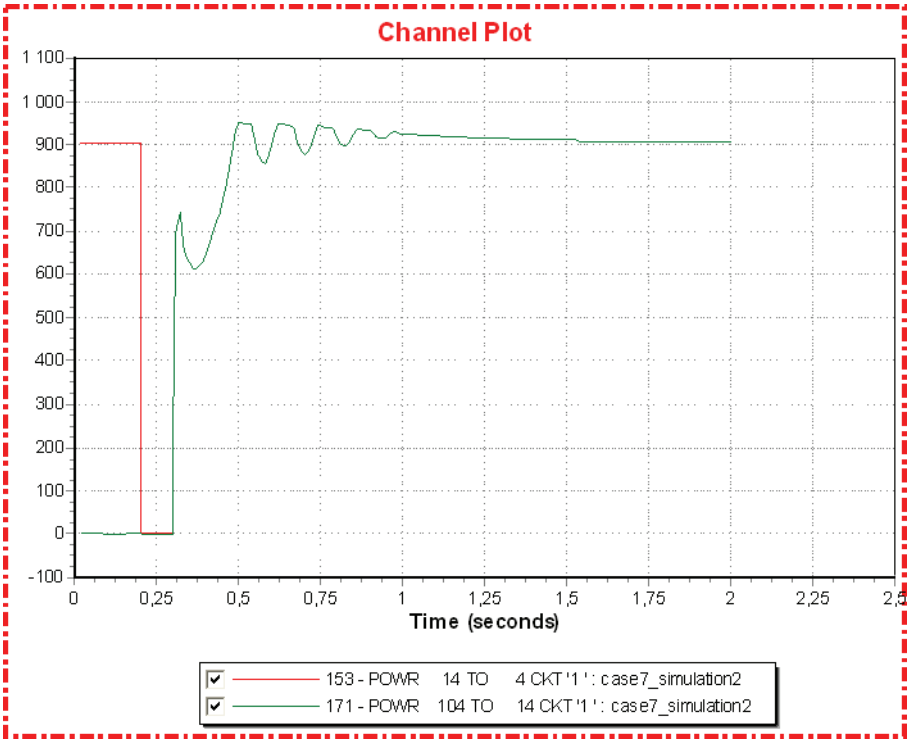

Figure 12.7.9: Onshore power flow [MW]

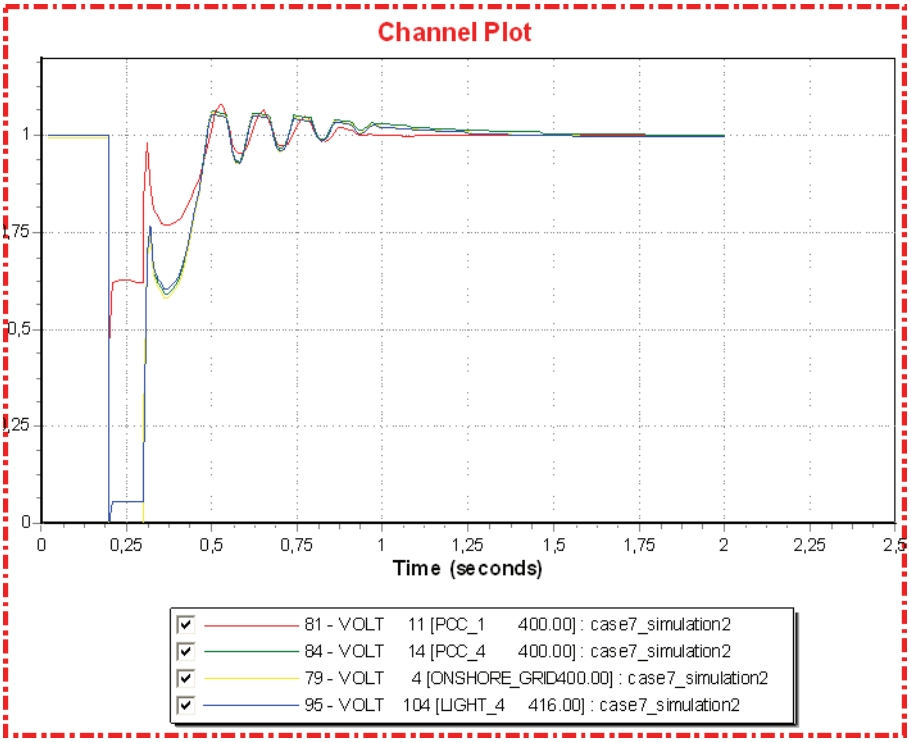

Figure: 12.7.10: Onshore AC voltages [pu]

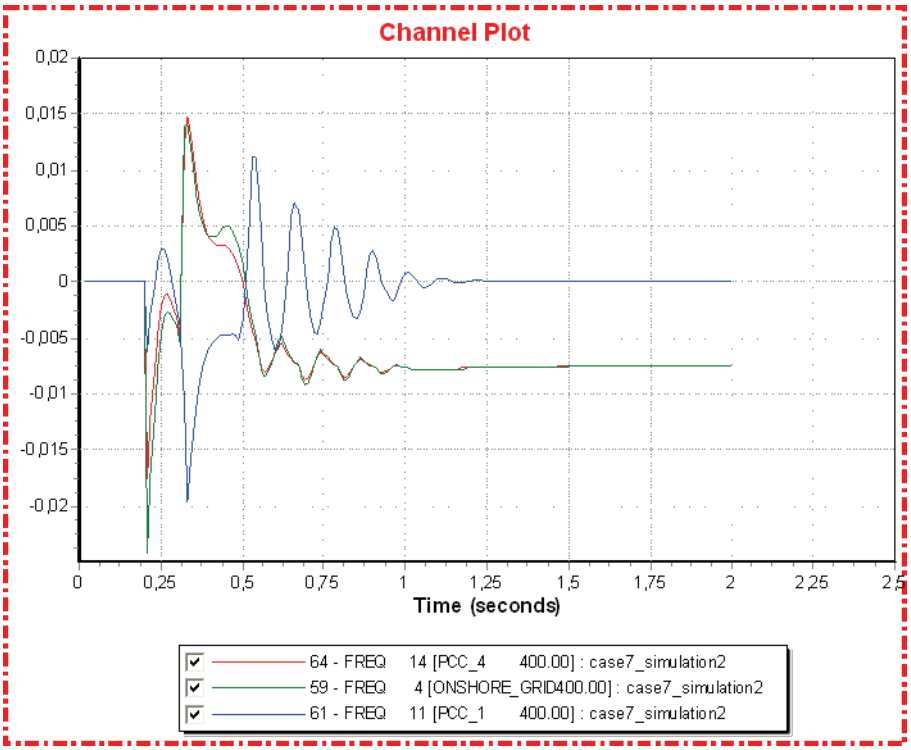

Figure 12.7.11: Onshore frequency [pu]

12.8 Case 8

Case 8 is an attempt to illustrate the stability improvements brought on by the presence of the VSC HVDC during various large power transfer scenarios.

The different large power transfer scenarios investigated are:

- The original large power transfer scenario
- The original large power transfer scenario, but with the disconnection of the entire VSC HVDC grid from the onshore AC grid at the start of the dynamic simulation.
- A power flow scenario where 50 % of the transferred power from bus 11 to bus 14 is transferred through the HVDC grid, i.e. a parallel AC/DC power transmission.

The described power flow situation with parallel AC/DC transmission is created with the large power transfer scenario as a basis. The power flow in the HVDC system is then altered so that converter 4 delivers 450 MW, i.e. half the power consumed at bus 4, to the onshore AC grid. The altered scenario is called “Large power transfer scenario modified”.

All the simulation performed in case 8 subject the system to the same disturbance, as seen in figure 12.8.1.

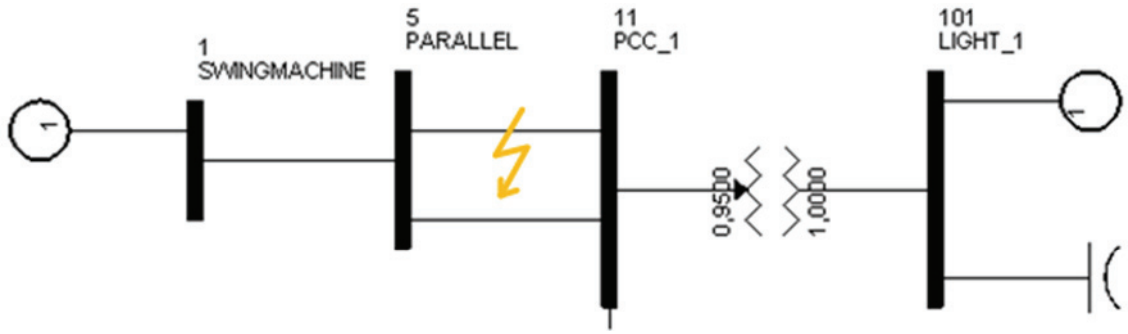

Figure 12.8.1: Dynamic simulation disturbance

Simulation 1 (Large power transfer)

Time	Event
0.00	Normal operation
0.20	Line fault on line 5 – 11 (id1)
0.30	Disconnect (Trip) faulted line

Simulation 1 demonstrates that the reactive power control option (Qoption) of the converters is set in AC voltage control. During the line fault and the following transient behavior, the onshore converters dynamically alter the reactive power delivered to the onshore grid to regulate the AC voltage. The MTDC improves as follows the power system performance in

the connected AC grid, as described in chapter 4.8. The performance of the onshore grid quickly recovers to its pre fault operation following the disconnection of the faulted line.

Converter 4, operating in Pctrl, displays the same unexplained performance as described in case 2, simulation 1 and 3, i.e. a small change in active power. The reason is most likely that the disturbance prohibits the correct operation of the control system for converter 1 and 4, just like in case 2.

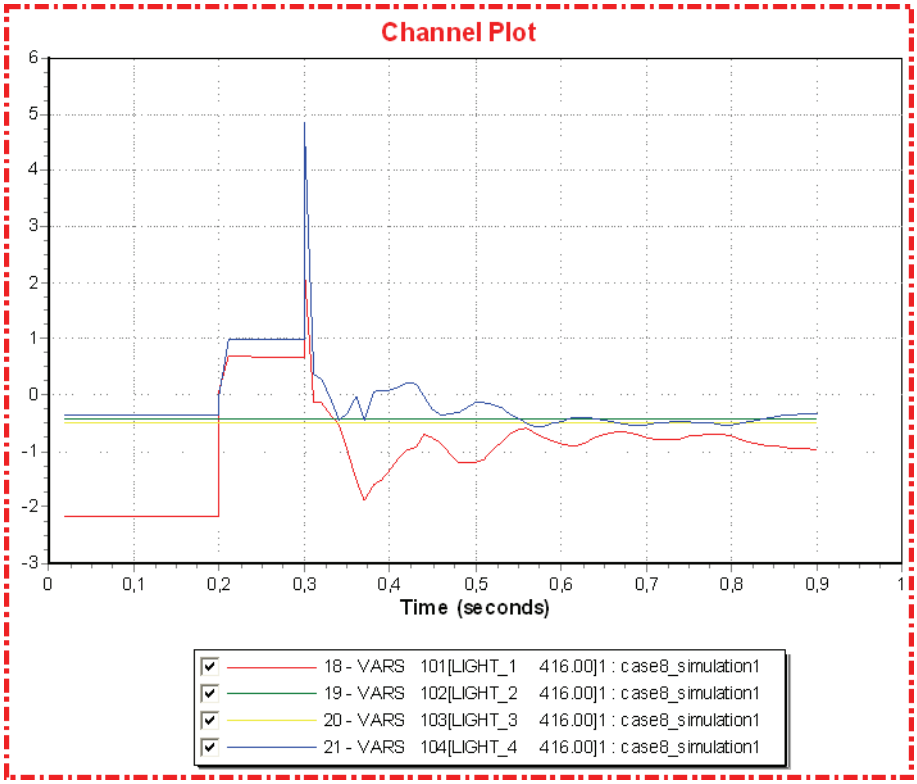

Figure 12.8.2: Converter reactive power [pu]

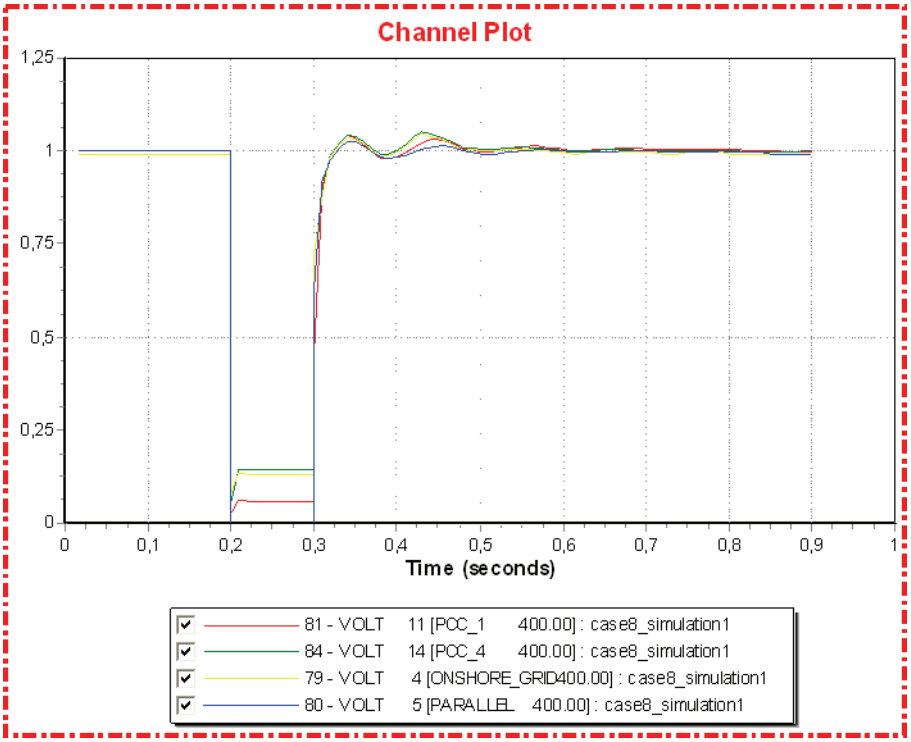

Figure: 12.8.3: Onshore AC voltages [pu]

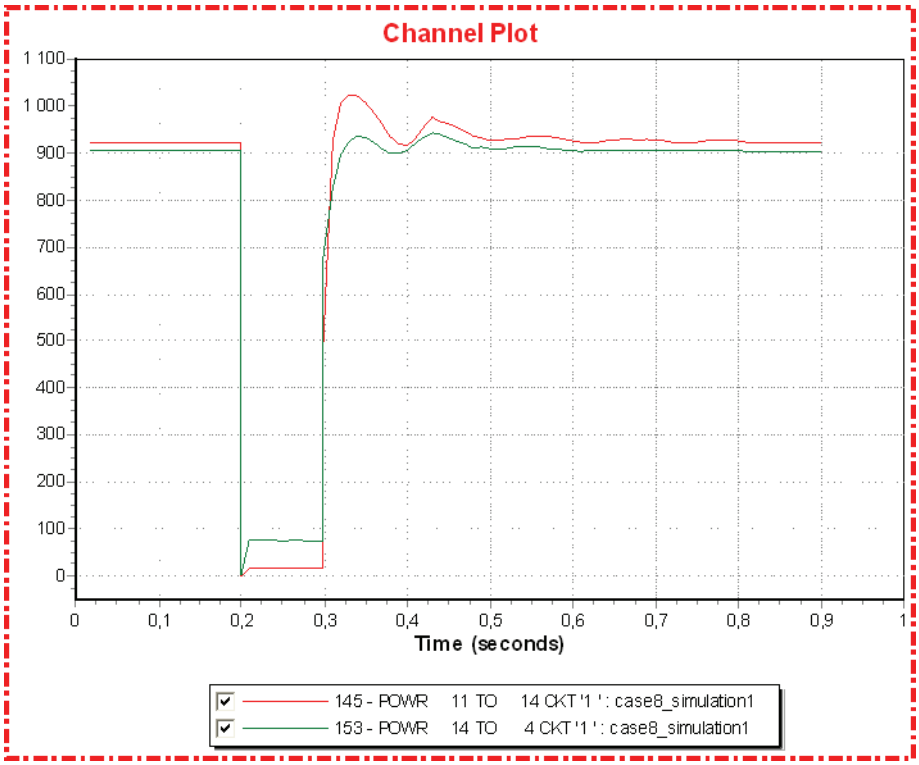

Figure 12.8.4: Onshore power flow [MW]

Simulation 2 (Large power transfer)

Time	Event
-0.00	Disconnect power transformers for converter 1 and 4
0.00	Normal operation
0.20	Line fault on line 5 – 11 (id1)
0.30	Disconnect (Trip) faulted line

The dynamic results from simulation 2 illustrate the important stabilizing effect of the voltage source converters for this specific grid model. The reactive support from the converters is crucial for maintaining acceptable voltages in the onshore AC grid. Prior to the simulation, the converters are removed from the onshore grid and the result is that even the pre fault voltage levels are too low, 0.9 pu at bus 1 and 0.823 pu at bus 4. Because the load at bus 4 is voltage dependant, as described in chapter 11, the pre fault load consumption is 778.2 MW. The system is not able to recover to its pre fault operating situation after the faulted line has been disconnected. The voltages stabilize at a lower level than pre fault, and as a result the voltage dependant load further decreases its power consumption to 605.8 MW at a voltage of 0.538 at bus 4. The reactive power generation at bus 1, the only generator in the onshore system, has a higher value post fault than pre fault, trying to increase the onshore voltages. The remaining onshore system analyzed in this simulation is not a realistic model for a power system, but it enables, together with simulation 1, a comparative view on systems with and without VSC.

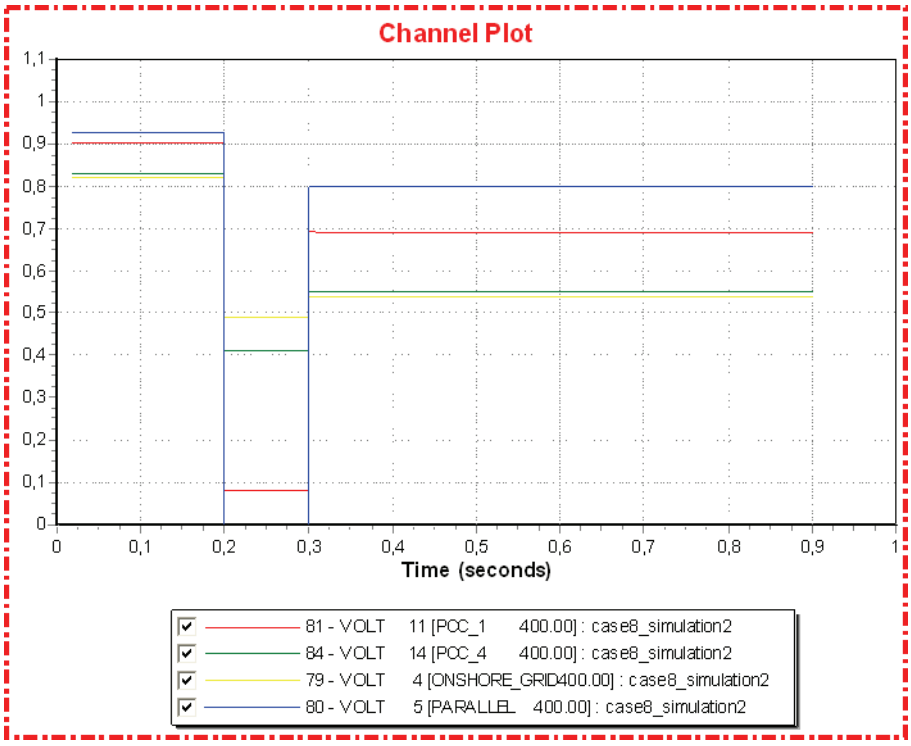

Figure: 12.8.5: Onshore AC voltages [pu]

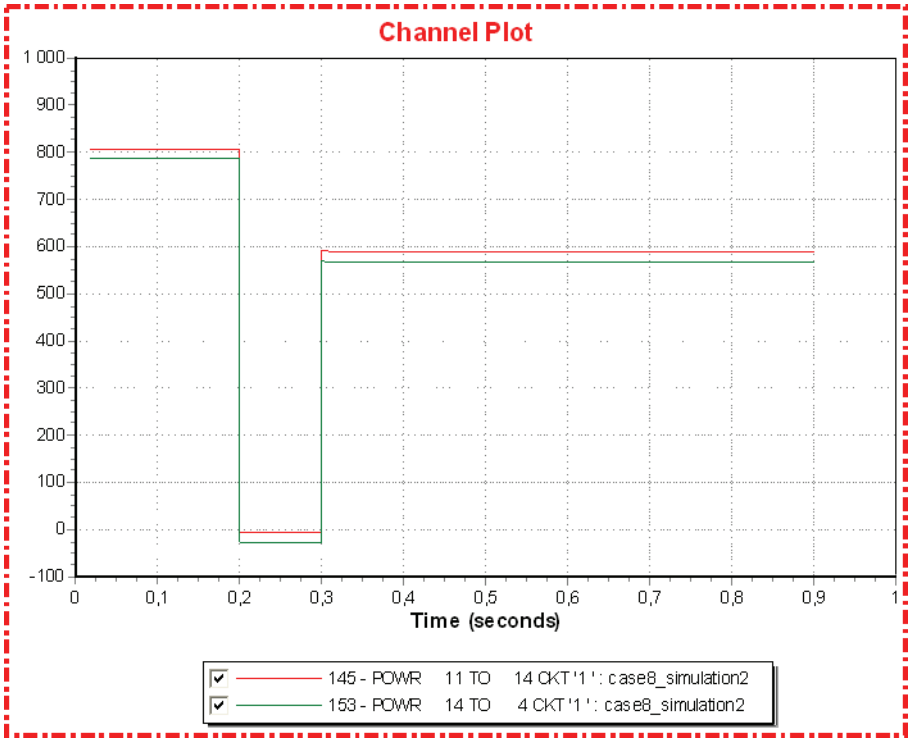

Figure 12.8.6: Onshore power flow [MW]

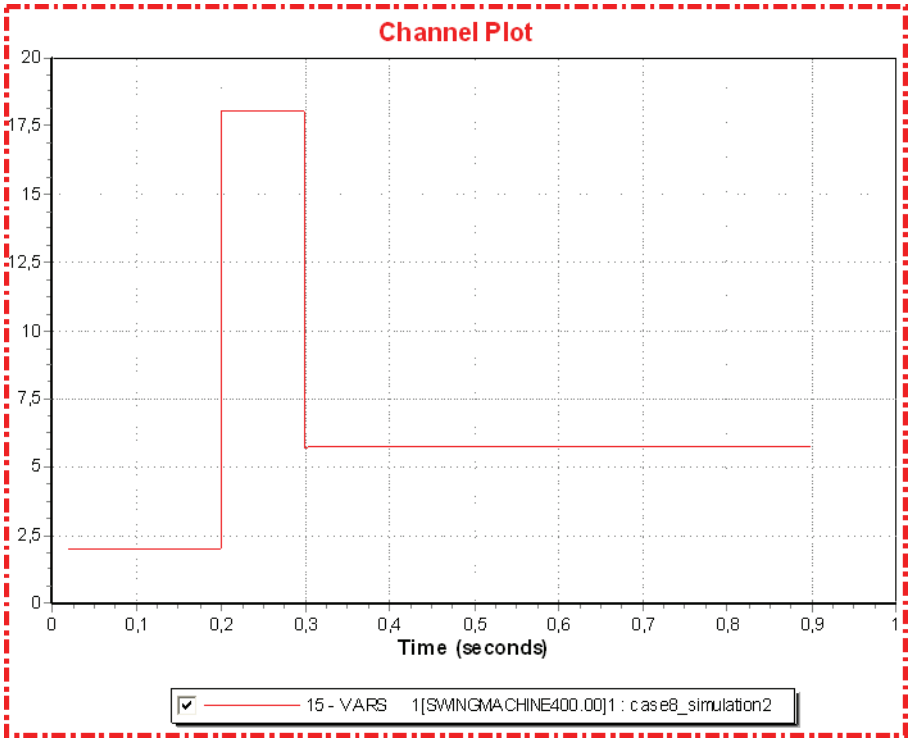

Figure 12.8.7: Onshore generator reactive power [pu]

Conclusively, the presence of voltage source converters in an offshore grid offers huge advantages to the system performance.

Simulation 3 (Large power transfer modified)

Time	Event
0.00	Normal operation
0.20	Line fault on line 5 – 11 (id1)
0.30	Disconnect (Trip) faulted line

Simulation 3 is included in the analysis in order to investigate whether the MTDC provides any additional benefits for the onshore AC system performance when 50 percent of the power consumed at bus 4 is transferred through the MTDC or not.

In comparison to simulation 1, the results show a very similar onshore behavior, when subjected to the same disturbance. The power delivered to bus 4 and the voltages experience a slightly larger initial overshoot in simulation 1 following the disconnection of the faulted line, but this is negligible.

Conclusively, it is the presence of the voltage source converters and their ability to interact with the MTDC that contribute to the dynamic performance in the onshore system, not the quantity of power transferred in the MTDC pre fault.

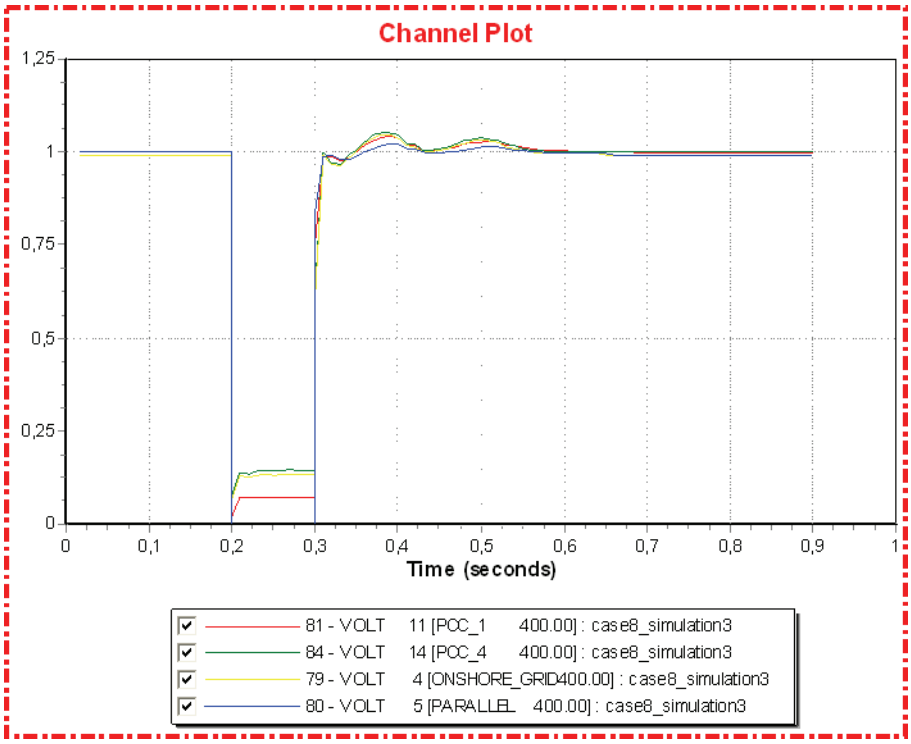

Figure: 12.8.8: Onshore AC voltages [pu]

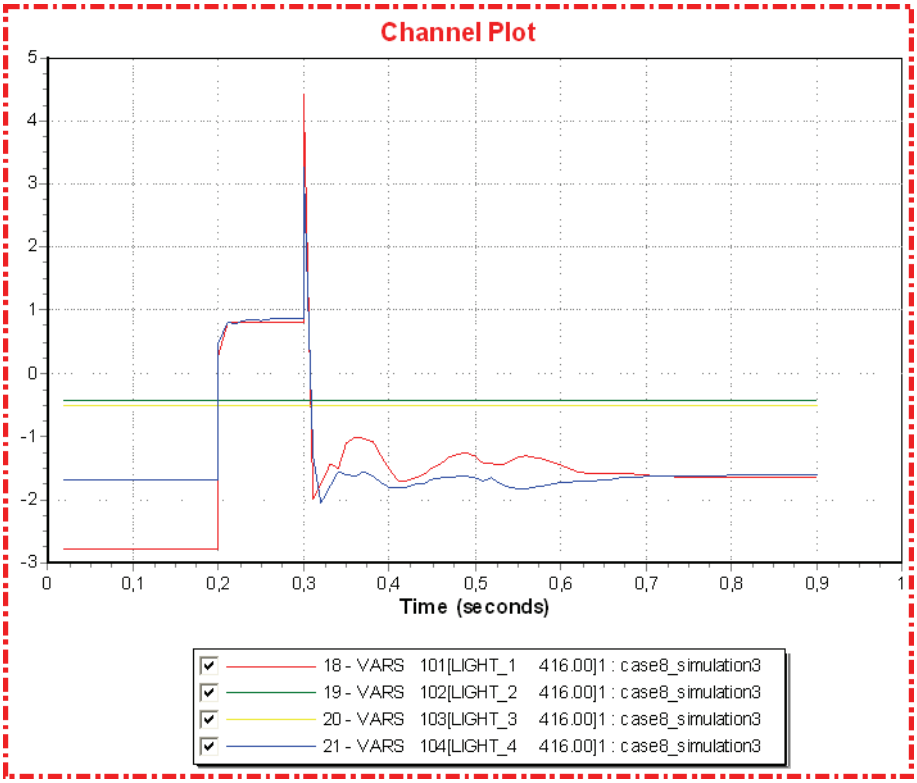

Figure 12.8.9: Converter reactive power [pu]

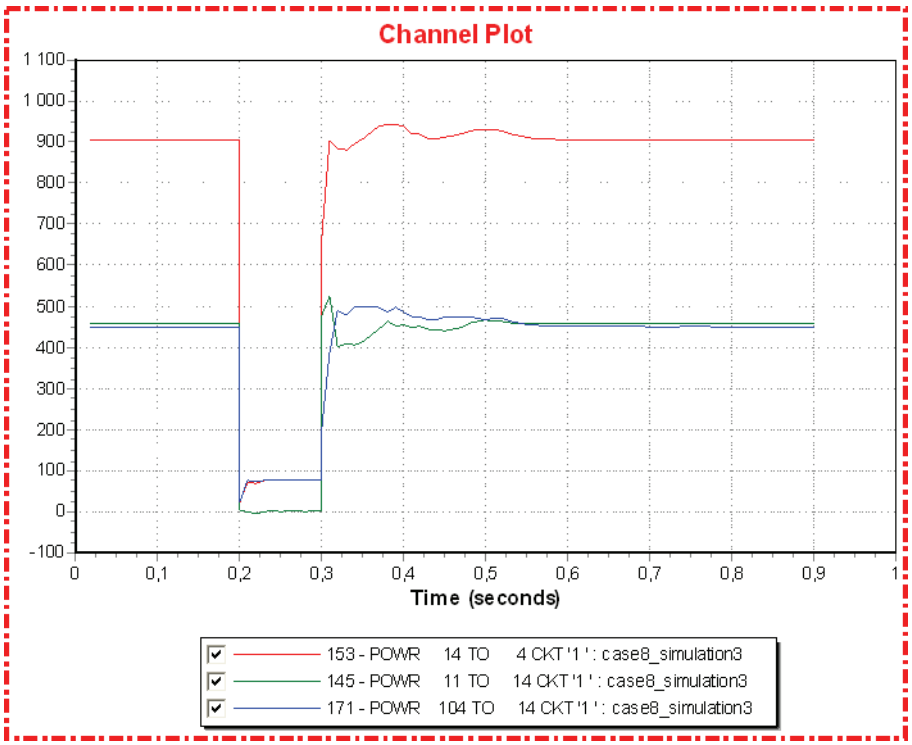

Figure 12.8.10: Onshore power flow [MW]

13 Discussion

13.1 Theoretical analysis

Results from the theoretical analysis conclude that VSC technology is a realistic solution for an offshore grid with the objective of supporting passive network installations far from shore. The main reason for this possibility is the fact that the VSC can convert the DC voltage of the DC side storage capacitor into an AC voltage by switching on and off the converter bridges according to the pre-determined switching pattern. The converter is able to fully control active and reactive power, voltage and frequency offshore without the requirement of a strong offshore AC grid.

Additional advantages with VSC for this area of application are:

- Black start capabilities of a dead system.
- Improved dynamic performance and stability, because the VSC provides the same dynamic power system support as a STATCOM.
- VSC can be used in multiterminal configuration because the system allow current in both directions without the need to change the polarity when the direction of power is changed.
- Lower space requirements compared with LCC, which is important in offshore installations.

An important topic for the realization of MTDC is the difficulties related to fault protection. The DC equivalent to AC breakers, that would serve the power and voltage ratings required in a DC grid of the scale investigated in this master thesis, does not exist today. For such a breaker to work, the fault current must have a zero crossing. Research is therefore in the process of developing a DC resonance breaker to superimpose a zero crossing on the DC current, for the necessary high ratings. An alternative solution involves the series connection of IGBTs in a “valve” that can be applied to break the current. This will be similar to a converter leg in a VSC, thus making the valve large and expensive compared to AC breakers from conventional power systems. In today’s two-terminal VSC systems without DC breakers, faults on the DC side are cleared by opening the breakers on the AC side in both converters. This solution is less attractive when more than two terminals are involved, as the entire DC side of the grid will lose its voltage for several hundred milliseconds. In other words, all interconnected passive AC systems would lose their power supply. They would have to shut down or operate in island operation until the fault is cleared and the DC system re-energized.

Possible protection schemes for fault clearing using AC breakers and IGBT-CBs have been described for multiterminal grids. When the DC breaker technology is commercially available, the protection of a MTDC should be feasible within the necessary requirements. In relation to

this theoretical analysis, simulations have been performed to investigate the effects of island operation for the time durations associated with the two protection schemes.

Further research on power flow control in MTDC is required before the implementation and construction of an offshore grid is realistic. The voltage margin method merged with DC voltage droop control appears to be a promising solution according to the theoretical studies. In order to further investigate power control of the MTDC, simulations have been performed to analyze the power control of the MTDC with the master-slave control scheme implemented in the HVDC Light model. Alterations in the power control have also been suggested and analyzed.

Statistical values for the operation of existing VSC transmission systems conclude that one petroleum platform supplied by one VSC connection would not experience reduced availability of power supply compared to a situation with local power generation. Provided that the difficulties concerning fault protection are resolved, petroleum platforms supplied by a MTDC would experience an increased security of supply. The faulted part of the MTDC would be disconnected, and the remaining MTDC would continue normal operation.

13.2 Modeling

The modeling of the offshore **wind farms** have been implemented with dynamic parameters provided in the PSS®E manual for a GE 1.5 MW wind turbine. In addition to the data set, the PSS®E manual includes block diagrams for the models and data sheets with a name that describes the meaning of each parameter. However, there is no further information concerning implementation of the wind model in power flow scenarios or a description of important conditions for normal behavior in dynamic simulations.

For these reasons, the information of the wind model is considered to be insufficient for a complete understanding of the applied wind model prior to the simulations.

To remedy this situation, a comprehensive analysis has been conducted on the block diagrams to better understand the dynamic behavior of the wind model. To carry out the power flow implementation, many assumptions have been made based on supplementary literature. These assumptions include power ratings and tap control of the interconnecting transformers, voltage levels, bus selection for voltage control and power factor for the generator.

Insufficient documentation and the necessity for the assumptions concerning power flow induce some uncertainty in whether or not the model is implemented correctly. This must be taken into consideration when interpreting the simulation results.

Dynamic analysis of the two possible generator models for the dynamic wind modeling resulted in a decision to use the older generator model, as the newest model displayed an unrealistic dynamic behavior. Simulations that verify and accept the aggregation of multiple

wind turbines into one dynamic model were also conducted. The wind farms were therefore modeled as a single generator in the power flow scenarios.

The **petroleum platforms** are modeled using PSS®E CLOD model to replace all constant power, current, and admittance loads with a composite load consisting of induction motors, lighting and other types of equipments. The CLOD model is being applied because it is developed for situations where it is desirable to represent loads at the dynamic level, as distinct from the algebraic characteristic level used in power flow, but where detailed dynamic data is not available. As the composition of different loads for the platform was the only information available, the CLOD model was a natural choice for the petroleum platform modeling.

Unfortunately, an unexpected dynamic behavior in the model was discovered. After a disconnection and following reconnection of neighbouring buses, it appears that the CLOD model disappears from the system. The simulation data sheets indicate that the model is still in service, but the effect of the model is no longer present, the power consumption falls permanently to zero. Around 26 percent of the load represented by the CLOD model is rotating machines, and the large amount of rotating masses should allow the model to ride through a short duration fault in island operation. The reason for this unrealistic dynamic behavior was not discovered, but it creates a problem for the intended dynamic simulations as a proper shut down of a converter involves a disconnection of the converter bus. The investigation of an offshore island operation is thus obstructed.

A solution to this problem was the implementation of more rotating machines in the offshore grid in the form of the wind turbines. The rotating masses of the wind turbines enable the offshore grid to remain operational following a trip of the interconnecting converter as the wind farm can regulate active and reactive power to support the grid.

However, this is not a completely satisfactory solution. Only the investigation of short duration island operation in offshore areas that consists of both petroleum platforms and wind farms is possible. Unfortunately, connected offshore AC systems that only consist of petroleum installations will probably be very dominant for a realistic implementation of VSC HVDC for interconnection of offshore installations.

An alternative solution would have been to model the petroleum platforms in more detail using specific models for the representation of rotating machines and compressor converters. The necessary platform parameter data was not available so this alternative was not chosen, but could be a possible approach for further work on the simulation model.

The **multiterminal VSC HVDC** system in the simulation model is represented using ABB's HVDC Light Open model Version 1.1.9-2. A detailed description of the model is made in chapter 8, along with explanations for the assumptions, considerations and choices made especially for the implementation in this specific system. A detailed understanding of the

HVDC Light model was acquired through the contents of the model documentation, simulations using the model and communication with Per-Erik Björklund at ABB. The HVDC Light model has proven to be a well operating external PSS®E model that displayed an expected and realistic behavior. The model has been the crucial component for the development of the simulation model used for the analysis in this master thesis.

13.3 Simulation results

The dynamic results from the different simulations are described and analyzed as they are presented in chapter 12. An overall discussion is made in this chapter as a summary.

Case 1 demonstrates the operation of the converter in DC voltage control (UdcCtrl) following a change in the MTDC power balance. The new power balance results in a charging or discharging of the DC capacitors and a subsequent change in DC voltage. The DC voltage alteration is detected by the UdcCtrl converter which changes its operating point in the P-Q diagram to create a new MTDC power balance, thus restoring the DC voltage to the desired value. The onshore AC system connected to the UdcCtrl converter will experience a change in the power exchange with the converter, and this change in power flow occurs very rapidly. This leads to the general rule for VSC HVDC systems that the converter selected for DC voltage control should be the converter connected to the strongest, and thereby most flexible AC grid.

The importance of an UdcCtrl converter present in the grid is also examined. The conclusion from the simulations is that without a converter operating in UdcCtrl connected to a strong AC grid, the DC system will lose its controllability and either be completely discharged or charged above protection limits of the equipment. In the HVDC Light model, an “emergency UdcCtrl” is implemented for the converters set in Pctrl. This emergency UdcCtrl is activated when the DC voltage exceeds the limits of 0.9 pu and 1.1 pu, and the converter stabilizes the DC voltage at the limit.

An alternative control strategy for the active power control (Poption) settings of the converters was also analyzed. The investigated idea was that the MTDC could operate with a control strategy where all the converters are ranked according to their ability to serve as the DC voltage controlling converter. In the case of a failure of the DC voltage controlling converter, the role of UdcCtrl is simply transferred to the highest ranked converter still operating in the MTDC. The conclusion from the simulations is that an advanced control system for the active power control operation (Poption) of all the converters in a MTDC may greatly improve the performance of the system following a disturbance. If the disturbance prohibits the Poption designated for a converter, the control system should be able to alter the Poption of the converters to the most suitable combination for the new system situation.

The motivation for the simulations performed in **case 2** and **case 3** is to illustrate the decoupling effect of using a VSC HVDC grid to connect separate AC systems. This was demonstrated by subjecting faults in one AC system and analyzing the response of the other AC grids. No fault current was drawn from one AC grid to feed the fault in another AC grid. The frequency and voltage behavior was also separated by the VSC HVDC. The main effects in the other AC grids were due to the response to the new power flow situation in the system as a consequence of the disturbance.

The only substantial consequence in another grid occurred when an onshore fault limited the power flow from the onshore AC system to the UdcCtrl converter as there was a net power deficit in the offshore grids. This prohibited the UdcCtrl converter from maintaining a satisfactory power balance in the MTDC and the energy in the DC capacitors were discharged. As the DC voltage fell, the offshore converters were unable to keep the power supply to the offshore AC grids constant. The offshore AC voltages experienced a small sag before the onshore fault was cleared.

To conclude, a connection of separate AC grids using VSC HVDC decouples the grids in the event of a disturbance as long as the active power control of the DC system is not compromised.

Case 4 investigated the temporary dynamic island operation of the offshore AC grids seen in relation to the protection schemes for a MTDC grid presented in the theoretical chapter 2.11.2. However, the quality of simulations in case 4 could not be conducted at the level intended early in the work, due to some unexpected problems with the simulation model.

Unfortunately, for most of the simulations performed in this case, offshore area 3 demonstrated an unrealistic behavior, and the reason for this behavior was not discovered. As a result, only offshore area 2 was used for the analysis in case 4.

The problem with the CLOD model is the most important limitation for the analysis of case 4. The model could not operate correctly in an island system without being connected to rotating machines. This made a comparative analysis of the protection schemes' effect on offshore island operation impossible using the CLOD model, for situations when the petroleum platform is the only component in the offshore system. Unfortunately, connected offshore AC systems that only consist of petroleum installations will probably be very dominant for a realistic implementation of VSC HVDC for interconnection of offshore installations.

The consequence of these problems is that the simulation results do not fully describe all the important situations, and the subsequent analysis is not able to create general conclusions for the protection schemes based on the simulations.

The simulations that were conducted in case 4 showed that the offshore AC grid was able to remain operational and deliver the necessary power to the petroleum platform during island operation, for both the time durations investigated. The wind farm dynamically adjusted its active and reactive power generation to support the grid. The offshore AC voltage was higher

than the desired set point due to reactive power generation in the cable connecting the wind farm to the rest of the offshore AC grid.

Despite the problems with the model, and the subsequent shortage of simulation results, a theoretical analysis can still be performed on the subject of island operation for passive systems consisting only of petroleum platforms, with regard to the protection schemes.

In Statoil, there is a requirement for the frequency converters powering compressors that they should handle a loss of power supply for 200 ms. Unable to determine the exact time duration that the DC system and power supply to the petroleum platform must shut down in relation to the protection scheme using AC breakers, it is most certainly longer than 200 ms. Estimations ranges from several hundred milliseconds to a minimum of a few seconds, and 2 seconds was assumed for the simulations. As a result, handling a fault in the DC grid by opening the offshore AC breakers is an unacceptable solution for protection, as the compressors will experience a surge that may cause damage and stop in production.

To improve system performance during island operation for passive systems, the use of a dynamic energy storage has been proposed, for instance ABB's product SVC Light with Energy Storage. It supports the grid continuously with reactive power, and in the event of loss of generation, the energy storage pushes active power into the grid until the grid is reconfigured.

If the offshore system with petroleum platform has a dynamic energy storage of the necessary rating installed, it would be possible for the isolated grid to maintain system performance for a longer duration of island operation. This improves the possibility of using the AC breaker protection scheme for VSC DC systems with few connected AC systems. However, the entire DC system would be discharged and shut down with this protection scheme, and this makes it inconvenient for larger MTDC. The protection scheme using IGBT-CBs is the preferred solution for MTDC.

The simulations of **case 5** are used to investigate the response in an offshore AC grid connected by a converter in passive net operation (PassNetOp) following the sudden disruption of a large offshore wind power generation. The actions taken by the converter to stabilize the offshore AC grid are analyzed.

In the case of an short-circuit fault in the offshore AC grid, the converter is unable to take any actions to stabilize the AC grid as long as the fault is present and prevents power transfer from the converter to the grid. Seen in relation to the petroleum platform requirements concerning loss of power, such a fault must therefore be cleared quickly.

After the disturbance has occurred and possible faults have been cleared, the converter immediately changes P-Q working point to support the AC grid. Due to the operation of the converter, connecting the offshore AC grid to the MTDC, there are no severe consequences for the offshore AC grid as long as the fault has been cleared and power transfer between the converter and petroleum platform is possible.

Case 6 examined the behavior of the MTDC following a disconnection of both the onshore converters. The onshore converters are operating in UdcCtrl and Pctrl, and after the disconnection there are no converters in the MTDC able to operate as the dynamic slack bus maintaining MTDC power balance and controlling the DC voltage. The offshore converters cannot assume this task because they are connected to weak AC systems with very limited flexibility in the power generation. Simulations were performed for situations with both a net deficit and a net surplus of power in the offshore AC grids. The simulations could then demonstrate both a discharging of the system until it collapsed, and a charging of the system until the DC voltage reached a level where the converters shut down to protect the equipment.

In addition, the functionality of onshore choppers was investigated. The choppers are essential for a situation where offshore wind farm create a net offshore power surplus, but at the same time the onshore converters are prevented from delivering the power onshore. The choppers will dissipate the excess energy in the MTDC in large power pulses, discharging the DC capacitances and thereby controlling the DC voltage.

The analysis of case 6 illustrates the functionality and necessity for control of a MTDC. They substantiate the technology as described in the theoretical chapters, and are useful for the understanding of multiterminal VSC technology.

Case 7 investigates the use of the MTDC as an alternative path for transferring large amounts of power in the case of an onshore disturbance that prohibits large power transmission within the onshore grid. The importance of a well developed, flexible control system for regulating the active power control option (Poption) of the converters has also been demonstrated. After the disturbance, the onshore grid included a small area with a large power consumption that was isolated from the generators onshore, but connected through the MTDC. By changing Poption for the interconnecting converter from Pctrl to PassNetOp, the converter acted as a dynamic slack bus in the passive part of the AC grid, supplying the necessary power and controlling voltage and frequency. After a short initial transient, the passive part of the onshore grid resumed normal operation, completely supplied from the converter.

Case 8 is an attempt to illustrate the stability improvements brought on by the presence of the VSC HVDC in the onshore system during various large power transfer scenarios. Three slightly different power flow scenarios have been subjected to the same onshore fault and the following onshore power system performances have been compared and analyzed. The conclusions from the simulations are that:

- The voltage source converters provide stability improvements to the connected AC grid, as explained in chapter 4.7 and 4.8.

- It is the presence of the voltage source converters and their ability to interact with the MTDC that contribute to the dynamic performance in the onshore system, not the quantity of power transferred in the MTDC pre fault.

14 Conclusion

In this master thesis, the possibilities for the interconnection of offshore installations with a multiterminal HVDC grid (MTDC) using voltage source converters have been investigated A comprehensive theoretical study of the VSC technology has been conducted based on existing literature. In addition, a power system model, consisting of four converters in a MTDC connecting three separate AC grids, has been developed in the power system simulation program PSS®E. A series of dynamic simulations have been performed using the model, and the simulation results have been analyzed to determine the principles of operation for a MTDC and interaction with the AC grids.

An overall conclusion is that the basic behavior and functionality of a MTDC, described in the theoretical analysis of the technology, is demonstrated and confirmed by the simulation results.

The theoretical analysis concludes that VSC technology is a realistic solution for an offshore grid with the aim of supporting passive network installations far from shore. This conclusion is supported by the dynamic simulations.

Simulations are carried out demonstrating the behavior of a MTDC, when the power control, and implicitly DC voltage control, is implemented with a master-slave control scheme. An improvement in the control philosophy were also suggested and analyzed. Simulation results conclude that an advanced control system for the active power control operation (Poption) of all the converters in a MTDC may greatly improve the performance of the system following a disturbance. If the disturbance prohibits the Poption designated for a converter, the control system should be able to alter the Poption of the converters to the most suitable combination for the new system situation. This suggested control philosophy improves the flexibility of the MTDC compared to the permanent master-slave control philosophy, where the entire MTDC collapses if the master converter is disabled.

It has been demonstrated that the connection of separate AC grids using VSC HVDC decouples the grids in the event of a disturbance as long as the active power control of the DC system is not compromised.

In the case of an onshore disturbance that prohibits large power transmission within the onshore grid, the possibility to use the MTDC as an alternative for transferring large amounts of power has been investigated. This was found to be beneficial for the system. In this respect, the importance of a well developed, flexible control system for regulating the active power control option of the converters has also been demonstrated.

Both theoretically and through simulations it has been demonstrated that the VSC MTDC provides stability improvements to the connected AC grid, by actively controlling the injected active and reactive power to the grid. A VSC HVDC connection with the objective of supporting the connected AC grid will essentially behave with the same functionality as a STATCOM combined with an energy storage.

The difficulties related to fault protection in a MTDC have been highlighted, and possible protection schemes have been described. An intended detailed analysis of the different protection schemes based on dynamic simulations was prevented due to problems with the simulation model. However, a theoretical analysis concluded that the protection scheme using IGBT circuit breakers is the preferred solution with present available technology.

15 Further work

The topic investigated in this master thesis of using VSC technology in a multiterminal HVDC grid for interconnecting offshore installations is a vast and complex area of research that requires further attention.

With a basis in this master thesis, the following suggestions for further work are presented, and may be used as input for formulating new projects.

The petroleum platforms should be modeled in detail, provided that the necessary parameter data is available. This would enable a more thorough investigation of the dynamic behavior in the offshore AC grids, as a result of the converter actions. Furthermore, the simulation model could be used to analyze island operation with only a petroleum platform in the offshore grid, in view of protection schemes for MTDC.

The onshore grid could be expanded to a larger and more realistic model of a main grid. A more detailed analysis of using the MTDC to relieve the main grid could then be conducted.

The HVDC Light model has the possibility to further improve the small signal stability of the AC grid connected to the voltage source converter. The converter model has the ability to receive an external auxiliary active power order from the AC grid. A possible suggestion for further work could be the development of a controller to create the set point for the active power order to the HVDC Light model.

16 References

[1] PSS®E v 32 User manual

[2] *"User guide PSSE HVDC Light Open model Version 1.1.9-2"*, ABB, 2010

[3] *"User guide PSSE multi terminal HVDC Light Open model Version 1.1.9-2"*, ABB, 2010

[4] Sigbjørn Sørbotten, Statnett SF, spring 2010

[5] Rolf Ove Råd, Statoil, autumn 2009

[6] Magnus Gustafsson, Statnett SF, 2009 and 2010

[7] ABB, Technical description of HVDC Light® technology *"It's time to connect"*, 2010

[8] N. Barberis Negra, J. Todorovic , T. Ackermann*, "Loss evaluation of HVAC and HVDC transmission solutions for large offshore wind farms"*, 2005

[9] Per-Erik Björklund, contact reference for [2] and [3], spring 2010

[10] Arne Nysveen, Professor at NTNU, conversations, April 2010

[11] Temesgen Mulugeta Haileselassie, "*Control of Multi-terminal VSC-HVDC Systems"*, Master thesis, Norwegian University of Science and Technology, Department of Electrical Power Engineering, June 2008

[12] Mohan N., Undeland T. M., Robbins W.P., *"Power electronics-Converters, Applications, and Design",*2003, John Wiley & Sons Inc.

[13] Michael P. Bahrman and Brian K. Johnson, *"The ABCs of HVDC Transmission Technology"*, IEEE Power and Energy Magazine, March/April 2007

[14] Infineon.com, accessed September 2009

[15] M. Molinas, Conversation regarding offshore wind configuration and power semiconductors, October 7. 2009

[16] Knut Magnus Sommerfelt, *"Offshore Wind Power in the North Sea, Grid Integration of 1000 MW Offshore Wind Power into the Norwegian Power System"*, Master thesis, Norwegian University of Science and Technology, Department of Electrical Power Engineering, June 2008

[17] Randi Aardal Flo, "*Configuration of large offshore wind farms"*, Master thesis, Norwegian University of Science and Technology, Department of Electrical Power Engineering, June 2009

[18] Michael P. Bahrman, Jan G. Johansson, Bo A. Nilsson, *"Voltage Source Converter Transmission Technologies - The Right Fit For The Application"*, ABB

[19] W. L. Kling, R. L. Hendriks, J. H. den Boon *"Advanced Transmission Solutions for Offshore Wind Farms"*, IEEE

[20] Jiuping Pan, Reynaldo Nuqui, Kailash Srivastava, Tomas Jonsson, Per Holmberg, Ying-Jiang Hafner, ABB, *"AC Grid with Embedded VSC-HVDC for Secure and Efficient Power Delivery"*, Paper presented at IEEE Energy 2030, 17-18 November, 2008 in Atlanta, USA

[21] Bengt Frankén, Yongtao Yang, Carl Öhlén, STRI AB, *"Pre-study of an Offshore Grid"*, feasibility study for Statnett SF, October 2009

[22] J. Dorn, D. Ettrich, J. Lang, D. Retzmann, *"Benefits of Multilevel VSC Technologies for Power Transmission and System Enhancement"*, December 2007

[23] Chengyoug, Z., *"A Control Strategy for VSC-HVDC System Based on Analytic Expression"*, IEEE

[24] Statnett, *"VSC HVDC Systemanalyser"*, internal report nr. 13111, 11.12.2008

[25] Tom Nestli, Adjunct Professor (Prof. II) at Norwegian University of Science and Technology, Dr. ing., Senior Adviser and General Manager of Nescon AS, autumn 2009

[26] Stefan G Johansson, Gunnar Asplund, Erik Jansson, Roberto Rudervall, *"Power system stability benefits with SVC DC-transmission systems"*, Cigré B4-204, 2004

[27] ABB, *"Capability Chart for an HVDC Light"*, accessed November 2009

[28] Ying Jiang-Hafner Hugo Duchen Michael Karlsson Leif Ronstrom Bernt Abrahamsson, *"HVDC with Voltage Source Converters, A Powerful Standby Black Start Facility"*, IEEE paper presented in Chicago, USA, April 2008

[29] Temesgen Mulugeta Haileselassie, conversations regarding MTDC, autumn 2009

[30] Gunnar Asplund, *"HVDC grids - possibilities and challenges"*, ABB Power Systems, Paper presented at Cigré SC B4 Bergen Colloquium, 2009

[31] Lianxiang Tang Hydro One, Boon-Teck Ooi, McGill University in Canada, *"Protection of VSC-Multi-Terminal HVDC against DC Faults"*, IEEE paper from 2002

[32] Christoph Meyer, Maurice Kowal, Rik W. De Doncker, Aachen University, *"Circuit Breaker Concepts for Future High- Power DC-Applications"*, IEEE paper, October 2005

[33] Stefan G Johansson, Gunnar Asplund, Erik Jansson, Roberto Rudervall, *"Power system stability benefits with VSC DC-transmission systems"*, Cigré B4-204, 2004

[34] United States Patent 3851219, *"Circuit-opening device for interrupting heavy currents by means of an explosive charge"*

[35] United States Patent 4284927, *"Method for breaking direct current and d.c. breaker for effecting same"*

[36] Lianxiang Tang Hydro One, Boon-Teck Ooi, McGill University in Canada, *"Locating and isolating DC faults in Multi-Terminal DC Systems"*, IEEE paper from 2007

[37] Temesgen Haileselassie, Kjetil Uhlen, Tore Undeland, *"Control of Multi- terminal HVDC Transmission for Offshore Wind Energy"*, Paper, Department of Electric Power Engineering, Norwegian University of Science and Technology

[38] Raphael Boinne, *"Stability Studies of an Offshore Wind Farms Cluster Connected with VSC HVDC Transmission to the NORDEL Grid"*, Master's thesis, Norwegian University of Science and Technology, Department of Electrical Power Engineering, April 2009

[39] Ulf Baur, Statnett SF, member of Cigré working group B4.52

[40] Geir Nordvik, Statoil, autumn 2009

[41] Gunnar Asplund, *"Utvikling av transmisjonsteknologi - Norge som svingmaskin"*, ABB Power Systems – HVDC, presentation September 2009 in Stavanger

[42] Prabha Kundur, *"Power System Stability and Control"*, McGraw-Hill, Inc, 1993

[43] Jan Machowski, Janusz W. Bialek, James R. Bumby, *"Power system dynamics: stability and control"*, 2008, John Wiley & Sons, Ltd

[44] Thomas Skaanøy, Siemens Trondheim, spring 2010

[45] Erling Ildstad, *"TET4160 High Voltage Insulating Materials"*, Compendium, fall 2008

[46] Arne Nysveen, *"Subsea Power Supply",* Compendium spring 2010

[47] Olivier Angoulevant, Nexans, *"Offshore Wind China 2010"*, presentation in Bergen, Norway, March 2010

[48] IEEE/Cigré joint task force, *"Definition and classification of power system stability"*, Report No. 321, June 2003

[49] M.H. Haque, Senior Member, IEEE, paper *"Stability Improvement by FACTS Devices: A Comparison between STATCOM and SSSC"*

[50] ABB Reliability and availability - HVDC Light® performance (HVDC Light), accessed December 2009

[51] P. Sandeberg, L. Stendius, "*Large scale Offshore Wind Power Energy evacuation by HVDC Light®"*, ABB, paper presented in 2008

[52] NORSOK standard, E-001, Rev. 4, 2001-07-01

[53] Jørgen Selmer Thon, Statnett SF, autumn 2010

[54] Ellen Hambro (SFT), Bente Nyland (OD), Olaf Thuestad (Ptil) og Agnar Aas (NVE), *"Kraft fra land til norsk sokkel"*, January 2008

[55] Cigré Working Group B4.39, *"Integration of Large Scale Wind Generation using HVDC and Power Electronics"*, February 2009

[56] Mukund R. Patel, "*Wind and Solar Power Systems: Design, Analysis, and Operation"*, Second Edition Taylor & Francis 2005

[57] Z. Chen H. Li, *"Overview of different wind generator systems and their comparison"*, Technical report, Institute of Energy Technology, Alborg University, 2007

[58] Timo Vekara Martti Hokkanen, Heikki J. Salminen, *"A Short Review Of Models For Grid-Connected Doubly-Fed Variable Speed Wind Turbines"*, Technical report, University of Vaasa, 2004

[59] Kjetil Uhlen, Professor at Norwegian University of Science and Technology, conversations spring 2010

[60] Terje Gjengedal, Adjunct Professor (Prof. II) at Norwegian University of Science and Technology, Dr. ing., manager of research and development at Statnett SF

[61] General Electric, 1.5 MW wind turbine documentation, 2009

[62] ABB document, *"SVC Light® with Energy Storage"*, 2010

[63] Sintef Energy, *"Planleggingsbok for kraftnett"*, published 1993, updated 2003.

17 Appendix A

17.1 Branch parameter values and SCR calculations

The short circuit ratio (SCR) for the system is calculated with respect to the connection point of converter 1 of the HVDC system. The explanation for this choice is that converter 1 is the DC voltage controlling converter, and therefore is the most crucial converter.

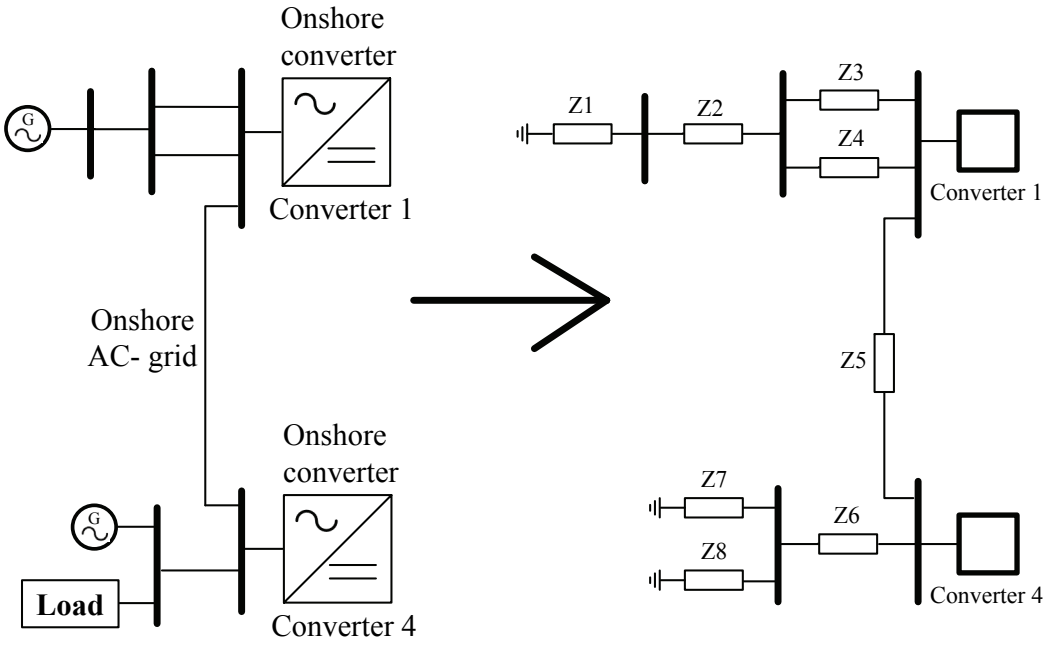

Figure A.1.1: Onshore system impedances

$$Z_{ref} = \frac{V_{ref}^2}{S_{ref}} = \frac{(400 \cdot 10^3)^2}{100 \cdot 10^6} = 1600\ \Omega \tag{17.1}$$

Line impedance values

Impedance	Distance [km]	R [Ω]	X [Ω]	B_{charg} [mS]	X_{charg} [Ω]
Z2	100	1.80	26.50	0.54	1866
Z3	100	1.80	26.50	0.54	1866
Z4	100	1.80	26.50	0.54	1866
Z5	200	3.60	53.00	1.07	933
Z6	50	0.90	13.25	0.27	3731

The impedances associated with the shunt capacitance are ignored when computing the Thevenin impedance used to find the SCR of the system. This is because these impedances are very much larger compared to the impedances of the lines and generators. As the shunt impedances are seen in parallel to ground with the line and generator impedances, the effect of the capacitance will be negligible.

$$Z1 = Z7 = jX_{pu} \cdot Z_{ref} = j0.01371 \cdot 1600 = j21.936\ \Omega \tag{17.2}$$

$$Z8 = Z_{load} = \frac{V_{AC}^2}{S_{load}} = \frac{(400 \cdot 10^3)^2}{900 \cdot 10^6} = 177.77\ \Omega \tag{17.3}$$

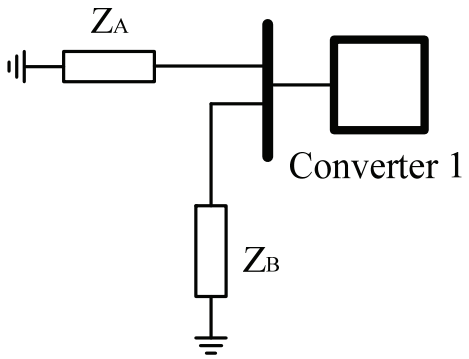

Figure A.1.2: Simplified onshore grid for SCR calculations

$$Z_A = Z1 + Z2 + Z3//Z4 = Z1 + Z2 + \frac{Z3}{2} = 61.75\angle 87.50^\circ \tag{17.4}$$

$$Z_B = Z5 + Z6 + Z7//Z8 = 88.15\angle 85.34^\circ \tag{17.5}$$

$$Z_{Th} = Z_A//Z_B = 36.32\angle 86.61\ \Omega \tag{17.6}$$

$$SCR = \frac{SC\_MVA}{P_{HVDC}} = \frac{V_{AC}^2}{Z_{Th} \cdot P_{HVDC}} = \frac{(400 \cdot 10^3)^2}{26.32 \cdot 1216 \cdot 10^6} = 3.623 \tag{17.7}$$

Line parameter values for use in PSS®E

Impedance	R [pu]	X [pu]	Charging (B) [pu]
Z2 = Z3 = Z4	0.00113	0.01656	0.8576
Z5	0.00225	0.03313	1.7152
Z6	0.00056	0.00828	0.4288

Cable impedance values

Power [MW]	Distance [km]	Voltage [kV]	R [Ω]	X [Ω]	C [μF]	B [mS]
250	30	245	1.80	3.84	5.10	1.601
100	5	132	0.55	0.75	0.70	0.220
120	3	132	0.33	0.45	0.42	0.132

$$Z_{ref\_132\_kV} = \frac{V^2}{S_{ref}} = \frac{(132 \cdot 10^3)^2}{100 \cdot 10^6} = 174.24\ \Omega \tag{17.8}$$

$$Z_{ref\_245\_kV} = \frac{V^2}{S_{ref}} = \frac{(245 \cdot 10^3)^2}{100 \cdot 10^6} = 600.25\ \Omega \tag{17.9}$$

Cable parameter values for use in PSS®E

Power [MW]	Distance [km]	Voltage [kV]	R [pu]	X [pu]	B [pu]
250	30	245	0.002999	0.006397	0.96124
100	5	132	0.003157	0.004304	0.03830
120	3	132	0.001894	0.002583	0.02298

18 Appendix B

18.1 Onshore generators

The onshore generators were modeled with the PSS®E model GENCLS (Classical generator model), which is a constant internal voltage generator model.

The model parameters were copied from an example case in the ABB HVDC Light model package, where the generator represented an onshore swing machine. The model is very simple, especially with the given parameters, but it was considered acceptable for the simulations conducted in this master thesis, where focus was on the MTDC behavior.

Table 18.1: GENCLS parameters

Cons	Value	Description
J	0	H, Inertia
J+1	0	D, Damping constant

```
IBUS, 'GENCLS', ID, CON(J) and CON(J+1) /

1, 'GENCLS', 1, 0.0, 0.0 / AC Network generator

4, 'GENCLS', 1, 0.0, 0.0 / AC Network generator
```

Onshore generator representation in the dynamic model (.dyr)

18.2 Offshore transformer modeling

The offshore transformers connecting the filter bus and PCC bus are modeled with the same parameters as recommended in the HVDC Light model package.

The transformers between the offshore areas' PCC are modeled according to example parameter values given in reference [63]. The ratings of the transformers are set equal to the rating of the connected wind farms. The Xsource of the transformers are set on winding base, i.e. based on local impedance reference for each transformer. Rsource is set equal to zero.

Table 18.2: Offshore transformers parameter values [63]

From bus	To bus	Rating [MVA]	Xsource [pu]	Controlled bus
21	22	285	0.12	22
22	23	285	0.06	-
31	32	115	0.12	32
32	33	115	0.06	-
12	24	130	0.12	24

19 Appendix C

19.1 Dynamic wind model

This appendix contains the model parameters applied for the dynamic wind model. The parameter values are found in reference [1].

WT3G1

IBUS, 'WT3G1', ID, ICON(M), CON(J) to CON(J+4) /

Cons	Value	Description
J	0.80	Xeq, Equivalent reactance for current injection (pu)
J+1	30.00	Kpll, PLL first integrator gain
J+2	0.00	Kipll, PLL second integrator gain
J+3	0.10	Pllmax, PLL maximum limit
J+4	1.50	Prated, Turbine MW rating

Icons	Value	Description
M	67 or 167	Xeq, Equivalent reactance for current injection (pu)

WT3E1

IBUS, 'WT3E1', ID, ICON(M) to ICON(M+5), CON(J) to CON(J+30) /

Icons	Value	Description
M	21 or 31	Remote bus # for voltage control; 0 for local voltage control
M+1	1	VARFLG: 0 Constant Q control 1 Use Wind Plant reactive power control -1 Constant power factor control
M+2	1	VLTFLG: 0 Bypass terminal voltage control 1 Eqcmd limits are calculated as VTerm + XIQmin and VTerm + XIQmax, i.e., limits are functions of terminal voltage 2 Eqcmd limits are equal to XIQmin and XIQ max
M+3	21 or 31	From bus of the interconnection transformer
M+4	22 or 32	To bus of the interconnection transformer
M+5	1	Interconnection transformer ID

Cons	Value	Description
J	0.1500	Tfv, Filter time constant in voltage regulator (sec)
J+1	18.000	Kpv, Proportional gain in voltage regulator (pu)
J+2	5.0000	KIV, Integrator gain in voltage regulator (pu)
J+3	0.0000	Xc, Line drop compensation reactance (pu)
J+4	0.0500	TFP, Filter time constant in torque regulator
J+5	3.0000	Kpp, Proportional gain in torque regulator (pu)
J+6	0.6000	KIP, Integrator gain in torque regulator (pu)
J+7	1.1200	PMX, Max limit in torque regulator (pu)
J+8	0.1000	PMN, Min limit in torque regulator (pu)
J+9	0.4360	QMX, Max limit in voltage regulator (pu)
J+10	-0.4360	QMN, Min limit in voltage regulator (pu)
J+11	1.1000	IPMAX, Max reactive current limit
J+12	0.0500	TRV, Voltage sensor time constant
J+13	0.4500	RPMX, Max power order derivative
J+14	-0.4500	RPMN, Min power order derivative
J+15	5.0000	T_Power, Power filter time constant
J+16	0.0500	Kqi, MVAR/Voltage gain
J+17	0.9000	VMINCL, Min voltage limit
J+18	1.2000	VMAXCL, Max voltage limit
J+19	40.0000	Kqv, Voltage/MVAR gain
J+20	-0.5000	XIQmin
J+21	0.4000	XIQmax
J+22	0.0500	Tv, Lag time constant in WindVar controller
J+23	0.0500	Tp, Pelec filter in fast PF controller
J+24	1.0000	Fn, A portion of online wind turbines
J+25	0.6900	ωPmin, Shaft speed at Pmin (pu)
J+26	0.7800	ωP20, Shaft speed at 20% rated power (pu)
J+27	0.9800	ωP40, Shaft speed at 40% rated power (pu)
J+28	1.1200	ωP60, Shaft speed at 60% rated power (pu)
J+29	0.7400	Pmin, Minimum power for operating at ωP100 speed (pu)
J+30	1.2000	ωP100, Shaft speed at 100% rated power (pu)

A small increase has been made in CON(J+9), to match that of reference [17].

WT3T1

IBUS, 'WT3T1', ID, CON(J) to CON (J+7) /

Cons	Value	Description
J	1.2500	Vw, Initial wind, pu of rated wind speed
J+1	4.9500	H, Total inertia constant, sec
J+2	0.0000	DAMP, Machine damping factor, pu P/pu speed
J+3	0.0070	Kaero, Aerodynamic gain factor
J+4	21.9800	Theta2, Blade pitch at twice rated wind speed, deg.
J+5	0.0000	Htfrac, Turbine inertia fraction (Hturb/H)
J+6	1.8000	Freq1, First shaft torsional resonant frequency, Hz
J+7	1.5000	Dshaft, Shaft damping factor (pu)

WT3P1

IBUS, 'WT3P1', ID, CON(J) to CON (J+8) /

Cons	Value	Description
J	0.3000	Tp, Blade response time constant
J+1	150.0000	Kpp, Proportional gain of PI regulator (pu)
J+2	25.0000	Kip, Integrator gain of PI regulator (pu)
J+3	3.0000	Kpc, Proportional gain of the compensator (pu)
J+4	30.0000	Kic, Integrator gain of the compensator (pu)
J+5	0.0000	TetaMin, Lower pitch angle limit (degrees)
J+6	27.0000	TetaMax, Upper pitch angle limit (degrees)
J+7	10.0000	RTetaMax, Upper pitch angle rate limit (degrees/sec)
J+8	1.0000	PMX, Power reference, pu on MBASE

```
23 'WT3G1' 1
167 0.80000 30.000 0.0000 0.10000 1.5000 /

23 'WT3E1' 1 21 1 1 21 22 '1'
0.15000 18.000 5.0000 0.0000 0.50000E-01
3.0000 0.60000 1.1200 0.10000 0.43600
-0.43600 1.1000 0.50000E-01 0.45000 -0.45000
5.0000 0.50000E-01 0.90000 1.2000 40.000
-0.50000 0.40000 0.50000E-01 0.50000E-01 1.0000
0.69000 0.78000 0.98000 1.1200 0.74000
1.2000 /

23 'WT3T1' 1
1.2500 4.9500 0.0000 0.70000E-02 21.980
0.0000 1.8000 1.5000 /

23 'WT3P1' 1
0.30000 150.00 25.000 3.0000 30.000 0.0000 27.000 10.000 1.0000 /

33 'WT3G1' 1
67 0.80000 30.000 0.0000 0.10000 1.5000 /

33 'WT3E1' 1 31 1 1 31 32 '1'
0.15000 18.000 5.0000 0.0000 0.50000E-01
3.0000 0.60000 1.1200 0.10000 0.43600
-0.43600 1.1000 0.50000E-01 0.45000 -0.45000
5.0000 0.50000E-01 0.90000 1.2000 40.000
-0.50000 0.40000 0.50000E-01 0.50000E-01 1.0000
0.69000 0.78000 0.98000 1.1200 0.74000
1.2000 /

33 'WT3T1' 1
1.2500 4.9500 0.0000 0.70000E-02 21.980
0.0000 1.8000 1.5000 /

33 'WT3P1' 1
0.30000 150.00 25.000 3.0000 30.000 0.0000 27.000 10.000 1.0000 /
```

Wind farm representation in the dynamic model (.dyr)

20 Appendix D

20.1 SLD of simulation model

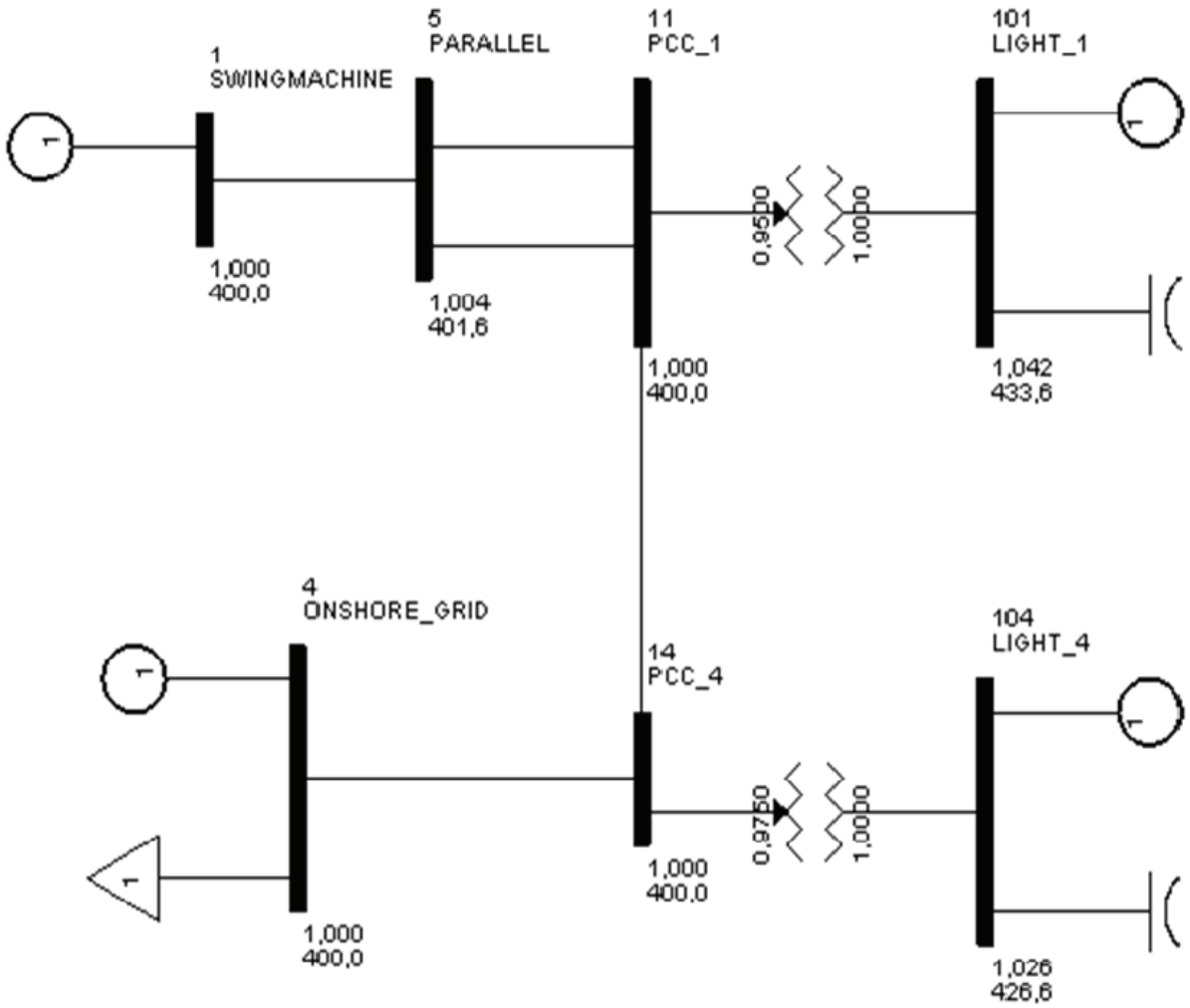

Figure D.1.1: SLD of simulation model, onshore system

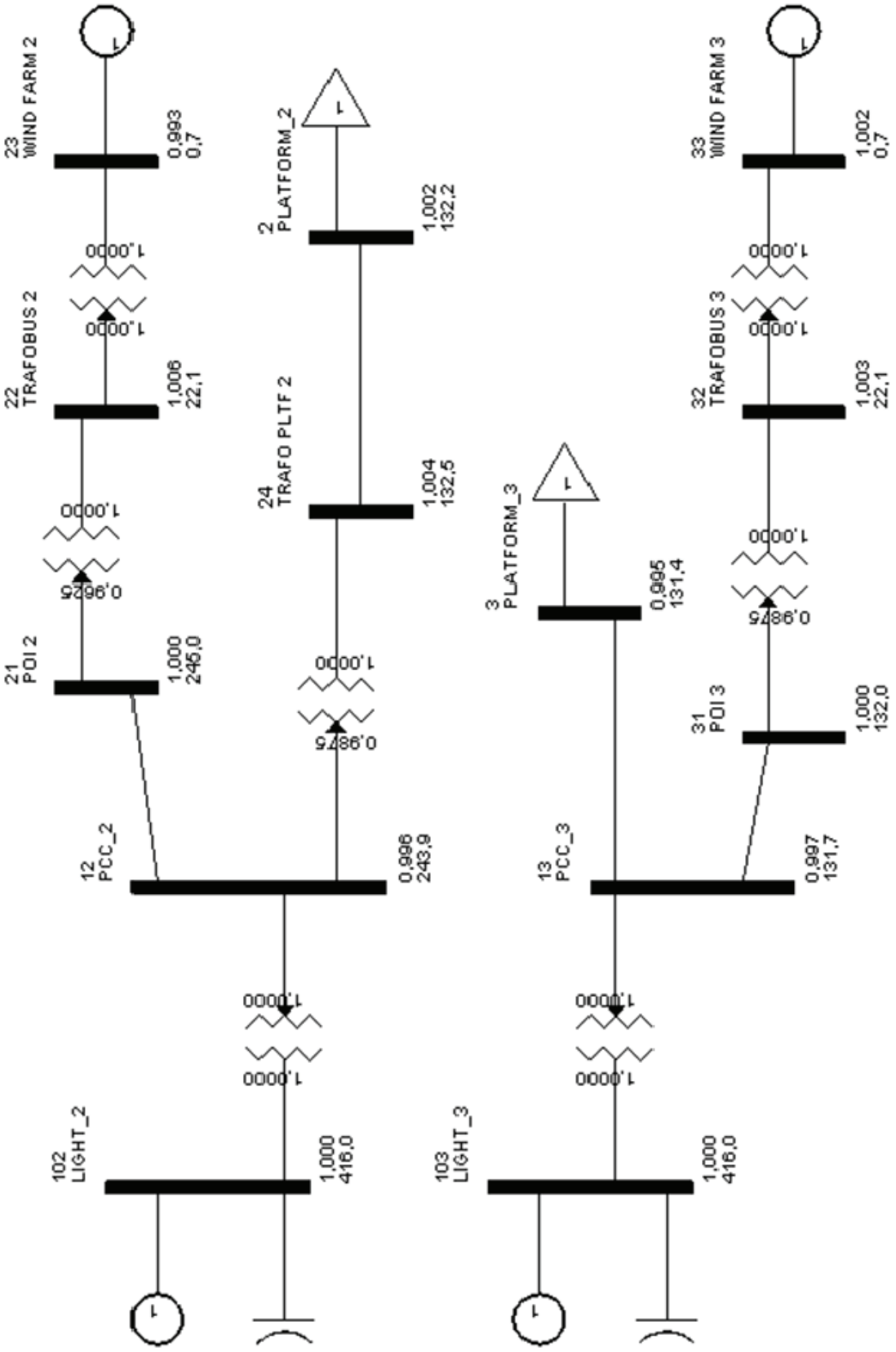

Figure D.1.2: SLD of simulation model, offshore systems

21 Appendix E

21.1 Energy calculations for case 6, simulation 1

The stored energy in a system capacitance with time constant T is:

$$T = \frac{2 \cdot \frac{1}{2} \cdot U^2 \cdot C}{P_{nom}} \rightarrow W_{stored\_energy} = 2 \cdot \frac{1}{2} \cdot U^2 \cdot C = P_{nom} \cdot T \tag{21.1}$$

$$T_{conv\_1} = T_{conv\_4} = 0.0040 \text{ seconds} \tag{21.2}$$

$$T_{conv\_2} = T_{conv\_3} = 0.0016 \text{ seconds} \tag{21.3}$$

$$T_{cable\_total} = 0.0039 \cdot 3 = 0.0117 \text{ seconds} \tag{21.4}$$

The stored energy in the system prior to the disturbance is:

$$W_{conv2} = W_{conv2} = 1216 \cdot 0.0016 = 1.9456 \text{ MWs} \tag{21.5}$$

$$W_{conv1} = W_{conv4} = 1216 \cdot 0.0040 = 4.8640 \text{ MWs} \tag{21.6}$$

$$W_{cables} = 1216 \cdot 0.0117 = 4.7420 \text{ MWs} \tag{21.7}$$

$$W_{total\_stored} = 27.846 \text{ MWs} \tag{21.8}$$

With the simplification that the delivered power from the offshore converters to the offshore AC grids falls linearly, the delivered power from the MTDC after the disturbance is:

$$W_{delivered\_conv2} = \left(\frac{(83-62)}{2} + 62 \right) \text{MW} \cdot 0.115 \text{ seconds} = 8.338 \text{ MWs} \tag{21.9}$$

$$W_{delivered\_conv3} = \left(\frac{(105-85)}{2} + 85 \right) \text{MW} \cdot 0.115 \text{ seconds} = 10.930 \text{ MWs} \tag{21.10}$$

$$W_{total\_delivered} = 19.268 \text{ MWs} \tag{21.11}$$

$$\frac{W_{total\_delivered}}{W_{total\_stored}} = 69.2 \text{ \%} \tag{21.12}$$

Collapse in the offshore simulation system occurs when approximately 69.2 percent of the stored energy in the MTDC is discharged.

The collapse occurred as the DC voltage reached approximately 0.5 pu. It has not been investigated what was the triggering factor for the total system collapse, the voltage drop or the energy discharge.

22 Appendix F

22.1 Dynamic simulation results

22.1.1 Case 1

Simulation 1 (Large wind generation)

Time	Event
0.00	Normal operation
0.20	Disconnect (trip) converter 2

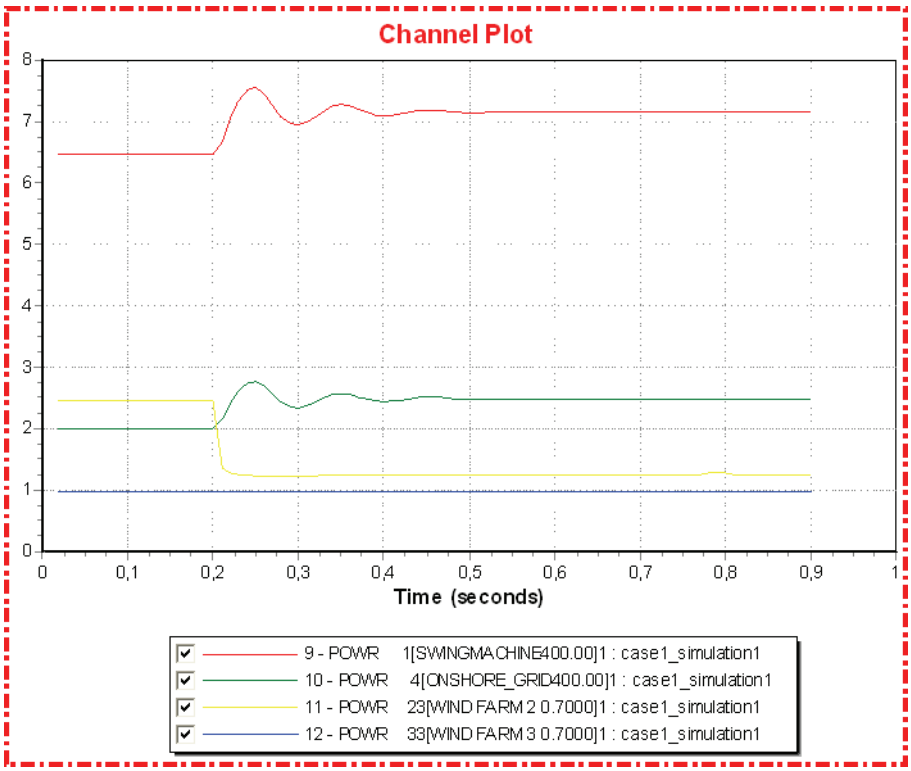

Figure F.1.1: Active power generation in AC grids [pu]

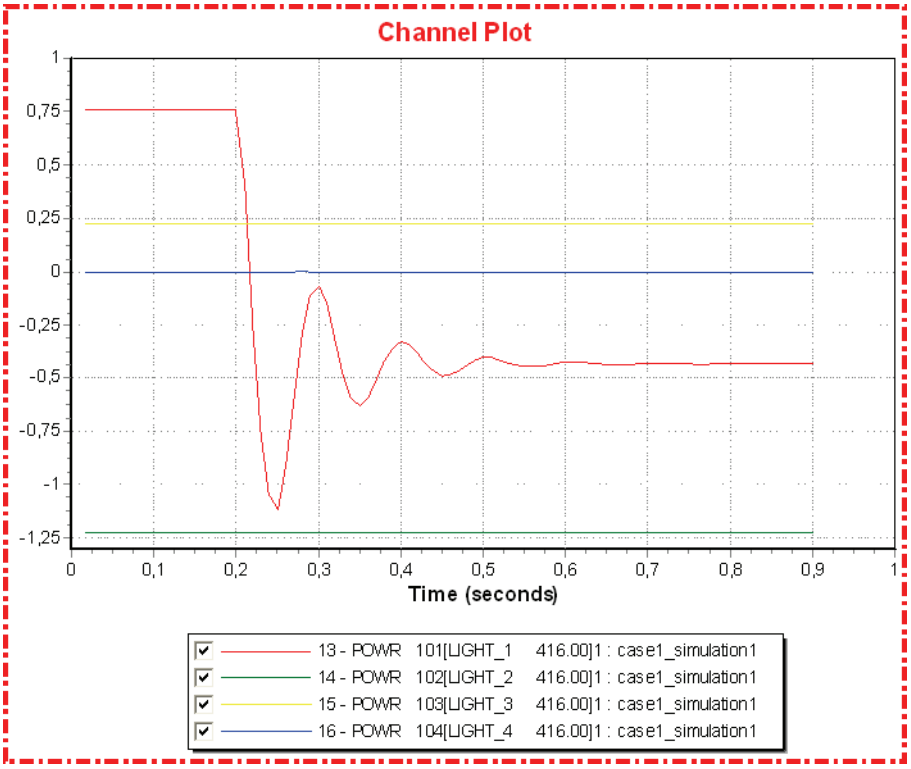

Figure F.1.2: Converter active power [pu]

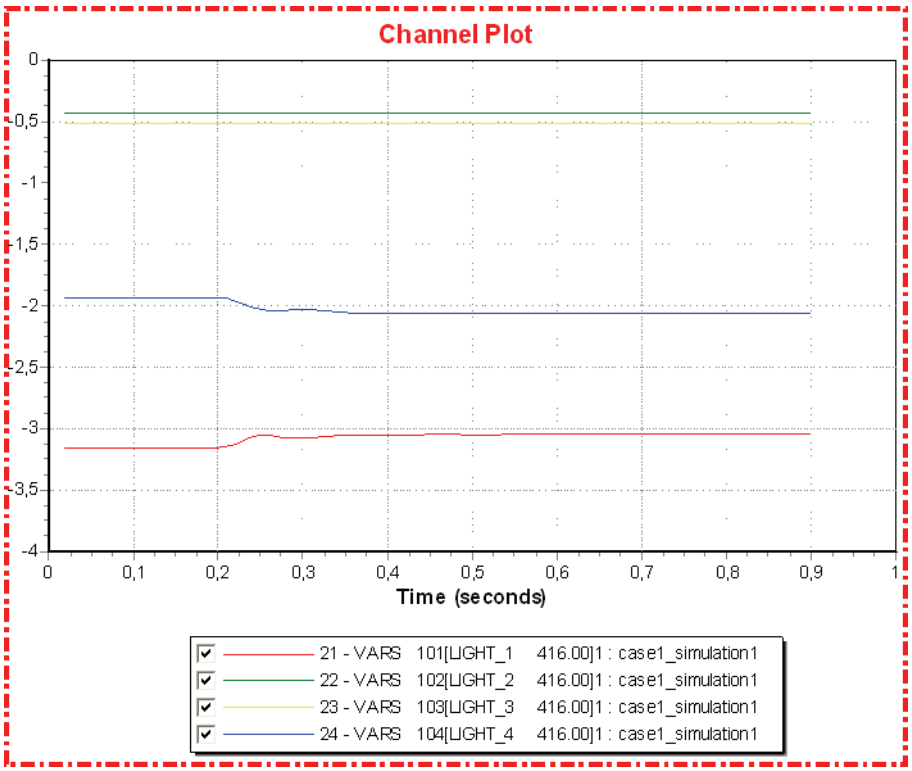

Figure F.1.3: Converter reactive power [pu]

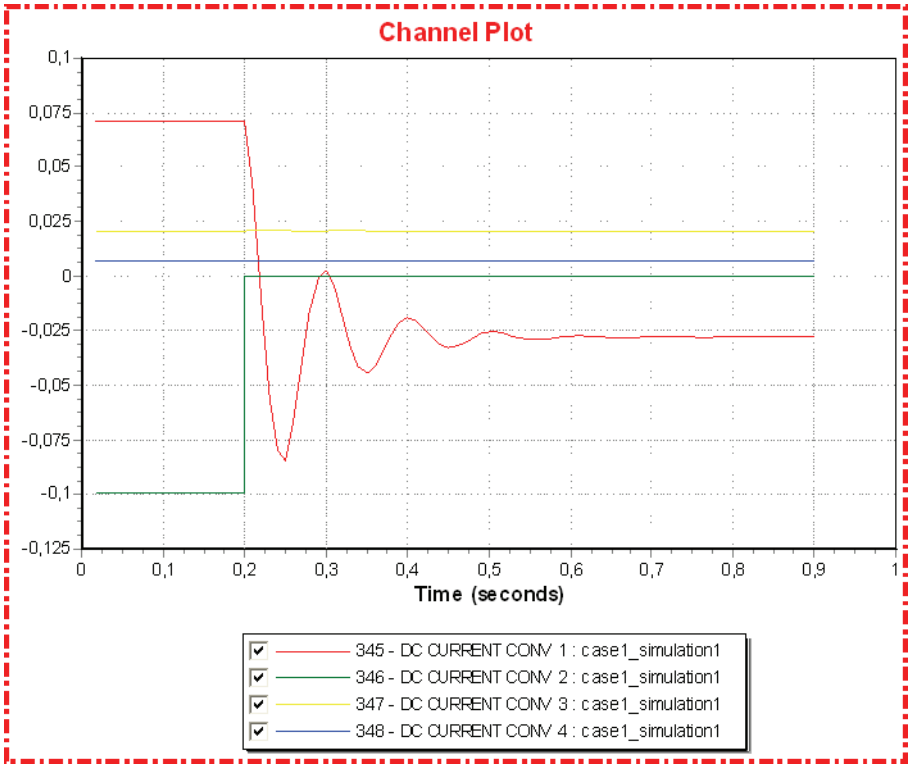

Figure F.1.4: Converter DC current [pu]

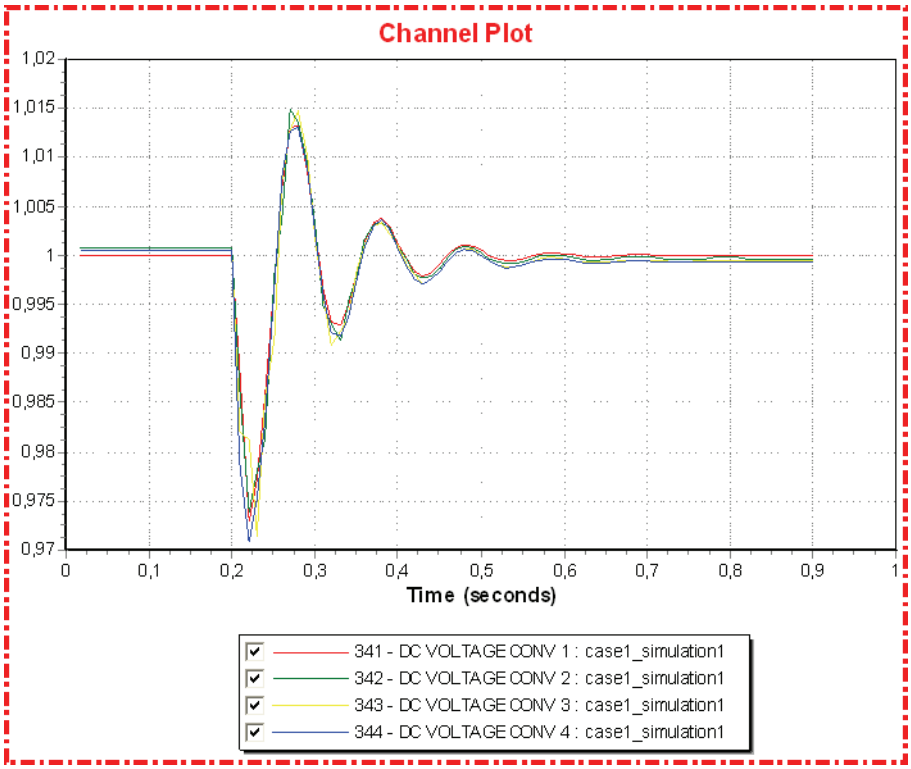

Figure F.1.5: Converter DC voltage [pu]

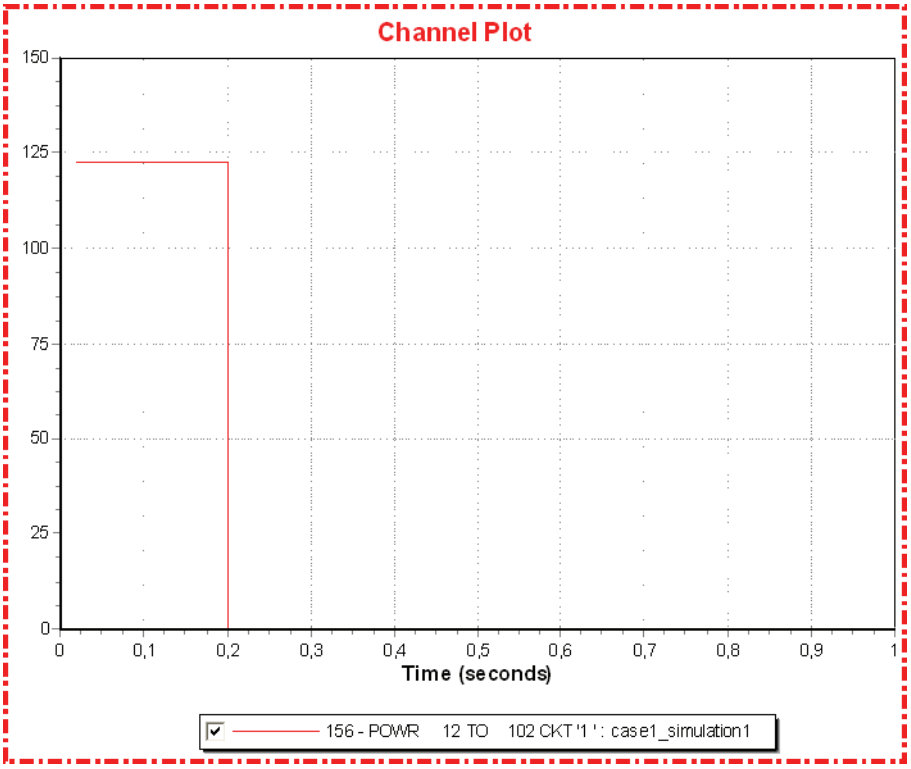

Figure F.1.6: Active power from PCC2 to converter 2 [MW]

Simulation 2 (Large wind generation)

Time	Event
0.00	Normal operation
0.20	Disconnect (trip) converter 1 (UdcCtrl converter)

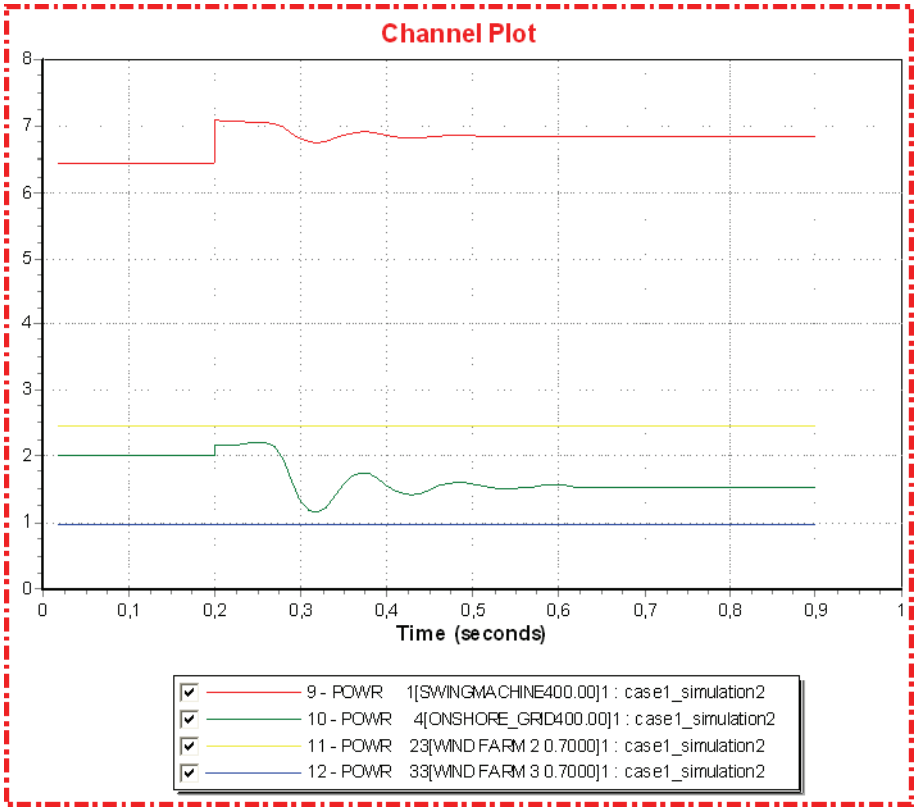

Figure F.1.7: Active power generation in AC grids [pu]

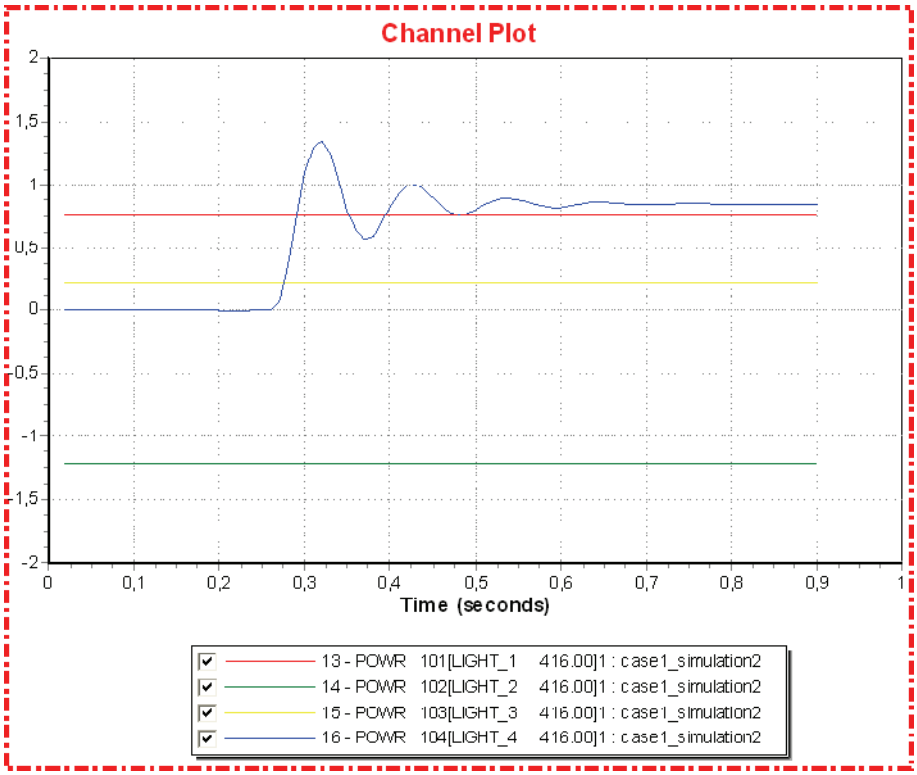

Figure F.1.7: Converter active power [pu]

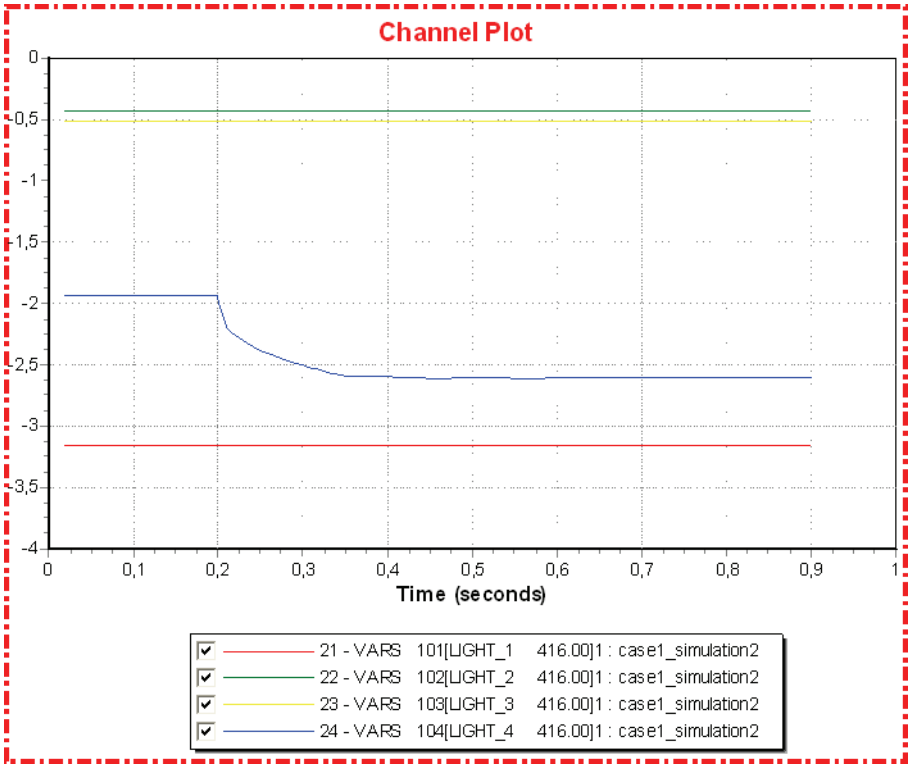

Figure F.1.8: Converter reactive power [pu]

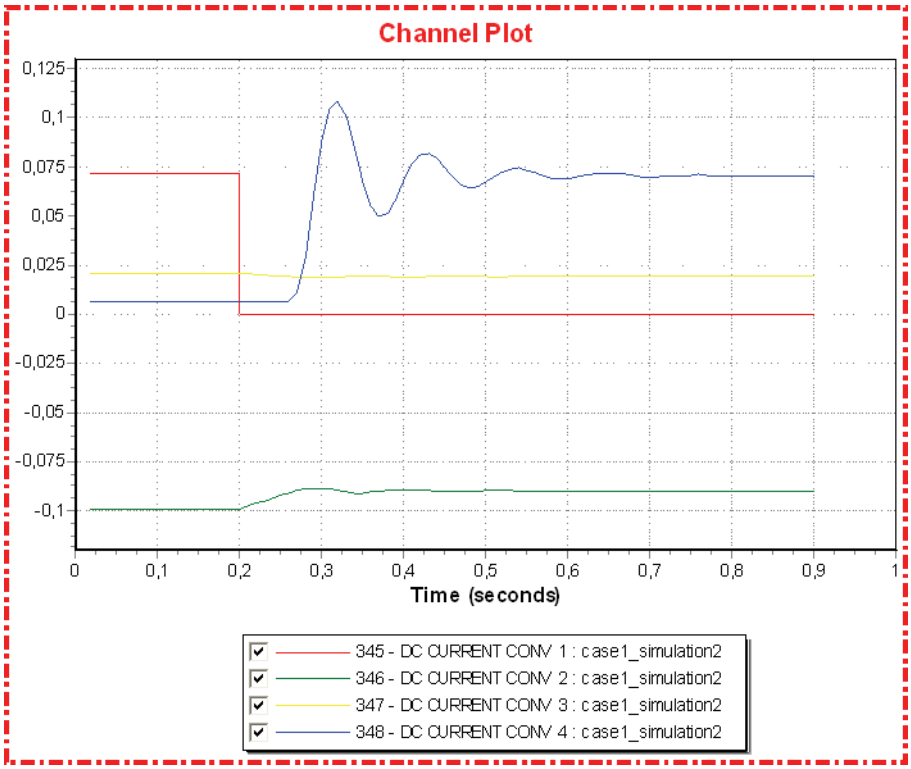

Figure F.1.9: Converter DC current [pu]

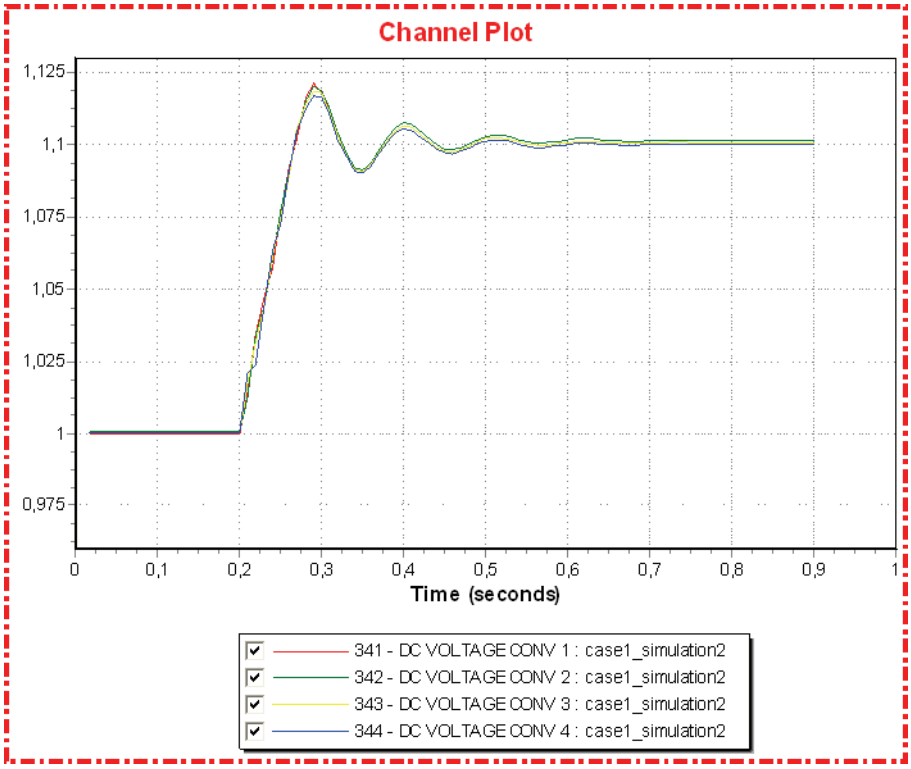

Figure F.1.10: Converter DC voltage [pu]

Simulation 3 (Small wind generation)

Time	Event
0.00	Normal operation
0.20	Disconnect (trip) converter 1 (UdcCtrl converter)

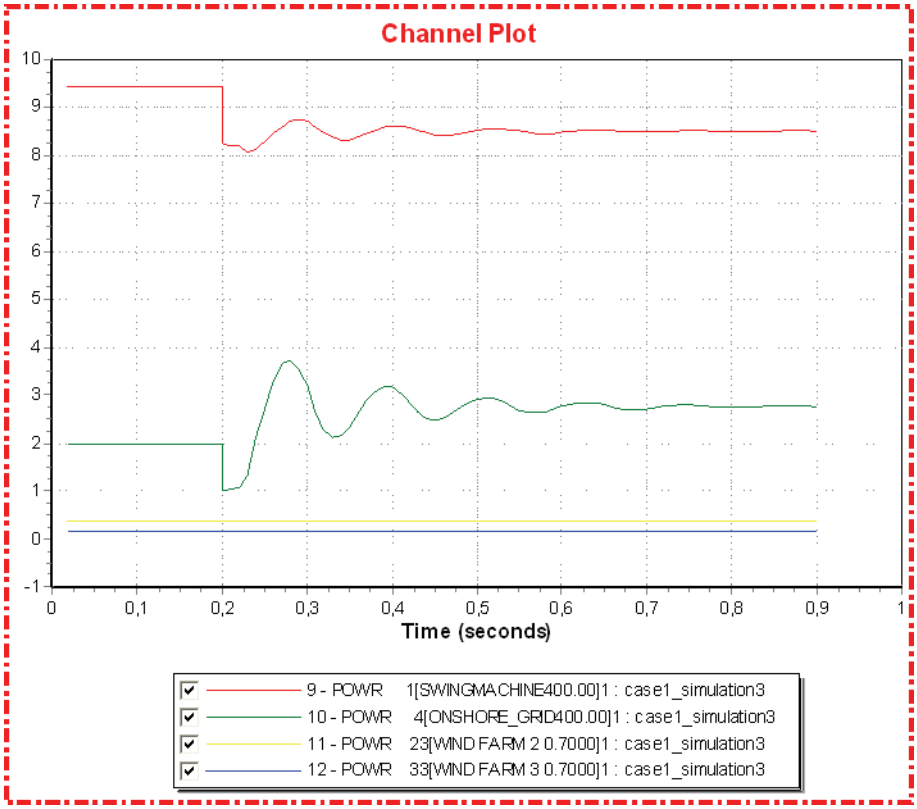

Figure F.1.11: Active power generation in AC grids [pu]

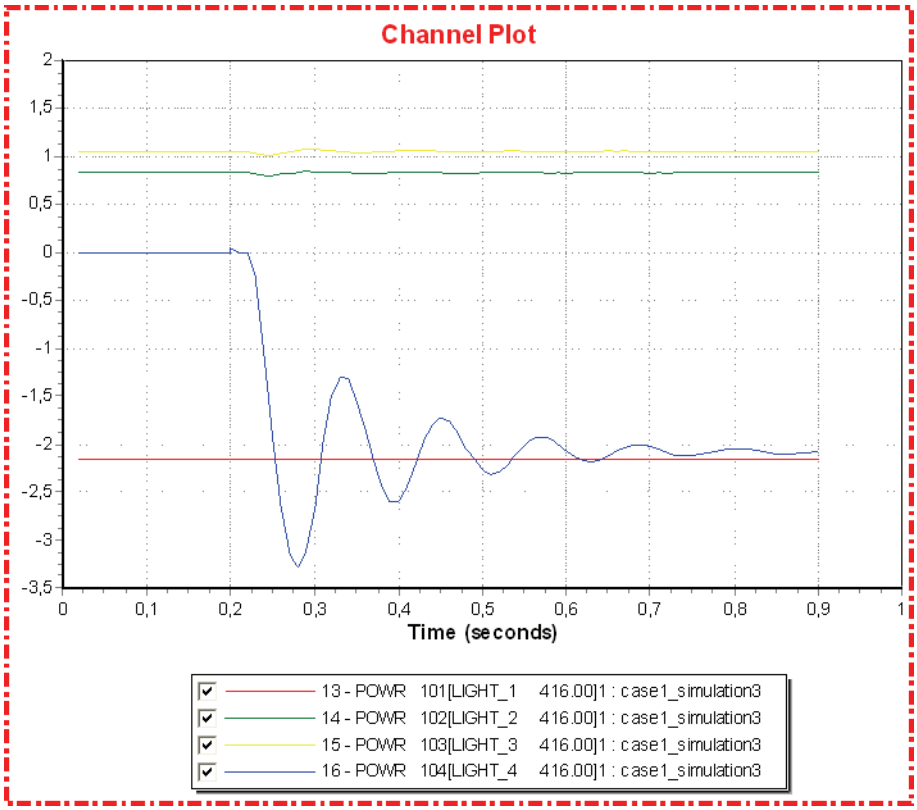

Figure F.1.12: Converter active power [pu]

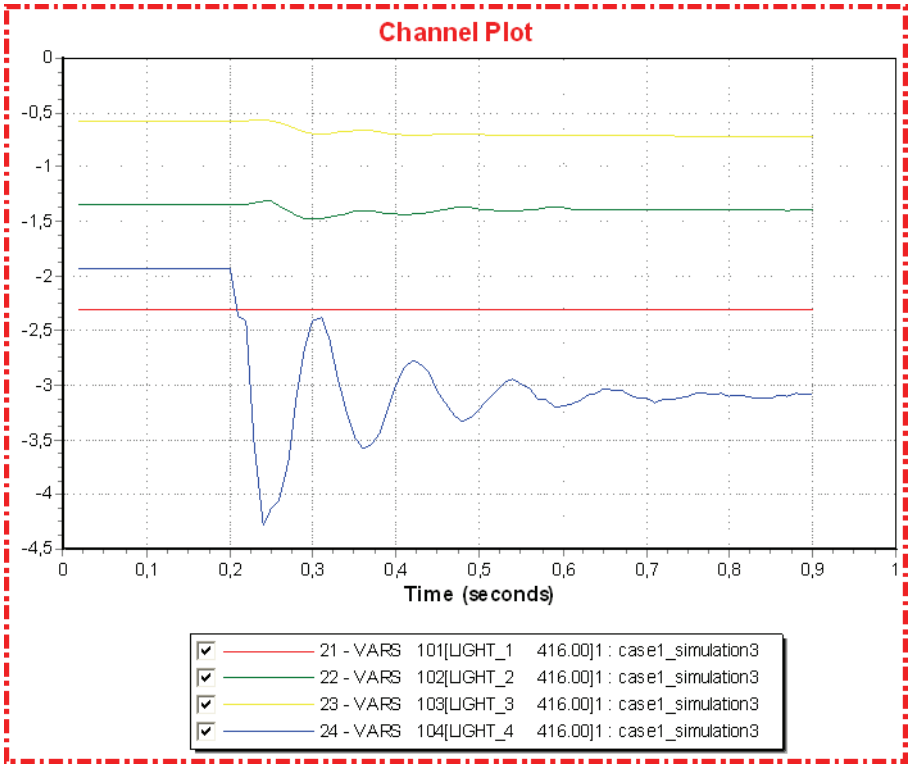

Figure F.1.13: Converter reactive power [pu]

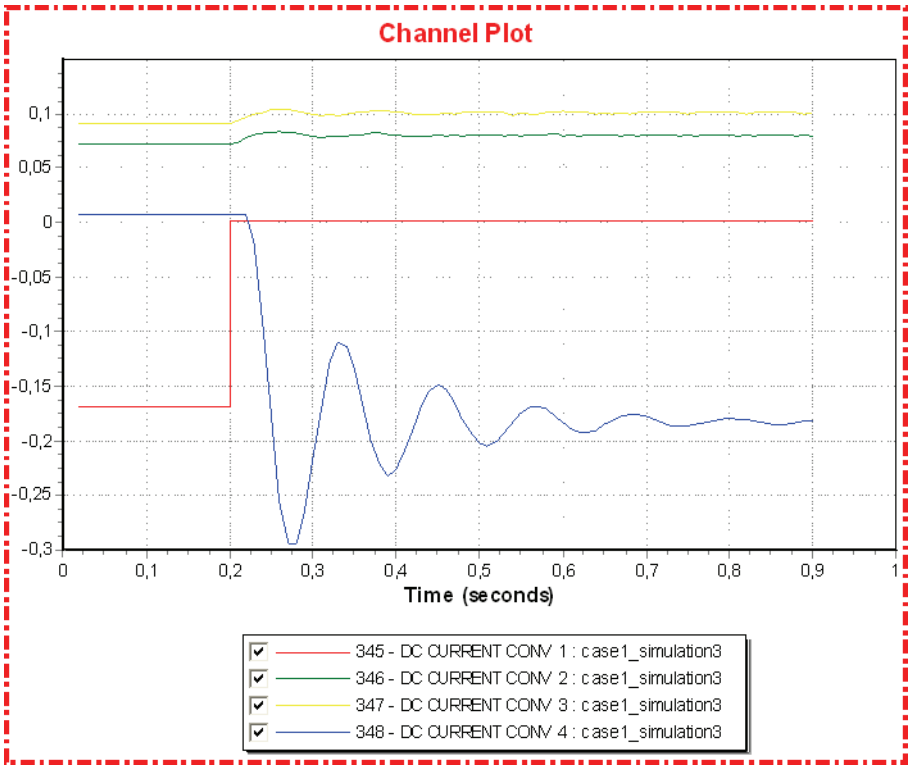

Figure F.1.14: Converter DC current [pu]

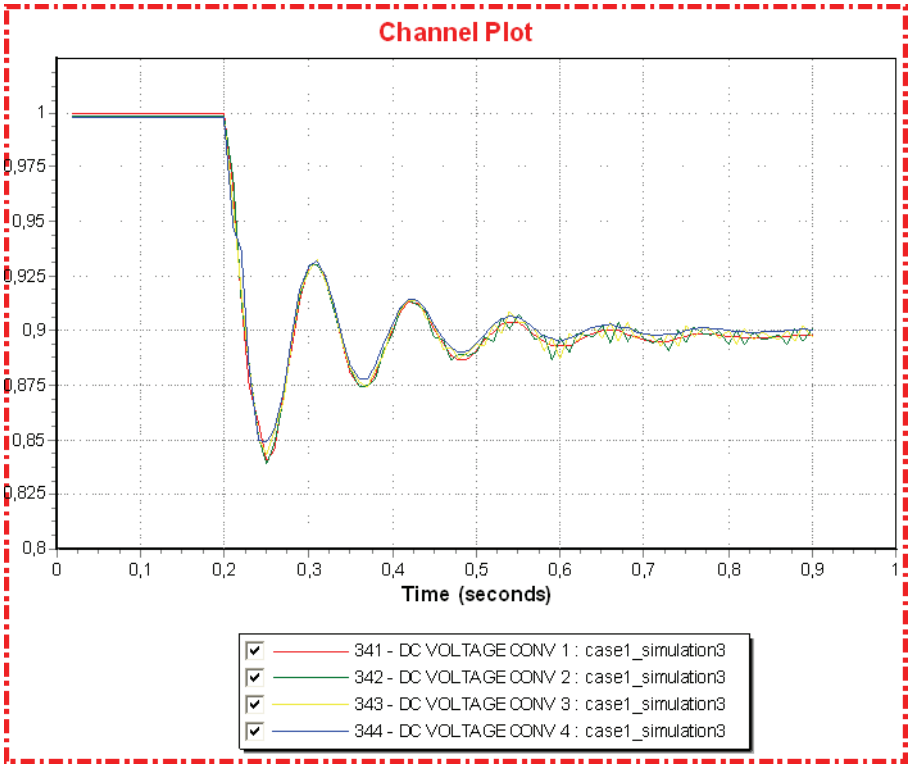

Figure F.1.15: Converter DC voltage [pu]

Simulation 4 (Large wind generation)

Time	Event
0.00	Normal operation
0.20	Disconnect (trip) converter 1 and change Poption for converter 4 to UdcCtrl

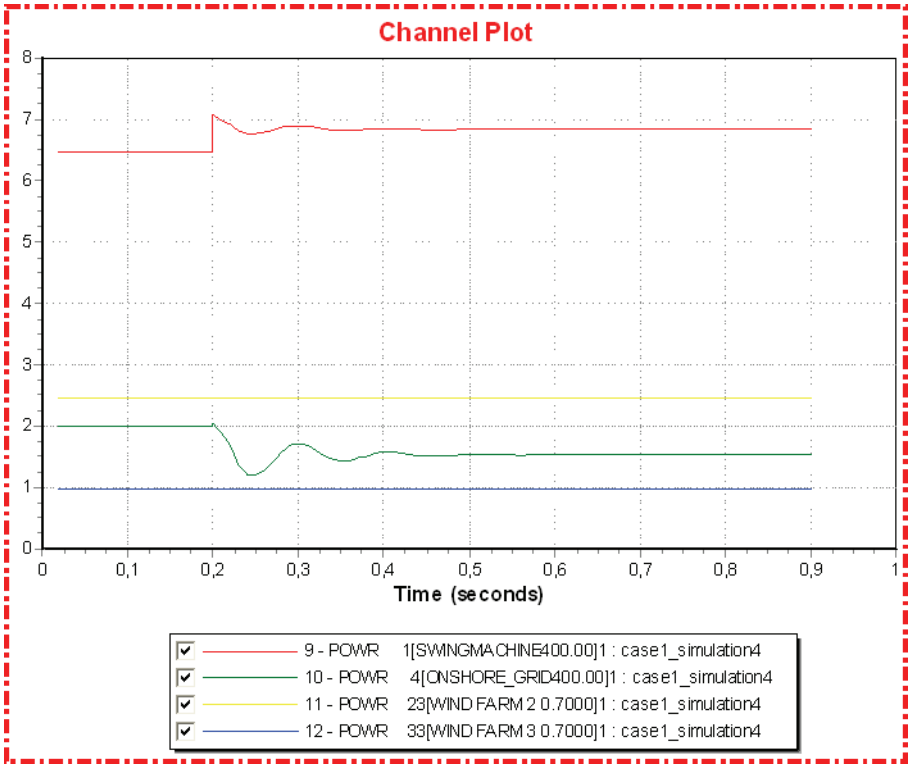

Figure F.1.16: Active power generation in AC grids [pu]

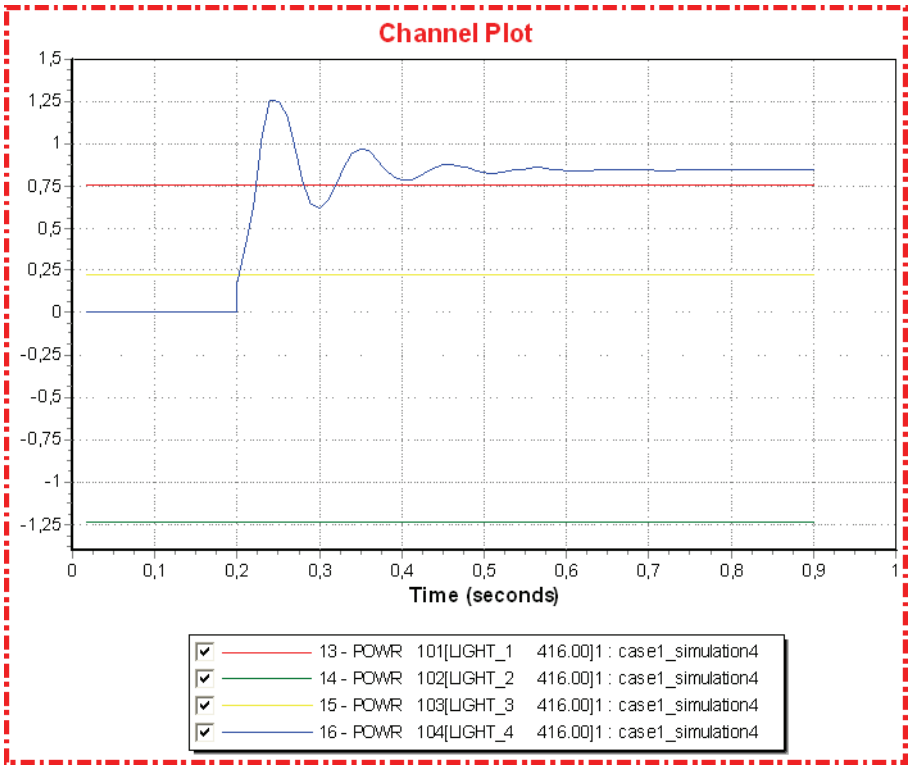

Figure F.1.17: Converter active power [pu]

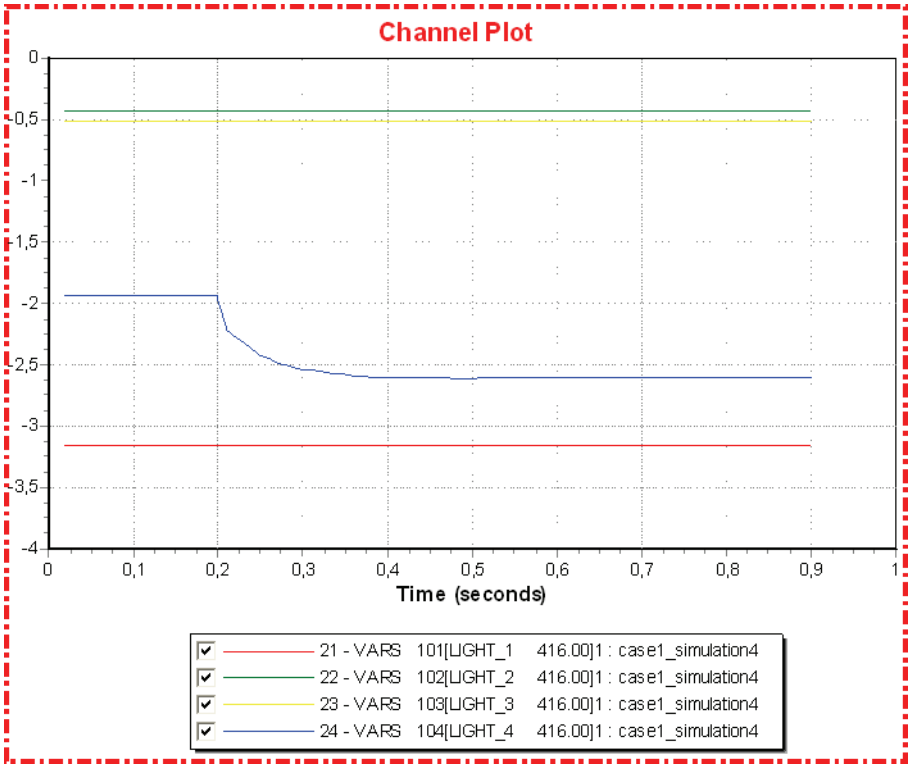

Figure F.1.18: Converter reactive power [pu]

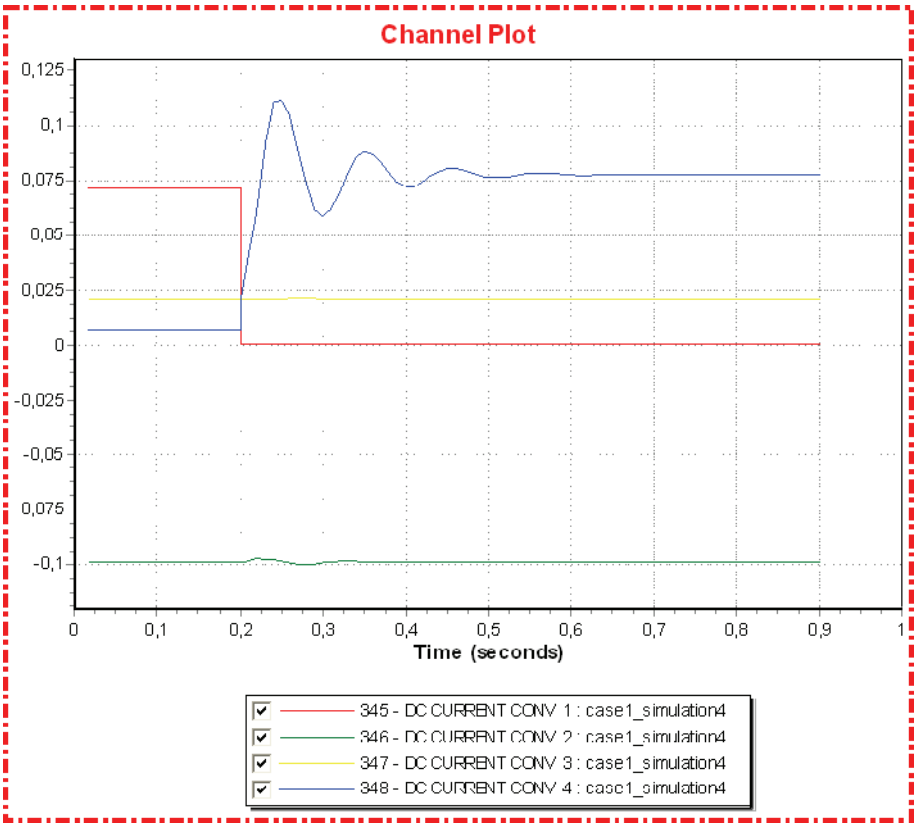

Figure F.1.19: Converter DC current [pu]

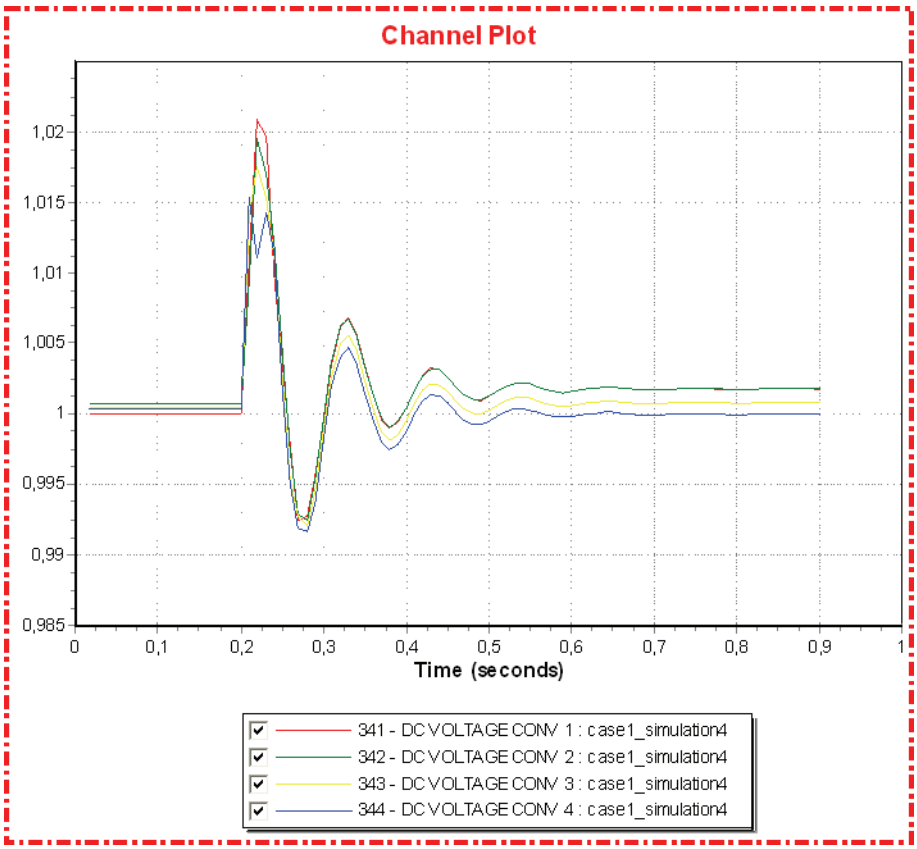

Figure F.1.20: Converter DC voltage [pu]

22.1.2 Case 2

Simulation 1 (Large wind generation)

Time	Event
0.00	Normal operation
0.20	Line fault on line 5 – 11 (id1)
0.30	Disconnect (Trip) faulted line

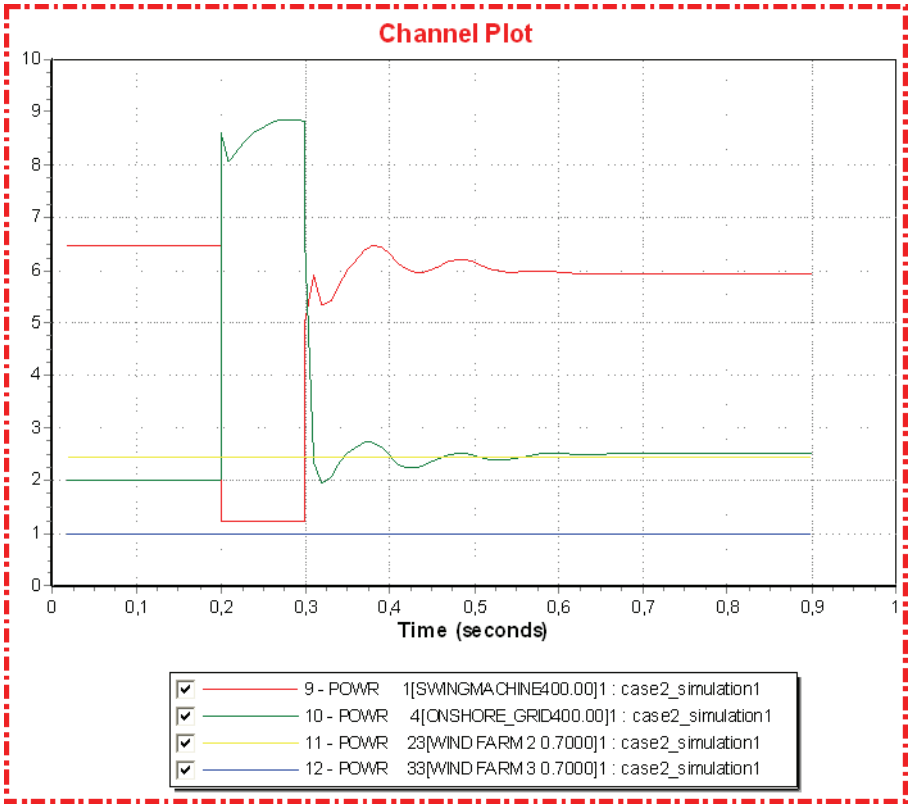

Figure F.2.1: Active power generation in AC grids [pu]

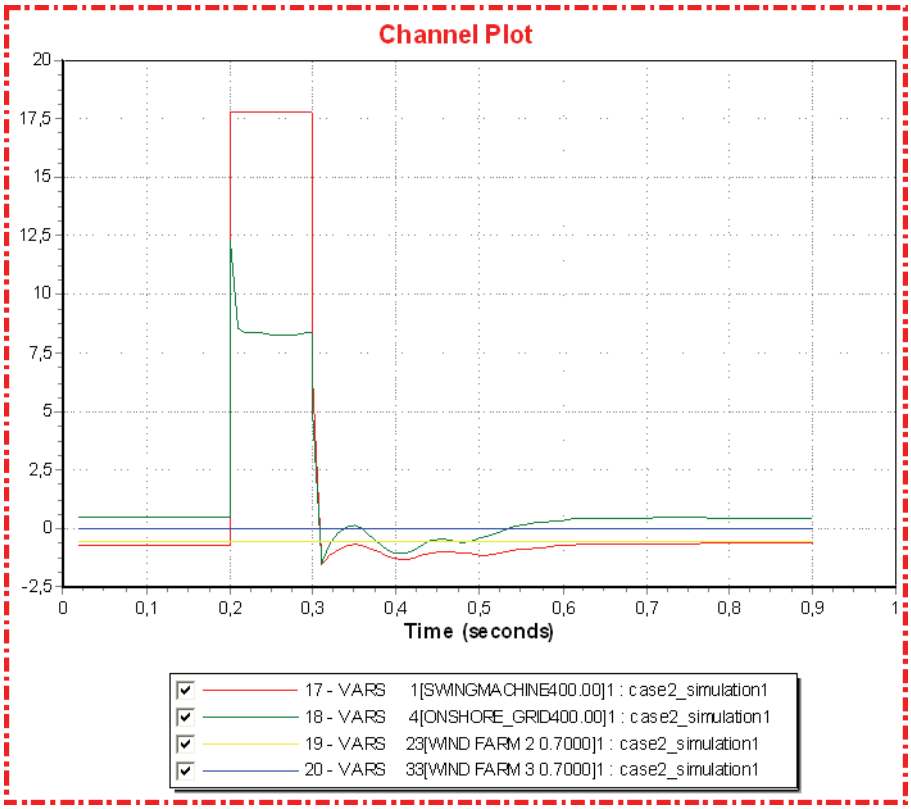

Figure F.2.2: Converter active power [pu]

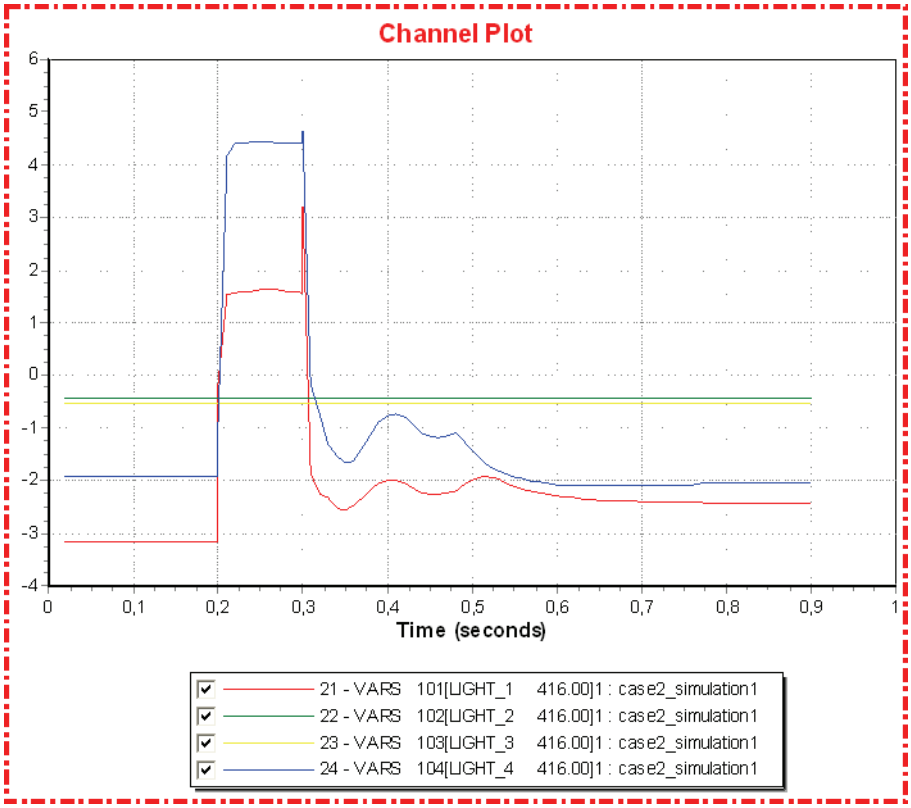

Figure F.2.3: Converter reactive power [pu]

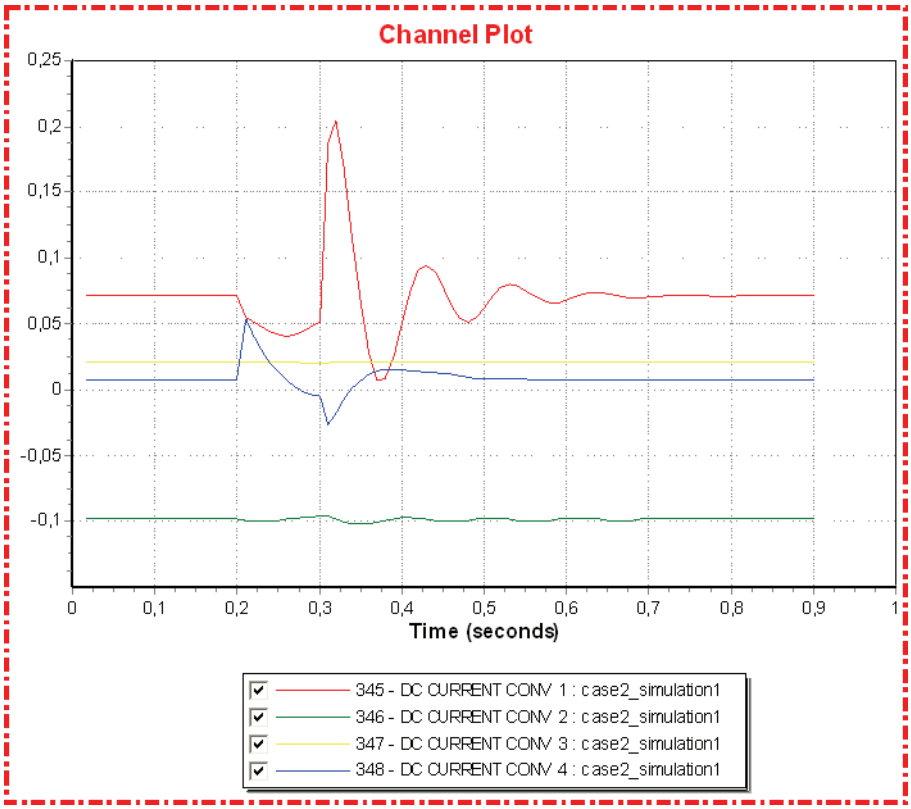

Figure F.2.4: Converter DC current [pu]

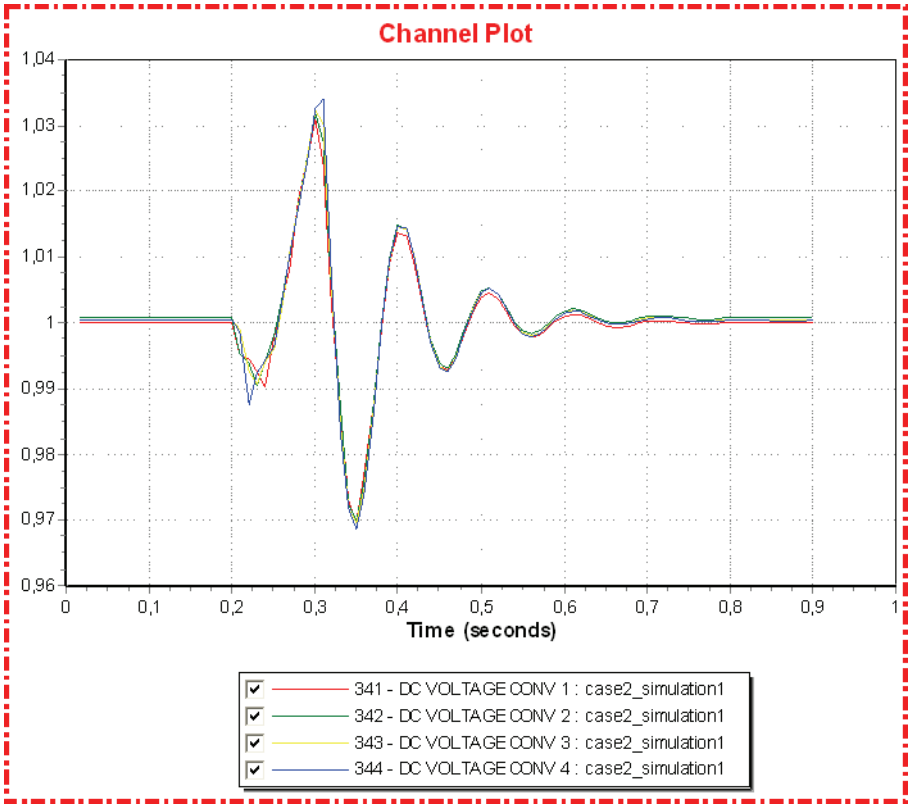

Figure F.2.5: Converter DC voltage [pu]

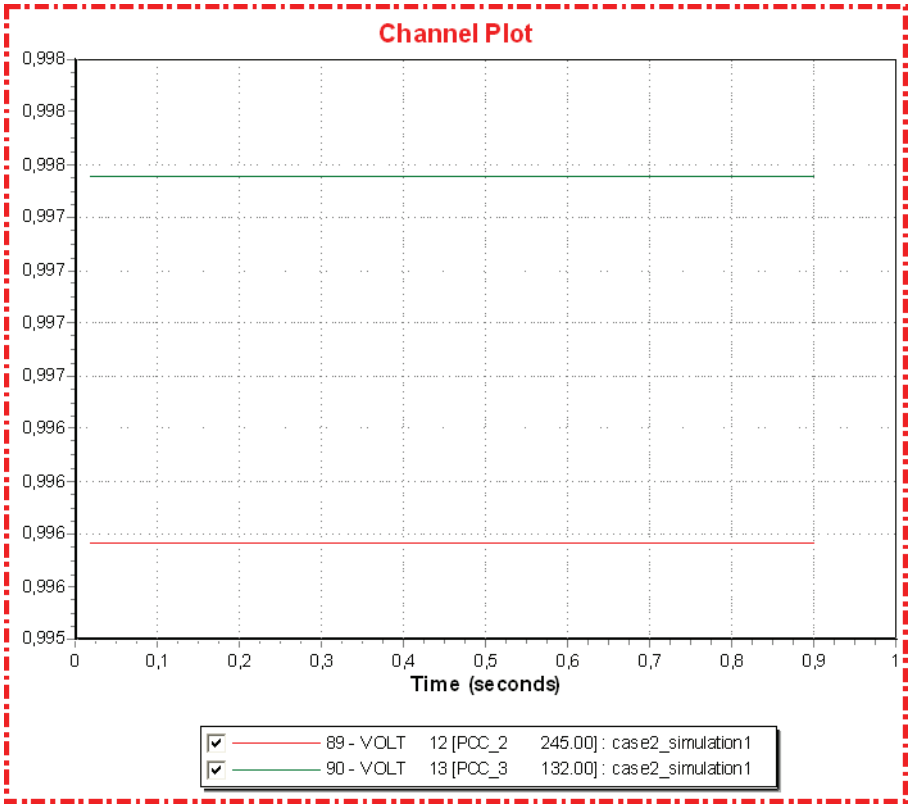

Figure F.2.6: AC voltage offshore [pu]

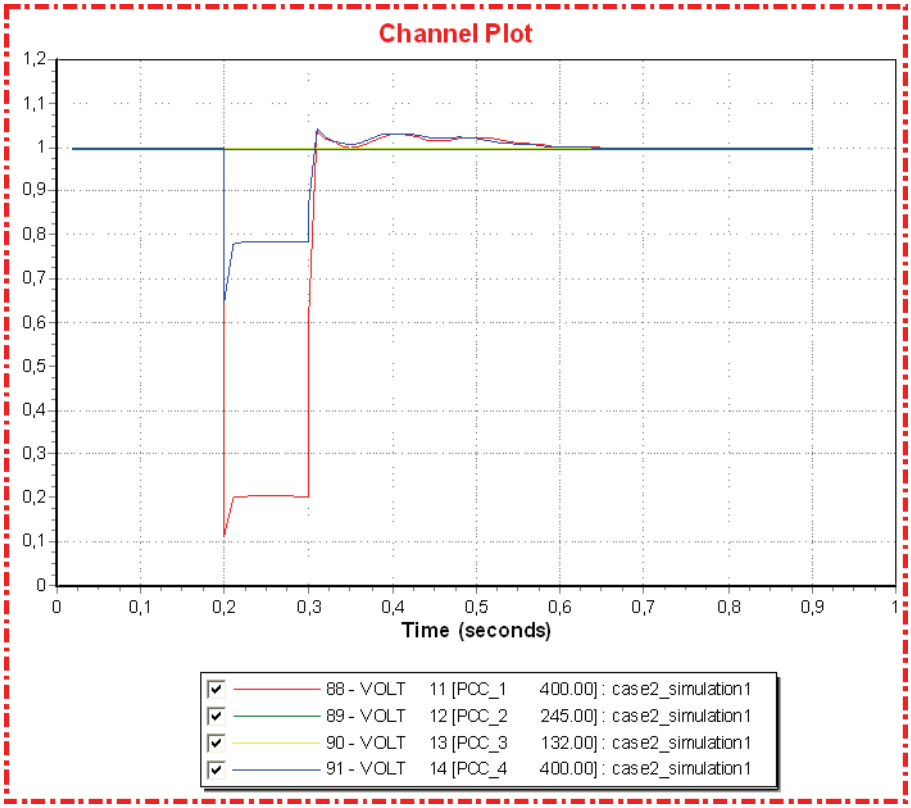

Figure F.2.7: AC voltages [pu]

Simulation 2 (Large wind generation)

Time	Event
0.00	Normal operation
0.20	Bus fault at bus 14
0.30	Clear bus fault

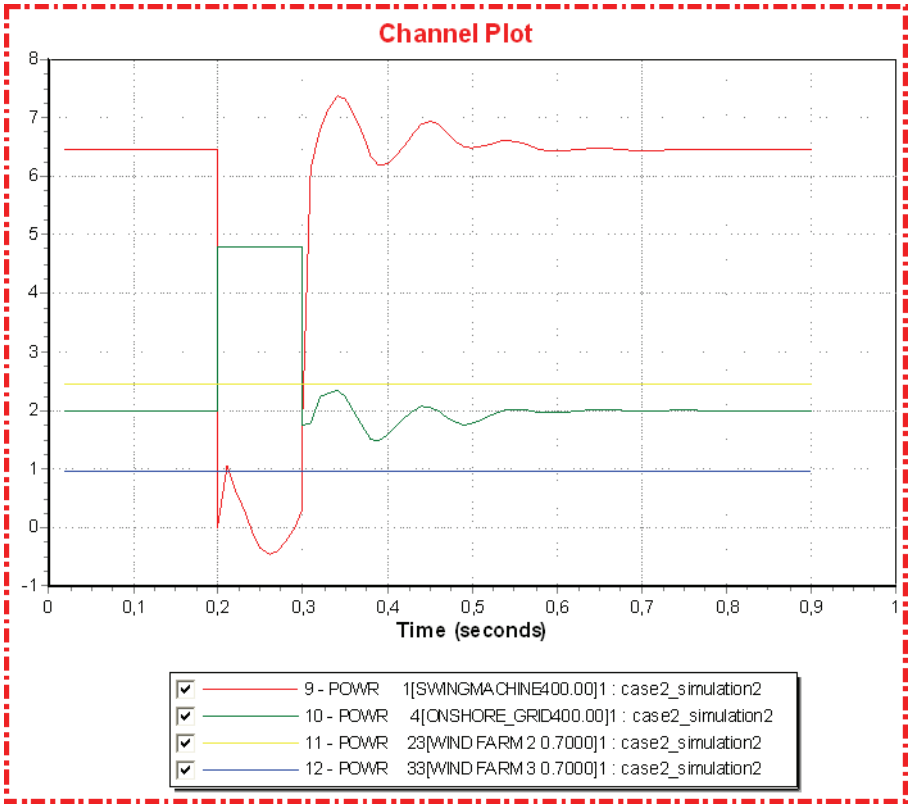

Figure F.2.8: Active power generation in AC grids [pu]

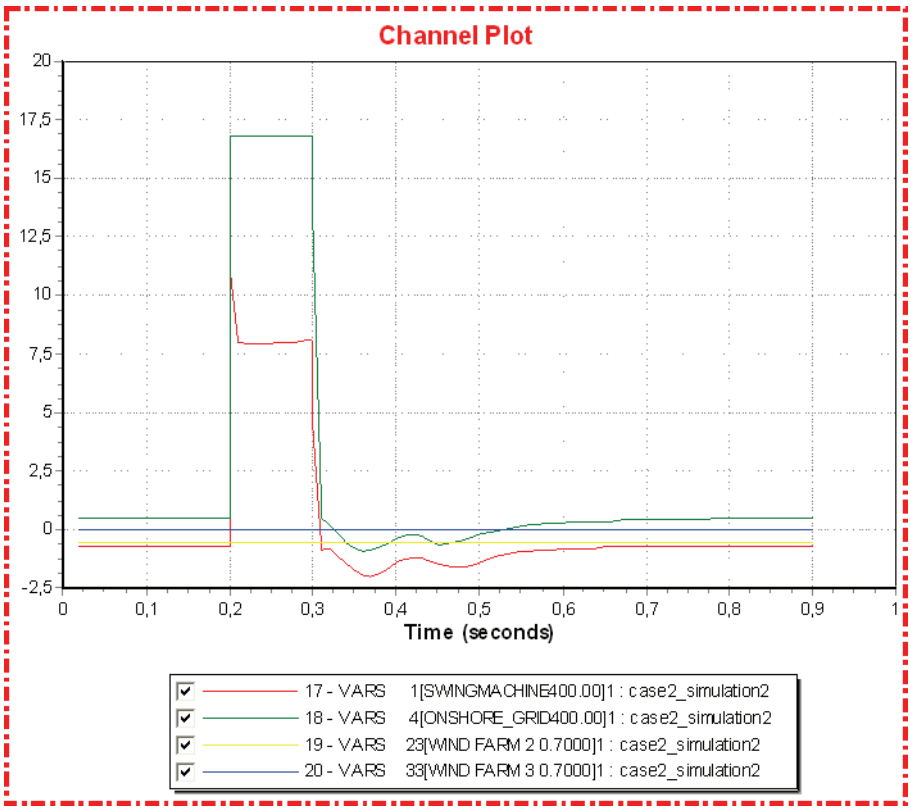

Figure F.2.9: Reactive power generation in AC grids [pu]

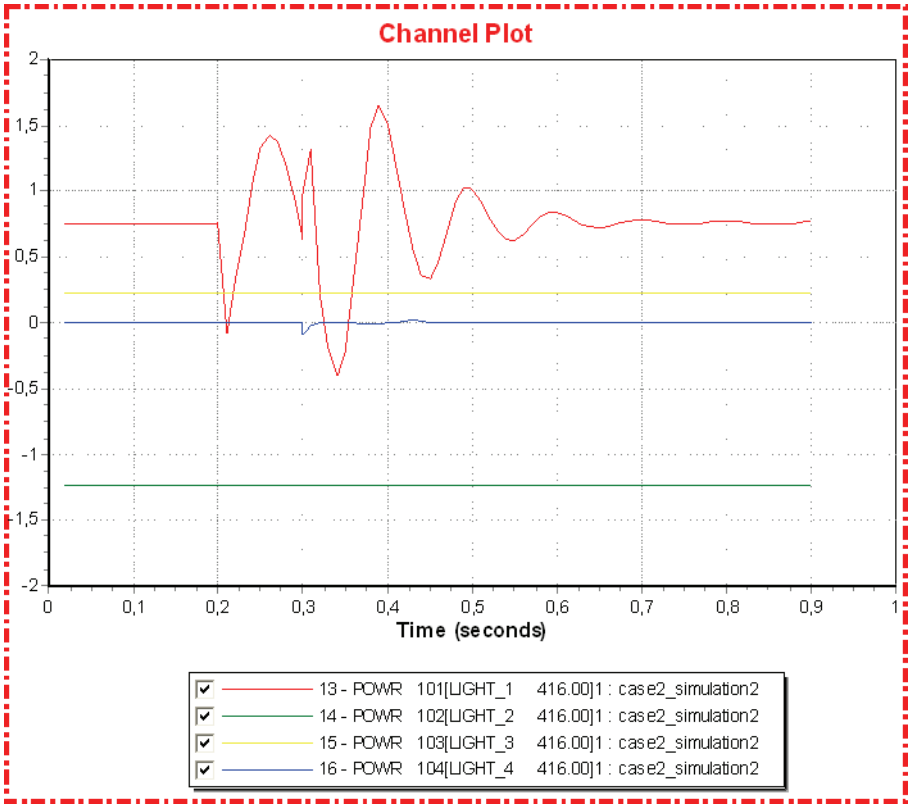

Figure F.2.10: Converter active power [pu]

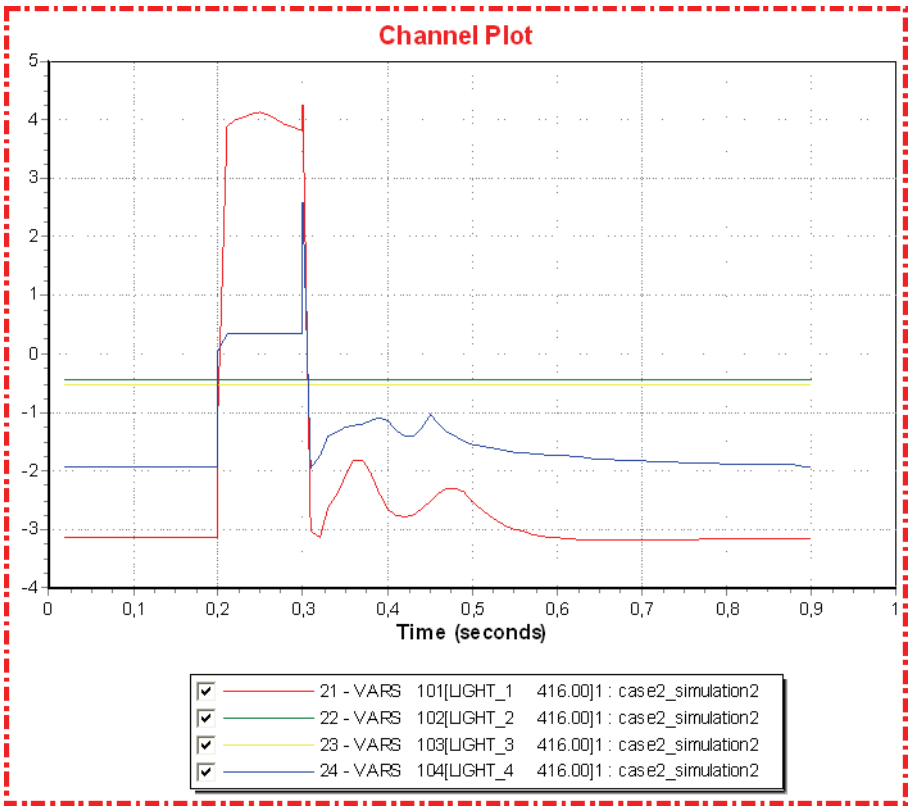

Figure F.2.11: Converter reactive power [pu]

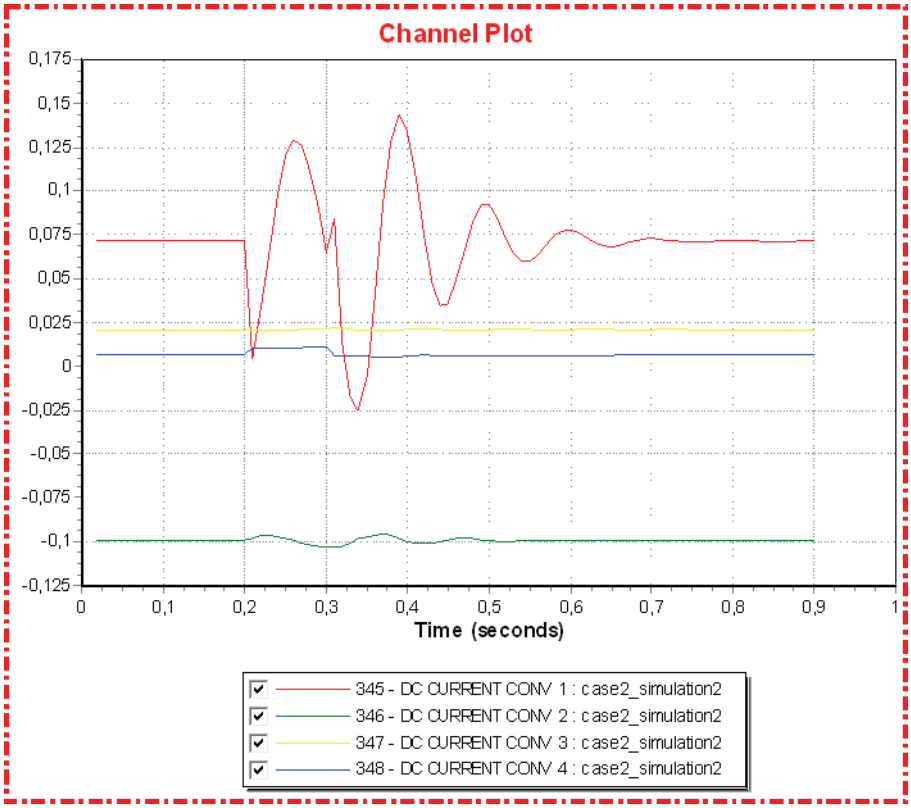

Figure F.2.12: Converter DC current [pu]

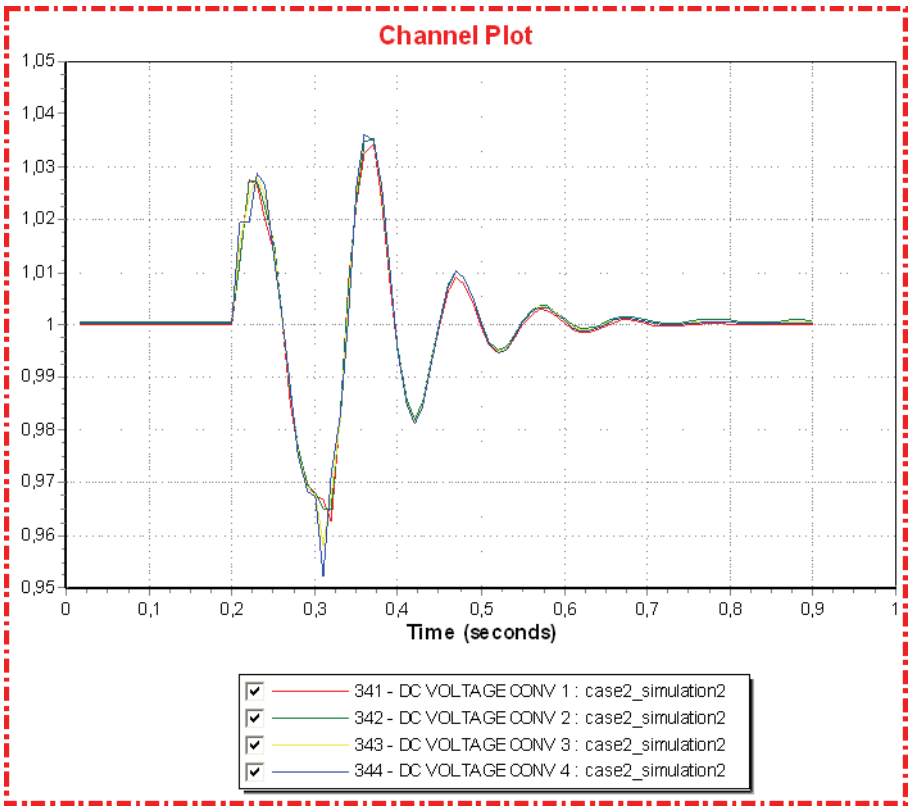

Figure F.2.13: Converter DC voltage [pu]

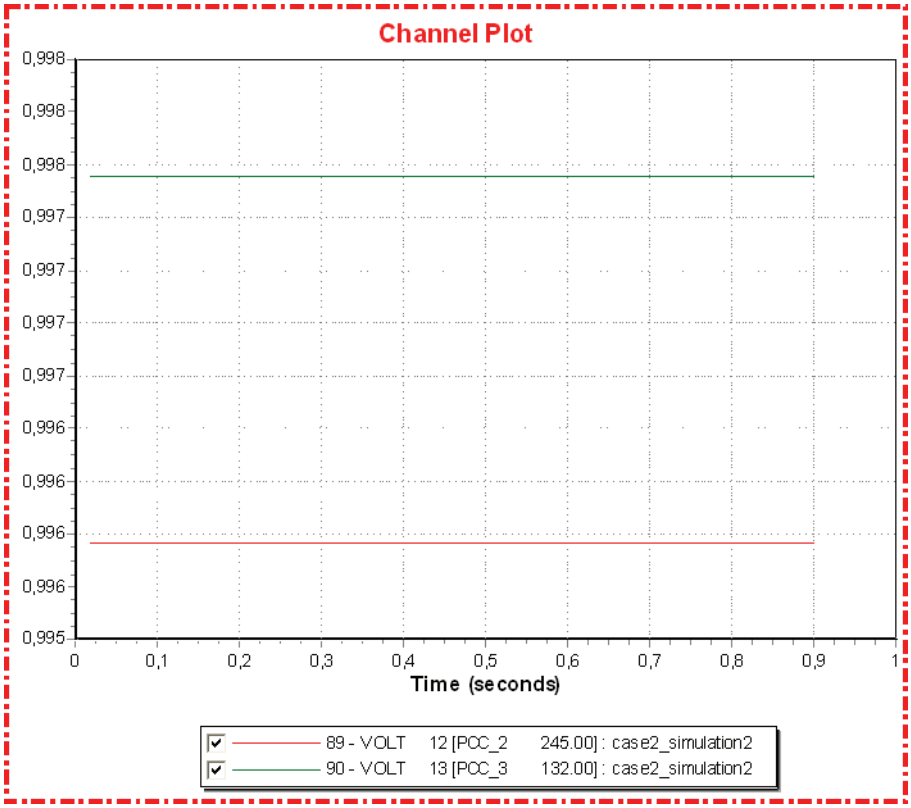

Figure F.2.14: Offshore AC voltage [pu]

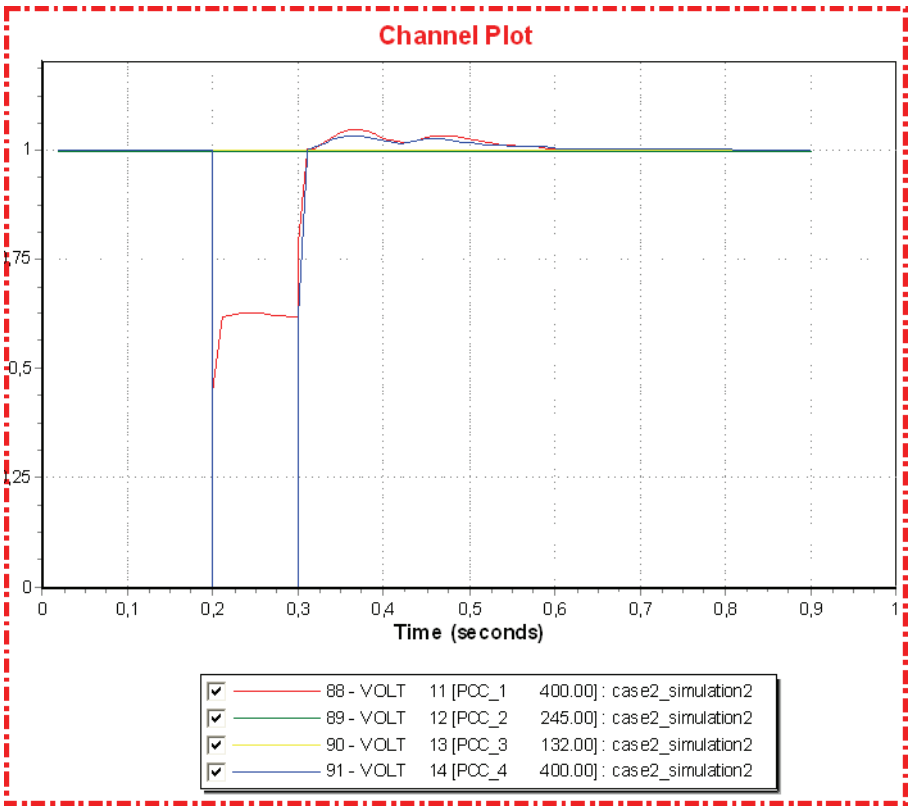

Figure F.2.15: AC voltages [pu]

Simulation 3 (Small wind generation)

Time	Event
0.00	Normal operation
0.20	Line fault on line 5 – 11 (id1)
0.30	Disconnect (Trip) faulted line

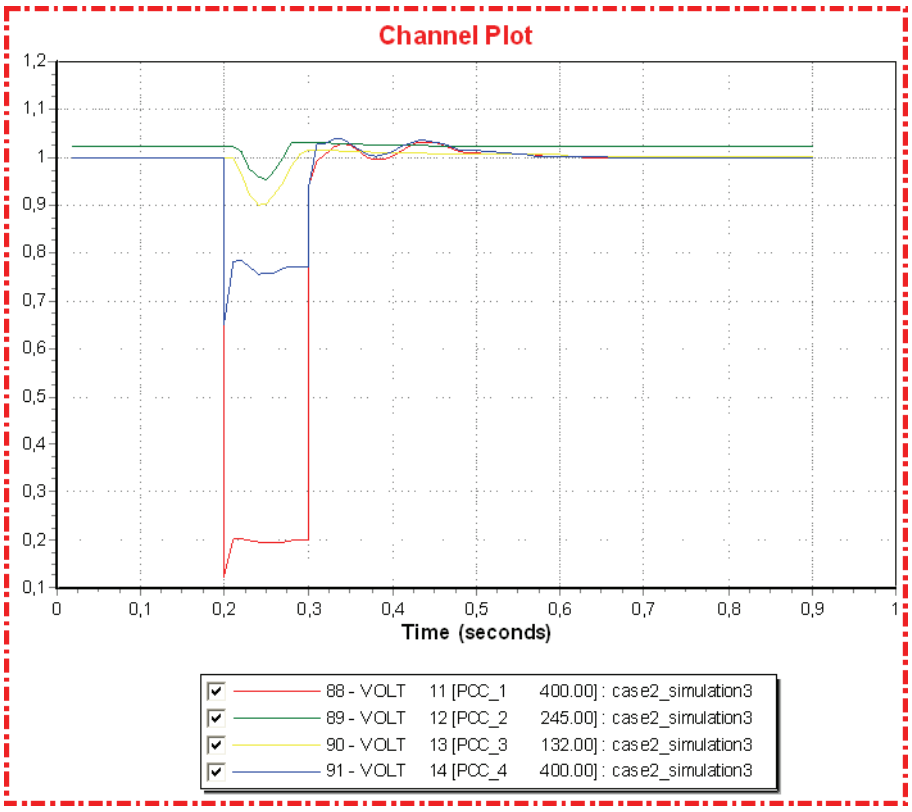

Figure F.2.16: AC voltages [pu]

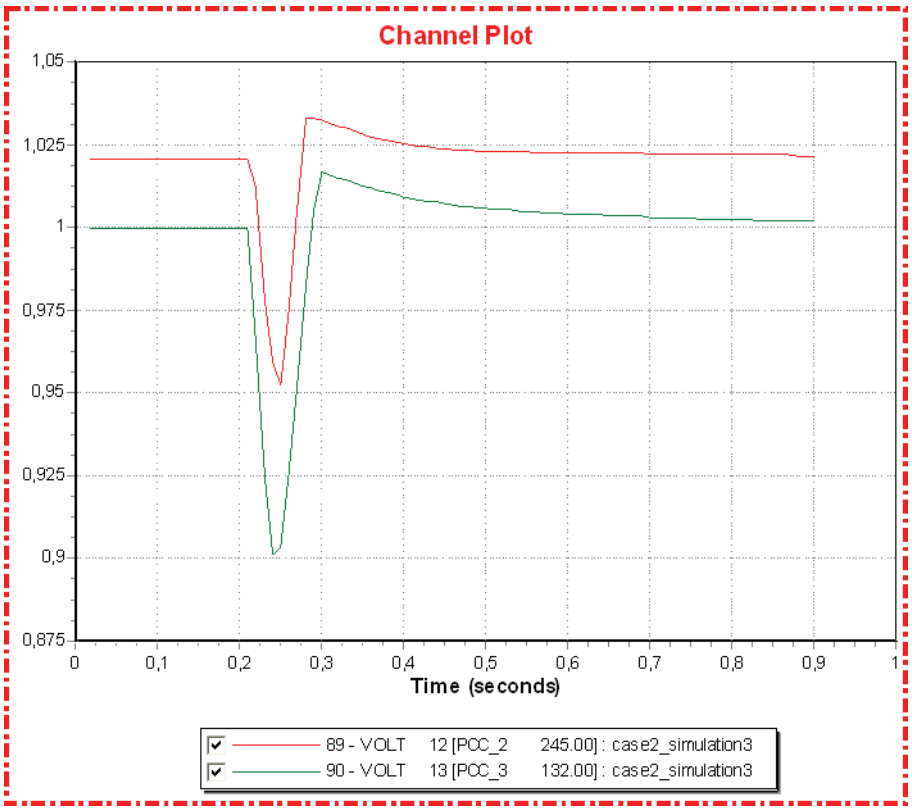

Figure F.2.17: Offshore AC voltage [pu]

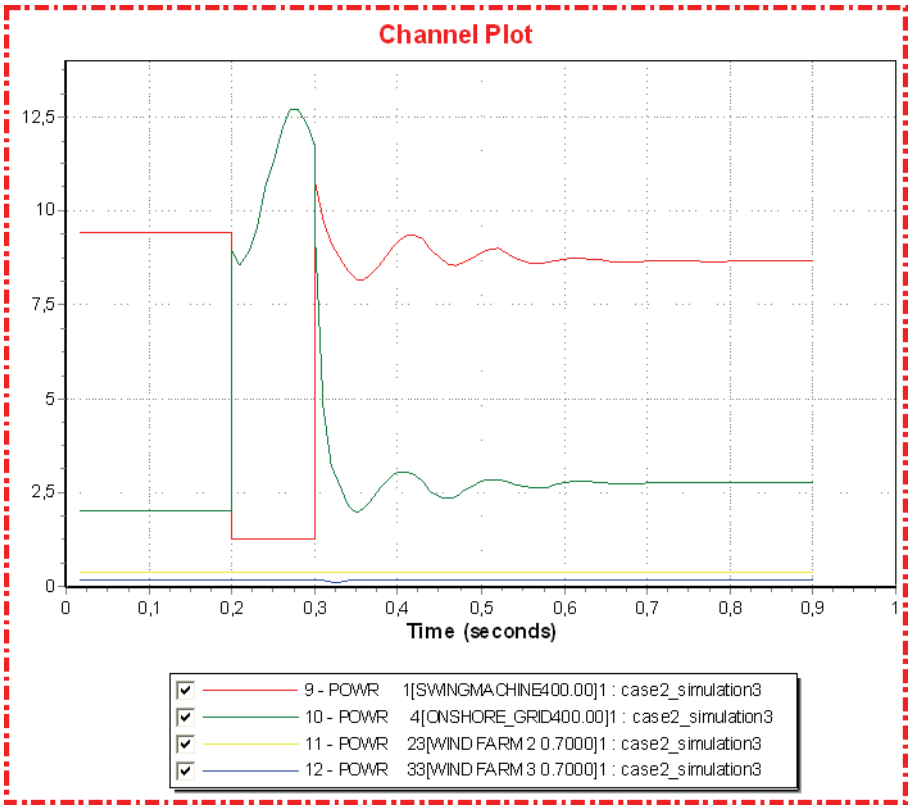

Figure F.2.18: Active power generation in AC grids [pu]

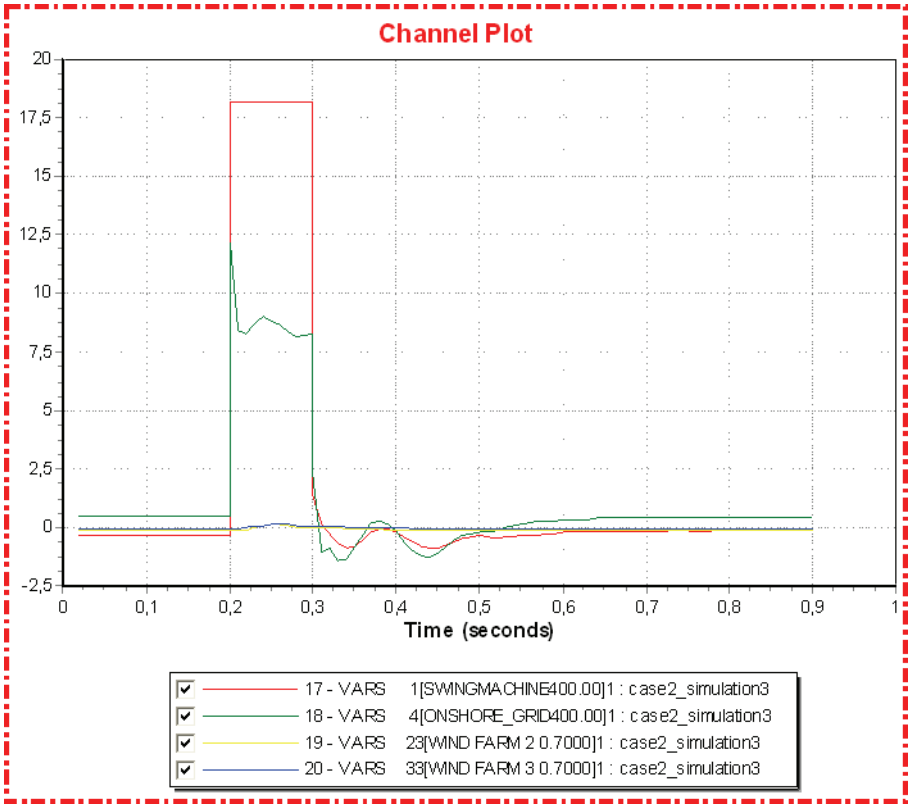

Figure F.2.19: Reactive power generation in AC grids [pu]

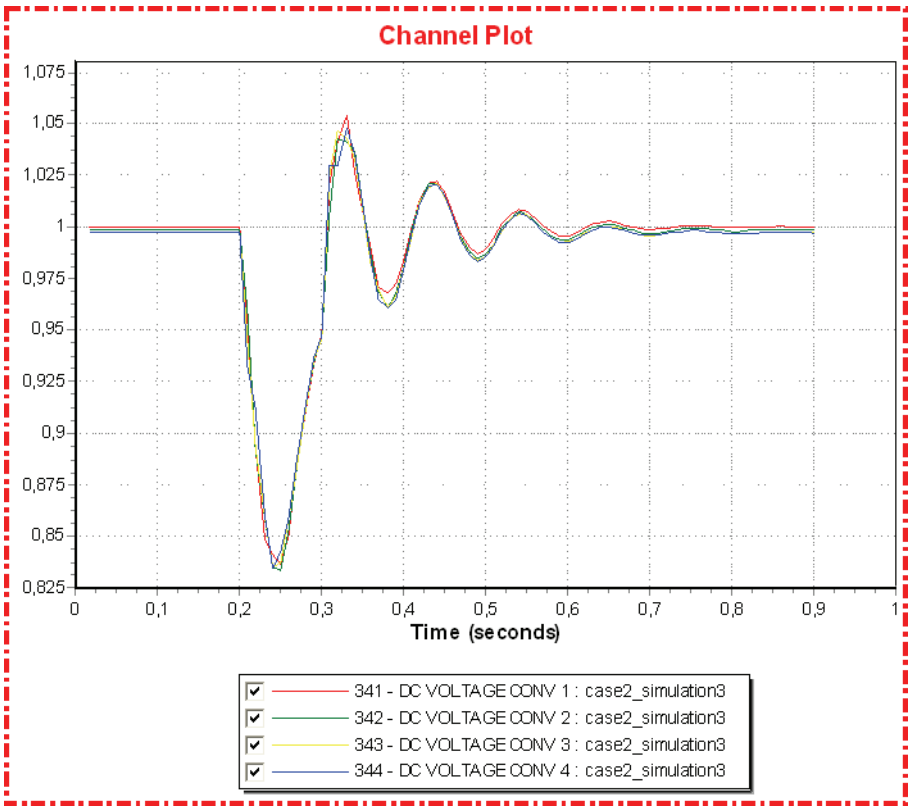

Figure F.2.20: Converter DC voltage [pu]

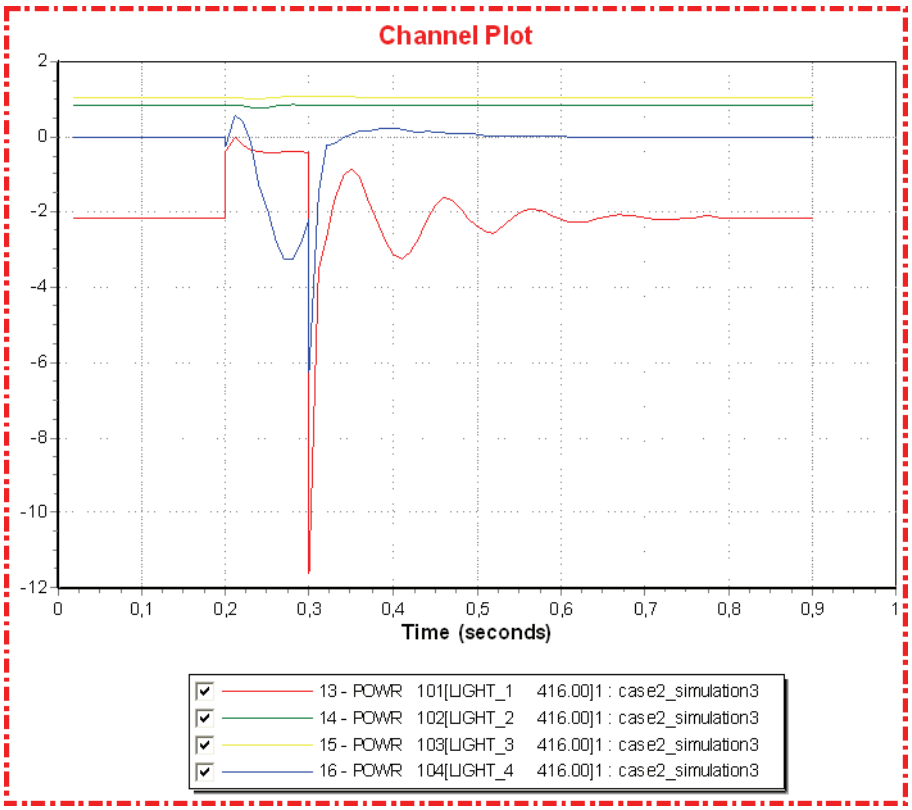

Figure F.2.21: Converter active power [pu]

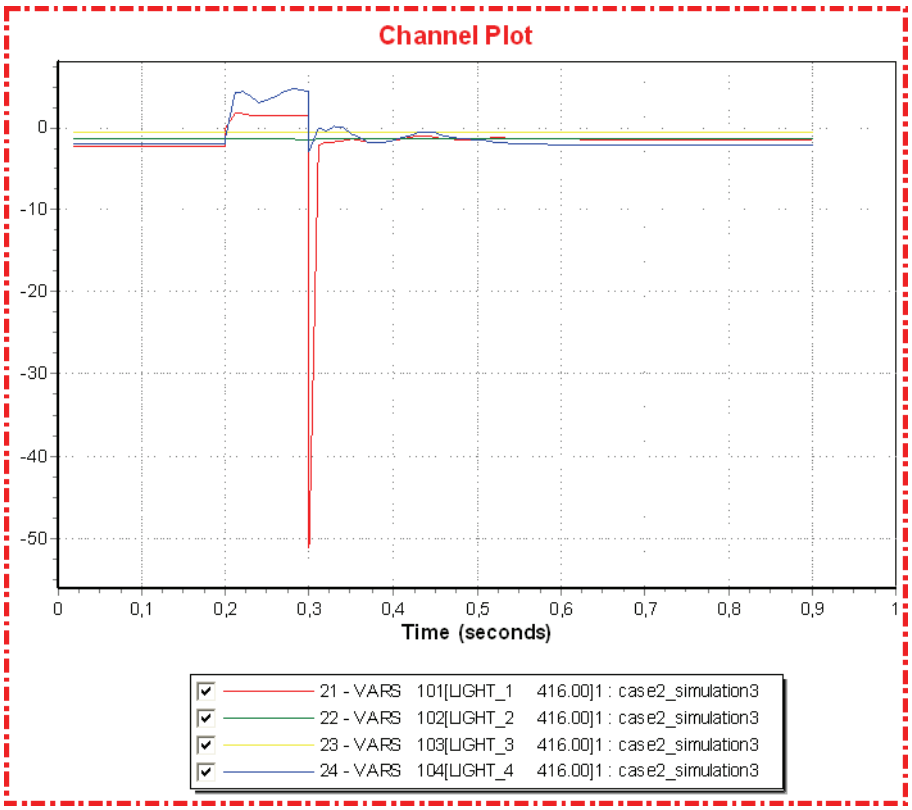

Figure F.2.22: Converter reactive power [pu]

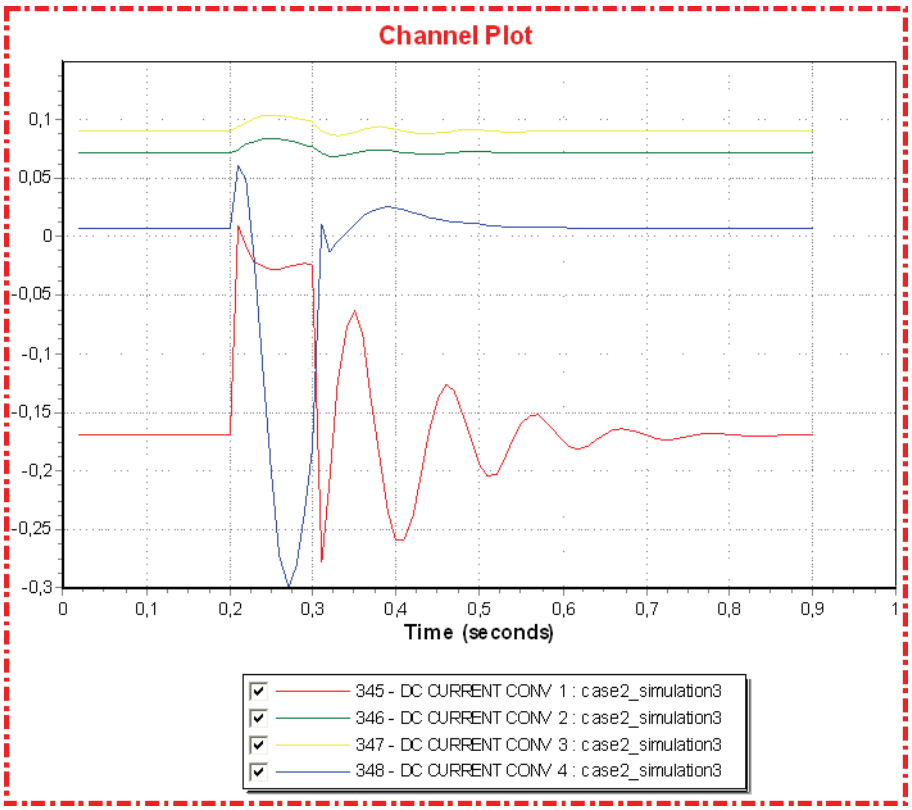

Figure F.2.23: Converter DC current [pu]

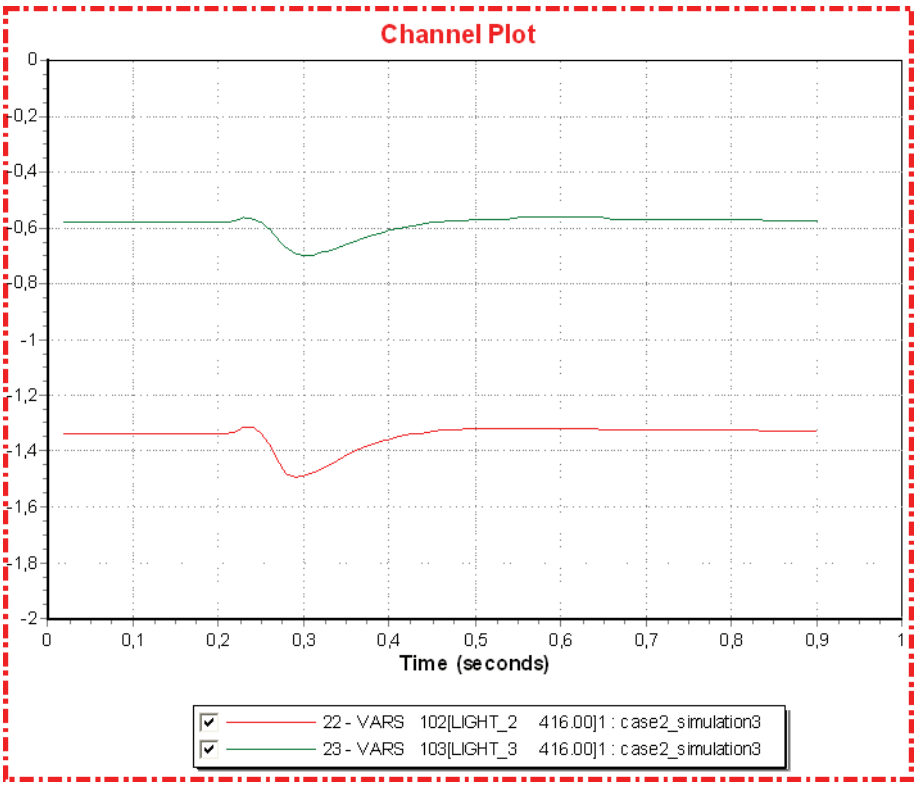

Figure F.2.24: Offshore converters reactive power [pu]

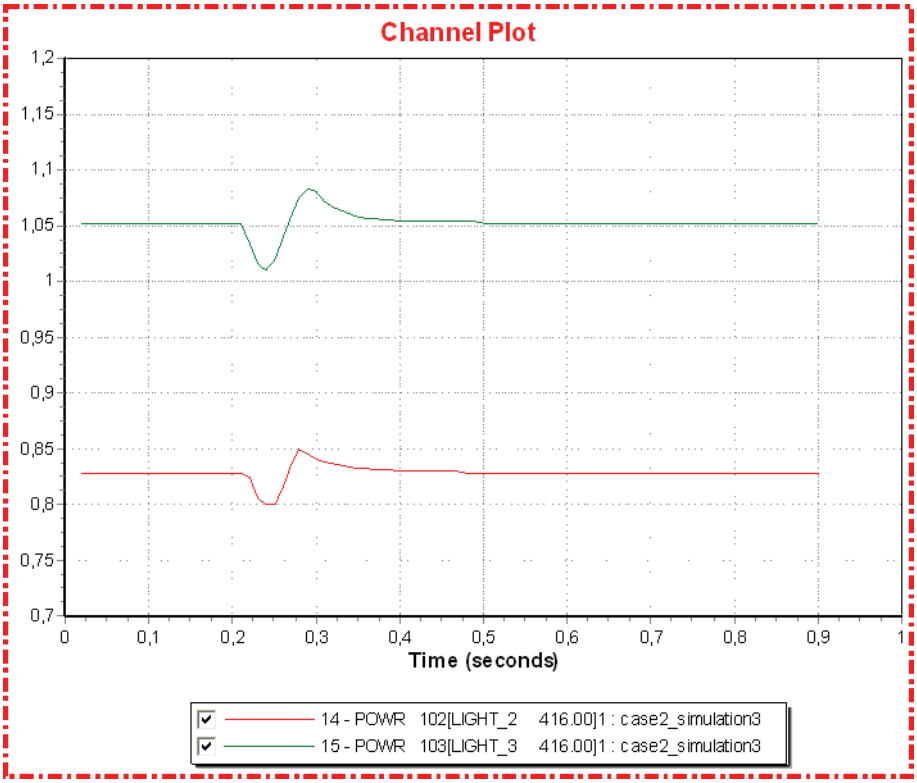

Figure F.2.25: Offshore converters active power generation in [pu]

Simulation 4 (Small wind generation)

Time	Event
0.00	Normal operation
0.20	Bus fault at bus 14
0.30	Clear bus fault

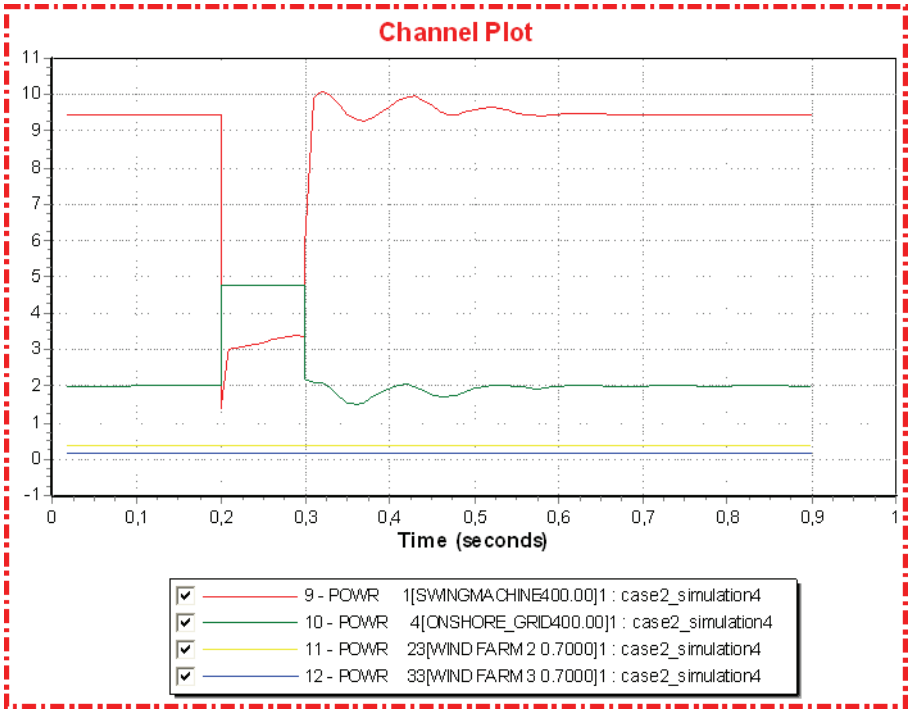

Figure F.2.26: Active power generation in AC grids [pu]

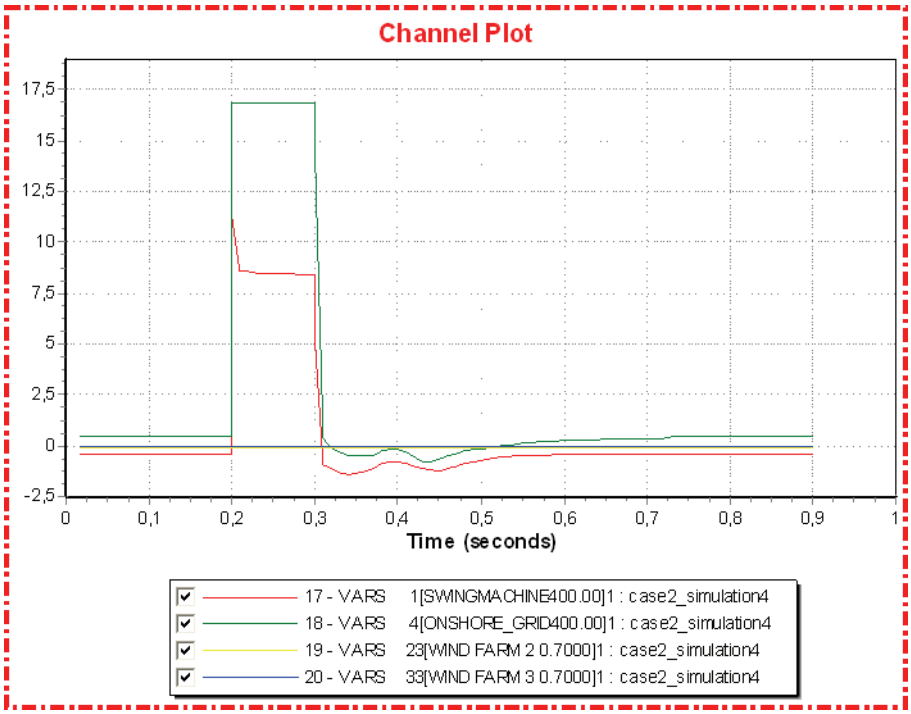

Figure F.2.27: Reactive power generation in AC grids [pu]

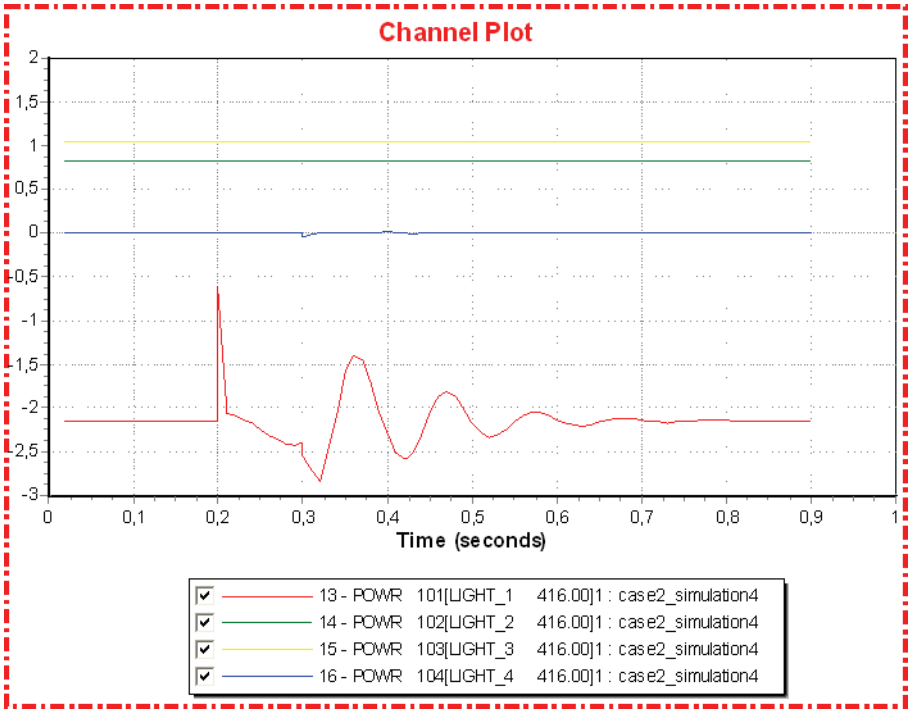

Figure F.2.28: Converter active power [pu]

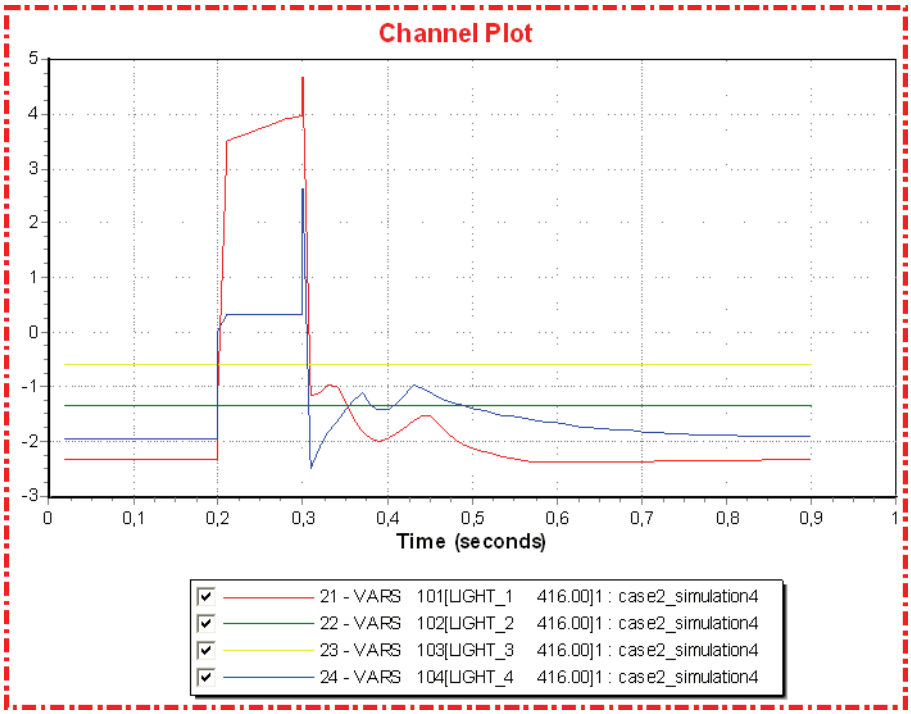

Figure F.2.29: Converter reactive power [pu]

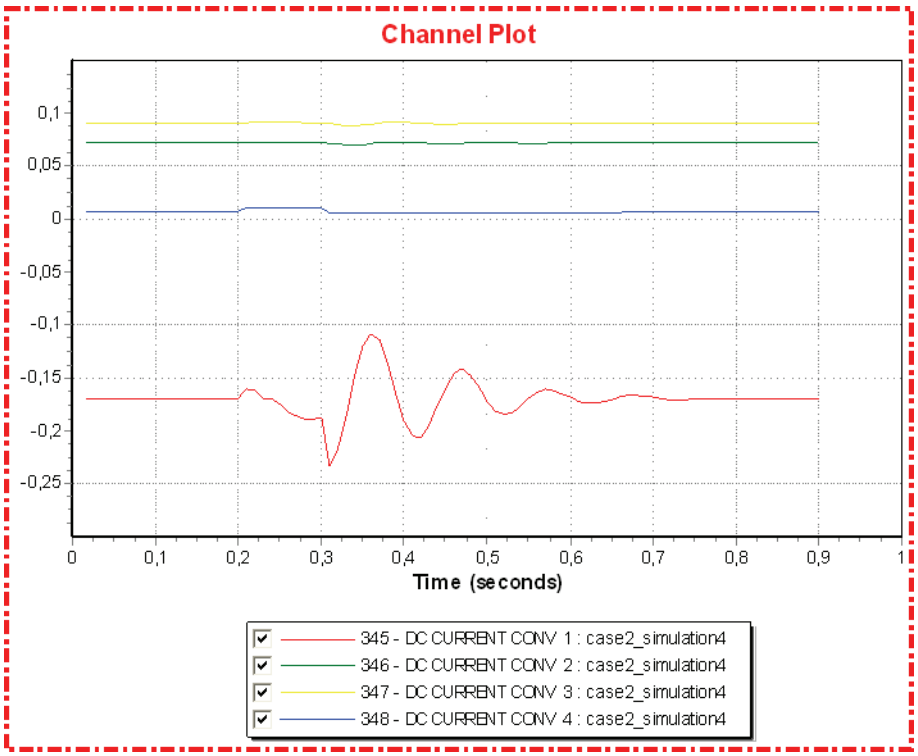

Figure F.2.30: Converter DC current [pu]

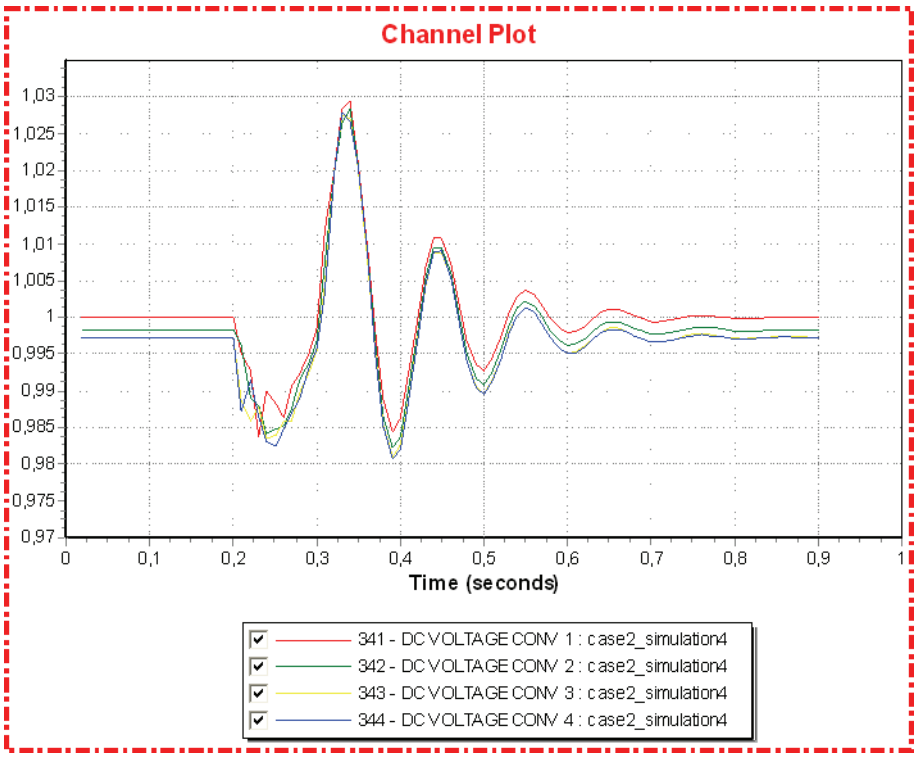

Figure F.2.31: Converter DC voltage [pu]

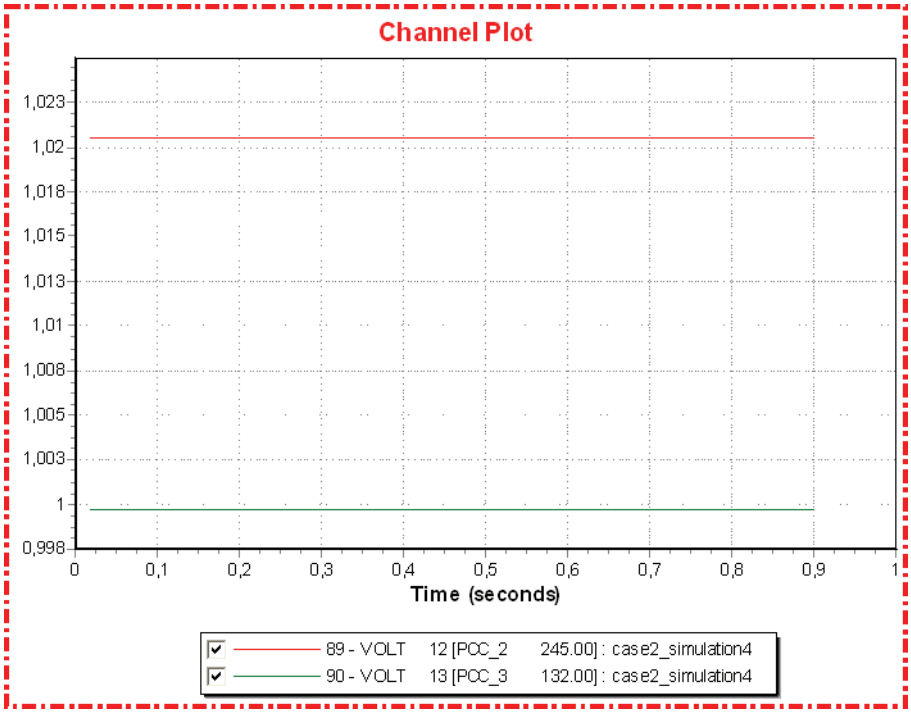

Figure F.2.32: Offshore AC voltages [pu]

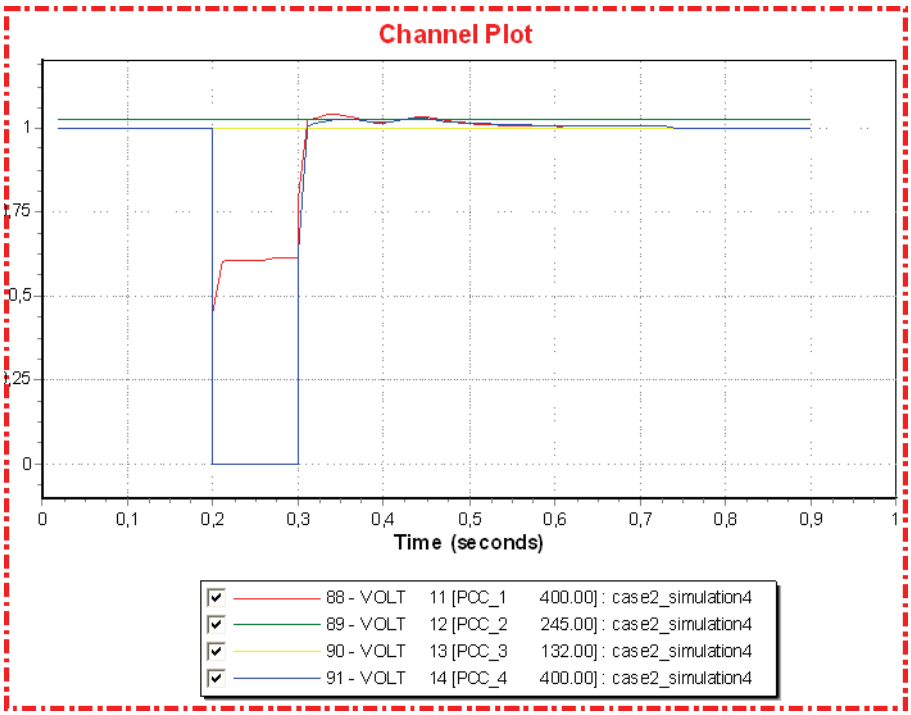

Figure F.2.33: AC voltages [pu]

22.1.3 Case 3

Simulation 1 (Large wind generation)

Time	Event
0.00	Normal operation
0.20	Bus fault at bus 12 (PCC 2)
0.30	Clear bus fault

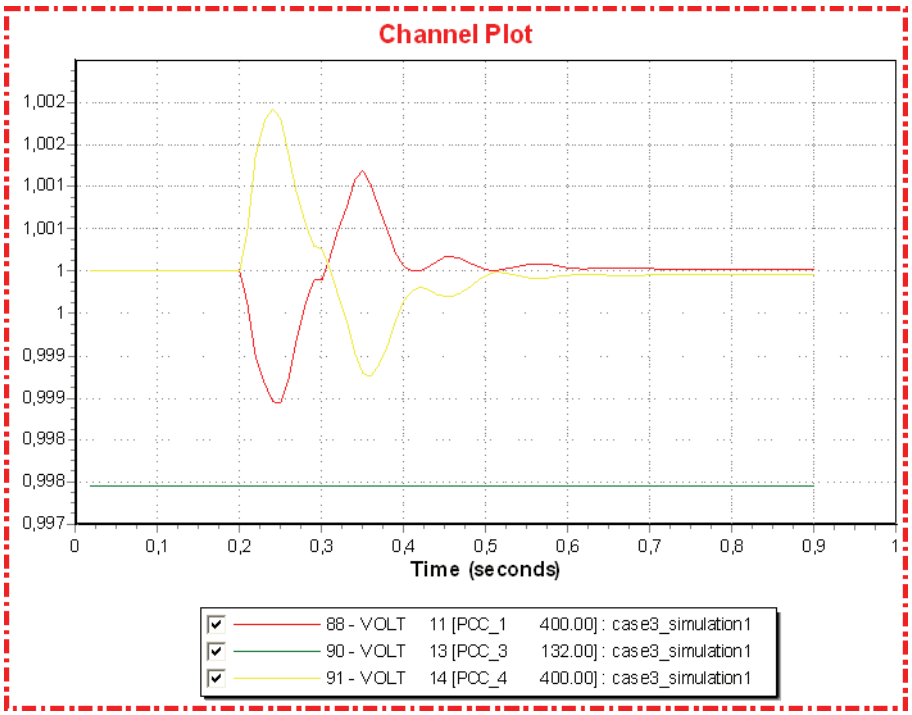

Figure F.3.1: AC voltages [pu]

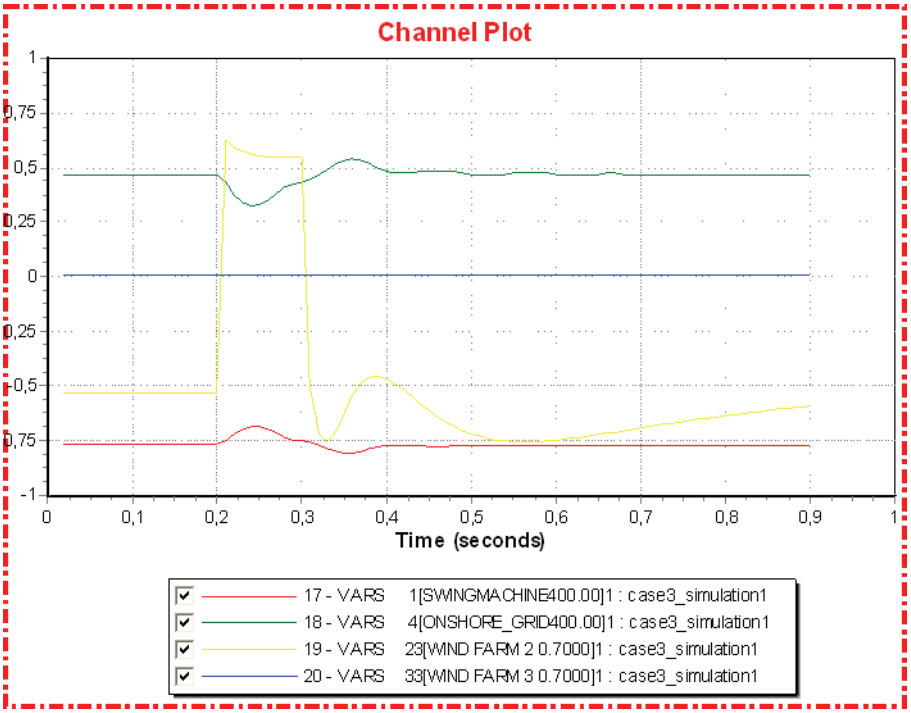

Figure F.3.2: Reactive power generation in AC grids [pu]

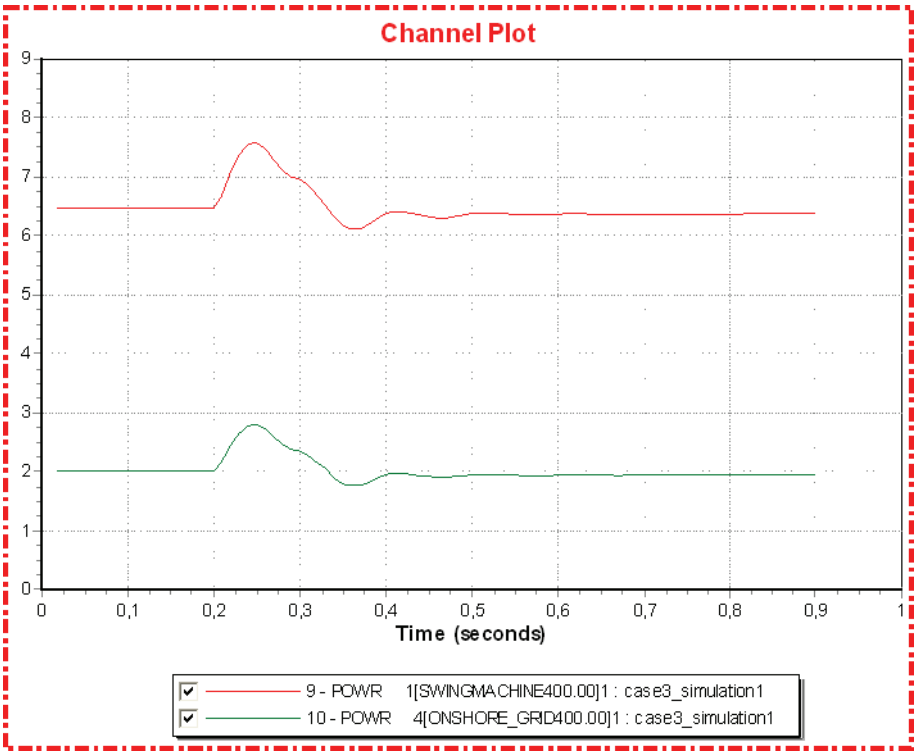

Figure F.3.3: Onshore active power generation [pu]

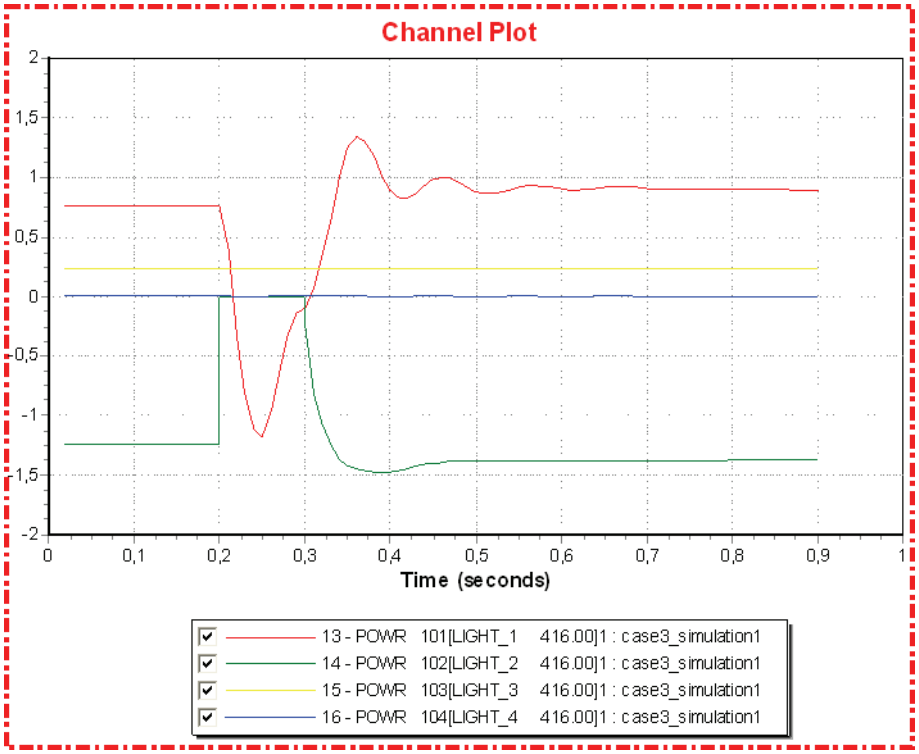

Figure F.3.4: Converter active power [pu]

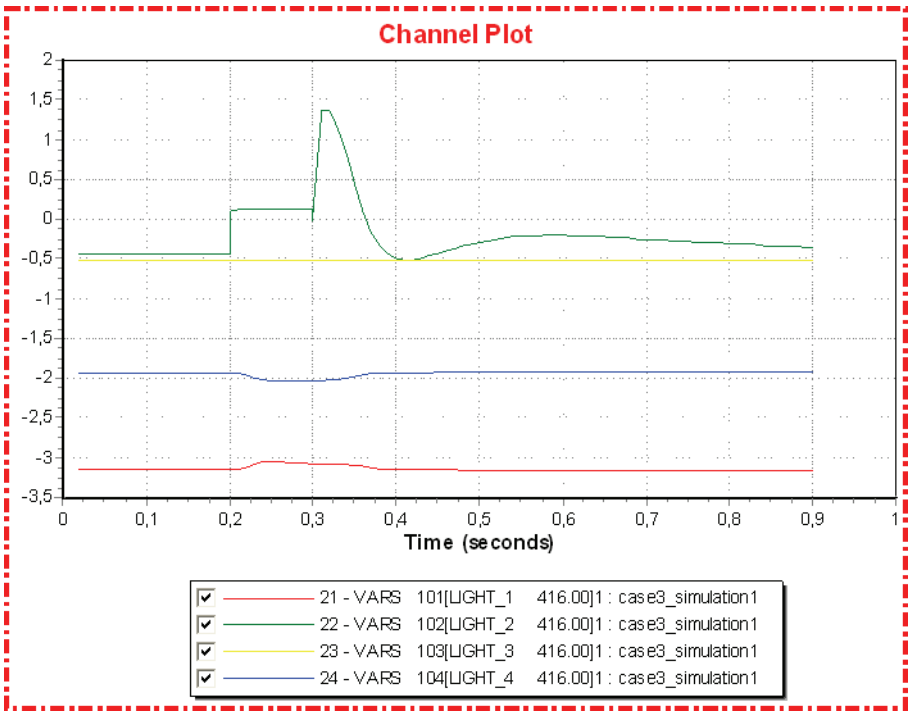

Figure F.3.5: Converter reactive power [pu]

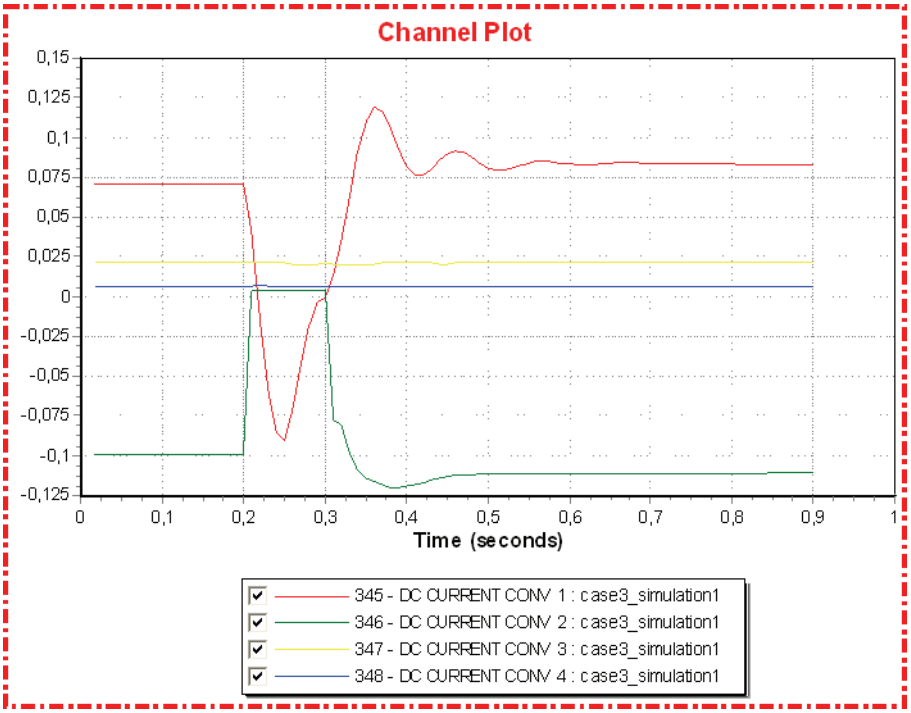

Figure F.3.6: Converter DC current [pu]

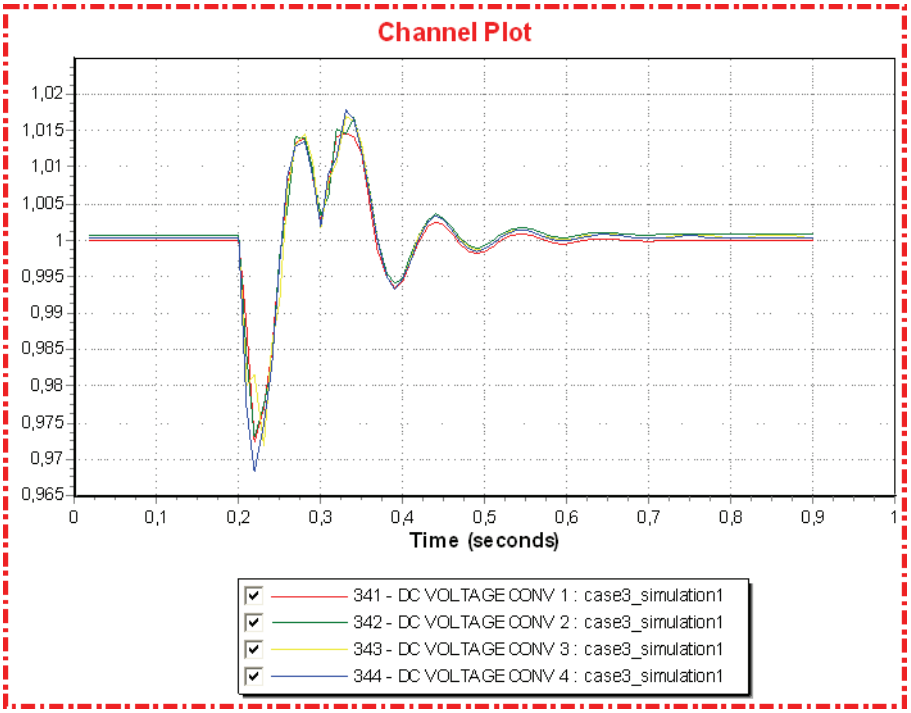

Figure F.3.7: Converter DC voltage [pu]

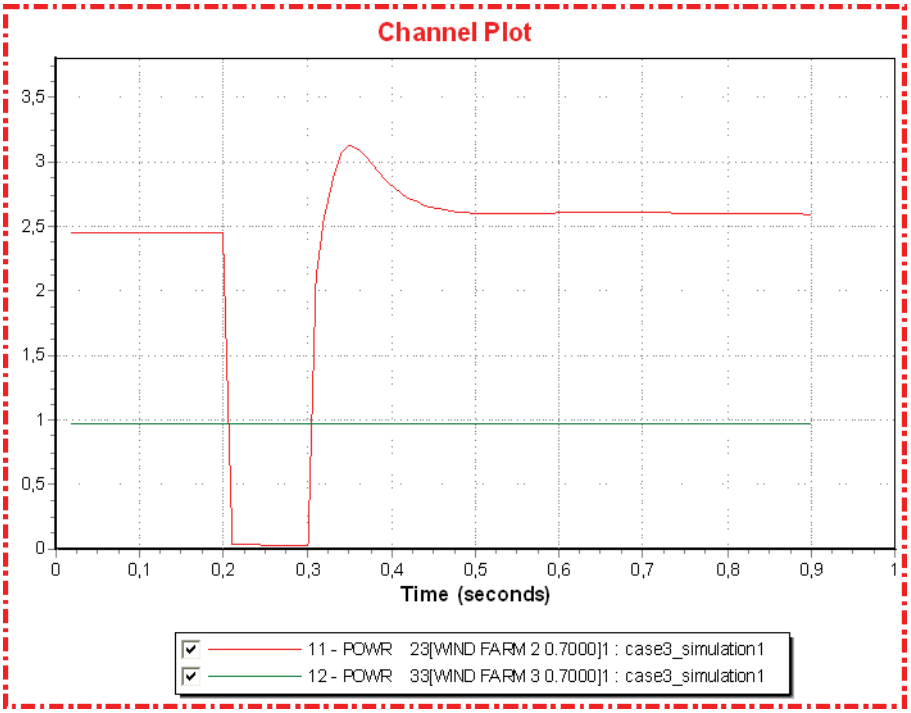

Figure F.3.8: Active wind power generation [pu]

Simulation 2 (Large wind generation)

Time	Event
0.00	Normal operation
0.20	Disconnect generator at bus 23 (wind farm 2)

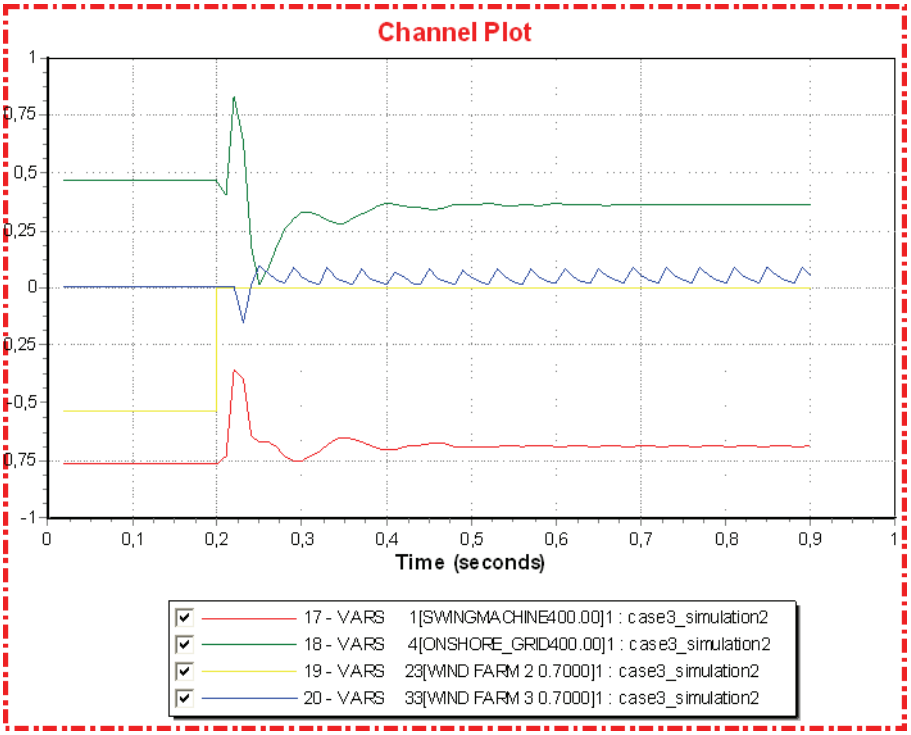

Figure F.3.9: Reactive power generation in AC grids [pu]

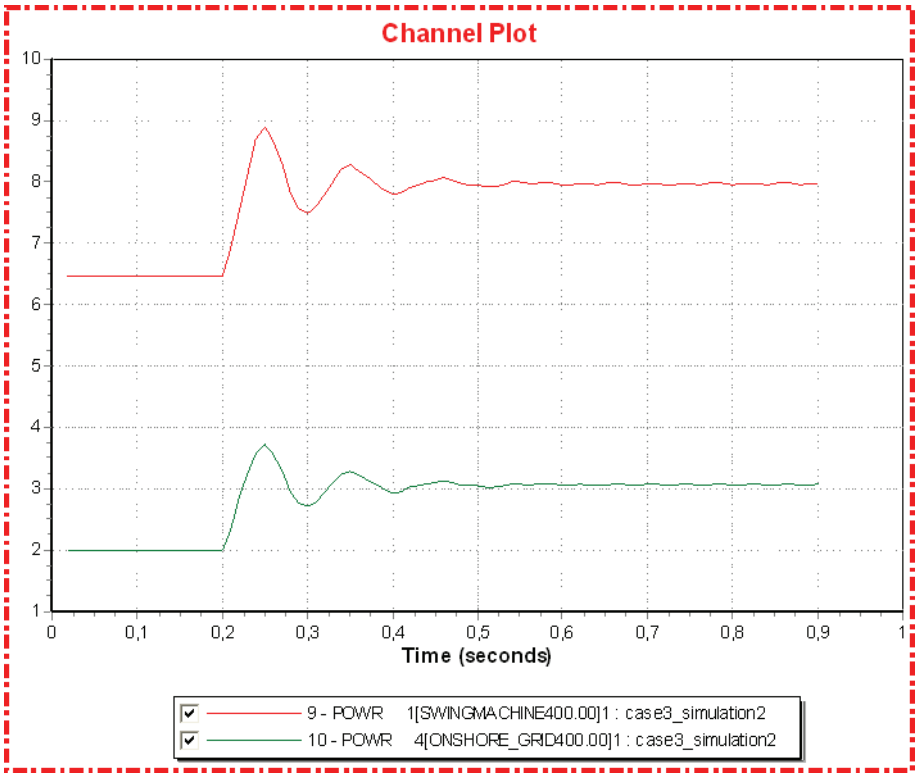

Figure F.3.10: Onshore active power generation [pu]

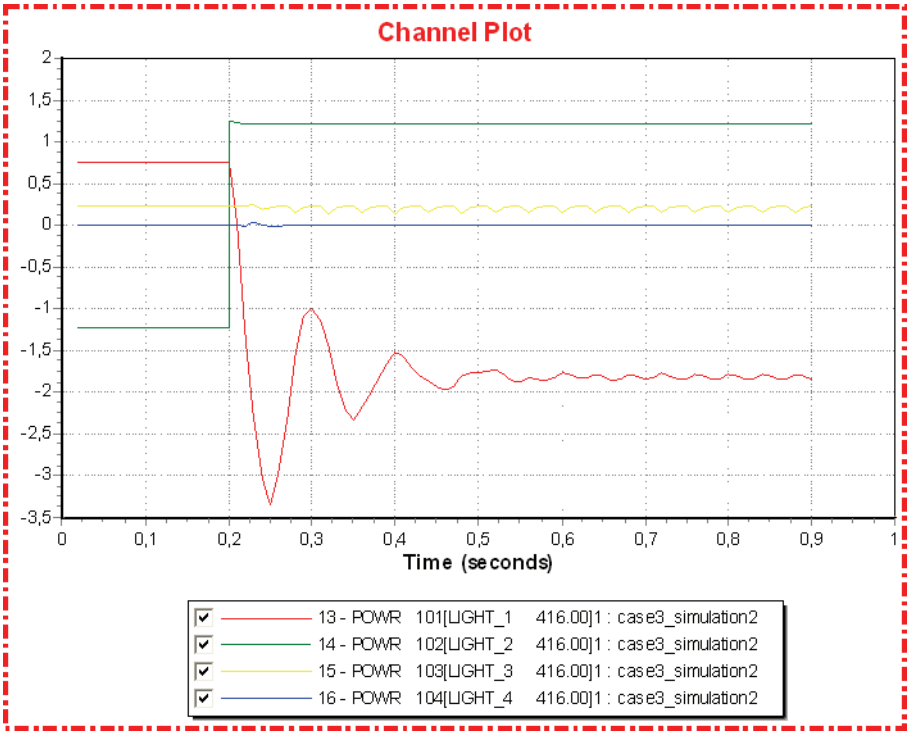

Figure F.3.11: Converter active power [pu]

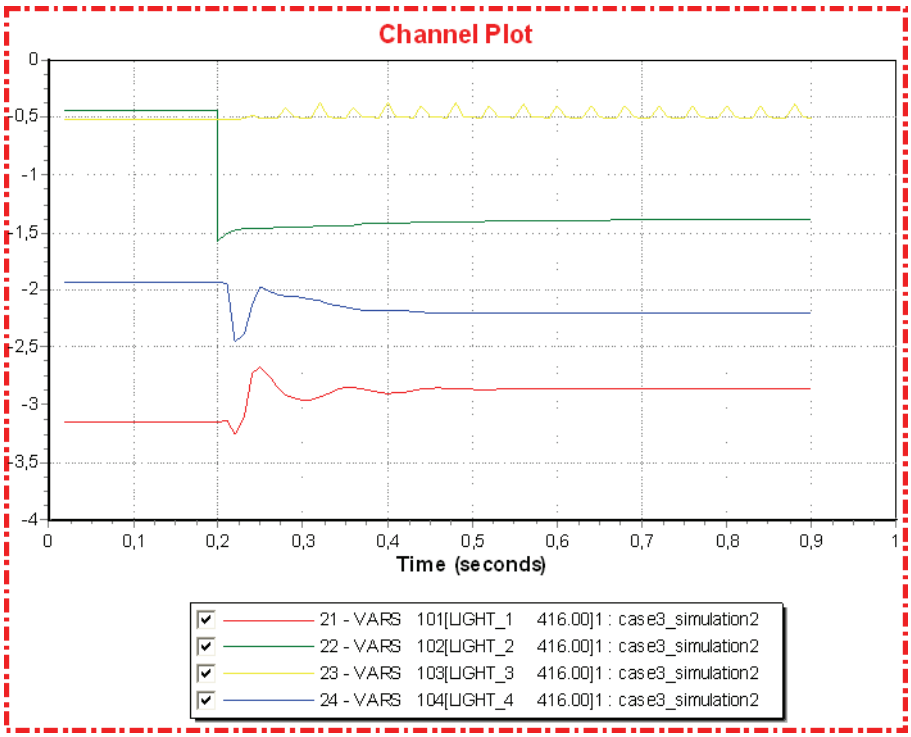

Figure F.3.12: Converter reactive power [pu]

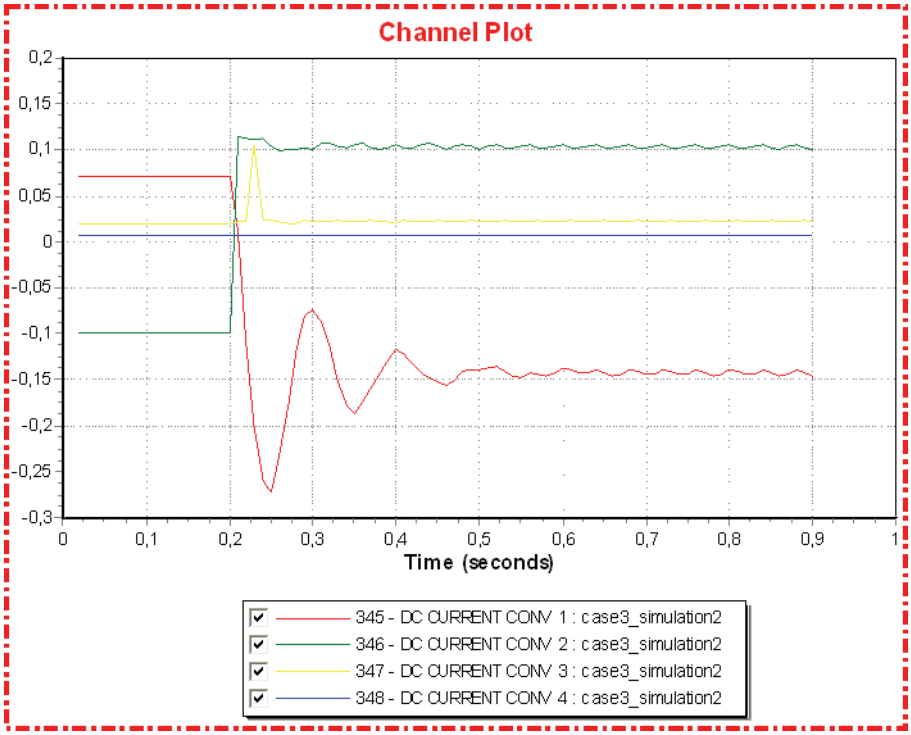

Figure F.3.13: Converter DC current [pu]

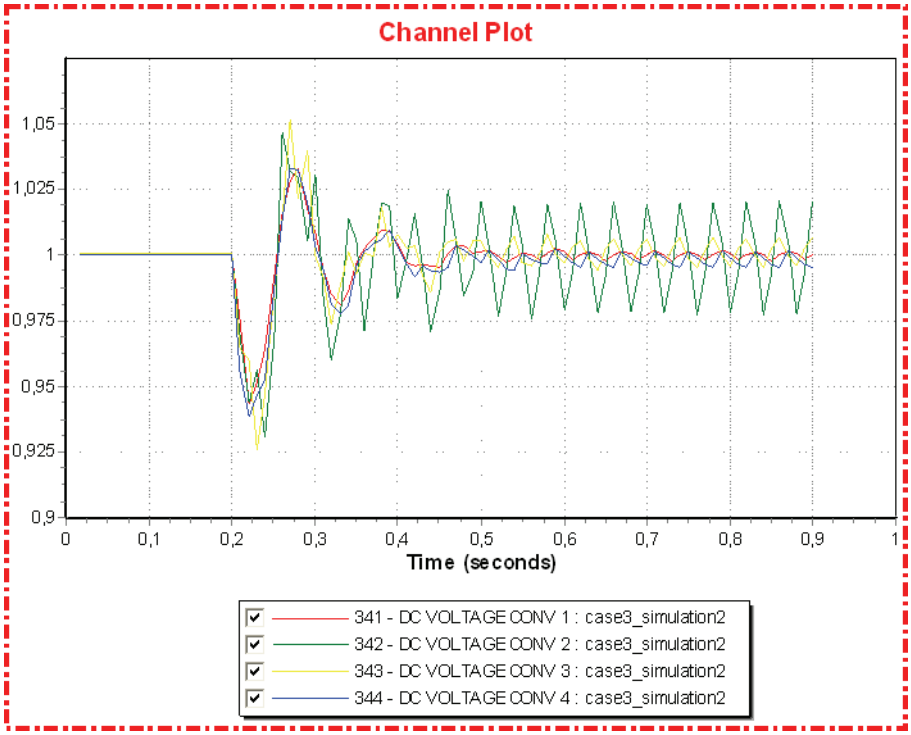

Figure F.3.14: Converter DC voltage [pu]

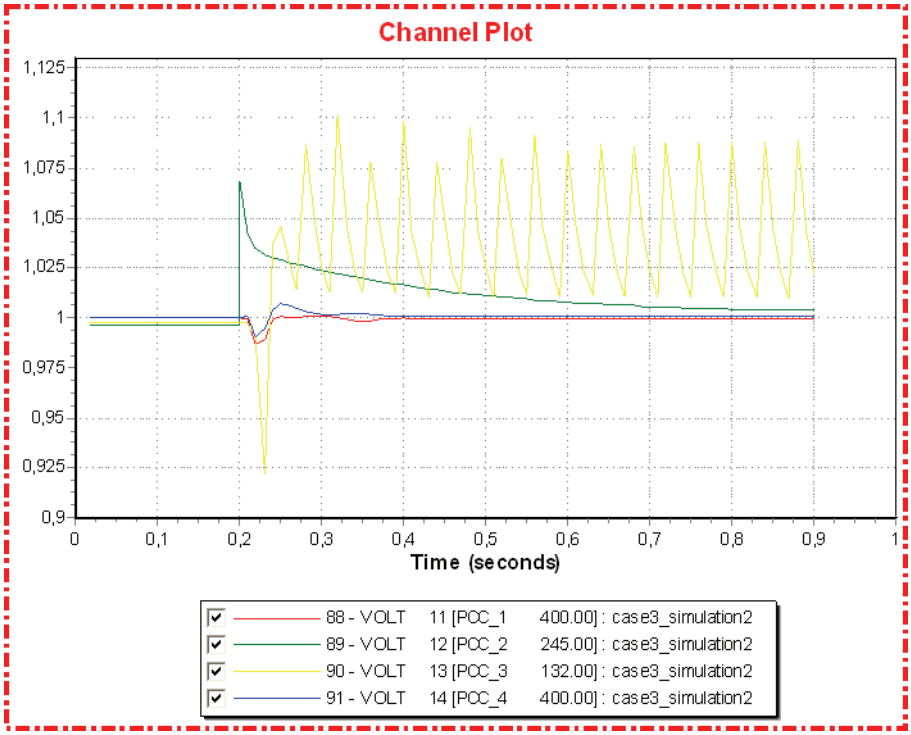

Figure F.3.15: AC voltages [pu]

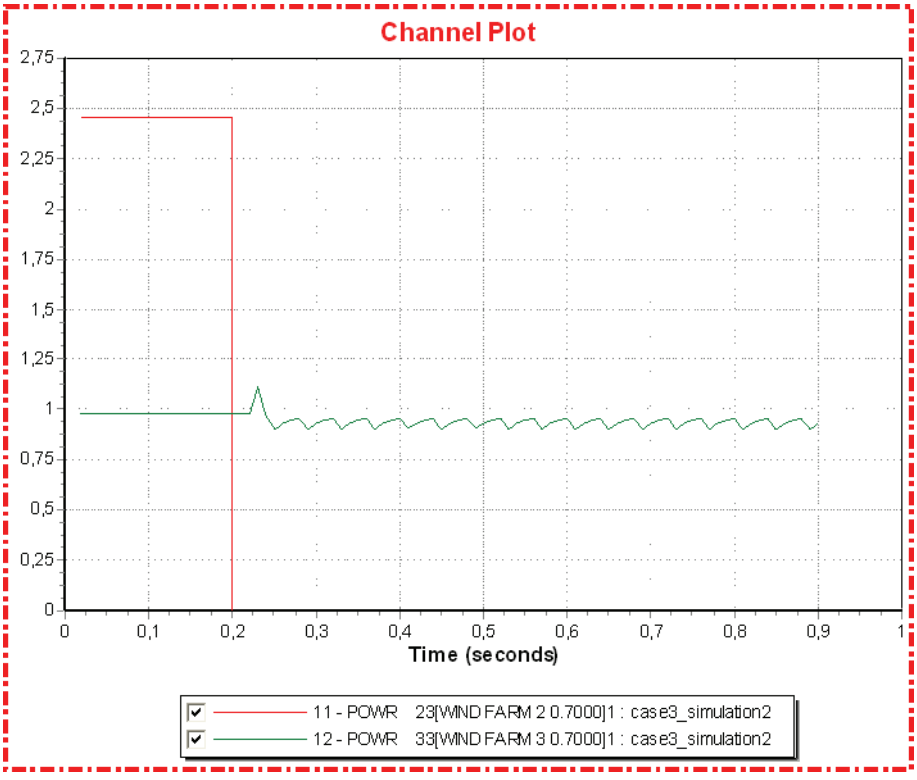

Figure F.3.16: Active wind power generation [pu]

22.1.4 Case 4

Simulation 1 (Large wind generation)

Time	Event
0.00	Normal operation
0.20	Disconnect (trip) converter 2 and 3
0.25	Reconnect converter 2 and 3 and the associated power transformers

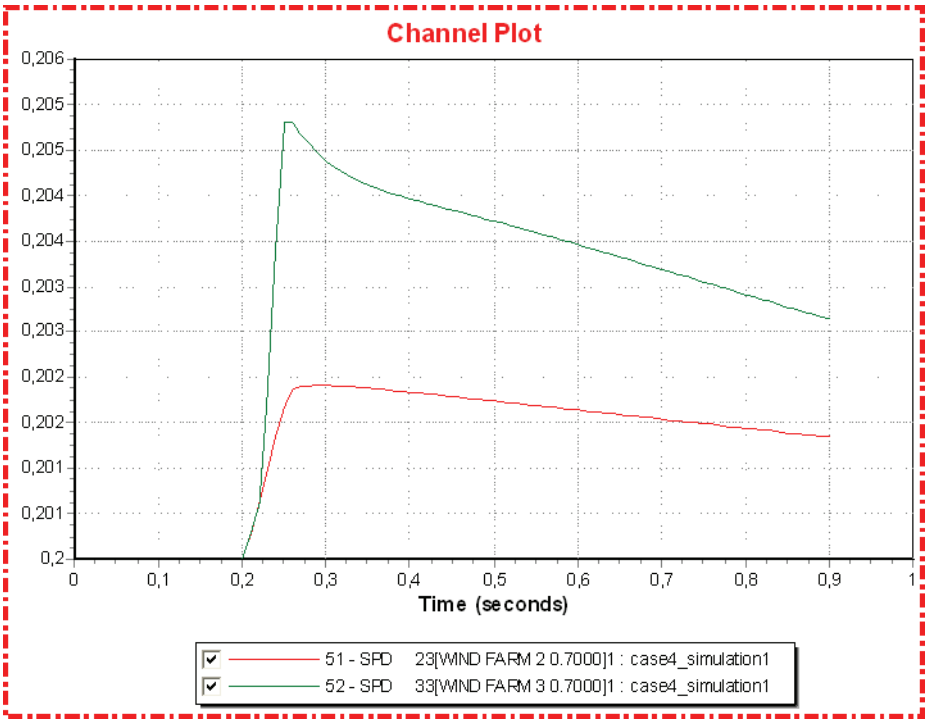

Figure F.4.1: Turbine speed, both wind farms [pu]

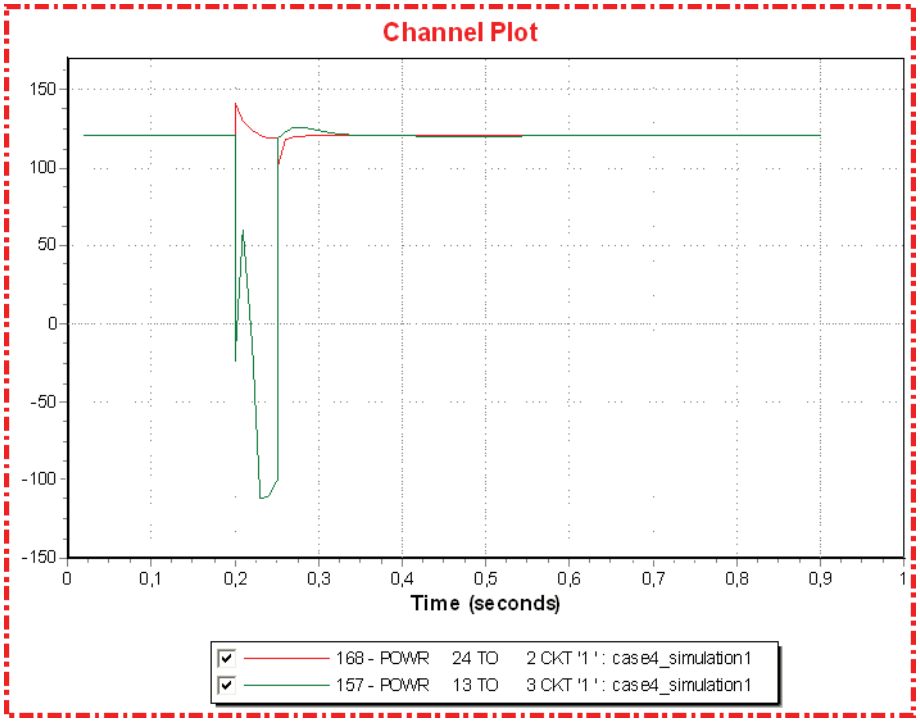

Figure F.4.2: Active power to the platforms [MW]

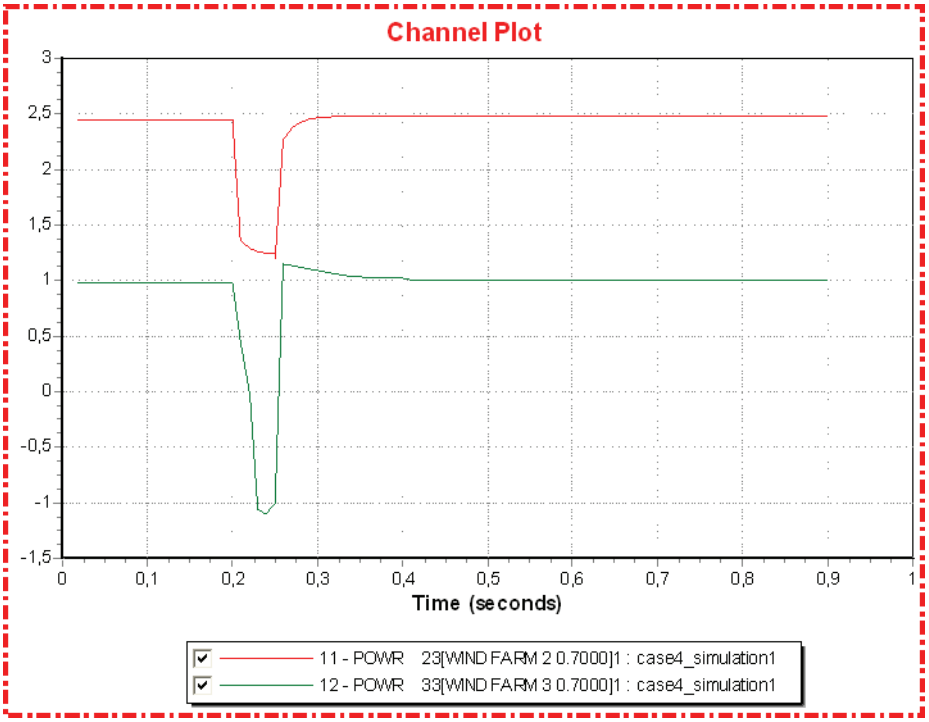

Figure F.4.3: Active wind power generation [pu]

Offshore area 2:

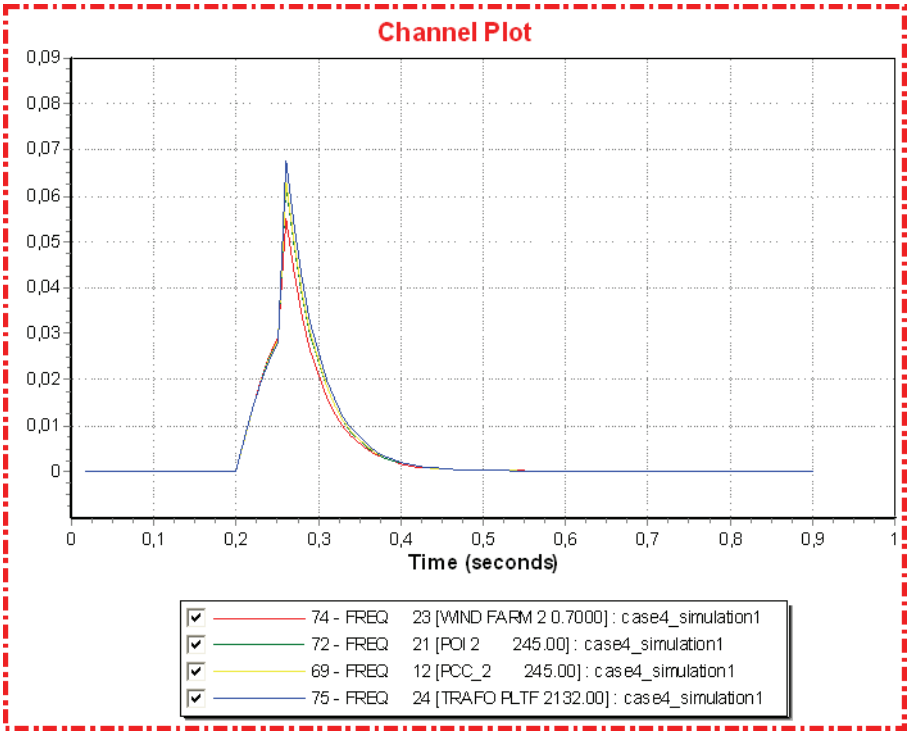

Figure F.4.4: Frequency offshore area 2 [pu deviation from 50 HZ]

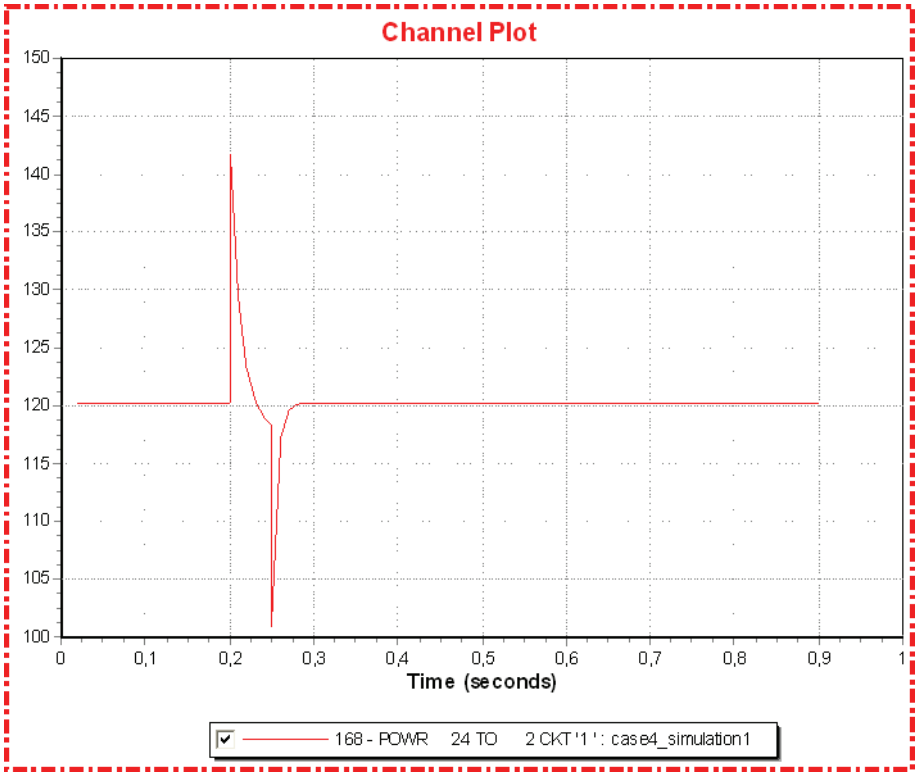

Figure F.4.5: Active power to platform 2 [MW]

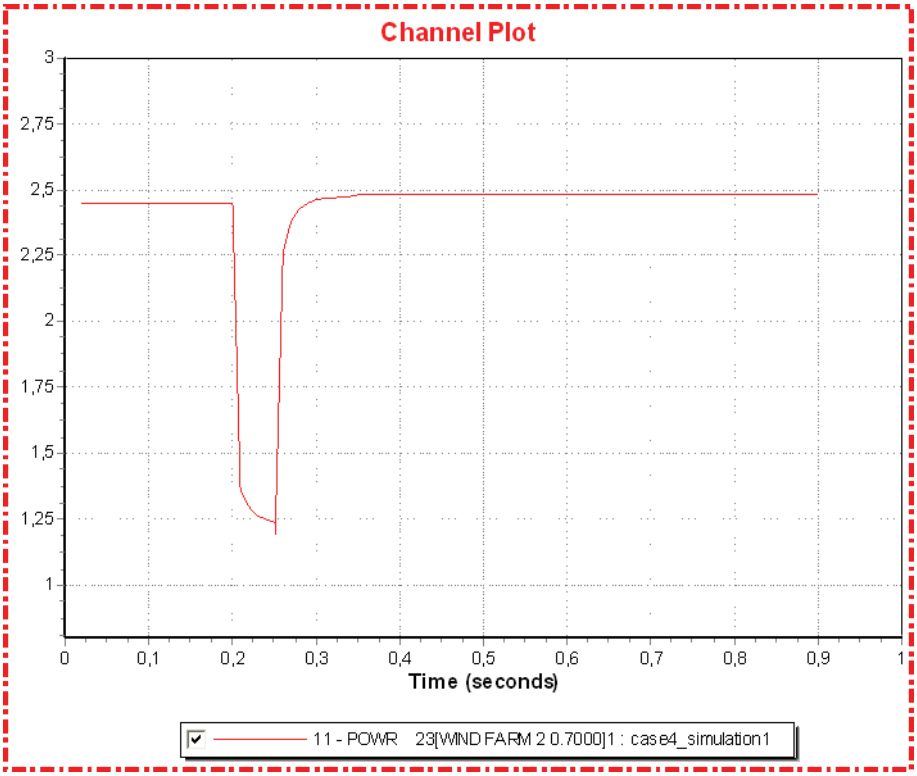

Figure F.4.6: Active wind power generation [pu]

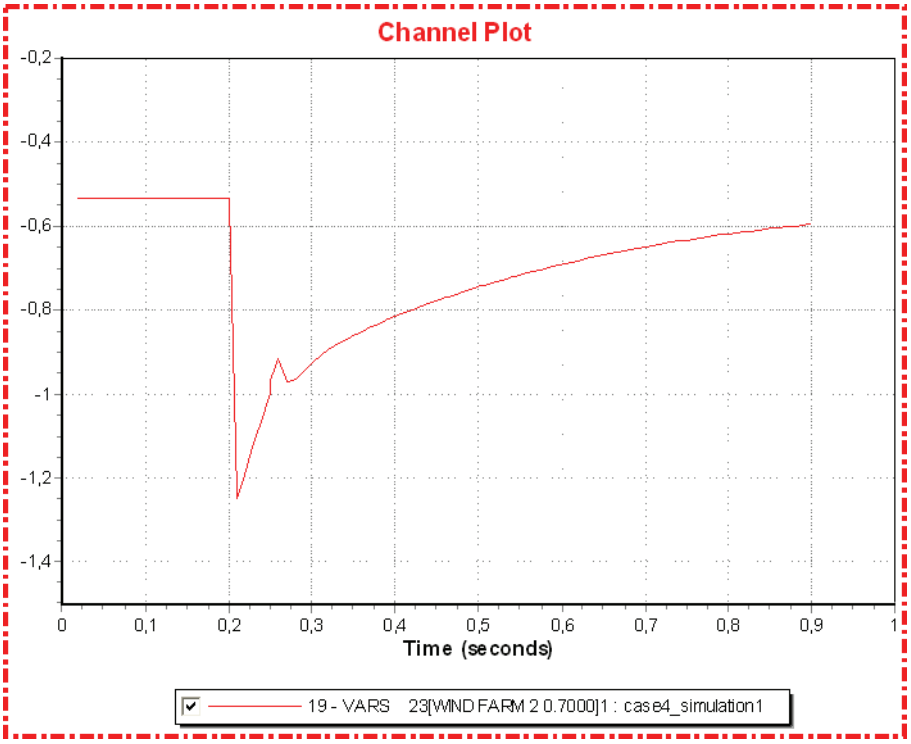

Figure F.4.7: Reactive wind power generation [pu]

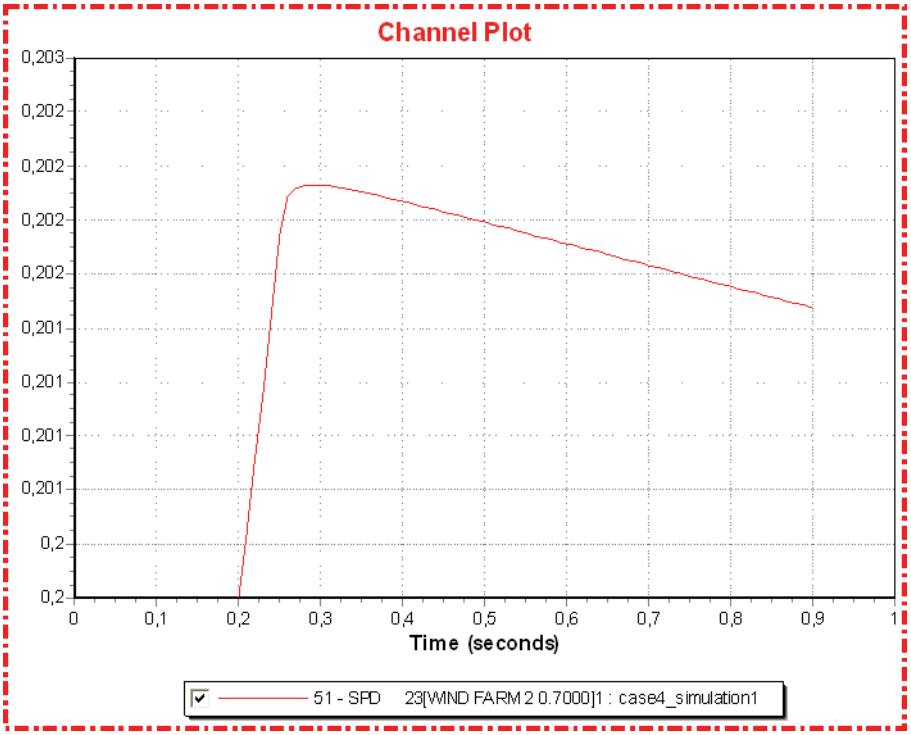

Figure F.4.8: Turbine speed, wind farm 2 [pu]

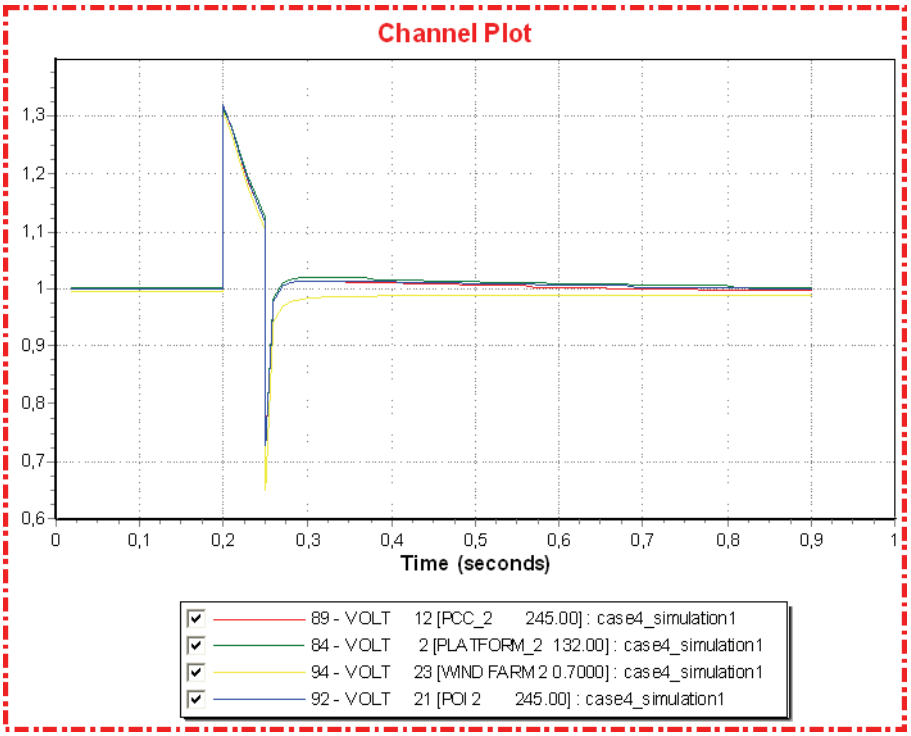

Figure F.4.9: Offshore area 2 voltage [pu]

Offshore area 3:

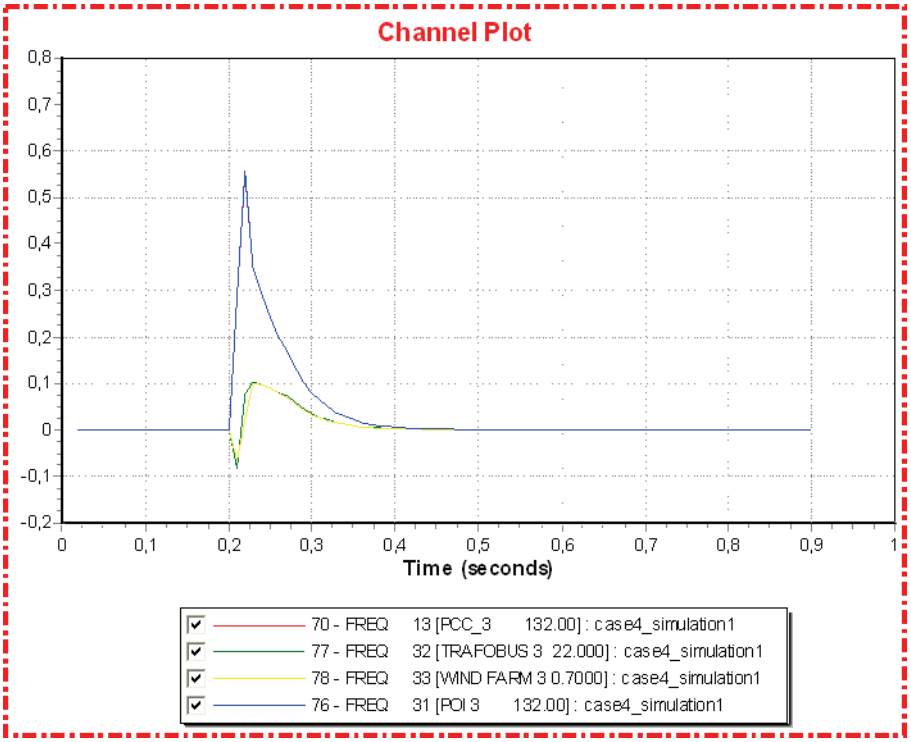

Figure F.4.10: Frequency offshore area 3 [pu deviation from 50 HZ]

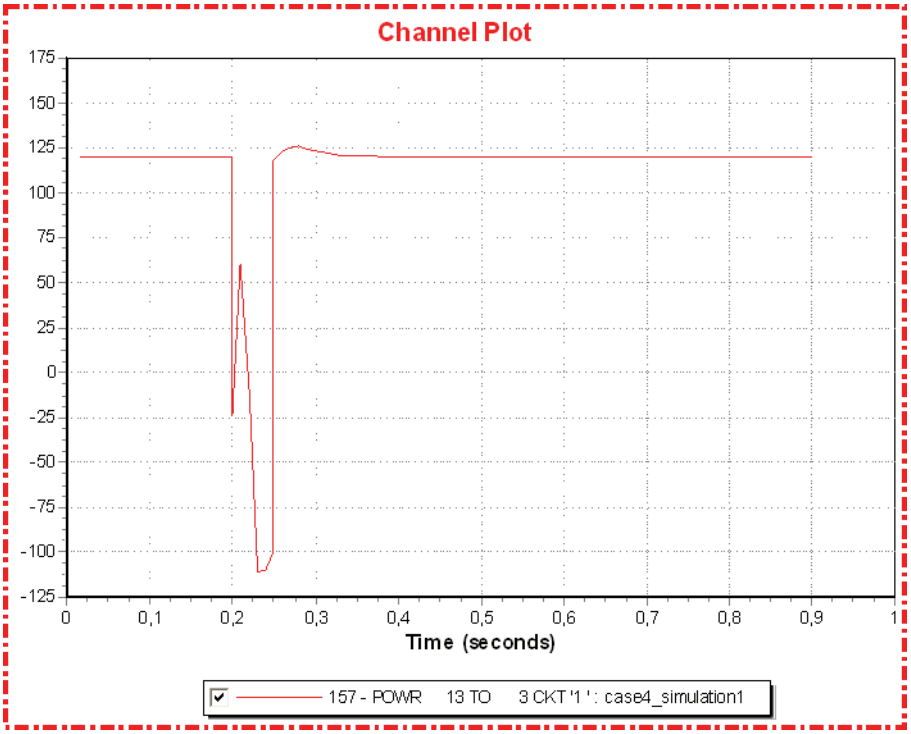

Figure F.4.11: Active power to platform 3 [MW]

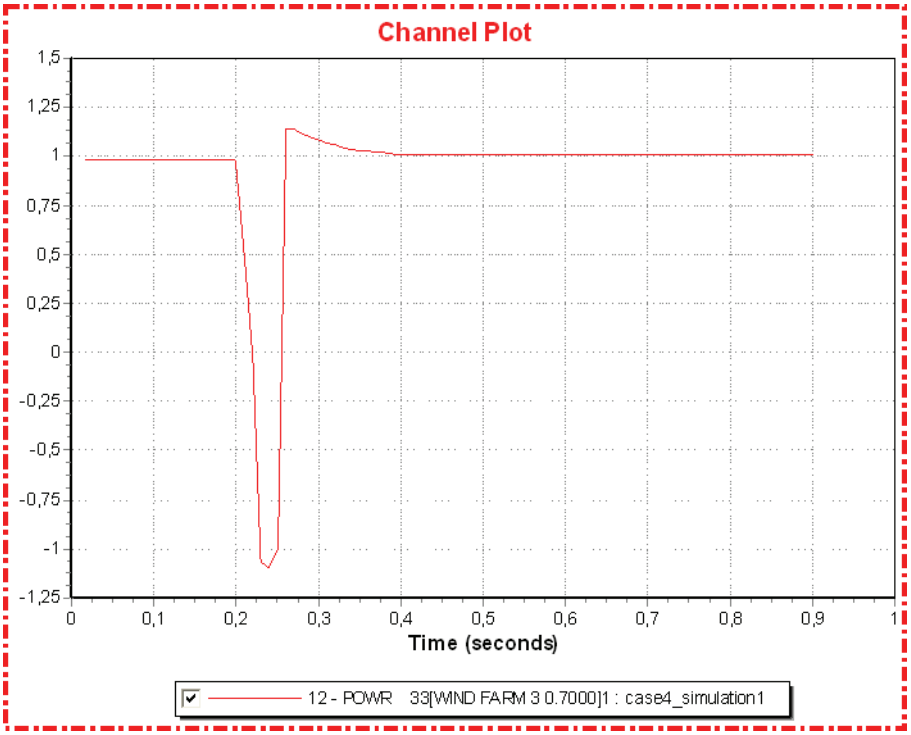

Figure F.4.12: Active wind power generation [pu]

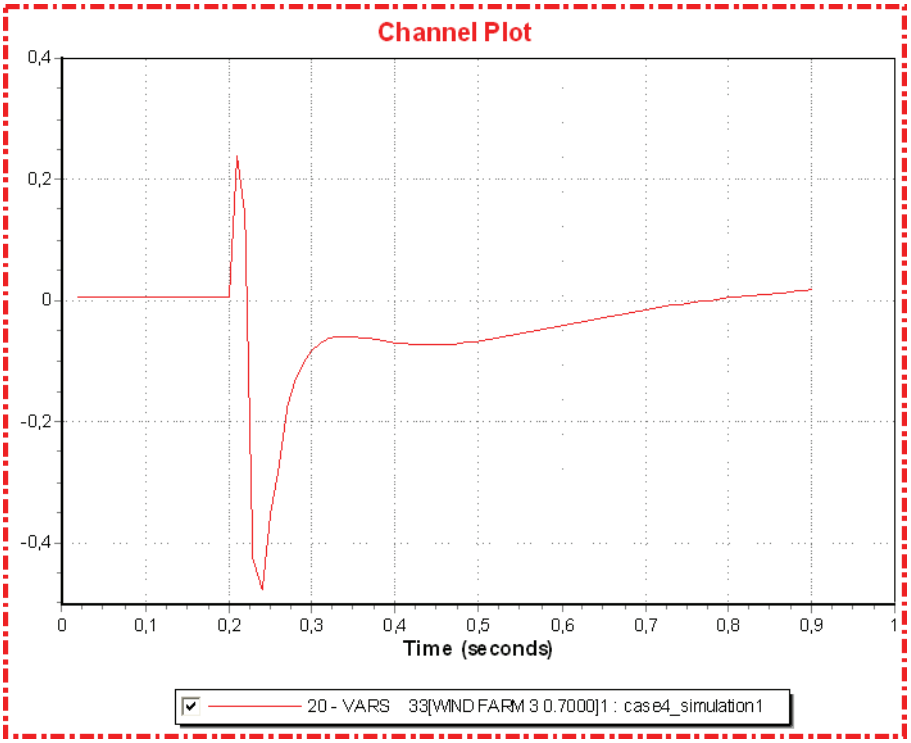

Figure F.4.13: Reactive wind power generation [pu]

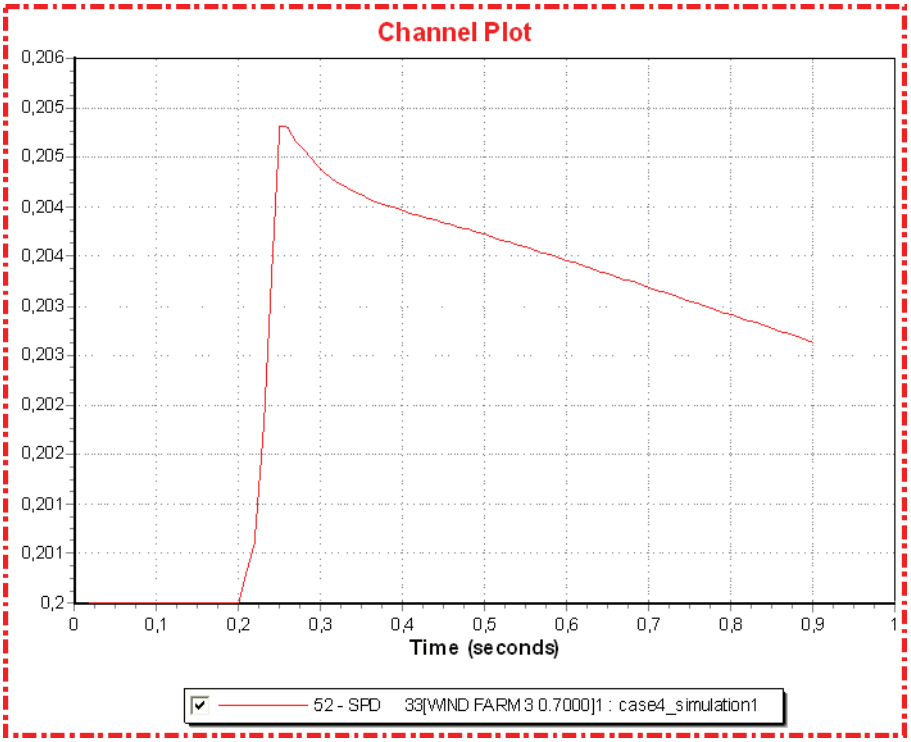

Figure F.4.14: Turbine speed, wind farm 3 [pu]

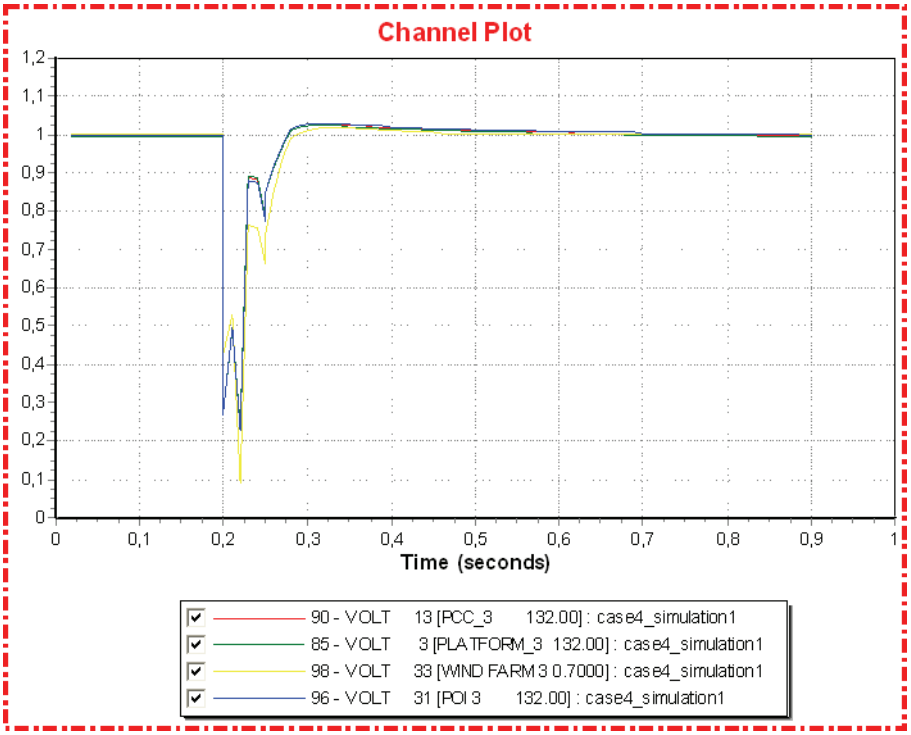

Figure F.4.15: Offshore area 3 voltage [pu]

Simulation 2 (Large wind generation)

Time	Event
0.00	Normal operation
0.20	Disconnect (trip) converter 2 and 3
2.20	Reconnect converter 2 and 3 and the associated power transformers

Only offshore area 2 is included, as described in chapter 12.

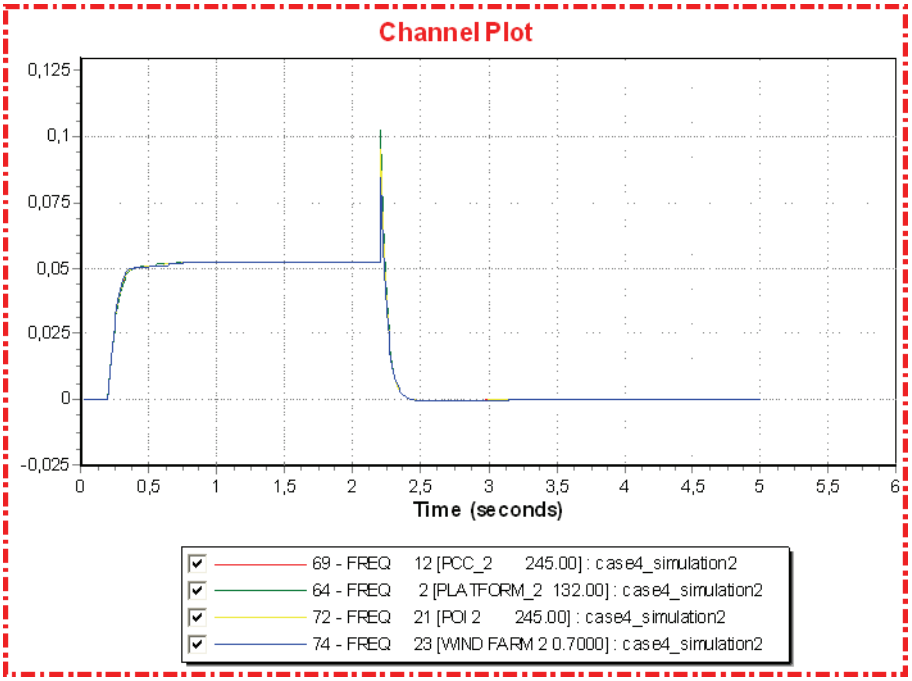

Figure F.4.16: Frequency offshore area 2 [pu deviation from 50 HZ]

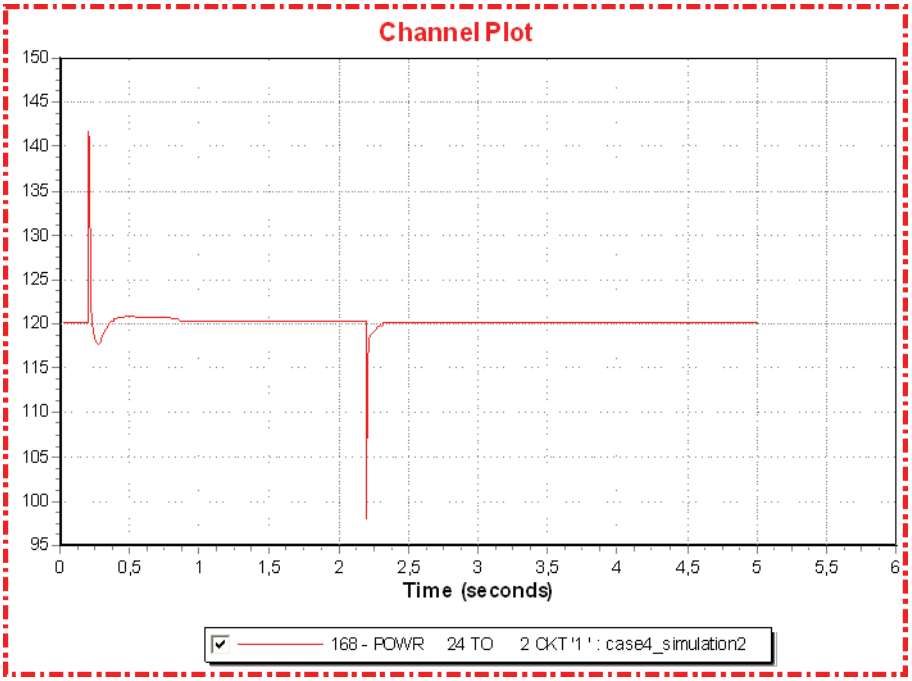

Figure F.4.16: Active power to platform 2 [MW]

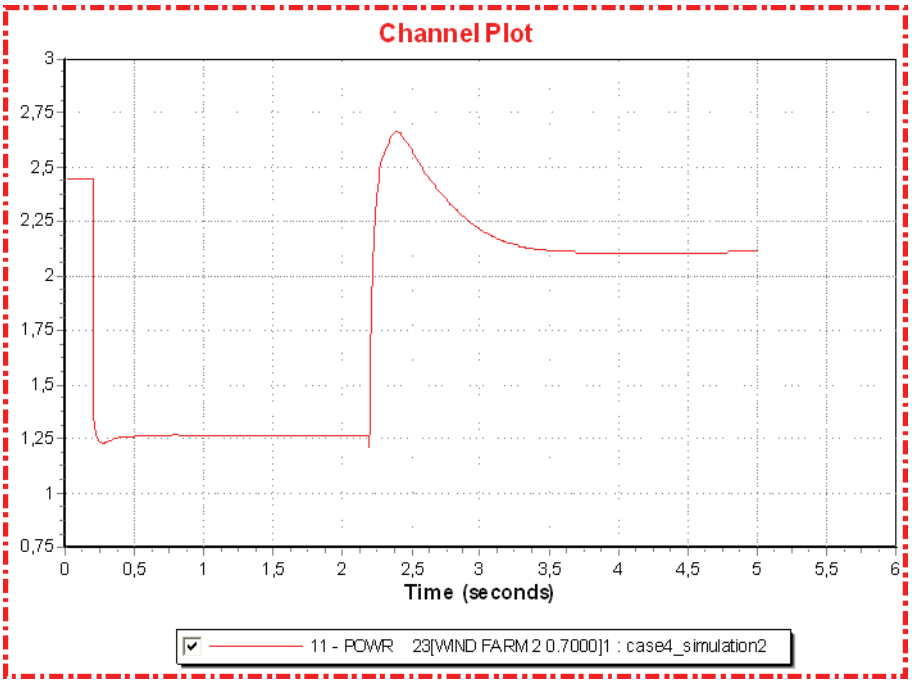

Figure F.4.17: Active wind power generation [pu]

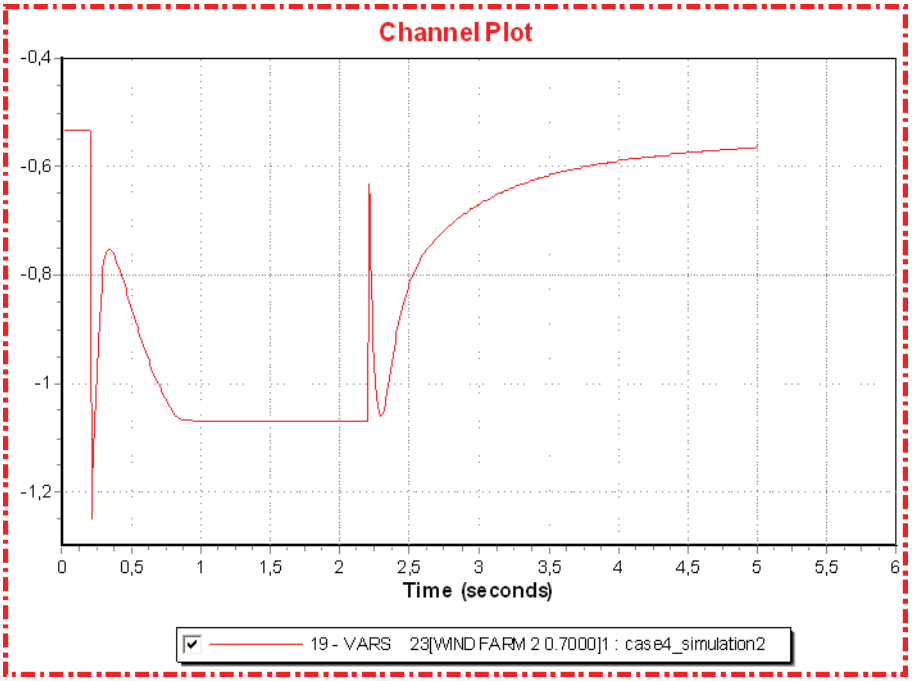

Figure F.4.18: Reactive wind power generation [pu]

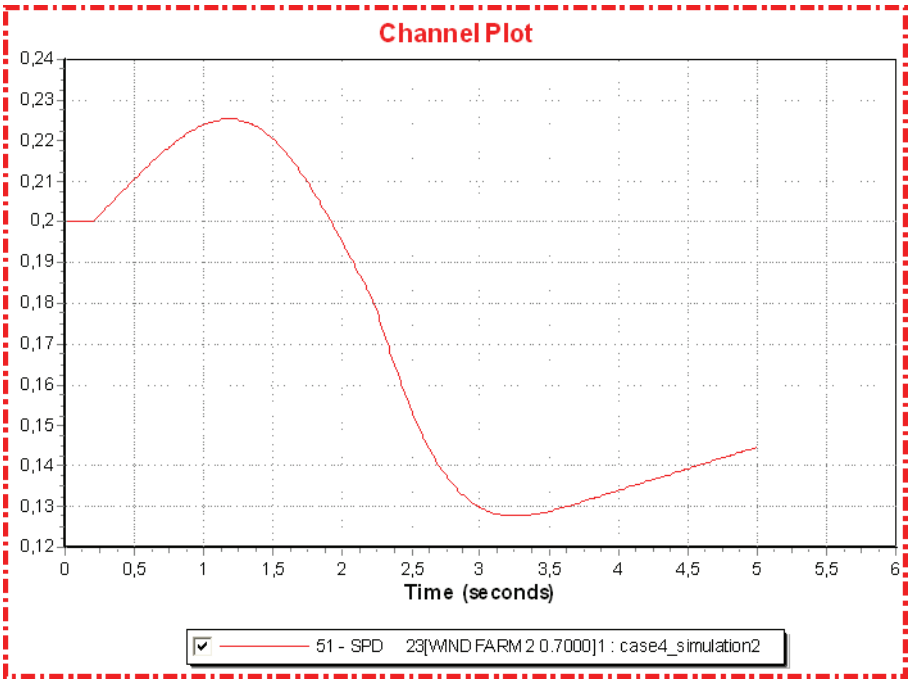

Figure F.4.19: Turbine speed, wind farm 2 [pu]

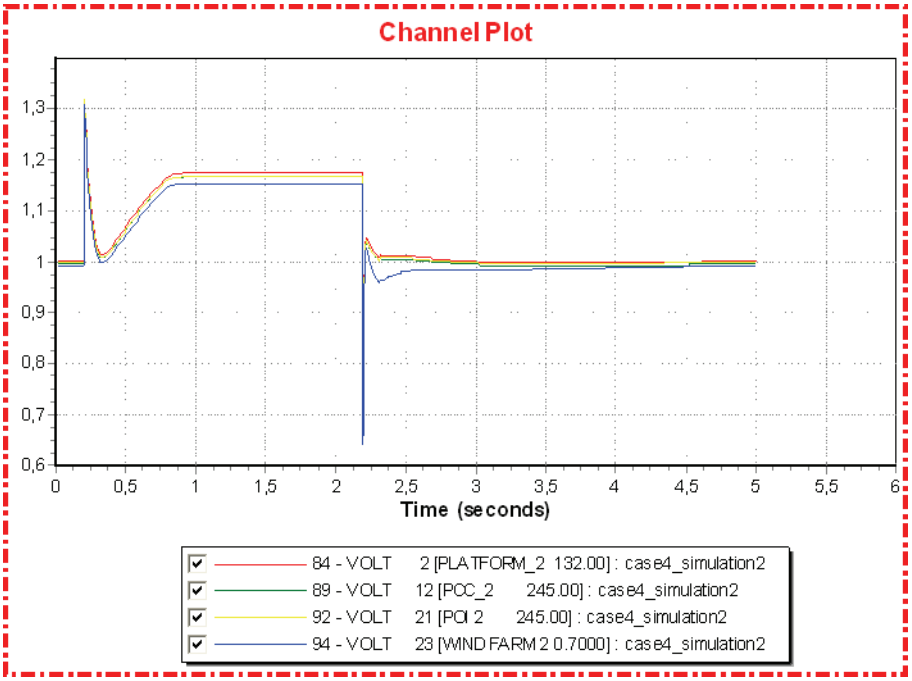

Figure F.4.20: Offshore area 2 voltage [pu]

Simulation 3 (Small wind generation)

Time	Event
0.00	Normal operation
0.20	Disconnect (trip) converter 2 and 3
0.25	Reconnect converter 2 and 3 and the associated power transformers

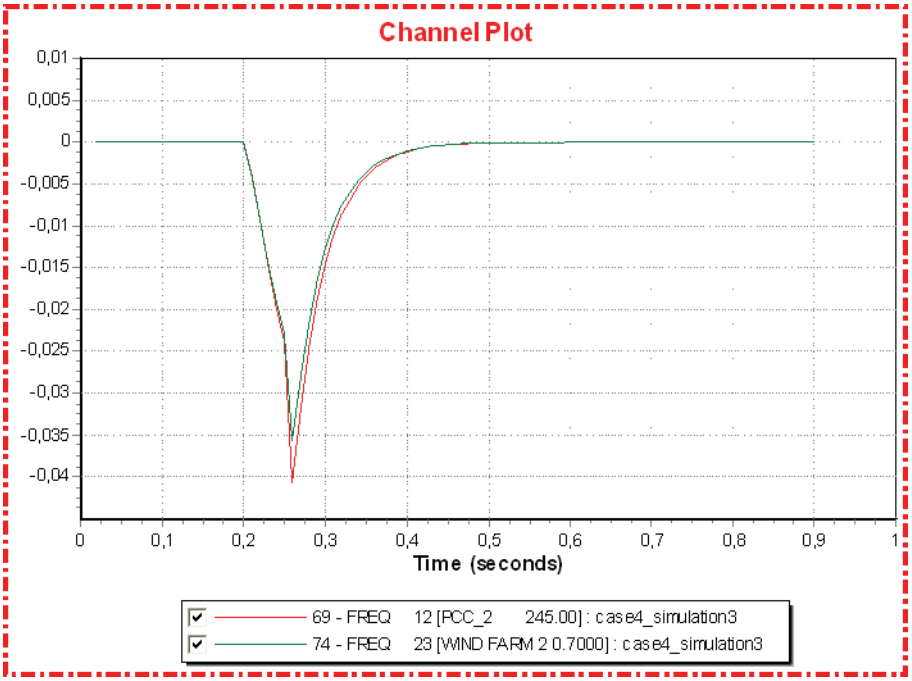

Figure F.4.21: Frequency offshore area 2 [pu deviation from 50 HZ]

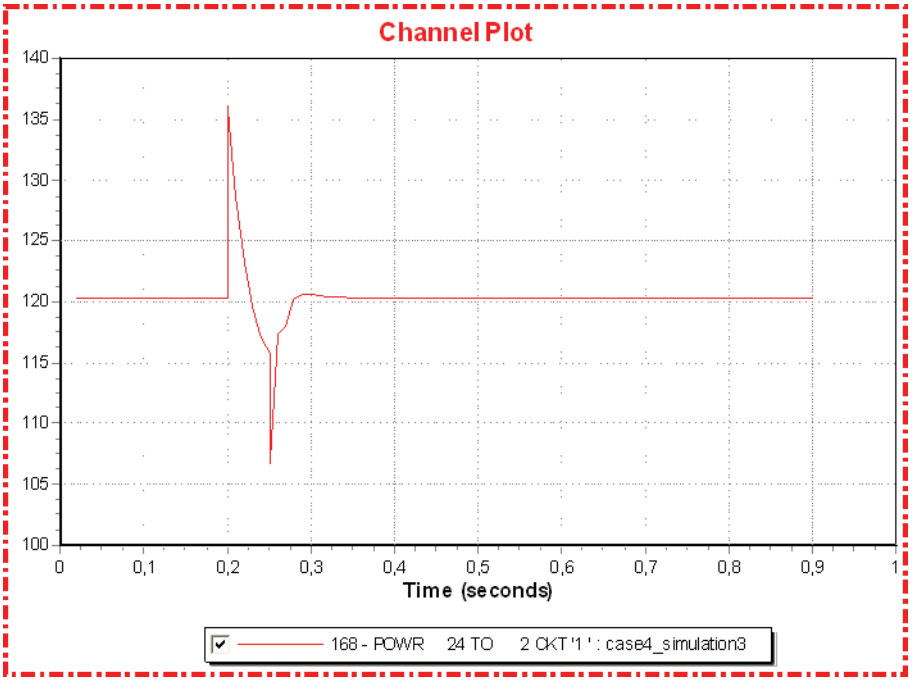

Figure F.4.22: Active power to platform 2 [MW]

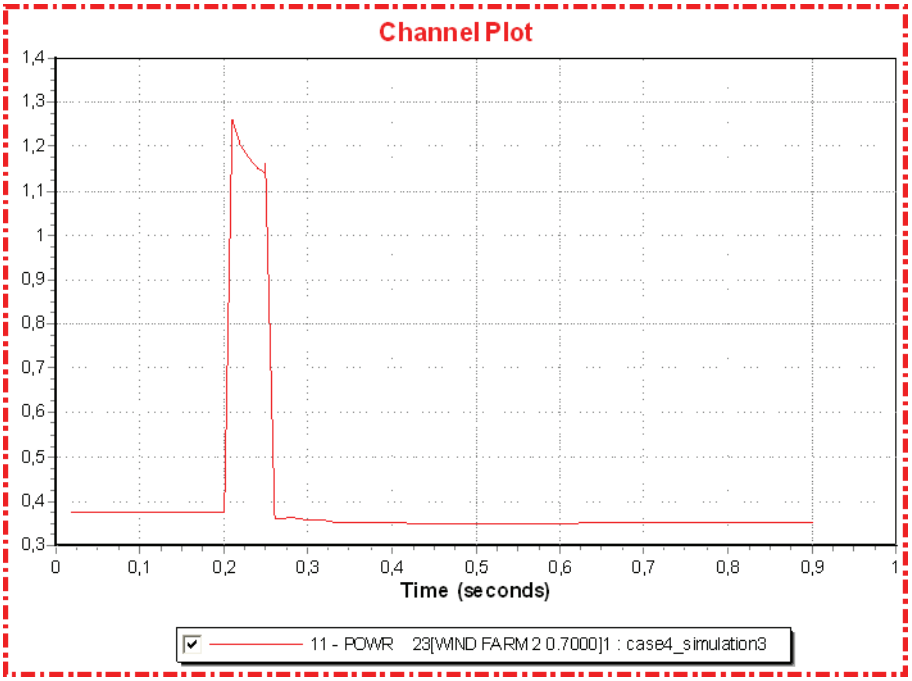

Figure F.4.23: Active wind power generation [pu]

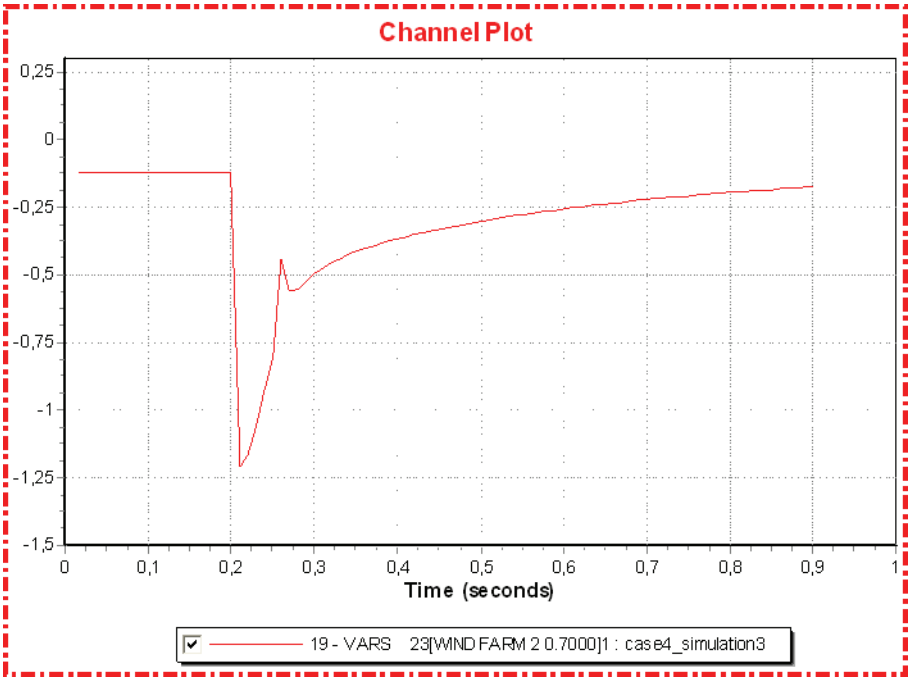

Figure F.4.24: Reactive wind power generation [pu

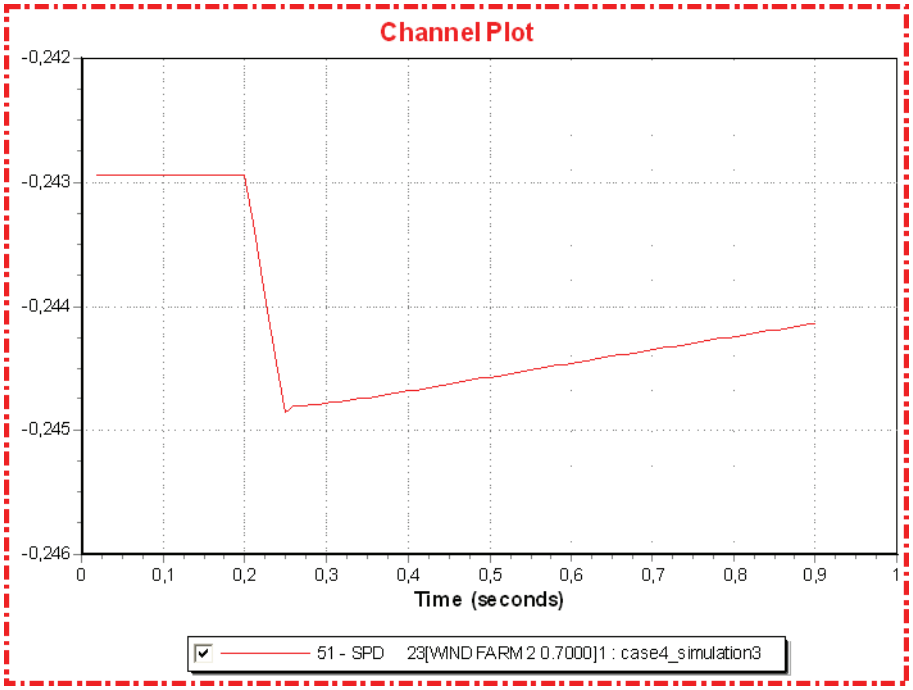

Figure F.4.25: Turbine speed, wind farm 2 [pu]

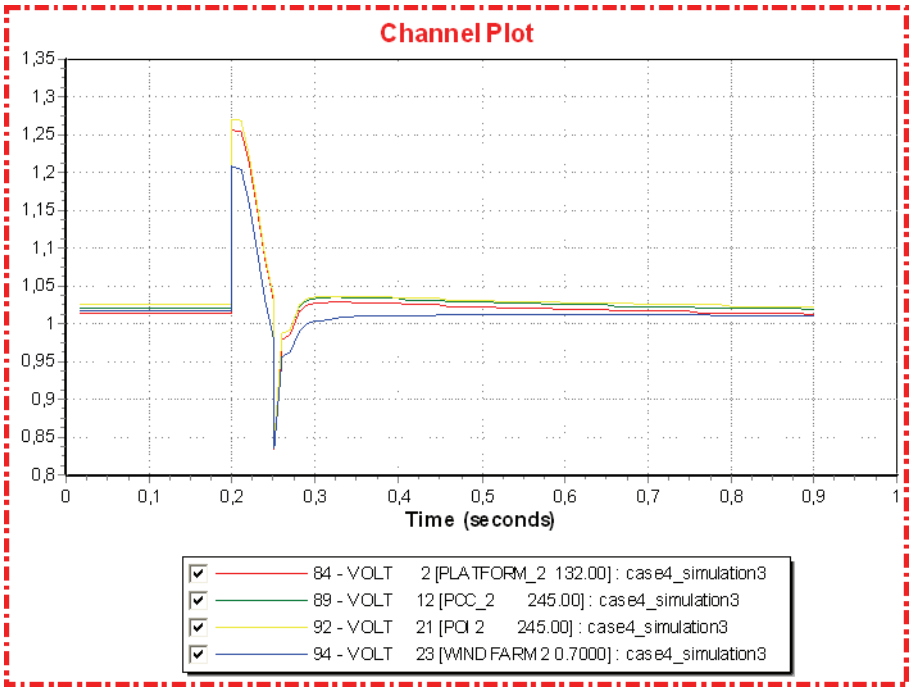

Figure F.4.26: Offshore area 2 voltage [pu]

Simulation 4 (Small wind generation)

Time	Event
0.00	Normal operation
0.20	Disconnect (trip) converter 2 and 3
2.20	Reconnect converter 2 and 3 and the associated power transformers

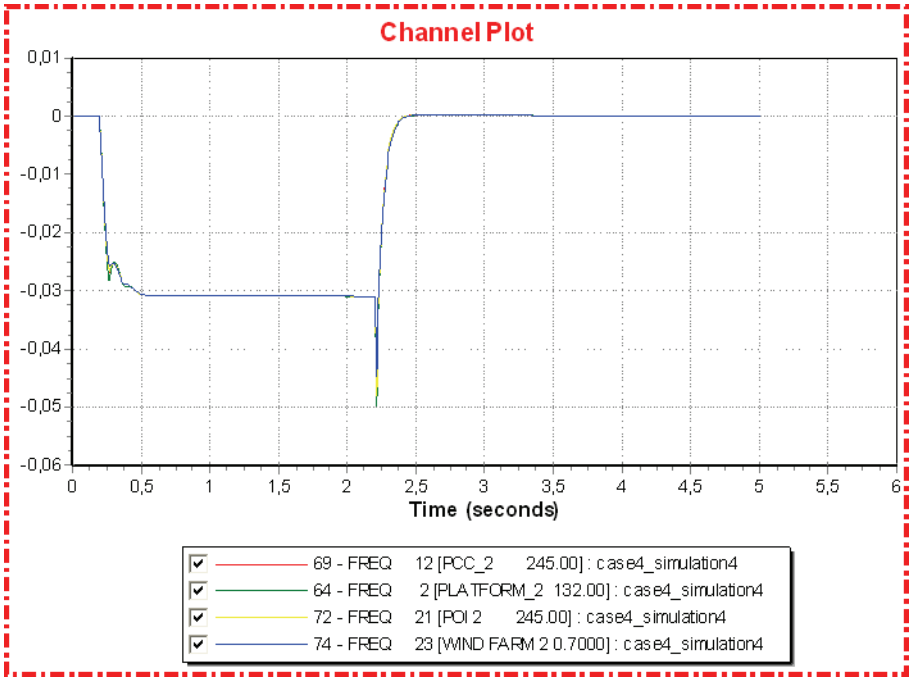

Figure F.4.27: Frequency offshore area 2 [pu deviation from 50 HZ]

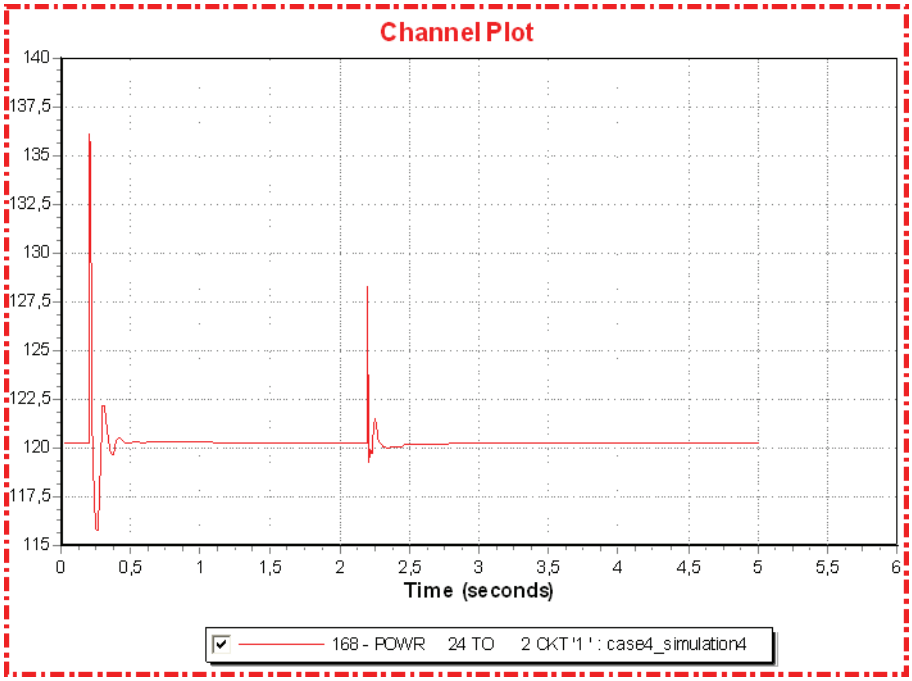

Figure F.4.28: Active power to platform 2 [MW]

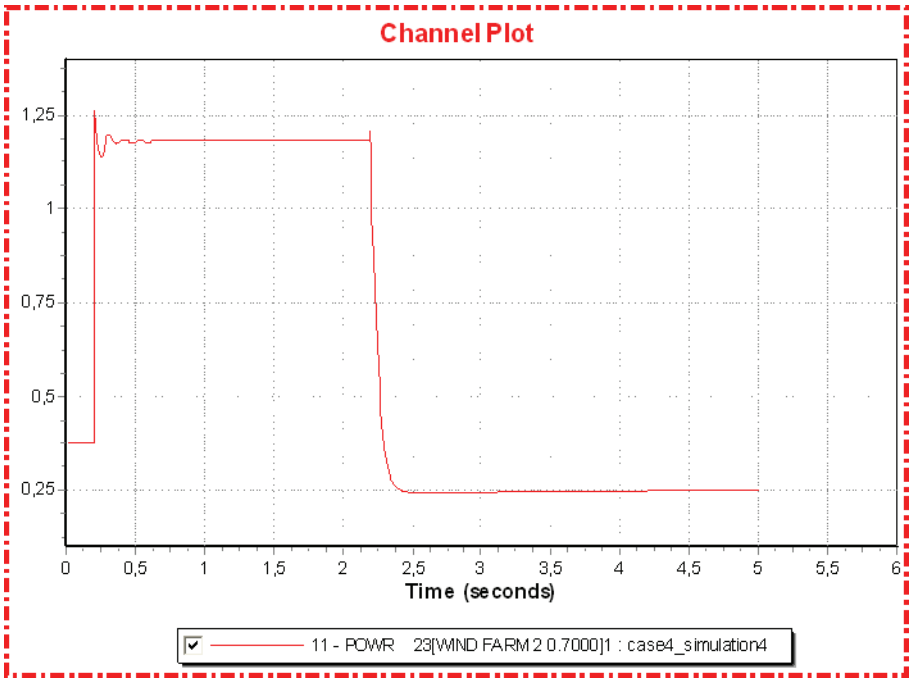

Figure F.4.29: Active wind power generation [pu]

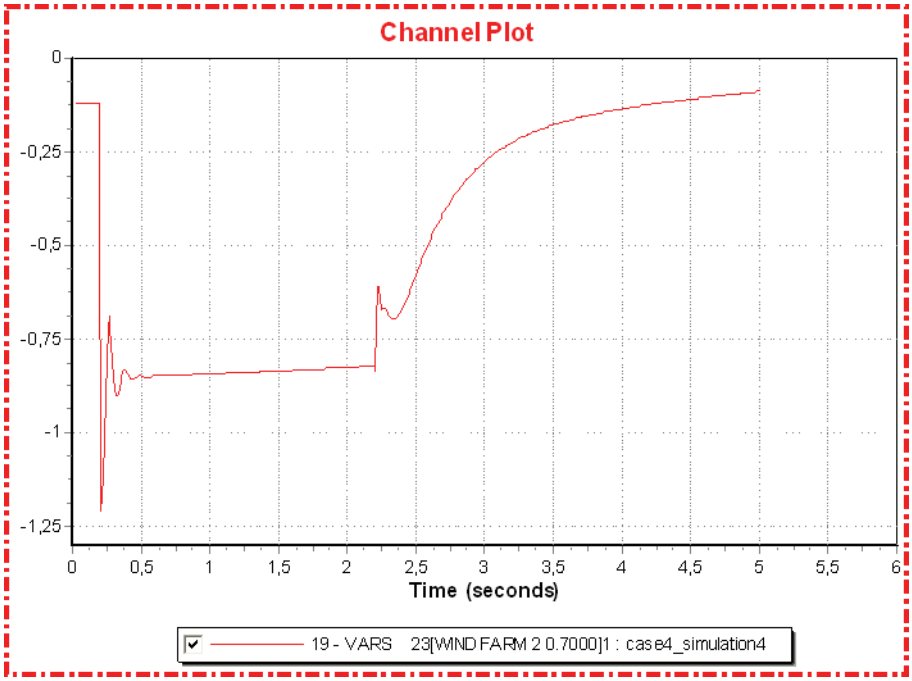

Figure F.4.30: Reactive wind power generation [pu]

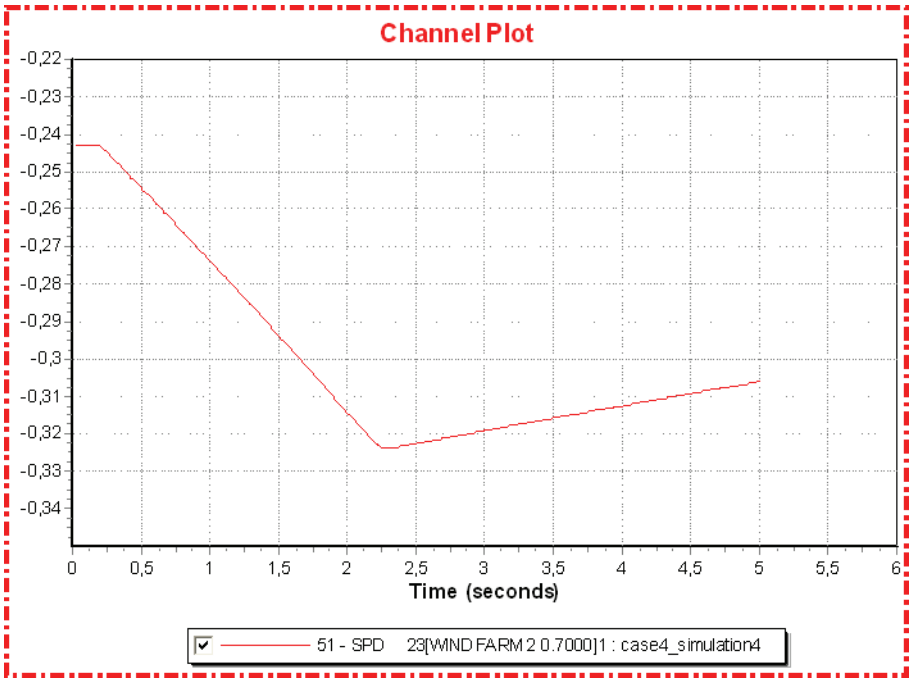

Figure F.4.31: Turbine speed, wind farm 2 [pu]

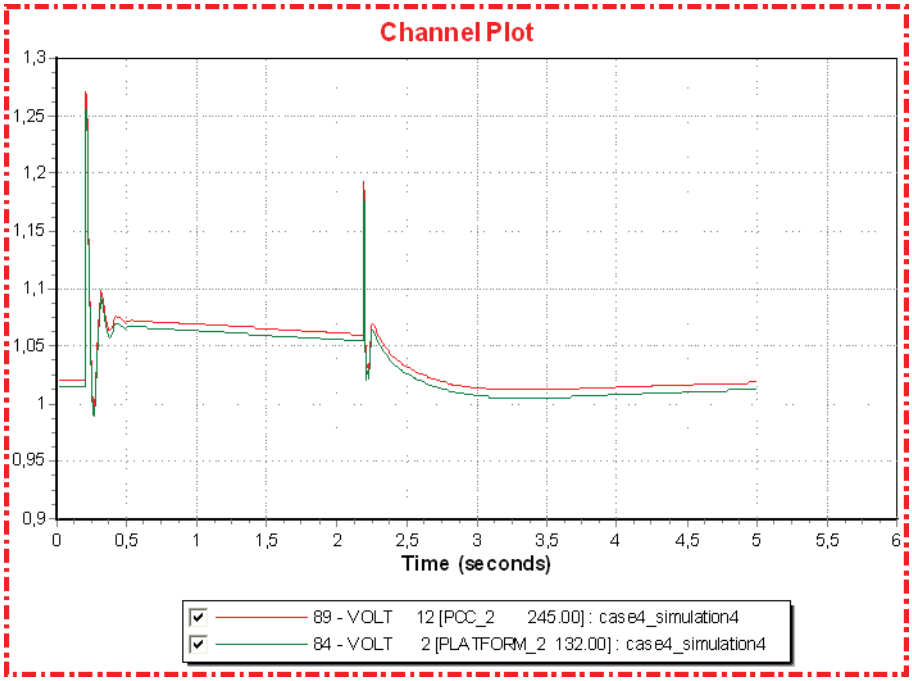

Figure F.4.32: Offshore area 2 voltage [pu]

22.1.5 Case 5

Simulation 1 (Large wind generation)

Time	Event
0.00	Normal operation
0.20	Disconnect generator at bus 23 (wind farm 2)

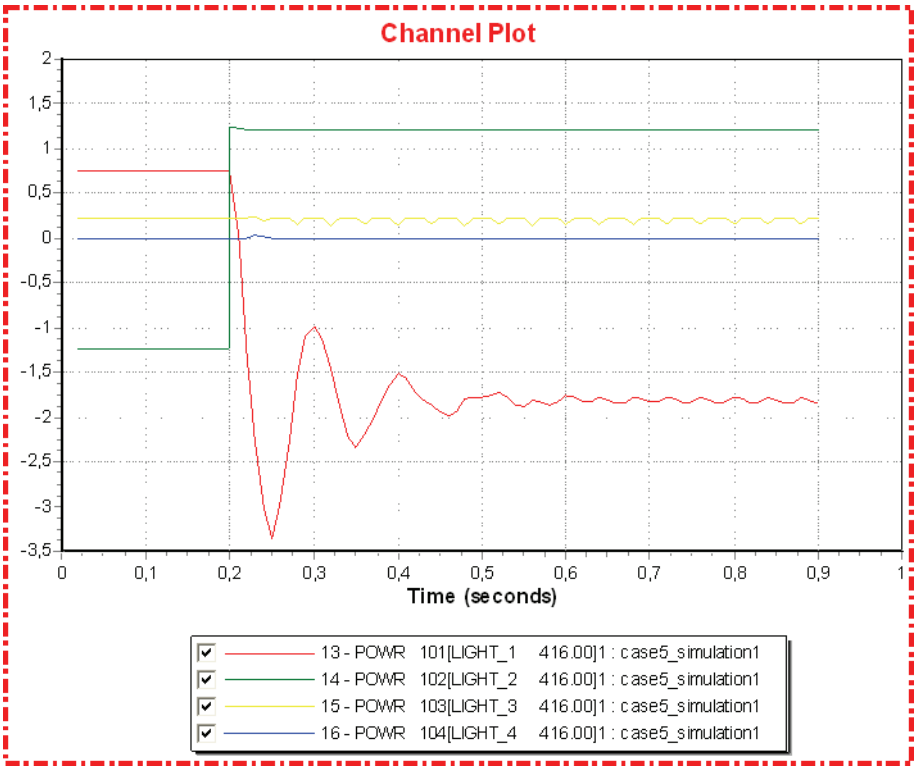

Figure F.5.1: Converter active power [pu]

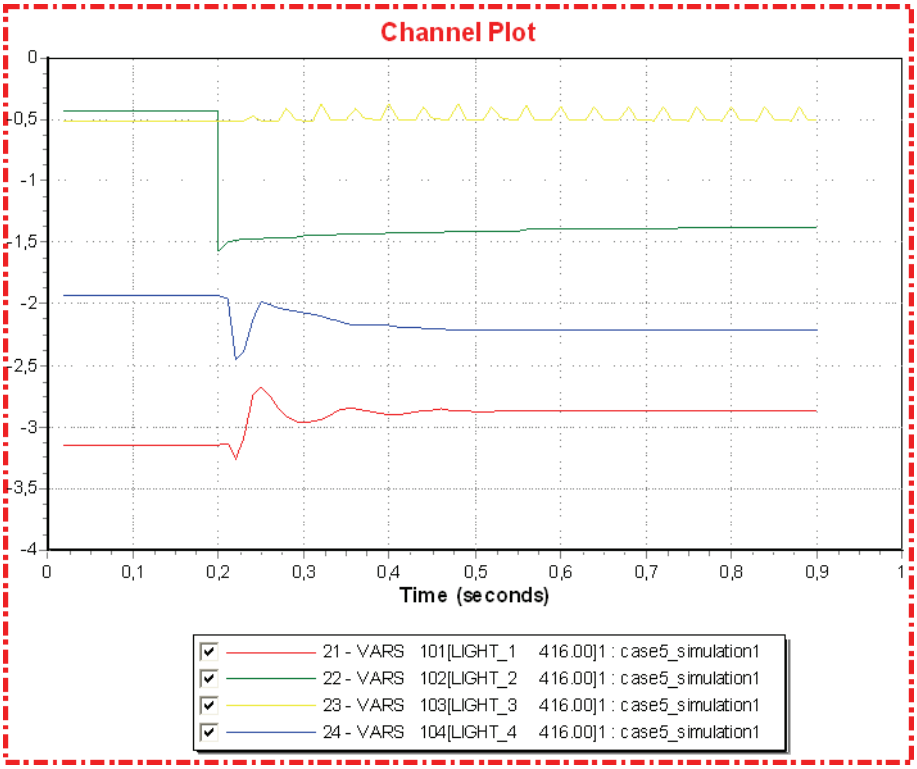

Figure F.5.2: Converter reactive power [pu]

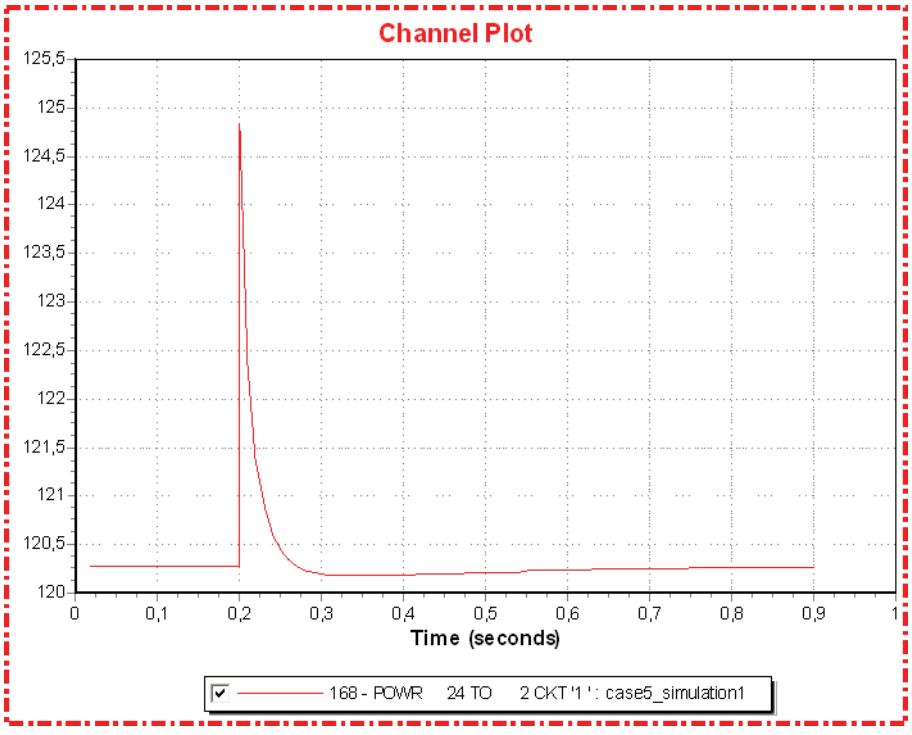

Figure F.5.3: Active power to platform 2 [MW]

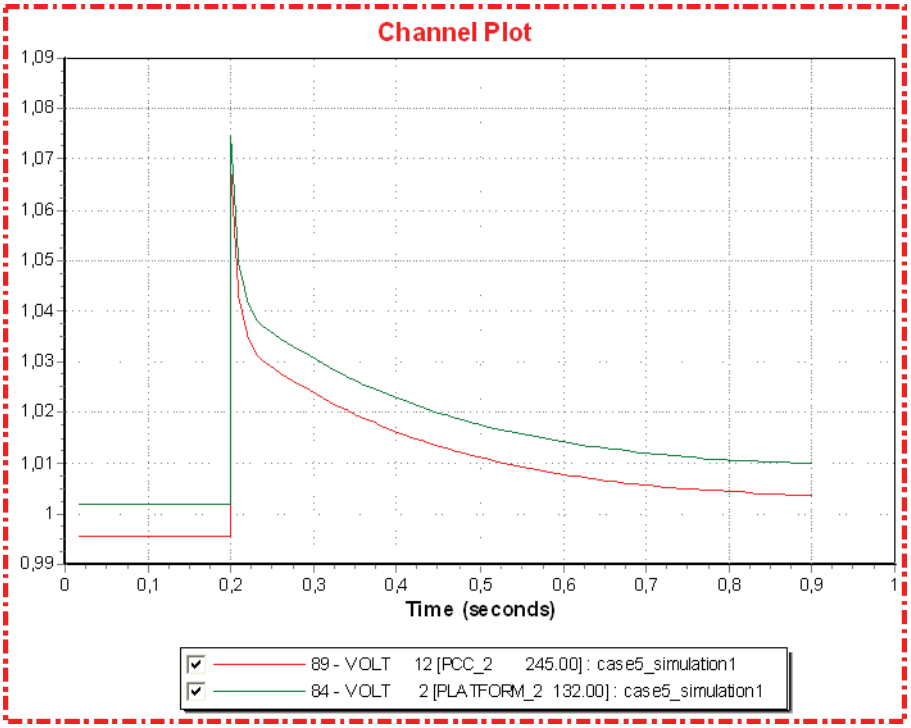

Figure F.5.4: Offshore area 2 voltage [pu]

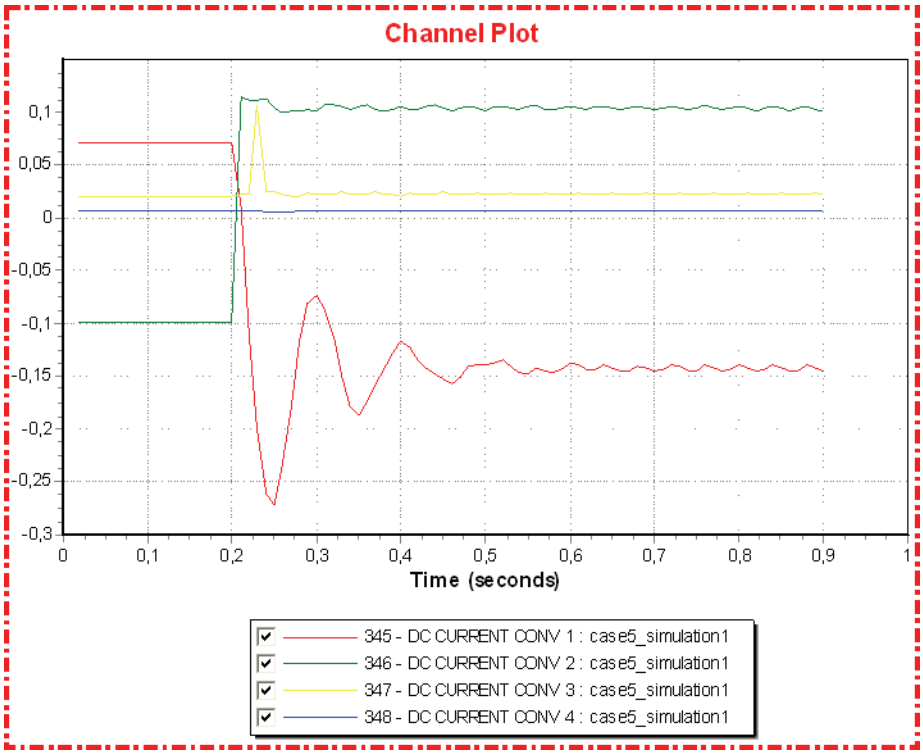

Figure F.5.5: Converter DC current [pu]

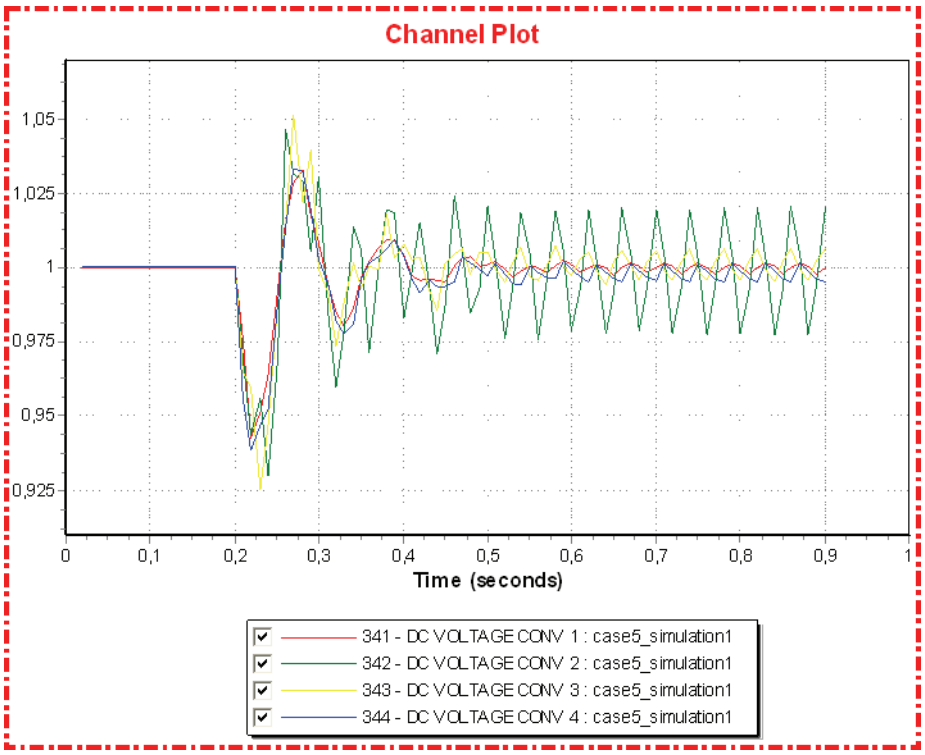

Figure F.5.6: Converter DC voltage [pu]

Simulation 2 (Large wind generation)

Time	Event
0.00	Normal operation
0.20	Line fault on cable 21 – 12
0.30	Disconnect (trip) faulted line

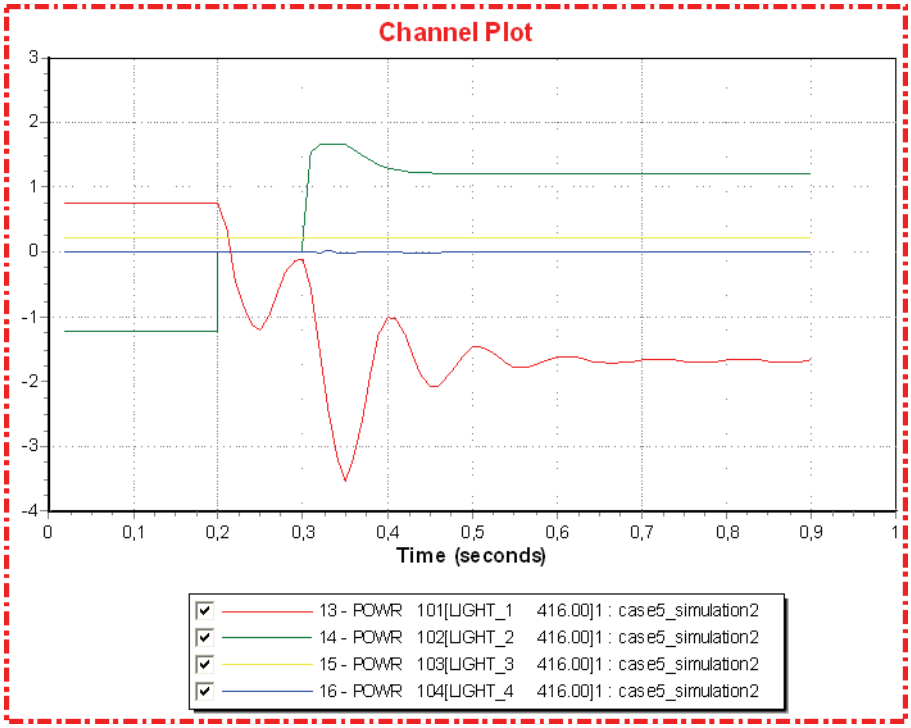

Figure F.5.7: Converter active power [pu]

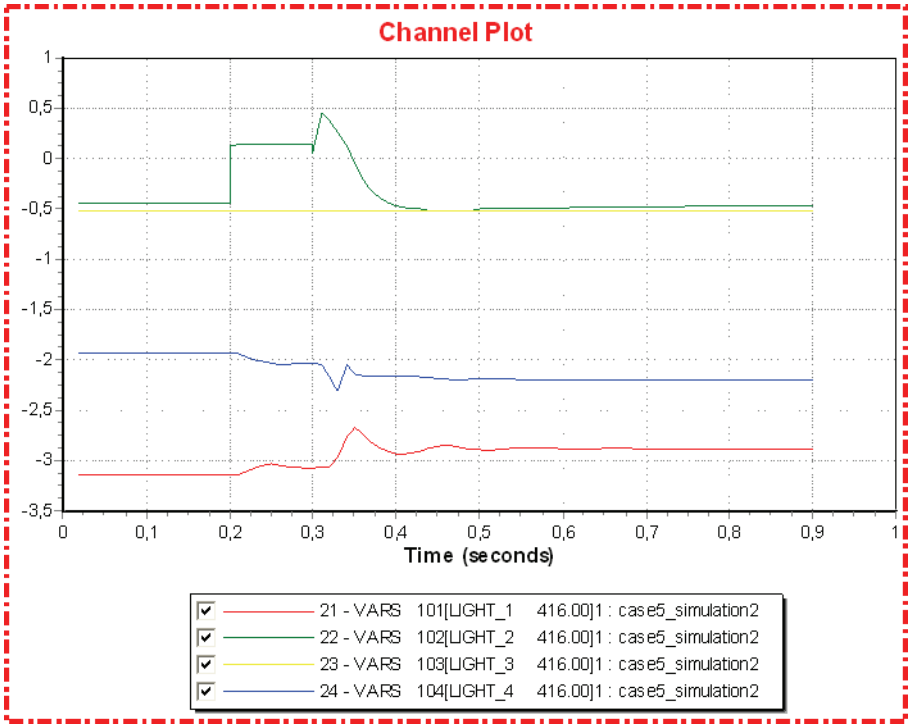

Figure F.5.8: Converter reactive power [pu]

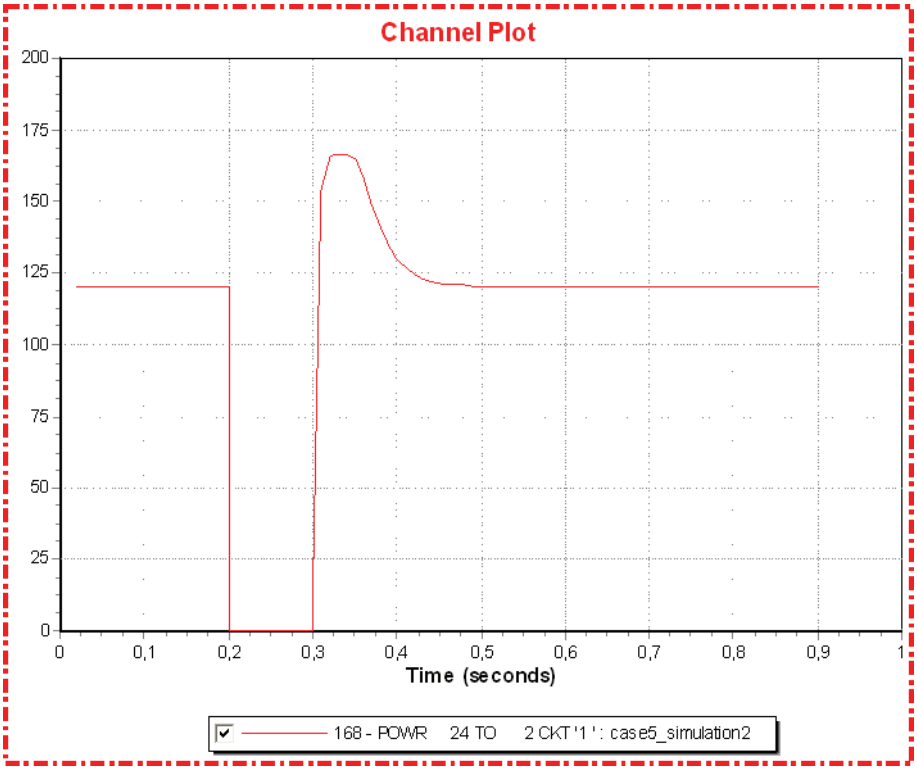

Figure F.5.9: Active power to platform 2 [MW]

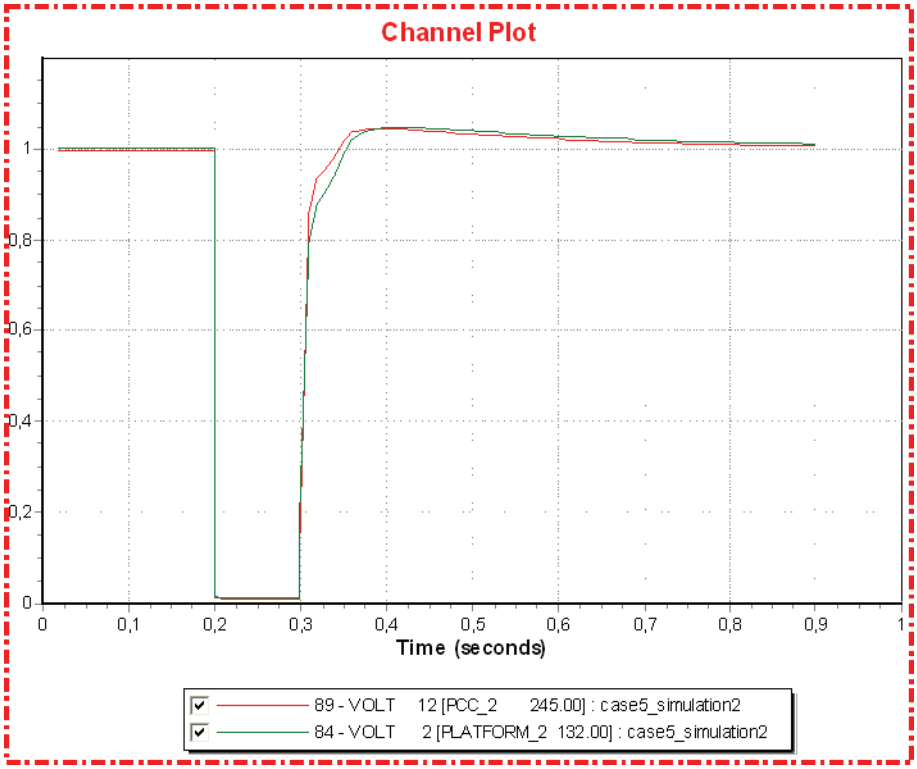

Figure F.5.10: Offshore area 2 voltage [pu]

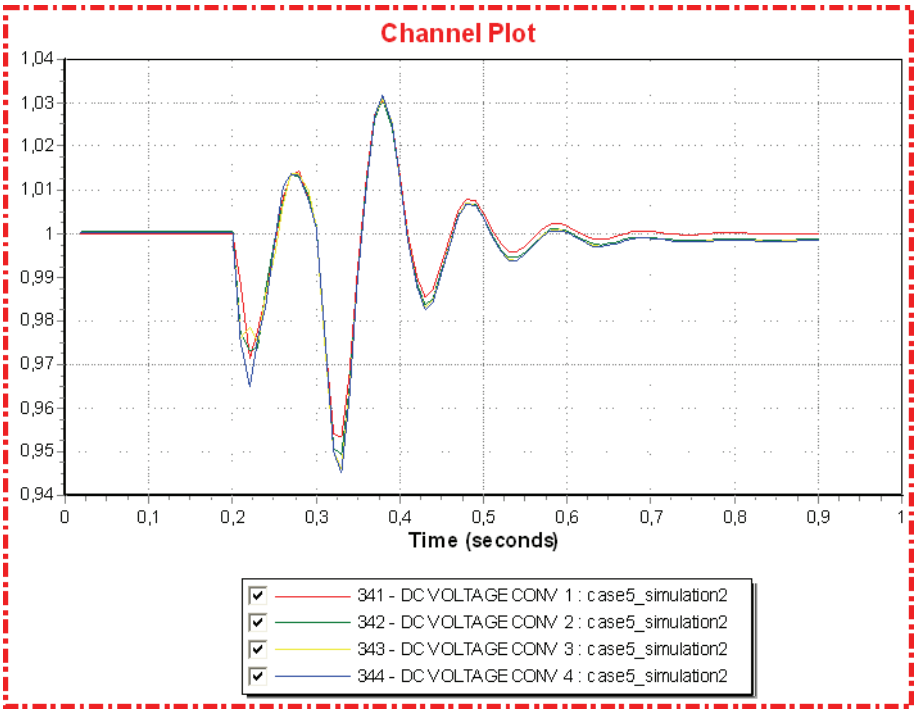

Figure F.5.11: Converter DC voltage [pu]

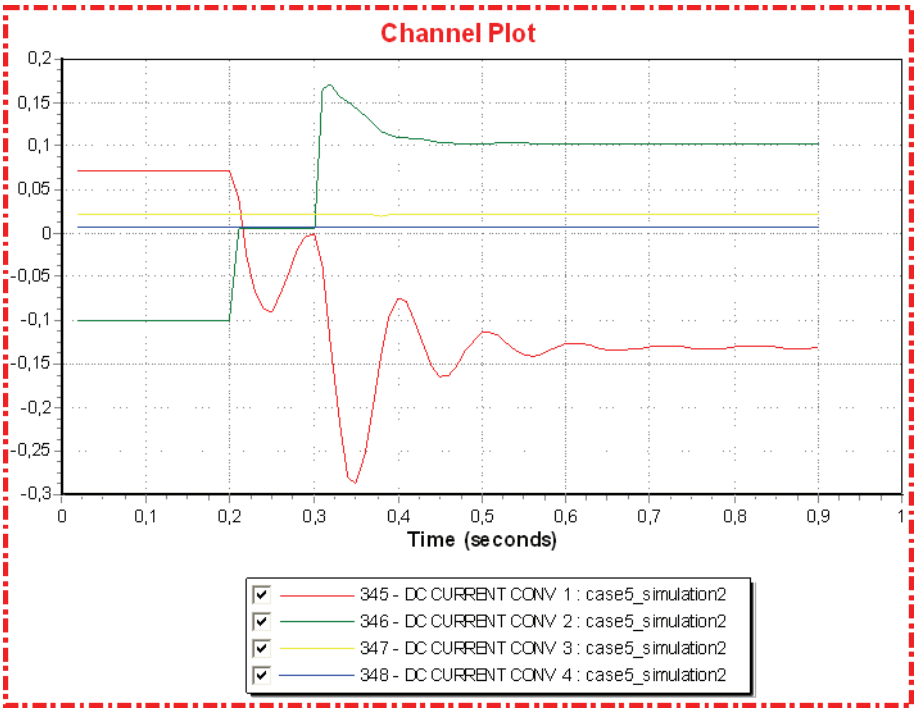

Figure F.5.12: Converter DC current [pu]

22.1.6 Case 6

Simulation 1 (Small wind generation)

Time	Event
0.00	Normal operation
0.20	Disconnect (trip) converter 1 and 4

The following figures depict the simulation results up to simulation time = 0.314 seconds.

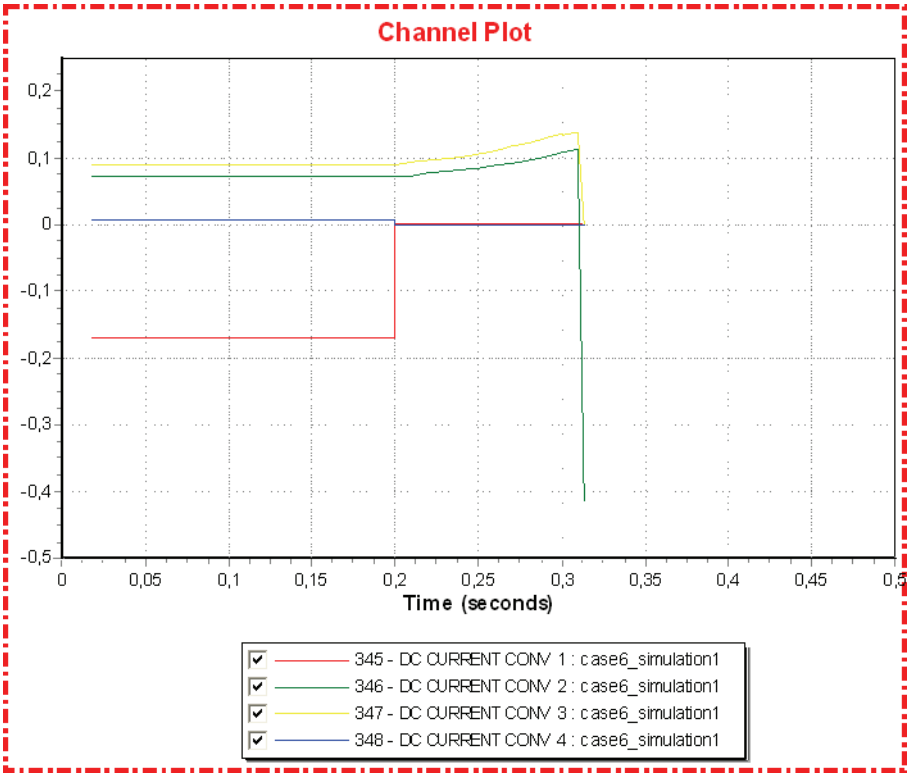

Figure F.6.1: Converter DC current [pu]

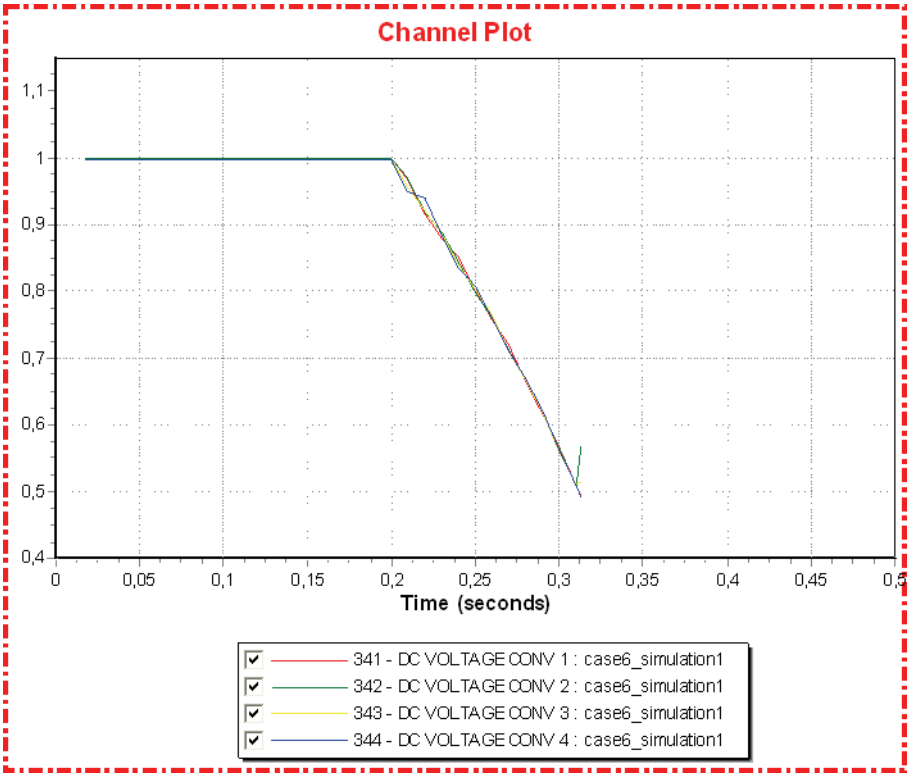

Figure F.6.2: Converter DC voltage [pu]

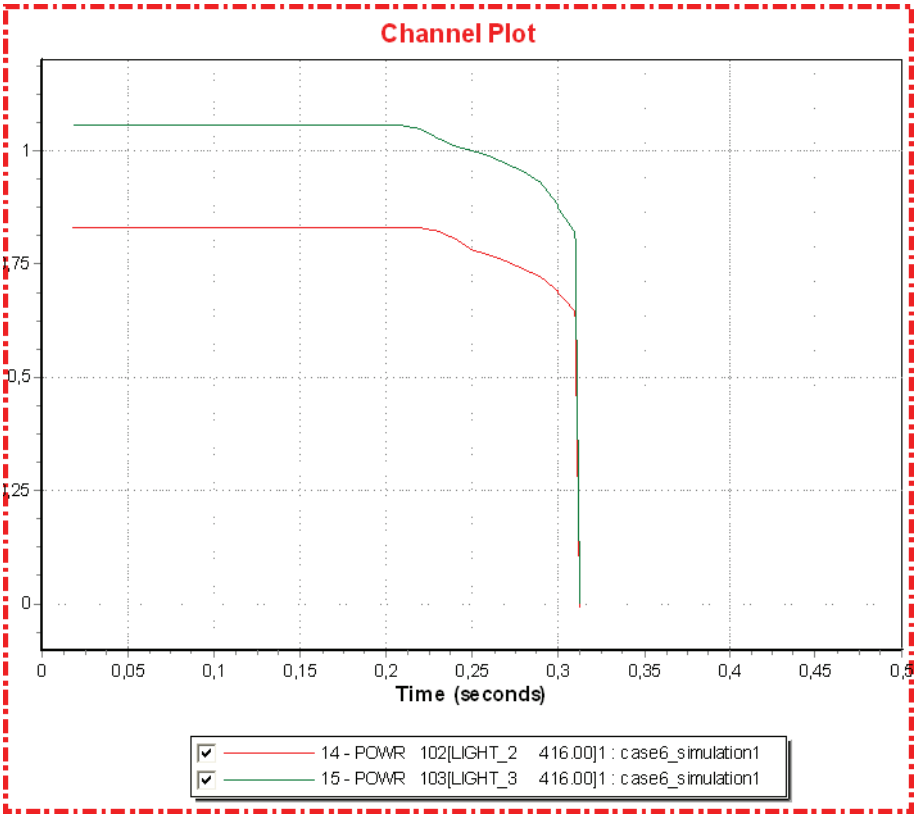

Figure F.6.3: Offshore converters active power [pu]

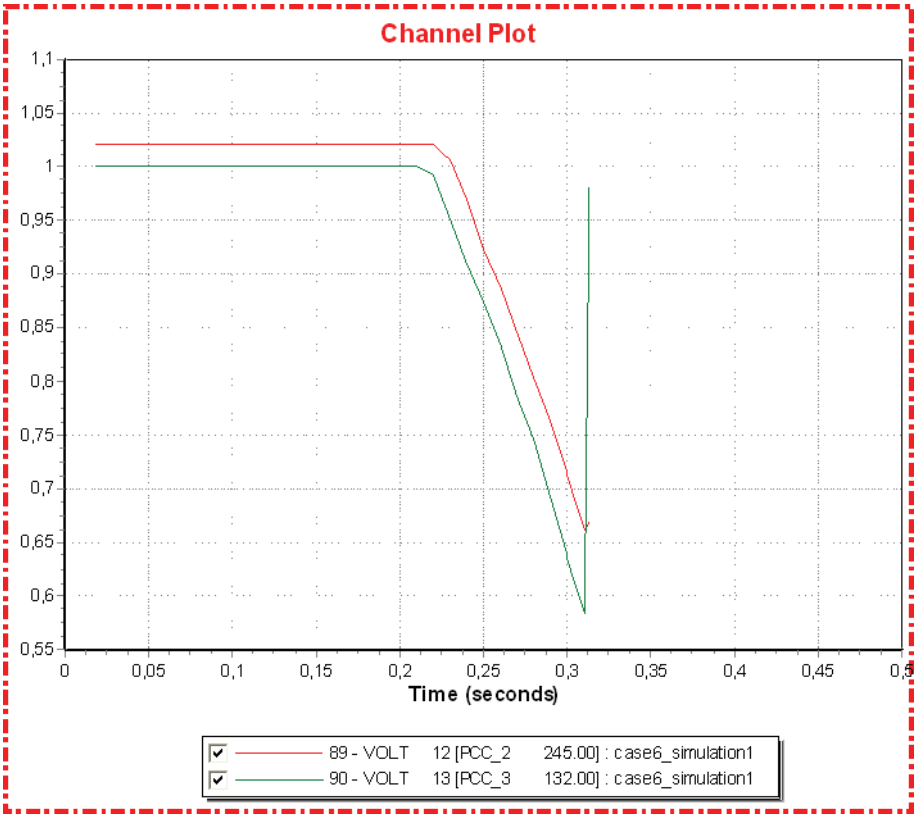

Figure F.6.4: Offshore AC voltage [pu]

The following figures depict the simulation results up to simulation time = 0.500 seconds.

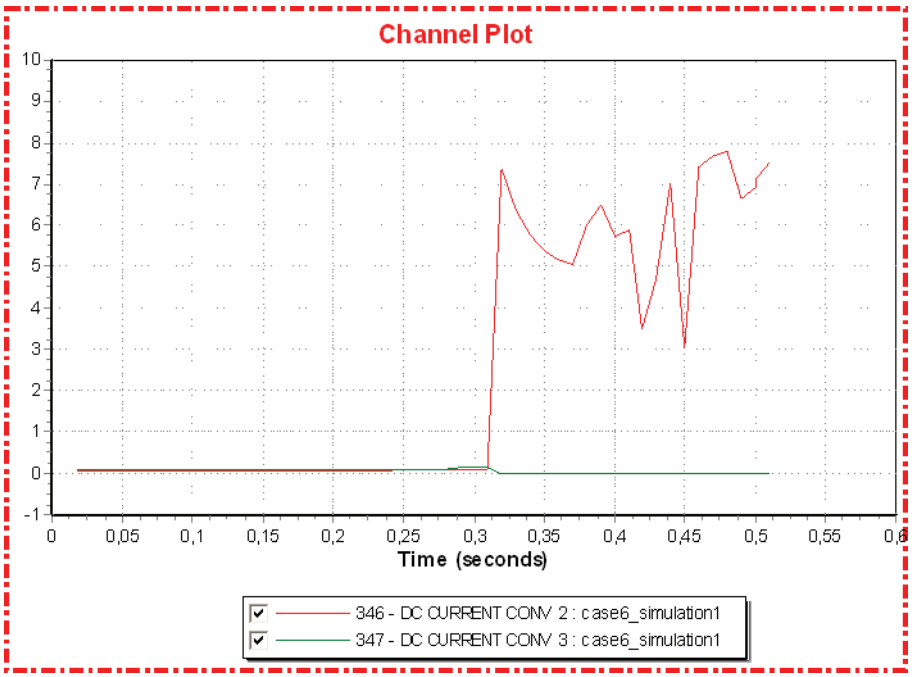

Figure F.6.5: Converter DC current [pu]

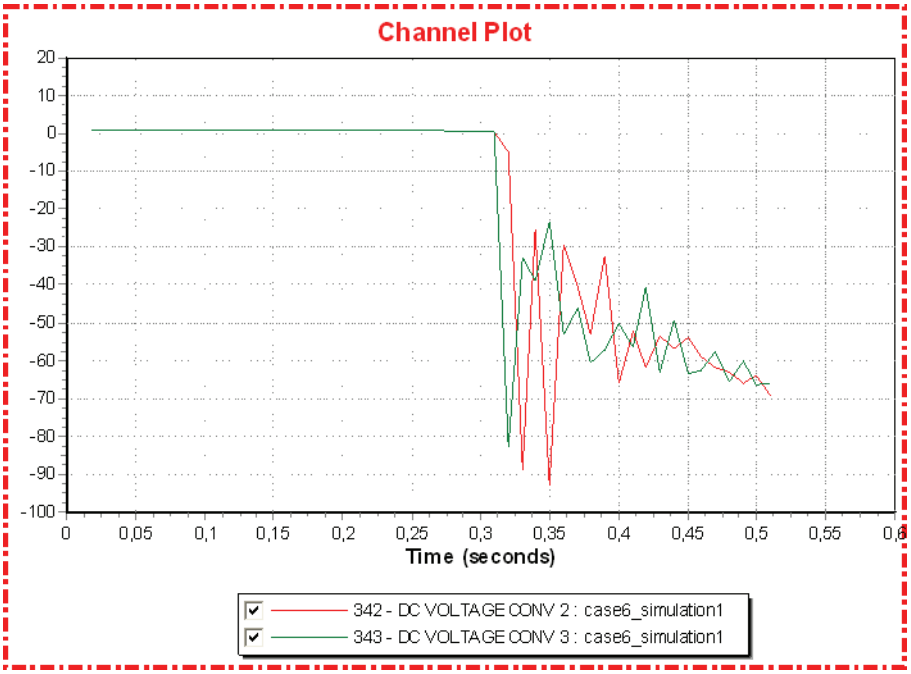

Figure F.6.6: Converter DC voltage [pu]

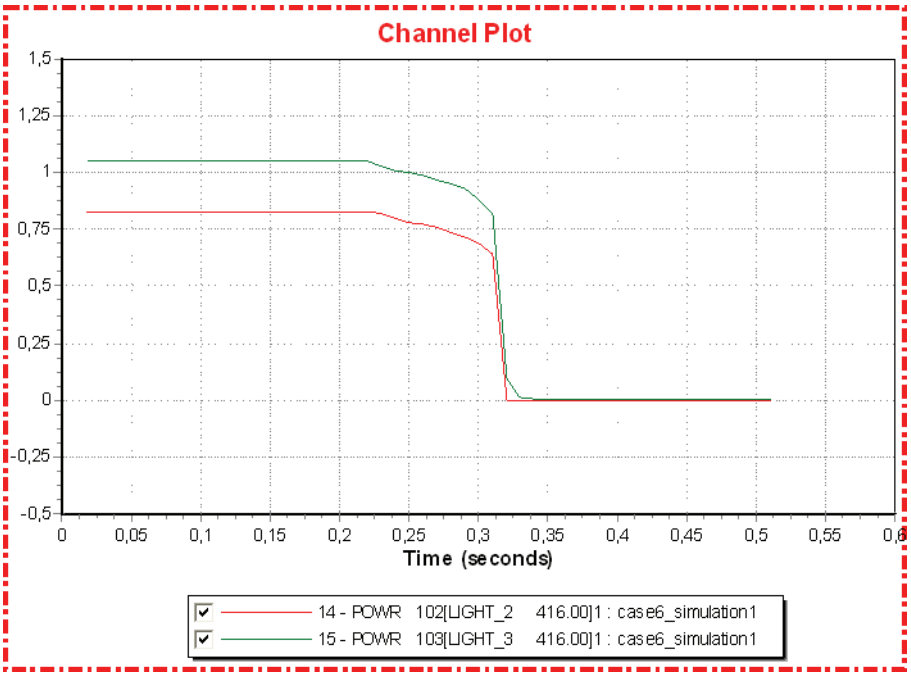

Figure F.6.7: Offshore converters active power [pu]

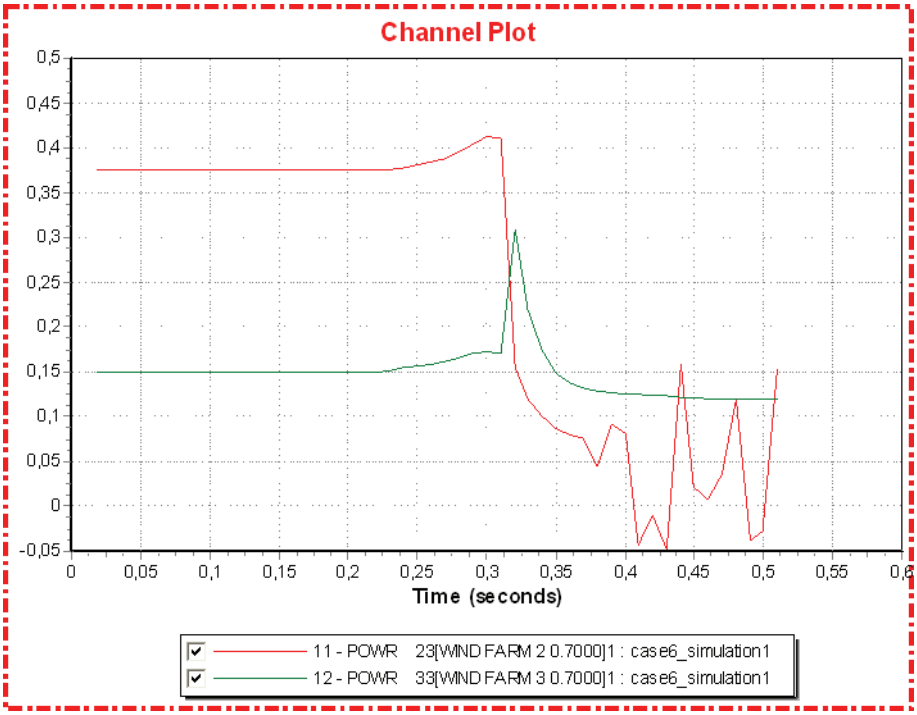

Figure F.6.8: Active wind power generation [pu]

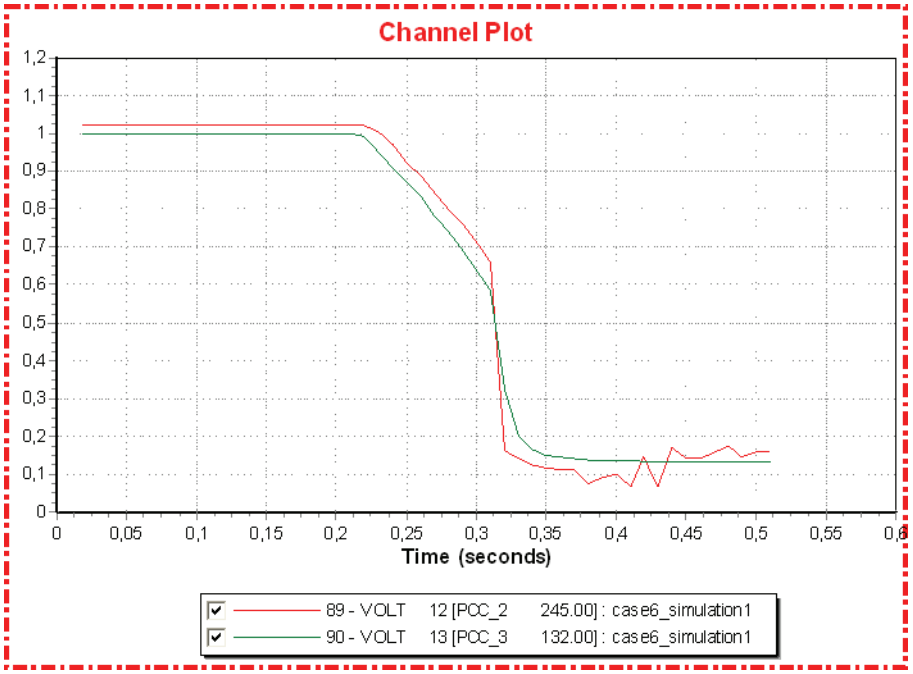

Figure F.6.9: Offshore AC voltage [pu]

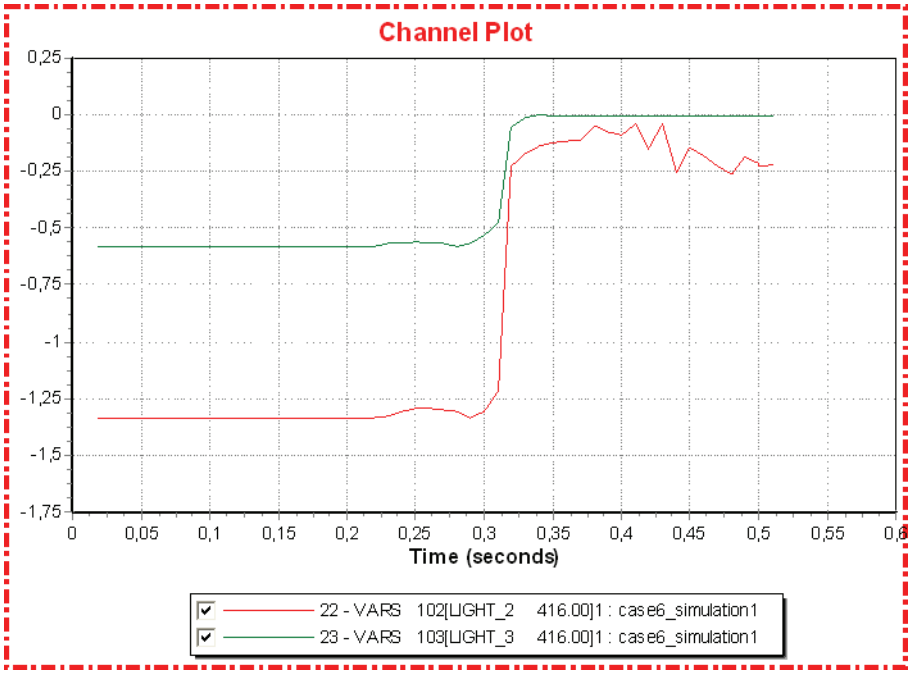

Figure F.6.10: Offshore converters active power [pu]

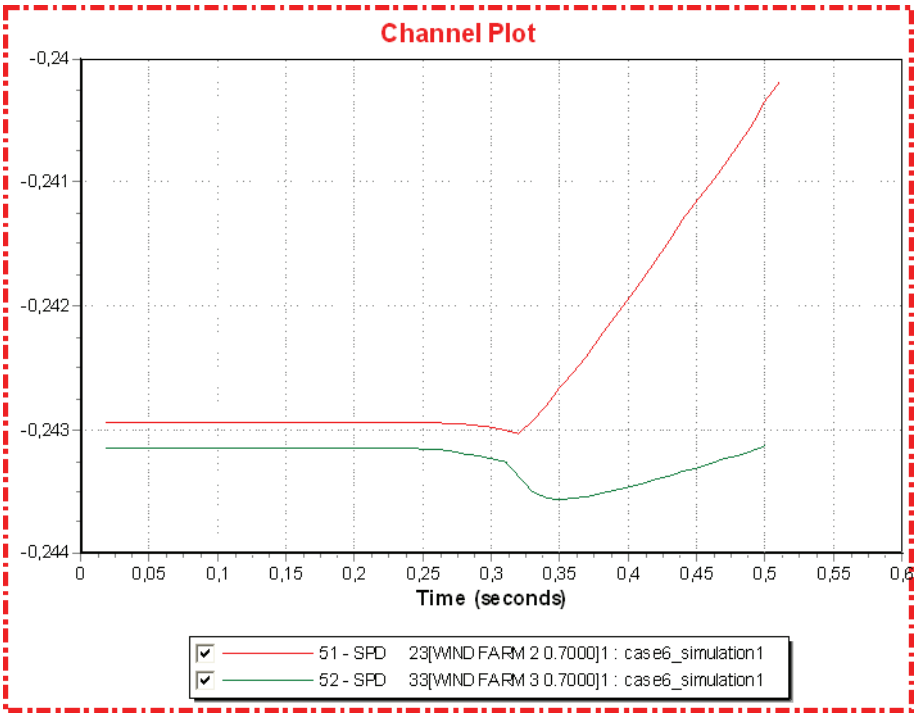

Figure F.6.11: Turbine speed, wind farms [pu]

Simulation 2 (Large wind generation)

Time	Event
0.00	Normal operation
0.20	Disconnect (trip) converter 1 and 4

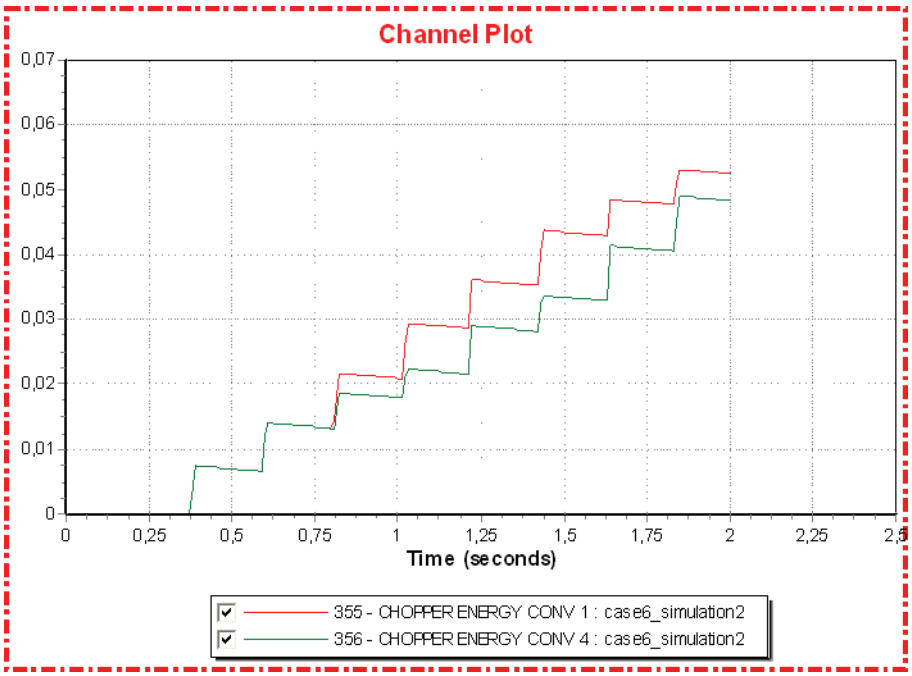

Figure F.6.12: Dissipated chopper energy [pu]

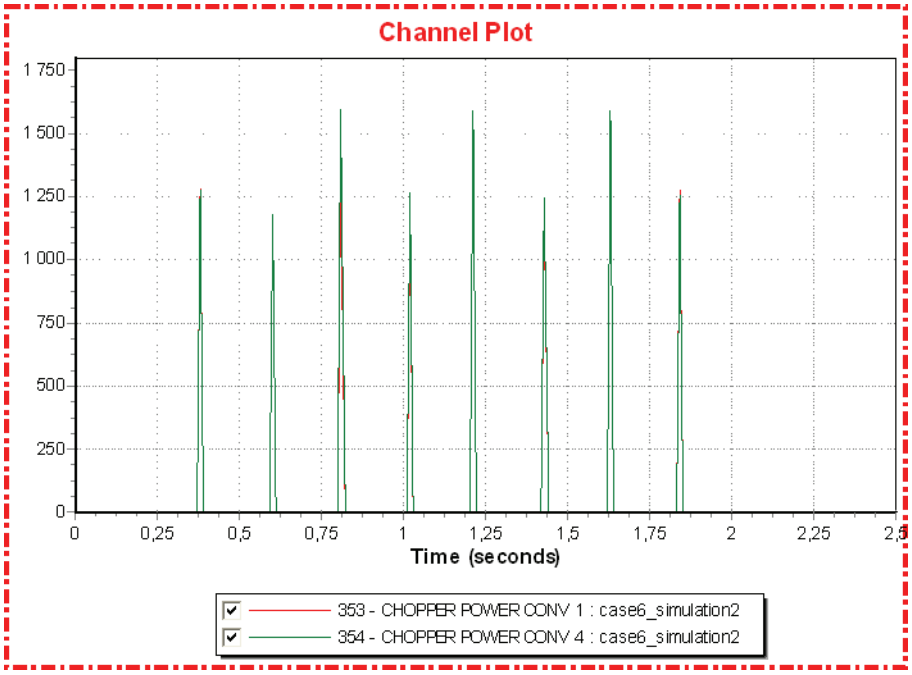

Figure F.6.13: Dissipated chopper power [pu]

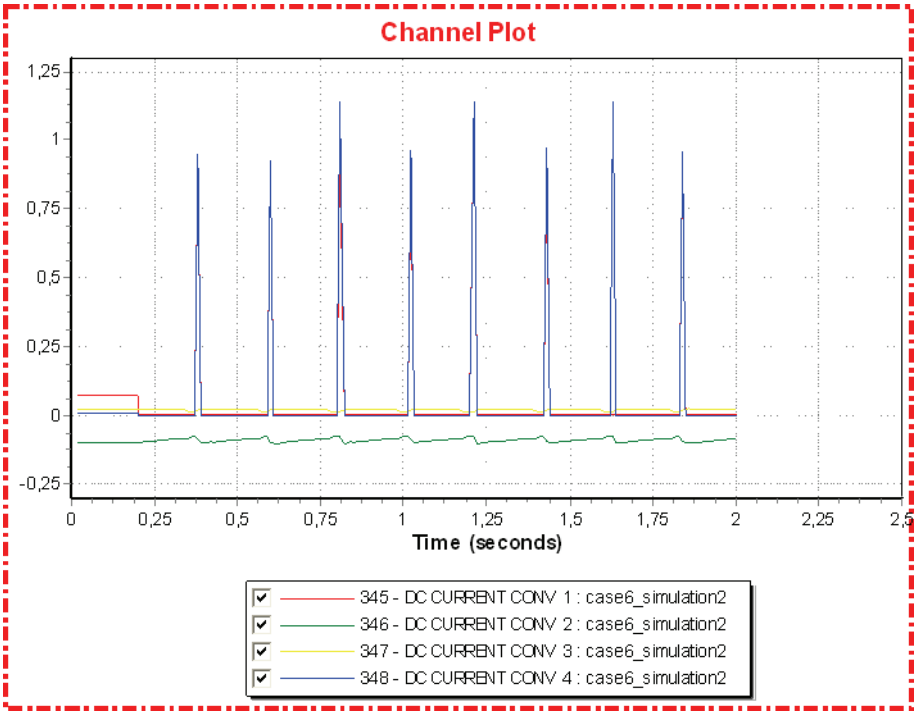

Figure F.6.14: Converter DC current [pu]

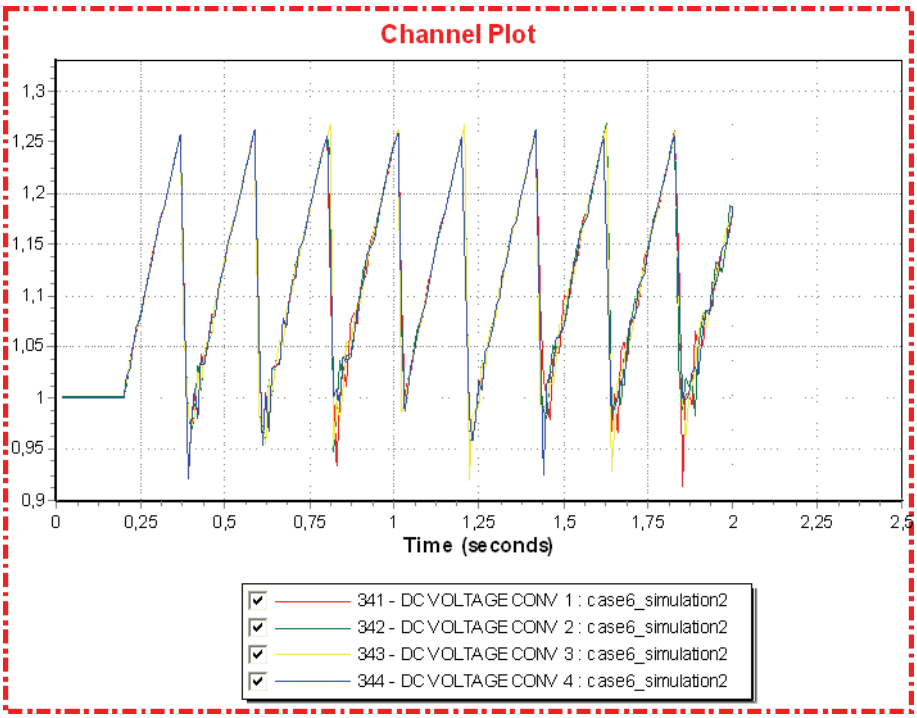

Figure F.6.15: Converter DC voltage [pu]

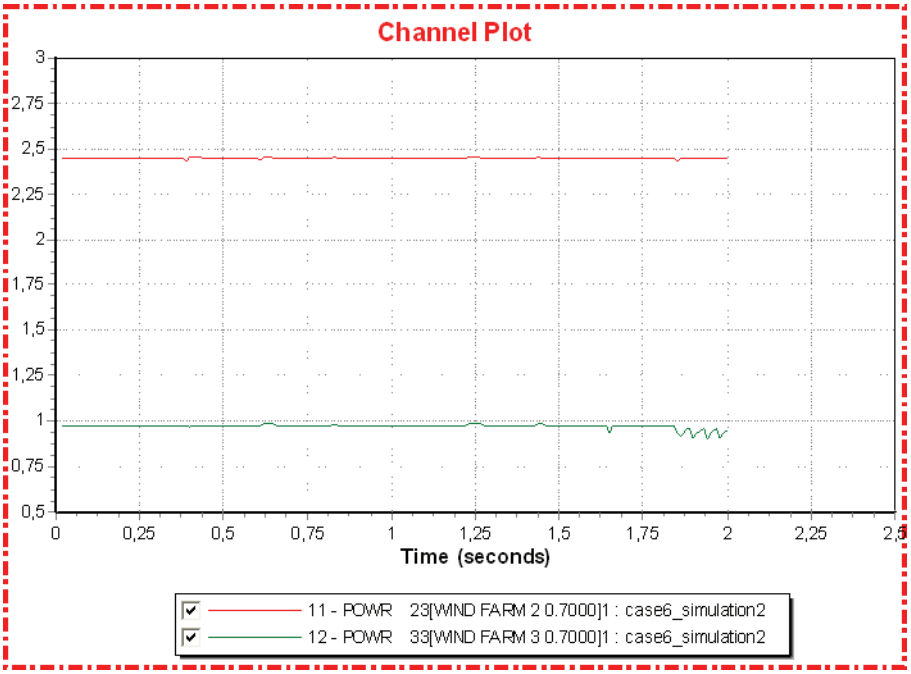

Figure F.6.16: Active wind power generation [pu]

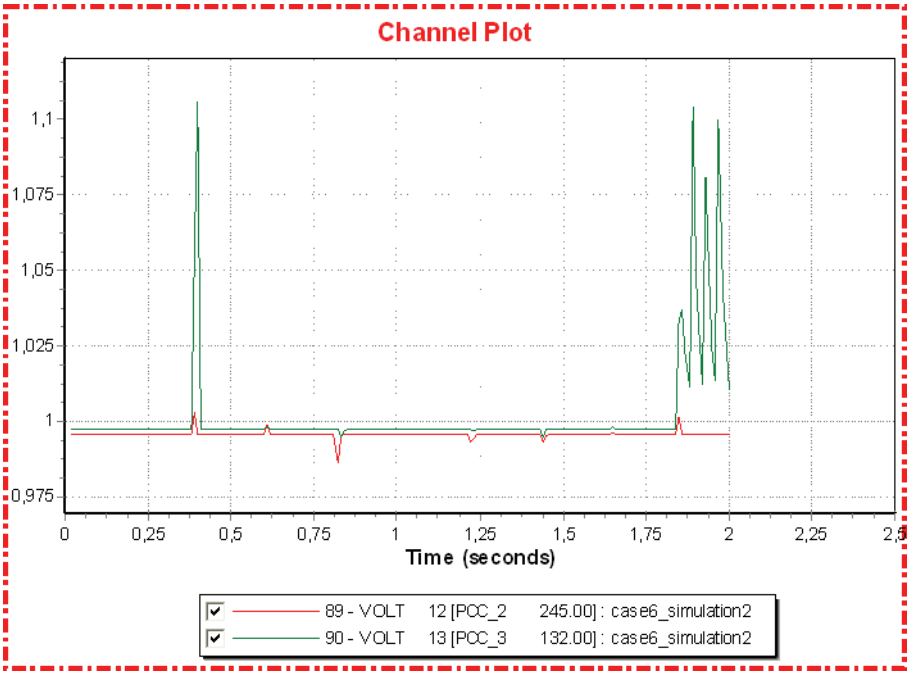

Figure F.6.17: Offshore AC voltage [pu]

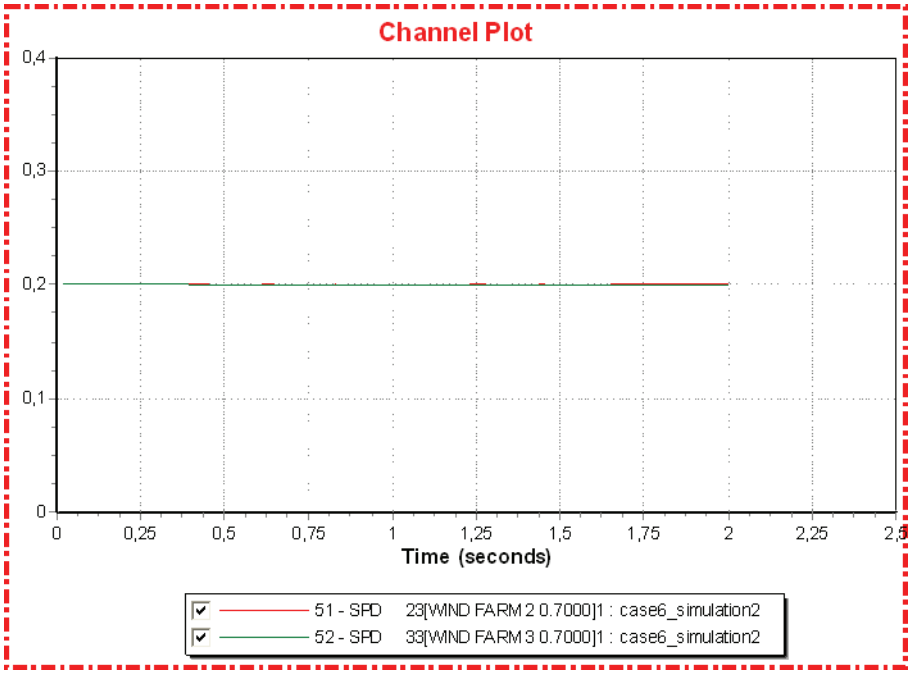

Figure F.6.11: Turbine speed, wind farms [pu]

Simulation 3 (Large wind generation)

Time	Event
-0.00	Remove the choppers connected to the onshore converters
0.00	Normal operation
0.20	Disconnect (trip) converter 1 and 4

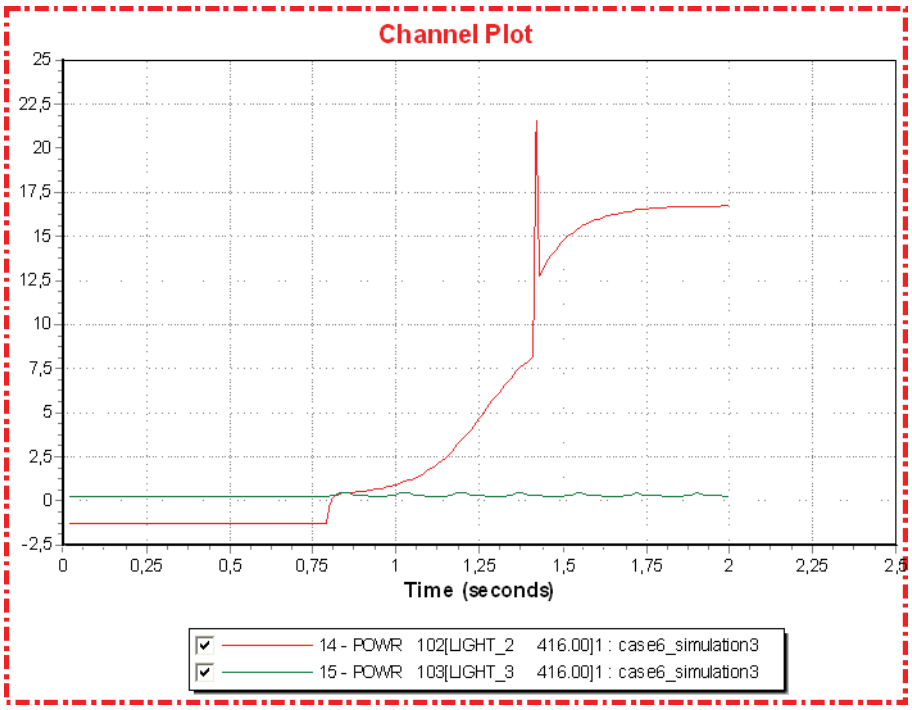

Figure F.6.19: Offshore converters active power [pu]

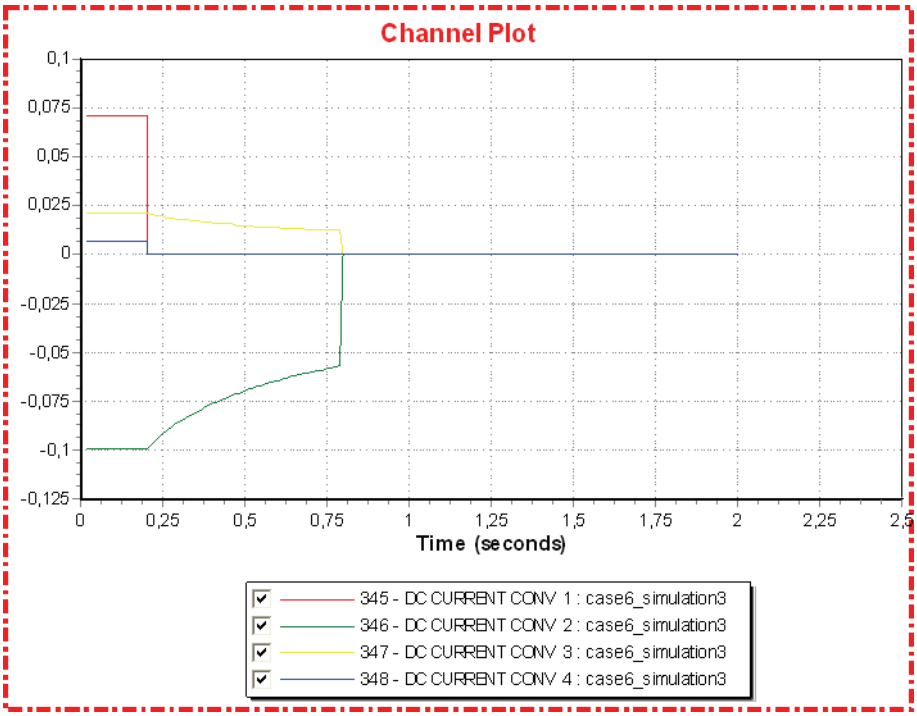

Figure F.6.20: Converter DC current [pu]

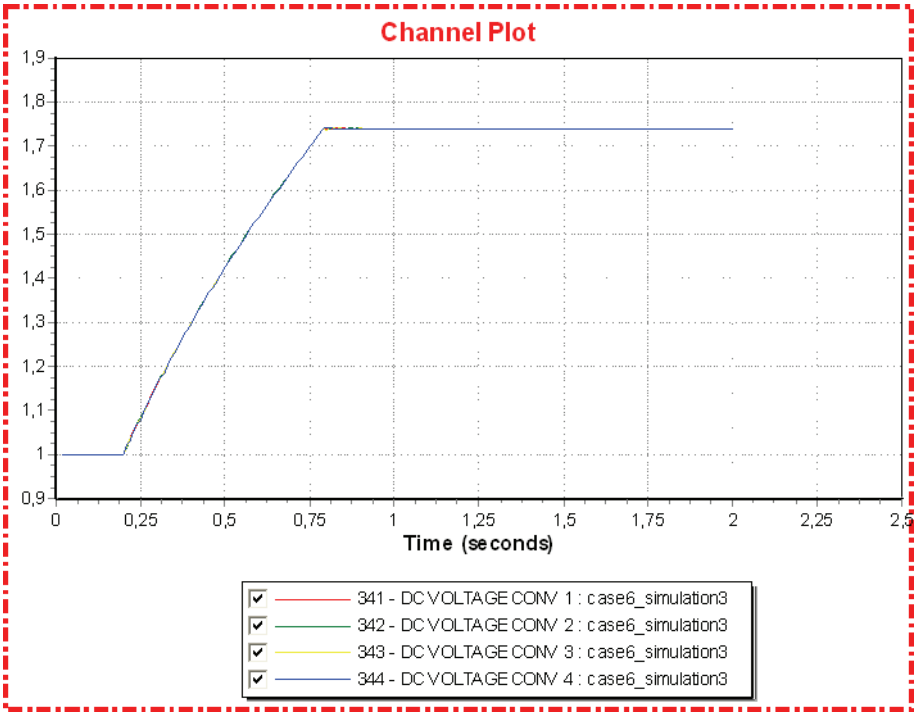

Figure F.6.21: Converter DC voltage [pu]

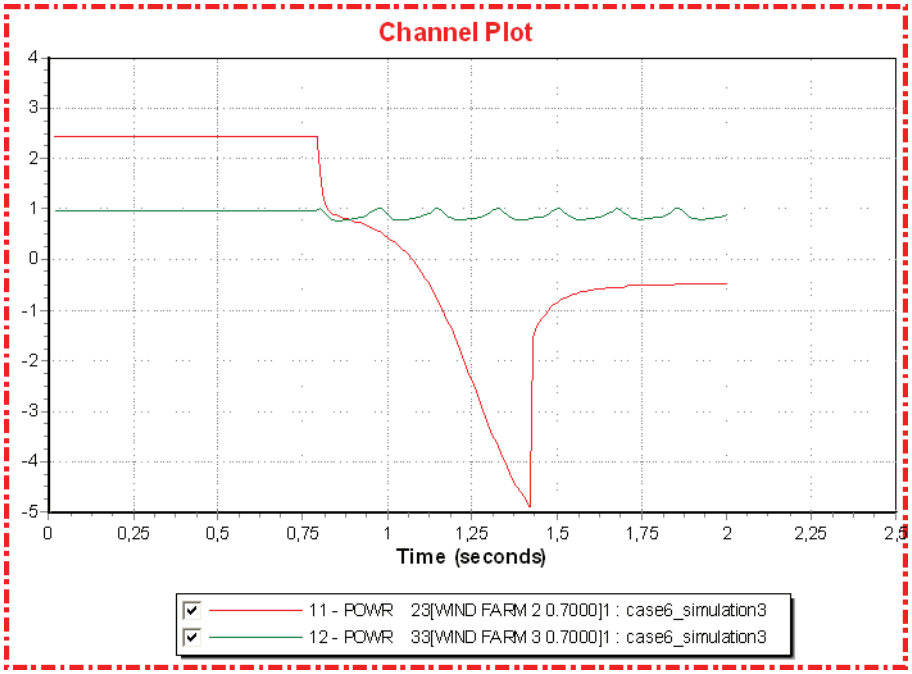

Figure F.6.22: Active wind power generation [pu]

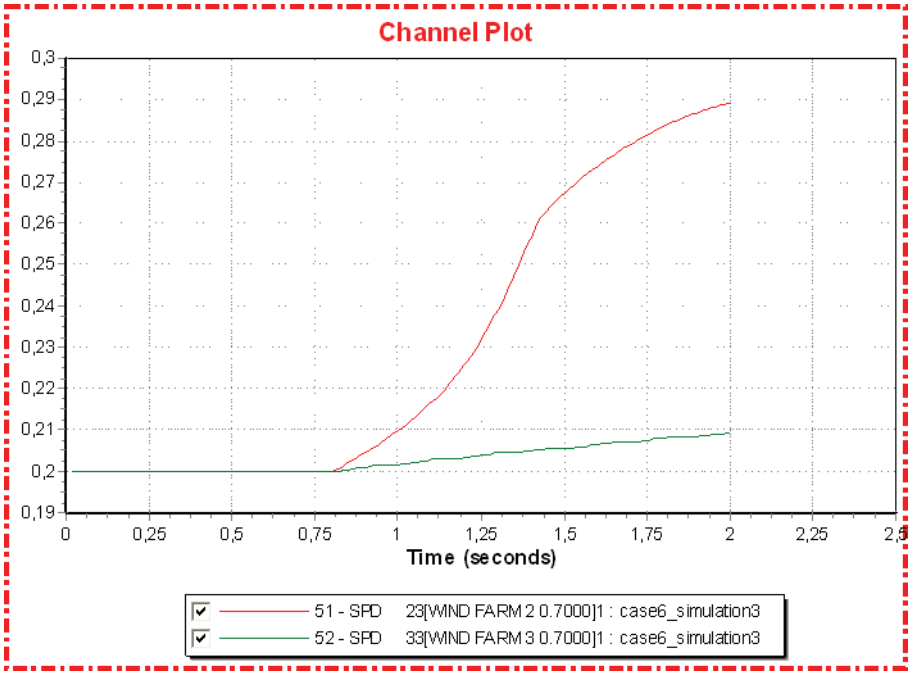

Figure F.6.23: Turbine speed, wind farms [pu]

22.1.7 Case 7

Simulation 1 (Large power transfer)

Time	Event
0.00	Normal operation
0.20	Line fault on line 14 – 11
0.30	Disconnect (trip) faulted line

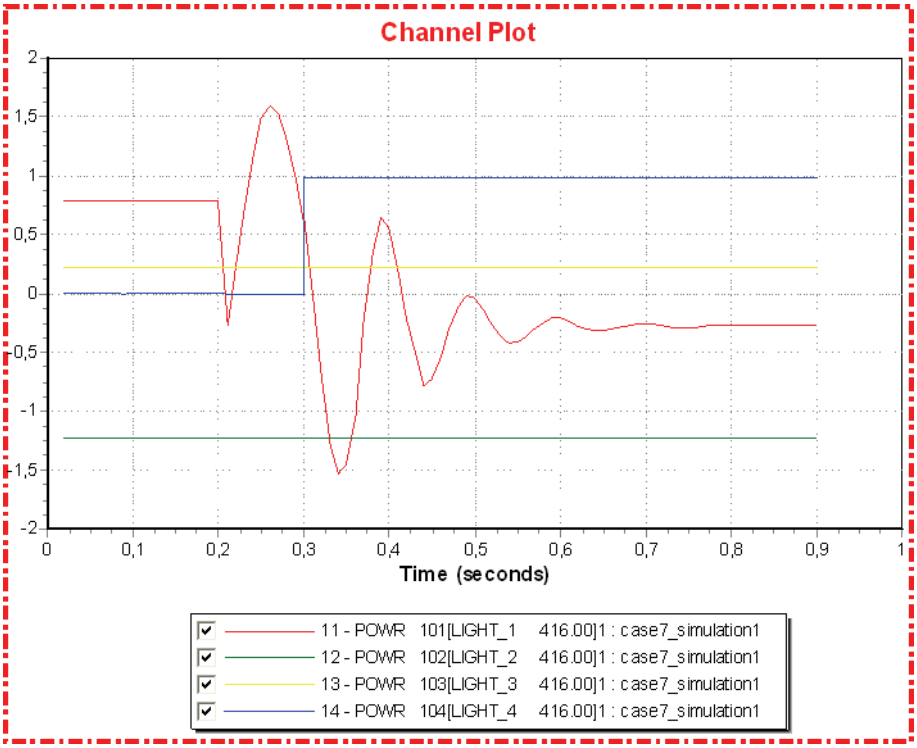

Figure F.7.1: Converter active power [pu]

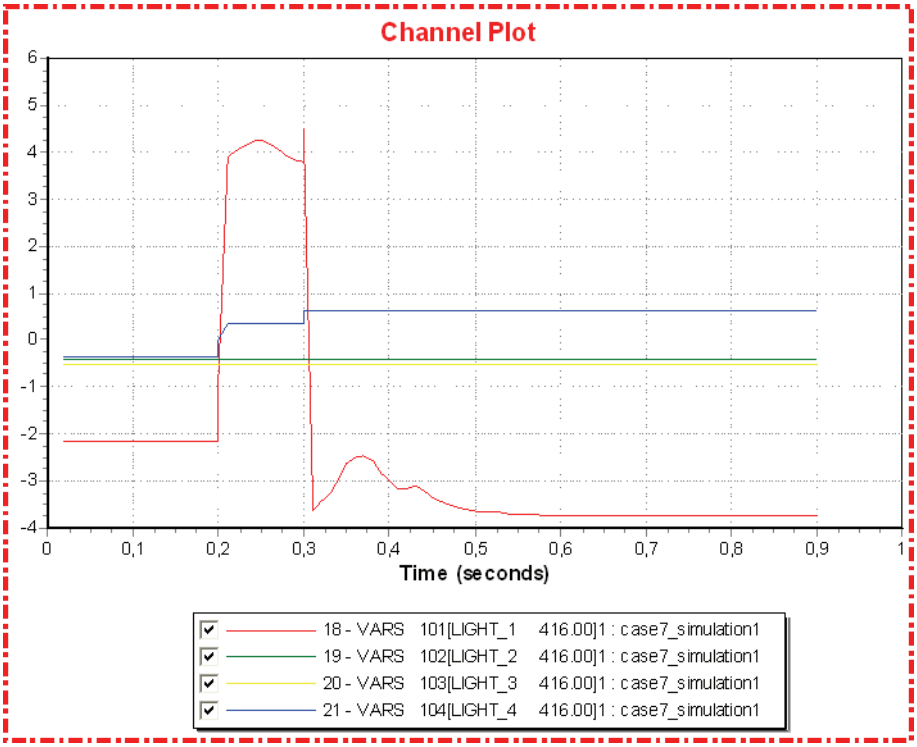

Figure F.7.2: Converter reactive power [pu]

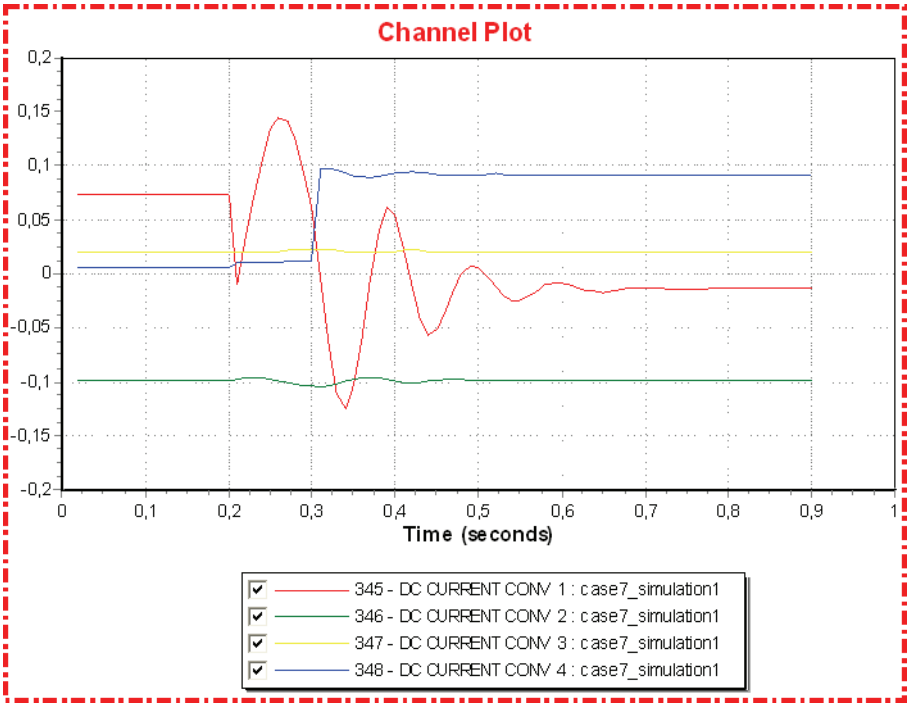

Figure F.7.3: Converter DC current [pu]

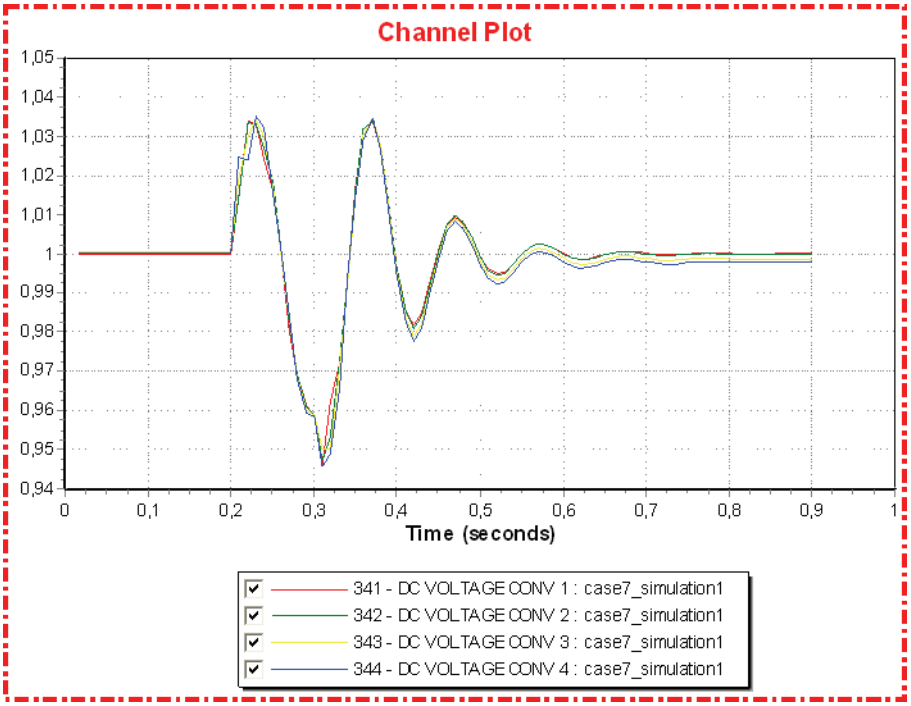

Figure F.7.4: Converter DC voltage [pu]

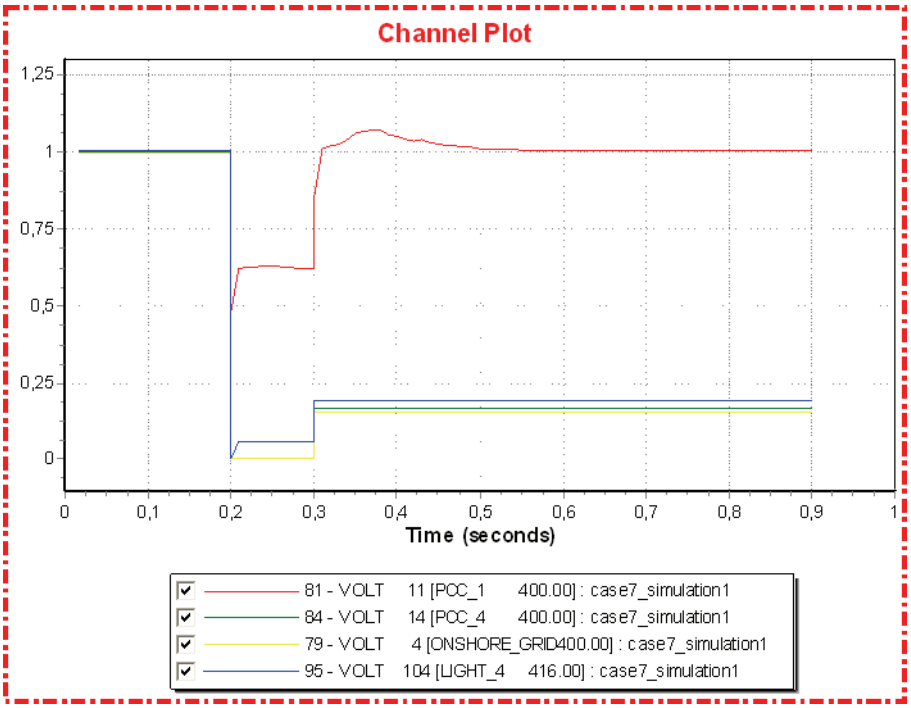

Figure F.7.5: Onshore AC voltage [pu]

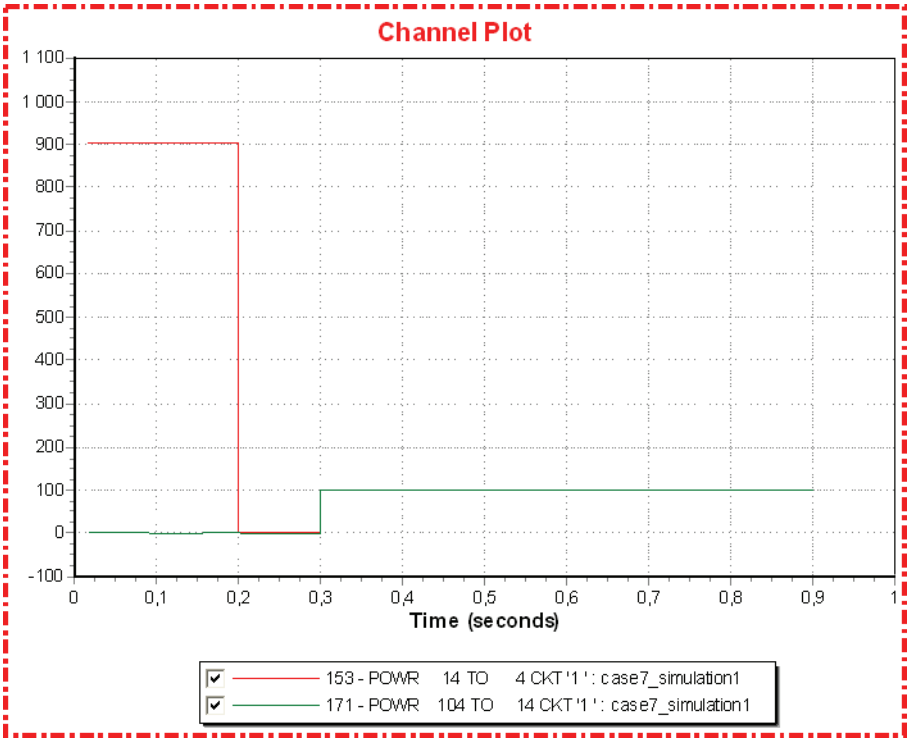

Figure F.7.6: Onshore active power transfer [MW]

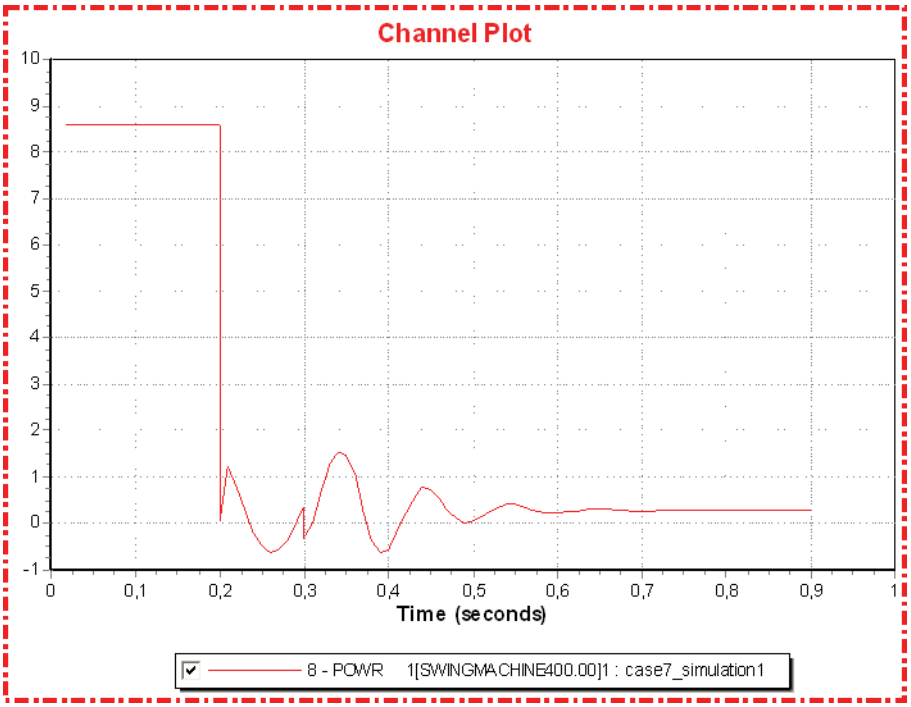

Figure F.7.7: Onshore active power generation [pu]

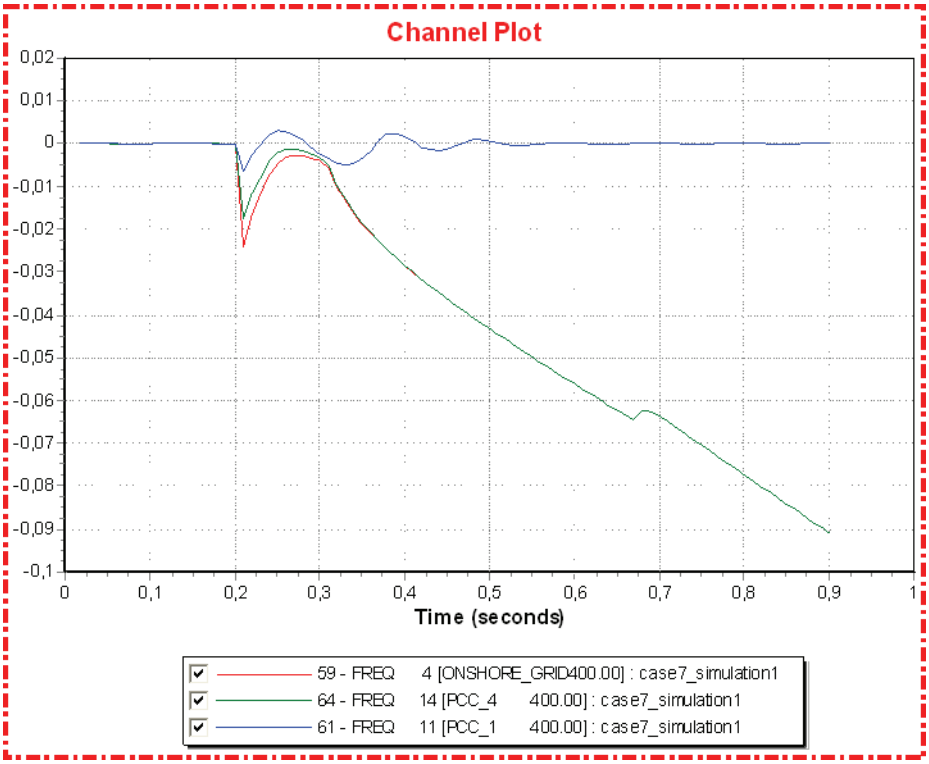

Figure F.7.8: Onshore frequency [pu deviation from 50 HZ]

Simulation 2 (Large power transfer)

Time	Event
0.00	Normal operation
0.20	Line fault on line 14 – 11
0.30	Disconnect (trip) faulted line and change Poption for converter 4 to PassNetOp

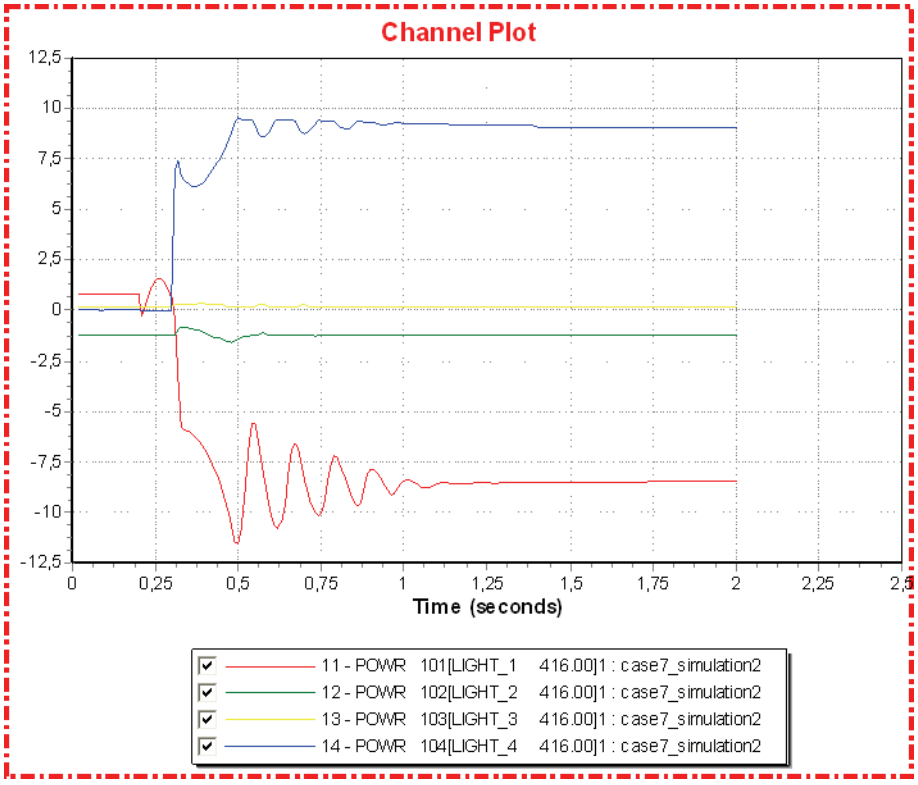

Figure F.7.9: Converter active power [pu]

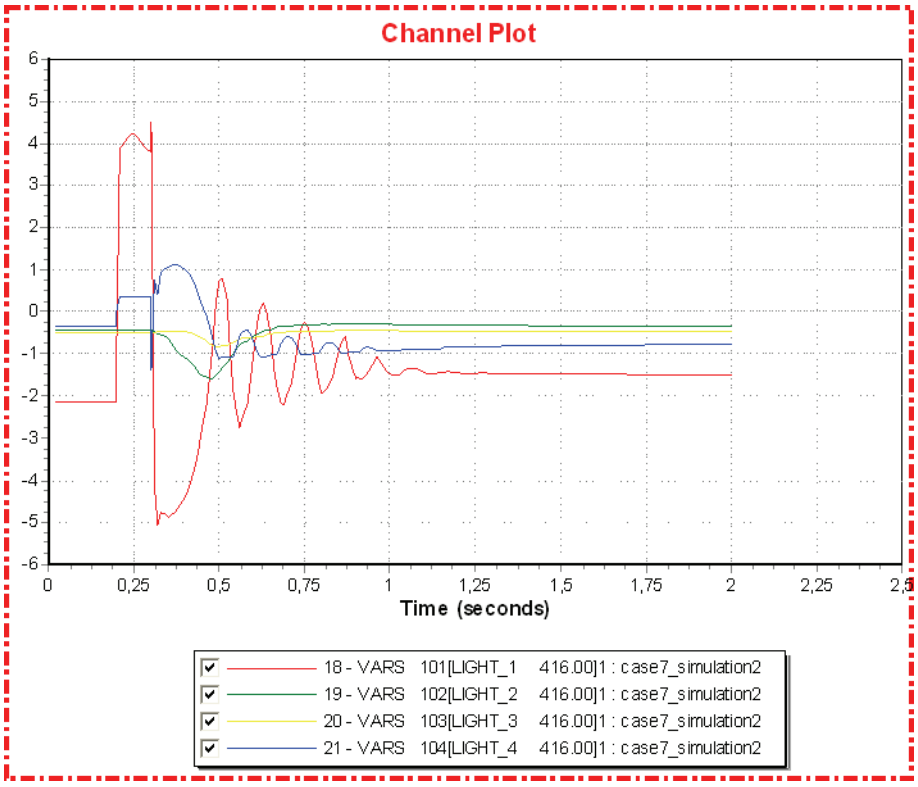

Figure F.7.10: Converter reactive power [pu]

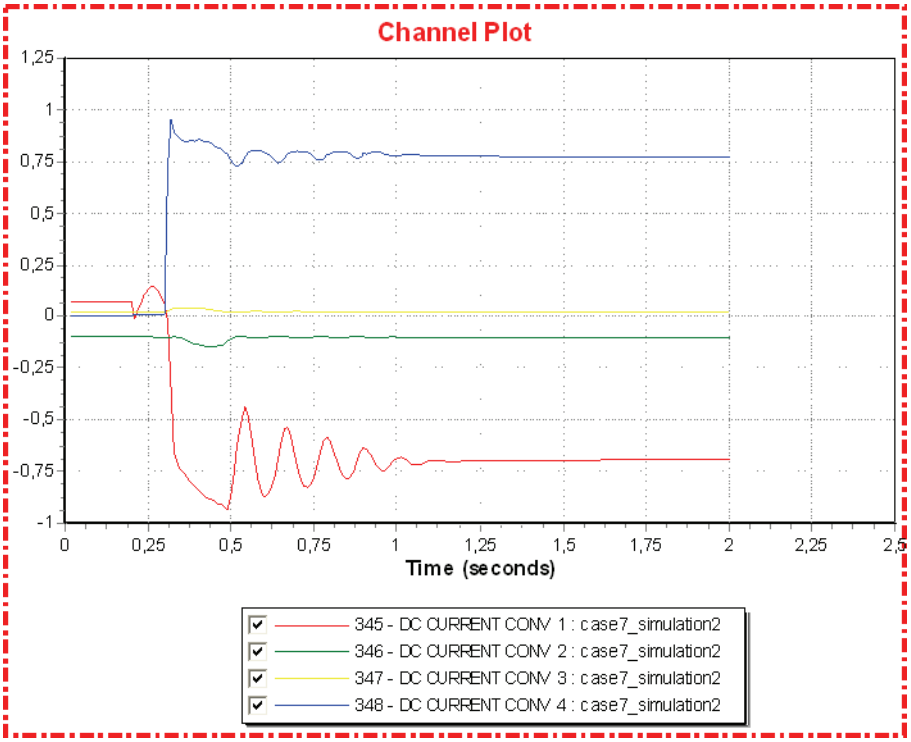

Figure F.7.11: Converter DC current [pu]

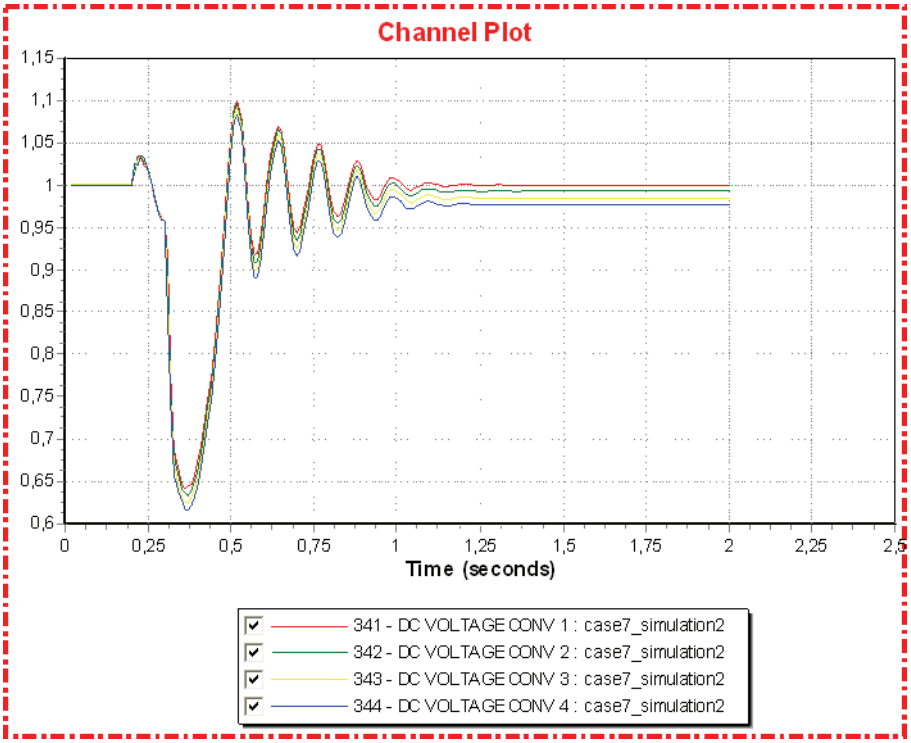

Figure F.7.12: Converter DC voltage [pu]

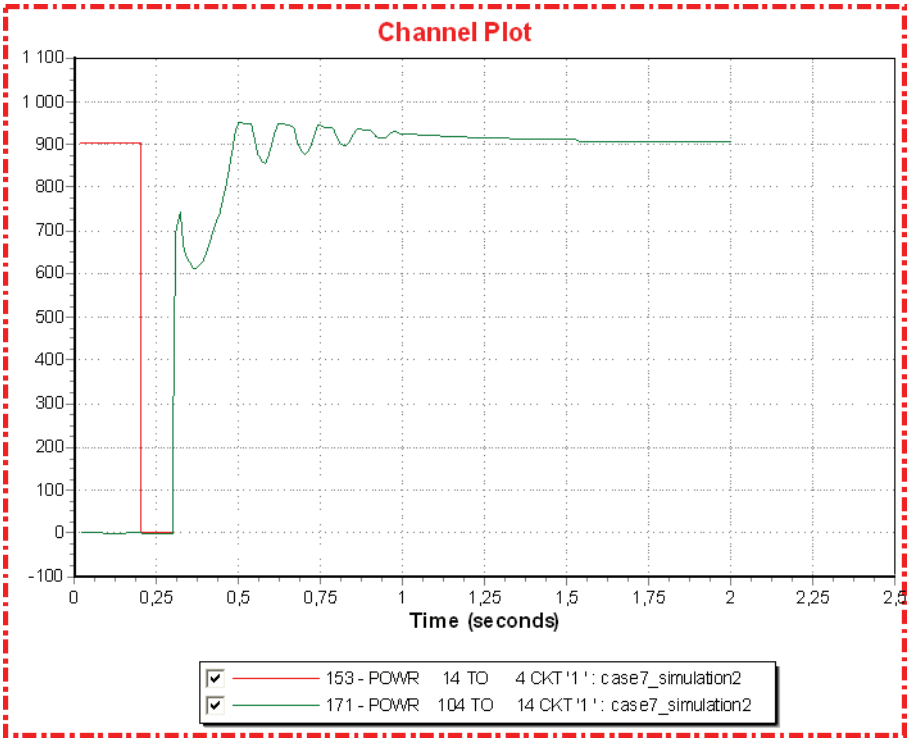

Figure F.7.13: Onshore active power transfer [MW]

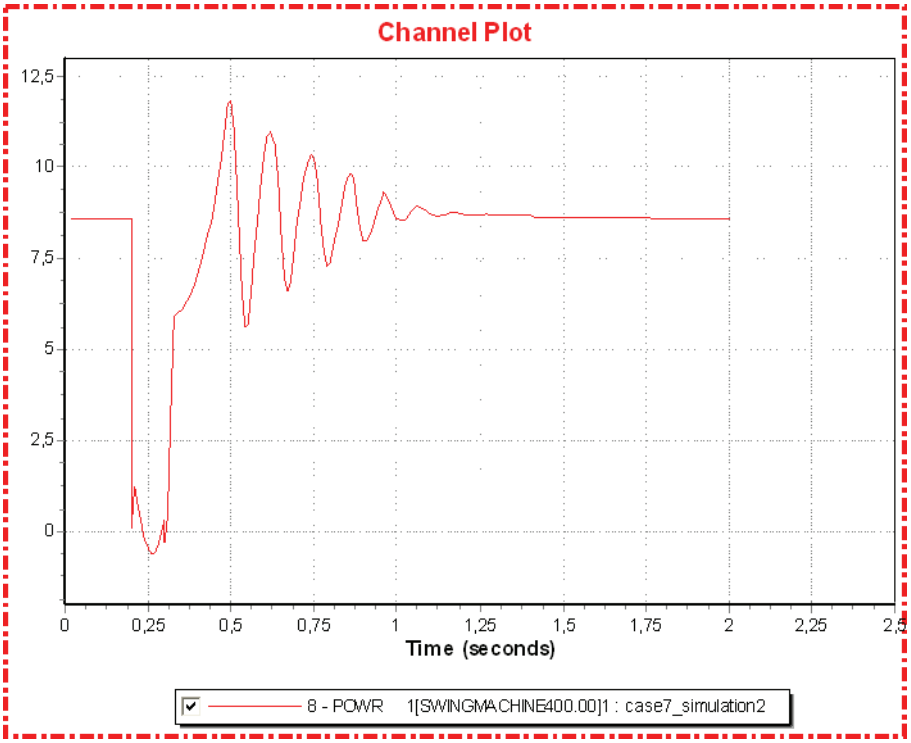

Figure F.7.14: Onshore active power generation [pu]

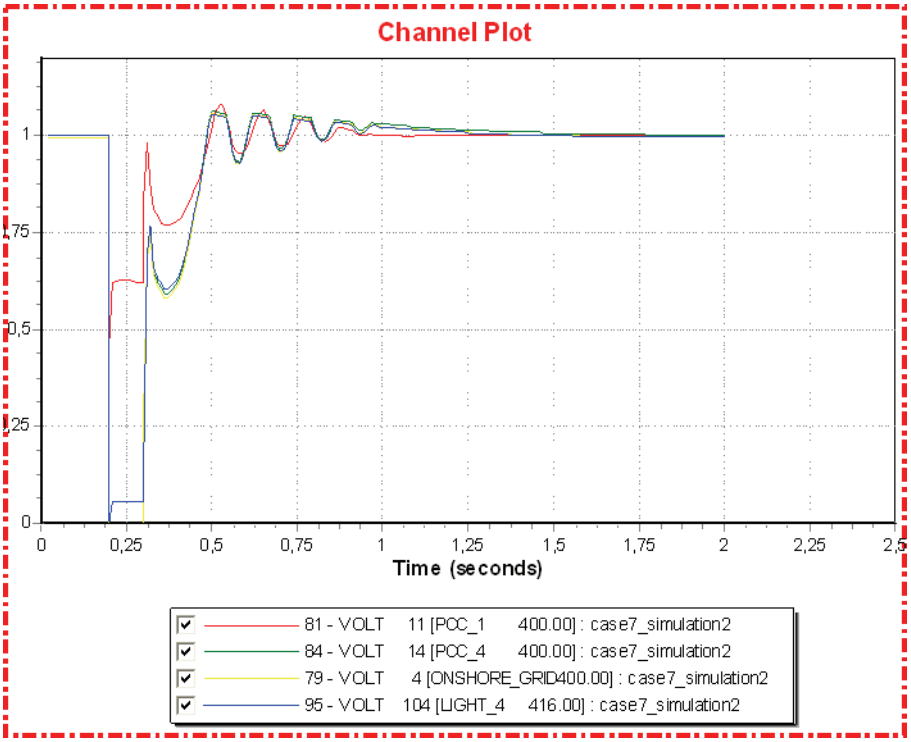

Figure F.7.15: Onshore AC voltage [pu]

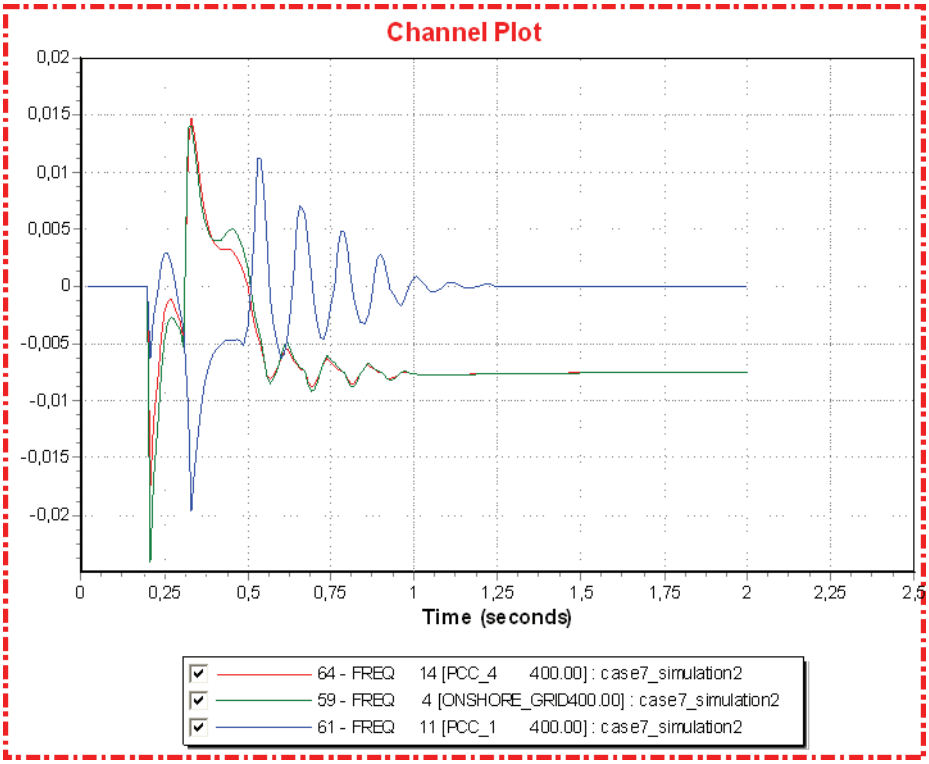

Figure F.7.16: Onshore frequency [pu deviation from 50 HZ]

22.1.8 Case 8

Simulation 1 (Large power transfer)

Time	Event
0.00	Normal operation
0.20	Line fault on line 5 – 11 (id1)
0.30	Disconnect (Trip) faulted line

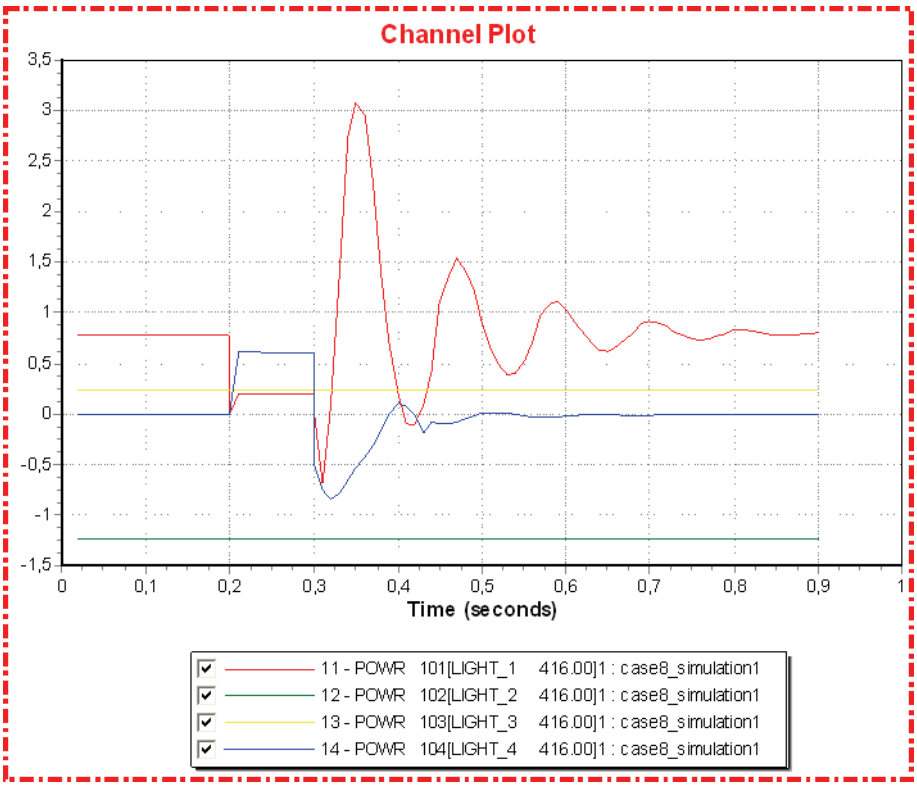

Figure F.8.1: Converter active power [pu]

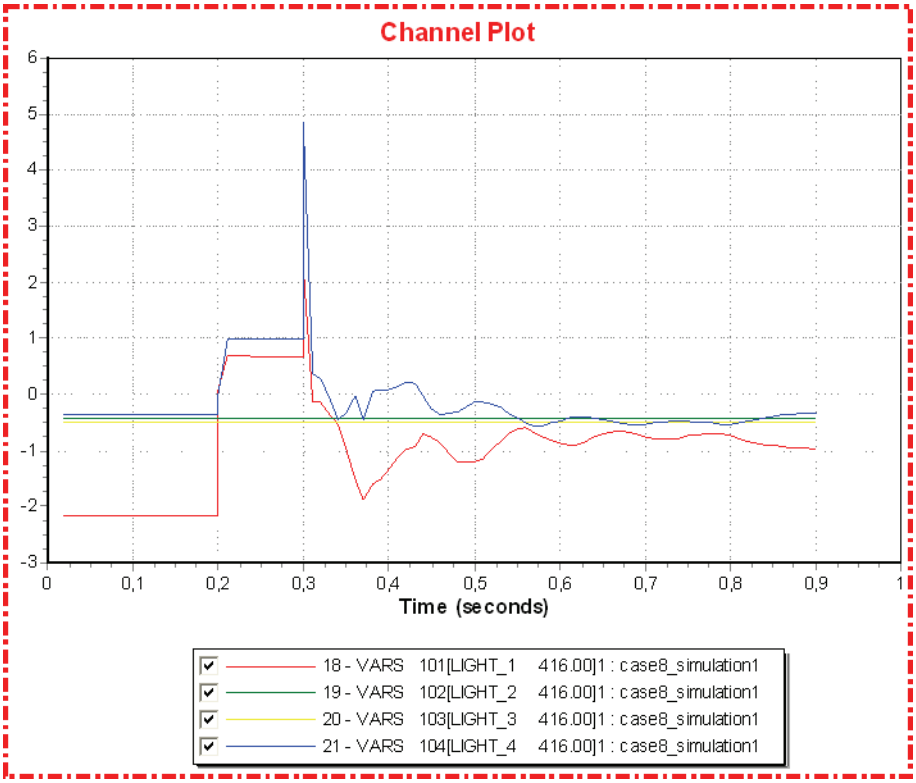

Figure F.8.2: Converter reactive power [pu]

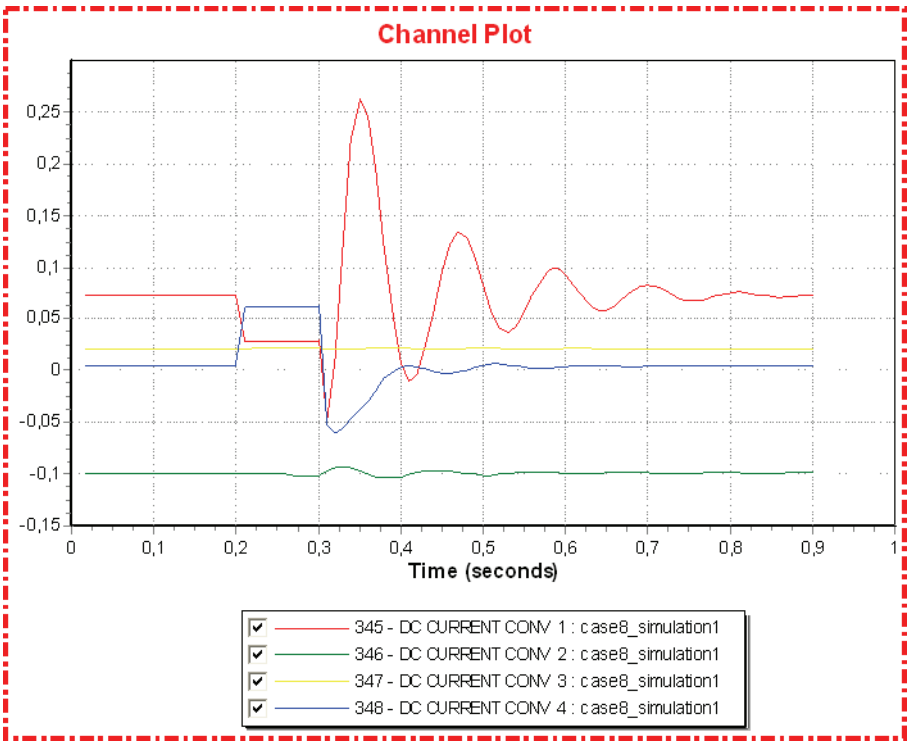

Figure F.8.3: Converter DC current [pu]

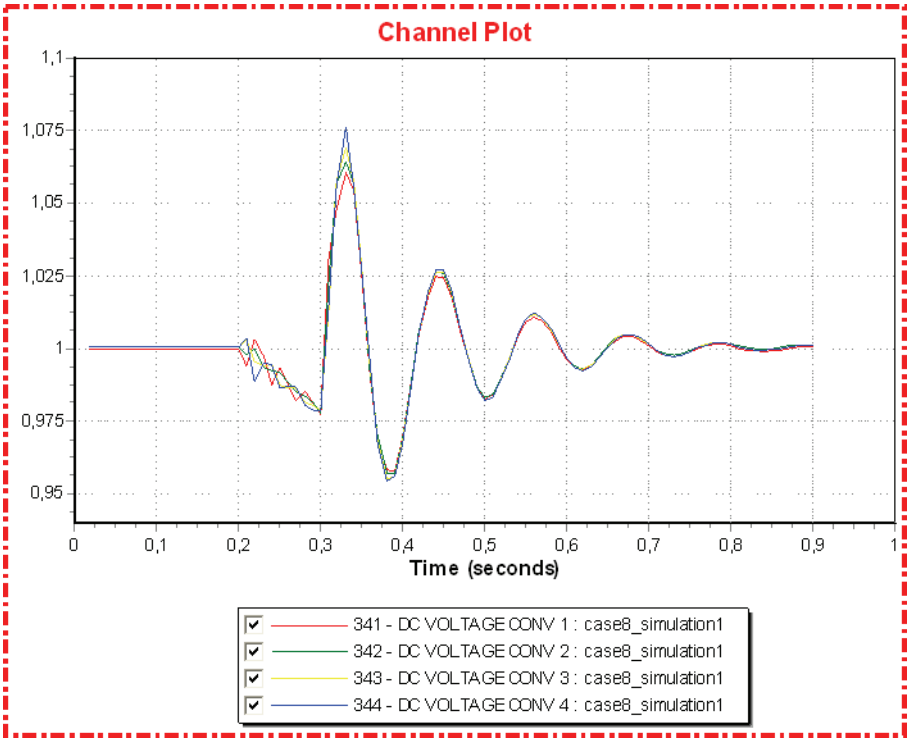

Figure F.8.4: Converter DC voltage [pu]

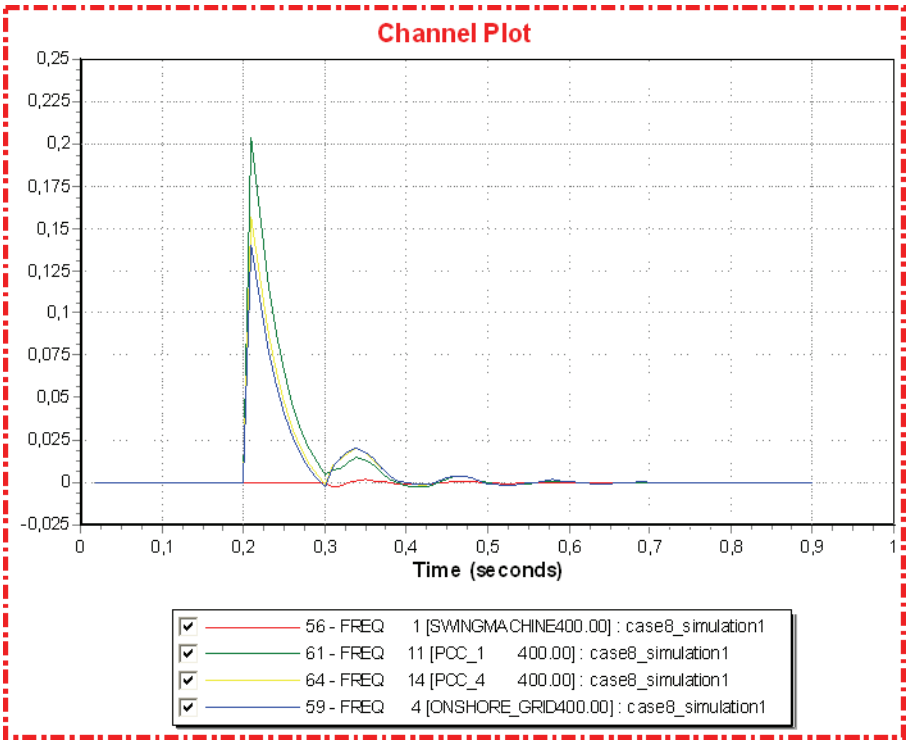

Figure F.8.5: Onshore frequency [pu deviation from 50 HZ]

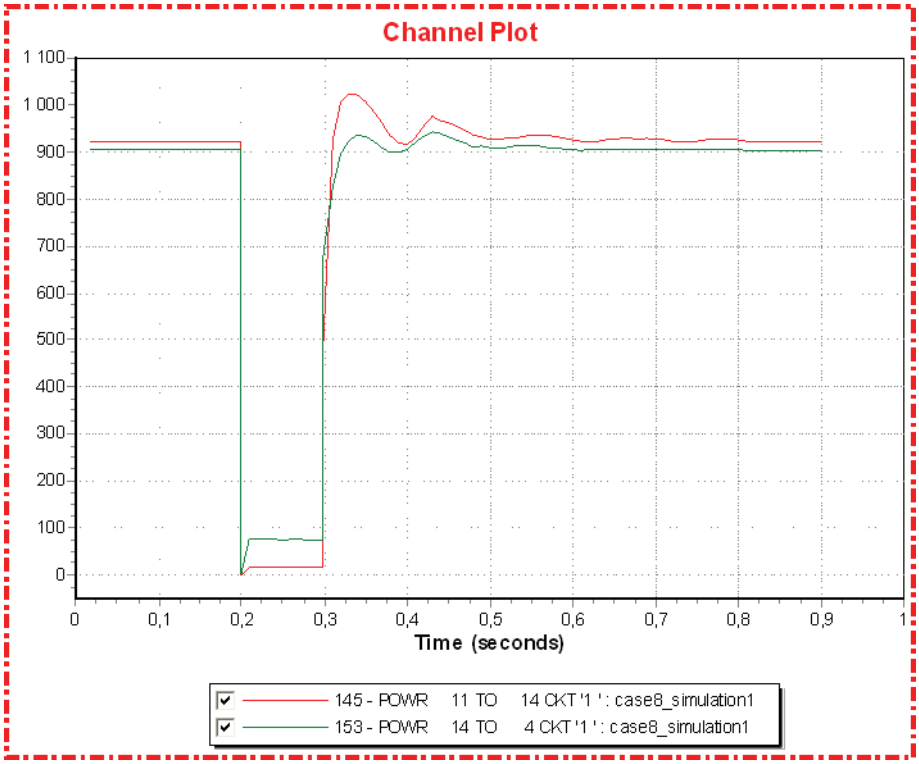

Figure F.8.6: Onshore active power transfer [MW]

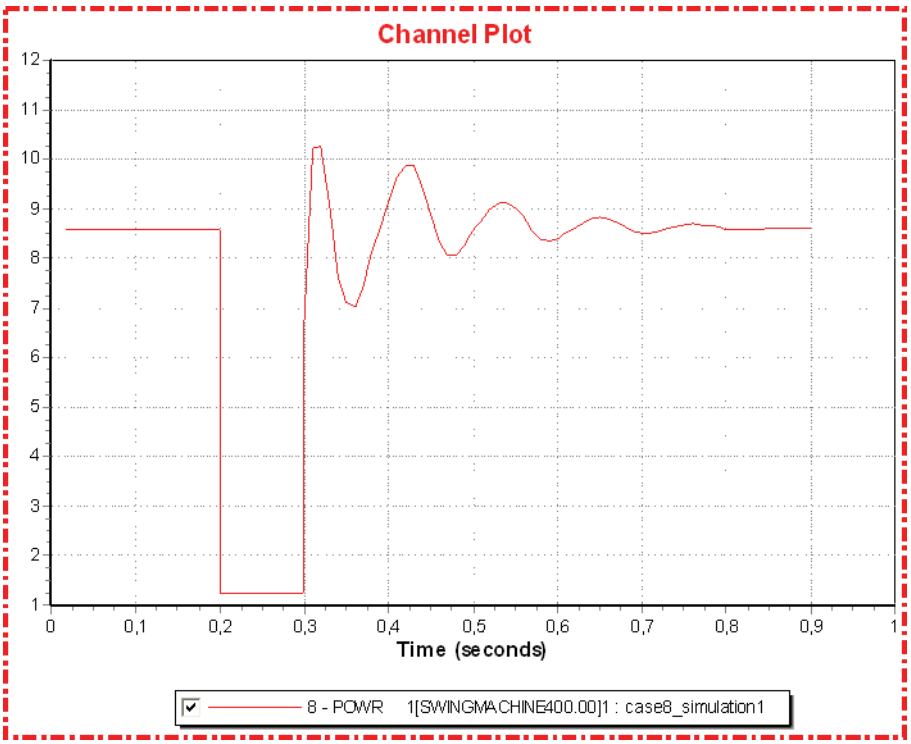

Figure F.8.7: Onshore active power generation [pu]

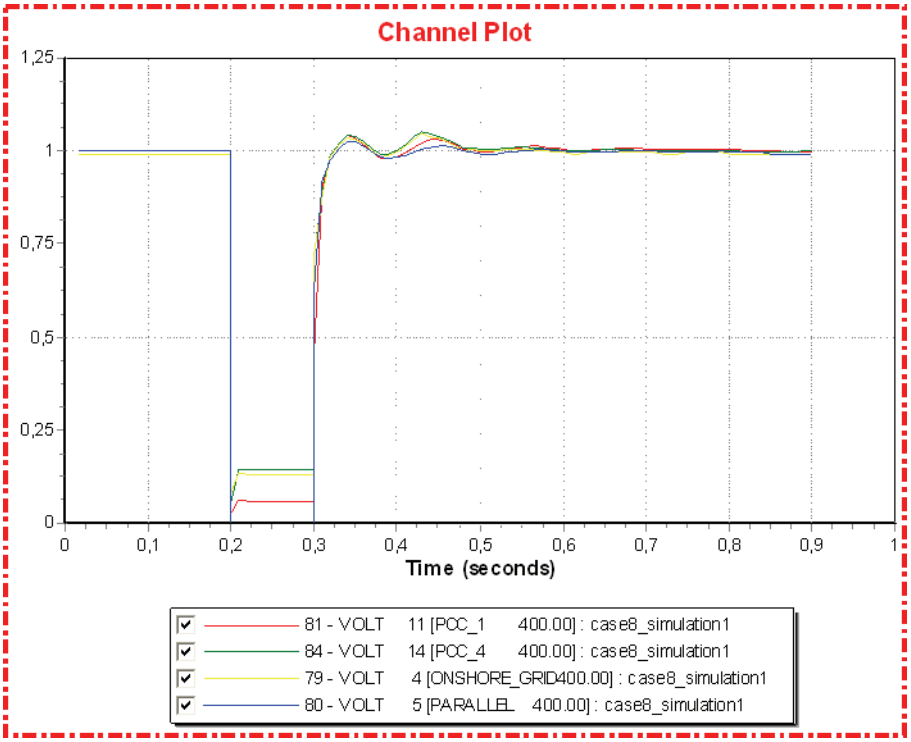

Figure F.8.8: Onshore AC voltage [pu]

Simulation 2 (Large power transfer)

Time	Event
-0.00	Disconnect power transformers for converter 1 and 4
0.00	Normal operation
0.20	Line fault on line 5 – 11 (id1)
0.30	Disconnect (Trip) faulted line

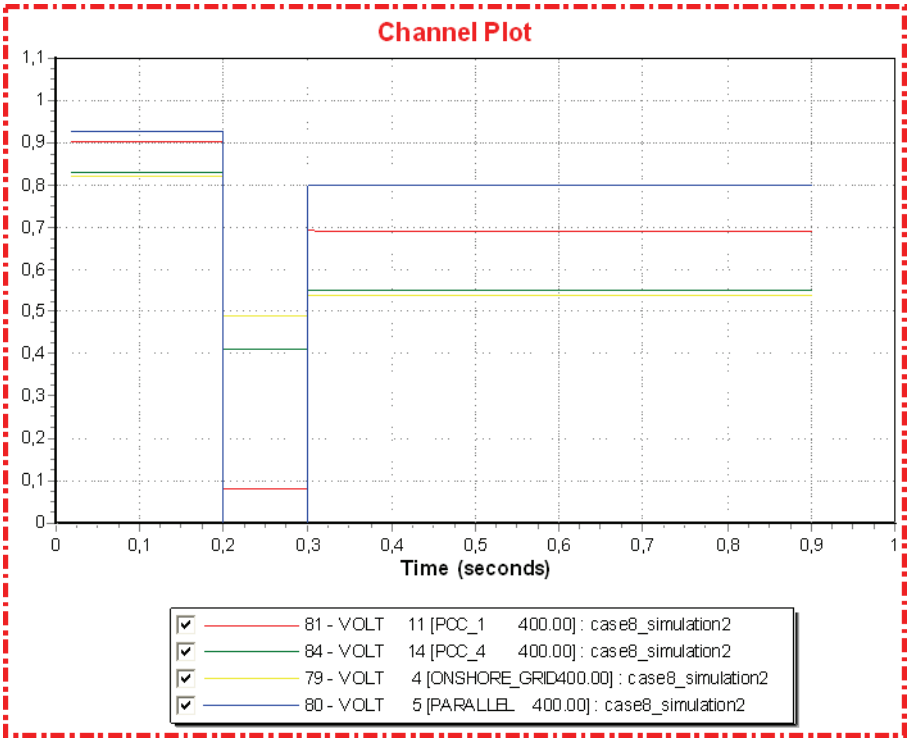

Figure F.8.9: Onshore AC voltage [pu]

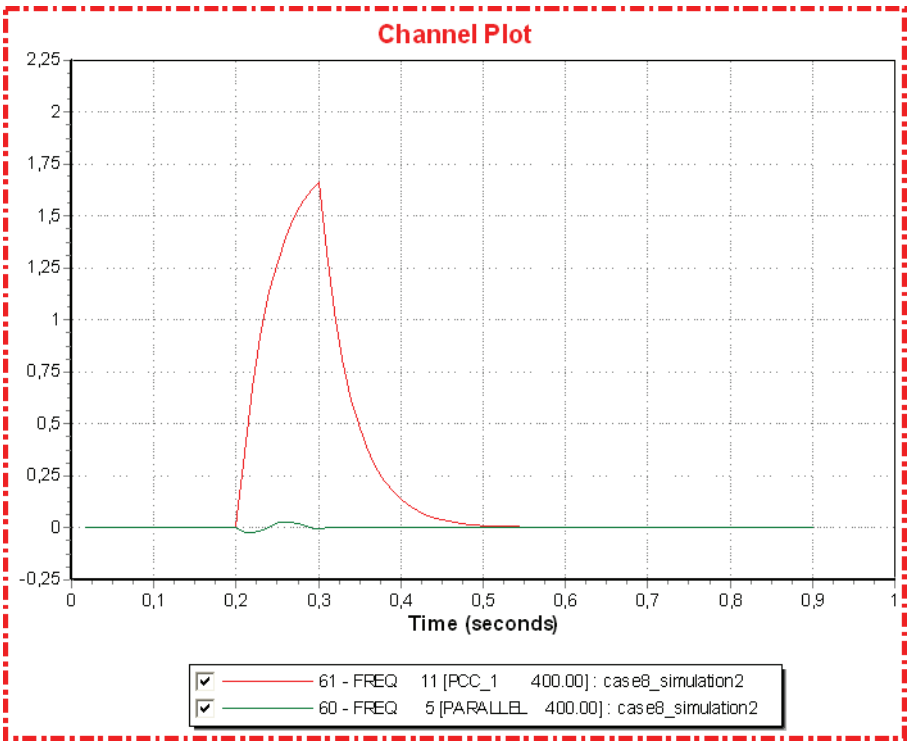

Figure F.8.10: Onshore frequency [pu deviation from 50 HZ]

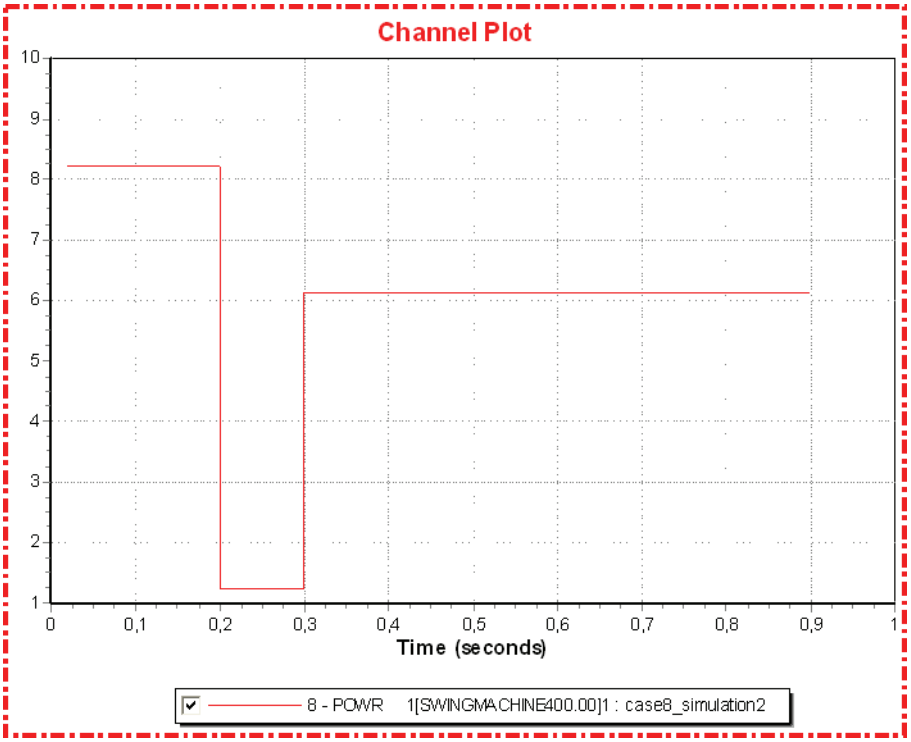

Figure F.8.11: Onshore active power generation [pu]

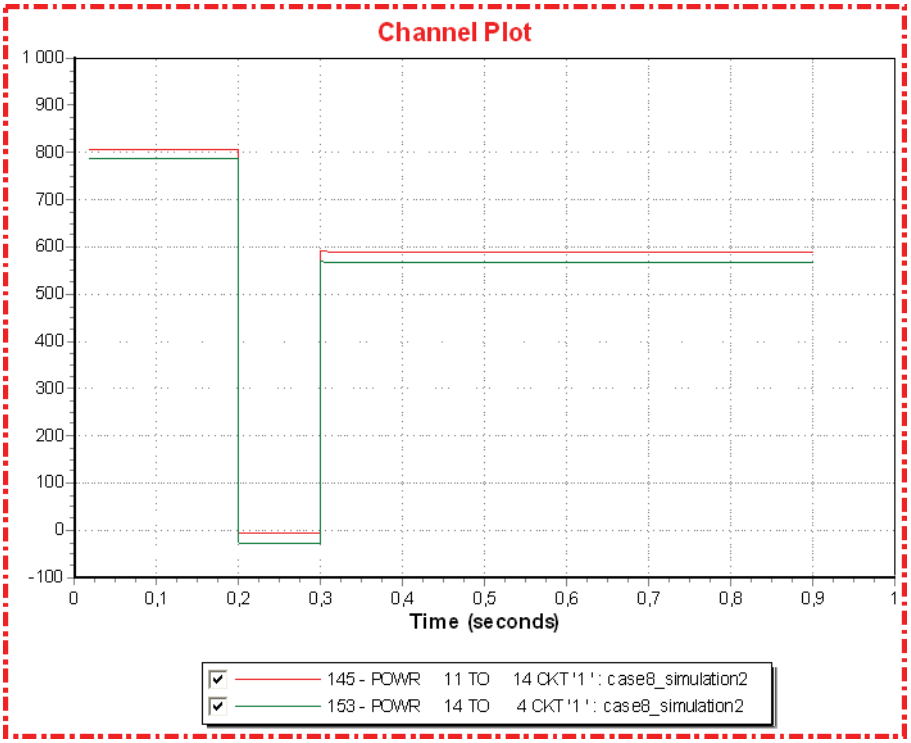

Figure F.8.12: Onshore active power transfer [MW]

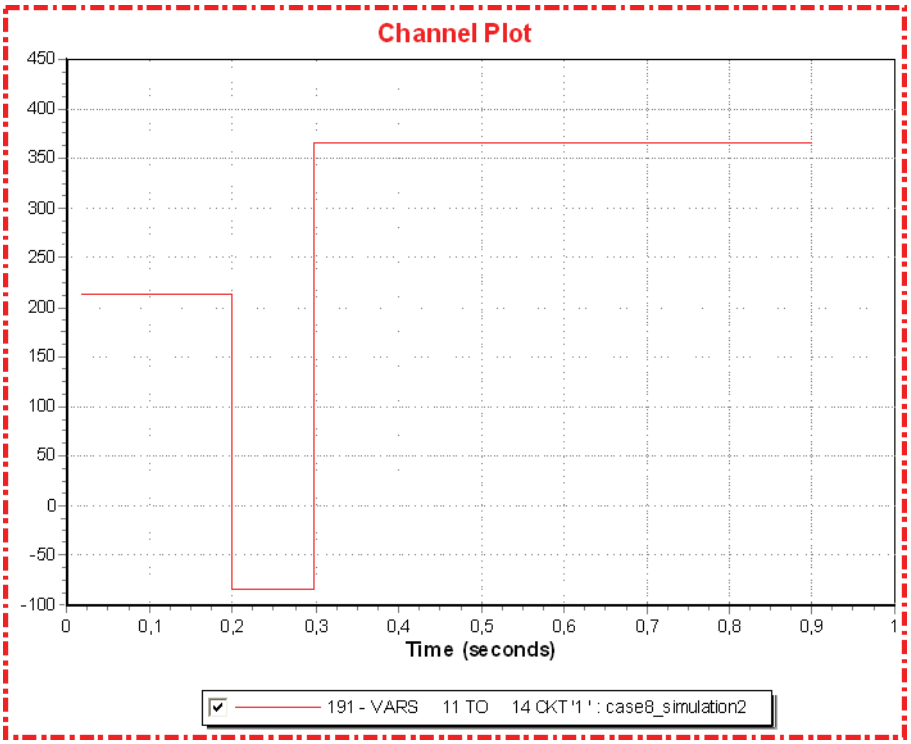

Figure F.8.13: Onshore reactive power transfer [MW]

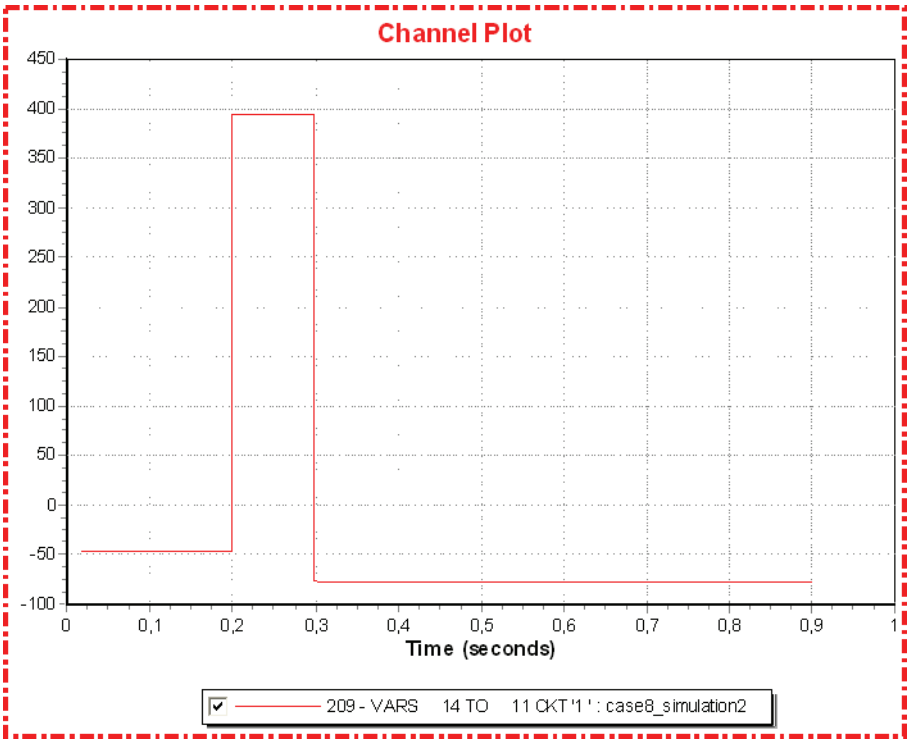

Figure F.8.14: Onshore reactive power transfer [MW]

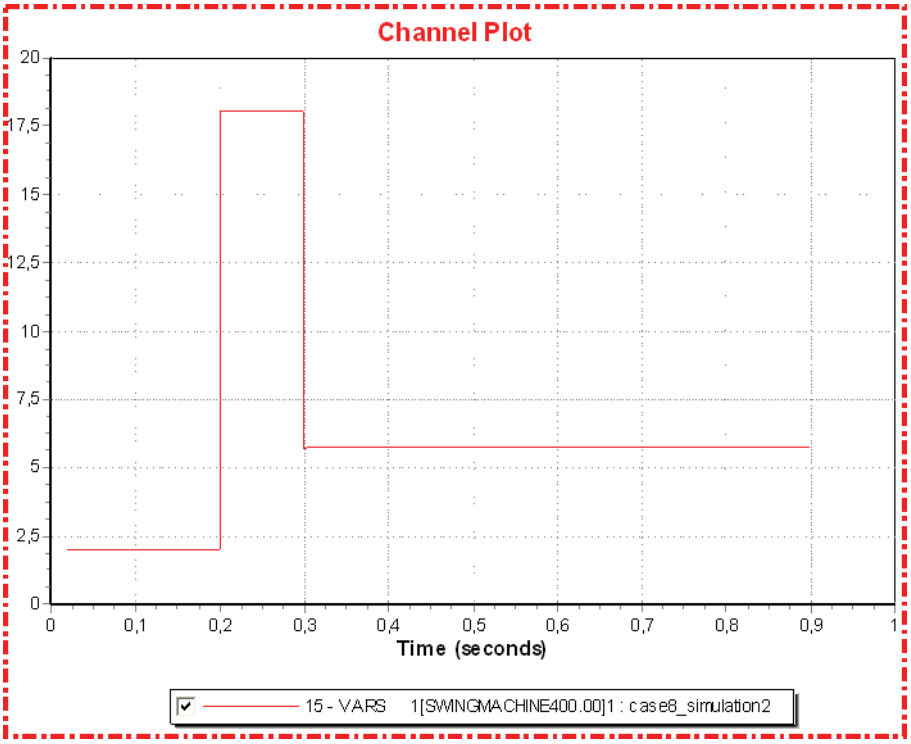

Figure F.8.15: Onshore reactive power generation [pu]

Simulation 3 (Large power transfer modified)

Time	Event
0.00	Normal operation
0.20	Line fault on line 5 – 11 (id1)
0.30	Disconnect (Trip) faulted line

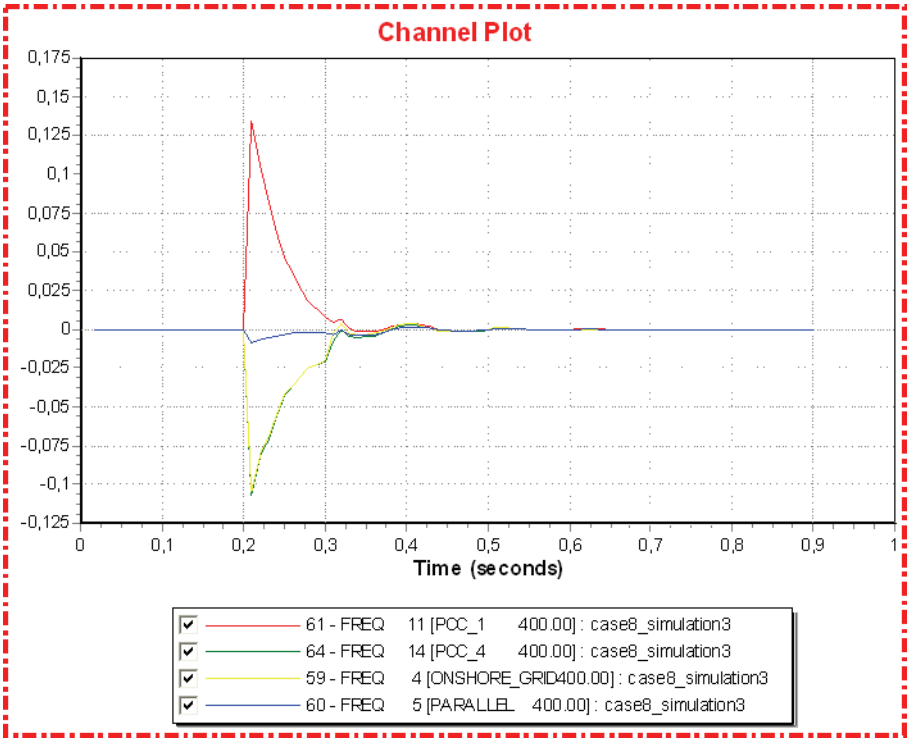

Figure F.8.16: Onshore frequency [pu deviation from 50 HZ]

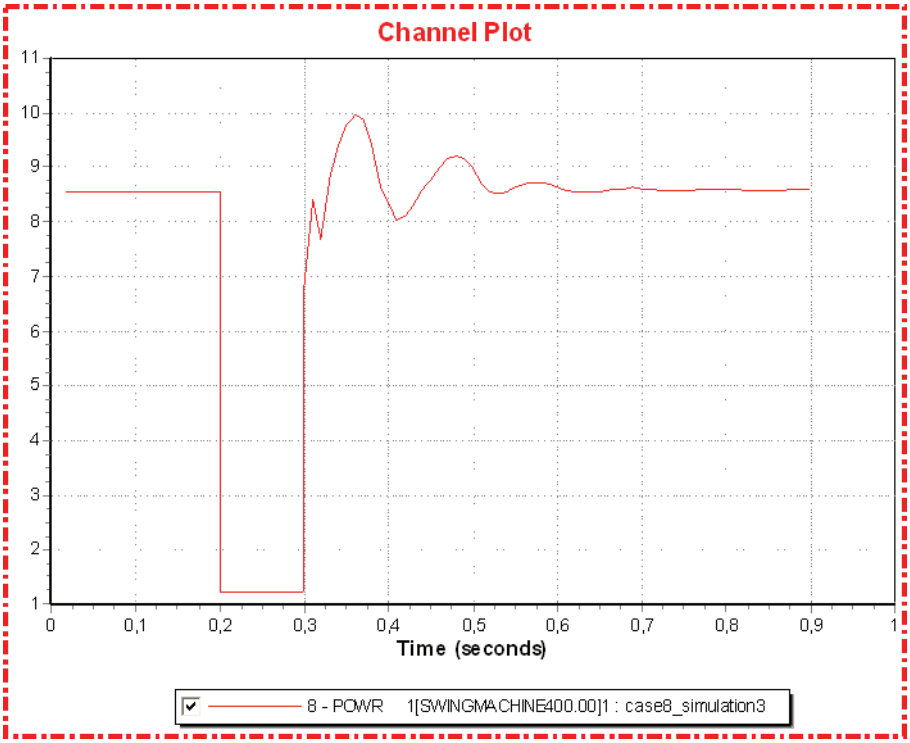

Figure F.8.17: Onshore active power generation [pu]

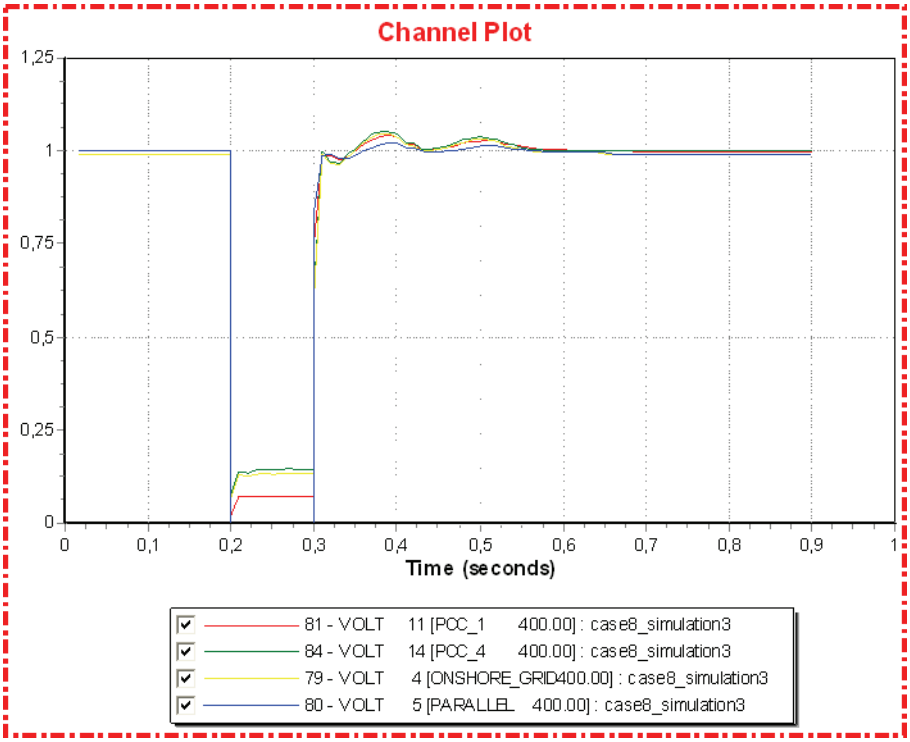

Figure F.8.18: Onshore AC voltage [pu]

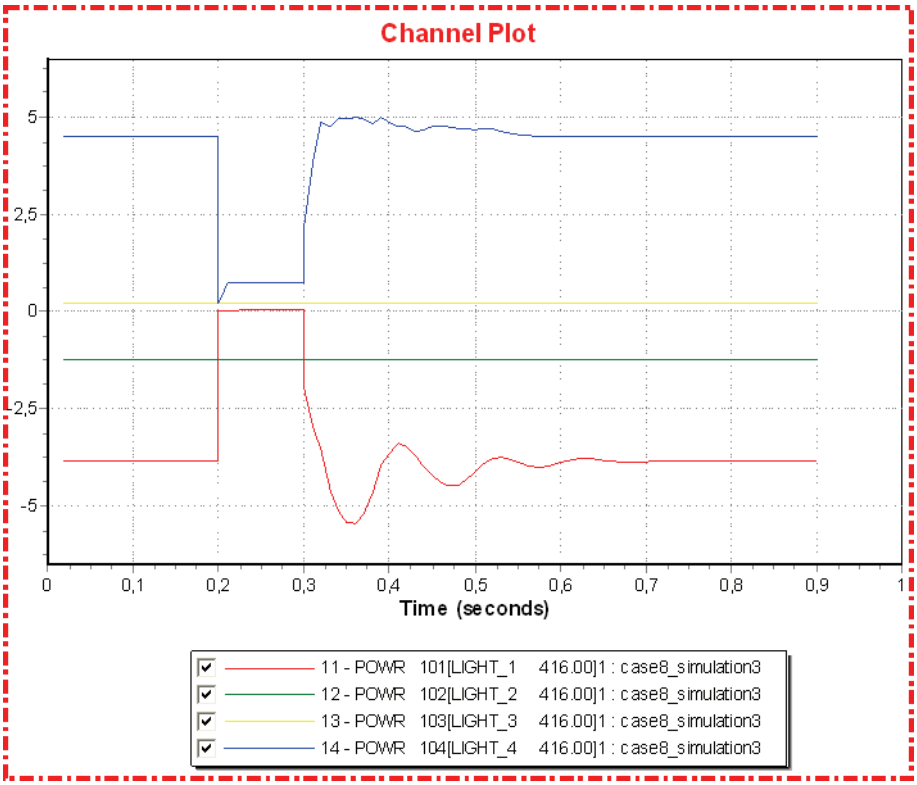

Figure F.8.19: Converter active power [pu]

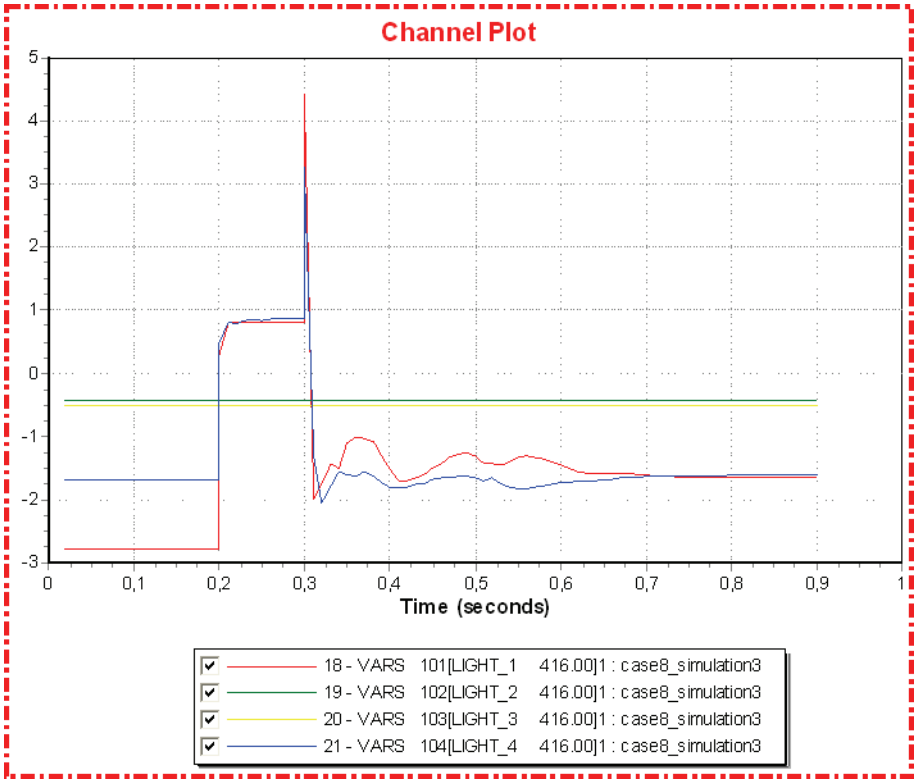

Figure F.8.20: Converter reactive power [pu]

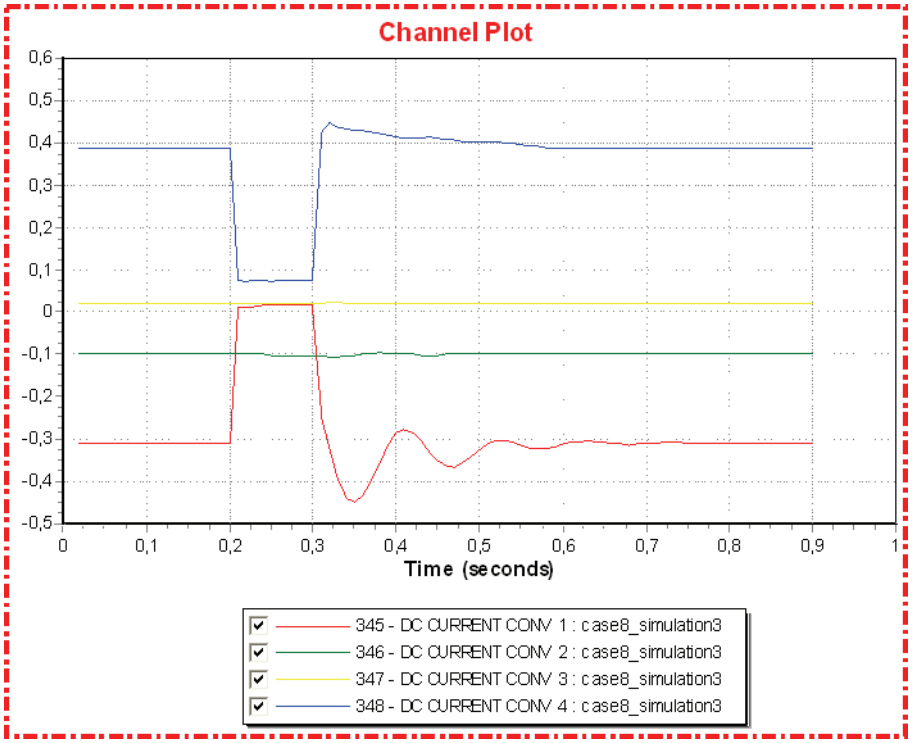

Figure F.8.20: Converter DC current [pu]

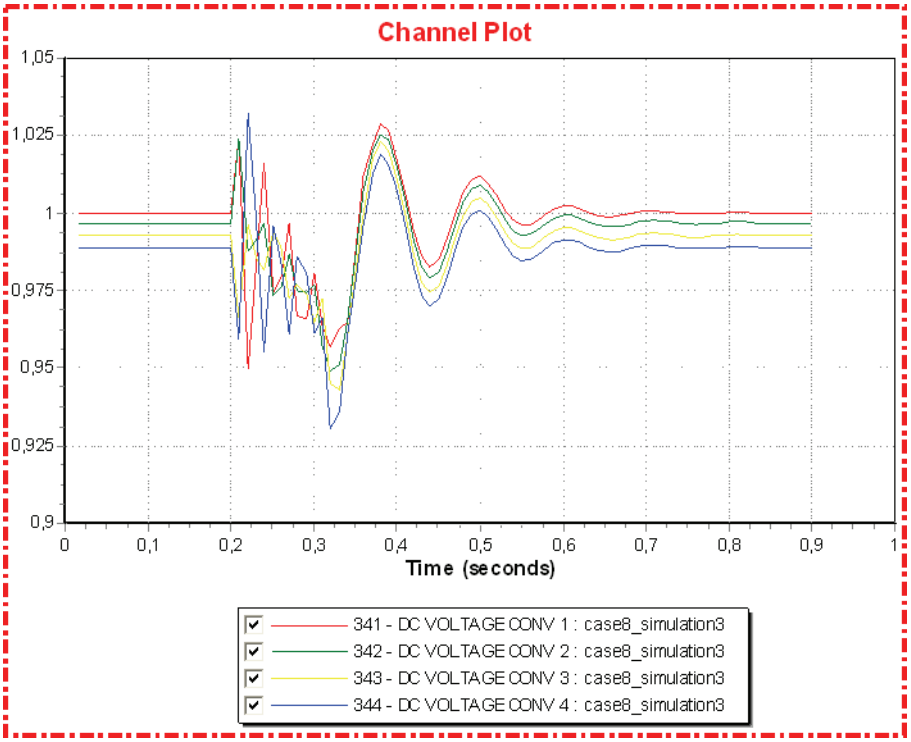

Figure F.8.21: Converter DC voltage [pu]

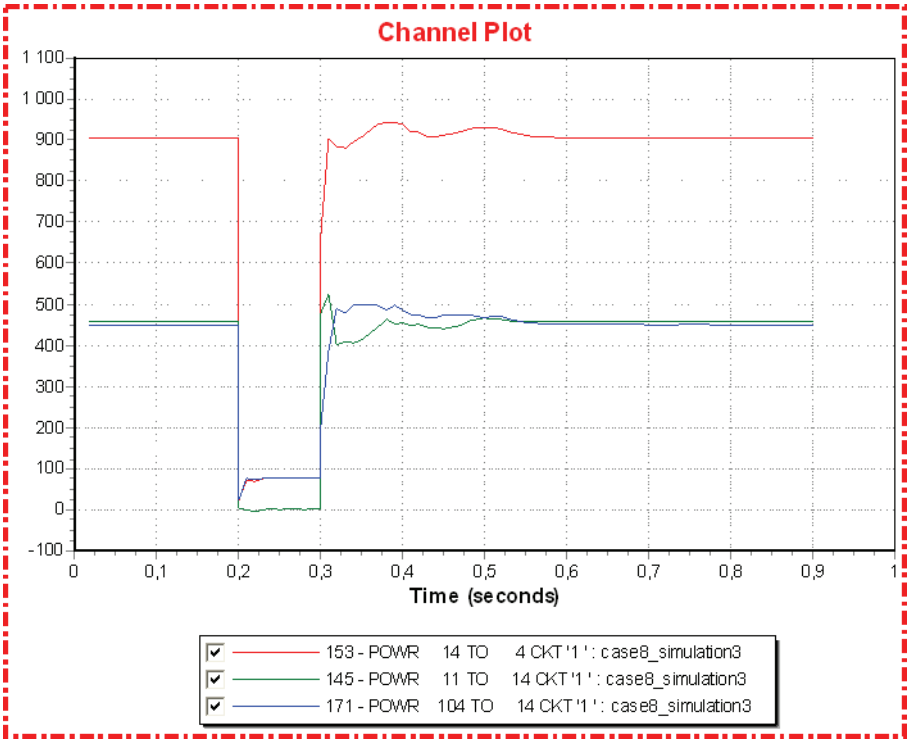

Figure F.8.22: Onshore active power transfer [MW]